This electronic thesis or dissertation has been downloaded from the King's Research Portal at https://kclpure.kcl.ac.uk/portal/

KING'S College LONDON

An instrument for the measurement of body/support interface stresses : with particular application to below-knee prostheses.

Williams, Robin Bede

The copyright of this thesis rests with the author and no quotation from it or information derived from it may be published without proper acknowledgement.

END USER LICENCE AGREEMENT

Unless another licence is stated on the immediately following page this work is licensed

under a Creative Commons Attribution-NonCommercial-NoDerivatives 4.0 International

licence. https://creativecommons.org/licenses/by-nc-nd/4.0/

You are free to copy, distribute and transmit the work

Under the following conditions:

- Attribution: You must attribute the work in the manner specified by the author (but not in any way that suggests that they endorse you or your use of the work).
- Non Commercial: You may not use this work for commercial purposes.
- No Derivative Works - You may not alter, transform, or build upon this work.

Any of these conditions can be waived if you receive permission from the author. Your fair dealings and other rights are in no way affected by the above.

Take down policy

If you believe that this document breaches copyright please contact librarypure@kcl.ac.uk providing details, and we will remove access to the work immediately and investigate your claim.

Download date: 05. May. 2023

An Instrument for the Measurement of Body/Support Interface Stresses: with particular application to below-knee prostheses

by

Robin Bede Williams

A thesis submitted for the degree of
Doctor of Philosophy

Based on research carried out in the
Department of Medical Engineering & Physics
Kings College Hospital School of Medicine & Dentistry
University of London

October 1993

B LON IN. UNIV

ABSTRACT

The socket of the prosthesis forms a critical interface between the amputee and their replacement (prosthetic) limb. Current socket design principles emphasise the importance of redistributing the normal stresses (pressures), present at the interface, to areas of the residual limb which can tolerant them. However, shear stresses, which are thought to have equal potential for causing tissue damage have been ignored. Little is known about the duration, magnitude and distribution of concurrent shear and normal stresses imposed on the limb during normal activities. This is primarily due to the lack of instruments to characterise them.

To address this a unique three axis transducer and data acquisition system have been developed during this research. It is the first of its type to be demonstrated as suitable for continuous simultaneous measurement of normal and shear stresses occuring at any site on the residual limb/prosthetic socket interface. The transducer (*16mm* diameter *x 4.9 mm* thick) detects stresses applied normal to, and shear stresses applied in the plane of, the limb/socket interface. It is designed to be recessed into, or inserted through, the socket wall. The accuracy of the shear and normal axes are *6%* indicated stress or *2.25KPa* (whichever is the greater) and *1.75%* or *5.5KPa* respectively. The frequency response (*-3dB* Bandwidth) of the transducer is better than *0.1mHz-1000Hz.*

Transducer interface circuitry, microcomputer controlled data acquisition hardware and associated software have been designed and are described. The system is able to digitise, to *12bits*, and store *32* channels of data (*10* transducers and *2* footswitch signals) at a rate of *500Hz*, for about *30* seconds per trial. Data can be archived to disc file on a PC. Overall system noise and uncertainty is better than *0.25%FSO.*

Preliminary clinical trials provide data not previously seen. It indicates that shear stresses (*2-20KPa*) are smaller than normal stresses (*10-40KPa*), and interwalk variations in stress magnitude and phasing are minimal. The significant spectral components of the stress waveforms were all found to be below *15Hz.* Waveform timing indicates that a stress wave travels across the limb in a proximomedial direction. Slippage of the limb in the socket was also observed.

The understanding gained from acquired stress data is being/can be used to: increase knowledge on tissue response to combined shear and normal stresses; improve prosthetic design principles; and improve models of the mechanical behaviour of limb/socket structures for computer aided socket design.

DEDICATION

In memory of my
Mother and Father

ACKNOWLEDGEMENTS

I sincerely thank my wife Nicola, not only for the hours spent deciphering my illegible script whilst typing it, but principally for her enduring encouragement, strength and unreserved dedication to myself, without which this thesis would not be. I am grateful beyond words.

I am indebted to my colleague and good friend Mr. David Porter for his invaluable ideas, constructive advice, enthusiasm and good humour.

I wish to thank my supervisor Professor V.C.Roberts, Head of Department, for enabling me to undertake this work and for his guidance and support.

There are many friends and colleagues, past and present, from the Department which I thank for their helpful suggestions and discussions over the years. Several of them deserve particular thanks: Messrs Riad Hosein and Ming Zhang for their co-operation and ruthless critique of my work; Dr. Eduardo Costa for his often timely counsel; Mr. Andrew Healey for allowing me to bend his ear on many occasions and commission his sagacious perception; Dr. Sidney Leeman for his example, advice and confidence in me; Mr. Andrew Healey, Dr. Sidney Leeman and Mr. Nicolas Thomas for their stimulating discussions and physics-on-a-napkin over coffee; Ms. Beverley Conway for her friendship and support over many years; Messrs. Kevin Jennings, Philip Millward, and Paul Richardson for the meticulous production of the mechanical components for the transducers and calibration jigs - often at short notice; and Dr. Inigo Deane, Ms. Lindis Richards, Mrs. Eve Langford for their constant assistance.

I would like to thank Mr. Jim Regan, chief prosthetist, for his advice and skills proffered. Also, I am indebted to the patients who willingly donated their time and patience during the clinical trials

Finally, I thank (posthumously) Mr. Stanley Parsonage for his enthusiasm and volunteering his skills during the early development of the transducer.

TABLE OF CONTENTS

Title 1
Abstract 3
Dedication 5
Acknowledgements 7
Table of Contents 9
List of Illustrations 15
Table of Tables 19

Chapter 1
Introduction

1.1 Introduction 23
1.1.1 Historical Perspective 25
1.1.2 Current Trends 26
1.1.3 Summary 29
1.2 Anatomy of the Lower Leg 29
1.2.1 Bone and Muscle 29
1.2.2 Skin 32
1.3 Amputation Procedures 35
1.3.1 Discussion 41
1.4 Prosthesis Fitting 41
1.4.1 Design Considerations for Below-Knee Sockets 42
1.4.2 The P.T.B. Below-Knee Prosthesis 46
1.4.3 Conventional P.T.B. Socket Manufacture 48
1.4.4 C.A.S.D./C.A.M. in P.T.B. Socket Design 50
1.4.4.1 Shape Manipulation CASD 52
1.4.4.2 Tissue Compliant CASD 53
1.4.4.3 Computer-aided socket manufacture 55
1.4.4.4 Discussion 55
1.5 Prosthetic Assessment 57
1.5.1 Gait Analysis 57
1.5.1.1 Temporal and Spatial Parameters 58
1.5.1.2 Kinematic Parameters 59
1.5.1.3 Kinetic Parameters 60
1.5.1.4 Metabolic Parameters 61
1.5.1.5 Summary 62

1.6 Discussion 63

Chapter 2
Soft Tissue Mechanics & Interface Stress Measurements

2.1 Soft Tissue Mechanics 65
2.1.1 Skin 66
2.1.1.1 Experimental Considerations 66
2.1.1.2 Structural Components of Skin 68
2.1.1.3 Properties of Whole Skin 68
2.1.2 Fascia, Tendon and Ligament 74
2.1.3 Muscle 76
2.2 Stress Effects on Tissue 77
2.2.1 Friction Effects 77
2.2.2 Normal Stress Effects 78
2.2.3 Shear Stress Effects 80
2.2.4 Socket Design Influence on Stress 81
2.2.5 Tissue Adaption 83
2.2.6 Discussion 84
2.3 Previous Interface Stress Measurements - Methods 85
2.3.1 Sensors between Limb and Socket 85
2.3.2 Sensors Recessed in Socket Walls 90
2.3.3 Instrumented, Isolated Sections of Socket Wall 92
2.3.4 Special Sockets 93
2.3.5 Sensors Measuring Shear Stress 93
2.3.6 Concurrent Studies 96
2.3.7 Discussion 97
2.4 Previous Interface Stress Measurements - Findings 101
2.5 Temperatures in Prosthetic Sockets 106
2.6 Transducer Design Criteria 107

Chapter 3
Triaxial Stress Transducer - Prototype Design

3.1 Shear-Section Design 115
3.1.1 Principle of Operation 116
3.1.2 Force to Displacement Conversion 118
3.1.2.1 Rubber as a Spring 119

3.1.2.1.1 Rubber in Simple Shear 122
3.1.2.1.2 Rubber in Compression 123
3.1.2.2 Time Domain Behaviour of Rubber 123
3.1.2.3 Frequency Domain Behaviour of Rubber 127
3.1.2.4 Useful Types of Rubber 130
3.1.3 Displacement to Voltage Conversion 133
3.1.3.1 Magnet Types 133
3.1.3.2 Magnetoresistor Properties 133
3.1.3.3 Disc Materials 139
3.1.3.4 Other Materials 139
3.2 Normal Section Design 141
3.2.1 Principle of Operation 141
3.2.2 Strain-gauge Properties 142
3.2.3 Excitation Limits 145
3.2.4 Diaphragm Considerations 145
3.2.5 Indentor Mechanism 149
3.3 Prototype Device Assembly 150
3.3.1 Shear-section Assembly 150
3.3.2 Normal-section Assembly 151
3.3.3 Three Axis Device Assembly 151
3.4 Mounting Considerations 152

Chapter 4
Triaxial Stress Transducer - Development to Requisite Form

4.1 Shear-Stress Section Development 157
4.1.1 First Prototype Assessment - Design A 158
4.1.1.1 Test Regimes and Equipment 158
4.1.1.2 Static Stress Response 161
4.1.1.2.1 Linearity and Range 162
4.1.1.2.2 Creep and Hysteresis 164
4.1.1.3 Temperature Sensitivity 167
4.1.1.3.1 Magnetoresistor Contribution 168
4.1.1.3.2 Silicone Expansion 169
4.1.1.3.3 Magnet Contribution 172
4.1.1.4 Discussion 172
4.1.2 Component Reselection 174
4.1.2.1 Magnetoresistor Replacement 174

4.1.2.2 Magnet Replacement 175
4.1.2.3 Silicone Replacement 176
4.1.2.4 Dimensional Changes 178
4.1.3 Second Prototype Assessment - Design B 179
4.1.3.1 Test Equipment Modification 179
4.1.3.2 Temperature Sensitivity 182
4.1.3.2.1 Magnetoresistor Contribution 182
4.1.3.2.2 Silicone Expansion 183
4.1.3.2.3 Magnet Contribution 185
4.1.3.2.4 Component Summary 186
4.1.3.2.5 Device Temperature Sensitivity 186
4.1.3.3 Static Stress Response 188
4.1.3.3.1 Linearity and Range 189
4.1.3.3.2 Force Resolution 190
4.1.3.3.3 Repeatability 190
4.1.3.3.4 Creep and Hysteresis 190
4.1.3.3.5 Alignment Errors in Testing 193
4.1.3.4 Discussion 195
4.1.4 Further Component Reselection 196
4.1.4.1 Silicone Replacement by Natural Rubber 196
4.1.4.1.1 Natural Rubber Formulation 197
4.1.4.1.2 Bonding Considerations 197
4.1.4.2 Low-Friction Polymer Central Disc 200
4.2 Normal-Stress Section Development 201
4.2.1 Test Equipment and Methods 202
4.2.2 Temperature Sensitivity 202
4.2.3 Static Stress Response 204
4.2.3.1 Non-axial Loading of Diaphragm 206
4.2.4 Discussion 208
4.3 Requisite Triaxial Transducer Design - Design C 208
4.3.1 Device Construction 208
4.3.2 Dynamic Stress Response 215
4.3.2.1 Test Equipment 216
4.3.2.2 Dynamic Measurement Considerations 217
4.3.2.3 Range, Hysteresis, Linearity and Accuracy 224
4.3.2.4 Shear Stress Vectors and Crosstalk Errors 236
4.3.2.5 Creep and Frequency Response 238
4.3.3 Temperature Sensitivity 243
4.3.3.1 Test Equipment and Methods 243

4.3.3.2 Sensitivity Data 244
4.4 Summary 247

Chapter 5
Data Acquisition : Hardware

5.1 Transducer Interface Circuit 251
5.1.1 Transducer Excitation 252
5.1.1.1 Magneto-resistor Electrical Properties 252
5.1.1.2 Strain-gauge Electrical Properties 255
5.1.1.3 Excitation Circuit 256
5.1.2 Signal Conditioning 258
5.1.2.1 Amplification 258
5.1.2.2 Interference and Filtering 264
5.2 Signal Conversion and Data Storage 270
5.2.1 Analogue to Digital Conversion 271
5.2.2 Conversion Control and Data Storage 273
5.2.3 Power Supplies 274
5.3 Registration of Foot Contact Events 275
5.4 Interface to Kinematic Measurements 277
5.5 System Integration 278
5.6 Safety 281
5.7 Discussion 282

Chapter 6
Data Acquisition : Software

6.1 System Hardware and Programming Environment 286
6.2 Software Overview 287
6.3 Level1 - File Viewing 290
6.3.1 View Data Files 293
6.4 Level2 - Data Collection Unit Initialisation 293
6.4.1 Dos Functions 297
6.4.2 Monitor Functions 298
6.4.3 Programme Transfer and Execution 298
6.5 Level3 - Data Collection 299
6.5.1 Support Functions 302
6.5.2 Transfer Data Files 304

6.5.3 Collect New Data 307
6.5.4 View Data Files 311
6.6 Error Trapping 312
6.7 Discussion 315

Chapter 7
Clinical Evaluation

7.1 Introduction 317
7.2 Evaluation Study 1 - Limb/Socket Stresses in Amputees 318
7.3 Evaluation Study 2 - Plantar Stresses in Normals 328
7.4 Performance and Mounting Notes 333

Chapter 8
Discussion and Future Work

8.1 Overview of the Imperatives 337
8.2 Transducer Development 339
8.3 Data Acquisition System Development 343
8.4 Clinical Findings 344
8.5 Outline for Future Developments 346

Appendix
Data File Format & Memory Map

A.1 Data-File Format 351
A.2 DCU Memory Map 353

Publications 355

References 357

LIST OF ILLUSTRATIONS

Chapter 1

1.1 Section view of the leg from midway along the tibia. 30
1.2 Cross-sectional view of skin 33
1.3 Skin incisions for below-knee amputations 37
1.4 Stages of the Long Posterior Flap amputation 38
1.5 Stages of the Equal (skewed sagittal) Flap amputation 39
1.6 Pressure tolerant/sensitive areas of the residual limb 43
1.7 Forces acting on the limb and PTB socket during gait 45
1.8 Basic components of the PTB below-knee prosthesis 46
1.9 Temporal and spatial parameters of the gait cycle 58

Chapter 2

2.1 Stress-Strain curve for skin under uni-axial tension 70
2.2 Hysteresis in skin under uni-axial tension 71
2.3 Load cycle preconditioning for skin (uni-axial tension) 72
2.4 Stress strain curve for collagen 76
2.5 Normal stress sensors inserted between limb and socket 87
2.6 Stress sensors inserted through the socket wall 91
2.7 Stress measurements by isolating socket sections 93
2.8 Non-prosthetic body/support interface stress sensors 95
2.9 Triaxial stress sensor developed in concurrent research 96
2.10 Limb-in-socket temperature variation with exercise 107

Chapter 3

3.1 Principle of shear transduction mechanism 116
3.3 Schematic of biaxial shear transducer 117
3.2 Assembly of biaxial shear transducer 118
3.4 Structural formulae of some elastomers 119
3.5 Crosslinking and entanglements in long chain molecules 120
3.6 Shear stress v strain in Natural rubber (Treloar) 121
3.7 Schematic of rubber in simple shear 123

3.8 Viscoelastic response to constant stress/strain 124
3.9 Compliance v time for ideal rubber 125
3.10 Mechanical models for viscoelastic behaviour 126
3.11 Shear modulus v frequency for ideal rubber 129
3.12 Uncertainty of stress estimation with phase lag 129
3.13 Current path in magnetoresistor under a magnetic field 134
3.14 Resistance v induction for magnetoresistor 135
3.15 Resistance v temperature for magnetoresistor 136
3.16 Response of FP110D155 to magnet displacement 138
3.17 Dimensions of disc's - Design A shear section 140
3.18 Assembly of magnetoresistor PCB 141
3.19 Generalised diaphragm under distributed normal force 146
3.20 Operation of indentor mechanism 149
3.21 Transducer assembly jig 150
3.22 Schematic of Transducer mounted in socket wall 153
3.23 Dimensions of blanks for making transducer recessess 154
3.24 Method of making transducer blanks 155
3.25 View of finished recess and instrumented socket 156

Chapter 4

4.1 Transducer calibration jig 160
4.2 Stress response of Design A shear sections 163
4.3 Stress response with orientation Design A shear section 164
4.4 Stress response and relaxation, Design A silicones 166
4.5 Temperature response of Design A shear sections 168
4.6 Temperature response of FP110D155 magneto-resistor 169
4.7 Output v magnet (SmCo) / MR (FP110D155) separation 171
4.8 Temperature response of SmCo magnet (experimental) 173
4.9 Relative field exposure with magnet/MR size 176
4.10 Unidirectional response, MR(FP111L100) / magnet(NdBFe) 177
4.11 Shear stress response v thickness, RTV157(GE) silicone 178
4.12 Ridge/channel dimensions, Design A v Design B 179
4.13 Circuit for interfacing test equipment to A/D, Design B 181
4.14 Temperature response of FP111L100 magneto-resistor 183
4.15 Output v magnet (NdBFe) / MR (FP111L100) separation 184
4.16 Temperature response of NdBFe magnet (experimental) 185
4.17 Experimental setup, temperature response, Design B 187
4.18 Temperature response of Design B shear sections 187

4.19 Experimental setup, static stress response, Design B 188
4.20 Stress response with orientation Design B shear section 189
4.21 Hysteresis behaviour in Design B shear sections 191
4.22 Hysteresis behaviour in silicone disc under shear 194
4.23 Alignment errors in shear section calibration jig 195
4.24 Gauge patterns and diaphragm outlines, normal sections 201
4.25 Temperature response of prototype normal sections 203
4.26 Force sensitivity of normal stress prototypes 205
4.27 Effect of load spreading layers and indentor size 207
4.29 Dimensions of Design C PCB's 209
4.28 Dimensions of Design C shear section disc's 210
4.30 Dimensions of Design C normal section 212
4.31 Photograph of Design C before assembly 214
4.32 Dynamic test equipment setup 216
4.33 Rheological model of the dynamic test set up 218
4.34 Model for determination of calibration jig damping 221
4.35 Magnification and phase response - metal spring 224
4.36 Stress sensitivity of Design C shear section 226
4.37 Linearity of Design C shear section stress response 228
4.38 Conversion errors using 1st order polynomial - shear 229
4.39 Conversion errors using 5th order polynomial - shear 231
4.40 Stress sensitivity of Design C normal section 232
4.41 Linearity/conversion errors, 1st order poly - normal 234
4.42 Conversion errors using 5th order polynomial - normal 235
4.43 Error in derivation of shear stress vector angle 237
4.44 Magnification and phase response of Design C 241
4.45 Impulse response of Design C shear and normal sections 242
4.46 Temperature sensitivity of Design C - shear and normal 245

Chapter 5

5.1 Block diagram of system hardware interconnections 251
5.2 Schematic of Wheatstone bridge circuit 253
5.3 Transducer excitation circuit 257
5.4 Transducer signal amplifier circuit 260
5.5 Environmental noise measurement circuit 266
5.6 Transducer signal filter circuit 269
5.7 Frequency response of amplifier and filter circuit 270
5.8 Footswitch signal conditioning circuit 276

5.9 Footswitch signal interface to Vicon 279
5.10 Photograph of data collection system 281

Chapter 6

6.1 Block diagram of system units interconnection 287
6.2 System software diagram 289
6.3 User screens from Level1 menu 291
6.4 Programme sequences for Level1 menu options 292
6.6 User screens from Level2 menu 294
6.5 Programme sequence to synchronise the PC and DCU 296
6.7 Programme sequence for Level2 menu support options 297
6.8 Programme sequence to download code to the DCU 299
6.9 Programme sequence for commands received on DCU 300
6.10 User screen for Level3 menu 301
6.11 Programme sequence for Level3 menu options on the PC 303
6.12 User screen listing data files on DCU 305
6.13 Programme sequence to transfer a data file from DCU 306
6.14 User screen for defining trial parameters 308
6.15 Programme sequence for defining trial parameters 309
6.16 Programme sequence for data conversion 310
6.17 Programme sequence on unexpected input 313
6.18 Principle operation of error recovery 314

Chapter 7

7.1 Stresses at Popliteal with Multiflex/Quantum foot 321
7.2 Stresses at Lat Paratibial with Multiflex/Quantum foot 322
7.3 Frequency components of stump/socket interface stresses 327
7.4 Schematic of the transducer mounting in a shoe insole 329
7.5 Shear stresses under 1st Metatarsal - Normal subject 331
7.6 Frequency components of foot/shoe interface stresses 332
7.7 Alternative external mounting method for transducer 335

TABLE OF TABLES

Chapter 1

1.1 Aetiology of amputations Eng., Wales, N.Ire. in 1986 27

Chapter 2

2.1 Summary of previous interface stress findings 102
2.2 Proposed performance specification for triaxial sensor 111

Chapter 3

3.1 Predicted modal stress v strain relationship in rubber 121
3.2 Physical properties of some common rubbers 130
3.3 Field and temperature sensitivity with MR doping grades 137
3.4 Properties of suitable magnetoresistors - Siemens LTD 138
3.5 Diaphragm thickness & deflection at yield point stress 148

Chapter 4

4.1 Sensitivity of Design A shear sections 162
4.2 Hysteresis in Design A shear sections 165
4.3 Creep rate of silicones used in Design A 167
4.4 Thermal expansion of Design A silicones, pure v aerated 170
4.5 Design A temperature coefficient, component summary 174
4.6 Design A v Design B temp coeff, component summary 186
4.7 Hysteresis in silicone blank v Design B shear section 192
4.8 Creep rate in Design B shear section 193
4.9 Formulation for Natural rubber spring 197
4.10 Temperature coefficients of prototype normal sections 204
4.11 Force sensitivity and drift, prototype normal sections 204

4.12 Masses of the calibration jig components 221
4.13 Creep rate in Design C shear section 239
4.14 Gain/offset and drift, Design C shear section 246
4.15 Performance data final triaxial transducer design 249

Chapter 5

5.1 Environmental noise signal magnitudes 265
5.2 Specifications of Analogue to Digital convertor 272
5.3 State table of binary footswitch signal 275
5.4 State table of trinary footswitch signal 277

Appendix A

A.1 Data file format description 352
A.2 Memory map of the DCU address space 353

Chapter 1
Introduction

1.1 Introduction

Throughout our daily lives our bodies or some parts of them are in contact with a supporting structure. Whether it is the back of a sleeping man on a bed or the toe of a pirouetting ballerina on the stage, the soft tissues beneath the skeleton experience forces due to the ever present gravity. Sustaining the forces is something we are normally not conscious of until pain reminds us to relieve these tissues of stress. Ignoring pain signals, or not receiving them, or being unable to effect relief of the tissues from these forces will lead eventually to tissue damage. Many people daily find themselves in just this position. In order to mitigate their predicament much must be learnt about the nature of these stresses and their effect on the soft tissues of the body. Measurements of forces at the body surface are very problematical, and nowhere more so than when the tissue is enclosed as in a shoe or a prosthesis. In these situations a knowledge of the dynamics of the forces occurring at the body/support interface is a major component in designing efficient and safe load transfer from skeleton to the support surface. This is especially important in the case of prosthetic design.

In normal gait, body support forces are directed through the skeleton to specialised plantar tissues and then on to the support surface (floor). In the amputee those support forces are to be transmitted through soft tissues which are not biologically designed to sustain them. When tissues are subjected to stresses greater than they are capable of tolerating, they will experience an occlusion of their blood supply and possible direct mechanical damage. Without sufficient nutrient supply and waste product removal the tissue cells may become dysfunctional and die **[Husain 1953; Levy 1962]**. Mechanical damage may present as cell separation in the epidermal layer of the skin and possible blister formation **[Hunter et al 1974; Stoughton 1957]**. Rupture of the blister will leave an open wound susceptible to infection and ulceration. Treatment of these conditions may require (further) hospitalisation, loss of mobility or, in severe cases, re-amputation at a higher level **[Levit 1981]**. Alternatively some tissue adaption may occur, in a similar mechanism

to callous formation. **Brand [1975]** showed that the magnitude and duration of stress loadings was an important factor in whether plantar tissues (in rats) formed callous structures or suffered major structural failure and death.

The design of the interface between the residual limb and the prosthetic socket is a crucial factor in the amputees mobility, independence, 'quality of life', even livelihood. It must provide comfort, proprioceptive feedback, stable support and sustainable weight bearing during stance and gait. Load must be relieved from those parts of the limb which are easily damaged and transferred to those parts which can tolerate it. The shape of the socket is therefore not simply a geometric copy of the limb shape but will be unique to the topography of the load tolerant tissues of each individual. Interface stress measurements are essential for a clear understanding of the inter-relationship between the stresses (pressure and shear) and socket comfort, prosthetic and surgical variables and gait parameters. When this understanding is translated into effective socket design, the amputee may be able to return quickly to their normal environment with a minimum of disadvantage in having a prosthetic limb. To this end, there have been several investigations into the quantification of normal stresses in sockets, but only one early report on shear stressesin Above-Knee (**AK**) sockets and, coincident with the work of this thesis, one recent investigation into shear stresses in Below-Knee (**BK**) sockets.

It is the objective of the study documented in this thesis to:

a) present an overview of the current knowledge on tissue mechanics, amputation procedures and limb fitting practice.

b) develop an instrument capable of measuring normal and shear stresses in lower limb prosthetic sockets - specifically in BK sockets. Although, a secondary intention is to design the instrument so that it would be capable of making the same measurements at other body/support interfaces (Eg under feet, in shoes). The instrument should be capable of providing data to: enable a greater understanding of the interface stress fields and their effect on soft tissue; act as a catalyst for improvements in socket (and interface material) design; verify theoretical models of the stress/strain characteristics of soft tissue; improve CAD models for predictive stress simulations of socket shapes; and investigate the processes and limitations of tissue adaption to stress.

c) to assess the device performance and it's clinical appropriateness.

The format of this thesis is as follows. The remainder of this chapter presents a background to limb anatomy and limb amputation surgery to familiarise the reader with shape and construction of the residual limb. The prosthetic fitting options and assessment processes are also detailed. **Chapter 2** contains a review of current knowledge on the mechanical properties of the soft tissues of the lower limb. This is followed by a discussion of the factors and stress modes instrumental in tissue breakdown and their implication for socket design. A review of the previous methods and instruments for measuring stresses in lower limb prostheses is given, along with an overview of some interface transducer design criteria. A proposed specification for a transducer device, which overcomes most of the limitations of previous instruments and measures shear and normal stresses, is presented. **Chapters 3** and **4** detail the design philosophy, materials evaluation, development, and performance calibration of a unique three axis stress transducer suitable for measuring prosthetic socket/residual limb interface stresses. **Chapters 5** and **6** describe the transducer interface electronics, data collection hardware and control software, developed for the complete interface stress measurement system. **Chapter 7** presents the clinical assessment of the efficacy of the transducer performance, its mounting methods and the operation of the system as a whole. Also presented is some example clinical data. **Chapter 8** is a discussion of the work undertaken here with proposals for further development.

1.1.1 Historical Perspective

From early history lower limb amputation surgery has been performed to extend the useful life of the unfortunate individual **[Isherwood 1980]**. In the first century, a Roman, Celsus (*50AD*), wrote that amputation 'involves a very great risk for patients who often die under the operation ... but it does not matter whether the remedy is safe enough, since it is the only one' [cited in **Butler 1986**]. Artificial limbs have been developed and prescribed for almost as long with the aim of restoring or mitigating the lost function of the missing limb **[Ficarra 1943]**. Descriptions of prosthetic replacements from as early as *1800BC* have been recorded [cited in **Sanders 1985a**], and an artificial leg dating from *300BC* has been found in Italy [cited in **Vitali et al 1986**].

The Greeks and later the Romans developed some sophistication in amputation surgery, however the Dark Ages in Europe seemed to halt progress, and perhaps reverse some. With the spread of leprosy and the advent of gunpowder in the

Middle Ages the number of amputees began to increase dramatically **[Rang and Thompson 1981]**. Early prostheses to serve these new multitudes were mainly simple wooden constructions. Between the *15th* and the *18th* Centuries surgical techniques and prosthetic design slowly evolved. Much of the progress during this time in history stemmed from battlefield surgery. Many names from these centuries are associated with key developments, but perhaps the most notable is the great French army surgeon Ambrose Paré (*1510-1590*). In his book ('Apologie and Treatise') he described improvements to surgical procedures, including level selection with respect to prosthetics needs, as well as describing several prosthetic designs. By the late *18th* Century ankle and foot joints had been developed and skin flap operations to promote wound closure were in practice. The use of anaesthetics from *1840* allowed the surgeon more operating time and with this came improvements in surgical techniques. The Crimean War (*1854-1856*) and the American Civil War (*1861-1865*) gave great impetus to further improvements in surgical procedures and prosthetic design **[McCord 1963]**. However, the vast numbers of amputees from the First and Second World Wars, and the discovery of penicillin and sulphonamides, produced the greatest spur for surgical and prosthetic advances.

Today, the estimated rate of new amputees in the UK is approximately *10,000* per annum **[Dormandy and Thomas 1988]**, although only about half of these are referred for artificial limb fitting. The number of referrals in the UK has risen from *3500* per annum in *1961* to *5461* per annum in *1986* **[Ham et al 1989]**. Similar increases have been seen in: the USA, from *33000* amputations in *1965* **[Ham and Cotton 1991]** to *118,000* in *1983* **[Rutkow and Marlboro 1986]**; Sweden, from *170* per million population in *1962* to *410* per million in *1977* **[Renstrom 1981]**; and Finland, *154* per million in *1972* to *325* per million in *1984* **[Pohjolainen and Alaranta 1988]**.

1.1.2 Current Trends

Although previous to this century the majority of amputations came from the theatre of war trauma, recent European history records new major causes of the need for amputation. **Coddington [1988]** describes the breakdown of the latest statistics **[DHSS 1986]** collected from England, Wales and Northern Ireland. The aetiology of all the amputations is given in Table 1.1.

In *1986* there were *65,000* amputees known to the DHSS of which *5780* were newly registered that year. Of those, *97%* were leg amputations, and the majority of which were over *60* years (*75.5%*) and male (*2:1*).

	Male	*Female*	*Total*	*%*
Vascular	*2434*	*1262*	*3696*	*63.9*
Diabetes	*765*	*391*	*1156*	*20.0*
Trauma	*422*	*105*	*527*	*9.1*
Malignancy	*122*	*98*	*220*	*3.8*
Infection	*72*	*37*	*109*	*1.9*
Deformity	*46*	*26*	*72*	*1.3*
Total	*3861*	*1919*	*5780*	*100.0*

*Table 1.1 Aetiology of new amputations in England, Wales and N.Ireland in 1986 (from **Coddington 1988**).*

From Table 1.1, the major cause of amputation is vascular disease (*63.9%*) followed by diabetes (*20.0%*). This trend is similar in Scotland (*65%*) **[Knight and Urquhart 1989]** and Denmark (*61%*) **[Ebskov 1988]**. Although, the causes may have a different order of precedence in other parts of the world. This reflects their standard of living, life expectancy, disease patterns and social conditions. For example, in India *82%* of amputations are due to trauma **[Narang and Jape 1982]**, where the average age of the amputee is *25* years.

It is widely accepted that where amputation is considered, conservation of the knee joint, whenever possible, significantly increases the amputee's rehabilitation potential **[Burgess and Matson 1981]**. Also, at centres where appropriate lower limb rehabilitation services are closely linked to the surgical unit the ratio of Below Knee (BK) to Above Knee (AK) amputations should be a minimum of *2:5*.

Dormandy and Thomas [1988] showed in their review of *16* studies published over *30* years that the ratio is usually very much below the recommended figure and there has been no significant increase in this ratio over the last *20* years. Indeed the most recent data for England, Wales and Northern Ireland show that

the average ratio is *41:49* **[Ham et al 1989]**. There are however, a number of extenuating circumstances which belie these figures. Because of the high incidence of vascular amputations, centres with less experience in these amputations may opt for an AK level believing it will increase the chances of successful primary healing. It is also believed that because some statistics indicate that the need for re-amputation (of previous BK operations) is about *16%* and that the delayed/secondary healing is about *15%*, then AK amputations will avoid potential long-stay patients and result in a quicker return to the community. There is undoubtedly a large number of vascular patients for whom AK amputations are the only recourse, or in whom there are other complicating factors such as diabetes - an increasing prospect as the average life expectancy increases. Nonetheless, there are established techniques for predicting the likely successful amputation level **[Holstein and Hansen 1988; Spence and McCollum 1985a; Fairs et al 1987]**. With training and experience of these more of the potentially successful BK amputations may be realised **[Malone et al 1979]**. In some centres where the techniques are also coupled with a committed team approach the predominance of AK over BK has been reversed as well as the mean number of in-patient days reduced **[Rush et al 1981; Ham et al 1987]**.

On discharge from rehabilitation the current long-term prospect for the amputee is poor. Of the vascular amputees *25-30%* have less than a *2* year life expectancy while *50-75%* have less than a *5* year life expectancy. However, this data probably reflects the inability to halt the primary disease rather than a major shortcoming in the rehabilitation process or change in the patient's environmental circumstance.

Despite major advances in the rehabilitation process the mobility statistics for amputees are dismal. From the vascular amputee studies reviewed by **Dormandy and Thomas [1988]** an average of *54%* of the BK amputees were fully mobile when discharged, and only *23%* of AK amputees. 'Fully mobile' was defined as walking freely or with the assistance of one stick. It is generally thought that mobility and independence decrease with time after discharge from rehabilitation training. It is also well accepted that many amputees stop using their prosthesis or only use it when attending the limb fitting centre. A *1986* survey has reported that *33%* of amputees interviewed complained of a poorly fitting or uncomfortable prosthesis **[McColl 1986]**. For the year *1984* each amputee made, on average, *3.2* visits to the limb fitting centre. In that year the total cost of all prostheses supplied was *£32m*. In the UK, in *1986*, the average time from amputation to delivery of

a definitive conventional Patellar Tendon Bearing (PTB) prosthesis was reported as *69* working days. This delay represents a significant proportion of some amputees remaining life.

1.1.3 Summary

In summary there are a great many lower limb amputations every year, with progressively more emphasis being placed on below knee levels of transection. Because of age and disease factors the majority of patients have a short life expectancy. However, many of these will have the prospect of full mobility and therefore greater independence. Currently there is a significant problem in realising a well fitting, comfortable prosthesis at an early stage of the rehabilitation process. This has a direct impact on achieving the full independence potential of new amputees. However, with functionally well designed, comfortable prostheses many more of the current and new amputees will be encouraged to attain their optimal mobility and therefore independence. This will in turn promote savings in facilities and services, of time and money that may be devoted to further improvements and more detailed individual consultations.

1.2 Anatomy of the Lower Leg

This section of the chapter describes the principal anatomy of the lower leg. It reviews the skeletal, muscular, vascular and nervous systems/groups found at the level of a typical below-knee transection. The material contained here references **Guyton [1981]**, **Gray [1989]** and **Tortora and Angnostakos [1990]** throughout.

1.2.1 Bone and Muscle

At the core of the leg are the skeletal structures - the fibula and tibia [Figure 1.1]. Their principal functions are: to provide structural support for the body; to provide points of attachment for the muscles; to act as levers in the process of locomotion; and for the production/storage of blood cells, minerals and energy. The bones are not completely solid but contain both macrospaces and microspaces. At the level of a typical trans-tibial amputation, the bones have a soft central area surrounded

by more compact rigid tissue. Covering this are two fibrous layers which make up the periosteum. The inner of these layers contains elastic fibres and bone growth cells. It also acts as the site of a attachment for ligaments and tendons. The outer layer is primarily composed of connective tissue, blood and lymphatic vessels.

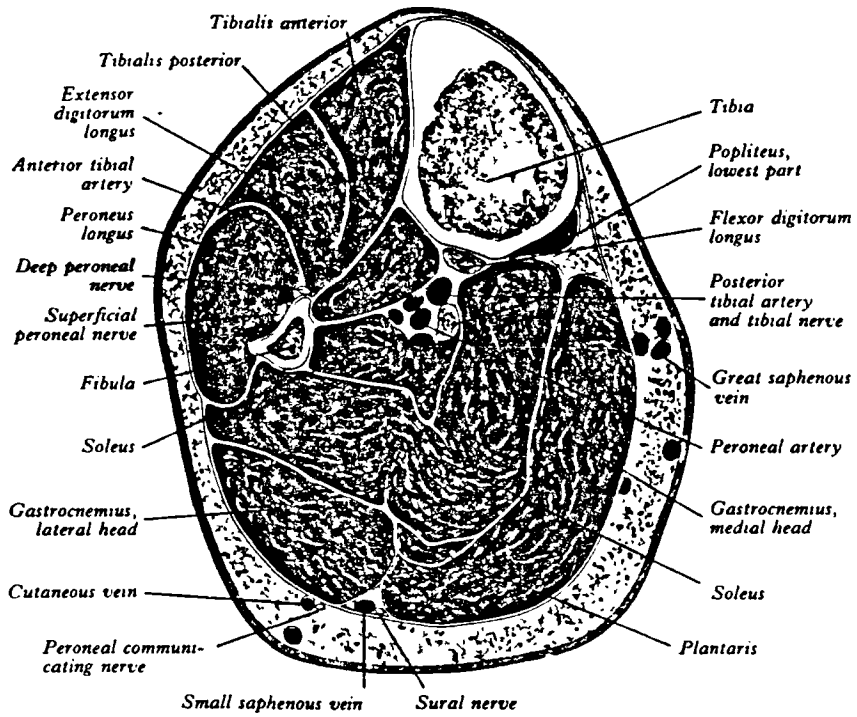

Figure 1.1 Section view of the leg 10cm distal of the knee joint. Each of the muscles are contained within an envelope of deep fascia. A layer of superficial fascia and adipose tissue enclose all the muscles and form attachments between them and the skin (from ***Gray1989****).*

There are three groups of muscles in the lower leg, each of which is compartmentalized by deep fascia. All the muscles in the respective group are activated by a single nerve. The anterior group consist of muscles which dorsiflex the foot (*tibialis anterior, extensor hallucis longus, extensor digitorum longus*) and are innervated by the deep peroneal nerve. The lateral group plantarflex and evert the foot (*peroneus longus* and *brevis*). These are activated by the superficial peroneal nerve. The posterior group is subdivided into deep and superficial subgroups. All are activated by the tibial nerve. The superficial muscles (*gastrocnemius, soleus, plantaris*) plantarflex and invert the foot. Three of the deep muscles (*flexor hallucis longus, tibialis posterior* and *digitorum longus*) plantarflex the foot and toes. The

other deep muscle (*popliteus*) flexes the foot and rotates the leg. Enclosed in the groups or outside them run the nerves, arteries, veins and lymphatic ducts which service the leg and foot.

Each of the muscles is surrounded by sheets of fibrous connective tissue called fascia.

Superficial fascia is a layer found immediately below the dermis of the skin. It is generally inseparable from the dermis by blunt dissection. In the lower leg it is usually *5mm* thick **[Lee and Ng 1965]** but will vary with age and the individual. Here it also moves freely over the underlying deep fascia except where they both lie over bony prominences (Eg *tibial crest*). It is composed of a mixture of loose (*Areolar*) connective and fatty (*Adipose*) tissues. The connective tissue consists of a loose matrix of elastic, collagenous and reticular fibres interspersed with nonstructural cells in a semifluid ground substance. This provides strength elasticity and support. Adipose tissue is much thicker and consists of lipid filled cells which act as a thermal insulator and energy store. Both layers also protect the limb from mechanical impacts.

Deep fascia is a dense connective tissue which lines the limb wall, holds the muscles together and separates them into functional groups. Its other functions are to allow free movement of the muscles over one another, and connect them to other structures. The density of the tissue is related to the local stresses it is expected to sustain. It extends into muscle groups surrounding individual muscles (*epimysium*), bundles of muscle fibres (*perimysium*) and individual muscle fibres (*endomysium*). All these parts are continuous, contributing collagenous fibres which attach the muscles to bone or other muscles.

As the fascia becomes denser and extends beyond the muscle fibres it becomes a tendon - a cord of dense connective tissue which attaches muscle to the periosteum of a bone. Thus the deep fascia may: connect the superficial fascia to bone (Eg *tibial crest, tibial* and *femoral condyles, patella* and *fibular head*); extend to tendonous tissue (Eg from *semitendinosus* and *semimembranosus, gracilis, sartorius* and *biceps femoris*); or attach muscles to bone (Eg *posterior tibialis* to the *posterior tibia*).

In addition to fascia, but buried within it, are structures (bursae) designed to reduce friction between moving parts. These are fluid filled sacs made from connective

tissue and lined with synovial membrane. In the lower limb there are three groups: anterior bursae (supra-, pre- and infra-patellar); medial bursae; and lateral bursae. For example the infra-patellar bursa lies between the patella ligament and the upper part of the tibial tuberosity, where it reduces friction between the tibia and the ligament during knee flexion.

Dense connective tissue also forms ligaments which form strong attachments between bones across joints. These consist mainly of collagenous fibres arranged in bundles and interspersed by fibroblasts.

1.2.2 Skin

Skin is one of the largest organs of the body in terms of area. It performs six major functions. Regulation of body temperature, which is achieved by production of sweat (sudoriferous glands) and by modulations in skin blood flow. It forms a physical, bacterial, waterproof and light (UV) barrier. Temperature, pressure, pain and touch receptors detect external stimuli which are passed to the central nervous system (CNS). Perspiration allows excretion of water, salts, and other organic compounds. Vitamin D is synthesized in the skin layers from the action of UV on a precursor hormone. Some cells also form part of the immune response chain.

There are also two major classes of skin which have important differences in their detailed structure and functional properties. These are thick hairless skin found on the surface of the palms and soles, and thin hairy skin found in the majority of other surfaces of the body. Thick skin has a complex pattern of ridges with added strength and specific frictional properties to aid locomotion and resist manipulation. It also has numerous sweat glands for cooling during sustained activity and many sensory cells where spatial discrimination is unimpeded by hair follicles. Thin hairy skin performs the general cutaneous functions over the rest of the body surface.

The skin covering the leg (and elsewhere) is composed of two principle regions, the epidermis (superficial) and the dermis (deep). The following is a description of the structured layers within both these regions. Figure 1.2 shows a cross-section of a specimen of skin.

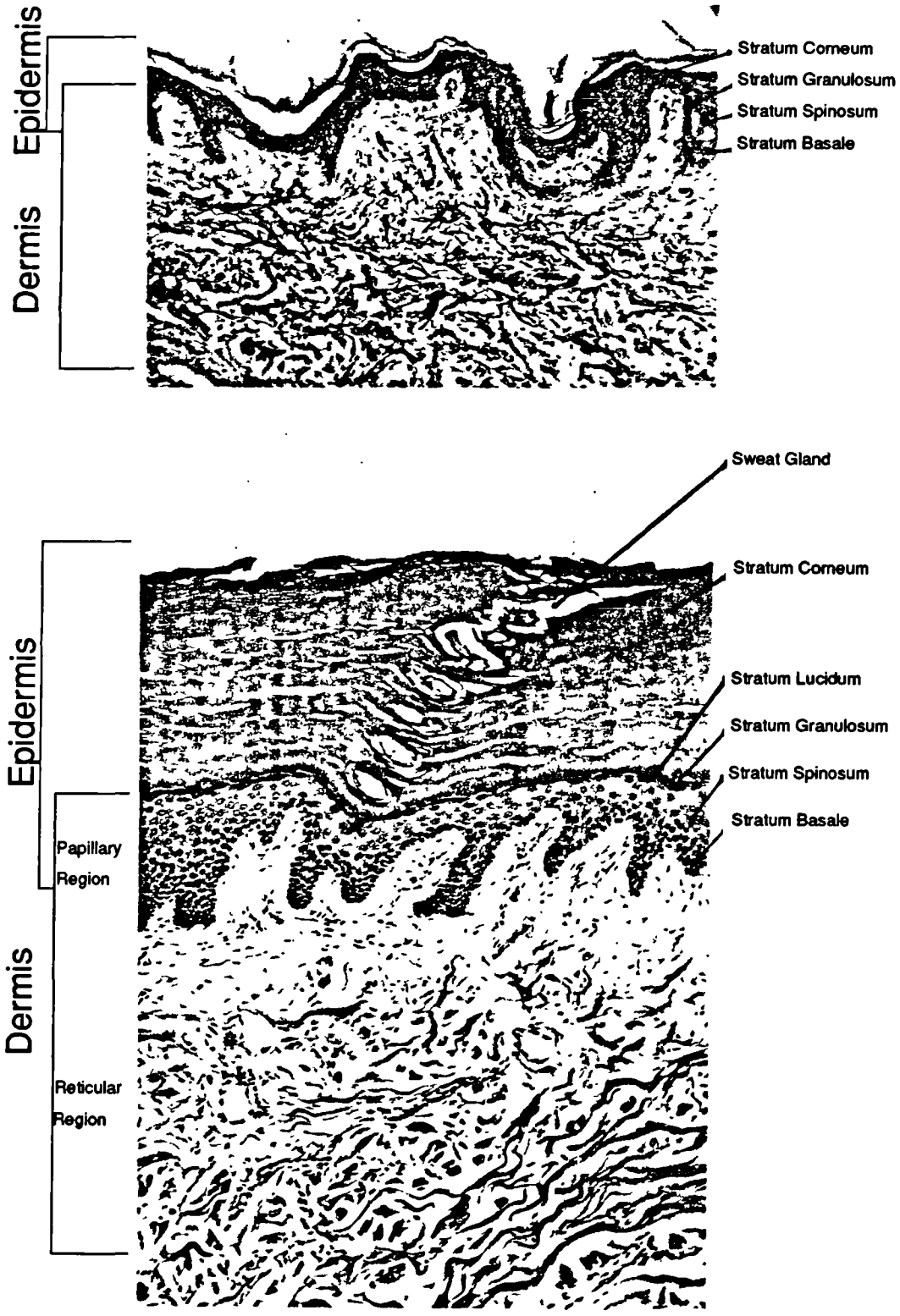

Figure 1.2 Cross-sectional view of the skin from thin hairy (top) and thick hairless (bottom) regions of the body. The epidermis and the dermis regions contain sub layers which are present to more or less degrees dependant on the area of the body observed. Below these skin sections lie the superficial and deep fascia (from ***Gray 1989****).*

The epidermis is composed of stratified squameous epithelium of four basic cell types; keratinocyte, melanocyte and two non-pigmented granular dendrocytes (Langerhan's and Granstein cells). It is normally *0.07-0.12mm* thick, however on the palms and soles it is thicker - up to *1.4mm* on the sole, and *0.8mm* on the palms **[Fawcett 1986]**.

The epidermis is divided into four or five sublayers: stratum basale, stratum spinosum, stratum granulosum, stratum licidum and stratum corneum. In the palms and soles where friction is greatest, all five layers are present. Over the rest of the body the stratum lucidum is not present. All layers are composed mainly of keratinocytes. Their principal function is to produce the protein keratin which aids in waterproofing and physical protection of the underlying tissues. At the deepest layer (stratum basale) a single layer of cuboidal/columnar epithelial cells divide and multiply. They push toward the surface layer (stratum corneum) degenerating on the way. This migration takes about *31* days. The stratum spinosum is about *8-10* rows deep. The migrating cells become polyhedral and tightly interlinked in a spine-like way with inter-digitated cell membranes. The stratum granulosum consists of *3-5* rows of flattened cells which contain dark granules of the first stage of keratin formation. Stratum lucidum consists of *3-5* rows of clear flat dead cells. These contain a clear substance which is the second stage of keratin formation. The stratum corneum layer is *25-30* rows of tightly bound flat dead cells filled with keratin. Migration through this layer takes about 14 days, ending in the cell being shed.

The dermis is composed of connective tissue containing elastic (*0.2-0.6%*) and collagenous (*27-39%*) fibres, water (*60-72%*) and a high viscosity ground substance of glycosaminglycans (**GAG's**) (*0.03-0.35%*). It is normally about *1-2mm* thick, although it may be up to *3mm* on the palms or soles **[Fawcett 1986]**. There is a tendency for it to be thicker on the dorsal aspect of the body and the lateral aspects of the extremities. The superficial fifth of the dermis (papillary layer) consists of loose connective tissue containing sparse fine elastic and collagen fibres embedded in a gel of ground substance. Finger-like loops (rete ridges) of dermis project into the epidermal layer carrying capillaries, nerves and touch receptors. Each elastic fibre (*1.0-0.2μm*) consists of amorphous elastin protein surrounded by microfibrils (*10nm* diameter) **[Sandberg et al 1981]**. Amino acids in the long elastin molecules form random widely spaced crosslinks with other elastin molecules.

With these molecules linked in a loose three dimensional network, elastin has a structure similar to that of natural rubber. This is linearly elastic up to *≈100%* strain.

The remaining four fifths of the dermis (reticular layer) consists of dense irregularly oriented connective tissue containing coarse elastic fibres and bundles of collagen fibres. The collagen bundles form into sheets in an interlaced irregular matrix. Spaces in the matrix are occupied by adipose tissue, hair follicles, nerves and sebaceous oil glands. Each collagen fibre (*0.5-20μm* diameter) is composed of many collagen fibrils (*30-60nm*) lying parallel to one another. They are coated with a chemical sheath which allows them some movement relative to each other and reduces their stiffness. Each fibril is formed of a right-handed helix of microfibrils (*3-5nm*) formed as a left-handed helix of *3* to *5* collagen molecules (*≈1.4nm*). Each of these molecules is a right-handed helix of three polypeptide chains arranged in individual left-handed helix's. Adjacent molecules link together at sites along their length, each being overlapped with it's neighbour - presenting a banded appearance under a light microscope. Collagenous fibres are very strong but allow some flexibility due to their partially contracted spatial arrangement, and small amount of viscoelastic stretch (*2-4%*). The elastin fibres loop about the collagen bundles and probably bond with them **[Gibson et al 1965]**. The combination of elastic and collagenous fibres in a matrix provide the skin with extensibility, elasticity and strength. The aggregate directionality of the fibres in the matrix determine the skin's local anisotropy.

1.3 Amputation Procedures

The following section is a summary of the current principles and procedures for below knee amputation surgery.

Amputation has as its primary intention: the arrest of disease; the stabilising of a traumatic condition; or the remedy of the result of a disease or congenital deformity. Secondly, it aims to fashion a residual limb which is amenable to the fitting of an effective prosthesis which may restore functional mobility.

Where a patient presents for amputation it is important for their optimum rehabilitation that all members of the surgical, care and rehabilitation 'team' consult on the best surgical procedure for that individual, and for the patient to be counselled. There are many contra-indications which may place a patient in a category which is unsuitable for below knee amputation. These include: previous cerebrovascular accident with residual spasticity; severe knee flexion contracture; senility; diminished functional capacity; ablation of the opposite limb; long term immobility; and poor vascular status **[Waddell 1981]**.

When a below knee amputation is confirmed there are currently two major choices of surgical technique practiced. The long posterior flap (LPF) **[Kendrick 1956; Burgess 1968]** and the equal flap (EF) **[Robb et al 1965; Termanson 1977; Robinson 1982]** methods. These are general techniques which have their variations. The LPF method is most often used as the posterior tissues are generally better vascularised by collateral arteries than the anterior tissues. Where there is insufficient viable posterior tissue, through trauma or ulceration, the EF method is used. **Robinson [1988]** and **McCollum et al [1985]** suggest that skewed sagittal flaps version of the EF method may usefully divide the limb into an anteromedial flap supplied by the saphenous artery and a posterolateral flap supplied by the sural artery. This also produces a tapered stump with an hemispherical end which permits early socket casting. Figure 1.3 shows the line of incision for both techniques.

Figures 1.4 and 1.5 describe the surgical sequence for the long posterior flap and the skew(equal)-flap methods respectively.

For the LPF method the anterior skin incision is made to the level of the deep fascia, *8-12cm* distal of the tibial tuberosity. The level of the transection is somewhat dependant on the viability of the tissues and the blood supply. An optimal length of *12-18cm* with a minimum of *8cm* is suggested **[Burgess 1985; Vitali et al 1986]**. **Quesada and Skinner [1992]** suggest that any extra length of the limb retained at surgery theoretically reduces the average normal stress experienced by the limb in a socket. Too long a limb will cause prosthetic and perhaps vascular problems as the muscle flap (gastrocnemius) used to pad the distal end of the tibia, becomes tendonous over its distal third. Short limbs will be unstable in a prosthesis, and the small leverage will make knee flexion difficult. It may be possible however to post-operatively lengthen short stumps to a useful size **[Keier et al 1988]**. Some

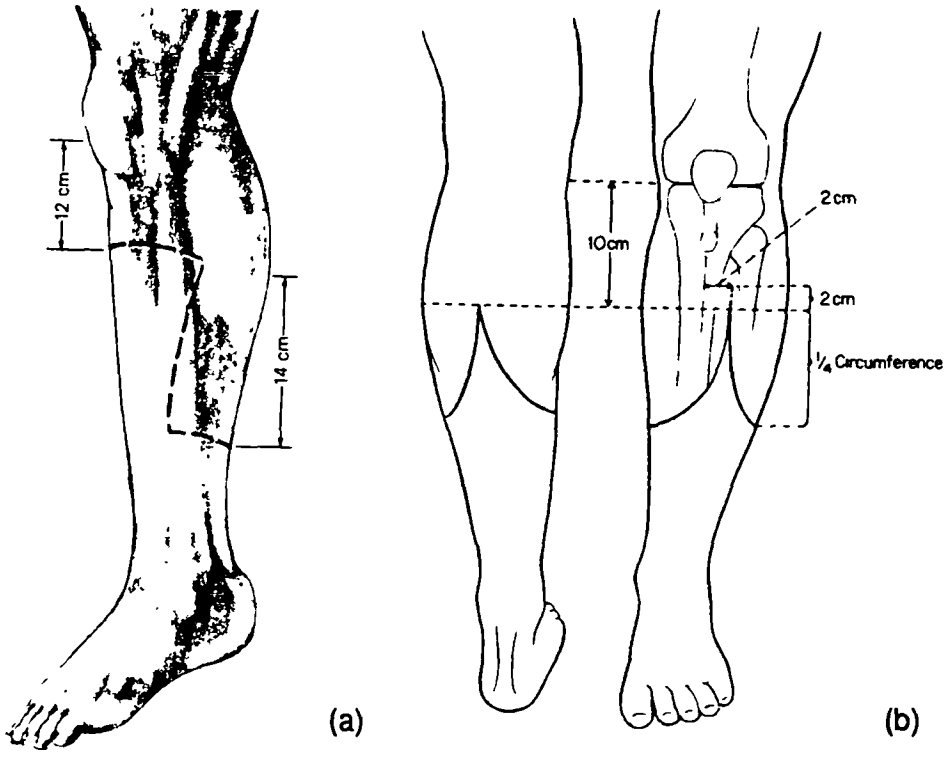

Figure 1.3 Skin incisions for the long posterior flap (a) and the (equal) skew-flap (b) below knee amputations.

surgeons divide the lower leg into thirds and amputate at the level of the proximal third. This ensures that all patients are left with a limb in proportion to their height.

The incision is carried transversely across the leg both medially and laterally one-half the way around the circumference of the limb. The flap is created by extending the incision distally by about *14cm* on both medial and lateral sides, and completed by joining both sides posteriorly. The posterior skin flap should be sufficiently long to allow closure without tension, and will be cut to size later.

The anterior tibial compartment is sectioned. Ligation and sectioning of the common peroneal nerve, anterior tibial artery and vein is carried out, before exposing the fibula. Nerves are brought under moderate tension before sectioning so that they retract into the tissues, in order to avoid neuromas developing.

With the EF method the skin incision is begun *10-14cm* distal from the tibial plateau, *2cm* lateral of the tibial crest, and *2cm* distal from the proposed tibial transection. This is the junction of the anteromedial and posterolateral skin flaps.

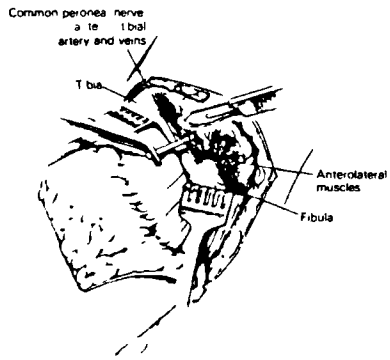

(a)

Skin incision.

Section of anterior tibial muscle groups.

Ligate and section arteries and nerves.

(b)

Place leg in traction.

Section tibia and fibula.

Bevel anterior edge.

Wash out bone chippings.

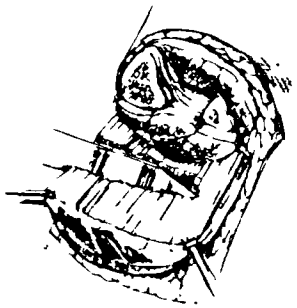

(c)

Section lateral muscle group.

Ligate vessels and nerves.

Fashion posterior muscle tounge.

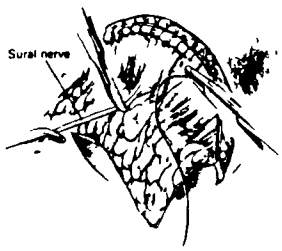

(d)

Insert drain.

Suture muscle tounge to muscle or bone.

Ligate, retract and section sural nerve

(e)

Suture skin under mild tension

*Figure 1.4 Stages of the Long Posterior Flap method of lower limb amputation (from **Burgess 1985**).*

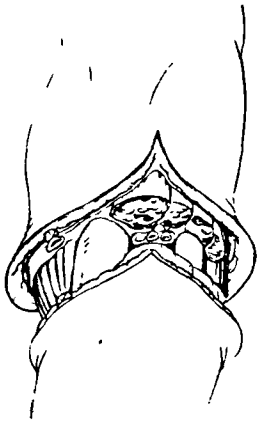

(a)

Skin incision.

Section of anterior tibial muscle groups.

Ligate and section arteries and nerves.

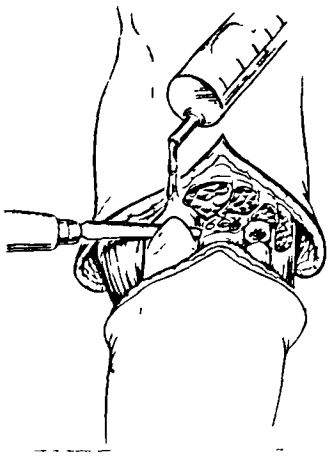

(b)

Place leg in traction.

Section tibia and fibula.

Bevel anterior edge.

Wash out bone chippings.

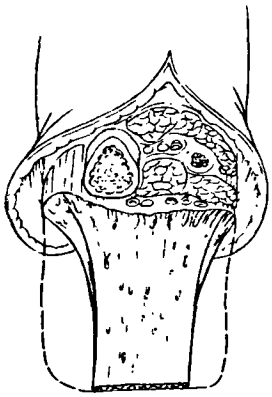

(c)

Section lateral muscle group.

Ligate vessels and nerves.

Fashion posterior muscle tounge.

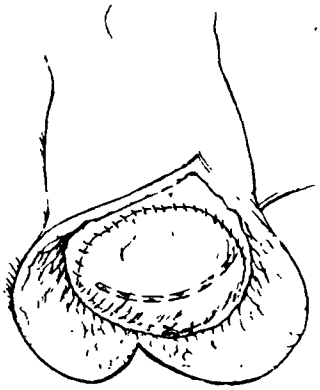

(d)

Insert drain.

Suture muscle tounge to muscle or bone.

Ligate, retract and section sural nerve

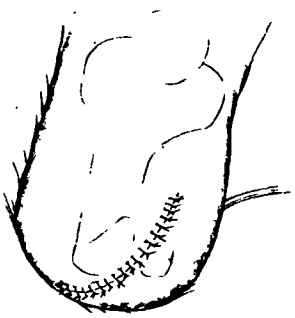

(e)

Suture skin under mild tension

Figure 1.5 Stages of the Equal (skewed sagittal) Flap method of lower limb amputation (from ***Robinson 1988****).*

The limb is marked from the anterolateral point to the diametrical posteromedial point in a semicircular arc. The radius of the arc is one-quarter of the circumference of the limb. This line denotes the extent of the skin flap. The long and short saphenous veins in the fascia layer are ligated and sectioned followed by sectioning of the saphenous and sural nerves. The anterior tibial and peroneal muscles are sectioned until the anterior tibial artery and nerve are uncovered and ligated.

The fibula is sectioned *2-4cm* proximal of the proposed tibial transection. It is considered advantageous to retain the fibula to create a triangular shaped residual limb, which is more resistant to rotation in the prosthetic socket. With its ligumentae and surrounding muscle bulk there may be some resilience in the limb during rotation. The periosteum around the tibia is divided and elevated on the anterior aspect. Care must be taken to avoid disturbance of the precarious anterior blood supply. Tibial division is followed by the cutting of a bevel on the anterior surface of the distal end, which is rounded by file. This is essential because in total contact sockets high stresses will develop over the distal anterior tibia. Care is taken to remove all sawdust and filings with a saline rinse. For the LPF method, the distal part of the limb is removed by disection of muscle from the posterior surfaces of the tibia and fibula. The deep flexor muscles are sectioned 3cm below the level of the tibial section, and the underlying peroneal and tibial vessels ligated and sectioned. **Angel [1979]** and **Burgess [1985]** recommend bevelling the remaining gastrocnemius-soleus muscle flap from just distal to the deep flexor muscles to the level of the fascia at the distal *end* of the flap. However, others **[Waddell 1981, Little 1985, McCollum 1989]** advocate the complete removal of the soleus muscle, as it derives its blood supply from the anterior arteries which may be weak.

In the EF method downward traction is applied to the distal section of the limb, and the tibialis posterior muscle sectioned to the level of the neurovascular bundle. These vessels are ligated and sectioned. A length of the gastrocnemius-soleus muscle equal to the vertical thickness of the stump is extricated from the distal limb section and sectioned at the appropriate length. This muscle tongue is shaped by a bevelled section on the anterior, lateral and medial aspects, to fit the limb cross-section once folded. It is important to reduce the muscle bulk before folding the flap, as this will otherwise result in a 'bulbous' stump which is difficult to fit to a prosthetic socket and will cause instability during gait. After appropriate fashioning the gastrocnemius muscle flap is pulled forward under slight tension and cut to the appropriate shape. It is then sutured to the periosteum of the tibia

(myodesis) and the aponeuroses of the anterior tibialis muscle (myoplasty). This closes the medullary cavity of the tibia and provides a muscle padded load transfer surface from the skeleton to the prosthesis. It also retains opposed muscle contraction to aid knee flexion and venous return. The sural nerve is sectioned and retracted. A drain is placed deep into the myofascial flap, to remove fluid build up during healing. This is later removed. Superficial fascia from the posterior surface of the flap is opposed to the anterior superficial fascia. These are sutured and steri-stripped to close the skin of the limb.

The resultant healed stump will shrink in size, from reduced odema and muscle wastage, over the *6-12* months post operative. In some cases it may continue for up to *2* years. These changes can be accommodated for, within PTB sockets, by stocking or liner changes or recasting.

1.3.1 Discussion

The two principle intentions of modern amputation surgery are to arrest the disease or stabilise the traumatised tissue and to form a residual limb which is optimal for a prosthesis. The general considerations of the surgeon in achieving these are: the prevention of neuralgias, by attention to nerve length; salvaging a residual limb length of *8-12 cm* sufficient for good prosthesis control; retaining the fibula for a limb shape which resists axial torsion; to provide sufficient muscle padding over the distal end of the tibia; to ensure adequate muscle fixation for resistance to muscle action during muscle retention exercises; and to fashion an hemispherical distal end to the residual limb for an even loading pattern in the socket.

1.4 Prosthesis Fitting

Ham and Cotton [1991] divide the post operative period of amputation rehabilitation into an early and a late phase. In the early phase while the limb is healing under soft dressings or plaster cast **[Mensch and Ellis 1987]** it is placed horizontal with the knee in full extension. Over the first two days post amputation both limbs are given regular physiotherapy to strengthen muscles and avoid flexion contractures. From the third day when the medical condition stabilises the patient moves on to a gymnasium and group interaction. Throughout the whole rehabilitation period the patient also works with occupational therapy to improve their general condition

and practice activities for daily living. To improve their chances of successful rehabilitation, patients are mobilized to bipedal gait as soon as possible **[Wiess 1969; Burgess et al 1971]**. Early walking aids are utilised to introduce the patient to standing and walking and to help assess their ability, motivation and physical capability. These may be pneumatic **[Redhead 1983; Rausch and Khalili 1985]**, contact vacuum sockets **[Henriksen et al 1978]** or other local variants **[Hutton and Rothnie 1977; Ruder et al 1977, Callen 1981, Wu et al 1981; Acton et al 1984]**.

In the late phase the exercise programme is extended and the patient encouraged to monitor their own progress. Those that are suitable for prosthetic fitting have their stump volume monitored and are sent for measurement at the earliest feasible time. This can be by simple tape measurements or more complex instruments **[Renstrom 1986; Rockborn and Jernerberger 1986]**. After the patient has received their prosthesis an intensive daily programme of gait training is undertaken **[Steinberg et al 1985]**. These will include training over a variety of surfaces, stairs and slopes. The patient's family are also involved. When the patient is optimally independent they are moved back to the community, ensuring that any additional facilities required there are organised. Follow-up visits, work liaison and outpatient physiotherapy should be implemented on a regular basis.

1.4.1 Design Considerations for Below-Knee Sockets

The socket forms the interface between the amputee and their prosthesis and as such, if its design is not optimal then the prosthesis will not be acceptable nor will it function properly. As stated earlier the soft tissues of the lower leg are not specifically designed for the sustained transmission of body support forces. So achieving this transference in a controlled manner is at the core of socket design.

The function of the socket in a prosthesis is threefold. Firstly, it must provide for the safe, healthy and comfortable transmission of limb forces to the prosthesis. Secondly, it must maintain the stability of the prosthesis on the limb. Thirdly, it must enable the amputee to exert sufficient control over the prosthesis.

Now, the forces which act on the residual limb are both static and dynamic in nature and have a normal and shear component. They are distributed over areas of the limb rather than at specific points. Also, tissue thickness and characteristics

can vary considerably from point to point on the limb and from patient to patient. So an understanding of the dynamic pressure and shear distributions and the biomechanical properties of the limb tissues are equally important for effective socket design to begin. It has been shown that some areas of the residual limb are tolerant of pressures while others are pressure sensitive **[Radcliffe and Foort 1961]**. Figure 1.6 shows these areas as mapped onto the limb.

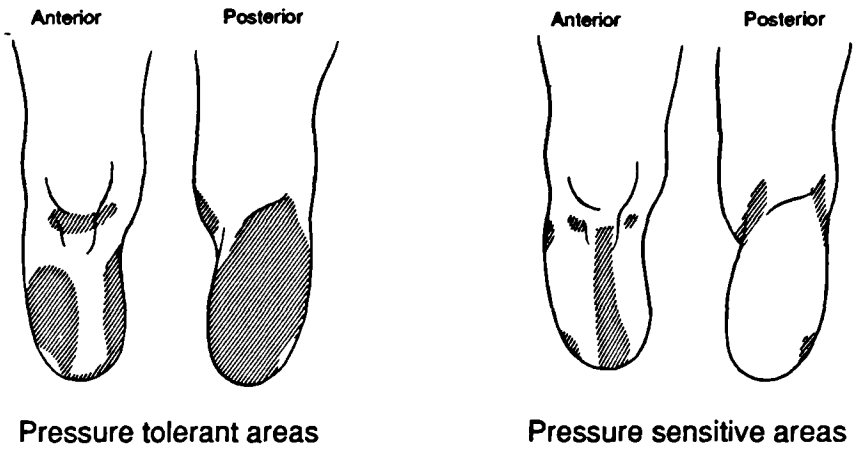

*Figure 1.6 Areas of the residual limb which are pressure tolerant (a) and pressure sensitive (b) (from **Rae and Cockrell 1971**).*

Until recently **[Sanders et al 1989, 1990, 1992; Williams et al 1989, 1992]** there have been no studies performed to investigate the shear stresses which are exerted on the limb during support or gait. This is principally due to the lack of suitable transducing instruments. With the advent of further studies in this area and that of torsion stresses a more comprehensive understanding of the stress fields applied to the residual limb will be gained.

The socket, therefore, must be designed to redistribute load to areas which are relatively pressure tolerant and away from areas which are sensitive to pressure. In the prosthetic manufacturing process this is achieved by adding or removing material from a positive model of the limb, from which the socket will be cast. Although these areas may be generalized, their exact extent and sensitivity must be identified for each individual.

Secondly adequate stiffness and contact must be present at those areas of the socket where nett force vectors will be applied during the gait cycle. These vectors will occur in both the anteroposterior and mediolateral planes. Examples of these nett force vectors in a PTB socket are given in Figure 1.7. Without this the stability of the prosthesis will be compromised and may make it unusable.

Care must also be taken, in the design phase, to allow relatively unrestricted movement of the knee joint.

Thirdly, the other major field of prosthetic component design is that of the method of suspension or attachment to the amputee. During stance phase the limb is forced into the socket, however, during swing phase, gravity and centrifugal forces will attempt to separate the limb from the socket. Adequate suspension should exert firm holding forces to combat 'pistoning' without causing discomfort or difficulties for cosmesis. The fit should be such that the limb does not move within the socket, so as to provide stable control over the prosthesis direction.

However, the interaction of changes in prosthetic variables (E.g. alignment **[Appoldt et al 1968]**, socket liner material **[Sonck et al 1970; Silver-Thorn and Childress 1992a]**, prosthetic feet **[Leavitt et al 1972; Barth et al 1992]**) can also have a significant effect on the magnitude and timing of the stress fields in the socket.

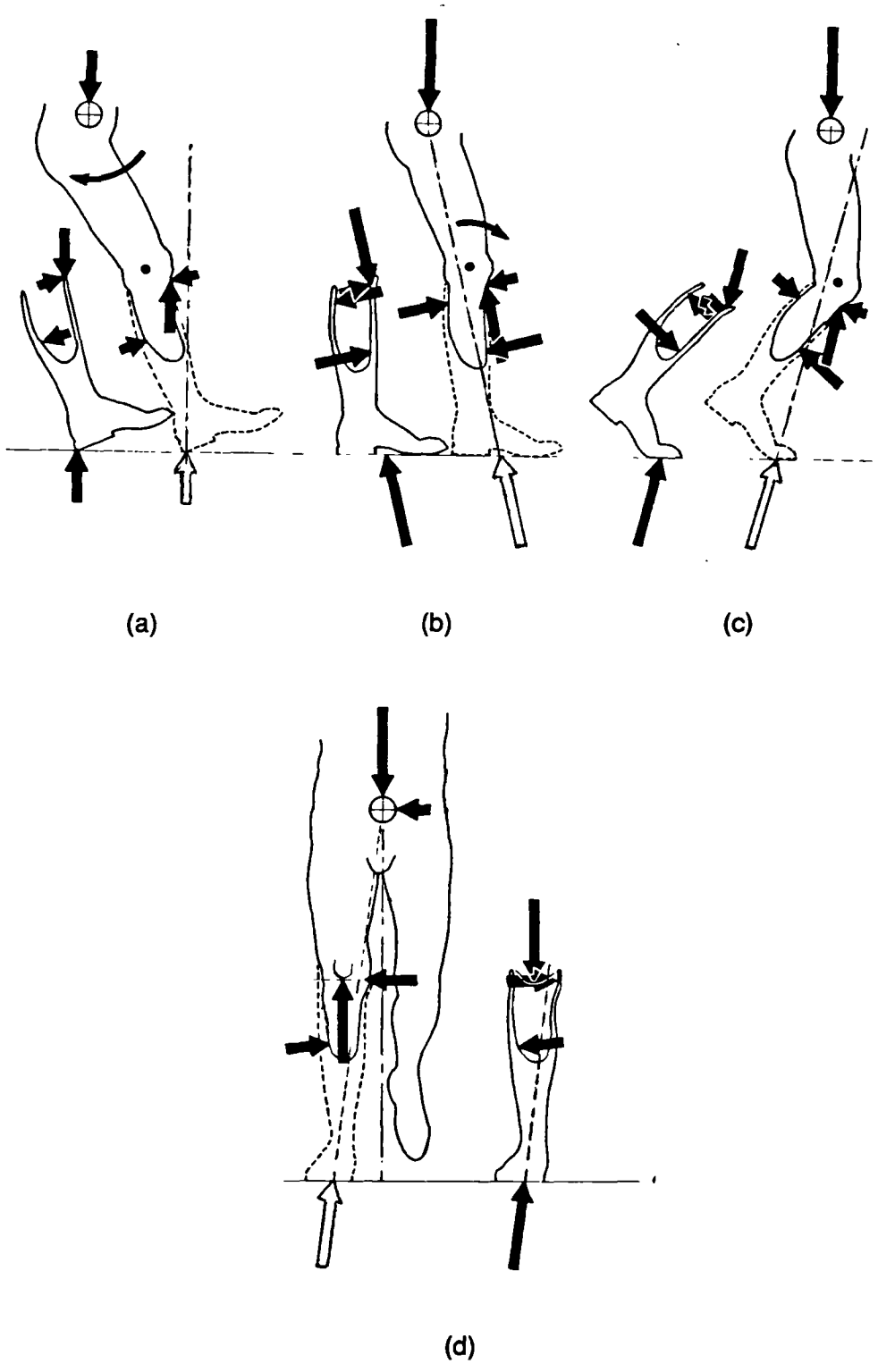

Figure 1.7 Force diagrams showing the nett forces acting on the limb and on the PTB socket during gait. Anteroposterior plane: heel strike (a) stance phase (b) and toe-off (c), mediolateral plane (d) (from ***Hughes and Taylor 1989).***

1.4.2 The P.T.B. Below-Knee Prosthesis

In the United Kingdom the standard prosthesis fitted for the below knee amputee is the Patellar Tendon Bearing (PTB) limb. Its present form is based on the original design by **Radcliffe and Foort [1961]**. The limb consists of five basic components: a suspension device, a limb socket, socket liner, shank and a foot-ankle assembly. These are represented in Figure 1.8.

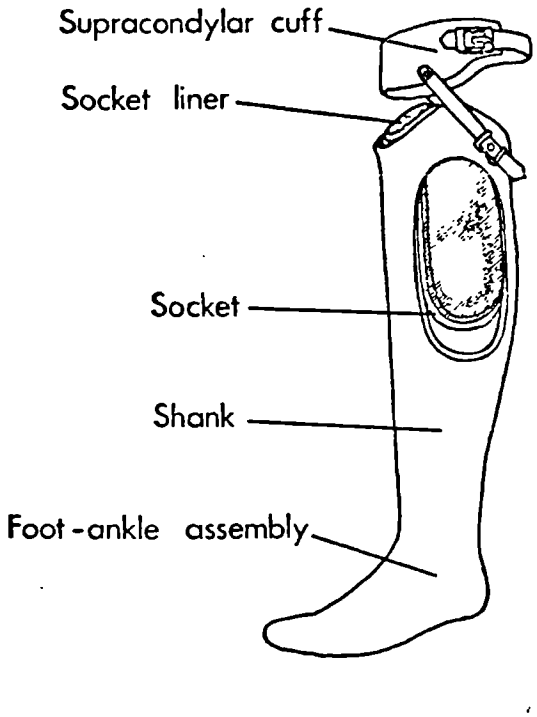

Figure 1.8 Basic components of the patellar-tendon-bearing below-knee prosthesis.

Suspension

The suspension device is primarily intended to hold the prosthesis onto the limb during swing phase. The original leather cuff suspension is still the most common in England and Wales. Two straps attach to the top of the socket in the posterolateral and posteromedial regions. They pass up and across the knee to join to the cuff which buckles around the thigh just above the knee. The straps must be long enough to allow unhindered extension and flexion of the knee, which is polycentric, but not so long as to allow piston motion of the limb in the socket to occur. Occasionally a thigh corset is prescribed to provide extra stability during stance phase. This is a longer leather cuff which laces up the front and additionally has

elastic check straps to the socket. The cuff suspension can provide good proximal/distal control but has poor mediolateral support. This aspect may cause instability of the knee during gait when mediolateral moments are generated.

Alternatively the socket itself may be designed to provide suspension. This may be a French variation of the PTB, termed PTS (*Prothèse Tibiale Supra-condylienne*) where the whole of the patella and the medial and lateral condyles are enclosed. Or it may be the German variation KBM (*Kondylen Bettung Münster*) which extends over the medial and lateral condyles of the femur. Or they may be variations of these **[Murdoch 1968; Lyquist 1970]**. These supra-patella or supra-condylar sockets are issued as the standard prosthesis in Scotland and the USA. They are formed with high medial and lateral walls which fit over and conform closely to the bulge of the femoral condyles. This grip is sufficient to hold the prosthesis on during swing phase. If the socket material is made sufficiently pliable then the limb may be inserted by pulling the walls outward by hand. If the material is more rigid then the conformity must be relaxed during manufacture and inserts used to lock the limb into the socket.

Socket and Liner

In recent years sockets were made from rigid fibreglass materials and lined with a soft elastic closed cell polymer foam. This was moulded to conform closely to an adjusted model of the patients stump. The liner was cut to ensure that there was total surface contact over the limb. The aim of this was to maximise the support area, aid in reducing oedema and provide a pumping action over the gait cycle which aids venous return. It was also thought that the total contact would improve the sensory feedback of the limb, thus aiding control and stability. There have been modifications to the original form of the PTB socket. The supra-condylar aspect of the socket modification provides added mediolateral stability, while the supra-patella modification aids in combating hyperextension of the knee and provides an anteroposterior reaction force. In the United Kingdom PTB's are generally made of a polyester laminate or polypropylene which are lighter, less rigid than the glass reinforced plastics but quicker and cheaper to produce.

1.4.3 Conventional P.T.B. Socket Manufacture

The manufacture of a PTB socket progresses through the following stages: taking a cast of the patient's residual limb; creation of a plaster positive from the cast; alteration or rectification of the positive; and fabrication of the socket from the modified positive. Each of these stages is detailed below.

Before the casting procedure the prosthetist makes various physical measurements of the stump shape. He also makes subjective assessment of such factors as tissue compressibility, pressure tolerance, skin mobility, and range of skin motion. These are for patient records and for use during the rectification phase. A record may typically take the form described by **Persson and Liedberg [1983]** or **Wall [1988]**. The limb is fitted with a nylon stocking which is adjusted to be a snug fit without distorting the limb shape.

Anatomical features such as the patella, tibia, patellar tendon and fibula head are marked on the sock with indelible ink. These markings are transferred to the positive during later stages and used by the prosthetist during rectification. During wrapping of the limb the knee is usually slightly flexed. Plaster of Paris bandages are then wrapped around the limb and sock. Care is taken not to compress the limb generally. As the plaster begins to set the prosthetist begins to shape the cast by hand. This procedure imparts to the cast a form coarsely suitable for load bearing. The regions either side of the patellar tendon are indented to form an anterior load-bearing shelf. The central area of the popliteal is indented opposite and slightly distal of the patellar tendon indentations. This encourages the limb to sit forward on the patella shelf and also provides a posterior load-bearing shelf. The depth and size of these indentations are subjectively determined by the prosthetist, based on the compliance of the patient's stump. When the cast is fully set it is removed from the stump and the stocking removed from inside the cast.

Prior to the making of the positive model, the inside of the cast is coated with a thin film of Vaseline or other parting agent. The cast is placed in a container which holds it upright (a box of sand has been used). A mandrill (*25mm* wooden rod or iron pipe) is positioned within the cast. This establishes an axis for the positive model and a convenient mounting handle. This axis is also a reference for rectification and for the initial alignment of the socket on the limb. It is recommended practice to set the mandrill with a sagittal and ventral inclination to

the vertical. This tends to cause flexion and adduction about the knee during stance. The degree of the inclination is subject to the preference of each prosthetist. A solid positive is made by pouring plaster into the cast. Alternatively a hollow positive may be made by adding successive layers of plaster to the inside of the cast (up to *22mm* thick). The mandrill is bonded in and the cast filled with waste paper. A cap of plaster is added to seal the positive and fix the mandrill. When the plaster has set the cast is cut away.

The anatomical features marked on the stocking will have been transferred to the cast and then to the positive. Using these and the earlier measurements the prosthetist makes a judgement on how to modify/rectify the shape of the positive. By adding or removing plaster he alters which regions of the stump will have an increased load-bearing role and which regions are relieved of load. Also flexion and adduction angles may be altered. The positive is sanded smooth to produce a smooth socket.

Socket manufacture, in England and Wales, involves the fitting of a liner (typically *7mm* Pelite) to the positive before the hard socket is formed. The liner allows for close firm support over the entire skin surface. It provides some minimal load spreading in stress tolerant areas as well as relief in stress intolerant areas. It also absorbs some shock during gait. The socket is formed from a polypropylene sheet or pre-formed proto-socket (bucket-like shape) which is heated until soft then pulled down over the pelite covering the positive. The sheet or proto-socket is clamped at its periphery and a vacuum applied between it and the positive, to encourage an intimate fit. The process is carried out by hand or by a semi-automatic machine. When the polypropylene has cooled the positive is broken out. The socket is trimmed and smoothed. In Scotland and the USA, rather than using polypropylene, Dacron felt, nylon stockinettes and glass reinforced plastic layers are sandwiched between PVA sheets and resin bonded together. A vacuum is also used to encourage an intimate surface conformance with the positive.

It has become increasingly popular in the USA and Northern Europe for transparent plastic check sockets to be fabricated from the positive, before the final prosthesis socket. **Pritham [1988]** argues that its use potentially leads to a better fit for the following reasons:

(a) its disposable temporary nature encourages the prosthetist to objectively refine the fit.

(b) as an isolated component the attentions of both prosthetist and patient will be focused on fit and not distracted by attempts at locomotion.

(c) both parties can see aspects of the confined limb.

(d) discussion is encouraged as the patient can illustrate his points.

(e) inexpensive iterative design methods promote innovation and change.

Their use in the UK is, however, not widespread.

Before issuing the amputee with his new prosthesis an assessment of the appropriateness, fit and function of the socket and limb is made. It is critical that all of these be met before the amputee begins training to regain limb function. The prosthetist then sets the limb alignment. By inspection of the residual limb and of the amputee's gait, and by discussion with the amputee he can determine the quality of the fit of the socket. If it is not satisfactory the prosthetist is able to make small adjustments to the socket fit by adding or removing material to the liner. If, however, this is not successful the entire manufacture process must be repeated since the limb shape information is lost when the cast and the rectified positive are destroyed.

1.4.4 C.A.S.D./C.A.M. in P.T.B. Socket Design

There are a number of disadvantages in the present method of manufacturing and fitting of below knee sockets. These hinder the early supply of temporary prostheses and make copies, for research, or replacement of existing sockets difficult.

Although the manufacture and design of below knee sockets is based on biomechanical foundations, there is a central craft element in the procedure. This craft element sets the quality of a fit and the absolute shape of the socket. Both of these are dependent on the skill of an individual prosthetist or team, and both of which are not consistent. The production process is also slow and labour intensive. Since exact shape and rectification information is lost when the wrap cast and positive model are destroyed, incremental changes in socket shape are impossible on all but the coarsest level. These difficulties may be exaggerated if more than one prosthetist is involved in a manufacturing chain. Thus there is a lack of accurate quantitative information which would allow objective modifications to be made to the fit of a

prosthesis or even to repeat a successful design. Without reproducibility it may be extremely difficult (as well as frustrating and painful for the patient) to ascertain the reasons why a fit is unsuccessful. Research and development are hampered by the inability to study the effects of changes in any one component when the others cannot be held constant. Even though a skilled prosthetist may be quite capable of producing a 'good' fitting socket on different occasions for the same limb, it may take several days to achieve this. Also, the craft-based skills needed take a significant time to acquire and require much costly practical experience. In fact, there is currently a shortage of trained personnel and a growing number of amputees.

These disadvantages of a craft-based system have been cited by many [Eg **Klasson 1985; Reynolds 1988**] as being incentives for the introduction of CASD/CAM techniques. The inherent benefits of which are shorter design times: quicker manufacture; precise control and recording of dimensions; higher quality and lower cost in sufficient numbers. These lead directly to patient benefits and support greater developments in fitting principles. With faster production the prosthetist can also devote more time to the assessment and fitting phases. The recorded shape data allows sockets of a successful fit to be replicated easily and quantified modifications to be made to the ill-fitting socket. In this way the improvement of fit becomes truly iterative. With shorter manufacture cycles, the effects of changes in residual limb shape may be easily accommodated. Also during training the prosthetist will be able to discern more clearly the links between design variables, assessment and quality of fit **[Fernie et al 1984]**.

There are essentially three processes in computer aided socket design and manufacture (CASD/CAM): the acquisition of a limited set of significant measurements of the residual limb; the transformation of these into a well fitting socket shape; and the physical realisation of this socket shape. The achievement of the integration of all these processes will revolutionise the implementation and quality of prosthetic supply **[Klasson 1985; Lord and Davies 1988]**. Some progress has been made in this direction by many centres **[Saunders and Fernie 1984; Dewar and Reynolds 1986; Krouskop et al 1987; Engsberg et al 1992]**.

CASD methods broadly fall into two categories. Those which consider only shape information and those which also take into account the deformation of limb, liner and socket when under stress.

1.4.4.1 Shape Manipulation CASD

In the first category the external geometry of a limb is captured as a number of discrete radial measurements at various axial distances up the residual limb. These may be obtained by: manual measurements of the limb **[Saunders et al 1985]**; mechanical measurement of the conventional plaster wrap **[Reynolds 1988]**; or optical scanning methods employing silhouette projection **[Smith et al 1986]**, laser line projection **[Fernie et al 1985]**, or moiré contour projection **[Tsuchiya and Morimoto 1986]**; or ultrasound CT **[Faulkner et al 1986]**.

With some of these methods there are measurement errors inherent in the way they are performed. During casting the limb is slightly compressed, thereby distorting the external geometry. In current CT and MRI machines the measurements of limb geometry are taken with the patient supine. There, the relation of the soft tissues to bone are distorted. Similarly with ultrasound methods probe or fluid bath pressures cause some distortion of the tissue with respect to the skeleton. Laser and silhouette projections may produce accurate external geometry but there remains the difficulty of registering it with internal geometry data.

Saunders et al [1985], **Dean and Saunders [1985]**, and **Torres-Moreno et al [1989, 1991, 1992]** selected a reference socket primitive from a computerised database and scaled it to the approximate shape of the limb. The dimensions of the primitive were described as a wire frame in terms of cylindrical polar co-ordinates. Scale factors were derived from the limb shape measurements. Its proximal end was scaled according to measurements made at the knee. The length was tapered to fit circumferential and anteroposterior measurements taken at one inch intervals down the limb. The prosthetist operated on these scaled primitives using interactive computer graphics software, adding or removing areas from the resultant wire frame shape by way of rectification.

This technique was improved by **Fernie et al [1985]** who described a laser line projector and optical sensor system for accurate and rapid capture of the patient's limb shape. **Engsberg et al [1992]** incorporated a optical/laser shape digitiser into a CASD system where the acquired shape was manipulated graphically by a prosthetist, in the same manner as above.

An attempt to automate the rectification process was begun by **Nakajima et al [1982]**. The shape of the patient's limb was digitised by mechanical measurement of a conventional positive limb cast and the resultant contours modelled by a mathematical function. From a knowledge base of measurements of successful socket designs, made by conventional methods, the functions were automatically modified to effect the socket rectification.

The impetus for the development of these CASD methods was to quantify and record the prosthetists process of socket design and to store the form of the definitive socket. From these records iterative improvements in an individual's socket can be performed and copies of a patient's socket can readily be produced. Also, a data base of many patients will lend quantitative insight into the rectification process, which can be used for teaching new prosthetists or the development of new techniques. Essentially, the shape manipulation techniques are still craft based but with the improvement of realising numerical data on the design and reducing the time to socket fabrication.

1.4.4.2 Tissue Compliant CASD

The above shape manipulation techniques tend to produce the same socket shape for a given limb shape, within operator variability and parameter selection. The other category of CASD/CAM system attempts to account for the way the limb tissues will deform under external stresses. As comfort depends upon the area and magnitude of the load transference from skeleton to socket, then without knowledge of the internal structure of the limb and its tissue characteristics the comfort of any given design must be partly circumstantial. The shape of a comfortable socket is critically determined by the distribution of bone in the limb. Pressure on thin tissues over bone must be minimised, while at the same time ensuring close contact to avoid excessive movement of the socket relative to the skin of the limb. Fleshy and tendonous regions of the limb are, by comparison, more tolerant of pressure. Now, external limb shape by itself yields only a minimal amount of information about the skeletal shape and tissue type of the limb. Thus, for comprehensive data from which to derive repeatable comfortable sockets separate internal structure information is required.

The internal geometry of the limb is generally determined by: radiographic methods, either Computer-aided Tomography (CT) **[Childress and Steege 1987]** or Magnetic Resonance Imaging (MRI); or ultrasonic methods **[Krouskop et al 1987ab, 1989]**. The mechanical properties of the limb tissues may be determined by indentation methods **[Childress and Steege 1987; Reynolds 1988; Lui et al 1992]**, or ultrasonics **[Krouskop et al 1987ab, 1989]**.

In tissue compliant CASD, an analytical model of the soft tissue of the limb is built from measurements of its internal and external boundaries and its Young's Modulus. Computer simulations of the model (usually implemented with Finite Element (FE) techniques) under various applied loads is then used to predict the shape of a comfortable socket. Two simulation methods are used. Either, the shape of a proposed rectified socket is impressed upon the measured limb shape and typical stance forces and moments are applied to the whole limb/socket complex. Computer simulations then calculate the nett stresses on the external surface of the limb **[Reynolds 1988]**. Or, desirable surface stress patterns are applied to the limb model and the resultant surface displacements are calculated **[Steege et al 1992]** If the limb model is realistic and the constraints imposed on it are valid, then the effect of socket rectifications can be assessed without recourse to manufacturing test sockets. Rectifications to the socket shape are applied manually, by a skilled prosthetist, or automatically, from a computer knowledge base, and the simulation run. This phase is repeated, iteratively. When a suitable load pattern is arrived at, the socket shape is archived and sent to a computer controlled facility for manufacture.

To assess whether current analytical limb models are realistic, the socket shapes used in present simulations are manufactured and instrumented. The predicted interface stresses on the models are then compared with those actually measured at the limb/socket interface of the manufactured socket. The model is then modified until the two sets of stresses approximate each other.

However, many of the computer simulations have been constructed to study and predict stresses which occur during standing with weight-bearing only **[Reynolds 1988; Krouskop et al 1988, 1989; Steege 1987a,b; Silver-Thorn and Childress 1992a]**. To the author's knowledge no studies have been conducted into simulating dynamic loading.

Also, in the modelling and simulation processes various assumptions and simplifications are made to minimise the model complexity and therefore reduce computation time. Some of these are: soft tissue is homogeneous and locally isotropic: the mechanism of deformation is compressive and independent of strain magnitude with a linear stress/strain relationship: the interface is uniformly frictionless or uniformly non-slip: Poissons ratio is approximately 0.45: and the skeleton and socket are considered rigid. Clearly some of these are gross approximations to reality. Moreover, modelling of the tissue deformations only considers normal stress (pressure) loadings and does not take into account shear loading or indeed of the shear and tension characteristics of soft tissue. As significant shearing action is imposed on the limb during ambulation, its lack of inclusion in the model is probably a serious shortcoming. A major reason for the lack of shear models is the sparsity of data on the shear stress fields and friction coefficient at the limb/socket interface.

1.4.4.3 Computer-aided socket manufacture

Rectified socket designs once archived are used as the basis of computer-aided socket manufacture. This is effected by several methods: machining a residual limb positive **[Lawrence et al 1985]** ready for drape forming of the socket **[Davies et al 1985]**; by directly carving a socket from a solid **[Rovick et al 1992]**; or by building a socket in a material additive process such as photo-curing liquid plastic **[Rovick et al 1992]**, plastic layer deposition **[Rovick 1992]**, or laser sintered powders **[Rogers et al 1992]**.

1.4.4.4 Discussion

The impetus for development of CASD/CAM techniques was primarily to quantify and record the rectification operation and to speed up the design-to-production phase. Additional intentions were to: enable iterative socket design; allow some standardisation of the rectification process; archive successful designs; facilitate the controlled study of the effect of changes in prosthetic variables on socket comfort, fit and function; and aid in the teaching of prosthetists skills.

Initially, techniques concentrated on assisting skilled prosthetists in their craft by providing them with computerised shape manipulation tools to use. These techniques were extended to make libraries of standard patterns available for rapid initial rectifications but retained a large manual design input. Currently, attempts are being made to automate the rectification process, through the use of computed mathematical models of the limb and socket mechanical behaviour, where the prosthetist has a more supervisory role. All these techniques are currently under development at various prosthetic centres around the world.

Several developers **[Wilkinson and Dewar 1990; Torres-Moreno et al 1991; Engsberg 1992]** and comparative studies **[Kohler et al 1989; Topper and Fernie 1990; Houston et al 1992]** have reported that patients fitted with CASD/CAM sockets (using computerised shape manipulation methods) expressed at least equal preference between them and traditional hand crafted sockets. The prosthetists involved felt that the CASD/CAM systems used could be improved and that currently they were not as efficient as manual methods. Criticisms were directed at: more expedient limb shape input and socket production output; and enhance the shape manipulation and visual presentation software. Nevertheless, there was general agreement that CASD/CAM was on the brink of being commercially feasible. **Houston et al [1992]**, further, suggested that "research can now be concentrated in the areas of: ...increasing knowledge of and developing devices for quantitative assessment of socket/prosthesis fit... ; developing methods and devices for quantitative assessment of the mechanical ... residual limb tissue properties of patients, and increasing the understanding of the effects of prosthetic socket stresses on these properties; ... applying computer-aided engineering methods, such as finite element analysis and stress distribution optimization, to achieve prosthesis designs matched to the characteristics and requirements of individual patients."

These CASD/CAM systems which employ mathematical models to predict limb and socket mechanical behaviour, under gait and stance stress, typically use finite element methods. These are only experimental systems and are still undergoing development. Researchers **[Krouskop et al 1987; Childress and Stege 1987; Reynolds 1988; Silver-Thorn and Childress 1992b; Reynolds and Lord 1992]** report that current models produce significant errors between predicted and actual limb/socket interface stresses and that "the extent to which the model quantifiably mimics the real situation remains to be proven". These models (and current prosthetic practice) are based on the compressive response of limb tissues and ignore its shear stress characteristics.

Although, it is recognised that shear plays an important role in the determination of interface pressures. However, there is a paucity of data on the nature of interface shear stresses occurring in sockets, so hindering advances in prosthetic design and model improvements by enabling comparison of predicted data with actual data. This paucity of data is due to lack of suitable instruments to simultaneously quantify the normal and shear stresses occurring at the interface. The development of the transducer described in this thesis will now allow these issues to be addressed. With the solution of the limb/socket model inaccuracies there will come the possibility of automatic socket rectification bringing time, cost, and quality of life benefits.

1.5 Prosthetic Assessment

Once a socket has been manufactured for a patient and attached to a prosthesis for their use, there remains the problem of assessing the quality of the fit, function, and comfort.

Final optimisation of socket fit and comfort is generally achieved by informed trial and error adjustments/rectifications to the socket or liner shape based on the verbal and visual communication between patient and prosthetist. This process may be enhanced by the use of transparent check sockets for visual inspection, or thermographic imaging of the limb **[Pye and Bowker 1976]**.

The functions of the lower limb are obviously support and locomotion, and successful rehabilitation of the amputee depends on the restoration of these. In order to monitor the progress of the amputee during prosthetic training [see 1.4] an assessment of their gait is made. In most centres, function is assessed by a visual inspection of the patients stance and gait, and informed adjustments to the prosthesis made. In most cases the skill of the prosthetist at this process appears to be adequate and patients leave with a functioning limb. However, if the assessment is inaccurate it will inevitably lead to discomfort and poor gait and therefore non-optimal rehabilitation.

1.5.1 Gait Analysis

There are many rapidly varying parameters occurring during the gait cycle some of which may be asymmetrical. The skilled prosthetist will be able to distinguish

gross and moderate anomalies in the patients gait, however, small and rapid deviations will be much more difficult to detect. **Saleh and Murdock [1985]** showed that visual assessment alone was an unreliable clinical skill, when they compared visual observation with quantitative measurements.

To gain an objective method(s) of assessment, medical engineering has investigated ways of analysing gait. These ways can be broadly split into the quantification and understanding of the following parameters: temporal or spatial; kinematic; kinetic, and metabolic cost **[Porter and Roberts 1989ab].** A brief overview of each of these parameters and the techniques employed to quantify them is given.

1.5.1.1 Temporal and Spatial Parameters

These are simple measures of gait: stride time, stride length, swing time, velocity and cadence. These are pictorially described as in Figure 1.9, although there are variations on this definition which have been noted by **Sienko-Thomas and Supan [1990].**

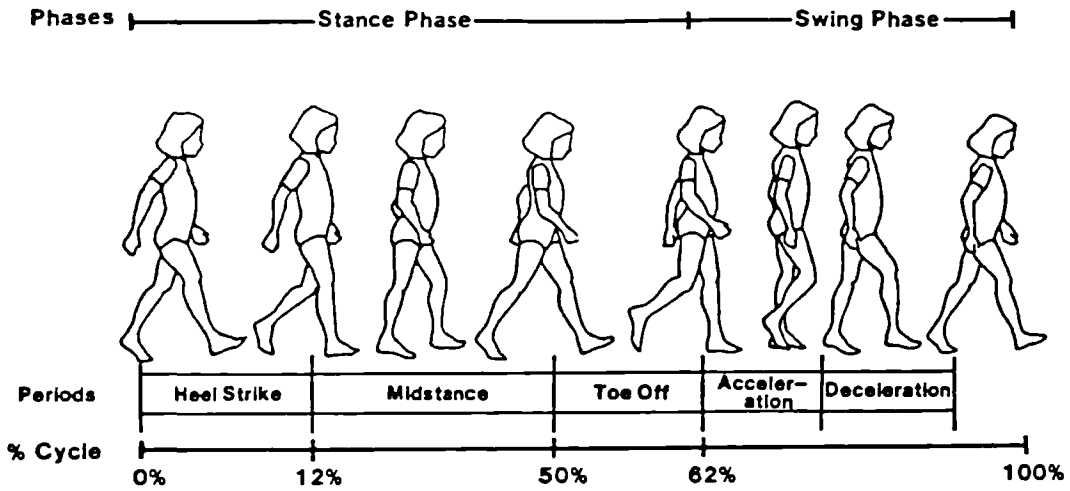

*Figure 1.9 Temporal and spatial parameters of gait as used by prosthetists (from **Sienko-Thomas and Supan 1990**).*

Distance and symmetry recordings between successive footsteps have been made using inked or absorbent paper, inked footpads, foil walkways and mats of electrical switches **[Kirkby et al 1985; Laughman et al 1984].** Temporal measurements

have been taken with stopwatches, electronically scanned foot/insole switches or conductive walkways **[Dewar and Judge 1980]**. Tachometers have been used to record velocity and cadence variations of the patients centre of gravity, during normal gait along a walkway **[Tibarewala and Ganguli 1982]**. The findings of these investigations typically were; single support phase was *37%* of the gait cycle for the prosthetic limb and *43%* for the normal limb; velocity, cadence and stride length were significantly lower than for normals; and the gait of a unilateral amputee was usually asymmetrical. However, with training cadence can be improved and a more normal gait pattern achieved, both of which have been assessed by temporal and spatial measuring techniques **[Laughman et al 1984]**.

1.5.1.2 Kinematic Parameters

Kinematics is the science of describing locomotion in terms of linear and angular displacements, velocities and accelerations of the body segments. Measurements are obtained by accelerometry, goniometry or photographic and cinematographic techniques.

Accelerometers have been used to directly measure acceleration of body segments, from which velocity and displacement are derived **[Robinson et al 1977]**. Alternatively, angular displacements have been recorded directly from goniometers attached about limb joints and angular velocity and acceleration are obtained by differentiation. Sophisticated three axis goniometers have been developed which may compensate for polycentric joints **[Frigo and Tesio 1986]**.

Photographic techniques employ periodically illuminated markers placed on significant anatomical landmarks. When the patient wears dark clothing and the camera is set for time exposure, the resulting photographs have equi-period dotted trajectories. Graphical methods can be used to derive displacement, velocity and acceleration of limb segments **[Cappozzo et al 1982]**. Cinematographic techniques follow the same principles but have a greater detail because of the frame rate **[Seliktar and Mizrahi 1986]**. In order to reduce the intensive manual data conversion associated with these latter two methods, semi-automated video based equipment has been developed for marker trajectory extraction **[Lanshammer 1982]**.

The following is a brief outline of some of the findings obtained using these techniques.

Acceleration patterns have been suggested as a measure of the smoothness of gait. In normals an harmonic analysis of gait cycle acceleration curves shows that even harmonics are obviously dominant over odd harmonics. However, for amputees this dominance is not so distinct. Also, amputee spectra exhibits higher active harmonics.

Body segment motion analysis shows that amputees produce less movement of their knee during swing phase. There may also be vaulting as the knee is held in extension during stance phase. Where this is significant there is deficient shock absorption causing unusual heel strike transients.

General observations were that hip movements, knee angles and upper body motion were exaggerated in the amputee. These findings were supported by goniometry studies. The effect of changes in prosthetic variables could also be observed. Experienced subjective setting of optimal alignment tended to coincide with maximised gait symmetry. Also adjustments to alignment in the prosthetic foot have the largest effect on symmetry than any other parameter. While variations in alignment tended to affect hip angle symmetries more than other symmetries.

1.5.1.3 Kinetic Parameters

In general the kinematic parameters are the result of muscle action, gravity and inertia etc. Kinetics is the study of forces and moments which act internally and externally on the body to cause movement. Internal forces and moments are not directly measurable and need to be derived from a knowledge of the external forces and a biomechanical model. External forces on the limb can be measured through the use of pedobarographs (normal forces) **[Symington et al 1979]**, force plates (normal and shear plane forces) **[Laughman et al 1984]** and instrumented pylons (normal, shear, moments and torsion forces) **[Jones and Paul 1978]**.

Characterisation of the ground reaction forces has been used to identify causes in gait abnormality. It was found that the anteroposterior force axis was particularly sensitive to deficiencies in gait. Deviations on braking are thought to be due to

amputee confidence and alignment variables. Variation in normal forces at push off are thought to mainly reflect alignment conditions. While, perturbations in vertical force curves are assumed to be more representative of the stability of the foot mechanism.

Measurements of ground reaction forces in amputees have shown smaller vertical and anteroposterior shear forces than normals, indicating smaller accelerations on the prosthetic side. Asymmetry of ground reaction forces have been observed for both adults and children. Speed of walking has a significant effect of both normal and shear forces.

Simple linked rigid bar models of limbs have been used to solve the force balance equations of gait and show moments about prosthetic limbs are significantly lower than normal limbs.

Accelerometers have been used to measure kinematic variables as it is directly related to applied force **[Gilbert et al 1984]**. Analysis of forces over the gait cycle show that prosthetic limb forces have a similar trend to normal limbs but with smaller magnitude and lower frequency components. It is thought this is due to the smaller mass of the prosthesis compared with that of a normal limb. This idea was supported by adding weights to the prosthesis and observing significant changes in its energy of motion, while that of the rest of the body was not significantly affected.

1.5.1.4 Metabolic Parameters

Under these procedures the energy expenditure during gait is evaluated. The methods used to measure expenditure are indirect and use: oxygen consumption **[Waters et al 1976]**; heart and respiratory rate **[Pagliarulo et al 1979]**: or electromyographical indicators **[Culham et al 1986]**.

It has been found that there is a relationship between assumed natural gait and minimising energy costs. The normal gait pattern tends to keep the vertical displacements of the body's centre of gravity and changes in its inertia to a

minimum. With a prosthetic limb, control over the motion of limb segments is degraded from normal. Because of the lack of efficiency in locomotion the amputee expends greater energy than does the non amputee.

The curve of energy expended per mass per distance *[cal/kg/m]* of a subject plotted against speed of walking *[m/s]* will have a minimum value. This value has been suggested as the 'natural' or optimum speed of locomotion for that individual.

Comparison of energy expenditure studies to date has been difficult as protocols and data presentation have not been standardised. However, an early review by **Fisher and Gullickson [1978]** summarise the findings of studies where the amputee walks at their own natural pace. The average amputee (BK) walks *36%* slower than normals, using *2%* more energy with time or *41%* more energy per metre.

1.5.1.5 Summary

Porter and Roberts [1989b] categorise the aims of performing gait analysis into three:

(i) the optimisation of the prosthesis
(ii) the monitoring of an amputee's rehabilitation progress
(iii) a greater understanding of the mechanisms of gait

A study of the ground reaction forces and joint moments have been reported as useful in optimising prosthetic variables. Energy consumption is probably more an indicator of the level of mobility. Kinetics and kinematics can be useful tools in assessing new prosthetic components. While gait symmetry, cadence and energy consumption can be employed by the rehabilitation officer to monitor a patients progress and highlight areas of deficiency.

1.6 Discussion

The number of new amputees in the UK is increasing at approximately 10000 per annum. About half of these are referred for artificial limb fitting. The primary causes of their need for amputation surgery are vascular disease (*64%*) and diabetes (*20%*). The majority are over *60 years* of age (*75.5%*) and the life expectancy of *50-75%* of them is only *5 years*. It is essential that optimum mobility and independence be achieved as soon as possible after amputation.

The informed skill of the surgeon is central in fashioning stable well shaped residual limb suitable for a *standard* prostheses. They must ensure a good limb length with sufficient muscle bulk fixed over its distal end in a neat hemisphere. Adequate blood, lymph and nerve supplies need to be secured to effect the long term health of the remaining tissues.

Following amputation, intensive physio- and occupational therapy is given to help the amputee rehabilitate to their previous way of life. Gait training with a definitive prosthesis is undertaken to achieve optimum mobility for the amputee before their discharge. In order to improve their chances of successful rehabilitation, prosthetic fitting and gait training must occur as soon as possible after surgery.

The below-knee prosthesis used in the UK consists of a socket and suspension, a shank or pylon and a foot-ankle assembly. The socket forms the interface between the amputee and their prosthesis. Its function is threefold: to provide safe and comfortable transmission of ambulatory and stance forces from the limb to the prosthesis; to afford stability of the prosthesis on the limb; and it must enable the amputee to exert sufficient control over the prosthesis. It is known that some areas of the residual limb are tolerant of pressures while others are pressure sensitive. The socket must be designed to accommodate these areas.

Both normal and shear forces act on the limb during ambulation and they are static and dynamic in nature. These forces may be modified by prosthetic variables such as component alignment and type of foot-ankle assembly. Current socket design principles are referenced to the normal force tolerance of the limb tissues and are ignorant of the shear force component at the limb/socket interface. However, socket comfort, fit and function are dependent on appropriately distributing or minimising both forces at the interface. There is presently a lack of knowledge about the

duration, magnitude and distribution of shear stresses imposed on the limb during ambulation. Perhaps more importantly, little is known of effect of the interaction of shear and normal forces on limb tissues. This situation is due primarily to an absence of instruments to measure both forces simultaneously. The transducer described in this thesis fills this technology gap and will be able to provide such knowledge.

Socket design methodology is currently craft orientated, relying on the skill of a trained prosthetist(s) to fashion a comfortable, functional socket from a plaster cast of the patients limb. This process is long and labour intensive and without sufficient recorded data for accurate iterative design improvements or socket replication. Because of the lack of reproducibility, socket design research is severely hampered. Computer aided socket design (**CASD**) and computer aided manufacture (**CAM**) are being introduced to prosthetic practice which will bring time and cost improvements and enable precise socket reproduction and true design iterations. These processes are still craft based with the prosthetist manipulating computer graphical limb shapes as opposed to solid plaster limb shapes. Again, in order for the prosthetist to be able to design comfortable, functional sockets they must know what stress magnitudes constitute the limits of comfort and how socket shape relates to it.

Attempts are being made to minimise the craft element in socket design and to automate the process. Computerised mathematical models of the limb and socket mechanical behaviour have been employed to predict the stresses generated in the limb tissues when gait cycle stresses are applied to a prospective socket shape. With accurate models and effective simulation techniques socket, and even total prosthesis design, can be rapid, predictably comfortable and functional at low cost. Also, they would provide objective methods of assessing new prosthetic components/materials without resorting to socket fabrication. However, the present models are immature and are based only on the response of the limb and socket to normal stress. Improvements to them will come as they are expanded to include shear stress response characteristics. Also, when instruments are available to compare predicted data with actual limb/socket interface stresses. The development of the triaxial stress transducer (and system) described here will address this need for real data and aid in determining the shear stress response of limb tissues.

Chapter 2
Soft Tissue Mechanics & Interface Stress Measurements

Section 2.1 presents a brief outline of the mechanical behaviour of soft tissues of the residual limb. This is followed [2.2-2.3] by an overview of the methods and results of other researchers who have attempted to define the effect of stress on tissue and to measure the stresses in lower-limb prosthetics. Section 2.4 reviews the literature on the range of temperatures to be found at the limb/socket interface - that which stress transducers will experience. Finally 2.5 discusses the major considerations of the transducer design process.

2.1 Soft Tissue Mechanics

The whole human body is subjected to external and internal stresses and strains, which establish themselves as actions and reactions on tissues. It is becoming increasingly possible to characterise the way in which these tissues tolerate, deform or degrade under the imposed loads, whether in a healthy or diseased state.

The characteristics of any organ are related to both the mechanical properties of its constituent tissues and its relation to neighbouring organs. Similarly the properties of its tissues are dependant on their chemical composition and their infrastructure. It is possible to analyse the individual properties of the constituent elastin, collagen, ground substance, muscle and other cells and interstitial fluids of tissue. When this is coupled with a knowledge of their structural relationship, it may be possible to deduce theoretical mechanical or mathematical models of the tissue's behaviour. This knowledge can form the basis of improvements in diagnosis, surgical technique, therapy, treatment monitoring and tissue prostheses.

In the pursuit of the formulation of these models and a qualitative appreciation of the form and function of tissue much has been learnt. However, **Kenedi et al [1975]** express the opinion that very little of the, then, current work was applicable in a clinical sense, particularly regarding ... "the bulk of the biomechanical animal work, which forms such a substantial portion of the literature and yet is virtually

inapplicable to the human case". However, in the authors' opinion, although a comprehensive tissue model has not yet emerged, much value has been gained in a qualitative sense from the work which has been done.

An in-depth analysis of all the findings would be beyond the scope of this thesis. Several excellent texts and reviews of the field can be found elsewhere **[Stevens and Jones 1972; Kendi et al 1975; Fung 1972, 1981; Barbenel and Payne 1981; Skalak and Chien 1987].** However, an overview is necessary to illustrate the nature of the materials which will be instrumental in supporting body forces transmitted to the skin/support interface.

The principal layers of the soft tissue found in the lower limb were described in [1.2]. The following sections, dealing with the skin, fascia and muscle, outline the main findings of investigations into their, or their components, mechanical properties.

2.1.1 Skin

2.1.1.1 Experimental Considerations

The majority of investigations on skin have been carried out in-vitro and the greater part of these have been studies of its uniaxial stress-strain relationship. Ideally, tests would be multiaxial and conducted in-vivo, however, this is difficult to achieve, especially while maintaining uniform strain fields. In-vivo measurements also have difficulties in that boundary conditions cannot easily be controlled, and skin thickness and resting tension may not be accurately assessible. Conditions in-vitro are much easier to control. The disadvantage of this regime is that the effects of the physiological conditions of blood, blood pressure, nervous and hormonal controls, metabolism and lymphatic drainage cannot be evaluated. Also, under tension experiments in-vitro **Kenedi et al [1965ab]** noted the expulsion of liquid from the specimen resulted in a change in volume. Care must be taken, however, as the common practice of storing specimens in saline, results in its swelling and an alteration of its mechanical properties **[Lanir and Fung 1974].**

It is accepted that it is difficult to compare in-vivo and in-vitro responses even of the same tissue specimen. **Kendi et al [1965a]** found that in-vitro tissue may be stiffer than the same tissue in-vivo. However, **Cook et al [1977]** found evidence

of the opposite relationship. While **Vogel and Denkel [1982]** and **Vogel [1982]** showed that the stress-strain relationship may be similar if the same gripping methods were used for both in-vivo and in-vitro studies.

Comparable parametric studies may be conducted in-vitro provided certain experimental controls are observed.

The method of gripping specimens and the mode of measuring strain can introduce errors. Grips may cause local stress concentrations and non-uniformities in strain. This non-uniformity in strain is a particular problem with in-vivo studies which use adhesive tabs. To minimise this during in-vitro studies 'I' or dumbbell shaped specimens are often used. Also, if strain measurements are taken from grip displacement then any slippage of the grips will introduce errors. Measurements of strain are best taken directly from the tissue surface at a site sufficiently remote from the grips.

Without a uniform strain field it is extremely difficult to form accurate constitutive equations for a model of skin behaviour. Uniaxial tension tests in-vivo have non-uniform strain fields but have been used to provide information on skin anisotropy. Improved field uniformity can be obtained by the use of biaxial tests. Torsion, circular cup tension and skinfold compression tests in-vivo have highly non-linear strain fields but lend parametric data for healthy and diseased tissues studies.

Temperature and humidity very significantly affect the stiffness of epidermal specimens under test **[Papir et al 1975]**.

Also the stiffness of skin is very low at low strain levels and the in-vitro specimen should be tested floating on a physiological solution so that it does not deform under its own weight. This testing condition also mimics the in-vivo state where skin is hydrated only from the dermal side **[Lanir and Fung 1974]**.

For comparison of results between workers, tissue specimens must be shape and treatment matched and taken from subjects of similar age, health and environment. Skin properties will also vary with site and orientation on the body.

2.1.1.2 Structural Components of Skin

The major structural components of skin are collagen, elastin and ground substance.

Collagen is the major mechanical element of the skin. The alternate-handedness of its helically wound infrastructure is very resistant to axial elongation. It has great tensile strength (Youngs Modulus ≈ *1GPa*) and has a reversible stretch ratio of only *2-4%* **[Fung 1981]**. In general it behaves more crystalline than rubber-like.

Elastin on the other hand is quite rubber-like in its behaviour and is considerably less stiff than collagen (Youngs ≈ *600kPa*) **[Fung 1981]**. It can be reversibly stretched to more than *100%* **[Lee and Kopping 1971]** and fails at *130%* **[Bergel 1961; Carton et al 1962]**. Because of its elasticity it is able to store energy on stretching and release it on contraction.

Ground substance is an hydrophilic gel which has a complex viscosity. It is suggested that it plays a role in the viscoelastic behaviour of the skin at very low tension strain levels (*0.6%*) as it exudes from between the fibres as they align **[Potts and Brewer 1983]**.

2.1.1.3 Properties of Whole Skin

Skin in-vivo is naturally in a state of tension. This may range from *0-20N/m* depending on the body site, specimen direction and body posture **[Dick 1951]** . This tension is not isotropic over the whole body but is directional and varies with site. **Lanir [1987]** notes that these directional effects have been known since 1834 **[Dupuytren 1834]** and studied in detail by **Langer [1861]** and more recently by **Cox [1944]**. The tension direction has been mapped as the elongation of circular puncture wounds, forming lines on the body known as Langer lines. These are closely related to the crease and wrinkle lines on the skin. It has also been shown histologically and by electron microscopy that the lines correspond with the predisposition and slight tension of collagen and elastin fibres **[Ridge and Wright 1966; Flint 1976]**. However, it is thought that the pretension is most likely due to the elastin fibres under strain **[Finlay 1969; Pierard and Lapiere 1987]**. The

skin has lower extensibility and a higher initial stiffness along these lines when in the in-vivo **[Gibson et al 1969]** or in-vitro states **[Barbenel et al 1973; Daly 1982]**.

Testing of the skin mechanics in-vivo is complicated by its binding to deeper layers of tissue. **Cook et al [1977]** found that adhesion of the dermis to fascia affected the results of his suction tests by *10-20%*. However, little work has been directed at assessing this effect generally. The binding of the dermis to deeper layers varies from site to site and possibly with age and disease.

The skin does not behave as a homogeneous material from a bio-engineering viewpoint, but is regarded as a series of networks in a gel, the variable pattern of which gives it its mechanical characteristics **[Gibson 1965; Gibson et al 1965]**. Five networks in the dermis are identified: collagen fibres; elastin fibres; capillaries; lymphatics; and nerve fibrils. The skin is further made non-uniform by the presence of hairs, sweat glands and ducts at non-regular intervals. The networks are also regarded as mobile in the gel of ground substance. However, on the clinical level it may be considered statistically homogeneous, although, this may not be a valid assumption for modelling studies such as CASD. Skin is viscoelastic and hysteretic with a non-linear stress-strain response.

Fung [1972] describes the viscoelasticity of skin as pseudo-elastic because under periodic steady state load cycling a steady state stress-strain relationship is evident. This relation is described by a hysteresis loop - the loading and unloading curves of which may be treated separately and described by the theory of elasticity.

Figure 2.1 describes a typical load deformation curve from an in-vitro skin specimen subjected to uniaxial tension. The curve can be considered to have three phases. Phase 1 is where the stiffness of the skin is very low (small stresses cause large strains) and lateral contraction is gradual. In Phase 2, or the 'elbow' of the curve, the stiffness increases rapidly and lateral contraction accelerates. Phase 3 is quickly reached where the stiffness becomes large and constant such that very little extension occurs even for large loads. During this phase the rate of lateral contraction slows down to a minimal level.

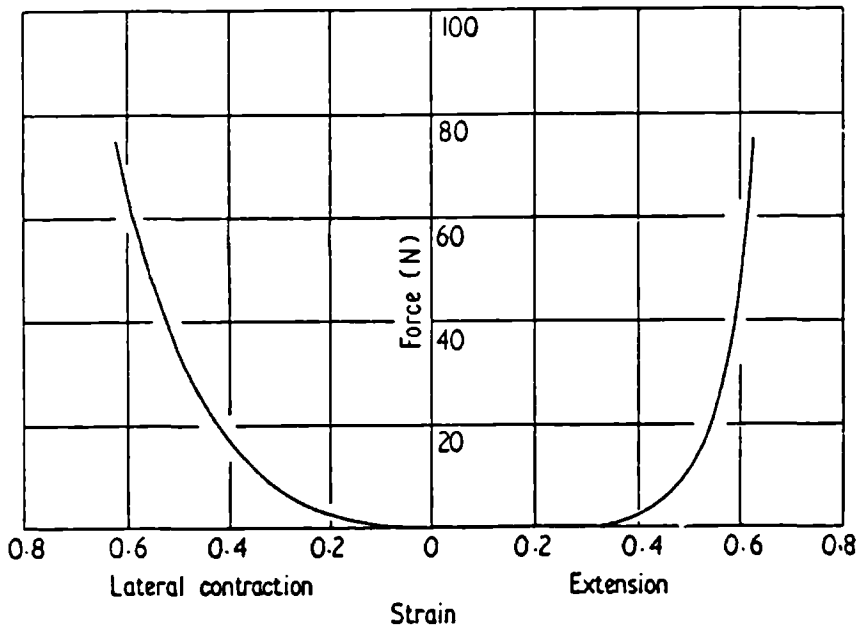

*Figure 2.1 Load deformation curve for skin specimen in-vitro under uniaxial tension. Increasing tension extends the skin axially but contracts it laterally (from **Kenedi et al 1975**).*

Figure 2.1 shows the skin to be nonlinear. **Lanir and Fung [1974]**, among others, have shown it to also be anisotropic but displaying some form of orthotropy or transverse isotropy depending on its site - Figure 2.2.

The cause of these phenomena have been described in terms of the behaviour of the components of the skin and their interaction.

The Phase I region of the stress-strain relation is dominated by the characteristics of elastin **[Dick 1951; Daly 1969; Lanir and Fung 1974]**. In this phase the collagen fibres are re-orientating to align with the axis of tension and do not yet bear any load. The elastin fibres are under tension and storing energy as they deform elastically. This description is supported by electron microscope studies **[Finlay 1969; Brown 1973]** and uniaxial tests which show the specimen to contract laterally. Also, hysteresis in this region is virtually absent. As the elastin fibres attach to the collagen fibres and/or loop around them, it is thought that the elastin network assists in restoring the original morphology of the collagen network after stresses are removed.

During Phase II some collagen fibres begin to bear load and the stiffness of the skin geometrically increases **[Markenscoff and Yannas 1979]**. Hysteresis is observed in this phase, which has been attributed to motion of the collagen fibres in the ground substance **[Minns et al 1973]**, although this is not certain.

Phase III response is due principally to the stretching of aligned collagen fibres. The stiffness of the skin being similar to that of isolated collagen fibres. The tensile strength of skin ranges from *2.5* to *16 MPa*, however, it varies with site, age, sex, and fibre direction. Apart from penetration induced failure of skin structure, partial damage may occur under long-term moderate tensions, not high enough to cause arrest of blood supply, such as found during pregnancy (gravidarum striae).

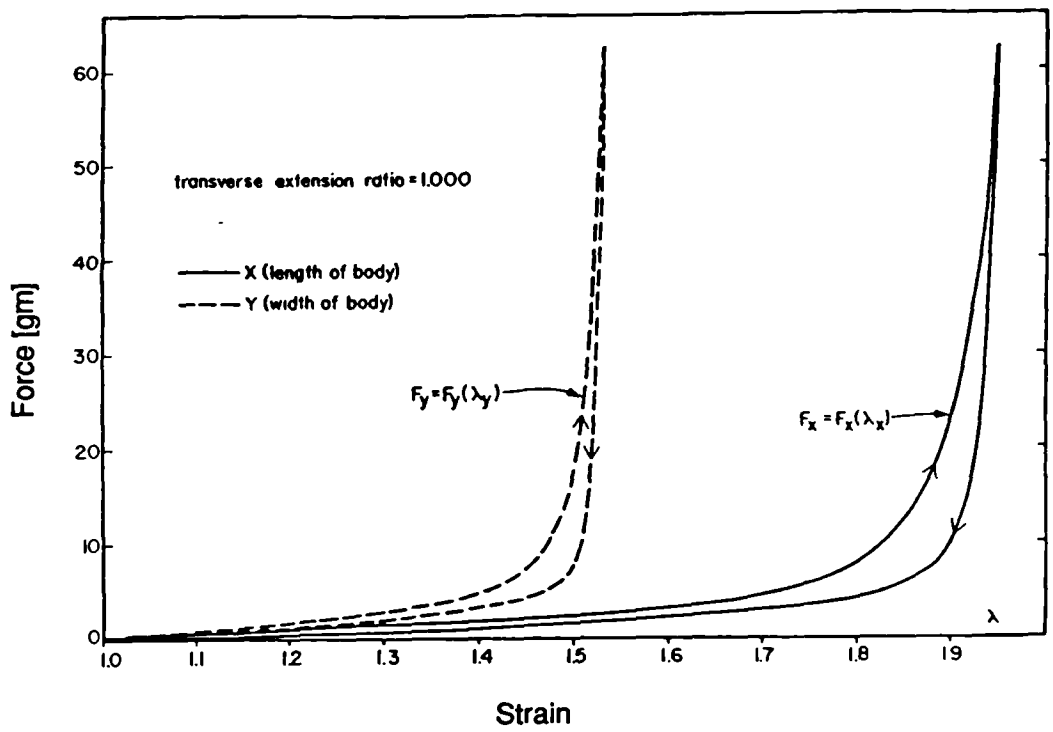

*Figure 2.2 Hysteretic behaviour of skin under uniaxial tension load cycling and some orthotropy or transverse isotropy (from **Lanir 1987**).*

Figure 2.2 describes the hysteretic behaviour of skin under a uniaxial tension load cycle **[Gibson and Kenedi 1970]**. It is known that during stress cycling the stress-strain curve of successive cycles shifts to positions of higher strain for a given stress. This shift decreases quickly so that after a few cycles a stable curve is established. Figure 2.3 describes this phenomena - which is called preconditioning.

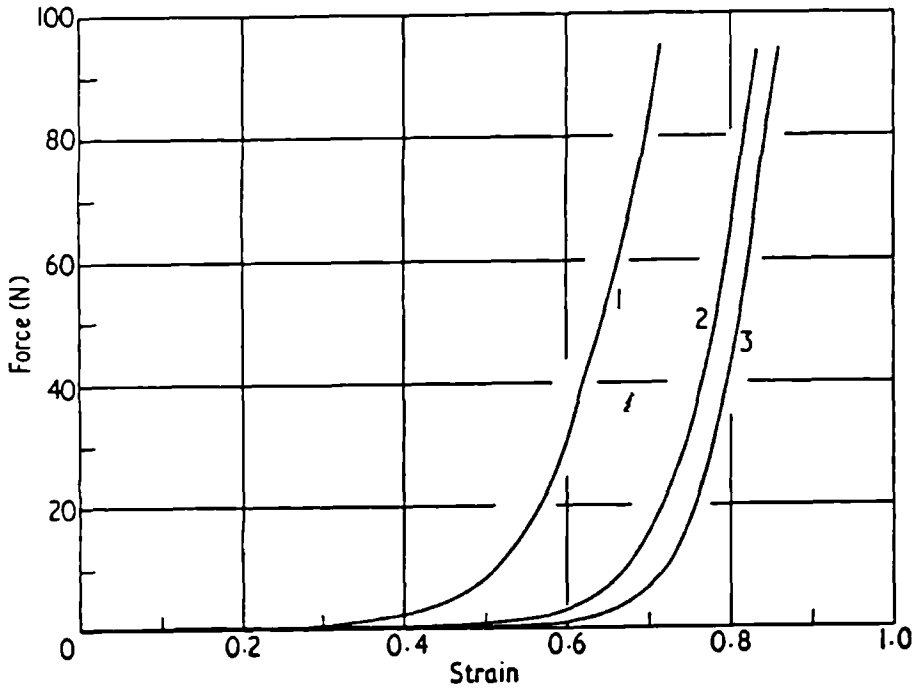

Figure 2.3 Characteristic shift in the stress-strain curve with load cycle of skin under uniaxial tension (from ***Kenedi et al 1975****).*

Figure 2.2 also indicates that skin is viscoelastic. This viscoelastic response is nonlinear and dependent on strain level. At low strain levels (Phase I) hysteresis, creep and stress relaxation are very small and skin behaves more or less elastically. At moderate to high strain levels (Phase II, III) a load cycle exhibits large hysteresis. The energy lost in this process may be dissipated as heat or microstructure alterations. Skin also exhibits stress relaxation and creep processes.

In general the skin's response to compressive loading is nonlinear and viscoelastic, although the magnitudes vary with age, sex, site, obesity and hydration. The components of the skin which predominate during compression are the elastin fibre network and the ground substance. **Vossoughi and Vaishnav [1979]** claim that the relative compressibility of skin (bulk modulus/shear modulus) in-vitro, which is of the order of *1000*, confirms that skin is incompressible. In-vivo studies however, tend to be unclear as yet **[Lanir 1987]**. This is an important parameter to establish as the constitutive equations for incompressible materials are significantly simpler that for the general case. Thus models of skin behaviour may be easier to use.

Moore [1970] in his review on the vibration studies of the skin indicates that at low frequencies (*<5KHz*) the compression response is dominated by shear waves, while at higher frequencies compression waves are important. The impedance characteristics therefore vary with frequency and also with humidity, body site, probe dimensions, and static pre-loads **[Franke 1950; Hussein et al 1978]**.

The epidermis is only about one tenth of the thickness of the dermis and is thought not to play a significant part in the skin's resistance to tension **[Lanir 1987]**. Its mechanical properties are known to be significantly influenced by temperature and humidity **[Wildnauer et al 1971; Middleton 1973; Papir et al 1975]**. There may be up to a *1000*-fold decrease in stiffness and a shift from linear to nonlinear response when the humidity increases from *25%* to *100%*. A similar change occurs with increasing temperature. Its breaking strain increases by *2*-fold over the same ranges although it has been observed that its tear strength is less than that of the dermis. The stratum corneum is viscoelastic becoming more lossy [see 3.1.2.3] with increasing humidity and temperature.

A review of various investigations found that skin becomes less compliant with age **[Lindner 1972]**. Also the skin's resilience and rate of recovery after load decrease with age. As collagen ages the degree of cross links increase making the fibres less extensible, and the total amount of collagen in skin appears to decrease with age **[Shuster et al 1975]**. The elastin content of the skin increases with age, but the elastin itself becomes calcified and irregular such that the nett amount of functional elastin decreases **[Dick 1951]**. It is also thought that the ability of the ground substance to bind water decreases with age, thus altering its viscosity **[Lindner 1972]**. Skin anisotropy and nonlinearity remain constant with age **[Lanir 1987]**.

Friction and surface adhesion coupled with normal (compressive) stresses are the major factors in determining the amount of shear stress able to be sustained at the skin surface. Unfortunately there is not the amount of data available about this property as there is with tensile and compressive properties. **Naylor [1955ab]** demonstrated that approximate linear relations exist in-vivo between frictional force and normal loading (Amonton's law). He also determined that for some materials (polythene, silver) the co-efficient of static friction is equal to the co-efficient of dynamic friction. However, **Comaish and Bottoms [1971]** describe higher static than dynamic friction with textile materials in contact with skin. They found that over a limited normal load range skin obeys Amonton's law, but deviations did occur with some materials approximating more toward $F = \mu W^n$, $n < 1$. This was thought to be because skin deformation under normal loads was not plastic but viscoelastic, thus contact area was not proportional to load. The co-efficients of dynamic friction for any given material were also found to vary with the presence of agents on the skin surface (Eg. sweat, water, talc, or oil). More recently **Cua et al [1990]** studied the frictional properties of skin in relation to age, sex and anatomical site. They did not find a significant variation in friction co-efficient with age or sex but a nearly three-fold variation with body region (abdomen = *0.12*, forehead = *0.34*).

2.1.2 Fascia, Tendon and Ligament

The mechanical properties of human connective tissue have been studied both in-vivo and in-vitro. Recall from Chapter 1 that fascia can be divided into two forms, superficial and deep fascia.

Superficial fascia acts as a lining to the body, attaching the skin to muscle or bone and to deep fascia. It also acts as a fat storage layer and may have up to several centimetres of adipose tissue - in obese subjects. At most sites it is able to move freely with respect to deep fascia or muscle. Although, at some sites it is closely bound to bone or deep connective tissue. An in-vitro study on isolated porcine superficial fascia yielded a bulk modulus and shear modulus of *70kPa* and *4kPa* respectively. Most studies have not isolated the superficial fascia from skin. Under compression in-vitro fluid was expressed from the tissue. This was presumed to be connected with ground substance. Its affect on the mechanical properties is still unclear. It has been found that oedema in the surface tissues affects its

stiffness at quasi-static indentation rates although at frequencies above *100Hz* the dynamic response is similar to that of normal tissue **[Mridha and Odman 1985]**. Various researchers have attempted to measure subcutaneous fluid pressure using needles, implanted capsules and wick catheters. There are however, disagreements over the findings. **Guyton [1963]** has proposed that interstitial fluid pressures are normally negative, *-0.5* to *-1kPa* and that induced positive fluid pressures meet with spontaneous flow. Positive pressures are said to induce the adipose cells to adopt a spherical shape, rather than cuboid, and thus opening intercellular spaces.

Deep fascia is principally composed of collagen and a few elastin fibres. It envelopes muscle groups and compartments, and may fuse with the periosteum and tendon. It forms in layered sheets and may be highly directional. Again comparatively fewer attempts have been made to characterize the mechanical properties of deep fascia compared with those of skin. In-vitro tension experiments, on fascia lata from the thigh, show a stress-extension relation which has three phases **[Butler et al 1984]**. The initial and final phases are linear - the final being much stiffer. The middle transitional phase is nonlinear. The change in modulus from first to third phase is much smaller than that seen in skin ($\approx$ *50%* increase). During the first phase it appears that the collagen fibres are aligning and the fibres begin to straighten. By the third phase the full load is borne on the fibres as the fibrils and molecules extend. The modulus in this region is about *400MPa*, which is similar to that of tendon. **Garfin et al [1981]** found that fascia appeared to contribute to the maintenance of muscle compartment pressure in dogs. After the fascia was removed the pressure fell by *50%* and muscle force decreased by *10-16%*.

The physiological role of tendon is to transmit muscle forces to bones, while ligaments provide stability to joints and limit their range of movement. The primary component of these structures is collagen, with small amounts of elastin and ground substance. The ultimate tensile strength of collagen is in the region of *45* to *125MPa* with a maximum strain of *0.08* to *0.35* **[Viidik 1987]**. There appears to be good correlation between the size of a tendon and the size of the force which its corresponding muscles can produce. The normal isometric muscle tension is about a quarter of the ultimate tensile strength of the tendon.

The parallel arrangement of collagen fibres in tendons is the basis of their strength, compared with the lower strength of fascia or skin. Also, because of this all the

fibres load bear simultaneously and evenly, where as fascia and skin with a less pronounced fibre direction are subject to more uneven stress distributions. The stress-strain relationship for parallel fibred collagenous tissue is given in Figure 2.4.

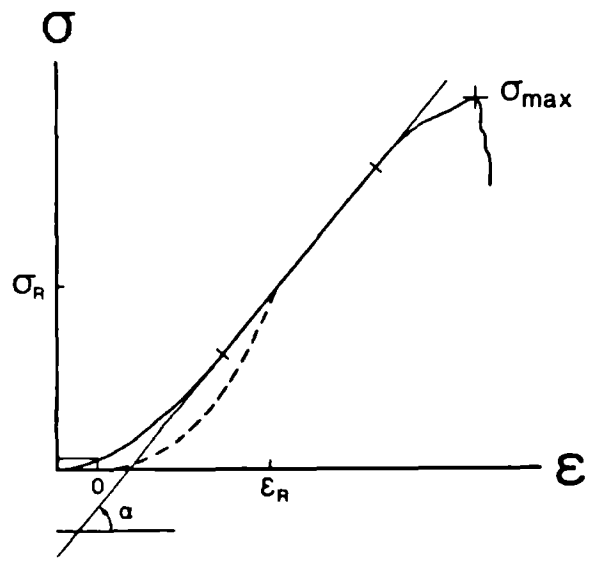

Figure 2.4. The stress-strain curve for parallel fibred collagenous tissue. It shows one loading cycle and stress loading to failure. The centre region of the curve is linear (marked). The dashed curve is an unloading line from the linear region. (from ***Viidik 1987****).*

This figure describes a linear region flanked by nonlinear regions at the start and end. Extension occurs as described for fascia. Most of our normal physiological activity only effects strains in the initial region, while strenuous activity strains may move into the linear region. A toned muscle may induce a pre-stress tension in the tendon moving the in-vivo resting state into the initial nonlinear region. Tendon and ligament stress-strain response is viscoelastic and hysteretic with the preconditioning effect described earlier in the chapter. They also exhibit a moderate strain rate dependence. With age the collagen molecules form more crosslinks and consequently the tendon has increased stiffness and strength.

2.1.3 Muscle

Despite there being a significant amount of literature devoted to muscle mechanics under their normal stimulation mode, there is very little information on its bulk properties as far as prosthetics is concerned.

Due to the compartmentalisation of muscle by deep fascia there is some limited relative mobility of muscle compartments and groups. From a prosthetics point of view the implication is that muscle will remain in place over bone when subjected to external stresses. **Shock et al [1982]** conducted compression studies on porcine muscle in-vivo. They measured the bulk and shear modulii to be *78kPa* and *82kPa* respectively. Measurements of the pressures inside muscle compartments by **Mubarek et al [1976], Hargens et al [1977],** and **Baumann et al [1979]** showed intra-compartment pressure variations to be small, and that pressures increased significantly during muscle contraction.

2.2 Stress Effects on Tissue

In a lower-limb prosthesis body support forces are transmitted through soft tissue which is not adapted to bearing them. Central to the design of effective sockets is an understanding of what modes, magnitudes, areas and durations of stress may be injurious to soft tissue. Modes of mechanical stresses which may cause tissue damage include friction, normal, shearing and torsion stresses. These are imposed by forces applied perpendicular (normal), obliquely (shear and normal) or planar (shear) to the skin surface.

2.2.1 Friction Effects

The mechanism of blister formation is unclear although there are two identifiable phases in their formation **[Naylor 1955ab]**. The first is where epithelial cells suffer necrosis and intra-epidermal splits form. Secondly the splits fill with fluid, probably from the dermis, and distend before rupturing. It appears that their formation is not related to local heating or enzyme action, however it is related to the number of surface rubbings, co-efficient of friction and applied normal load - there being an inverse relationship between the frictional force and the number of rubs required to form a blister. The implication of this being that repeated mechanical distortion of epidermal cells causes their failure and death. However, for a full contact prosthetic socket with no slip, friction may not be a significant contributor to tissue damage.

2.2.2 Normal Stress Effects

The effects of pressure (normal stress) on the viability of tissues - in rats and guinea pigs - was studied by **Husain [1953]** who found that:

(a) localised pressures were more damaging than large area distributed pressures.

(b) the duration of applied pressure was more critical than its magnitude although there appeared to be a *pressure x time* threshold for tissue damage.

(c) localised pressure led to tissue injury by: increasing capillary permeability during compression and upon release causing interstitial oedema, lymphatic and venous blockages; decreasing blood flow (causing ischaemia) resulting in inadequate nutrition and oxygenation; and trapping blood borne bacteria at local sites increasing local damage.

(d) reactive hyperaemia, oedema and even capillary and venous haemorrhage followed pressure release. This may lead to the release of blood borne bacteria to the interstitium and lead to ischaemia of downstream tissues.

(e) pathological changes are induced in tissues under pressure (ie. structural degradation, necrosis and absorption of muscle). Muscle tissues appeared to be affected to a much larger degree than skin and subcutaneous tissues.

(f) *pressure x time* thresholds were significantly reduced by vascular insufficiency, neurological deficiency or scorbutic conditions.

(g) decubitus ulcers were preceded by deep muscle damage and were more common near bony protuberances.

These findings have particular relevance to the amputee, indicating that emphasis in socket design should be placed on load spreading and instructing patients on the *pressure x time* threshold for tissue damage. Particular care should be shown to the fit and function of sockets for the vascular or diabetic amputee as they are more susceptible to tissue damage from pressure induced ischaemia.

Kosiak et al [1958] were of the opinion that decubitus ulcers are due to tissue ischaemia caused by external mechanical pressures which exceed the tissue capillary pressure. They conducted a study of the magnitude and distribution of pressures under the sitting area of normals seated on a number of plain or padded surfaces. They found that pressures under the ischial tuberosities were greatest. These, along with pressures at ten other sites, were commonly greater than arterial diastolic pressure and were far in excess of mean resting capillary pressure.

They made no conclusions as to the magnitude and duration of pressure required to produce ischaemic necrosis. Nor did they attempt to ascertain at what pressures the tissues ceased to be perfused. They did, however, demonstrate that even during normal activity tissue viability may be compromised easily. This illustrates the potential problems which face the amputee when tissues which are not normally expected to bear such stresses are exposed to prolonged pressures. However, some attempts to set thresholds, beyond which tissue breakdown occurs **[Daniel et al 1981]**, have not been supported by all clinical evidence **[Merbit et al 1985]**. This highlights that there may be many other factors than purely stress magnitude and time, which influence tissue susceptibility.

A recent review **[Crenshaw and Vistnes 1989]** of pressure sore research sustained much of Husain's findings, but suggested that ischaemia is only one of the factors responsible for necrosis in tissues under external pressures. Histological studies show that early damage occurs internally (sub-dermally) **[Whitkowski and Parish 1982]**. Adipose cells necrose before other cell types, while capillaries and venules dilate separating their endothelial cells and haemorrhaging. The displacement of ground substance away from blood vessels during loading could play a role in vessel haemorrhage on load release. Additionally, traumatised tissue has decreased fibrinolytic activity, resulting in deposits in interstitial spaces and capillaries - causing vessel occlusion, lymphatic and venous congestion, fluid cysts and localised bacteria. This was particularly evident in tissues exposed to shear stresses **[Bader et al 1986]**.

There appears to be a correlation with some medical conditions and increased sensitivity to stresses (E.g. low serum albumin and lymphocyte counts, anticoagulant medication, smoking related diseases). Some medical conditions significantly impair the tissues ability to re-perfuse with oxygen following the removal of external stresses **[Bader 1990]** . Observations made of the changes in transcutaneous oxygen

tension (gaseous) of areas of tissue subjected to repeated moderate normal stresses showed that oxygen levels decreased and carbon dioxide levels increased. For normals these resultant levels rapidly reversed on relief of the pressure and exhibited diminishing sensitivity on subsequent cycles. However, some spinal injury and multiple sclerosis patients showed incomplete recovery during moderate periods of relief and demonstrated a considerable build-up of CO_2 during loaded periods. Response and inability to adapt was suggested as being due to an impaired physiological control mechanism. Subjects demonstrating this response are at particular risk and require adequate pressure relief mechanisms. It was also suggested that it may be possible to establish the intervals of pressure relief necessary to avoid tissue compromise.

2.2.3 Shear Stress Effects

Although many studies have been performed into the effects of stress on tissue the vast majority have concentrated on the effects of normal stress only. Some of the authors of those works **[Reichel 1958; Roaf 1976]** have speculated that the role of shear stresses in causing soft tissue damage is of equal importance as that of normal stresses. Support for this proposition was brought by **Cockrell [1971]** and **Meier et al [1973]**, who reasoned from their studies, that shear is a major unmeasured factor in the cause of tissue damage and comfort in prosthetic sockets.

Cockrell [1971] studied the variation in average normal stress, at four sites of the limb/socket interface, with three different liner materials. It was observed that, although there were only small differences in normal stress between the materials, there was a very significant, subjective, patient preference for a gel liner. This was ascribed to the unmeasured shear stress component being a significant variable on the perceived liner comfort. **Meier et al [1973]** observed that some patients' limbs exhibited areas of tissue damage where the measured normal stress was low. However, a dye loaded limb sock [see 2.3] showed that these were areas of high stress (normal and/or shear) implying that shear stress was the causative factor in the tissue damage.

The extent and degree of influence of shear forces on deep tissues is dependent on the strength and thickness of the stratum corneum and the strength in the dermal-epidermal and dermal-fascia junctions. Mild shear produces tension in the

dermal collagen network stretching or pinching small vessels, causing ischaemia and associated hyperaemia. This may not cause permanent damage, however, greater forces for longer durations may cause rupture of the collagen fibres and small vessels resulting in hemorrhage and ischaemia - possibly leading to necrosis and ulceration. **Bader et al [1986]** identified shear stress as the main stress mode instrumental in the reduced fibrinolytic activity found in damaged tissue. Despite this, little experimental work has been undertaken to investigate shear stress fields at the limb/socket interface.

One of the earliest studies on the in-vivo effects of combined shear and compressive (normal) stresses on soft tissue function was that carried out by **Bennett et al [1979]**. They performed a comparison of shear and normal stresses as causative factors in vessel occlusion. It was observed that shear played a very significant role, such that 'the value of pressure (normal stress) necessary to produce occlusion could be nearly halved when accompanied by sufficient shear'. **Bennett et al** did not specify any preparation of the skin surface before their trials. The maintenance of shear stresses at the skin surface is dependent on the co-efficient of skin friction and the applied normal stress. Large co-efficients (*0.5-1.0*) are associated with high friction properties where large shear stresses may be sustained with low co-incident normal stresses. Under these conditions shear alone (ostensibly) may cause significant vessel occlusion and tissue damage.

The single shear axis device developed by **Appoldt et al [1970]** and the dual axis (normal and shear) device developed by **Bennett et al [1979]** are the only instruments, known to the author, which were designed to measure shear stresses applied to the skin. Furthermore, **Bennett et al [1979]** were the only workers to measure and investigate the interaction of shear and normal stresses on tissue viability. Until the further development of multiaxis devices and their wide use the relative significance of the two stress modes will remain speculative.

2.2.4 Socket Design Influence on Stress

Levy [1956] presented dermatological evidence that the focus of a significant proportion of cysts in skin failure was in the proximity of the edge of load bearing areas. Amputees often complain of pain at the socket brim or strap where the stiff prosthesis abuts the soft tissue. **Murphy [1971]** argued that this was because

stress concentrations are induced where there are transitions in stiffness, thus, socket design should incorporate stiffness gradients. The appliance could be made stiff at the central loaded areas and have tapered stiffness toward the brim.

Bennett [1971, 1972ab] performed a simplified analysis of transferring compressive and shear loads to soft tissue with particular emphasis on the prosthetic problem. This provided a simplified theoretical basis of Murphy and Levy's work, and showed that: large stresses exist proximal to the brim of a prosthetic socket; the stress levels could be controlled by controlling the local stiffness of the structure; and membranes could be used to spread shear stress uniformly. Pressure induced in tissues (theoretically), is dependent on the area of the indentor and not so dependent on radius of indentor curvature. They indicate that the tissue reaction is roughly divided into half normal stress and half shear stress about the indentor edge. The ratio (shearing/normal) increases with tissue thickness and indentor curvature. This theoretical analysis was qualitatively verified by experimental work **[Bennett 1973]**.

Bennett applied these theoretical findings to socket design principles. He modelled the (AK) limb/socket interaction using rigid plates indenting simulated flesh. These experiments confirmed that increasing brim radius reduces the local compressive stress but distributes it, raising the mean compressive stress in the tissues inside the socket brim. It also shifts the focus of shear stresses from just outside the brim to just inside it. Thus, there is a compromise between reduced brim stress and increased internal stress. An optimum brim radius of 12mm was suggested.

The effectiveness of liner materials in reducing tissue stresses, and therefore damage, was investigated by **Sonck et al [1979], Cockrell [1971],** and **Rae and Cockrell [1971]**. These studies showed that soft liners, especially gel types, consistently reduced peak normal stresses at many regions of the limb/socket interface. Also, that patient subjective evaluation showed preference to these soft liners. However, **Silver-Thorn et al [1992]** present data which indicates that liners may decrease peak normal stresses in some areas of the limb/socket interface, but may also increase stresses in other areas. **Bennett [1974]** formulated a simplified theory of the effect of gel liners on stress distributions in the limb. Experimental models of the interface showed that gel liners act to spread compressive and shear forces more uniformly over all the interface tissues. This had the effect of raising the stress levels in the deep tissues as well, but this was thought to be acceptably low.

Current design practice emphasizes the need to distribute loads on the limb over a wide area, in order to reduce peak stresses. Regions of thin tissue over bony prominences are relieved of load as these are more susceptible to damage. Muscular and tendonous areas tend to receive the majority of the load. Although, tendon is favoured as it is more resilient to stress than muscle, due to a highly parallel collagen structure. Its sparse innervation also keeps pain sensation to a minimum.

2.2.5 Tissue Adaption

Tissue adaptation to applied stress occurs commonly in the process of normal activities. Corns (clavus') and calluses of the palms and feet in response to friction and pressure are examples of tissue adaptation. **Brand [1975]** conducted an animal study on the response of tissue to mechanical loading. The foot pads of rats were subjected to repetitive applications of normal ambulatory stress levels (*20psi = 138kPa*). On applying 10 000 repititions/day 7 days a week for 10 days, the tissue exhibited ulceration, epithelial destruction and necrosis. This rate is equivalent to a daily 7 mile walk at a fast pace over hard ground. The same stress applied 8000 times/day for 5 days a week for 28 days, resulted in epithelial hypertrophy and a resistance to further loading damage. Thus, fewer loading cycles and occasional rest leads to adaption, highlighting the need for recuperative periods, both in the immediate term and in the longer term. There is also an inverse relation between magnitude of the applied stress and the number of regular applications before damage occurs **[Naylor 1955ab]**. This may imply that the recuperation periods should be longer for larger transient stresses.

Although, mechanical stresses imposed on healthy tissues may lead to damage situations, it has been demonstrated, on animal models, that regular controlled stresses applied to healing wounds can improve their resultant mechanical properties. When wounds are clipped closed under small amounts of tension, the collagen fibres are regenerated in a biaxial network. Open wounds grow wavy parallel collagen which have inferior mechanical properties **[Doillon et al 1988]**. Passive motion of healing wounds and physical activity can improve the mechanical properties and healing rates of the new tissue **[Vailas et al 1981, VanRoyen et al 1988]**. Thus with a sufficient understanding of the mechanisms of tissue growth it may be possible to design mechanical stimulation or surgical regimes to modify the stress tolerance of limb tissues.

With the instrument described in this thesis measurements of the magnitude and duration of the normal and shear stresses at the limb/socket interface can be obtained. This data can then be used to conclude whether breakdown or adaption will occur or to what extent tissue 'modification' regimes may be useful.

2.2.6 Discussion

The mechanical stress induced breakdown of soft tissue is a complex degenerative process involving more than just hypoxia and necrosis - due to vessel occlusion. A whole set of chemical and physical dysfunctions can result directly from stress actions on organs, cells and intra-cellular structures. These dysfunctions may be precipitated by a number of concurrent medical and nutritional conditions. Both normal and shear stresses are instrumental in causing damage, each affecting the tissue in a different manner. There appears to be a *stress magnitude x time* threshold beyond which dysfunction is evident.

There are two generalised responses in soft tissue to applied stresses: breakdown or adaption. Breakdown is a degenerative process where the ability of the tissue to tolerate further applied stress is reduced and aggravation of the existing damage occurs. Adaption is modification of tissue structures so that they become more tolerant to the applied stress.

Significant and continuing experimental work, in-vivo and in-vitro, is being carried out into the effects of normal stresses on tissue health. Already some of the findings in stress related tissue damage have had influence on facets of socket design. However, comparatively little quantitative assessment has been made of the effect of shear stresses on soft tissue. In particular, the magnitude and duration of the shear stress present at the limb/socket interface has not been known in sufficient detail for correlation with observed tissue damage. Indeed, little is known of the combined effect of concurrent normal and shear stresses and its impact on the apparent *magnitude x time* threshold. The principle reason for this is the lack of suitable instruments with which to measure the concurrent normal and shear stresses at the interface.

2.3 Previous Interface Stress Measurements - Methods

From earlier this century a variety of methods have been employed to qualify or quantify the residual limb/prosthetic socket interface stresses. These have included dye loaded stump socks, fluid or pneumatic membranous cells, variable capacitance stress sensors, strain gauged diaphragms/beams, and optical methods. The devices employed have been designed to be either inserted between the limb and socket of a standard prosthesis, recessed into the wall of an adapted socket, or mounted on the supports of isolated sections of adapted prostheses or integral to special sockets. The following briefly reviews the previous methods employed to measure interface stresses.

Similar devices and other methods have been used to investigate stresses at other body/support interfaces. Most notably: with reference to stresses under the normal and pathological foot **[Lord 1981; Alexander et al 1990]**; and for evaluating seating and bedsore problem **[Ferguson-Pell et al 1976]**. Significantly, all but two of these devices **[Appoldt et al 1970; Tappin et al 1980]** have been designed to investigate only the normal stress at the body/support interface.

2.3.1 Sensors between Limb and Socket

Of the various techniques, the printing method using the dye loaded socks **[Meier et al 1973]** is the only quasi-static technique. It records the stress distribution and provides a measure of the peak stress experienced at each point at any time during the period of the trial. The disposable sock is impregnated with microcapsules of dye. The capsules are designed to rupture under applied load. Thus the intensity of the, removed, stocking colour is related to the magnitude of stress and the number of pistoning repetitions of the limb into the socket. Unfortunately this technique is unable to distinguish between normal and shear stresses and is also sensitive to loading rate and temperature. Although, they do provide a permanent visual map of the stress distribution inside the socket it is, however, difficult to quantify the stress magnitudes.

In order to obtain repeatable, accurate (quantifiable) and continuous monitoring of limb-socket interface stresses the majority of early design effort focussed on discrete

transducers. Some of these took the form of flexible fluid filled **[Naeff and Van Pijkeren 1980; Van Pijkeren et al 1980]** or pneumatic **[Krouskop et al 1987ab; Barbenel and Sockalingham 1990]** cells with remote pressure transducers.

Van Pijkeren et al and **Naeff and Van Pijkeren** developed their own pneumatic device. Figure 2.5 contains a schematic of the cell. A turned rod with two diameters *(1mm and 0.2mm)*, was interposed between two *0.25 x 30mm* diameter PVC sheets before they were heat-sealed. The rod diameters formed the fluid channel to an external pressure transducer and a vent capillary for filling the fluid chamber, respectively. A *7mm* disc was cut from one of the PVC sheets to form the fluid chamber, and a *0.1 x 30mm diameter* PVC sheet heat sealed as its top surface. This top sheet formed a low stiffness lid to the chamber *(0.25 x 7mm diameter).* A lead tube *(1.2mm* OD) to the external pressure transducer (LX1600, National Semiconductor Corp) was joined to the cell by a 1mm diameter dowel tube. A flange was included in the PVC moulding to effect a strain relief at the tube inlet. The lead and chamber were filled with low viscosity silicone oil. Each device was fixed in place on the limb with double-sided adhesive tape. The lead tube extended from the chamber along the interface region to the socket brim and on to the pressure transducer. Resonant behaviour was assessed by dropping a ball onto the sensor to apply an impulse pressure. The system time constant was dominated by the fluid cell and its lead tube and was estimated as *20mSec*, giving an overall bandwidth of *8Hz*. This range was not sufficient to record all the significant frequency components occurring during gait.

The system of **Van Pijkeren et al [1980]** was improved by **Barbenel and Sockalingham [1990]** by: employing temperature compensated, low cost, high accuracy solid state pressure transducers with direct electric outputs; and using commercially available large area sensor cells (Talley Group LTD, UK). Each cell was made from *0.25mm* PVC sheets heat sealed to form a *28mm* diameter chamber. The lead tube was *1m* long (*2mm* ID, *3mm*OD) and 'considerably stiffer than the sensor cell'. Both the lead and cell were filled with vegetable cooking oil. The pressure transducer was a piezoresistive gauged silicon diaphragm (SCX05DN, Sensor Technics, UK). The transducer linearity was approximately *±0.23mmHg (0.03kPa)*, while hysteresis was less than *0.06kPa*. Long term drift was less than *2%FSO*. Sensor calibration was by hydrostatic means and verified by pressure measurements between the skin (forearm) and a sphygomanometer cuff.

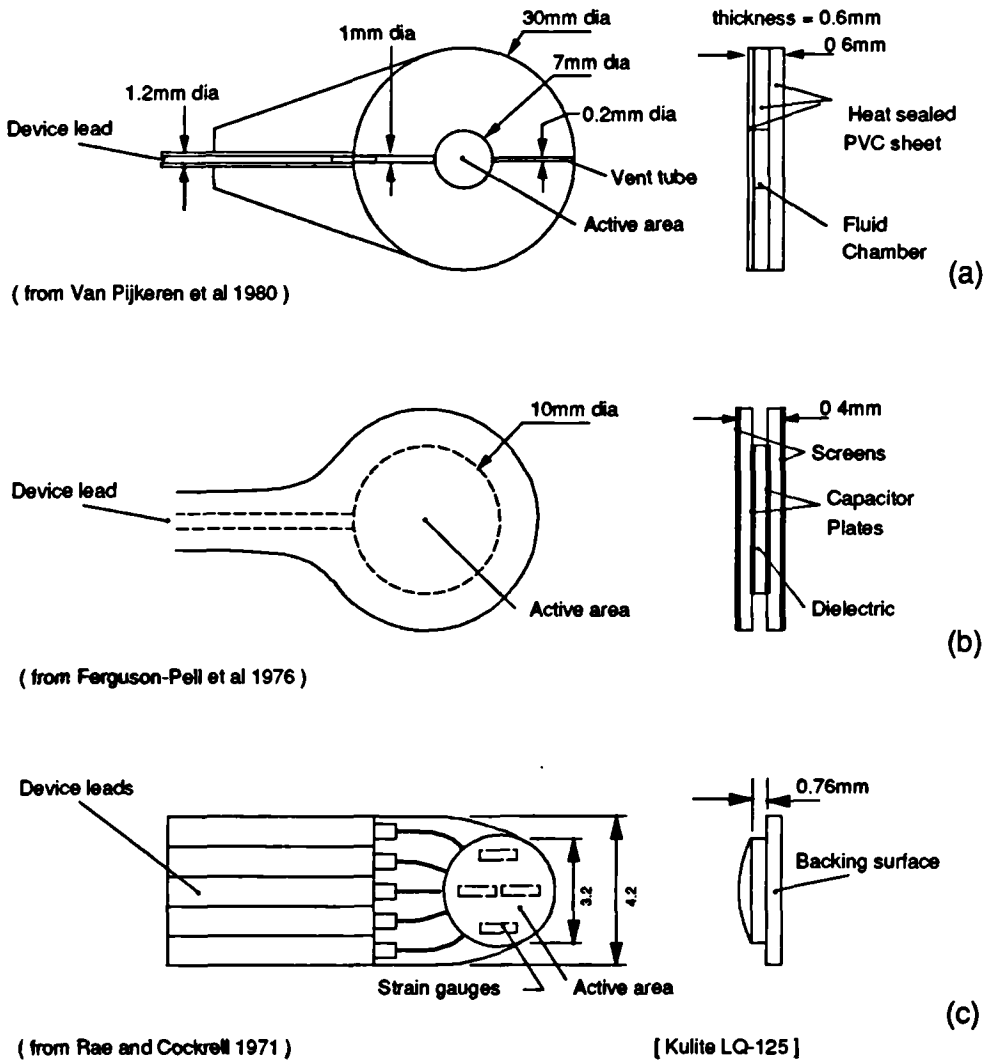

Figure 2.5 Examples of the types of normal stress sensors designed to be inserted between the residual limb and the socket. A fluid filled or pneumatic membrane cell (a); capacitive mode sensor (b); and strain gauge diaphragm type (c).

A linear array of electro-pneumatic membrane cells was developed by **Krouskop et al [1987ab]** to measure interface pressures at fixed intervals along the limb. Each cell was *1.6cm* diameter by *0.01cm* **[1987b]** or *0.5cm* **[1987a]** thick, made from urethane film, and had opposing metallic contacts fixed on inner walls. An external pressure source inflated or deflated each cell until the electrical contacts broke or made conduction, indicating that the source pressure equals the pressure at the interface. Four to six arrays were fixed to the socket with double-sided tape at *2.5cm* intervals. Pressurisation and contact leads were conducted across the

interface to exit at the socket brim where they were attached to an (undescribed) 'electronic readout'. The pressure detection of this device was only quasi-continuous as it was dependent on the rate of the inflation cycles.

The shear stress and temperature response of these devices was not evaluated, nor was the effect of lead tube compressibility on accuracy. Also, it was noted that the vertical elevation of the sensor above the transducer produced an hydrostatic pressure and a change in transducer output.

The other sensor types used by previous investigators and mounted between the limb and the socket, used a mechano-electric transduction principle. Stress sensitive variable capacitance transducers were developed and/or used by **Monster [1972], Meier et al [1973]** and **Ferguson-Pell et al [1976]**.

Monster developed a three plate differential capacitor (*0.001in* brass shim) with two layers of compressible dielectric (#4416 Scotch mount tape, 3M Co, USA). The centre plate was the active terminal and the outer plates the reference or ground terminals of the capacitor. The sensor capacitor formed part of an oscillator circuit. With applied stress the dielectric compresses, increasing the capacitance and thus the oscillator frequency. A comparison between that frequency and another fixed frequency, produced an error signal. That signal was filtered and used as the system output. Bootstrapping techniques were used to reduce cable capacitance and noise. The unstressed capacitance of the transducer was approximately $233pF/m^2$. The same transducer was used by **Meier et al [1973]** to measure interface pressures in below-knee sockets. Transducer attachments were to the limb or socket with double-sided adhesive tape. The sensor had an active surface of *2cm* diameter, and a thickness of *2mm*. Accuracy of the device is given as *±20%*. Some hysteresis was demonstrated but never quantified. The device's shear stress and temperature sensitivity was not reported. The response curves given in the paper are the same as those given by Monster.

A similar three plate capacitor arrangement [see Figure 2.5] was described by **Ferguson-Pell et al [1976]**. The compressible dielectric used was a thin layer of polyester adhesive giving an unstressed capacitance of about *200pF* and a full-scale change of *5pF* (at *500mmHg-66kPa*). Calibration curves, obtained by deadweight loading over a foam load spreading layer, showed the device had better than *1%*

linearity up to *60kg* loading. The device was, then, still under development and detailed performance curves were not presented. No further publications on it have appeared since.

Several researchers have used commercial normal stress transducers employing a strain-gauged silicon diaphragm (LP125, LQ125 : Kulite Semiconductor Products Inc, USA). These devices are disc shaped sealed chambers with a diaphragm sensing surface gauged to respond to circumferential and radial strains. Figure 2.5 describes the transducer outline.

Sonck et al [1970] and **Rae and Cockrell [1971]** developed a system for investigating the effect of liners on the interface stresses in BK sockets. The system was based on digital processing of signals from pressure sensors, goniometers and foot switches. Two commercial pressure sensors were assessed for suitability (M-7F-100 : Scientific Advances Inc, USA and LPS-125-500 Kulite Semiconductor Products Inc, USA) before a joint design effort with Kulite resulted in a revised version of their earlier device (LQS-125-500). Figure 2.5 has a diagram of the dimensions of this sensor. Its natural frequency was given as *350kHz*. The device was calibrated in a pressure vessel by the manufacturer, and all sources of error were less than *1%* full scale (*500psia*). Again, no shear stress or temperature sensitivity was given and errors due to non-hydrostatic loading in the socket were not assessed. The sensors were attached directly to the limb by tape over their leads.

Their revised transducer was used later by **Pearson et al [1973, 1974]** and **Burgess and Moore [1977]**. **Pearson et al [1973]** investigated the effect of alignment changes on the interface pressures in BK PTB prostheses. The transducers were taped directly to the limb at the patellar tendon, medial/lateral tibial condyle, and distal anterior tibia. No mention was made of any calibration procedures. A year later they extended their studies **[Pearson et al 1974]** and developed an analytical model for predicting stresses in PTB suction sockets. The model was verified by performing actual pressure measurements. The positive pressures were measured with the same transducers (LQS-125-500 Kulite), while negative pressures - in the distal socket cavity - were measured with another commercial pressure transducer **(TKM-1 Borfors AG)** mounted externally. Again, there was no mention of any calibration procedures. The positive pressure devices were taped to the limb with

the leads exiting from the brim. While the negative pressures in the socket cavity were conducted by a flexible tube passed through a modified socket suction valve to the external device.

Burgess and Moore [1977] investigated the factors allowing some amputees to ambulate normally without auxillary suspension mechanisms (i.e. only physiological suspension). Six pressure sensors (LQS-125-500 Kulite Inc) were taped (Micropore-3M Corp, USA) to the limb in a line centrally to the gastrocnemius muscle. Five were at *2cm* intervals across the centre of peak muscle movement. The sixth was at the most distal end of the limb. EMG activity, foot switch signals and motion of the limb end into the socket were also monitored. Lead wires exited from the socket brim and were connected to an interface unit worn at the subjects waist. Again no calibration processes were given. A nylon stocking was worn on the residual limb.

2.3.2 Sensors Recessed in Socket Walls

Many workers have attempted to measure limb/socket interface stresses by inserting devices through holes cut in the socket wall **Appoldt et al [1967, 1968a, 1969, 1970; Redhead 1979; Steege et al 1987]**. Their devices were mounted after the subject had donned the socket, and were inserted to a known depth until the interface is just reached. In the earliest study using this technique, **Appoldt and Bennett [1967]** and **Appoldt et al [1968a, 1969]** mounted interface pressure transducers in the socket wall so that their active faces terminated flush to the inside surface and abutted the limb. Each subject (AK amputee) wore their total contact socket without stockings or liners.

The transducer used by **Appoldt and Bennett [1967]** was a commercial strain gauged diaphragm device (Micro-systems Inc, USA). This was a *10mm dia* cylinder *40mm* long with a four gauge (semiconductor) diaphragm at one end and open to the atmosphere at the other. In their follow up study **[Appoldt et al 1968a]** this device was complimented by one of their own design which had improved damping response and pressure gradient sensitivity. The second transducer employed a piston in contact with the limb, the lower end of which was attached to a transverse beam upon which four strain gauges (foil) were bonded. Applied stresses force the piston to bend the beam and cause an increase in gauge resistance. Figure

2.6 describes this design. The natural frequency of both devices was *1kHz*. Calibration of both sensors was by gas pressure behind a rubber diaphragm, which was checked by dead weight loads. Combined hysteresis, repeatability and non-linearity error sources were given as *3%* of indicated load or *±0.5psi* whichever is the larger. No shear or temperature sensitivity was assessed.

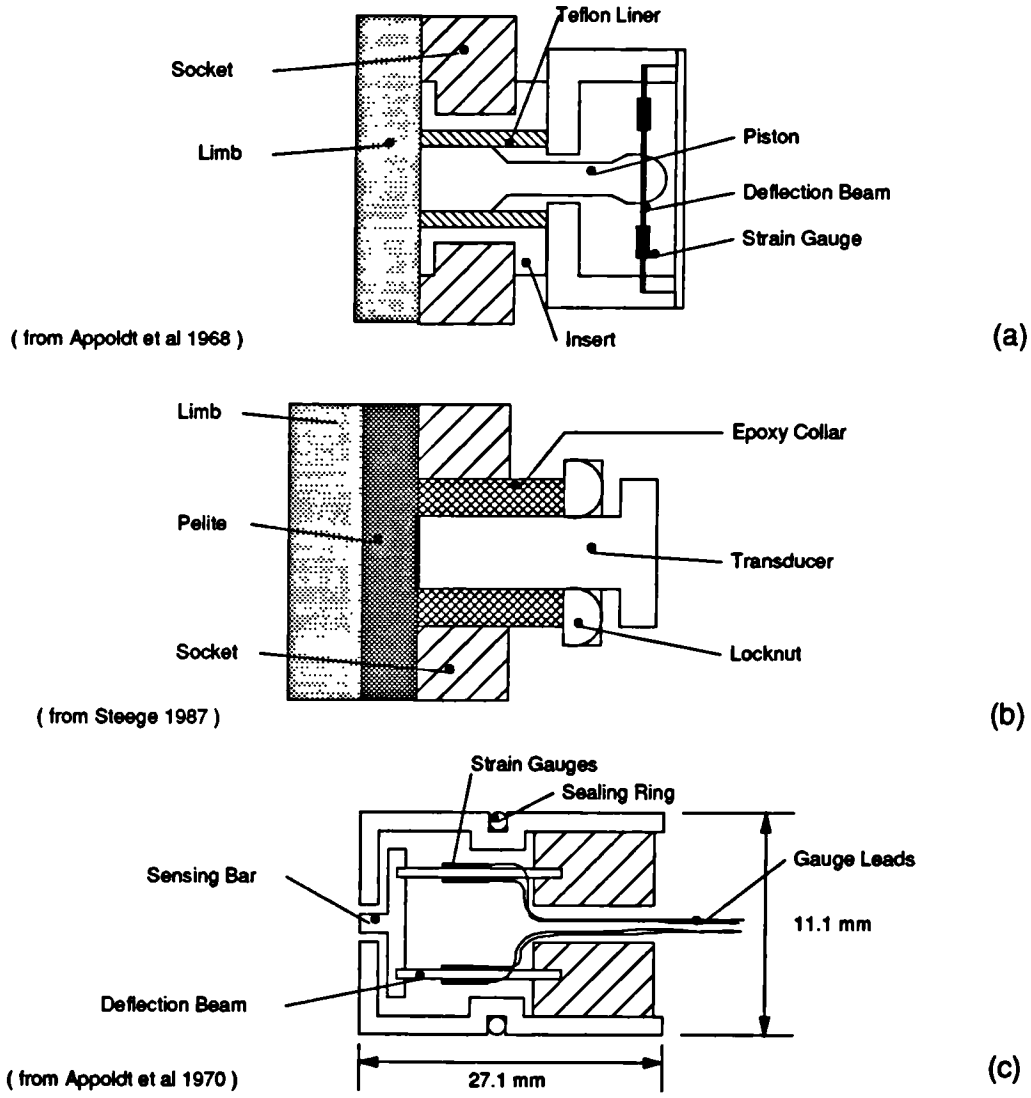

Figure 2.6 Interface stress sensors placed external to the socket with their active surface protruding through holes cut in the socket wall. Piston attached to internal strain gauged beam (a); external strain gauged diaphragm (b); single axis tangential (shear) stress sensor employing a pair of strain gauged deflection beams (c).

The same piston type sensor was used by **Appoldt et al [1969]** to study the effect of transducer protrusion on measured pressures.

Etched silicone diaphragm transducers were used by **Redhead [1979]** and **Steege et al [1987]**. **Redhead [1979]** used transducers (ZPT50A-Ferranti UK), fixed in holders in the socket walls, to measure pressures in total contact self suspending AK sockets. The subject was suspended and the socket applied to the limb with various axial forces.

The etched diaphragm pressure transducers (XTM-190, Kulite, USA) used by **Steege et al [1987]** were inserted through holes in the socket wall, to abut the intact Pelite liner. Figure 2.6 shows the transducer arrangement. The measurement of interface stresses obtained during stance were used to verify finite element models of the limb/socket structure. Calibration was by hydrostatic means with dead weight loading for confirmation. The effect of a layer of Pelite between the dead weight and transducer was to underestimate loads by as much as *30%*.

2.3.3 Instrumented, Isolated Sections of Socket Wall

In a study to determine the patient tolerance levels for bearing normal stresses on the distal end of the limb in a PTB sockets, **Katz et al [1979]** isolated the distal sixth of their sockets. Structural braces were fitted between the prosthesis shank and the remainder of the socket, to maintain rigidity and alignment. Guide rods were attached to the upper socket such that the cut section may be re-inserted and be able to slide axially. A loadcell placed under the section measured the axial stresses applied to the section by the limb. Loadcell calibration was by dead weights in the axial direction. No shear or temperature sensitivity was assessed. Figure 2.7 describes this arrangement. The height of the end section was adjustable to effect increases in end-bearing loads.

The patella tendon depression of the socket wall has been isolated by **Mizrahi et al [1985]** in order to measure the sagittal stresses imposed on it. A section *(5 x 2.5cm)* was cut from the socket and mounted on an external frame. The lower section of the frame was attached to the socket and the prosthesis shank, in such a way as to present the cut section back into its original position. A strain-gauged plate behind the section registered axial and radial stresses applied to the section. Figure 2.7 describes this arrangement.

A similar arrangement was used to study the optimum geometry of the patella tendon depression with respect to load bearing and gait performance by **Vachranukunki et al [1986]**. Additionally to the biaxial stress measurement, force plates measured ground reaction forces and cinematic equipment recorded kinematic data.

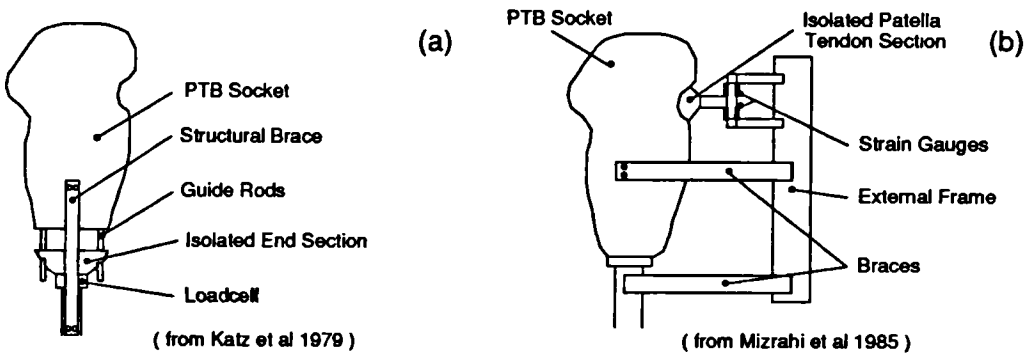

Figure 2.7 Examples of the arrangements used to measure limb/socket stresses by isolating sections of the socket and attaching them to external instruments. Loadcell measurement of limb endbearing stresses (a). Measurement of the biaxial (normal and shear) stresses on the patellar tendon, using a straingauged plate on an external frame (b).

2.3.4 Special Sockets

Akashi et al [1986] briefly describe a special socket fabricated to allow observation of the continuous stress distribution in the socket. A photo elastic material (CY230 epoxy resin) was used to build copies of subjects BK sockets. During full weight bearing stance photographs were taken through a polariscope. Strain-gauges were mounted on the socket at regions of high stress. During normal level gait the strain was recorded continuously. The distribution of stress concentrations varied with each socket, although, the anterior aspect of the tibia, the fibular head and the notches for the hamstrings were common stress points.

2.3.5 Sensors Measuring Shear Stress

There has only been one attempt, to the authors knowledge, to measure shear stresses at the limb/socket interface. **Appoldt et al [1970]** devised a transducer to measure 'tangential pressure' (shear and friction forces). This was designed to be

interchangeable with the transducers used in their earlier work, of measuring normal stresses. Figure 2.6 describes the construction of the transducer. The sensing face is circular with a narrow slit cut across the circumference. A bar *1.6mm* wide is held centrally in the slit by two thin steel deflection beams *(4.76 x 0.41mm).* Four strain gauges on the beams measure the deflection due to applied tangential forces. The transducer was rotated *90%* on successive trials in order to measure both horizontal and vertical 'tangential pressures'. Calibration of the device was by applied static loads in the normal and shear planes. The maximum error from linearity, hysteresis and crosstalk moments from normal stresses was less than *0.2psi (1.4kPa).* However, a limit of *0.4psi (2.8kPa)* was established as the minimum reliable measured stress. Two middle aged AK amputees had copies of their normal sockets (suction type) fitted with *10* to *15* transducer test sites.

Other attempts to measure shear stress fields at the body/support interface are those reported by **Bennett et al [1979], Tappin et al [1980],** and **Pollard et al [1983].**

To study the effectiveness of combined shear and normal stresses in occluding skin blood flow - at the thenar eminence - **Bennett et al [1979]** developed a four sensor device (*2* normal, *1* shear, *1* blood flow). Both the shear and normal stress sensors were the strain-gauged cantilever beam type [see Figure 2.8] and monitor adjacent areas of tissue. A small pad on the end of each cantilever beam, sits flush with the surface of the body of the device - a *77mm* diameter aluminium cylinder. Strain-gauges mounted on the lower section of the cantilever beams converts the beam strains into electrical signals. The maximum displacement of the sensing surface of the shear-stress beam was *0.025mm.* Calibration was by dead weight loading. Shear stress interaction on the normal stress beam was less than *6%.* Normal stress interaction on the shear stress beam was negligible. No further error sources or accuracy values were given.

A small single axis shear stress sensor was developed, for plantar stress studies, by **Tappin et al [1980]** and **Pollard et al [1983].** Although, later **Pollard** added a commercial strain-gauged normal stress sensor (un-named : Kulite Inc, USA) to the top of the shear stress device, in order to record simultaneous normal and shear stresses. These devices were specifically designed as low profile sensors suitable for inserting in shoes or placing under bare feet. Figure 2.8 shows a plan view and exploded assembly sketch of the shear stress transducer. This device is formed from two stainless steel discs bonded together by an elastic medium (silicone rubber).

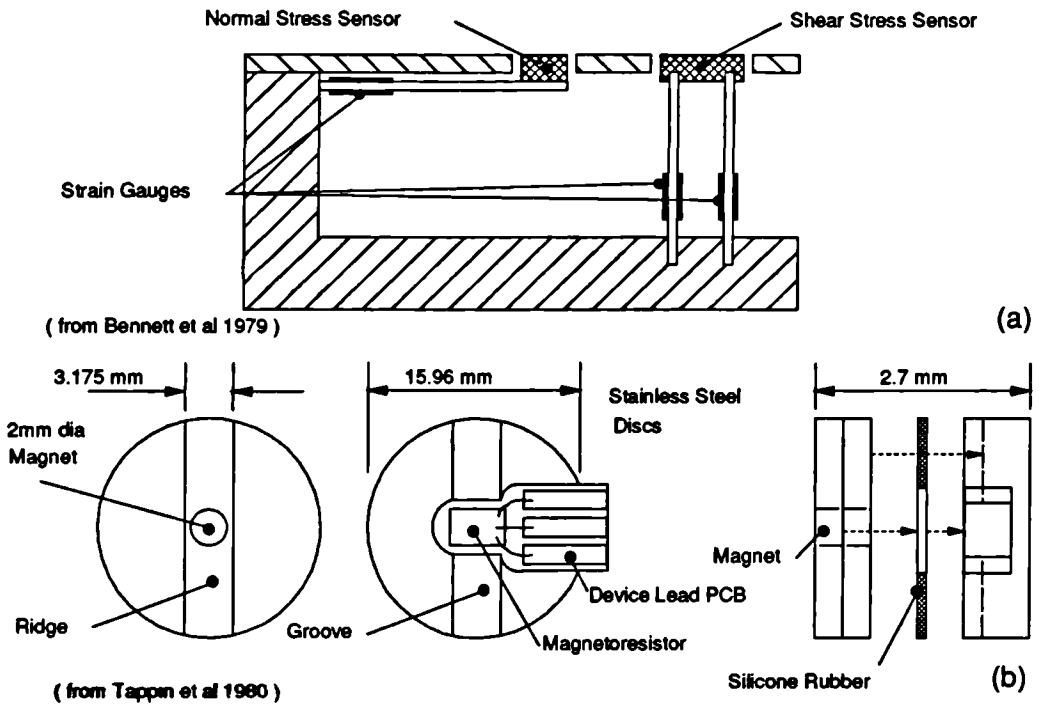

Figure 2.8 Shear stress sensor mechanisms employed in non-prosthetic body/support interface stress studies. Cantilever beam biaxial (normal and shear) stress sensor used on the thenar eminence (a). Single axis device sensing shear by measuring the amount of stretch in a silicone rubber layer (b). A magnet - magnetoresistor pair detect the displacement between discs bonded either side of the rubber layer. This device was employed to measure stresses at the plantar interface.

A ridge across the diagonal of one disc locates into a groove cut across the diagonal of the other disc. The effect of these are to restrict relative displacement of the discs to being along the axis of the ridge. The silicone rubber elasticity acts against the shear force applied between the discs, causing them to displace relative to one another. A magnet is fixed into one disc and a differential magneto-resistor fixed opposite it on the other disc. The relative displacement of the discs, and therefore applied shear force, is detected by a change in the magneto-resistor resistance as the magnet is moved across it. Calibration was by dead weight loading. The device response to load was stated as linear, up to *40N*. Frequency response was assessed by observation of the impulse response and found to be of the order of *500Hz*.

2.3.6 Concurrent Studies

With the exception of the work of **Mizrahi et al [1985]** and **Vachranukunki et al [1986]** all previous studies of interface stresses have employed uniaxial transduction devices. Also only **Appoldt et al [1970]** have attempted to measure shear stresses at the limb socket interface. The author was attempting to address the lack of simultaneous multiaxis data by the development of a triaxial transducer to measure both normal and planar shear stresses. However, the author has since discovered that during the course of this development, concurrent work by **Sanders et al [1989, 1990, 1992]** was being undertaken. Their device is described in Figure 2.9. A strain-gauged diaphragm for detection of normal stresses is fixed on the end of a cantilever beam, which detects biaxial shear stresses. A disc of liner material is affixed to the end of the diaphragm and the transducer inserted through a hole cut in the socket wall until it is flush with the inner socket face. The diaphragm *6.4mm* diameter by *0.17mm* thick. The cantilever beam was *1.6mm* square. Calibration was by static loading. Nonlinearity and crosstalk for the shear axes were less than *1%* and for the normal axes less than *2%*. The largest errors were from cable motion during gait - *5%*. However, due to the length of the device, measurements at the medial aspect of the prosthetic socket are highly improbable.

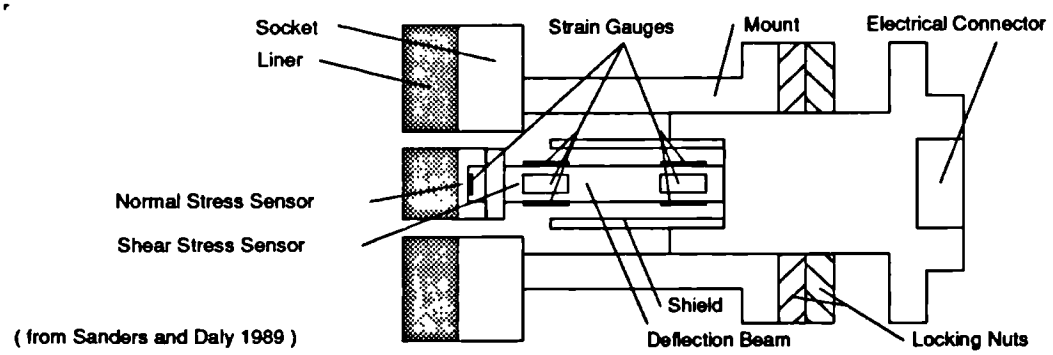

*Figure 2.9 Triaxial stress transducer developed by **Sanders and Daly** [1989] concurrently with the authors. A strain gauged beam detects two orthogonal axes of shear stress. Normal stress is measured by a straingauged diaphragm mounted on the end of the beam. The transducer is inserted through a prepared hole in the socket wall.*

2.3.7 Discussion

The following discusses the suitability of incorporating the mechanisms, previously used to transduce interface stresses, into the three axis stress sensor being developed here.

Although the pneumatic cells developed/used by **Naeff and Van Pijkeren [1980], Krouskop et al [1987]** and **Barbenel and Sockalingham [1990]** are robust and thin, they have potential error sources which have not thoroughly been investigated: their sensitivity to temperature and shear stress have not been evaluated; the curvature of the interface may cause a zero-load pressure offset; compression of the lead tube may produce artifacts, especially as the lead volume is comparable or greater the chamber volume; chamber collapse under local stress concentrations will affect device linearity; vertical elevation of the (fluid filled) sensor above the external transducer will produce hydrostatic pressure errors; the frequency response of these devices may be lower than the bandwidth of the measurand; and the electro-pneumatic type device used by **Krouskop et al [1987]** is only quasi-continuous as it is dependent on the rate of the inflation cycles.

In the context of the three axis transducer required here it would be practical and cost effective to use a common transduction mode for all axes (i.e. all mechano-pneumatic or all mechano-electric). Currently, no mechano-pneumatic transducers exist for the measurement of shear stresses, whereas devices using a mechano-electric principle do exist. For this reason and the above known problems mechano-pneumatic transduction sensors were less preferred than mechano-electric ones.

The stress sensitive variable capacitors developed/used by **Monster [1972], Meier et al [1973]** and **Ferguson-Pell et al [1976]** are compact thin devices that have been proven to be effective. They can be designed to have a linear stress response by employing a dielectric with linear compression characteristics and using a three plate configuration. These devices exhibit a compromise between mechanical stiffness and stress sensitivity. Their temperature coefficient is dominated by that of the dielectric, which can be made extremely small, and they are inherently low noise devices - as the series-equivalent resistance is negligible. However, because the output impedance of the device is usually high, shielding is required on cabling

connecting it to the signal electronics. This may make the cabling of a three axis device complex. Also, consideration must be taken to restrict the device motion to compression as it may be shear sensitive.

Variable resistance strain sensors (strain gauges) are widely used and their technology is well understood. They have an inherently high natural resonance (*10-100kHz*), which is normally dominated by the resonance of the structure on which they are mounted. They are accurate, repeatable sensors with low shear, temperature and humidity sensitivity and good long term stability. Their low electrical impedance also imbues them with low noise sensitivity. Their small size has made them popular in prosthetics applications **[Appoldt et al 1967, 1968a, 1969, 1970; Sonck et al 1970; Rae and Cockrell 1971; Pearson et al 1973, 1974; Burgess and Moore 1977; Redhead 1979; Katz 1979; Mizrahi et al 1985; Vachranukunki et al 1986; Steege et al 1987]**. Their manufacture is specialised so they are generally purchased in a kit form which allows them to be mounted with 'in-house' skills. However, very careful design and precise manufacture needs to be employed for the elastic straining element on which the gauges are mounted. These devices are widely implemented as strain-gauged diaphragms which are designed to measure hydrostatic pressures and will not specifically measure the contact pressure of solid media accurately. Although, the non-hydrostatic pressure measurement errors may be overcome by suitably arranged indentor mechanisms. Additionally, the device aspect ratio must be low to avoid indentation of the limb tissues at the interface, unless they are recessed into the lining or socket wall.

Although magneto-resistor sensors detect changes in the magnetic field applied to them, simple mechanical arrangements can translate mechanical stress to field strength, thus indirectly transducing stress to resistance. Devices based on these sensors have the similar advantages and disadvantages as strain gauge devices.

Another device type commonly used to measure stresses at other body/support interfaces is the compression sensitive variable resistor, also known as Force Sensing Resistors (FSR). This has conductive particles imbedded in a compressible substrate material, such that its resistivity is inversely related to the applied compressive strain. The stress-strain relation for the material is usually non-linear and may exhibit time-dependencies. An evaluation of the accuracy and properties of two leading FSR systems (Interlink Electronics Inc, USA and Teckscan Inc, USA) was

published by **Cardi et al [1991]** and **Ferguson-Pell and Cardi [1992]**. Both systems were shown to exhibit significant hysteresis (*19%, 20%* respectively) and creep rates (*7%/log(sec), 11%/log(sec)* respectively).

Piezo-electric effect devices have been used to measure normal stresses at the foot/shoe interface **[Hennig et al 1982; Nevill 1991]**. The effect occurs in many materials, although, the most commonly used are PZT (Lead Zirconate Titanate) ceramics and PVdF (Polyvinylidene Fluoride) films. Their piezo-electric properties are evoked by complex manufacturing processes. They are known to be sensitive to normal and shear stresses, bending moments and temperature. Although, with careful attention to design and calibration shear, bending and temperature sensitivities can be minimised or compensated for. Piezo-electric devices generate very small electric charges and require special cabling and precision amplifiers to accurately measure these charges without distorting them. The low frequency limit of a recent device was given as *0.01Hz* **[Nevill 1991]** which is inadequate for the monitoring of suspension stresses in sockets. Although shear stress can be transduced with piezo-electric devices, their sensitivity in this mode is very low.

In chosing the transduction methodology for each axis of the stress sensor it was prudent, for efficiency and cost, to employ transduction methods which were related in terms of: conversion mode; support circuitry requirements; and design skills. Also, adapting known transduction technology was preferable to engaging in basic transduction science research. Based on the above review and discussion, mechano-electric transduction principles were used for both the normal and shear stress measurement sections of the tri-axial device.

In the majority of mechano-electric transduction instruments there is a mechanism to convert, in a well behaved manner, the applied force into a mechanical displacement or strain. It is then the strain or displacement which is measured. However, the stiffness of the material which is strained or displaced should bear a reasonable similarity to the surrounding materials at the body support interface. Otherwise the measuring device may cause a significant perturbation to the stress field it is trying to measure.

A strain gauged diaphragm was preferred for the normal stress measurement section of the transducer. This technique, as discussed above, has been well used in prosthetics and is an accurate, low error method that is relatively cheap to make.

The electronics required to excite and buffer the gauges are common and inexpensive. However, to avoid errors due to non-hydrostatic or non-concentric loading an indentor mechanism was used.

Shear stress transduction mechanisms were not previously well explored, so several implementations were considered. Cantilever or simply supported beams could be made as integral members of the section body. Applied shear forces act to strain or displace the beams laterally, and the very small strains which occur may be measured accurately, with strain-gauge technology. However, in order to keep the thickness of the transducer to a minimum, transverse beams and very small strain-gauges are needed. The complexity of design and the manual dexterity required to mount those gauges is considerable. Also, the actual displacements which occur are also generally small, unless long beams are employed - which would compromise the device size. In comparison, thin displacement-sensors are available which are less difficult to handle. They generally incorporate working ranges of *1-2mm.* To utilise the range fully, larger movements are required than are typically achieved with strained beams, so less stiff spring materials must be used. Suitable materials to achieve this are found amongst the elastomers. Thus it was decided to pursue the method used by **Tappin et al [1980]**. This implementation would not compromise the size of the three-axis device as a whole. It is a method of transduction that is cheap, accurate, and compact but relatively easy to construct. It is also resistant to vibration and shock and can be made reasonably insensitive to electrical interference. Further, the equipment and skills necessary to assemble this device could commonly be found in the type of organisation or institution that might use it. Additionally it had been used previously and proved effective under simple calibration and clinical trials.

Clearly a three axes device based on these principles and technologies will not have a suitable size or aspect ratio to be inserted between the limb and socket. It must therefore be designed to be recessed into or inserted through the socket wall.

2.4 Previous Interface Stress Measurements - Findings

It has been observed that well fitting comfortable sockets when coupled with gait training can result in gait patterns that are very similar to normals **[Sonck et al 1970]**. However, there is still no consensus as to what range and patterns of normal and shear stresses constitute comfort. **Krouskop et al [1987ab]** report that amputees felt discomfort at normal stresses of *150mmHg (20kPa)*, while other researchers **[Meier et al 1973; Leavitt et al 1972; Sonck et al 1970]** report amputees able to tolerate normal stresses in excess of *400kPa*. The variation in the magnitude of sustainable stresses between amputees is due to a number of factors, such as: stressed area; stress duration; body weight; thickness of limb tissue; and pain threshold - all of which may be individual to the amputee. So, although the majority of investigators describe their findings in terms of absolute units of mechanical stress (E.g. *psi, mmHg, KPa*), some relate their findings to subject parameters (E.g. percentage of their body weight or peak standing stress).

Comfort limits have been suggested for different sites on the limb. **Katz et al [1979]** suggest that during normal level gait the maximum tolerable load, borne on the limb end, is *11-55%* of the total standing stress on the whole limb. **Vachranukunki et al [1986]** found that subjects could tolerate up to *60%* of their total body weight, in vertical stress, on their patella tendon without pain. Investigators have even attempted to define minimum stress levels as the functional limit of a prosthesis. **Krouskop et al [1987ab]** found that when the peak normal stress (radial), in AK amputees, fell below *12.5kPa* then significant slippage occurs.

A summary of the peak and average stresses measured at any site on the limb, by the investigators reviewed in [2.3], is given in Table 2.1. This describes: the number of subjects studied; the socket type; if a liner was used; the number of sites monitored; the site where maximum stresses mainly occurred; the peak - and (average) - normal and shear stress values observed; and if the study was on static or dynamic stresses. Clearly, the majority of data describes the normal stresses found at the limb/socket interface, while little is known of the shear stresses.

Level	Investigator	Year	# Subjects	Socket type	Liner	# Sites	Site (Peak)	Normal	Shear long'	Shear circum'	Static / Dynamic
AK	Appoldt	1968	2	TP/SS	N	23	B	413(52)			D
	Appoldt	1970	2	TP/SS	N	26	AD		25(9)	31(9)	D
	Leavitt	1972	35	TP/SS	N	5	B	880(170)			D
	Redhead	1979		TP/SS	N		B	160			
	Naeff	1980	2	W/SS	N	100	B	330(50)			D
	Krouskop	1987	18	Q	N	35	B	20(67)			S
	Torres-Moreno	1992	3	Q	N	12	B	86			D
BK	Sonck	1970	26	TP	N/Y	4	PT/AD	830(200)			D
	Rae	1971	26	TP	Y	4	PT/AD	830(200)			D
	Meier	1973	8	TP/SC	N/Y	5	Various	455(151)			D
	Pearson	1973	10	TP	N	4	PT/AD	700(80)			S
	Pearson	1974	10	FG/SS	N	4	DC/MC	130(91)			D
	Steege	1987		TP	N		PT/AD	300			S
	Sanders	1989	1	TP	Y	1	PP	230	26	15	D
	Sanders	1990	1	TP	Y	4	PP	95	55(22)	20	D
	Sanders	1992	3	TP/SC	Y	4	PP	205	54(23)		D
Foot	Poliard	1983	10	-	-	6	-	300	175		D

FG = Fibre Glass Q=Quadrilateral SC=Supercondylar SS=Suction Socket TP=Thermoplastic W=Wooden
AD=Anterodistal B=Brim DC=Distal Cavity MC=Mid Calf PP=Posteroproximal

Table 2.1 A summary of previous investigators studies of residual limb/prosthetic socket interface stresses. The Table describes: the number of subjects studied; the socket type; if a liner was used; the number of sites monitored; the site where maximum stresses mainly occurred; the peak - and (average) - normal and shear stress values observed; and if the study was on static or dynamic stresses. The plantar shear stress measured by ***Pollard et al [1983]*** *is included as an indication of possible peak shear stress values. The data presented by* ***Sanders et al [1990, 1992]*** *is given here as a postscript for comparison with the findings of the work presented in this thesis.*

The peak normal stresses at the limb/socket interface, found by previous studies, vary quite significantly - from *880kPa* **[Leavitt et al 1972]** to *20kPa* **[Krouskop et al 1987ab]**. The margins of the load-bearing sites and the unloaded sites of the socket bear much lower stresses. These have been found to be: < *10%* of peak shear stress **[Appoldt et al 1970]**; < *15-30%* of peak normal stress in AK sockets **[Appoldt et al 1968a; Krouskop et al 1987ab]**; and < *12%* of peak normal stress in BK sockets **[Rae and Cockrell 1971]**. In suction sockets these values may be higher in order to create an effective pressure seal for prosthesis suspension.

Appoldt et al [1970] and **Sanders et al [1989, 1990, 1992]**[1] are, to date, the only other investigators to quantify shear stresses at the interface. They all indicate that shear stresses are much lower in magnitude than normal stresses, *25-55kPa*. The coefficient of friction which sustains the shear stresses varies with site, lubrication and subject. **Sanders et al [1992]** report a range of *0.01-0.55* while **Appoldt et al [1970]** found a range of *0.25-0.4* with an average value of *0.3*.

The general concensus of findings shows that stresses vary with: area of the limb studied; whether dynamic or static stresses are being measured; how much muscle activity occurs; whether liners are used; and prosthetic alignment. Thus, before data can be compared, between workers, there must clearly be a common protocol.

By design the load transfer from limb to socket is distributed over those areas of the limb which are thought to be load tolerant. Specific emphasis is directed at placing a significant portion of the load through the patella tendon shelf of the PTB socket, hence its name. However, **Rae and Cockrell [1971]** and **Meier et al [1973]** observed that the patella tendon shelf is not always the area bearing the largest weight. The anterodistal site (kickpoint) can often experience larger pressures **[Sonck et al 1970]**, highlighting the need for a well muscle padded end tibia - constructed during surgery. Indeed, there may be other problem areas in some patients sockets which, in error, are generating the largest stresses.

Mizrahi et al [1985] observed that approximately *33%* of ground reaction forces are directed through the patella tendon shelf. This was supported by **Vachranukunki et al [1986]** who observed that about *30%* body weight was supported normally and *5%* body weight supported in shear at the patella tendon shelf. They also

1 N.B. the work of **Sanders et al [1989, 1990, 1992]** is added here as a postscript, at the time of compiling this thesis, for comparison of data.

observed that subjects could tolerate up to *60%* body weight in normal stress at the site, and that gait performance and stability increased with increased load. Stresses in sockets are not always positive in magnitude. Large negative (suction) pressures can exist in the distal cavity of sockets. Indeed, suction sockets employ this as a means of socket suspension during swing phase. **Pearson et al [1974]** measured the persistence time of the negative pressure in the distal socket cavity to be of the order of *16 sec* during level gait. The repetitive load cycling during gait had a pumping effect that increased peak pressure to *-300mmHg (-40kPa).*

Individual variations in the observed stresses, at the limb/socket interface, during standing occur with day to day differences in socket donning or while establishing and maintaining balance. These are, however, relatively minor compared to changes due to muscle contraction and the inertial and leverage effects of gait **[Pearson et al 1973, Redhead 1979]**. The stresses generated during gait are known to be higher in magnitude than those found in normal standing. **Appoldt et al [1969]** suggested that standing pressures are approximately *45%* of peak gait pressures. Although, **Pearson et al [1973]** suggests that this ratio varies with site.

The stress fields at the limb/socket interface are periodic with the gait cycle. A peak in the field moves across and up the limb as the prosthesis is loaded at heelstrike **[Rae and Cockrell 1971]**. **Leavitt et al [1972]** and **Sanders et al [1990]** found that step to step variations in pressure are small. But, **Appoldt et al [1968a]** found significant differences in the stress patterns when taken weeks and months apart. This they attributed to socket donning procedures; fatigue; temporary changes in stump size; and instrumentation drift.

Muscle contraction alone can alter the interface normal stress by approximately *10kPa* **[Redhead 1979]**. **Pearson et al [1974]** observed that the negative pressure in the distal socket cavity could be increased by *16.75kPa* by the tensing of limb muscles. As the patient alters their gait pace and balance, the changes in muscle contractions will alter the measured interface pressures. **Burgess and Moore [1977]** showed that some amputees re-learn new muscle activity sequences for their gait cycles. Some were even able to generate sufficient stresses by muscle activity to provide socket suspension during swing phase.

Alignment of the prosthetic limb components was also found to affect observed interface stress patterns. **Appoldt et al [1968a]** were of the opinion that alignment

variations of *5°*, which were considered large, in AK prostheses produced a measurable stress difference but appeared not to affect the observed gait of the subject. Extreme changes in posterior alignment, observed by **Pearson et al [1973]**, resulted in elevated normal stresses at the patella tendon and lateral condyles, when the subject accelerates. But stress magnitudes during steady level gait did not seem to be effected. The phasing or time relationship of the stress waveforms over the gait cycle were altered, resulting in a large delay during steady gait and deceleration steps. Extreme lateral alignment offsets also produced large magnitude variations at some sites and resulted in waveform delays over the gait cycle.

Sonck et al [1970] demonstrated that soft liners can significantly reduce peak pressures at the limb/socket interface during gait. Gel liners were found to be specifically effective in this respect. They suggested that the gel liners achieve this by uniformly distributing the load locally. A simplified mechanical theory to support this suggestion, and substantiating laboratory experiments, were later effected by **Bennett [1974]**. The suggestion is still currently accepted. However, no experimental data is yet available on how liners may distribute shear stresses.

Of the investigators who have recorded interface stresses in BK prosthetic sockets [Table 2.1] only **Meier et al [1973]** did not present representative normal stress waveforms. The others report regular cyclic waveforms that are clearly biphasic during the stance phase of the gait cycle. The waveform has an initial peak at *20-35%* into the stance and a second peak at *60-85%*. **Sanders et al [1992]** suggests that the maximal stresses within the step usually occur at the first peak, except at anteroproximal or patella tendon sites. This observation appears to be bourne out by the example waveforms of other workers. **Appoldt et al [1968a]** showed that shear stresses in the longitudinal and circumferential axes of the socket occur concurrently with normal stresses. Also, that they too have regular patterns. **Sanders et al [1989, 1990, 1992]** are the only researchers to present shear stress data from BK sockets. They describe waveforms similar to the normal stresses but with less pronounced biphasism. The peaks of these waveforms occurred synchronously with those of the normal stress waves.

The frequency content of a typical normal stress waveform was calculated by **Rae and Cockrell [1971]**. It was found that the relative amplitude of the spectrum

fell below *10%* at approximately *20Hz*. Although, the method of calculation used and the sample window taken from the stress curve meant that higher harmonics appeared in the result. The true spectrum bandwidth was probably closer to *10Hz*.

2.5 Temperatures in Prosthetic Sockets

To the author's knowledge no studies of the temperatures to be found in prosthetic sockets, during ambulation, have been published. However, **Ferguson-Pell [1980]** writes that **Adamson [1978]** states the temperature at body/support surfaces usually varies little throughout the measurement period, within the range *32-37*℃. Also, that the difference between ambient and body temperature is significant (*0-15*℃) and requires the transducer to be stable over this range (say *17-37*℃)

Ferguson-Pell et al [1985] measured temperature and humidity changes between patients' buttocks and seating cushions. It was observed that the maximum change in temperature after two hours was *3.75*℃, and the maximum change in relative humidity was *39%*.

To confirm this data in relation to changes in limb/socket interface temperature during ambulation an experiment was carried out with an active unilateral BK amputee. A thermistor type temperature sensor (*1mm* diameter), was placed against the subject's skin and the sensor lead taped to his limb inside the pelite liner in his standard PTB prosthesis. The subject walked continuously for *400m* without resting. The temperature was recorded at the beginning of the trial and after every *10m*. Figure 2.10 describes the increase in temperature with distance walked. From an initial value of *33.2*℃ the temperature rose to *35.4*℃ in an asymptotic fashion. Extrapolation of the curve estimates the maximum rise to be of the order of *2.5*℃. No change in temperature over any given gait cycle was observed.

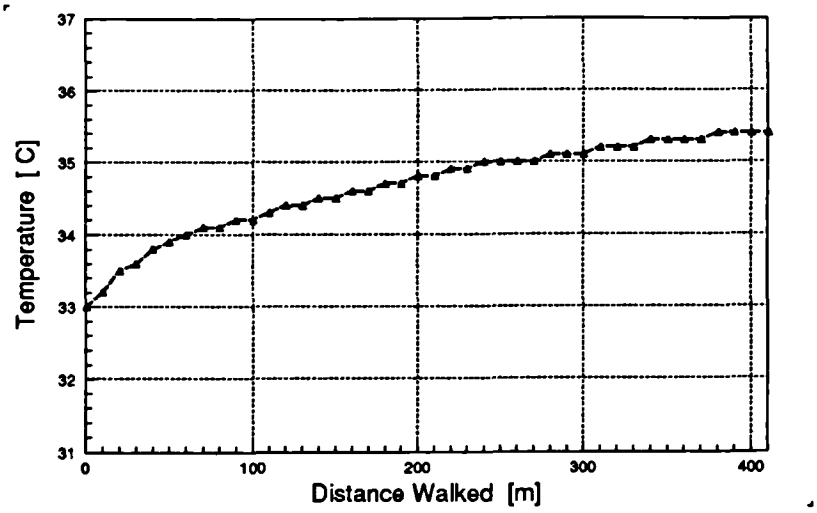

Figure 2.10 Measured temperature variation at the residual limb/prosthetic socket (BK) interface as a function of distance walked.

2.6 Transducer Design Criteria

The initial steps in the triaxial stress transducer design process were to observe the previously determined, or expected, nature of the measurands and then to set the performance/geometry specification of the device. The interface stress transduction system as a whole will be at its most useful if it is able to accurately transform stresses into a quantifiable property which is in turn recorded in a reviewable format.

From the discussion in [2.4] the magnitude, direction and frequency content of the stress field may be estimated. It is known that normal (radial) stresses, mediolateral (circumferential) and proximodistal (longitudinal) shear stresses occur at the limb-socket interface. Previous measurements of radial stresses vary greatly in the observed maximum magnitude, from *19.8kpa* **[Krouskop et al 1987]** to *827kPa* (*241kPa* average) **[Sonk et al 1970]**. Circumferential and longitudinal shear stresses are also active, simultaneously, in a regular pattern during the gait cycle **Appoldt et al [1968a]**. **Appoldt et al [1970]** were able to demonstrate that the shearing stresses at the limb/socket interface are much smaller (*2-8kPa*) than the coincident radial stresses. The stress sensitivity and range of the transduction mechanism, of the sensor described here, must reflect these findings. It is recognised that where stresses are derived from strains, there is an inherent compromise between range and sensitivity. There is a limit to the practical range of deflections over which

the stress-strain relationship in transduction materials is linear. Sensitivity requirements favour soft deflection beams, however stiff beams will allow a greater range of forces to be transduced. An additional consideration to be made in regard to transducer stiffness, is that if it presents a significantly different stiffness than the surrounding material of the interface region the transducer will distort the stress field it is attempting to measure.

Because three mutually orthogonal stress vectors are to be transduced it is important that there be three parts of the transducer device each sensitive to only one stress vector and insensitive to the other two. Each part should also be insensitive to other stimuli, such as temperature, humidity and chemical attack. The transformation characteristic should ideally be linear and exhibit minimal hysteresis.

The spectral content of recorded stress signals has been derived by **Rae and Cockrell [1971]**. The relative spectral amplitude was found to be significant (*>10%*) only in the range *0-20Hz*. **Antonsson and Mann [1985]** recorded the gait spectra of *12* normal subjects using forceplates. They observed that 'no amplitudes greater than *5%* of the fundamental [frequency] existed above *10Hz*, none greater than *2%* above *20Hz*, and all amplitudes greater than *1%* were contained below *50Hz*'. Also, *99%* of the power in the spectrum was below *15Hz*. In order for the transducer to respond to the rate of change of stress at the interface it must have a natural (resonant) frequency very much greater than the expected maximum stress frequency (*50Hz*). Ideally it should also be critically damped, for accuracy in following changes in stress.

Related to the frequency response, a constant group delay response, of the system as a whole, over the bandwidth of the measurand is desirable. In gait related stresses, step transients occur which have a wide spectrum content, each component of which must experience the same processing delay in order to maintain fidelity.

The accuracy of the conversion constant, or polynomial, associated with the transducer will generally incorporate errors due to nonlinearity, hysteresis, axes crosstalk and signal processing. Previous workers transducers have quoted accuracies of between *1%* and *20%*.

Calibration of the transduction device should be carried out in a mode under which it will be employed at the interface. It is unlikely that truly hydrostatic conditions

prevail at the limb/socket interface. The agency of stress transferral is dependent on: the proximity of bony prominences; the age and condition of the skin; the state of muscle and fascia tissues; and the frictional properties of the interface region. Therefore calibration techniques must mimic the way stresses are transmitted through semi-elastic mobile material like skin. They should also provide an estimate of the variation in transducer response to extremes of tissue compliance and to the proximity of bony prominences. Alternatively the device could be designed to avoid the requirement for limb tissue conformability.

Calibration data should hold for a reasonable period of time, in relation to the ease of recalibration. The useful life time (number of gait cycles) of the transducer must be relative to the capital cost and the ease of installation.

As friction is necessary for the formation of shear stresses, to minimise incongruity in the stress field due to the presence of the transducer, the sensing surface of the device must have a similar friction coefficient to that found locally at the interface.

Appoldt et al [1969] showed that when the stress transducer protruded from the socket wall into the flesh of the limb, it indicated larger pressures (*150%-400%*) than did a flush mounted transducer. This effect tends to be greater in areas of bony prominences or tensed muscle. It is thought that this is due to a membrane effect. As the membrane becomes stiffer its ability to conform to protrusions diminishes, causing a hammocking effect and thus concentrating local loading on the protrusion. Errors due to transducer protrusion also tend to be greater when the actual local pressure is high. This phenomena is probably due to the non-linear stress-strain relationship of skin. At high stresses it will increase in stiffness, and the hammocking effect will take place. Protrusion will also have an effect of the local shear stress fields - probably significantly - although these have not been quantified.

An evaluation of the accuracy of five small flat (*2.2-6.4mm x 1mm*) strain-gauge diaphragm transducers was carried out by **Patterson and Fisher [1979]**. In-vitro tests, under rubber and cloth surfaces, and in-vivo tests, under a blood pressure cuff at four sites of the lower leg, were carried out. From the in-vitro experiments the pressure measurement errors were least when the devices were compressed by the rubber balloon (condom). The largest errors were found in the devices with the smallest diameter (*15%* - rubber, *70%* - cloth). Adding a dome of rubber to

the sensing surface of the smallest diameter device was seen to reduce the measurement error, although it was still significant. During in-vivo tests errors were largest when the devices were placed over bony prominences (tibial crest) and least when placed over soft tissue (gastrocnemius). Again the small diameter transducers gave the largest errors. However, all the transducers performed poorly where the soft tissue thickness was minimal. Placing a small rubber dome on the sensing surface produced offset errors and large overestimates of applied pressure.

Ferguson-Pell [1980] attempted to analytically derive dimension recommendations for normal stress sensors placed between the body and its support surface. The analysis was concerned that the sensor itself did not perturb the stress field it was measuring and that it would indicate the peak pressures imposed on it, with a minimum of area averaging. This analysis was dependent on the mechanical properties of the interface materials. Skin was assumed to be homogeneous, isotropic, elastic, linear and time independent - clearly gross assumptions. Estimates of the support surface properties were made and a *5%* error in the measurement of peak pressure was taken as acceptable. It was suggested that the thickness to diameter ratio of *1:30* was appropriate. Where large interface stresses were to be measured this ratio could be reduced to *1:10*. Because there may be significant pressure gradients over the interface (*0.5kPa/mm* **[Kosiak et al 1958]**) the suggested sensor diameter should ideally be small (*1.4mm*). Although, the specified diameter here of *14mm* and thickness of *0.5mm* was considered as acceptable for most low pressure measurements (*0 - 40kPa*). Other considerations discussed were that: the radius of the transducer should be small relative to the radius of curvature of the interface; the hysteresis inherent in the device should be minimised; the frequency and magnitude response of the device should be greater than the expected stresses; the sensor stress response should be independent of temperature and humidity; and safety codes, electrical and mechanical, must be strictly adhered to in order to avoid possible hazards.

Summary

Small diameter, low aspect-ratio transducers would cause less disturbance and more accurately reflect the peak pressures to be found at the body/support interface **[Ferguson-Pell 1980]**. **Patterson and Fisher [1979]** also demonstrated that small diameter, high aspect-ratio transducers were most likely to produce greater errors than larger diameter, low aspect-ratio devices. Also, significant errors occurred

when any device was placed over bony prominences. These findings are confirmed by **Appoldt et al [1969]**. As it is unlikely that a three axis transducer could be made into a small diameter, low aspect-ratio package, the above difficulties could initially be avoided by designing the transducer to be recessed into the socket wall. The active face of the device being made flush with the inside surface.

By creating a predefined actuator for the normal stress section of the transducer, the problem of skin surface conformance was avoided. Also, to ensure friction and stiffness uniformity across the interface region, a layer of the interface material was bonded to the active face of the transducer.

Table 2.2 lists the major performance specifications to be aimed at during the design process.

Parameter	*Shear stress section*	*Normal stress section*
Measurement Range	*0 - 250 KPa*	*0 - 500 KPa*
Withstand Overload	*500 KPa*	*1000 KPa*
Accuracy	*The greater of: ± 5% indicated load or 2.5 KPa*	
Temperature Range	*20 - 40 ℃*	
Frequency Range	*0.5 mHz - 500 Hz*	
Lifetime (gait cycles)	*20000*	
Dimensions	*15 mm diameter x 5 mm*	
Mass	*< 10 g*	

Table 2.2 Proposed performance specification for the triaxial stress transducer.

Without much shear stress data from other investigators it was difficult to create a definite specification for the shear transducer. The values given in Table 2.2 represent conservative estimates for the expected shear stresses at any body/support interface. Those stresses found at the foot/shoe interface were most likely to be the greatest experienced by the body in its daily activities. Thus the measurement range for the shear stress transducer was an estimate arrived at from a consideration of the work of **Pollard et al [1983]**. From the results of studies on normal stresses

found at other body/support interfaces, the value given in Table 2.2 for the measurement range was a compromise between range and resolution. Although **Sonk et al [1970]** observed stresses outside this range, those were extreme values and it was felt less important to measure accurately their magnitude than it was to record their presence. Thus, to allow for their presence to be recorded the overload range was set to be greater than their magnitude. Also, it was felt that resolution at the lower ranges was important. The overload value was the maximum load up-to-which the transducer can be subjected without permanent damage or requiring recalibration. The measurement range was the expected range within which almost all of the stresses found at the body/support interface will fall. They included errors due to nonlinearities, hysteresis, creep and temperature sensitivities.

The accuracy figures given were targets to aim for. It was felt that data accurate to better than *10%* was adequate for early research work. However, it was thought that *5%* was achievable with the facilities available to the author.

The temperature range defines the temperatures over which the transducer calibration was to be constant. The expected range of temperatures at the limb/socket interface was approximately *32-37* ℃. While the temperature variation during a clinical trial was not expected to exceed *2.5* ℃ [see 2.4].

Frequency considerations were based around the frequency spectrum of gait cycle stresses and the period of typical clinical measurement sessions. **Antonsson and Mann [1985]** found that there were no significant frequency components in gait above *50Hz*. Thus, as the frequency response of the transducer should be much greater than that, a factor of ten was used to set the upper limit. The lower limit was arrived at from a composite argument. Firstly, for accurate quantitative stress measurements the transform characteristics of the sensor was to be stable during the measurement period (approximately *20-30* minutes). Secondly, if the device suffered from plastic (irreversible) deformation under stress, then to maximise the period between calibrations, this deformation must be very slow. Thirdly, there was strictly no such thing as *0Hz*, although practically speaking stress measurement devices are available with extremely stable characteristics. Thus, the lower frequency limit was set to the longest expected clinical trial period, and was viewed as the maximum acceptable value to aim for.

Values placed on the device's size and weight were only given as reasonable estimates based on minimising the weight of a transducer array and a compromise between construction complexity and radii of curvature in sockets.

The lifetime of the device reflects the period between calibrations (if complex) or major reconstruction. It is given in gait cycles and represents a period of over *100* clinical trials.

Chapter 3
Triaxial Stress Transducer - Prototype Design

Chapter 2 reviewed of the methodologies used by previous researchers and discussed other options for stress transduction mechanisms which could be employed in a transducer for this application. These are summarised in the discussion of [2.3.7]. Based on these reviews two mechanisms for the transduction of a) shear stresses and b) normal stresses were selected. This chapter details: the principle mode of operation of each of these mechanisms; and details the design considerations and initial development stages of transducer to meet the performance specifications proposed in [2.6].

Each axis of the transducer is essentially self contained and thus the overall device can be thought of as the combination of three separate sections. For this chapter the transducer will be referred to as two subassemblies; a biaxial shear-stress section and a uniaxial normal-stress section. An overview of the principle of operation of each section is presented in different divisions of the chapter [3.1 for shear section & 3.2 for normal section]. The chronological sequence of the many implementation and appraisal phases of the transducer development is summarised into three design stages:

a) the section design, operating principles, and the initial component selection for a prototype device;
b) the performance appraisal of the prototype and component reselection;
c) and final device performance tests.

The first stage is described here in Chapter 3 while the latter two are presented in Chapter 4.

3.1 Shear-Section Design

The following presents the general design of the section of the transducer which converts shear stresses into electrical signals. It describes the principle of operation

of this section and reports the process of selection of components for a prototype device. Details of the assembly equipment and procedures for the prototype are also given.

3.1.1 Principle of Operation

The sensing element is a semiconductor resistor (magneto-resistor) whose resistance varies with the strength of any magnetic field applied perpendicular to its face. The element is formed as two identical active regions connected in series with a centre-tapped output termination. It is a three terminal device whose output is proportional to the difference in magnetic field between the two active regions on the element. If a small magnet is suspended in close proximity and centrally above the element then its output will be half its input. Figure 3.1 is a schematic of this arrangement to illustrate this concept. Any lateral displacement of the magnet will alter the ratio of magnetic field experienced by the two active regions, and hence the element's output will change in proportion to the movement. Moving the magnet in one direction will have the effect of increasing the output, whilst movement in the opposite direction will decrease the output. Thus the direction and distance of any displacement of the magnet can be observed.

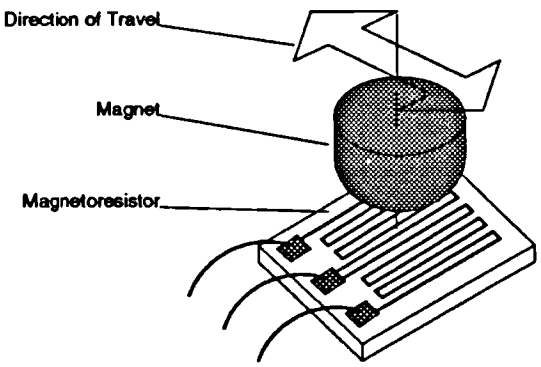

Figure 3.1 Principle of shear stress transduction using magneto-resistive element and magnet. Lateral displacement of the magnet changes the resistance of one active area of the element with respect to the other. This alters the ratio of the output to input.

The magnet is fixed into the centre of a rigid disc and the magneto-resistor (**MR**) fixed into the centre of another. The two discs are arranged parallel to one another with a fixed separation. They are then coupled together by an elastic medium that acts to maintain the discs central to each other. When a sliding/shearing force is applied to the discs it acts against the elastic medium and displaces one of the

discs a distance proportional to the applied force. This displacement is sensed by the magnet/element combination by causing the output of the MR to change in magnitude proportional to the displacement of the magnet and in sign relating to the direction of the applied stress.

Each magnet/element pair is uniaxial. That is, the element output will only change when the magnet is displaced transversely (movement away from one active region toward the other). To enable the overall transducer to discern the direction and magnitude (vector) of the stress component parallel to the shear plane, it is necessary to have at least two of these shear transducing elements at a fixed orientation to each other. The most effective way of achieving this is to fix the two elements orthogonally, and to restrict the relative motion of the magnet to be transverse to each element. This was accomplished by fabricating, a central ridge on the magnet disc and a corresponding groove in the element disc. When these are located the discs are mechanically constrained to slide over each other along one axis only. The second element is identical but the ridge and groove are orthogonal to the first. The magnet for the second axis is the opposite pole of the magnet for the first axis. An exploded assembly of the biaxial shear section is shown in Figure 3.2. and a schematic of it fully assembled is shown in Figure 3.3.

In using the sliding disk method of shear-stress transduction there are two fundamental mechanisms operating. The first is the conversion of the applied shear stresses into a displacement, via the elastic or spring material. The second is the transduction of displacement into an electrical signal. During the initial survey and design phase these were treated separately. Each being assayed and selected according to the predominant attribute they were required to have.

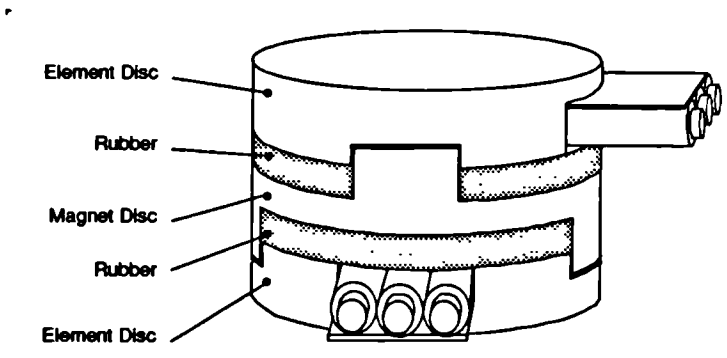

Figure 3.3 Schematic of fully assembled biaxial force transducer.

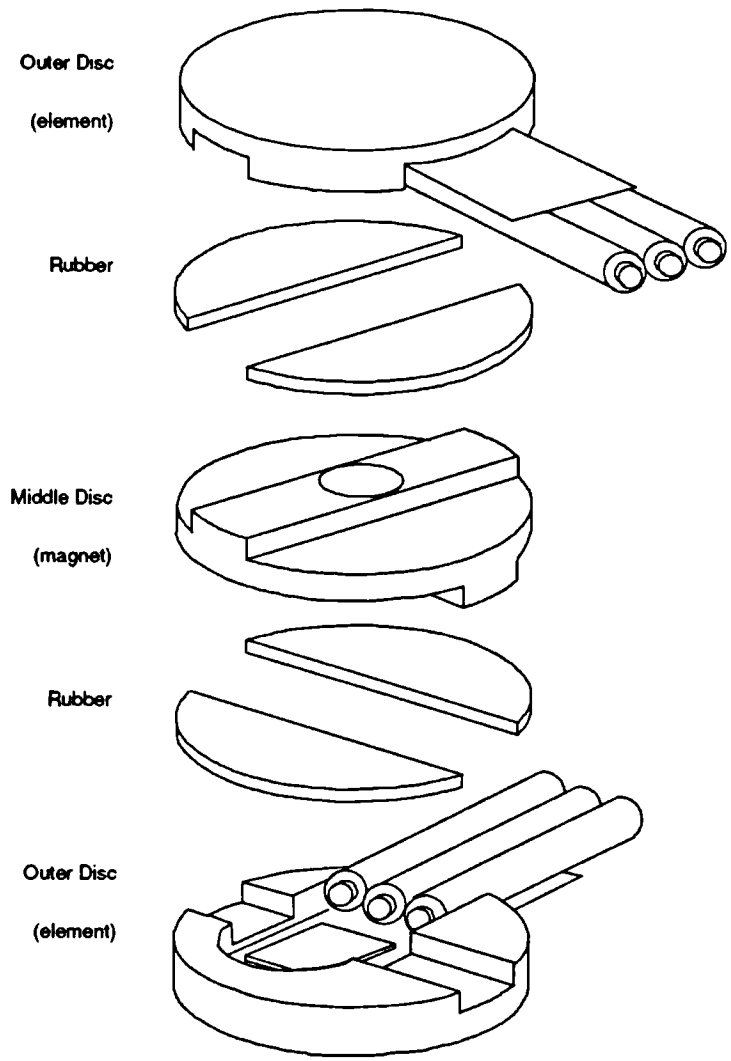

Figure 3.2 Schematic of the exploded assembly of the two shear sections.

3.1.2 Force to Displacement Conversion

The primary requirement of the first mechanism in the shear section is to provide a reproducible restoring force that opposes the applied shearing stresses. It must be truly elastic, that is, it must have a fully recoverable strain on release of the applied force. It should also usefully have a linear stress-strain relation. Or simply put what is required is a material that obeys Hooke's Law at large deformations. The useful measurement range of suitable commercial displacement-sensor elements

was *1-2mm.* The maximum expected clinical force range was approximately *±50N*, indicating a target stiffness of the elastic material of *25-50N/mm.* To meet that requirement in a compact size, elastomers was considered for their suitability.

The following subsections discuss the effective limitations of using an elastomer as a Hookean spring under static and dynamic stresses. This is followed by the selection of the most appropriate type for this application.

3.1.2.1 Rubber as a Spring

In leading up to the decision to utilize elastomers as the springing material, an investigation into their theoretical physical properties was carried out. The following section summarises the findings of these investigations.

The term 'Rubber' is commonly used to describe any material that can sustain large elastic deformations (strains), typically of the order of *500* to *1000%.* These materials include synthetics such as Teflon, Butyl rubber and Silicones, and naturals such as natural-rubber (polyisoprene), wool, silk and muscle. Figure 3.4 illustrates the structural formulae of the monomer units of some rubbers. Rubbers are members of the class of high polymers which are constituted of very long chain molecules that are both chemical interlinked and physically tangled at sparse irregular intervals. Figure 3.5 illustrates the concept of sparse cross-linking and tangled chains.

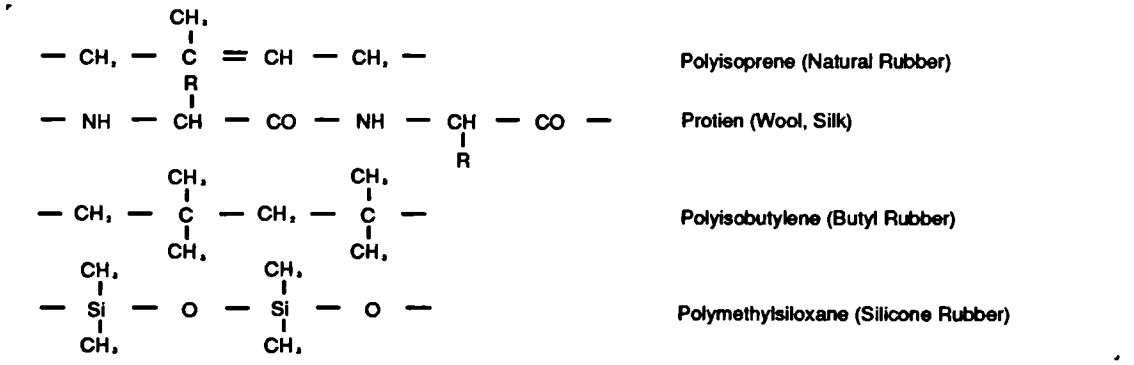

Figure 3.4 Schematic of the structural formulae of some typical elastomer materials (after ***Treloar [1958]*** *).*

The foundations of the theory relating the molecular structure of rubbers to their elastic properties were postulated by Meyer, von Susich and Volko as reported in **Treloar [1958].** They considered that the thermal or kinetic vibrations of each

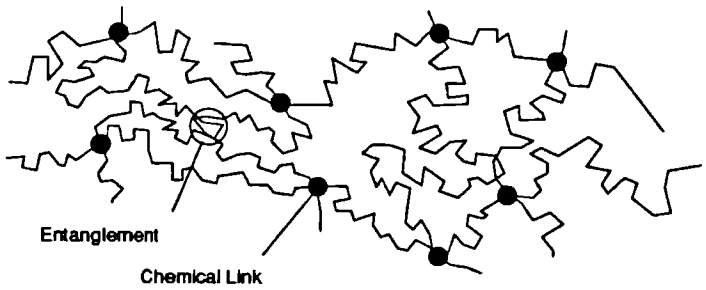

Figure 3.5 Schematic of the cross-linking and tangling between molecular chains of an amorphous polymer.

molecular chain tended to repel its neighbour and draw the ends of the chains together. This retraction occurs until an equilibrium is reached where the chains have a random statistically determinate arrangement and there is no nett force. These ideas were developed to formulate a statistical kinetic theory based on the configurational entropy of the chains. The assumptions of this theory were that the rubber was amorphous, isotropic and incompressible and the distribution of chain lengths between cross links is statistically related. All of which hold well for most rubbers. The kinetic theory accounted satisfactorily for the observed mechanical behaviour at equilibrium under relatively large elastic deformations. It also implies that the stress and strain relations can be simply derived from the equation for the elastic stored energy per unit volume. This energy is a function of the strain and one physical parameter or elastic modulus that is soley determined by the degree of cross-linking in the material **Treloar [1958]**.

$$W = \frac{1}{2}G(\lambda_x^2+\lambda_y^2+\lambda_z^2-3) \qquad (3.0)$$

Where W is the work of deformation or the elastically stored force energy per unit volume of the rubber. Here, $(\lambda_x,\lambda_y,\lambda_z)$ are the principle extension ratios along three orthogonal axes, and G is the elastic modulus.

This theory enabled the prediction of elastic behaviour of any rubber under all modes of strain [E.g. tension, compression, shear]. Table 3.1 shows the form of the stress strain relations for each mode, as calculated by the statistical theory. In its simplest form it assumes that the separation distances between each end of a chain is as a Gaussian distribution. This assumption holds as long as the rubber is less than moderately stretched.

Mode	*Approx Stress-Strain Relationship*
Simple Elongation	$t = G\left(\lambda^2 - \frac{1}{\lambda}\right)$
2D Extension/Compression	$t = G\left(\lambda^2 - \frac{1}{\lambda^4}\right)$
Simple Shear	$t = G\left(\lambda - \frac{1}{\lambda}\right) = G\sigma$
Pure Shear	$t_x = G\left(\lambda^2 - \frac{1}{\lambda^2}\right)$ $t_y = G\left(1 - \frac{1}{\lambda^2}\right)$

Table 3.1. Theoretical stress-strain relation for rubber's subjected to moderate deformations. Determined from the statistical kinetic theory assuming a Gaussian network.

The most significant point to note from Table 3.1 is that the Gaussian form of the theory predicts that in rubber, strain is proportional to the stress only in the simple shear mode. This is not the case for the other modes of deformation. **Treloar [1958]** in a review of his early work showed that the experimental data conforms quite closely to the theoretical values up to about *100%* strain. This is also described by **Lindley [1978]**. Figure 3.6 is an example of Treloar's data for natural-rubber under shear.

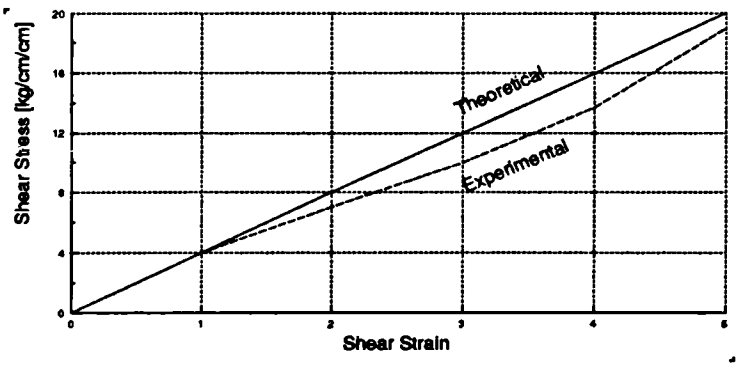

*Figure 3.6 The relation of shear stress to shear strain for a sample of Natural rubber. The theoretical line is calculated from the statistical theory assuming a Gaussian network (after **Treloar [1958]**).*

It is noted here as an adjunct that the assumption of a Gaussian distribution of chain lengths is only valid for moderate deformations. Other non-Gaussian statistics and internal-energy theories conform much closer to experimental data even at very large deformations. However, it may be sufficient in this case to use the simpler model to interpret any observed behaviour in the proposed transducer.

In summary, under equilibrium conditions rubber subjected to moderate simple shear deformations may behave like a Hookean spring. Furthermore this behaviour may be predicted and understood in a broad sense at the molecular level.

3.1.2.1.1 Rubber in Simple Shear

In general a cylinder of rubber that is subjected to a shearing force will experience both bending and shearing. **Love [1943]** and **Southwell [1953]** described how that if the total deformation is small compared with its diameter the conditions are similar to that of a loaded cantilever beam. The theory of superposition of the displacements, due to both mechanisms, will then hold provided certain end conditions are met. Figure 3.7 shows the situation that most closely approximates that found in the shear stress transducer developed here. Where: t is the thickness of the rubber layer (which has an area, A); x is the total deflection caused by the applied force, F.

The total deflection is found by **[Rivlin and Saunders 1949]**:

$$X = X_b + X_s = \frac{Ft}{AG}\left(1 + \frac{t^2}{36K^2}\right) \tag{3.1}$$

Where X_b and X_s are the deflections due to bending and shearing respectively, G is the shear modulus of the material and K is the radius of gyration about the neutral axis of bending.

For a cylinder $K = r/2$ where r is the radius of the circular section. Therefore for cylinders where the radius is very much greater than the thickness $t^2/9r^2 \ll 1$ and the conditions in the rubber approximate to:

$$X = \frac{Ft}{AG} \tag{3.2}$$

This means the displacement of the discs is approximately linear with applied shear force, and (3.2) represents a Hookean relationship. This is the desired property of the restoring force in the shear stress transducer.

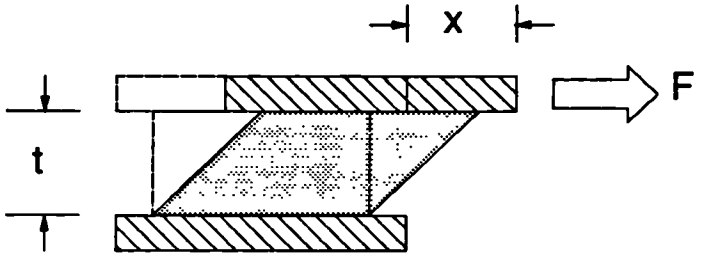

Figure 3.7 Schematic showing two rigid plates bonded by a rubber layer of thickness t and subjected to a shearing force, F. The resultant displacement is the distance x.

3.1.2.1.2 Rubber in Compression

An important property of some rubbers in this application is their very high bulk modulus. This means that it will exhibit only very small volume changes under compression load. Therefore, the rubber will attempt to displace or bulge. For rubber discs with a high diameter to thickness ratios there is very little unbound surface to do this. Thus the shape is virtually incompressible, and any normal stresses applied to the top of the shear section will be transmitted unchanged to the normal section. Also, magnet/magneto-resistor separation will remain relatively constant under normal stresses [see 3.1.3].

3.1.2.2 Time Domain Behaviour of Rubber

The previous discussion considered only the equilibrium behaviour of Rubber, that is, its response after a period of minutes under stress. In this particular application it will be necessary to be able to accurately measure stresses that may vary at rates up to about *50Hz*. Therefore the behaviour of rubber in the short time scale must be investigated.

In practise when a rubber is subjected to a given stress the observed deformation shows three phases **[Ward 1971]**. There is an immediate elastic phase (*e1*), then a time dependent continued deformation (*e2*) where the rate of strain decreases. This is followed by a stage (*e3*) where the strain rate becomes insignificant and the strain settles at some equilibrium value. These stages are illustrated in Figure 3.8. In the case of an applied constant strain, stresses are set up in the material instantaneously. These then decay away at a rate which decreases until they reach some equilibrium value.

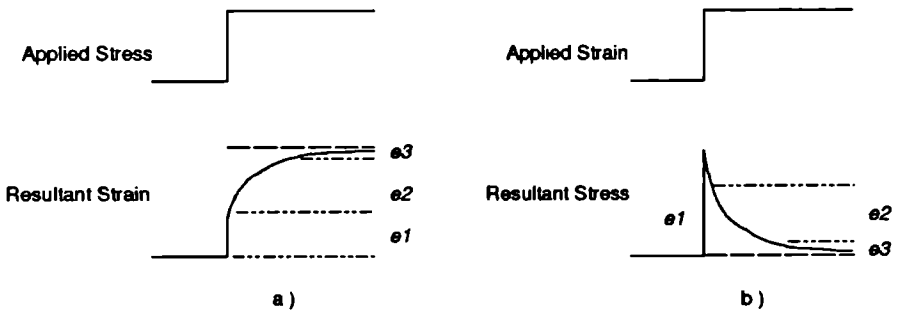

*Figure 3.8 Schematic of the response of a viscoelastic solid to a) constant stress and b) constant strain. Each response has three arbitrary phases; during **e1** there is an immediate elastic deformation; during **e2** the deformation is time dependent; during **e3** the rate of deformation is insignificant and equilibrium is achieved.*

Tobolsky and Andrews [1945] investigated the form of these phenomena and showed that the rate of decrease of either strain or stress conforms to an approximate exponential function of time. These cases are known as 'creep' and 'stress relaxation' respectively and for rubbers the overall process is reversible.
It is clear from this observed behaviour that there is a time dependent compliance in rubbers under load. **Mullins [1947]** in his study of the resilience of rubbers (i.e. its capacity to store and return energy under rapid deformations) showed that their response is more intimately related to the molecular structure than the gross structure of the material. In general, when stressed, rubbers may behave like glassy solids, viscous liquids or ideal elastomers dependent on the time scale of loading.

The three phases of the creep-type deformation , as outlined above, can to some extent be related to the dominance of the following molecular mechanisms **[Billmeyer 1971]**. During very short periods following the applied stress the rubber tends to act as a glassy solid, exhibiting Hookean elasticity. Here the main mechanism of

material deformation is bond stretching and bond rotation. This results in very low compliance and deformations of only a few percent. After longer periods the sections of the molecules between crosslinks and entanglements are able to uncoil. The effective compliance of the material in this phase is much higher. Deformations of several hundred percent are sustainable. For intermediate times the material is in transition between the other two phases and both mechanisms are operating. The compliance here is time dependent and akin to viscous flow. Although in all phases the deformation is reversible. A simplistic representation of the compliance variation with load time can be seen in Figure 3.9. The division between the glass and rubber states may be arbitrarily characterized by a transition time, *T*, which relates to the time required for the molecules to change their configurations.

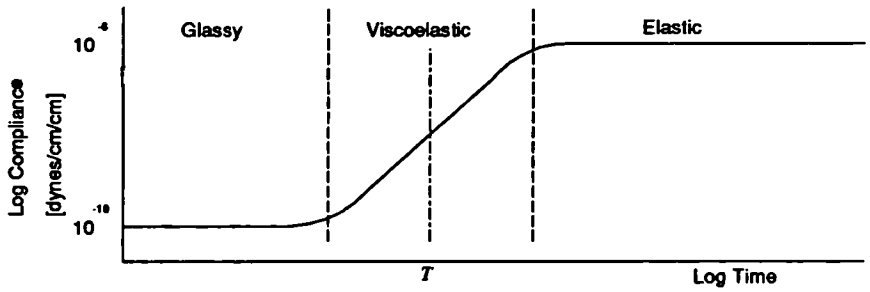

Figure 3.9 Schematic of the change in compliance of an idealised rubber as a function of time under load. T may be defined as the characteristic time constant of the material (after ***Ward [1971]*** *).*

If it is assumed that any incremental stresses applied to the rubber make an independent contribution to the strain then it can be said to be linearly viscoelastic. It is possible,then, to represent its behaviour by means of idealised spring-and-dashpot mechanical models. In its simplest form stress-relaxation may be expressed by the equations of state of a Maxwell element or model, which represents a liquid that has elasticity. Similarly creep deformation can be modelled by a Voigt model and represents a viscous solid. Both of these models are described in Figure 3.10.

It can be shown that the equation governing the stress strain relations in the Maxwell model has the form **[Ward 1971]**:

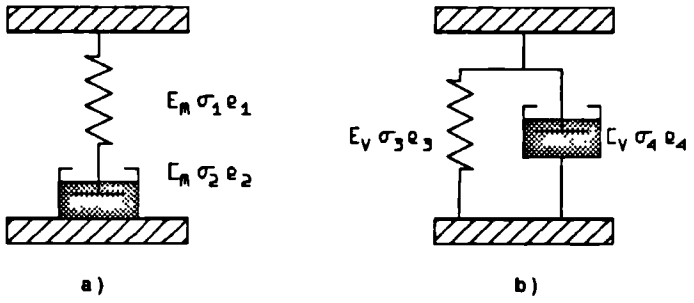

Figure 3.10 Schematic of the mechanical models used to represent the viscoelastic behaviour of rubbers; a) the Maxwell and b) Kelvin or Voigt elements (after ***Ward [1971]*** *).*

$$\dot{e} = \frac{1}{E_m}\dot{\sigma} + \frac{\sigma}{C_m} \tag{3.4}$$

Where the stress $\sigma = \sigma_1 = \sigma_2$ and the strain $e = e_1 + e_2$. E_m is the modulus of the spring and C_m is the viscosity of the dashpot. This is of value in modelling stress relaxation, where under constant applied strain, $\dot{e} = 0$, the solution to (3.4) describes an exponential decay of stress with time:

$$\sigma = \sigma_o \exp\frac{-E_m t}{C_m} = \sigma_o \exp\frac{-t}{\tau} \tag{3.5}$$

Here σ_o is the initial stress at $t=0$ and the characteristic time constant of the decay, $\tau = C_m/E_m$ is called the relaxation time. However under conditions of constant stress, $\dot{\sigma} = 0$, (3.4) resolves to :

$$\dot{e} = \frac{\sigma}{C_m} \tag{3.6}$$

describing constant flow. This is not true for creep behaviour in rubbers.

The Voigt alternative model is governed by the equation:

$$\sigma = E_v e + C_v \dot{e} \tag{3.7}$$

Here $e = e_3 = e_4$ and $\sigma = \sigma_3 + \sigma_4$. E_v is the elastic modulus and C_v the viscosity. The solution of (3.7) under conditions of constant stress, $\sigma = \sigma_o$, is found to be:

$$e = \frac{\sigma_o}{E_v}\left(1 - \exp\frac{-E_v t}{C_v}\right) \tag{3.8}$$

$$= \frac{\sigma_o}{E_v}\left(1 - \exp\frac{-t}{\tau}\right)$$

Where $\tau' = C_v/E_v$ is the characteristic time constant referred to as the retardation or orientation time. Equation (3.8) describes, to a first approximation, the observed creep behaviour of rubber. However its representation of stress relaxation behaviour is inaccurate. Under these conditions $\dot{e} = 0$ and the solution to (3.7) is:

$$\sigma = E_v e \tag{3.9}$$

which describes constant stress.

Kuhn [1954] proposed that the behaviour of real materials can be modelled using a distribution of time constants. This may be thought of as a network of Maxwell or Voigt elements each with their own unique time constant. Under this theory it is still possible to represent the material's behaviour, to a first approximation, by using a single element which has a time constant that is the mean value of the distribution.

So it can be seen that to a first approximation a Voigt model can be used as an analogy for creep behaviour while the Maxwell model describes stress relaxation.

3.1.2.3 Frequency Domain Behaviour of Rubber

For a more complete assessment of the suitability of the use of rubber as a spring it will be useful to expand briefly on the time domain concepts of the previous section. Here, the viscoelastic phenomena will be considered as a function of the frequency of applied stresses. It can be easily seen from the creep curve of Figure 3.8 that there is a time delay between maximum applied stress and the maximum strain. If the rubber sample is subjected to a sinusoidally varying stress then, under equilibrium conditions, the strain will vary sinusoidally but with a phase lag. So the stress and strain forms can be written as:

$$e = e_o \exp i\omega t$$

$$\sigma = \sigma_o \exp i(\omega t - \delta) \tag{3.10}.$$

Then a modulus of shear G can be defined where

$$\frac{\sigma}{e} = \frac{\sigma_o}{e_o}(\cos\delta - i\sin\delta) \tag{3.11}$$

$$= G_1 - iG_2$$

$$= G^*$$

The shear modulus can be described as having a real in-phase component, G_1, and an imaginary out-of-phase component, G_2. These are related to the elastic and lossy or resistive components of the deformation, respectively. The amplitude of the resultant displacement is then determined by the modulus of G^* or:

$$|G^*| = \sqrt{G_1^2 + G_2^2} \tag{3.12}$$

While the phase angle between the loss modulus and the elastic modulus is given by :

$$\delta = \tan^{-1}\frac{G_2}{G_1} \tag{3.13}$$

It is also possible to define a loss factor $\tan\delta = G_2/G_1$ which is a measure of the fraction of energy lost. For most rubbers this loss fraction is small, of the order of *0.01*. As before, it is possible to represent, to a first approximation, the dynamic behaviour of rubber with a Maxwell or Voigt model. For example, using the Voigt model to approximate creep processes it has been shown that **[Ward 1971]**:

$$G_1 = E_v\frac{1}{1+\omega^2\tau^2} \tag{3.14}$$

$$G_2 = E_v\frac{\omega\tau}{1+\omega^2\tau^2} \tag{3.15}$$

where $\tau = \frac{C_v}{E_v}$

Figure 3.11 represents these parameters as a function of frequency, for a typical rubber.

These relationships imply that during the viscoelastic phase where the resultant strain lags the applied stress, there will be uncertainty in deriving the causative stress from a simple observation of the strain. Furthermore this uncertainty will vary with rate of applied stress as the phase lag is a function of frequency. This concept can be best illustrated graphically as in Figure 3.12. The hysteresis loops describe a maximum uncertainty when the phase lag is $\pi/4$ and it becomes a minimum where there is zero lag.

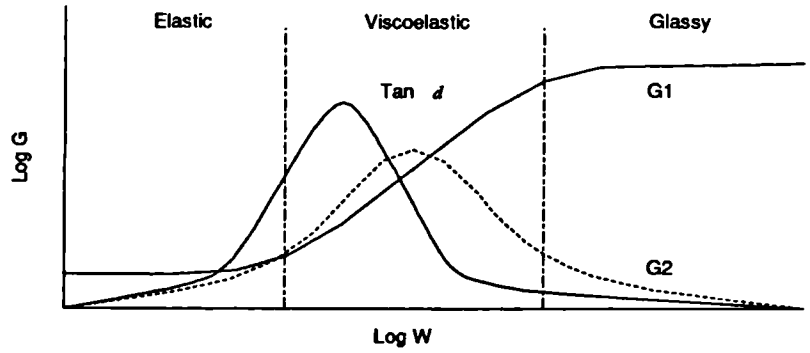

*Figure 3.11 Schematic of the shear modulus variation ($G^* = G_1 + G_2$) as a function of stress frequency for a typical rubber. G_1 is the elastic component and G_2 is the lossy component of the modulus. Tan d is a measure of the proportion of energy lost during a loading/unloading cycle (after **Ward [1971]**).*

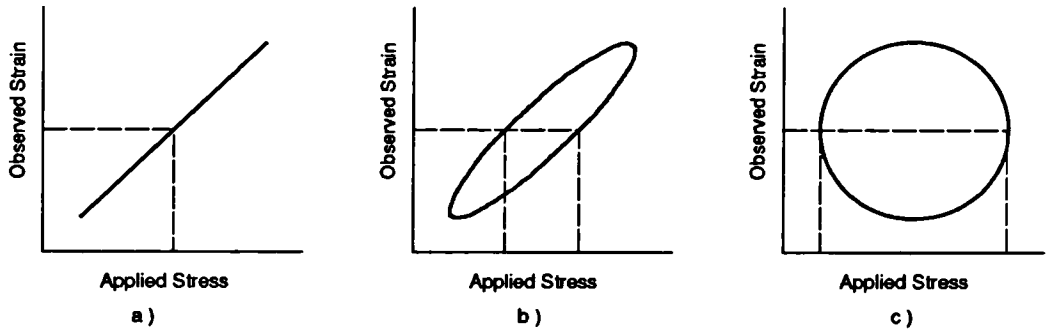

Figure 3.12 Uncertainty of deriving the causative stress from the observed strain, where the strain lags the stress by a) 0, b) π/8, c) π/4 under sinusoidal load cycles.

Theoretically it may be possible to derive the causative stress from an observed strain history, provided that the form of dynamic modulus is known for all frequencies. However, the complexity of the signal processing required and the complete characterisation of the material make this impractical. The form of the loss modulus predicts that: below the transition frequency of the material there will exist a frequency at which ther will be no viscous hysteresis; whereas the hysteresis in real rubbers will not diminish to zero at any frequency. It is suspected that this is due to finite energy losses during the changing of molecular orientations and the breaking (and reforming) of short links and chain defects. In general this form of hysteresis is quite small compared to the maximum viscous hysteresis and is more closely proportional to the amplitude of the deformation.

In summary at frequencies where a rubber exhibits elastic or glassy behaviour it will have a single modulus of elasticity (compliance). Under cyclic stresses there will be small hysteresis losses related to the stress magnitude. Additionally in the elastic region (low frequencies) creep processes will cause a variation in observed strain with frequency of applied stress. However in the viscoelastic region the modulus is frequency dependent and the observed strain will lag behind the applied stress to a significant degree. This lag which increases with frequency will be the cause of increasing uncertainty in deriving the magnitude of applied stress from observation of the strain in the material. Therefore in this application it is practical to use rubber as dynamic spring material provided a suitable type is chosen which exhibits a transition frequency above those of clinical interest.

3.1.2.4 Useful Types of Rubber

The above sections discussed the suitability and restrictions of the use of rubber (elastomer) as a spring in the shear-section of the required transducer. The following is a resume of types and properties of rubber in general use in industry. It has been difficult to find a direct comparison of the properties of all rubber types as each is sought for different applications. So, instead, a qualitative comparison is presented in Table 3.2 as derived from suppliers literature.

	Resilience	*Set*	*Strength*	*Hardness (°BS)*	*Cost**
Nitrile	5	8	4	40-90	7
Natural	9	7	6	40-90	8
Silicone	7	6	3	40-80	4
Neoprene	7	5	5	40-90	7
Flurocarbon	5	5	4	65-80	1
Polyurethane	6	5	9	-	5
Butyl	2	4	4	45-85	9

* *Bulk volume cost.*

Table 3.2 Qualitative comparison of some properties of commonly available rubbers. The highest value indicates the property is at its most advantageous.

It should be noted that the properties above can be varied by differences in processing and compounding. However the values given are an indication of the best that can be achieved for that rubber type.

The resilience of a rubber is a measure of its speed of recovery after deformation. This is particularly important for response to rapid changes in stress during the gait cycle. Set, is related to the degree of recovery from a deformation. As each of these rubbers is a non-ideal elastomer there will be some residual deformation that may take a significant time to diminish. It is very important in this application that all deformations are fully recovered to achieve accurate long-term stress measurements. The strength value given here is for the level tensile strength achievable, but gives an indication of the relative shear strength of each material. It should be noted that all of these rubber types will be able to sustain clinical loads. Hardness is a measure of the deformability of the material. In this application a moderate deformation is required for a fair range of displacements. But this must be limited to a range of deformation experienced by tissues under load. Cost values are based on cost per volume in bulk. In practice it is generally easier to obtain ready to use samples of some types over others - as is the case with silicone compared with Butyl. The bulk modulus of these rubbers is very much greater than its Young's modulus, thus they will not change their volume much under large loads and therefore are virtually incompressible. This feature is significant as it means that forces normal to the transducer will be transmitted unmodified by the shear transducer and there will be very little cross-axis interference (change in the shear axis output due to normal forces).

Natural-rubber (**NR**) is an organic compound derived from the sap of a tree (Hevea Brasiliensis). The raw form is vulcanised by mixing and heating with sulphur. During heating the sulphur aids in forming cross links between the long chain molecules. It is common to add in a range of chemicals, at the mixing stage, which alter the final properties of the rubber. These may be aids in the vulcanisation process, or used to alter the rubber stiffness or improve weathering properties. Rubbers containing only processing and protection chemicals are known as gum rubbers. However the majority of NR's used in heavy engineering contain various amounts and types of fillers. These are used to specifically increase hysteresis and creep and may improve tear and abrasion properties as well. The relaxation rates of all NR's are lower than those of other rubber types with gum rubbers exhibiting typical rates of *1.5%* per decade. For shear deformations in NR, creep and relaxation

rates are approximately equal. The hysteresis for gum rubbers is small compared to filled rubbers. However above *200%* deformation the hysteresis increases by orders of magnitude. In practice shear strains are normally limited to less than *100%*, although they are substantially linear up to *200%*.

A difficulty in using NR in the shear section is that of bonding. This is achieved either by a hot process or a cold process. The most common method is the hot one where the bond with the substrate is formed during the vulcanisation process. This is carried out at temperatures in excess of *120℃* and large pressures. Under these conditions post bonding assembly of the semiconductors in the section will be necessary to avoid their damage st high temperatures. This however would be a very difficult task. The cold bond method uses proprietary cements to bond sheets of NR to metal. This requires careful chemical preparation of both surfaces. There will be a surface boundary layer formed by this method that can be *80-150μm* thick - (this may represent up to *20%* of the total thickness of the proposed shear section rubber thickness).

Silicone rubber is a non-organic compound that has similar mechanical properties to those of NR - as far as this application is concerned. It is generally manufactured in a paste form which contains a stabiliser. When the paste is exposed to atmospheric moisture the stabiliser reacts with the silicone molecules to form the cross links. In contrast to NR the silicones form a bond with its substrate during the cold curing process. They are also commonly available with a range of properties, where as NR sheet must be formulated and made to order by specialist agencies.

In the prototype design of the shear section it was decided to use silicone in the first instance. This was also partly encouraged by the fact that **Tappin et al [1980]** used this in their device. Several manufacturers of silicone were approached for sample silicones suited to this application. Three of these samples were taken for testing, they were:

RTV738 (Dow Corning UK LTD);
RTV157 (General Electric UK LTD);
1039N (Ambersil LTD).

A final factor to be aware of, from a safety point of view, is the possible toxic or irritant nature of the rubber or its adhesives. Both silicone and natural-rubber are known to be non-toxic and non-irritant.

3.1.3 Displacement to Voltage Conversion

The primary requirement of the second mechanism operating in the shear stress section is to provide sensitive conversion of uniaxial displacement to a low noise electrical signal, over the full range of movement. It must also be insensitive to displacement in the other two axes. In order to achieve a large change in relative resistance of the magneto-resistor element with displacement, a combination of sensitive element and a high field strength magnet is desirable. The following sections describe the selection of the magneto-resistor and magnet materials.

3.1.3.1 Magnet Types

During the initial development phase a survey of the commercially available magnet types revealed that a resin bonded Samarium Cobalt rod magnet would best satisfy our requirement. These are very high energy, low cost magnets suitable for being made in small dimensions. They are also widely used to operate similar semiconductor devices (e.g. Hall effect switches). These were conveniently available in two millimetre long rods of two millimetres diameter. In this form the magnet was pressed into the hole in the centre disc (which is an interference fit) and cemented in place with a cyanoacrylate adhesive (see Figure 3.2).

3.1.3.2 Magnetoresistor Properties

The magneto-resistor elements were required to have high sensitivity to magnetic field changes as the magnet displacements were expected to be small. Especially as the dynamic range of expected shear forces spanned over two decades (*0.5N-50N*) where resolution of the smaller forces must be achievable. One of its primary advantages over other transducer mechanisms is that of low electrical impedance.

This has the advantage that in general noise signals may not have sufficient power to generate significant interference currents, and hence voltages, in low impedance circuits. Therefore the signal to noise ratio is greatly assisted.

Magneto-resistors (**MR**) are semiconductors of InSb/NiSb material whose resistance is influenced by magnetic fields in accordance with the Gauss effect. Charge carriers flowing in the material experience a lateral force when in a transverse magnetic field. The angle of deflection of the charge carriers is known as the Hall angle δ. This is dependent on the electron mobility μ and the magnetic induction β. The relation is:

$$\tan\delta = \mu\beta \tag{3.16}$$

InSb has a large electron mobility and produces a large defection angle. Unlike Hall generators it has low resistance NiSb needles grown transversely into it. These allow an even distribution of charge carriers throughout its cross section. The increase in the path length travelled by the carriers under a magnetic field effectively leads to increased resistance of the MR. Figure 3.13 illustrates this increased path length. The increase in resistance is independent of the polarity of the magnetic field.

Figure 3.13 The path of current flow under magnetic field influence in a section of InSb semiconductor. Imbedded NiSb needles act as low resistance conductors across the section.

The relation of resistance to magnetic induction, β, can be written to a first order approximation as:

$$R_\beta = R_o(1+K\mu^2\beta^2) \tag{3.17}$$

Where μ is the electron mobility, K is a material dependent constant and R_o is the base resistance at zero magnetic induction. The resistance increases in a quadratic manner up to about *0.3T* after which it is asymptotic to a straight line. This base resistance is dependent on the following factors:

the conductivity of the material, which is determined by the doping level of the NiSb needles [type D = $200\Omega cm^{-1}$, L = $500\Omega cm^{-1}$ and N (undoped) = $800\Omega cm^{-1}$];
the path width and thickness;
the total length of the path in the field (the tolerance of this value is dependent on the homogeneity of the material and the reproducibility of the dimensions of the path).

The relative change in resistance with magnetic induction for the three doping grades are illustrated in Figure 3.14. Also the resistance change is only effected by the component of the magnetic induction that is orthogonal to the element.

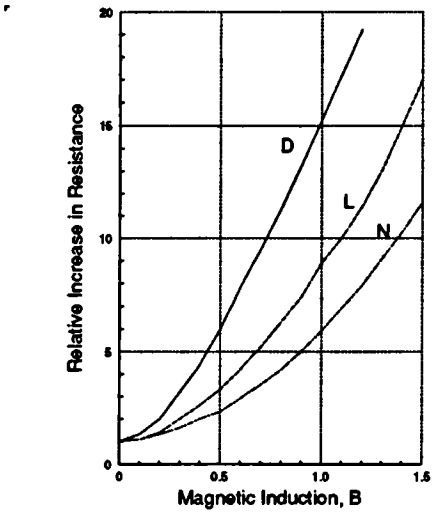

Figure 3.14 The relative increase in resistance of InSb/NiSb semiconductor with magnetic induction, β. Curves for three doping grades are shown; D (200 Ωcm^{-1}), L (550 Ωcm^{-1}), N (800 Ωcm^{-1}).

There is a temperature coefficient of resistance associated with each doping grade. It is generally non-linear with temperature itself and also dependent on the magnetic induction. Figure 3.15 describes the effect of this temperature coefficient by plotting the resistance at a given temperature as a percentage of the resistance at *25 ℃* for each doping grade and for a range of inductions. Although the response is generally non-linear it is seen that for small changes in temperature (*20-40 ℃*) it is approximately linear.

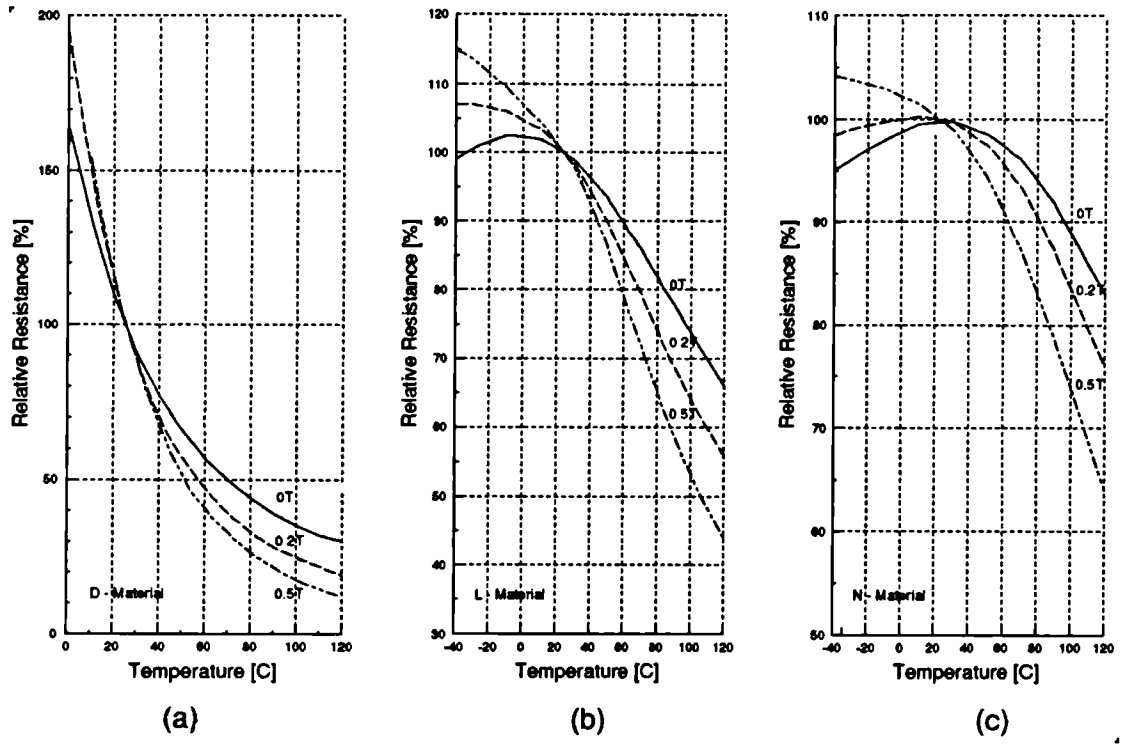

Figure 3.15 Resistance of magnetoresistors as a function of temperature and magnetic induction, relative to their value at 25 ℃, for doping grades a) D, b) L, c) N.

For differential type MR's where the output of the device is found as the Ratio of one resistance to another, temperature changes common to both resistances will produce the same relative change in each, and the output will be constant. The assumptions here are that; the resistors have identical temperature coefficients for a given temperature and induction; they experience the same temperature; and that the induction difference between them is small. This last point is problematical as the induction difference is the principle action. Therefore a device under shear stress will have a temperature coefficient difference between its arms which will lead directly to an apparent strain error under temperature changes. If the resistance change in a material is large for a small change in induction the effect of the coefficient difference can be minimised. There is, however, a compromise to be made as those doping grades with high induction sensitivities also have high temperature coefficient variations. Table 3.3 illustrates: typical variations in Ratio for changes in induction, at a fixed temperature; and the variation in Ratio with changes in temperature at a fixed induction.

	D	L	N
a) ΔR_B [%]	71	47	38
b) ΔR_T [%]	2.3	1.6	1.4

Table 3.3 A comparison of the expected change in Ratio for the three doping grades of differential magnetoresistor for a) a change in inductance of 0.5T at 25 ℃ and b) a change in temperature of 25 ℃ with induction constant at 0.5T.

As the displacements in the device under shear will be small and therefore also the induction changes, the doping grade D was used in the prototype as this will produce the largest output signals.

There are parameters of the assembled device that are difficult to measure, that mean an accurate analytical prediction of the device performance is impractical. These are namely; magnet-magnetoresistor separation; the homogeneity of the induction field; the lateral placement of the magnet; and the resistor tolerance and symmetry. Therefore the performance will need to be assessed experimentally.

In addition to the semiconductor performance trade-offs there are physical size considerations to be made. In order to reduce the overall device thickness each subassembly must have minimal thickness. The elements were to be recessed into a thin disc that already has a channel milled into it, so their thickness was critical. Similarly if the element occupies a relatively large surface area there will be more material removed from the disc which will affect the disc's rigidity. Elements are available in two forms; (a) encapsulated where it is moulded in a plastic block with an external lead frame; (b) unencapsulated where the active semiconductor is laid on rigid substrate, usually magnetically biased. The leads from the element are very fine (*0.08mm* diameter) resin insulated copper. The volume of the encapsulated form can be up to ten times that of the basic semiconductor element. In view of the size restrictions the unencapsulated form was preferred despite the greater handling complexities.

A survey of the semiconductor manufactures for suitable magneto-resistors resulted in the selection of the model FP110D155 by Siemens [see Table 3.4]

Type	Base Ω	Centre Symmetry [%]	Resistance Change 0.3T	Resistance Change 1T	Temperature Coefficient 0T	Temperature Coefficient 0.3T	Temperature Coefficient 1T	Thermal Conductance [mW/K]	Dimension [mm]
FP110D155	2x155	< 5	>2.8	>12	-1.8	-2.7	-2.9	10	1.2x3.2x0.4
FP111L100	2x100	< 5	>1.7	>7	-0.16	-0.38	-0.54	10	2.7x3.2x0.4

Table 3.4 Table of the properties of the Magneto-resistors available from Siemens LTD.

Although the ridge and groove constructs on the discs are designed to stop the magnet moving longitudinally along the element any *play* in the assembly may change the position of the field over the element's active areas. It is therefore important to ascertain if the elements are truly uniaxial. Also to ensure similarity of resting output between devices where there is a variation in the placement of the element during assembly. Figure 3.16 shows a map of the output from a typical element (with a *1* volt excitation) when the magnet is moved over its face at a separation of *0.1mm* this map verifies that the elements are sufficiently uniaxial.

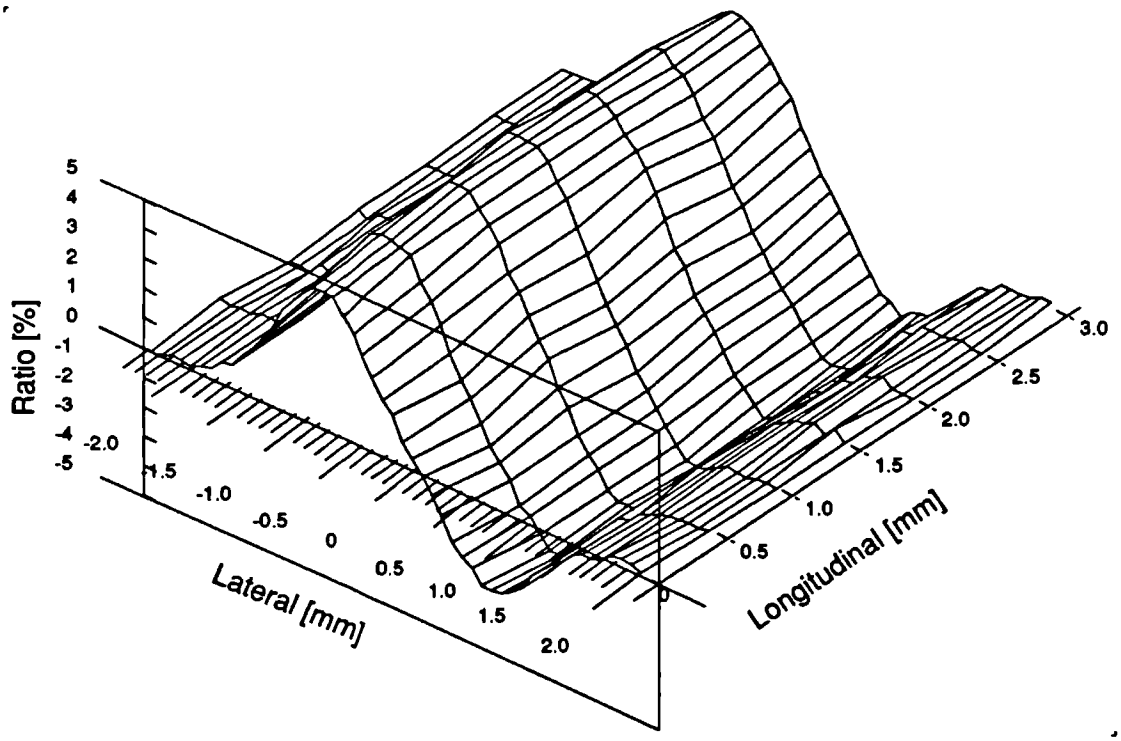

Figure 3.16 Map of the output response of a typical magneto-resistor element (Siemens FP110D155) when a small rod magnet (Magnet Developments Ltd., dia.2x2 mm resin bonded Samarium Cobalt) is moved parallel to its surface at a normal separation of 0.1 mm.

3.1.3.3 Disc Materials

The primary requirements of the disc materials were low weight, sufficient rigidity to resist point deformations, ease of fabrication and bonding compatibility. Materials considered were plastics, metals - namely steels and aluminium - and ceramics. Although the latter could provide a thinner, lighter and more rigid disc than the others, it is significantly more expensive and complicated to manufacture. The facilities for which are not commonly available. Some steels are ferromagnetic and although it was thought that this would have a minimal effect on the magnetic flux paths they were heavier than aluminium. Plastics can have good rigidity and bonding affinities but only at higher cost and less availability than metals. Aluminium in comparison is light, rigid, cheap and easily machinable. Silicone rubber will easily bond to it - provided it is degreased and the oxide layer removed. It was decided to use aluminium discs for the prototype shear transducer, the dimensions of which are shown in Figure 3.17.

3.1.3.4 Other Materials

In order to provide a degree of strain relief for both the device leads and magneto-resistor element leads the element is bonded to a printed circuit board and the leads soldered to tracks. The board is a thin flexible three layer laminate of double sided copper coated Kapton each of respective thickness *35, 50, 35*μm. A land for the element placement and three tracks for lead attachments were photo printed and etched onto the board. An exploded schematic of the board and how the components are placed onto it is given in Figure 3.18. The land for the element acts as a placement target to aid in the consistent positioning of the MR in the centre of the disc. Due to the very small component sizes involved all assembly work had to be carried out under an *8.75X* binocular microscope. When assembled, the leads, element and circuit board were located in the arch shaped slot milled into the magneto-resistor disc, and cemented in place with a cyanoacrylate adhesive. With this arrangement the accuracy of lateral placement of the element with respect to the centre of the disc is $\pm$ *0.25mm.*

The signal leads for the whole device are P.V.C. coated *7/0.13mm* copper wires laminated into a ten way ribbon cable.

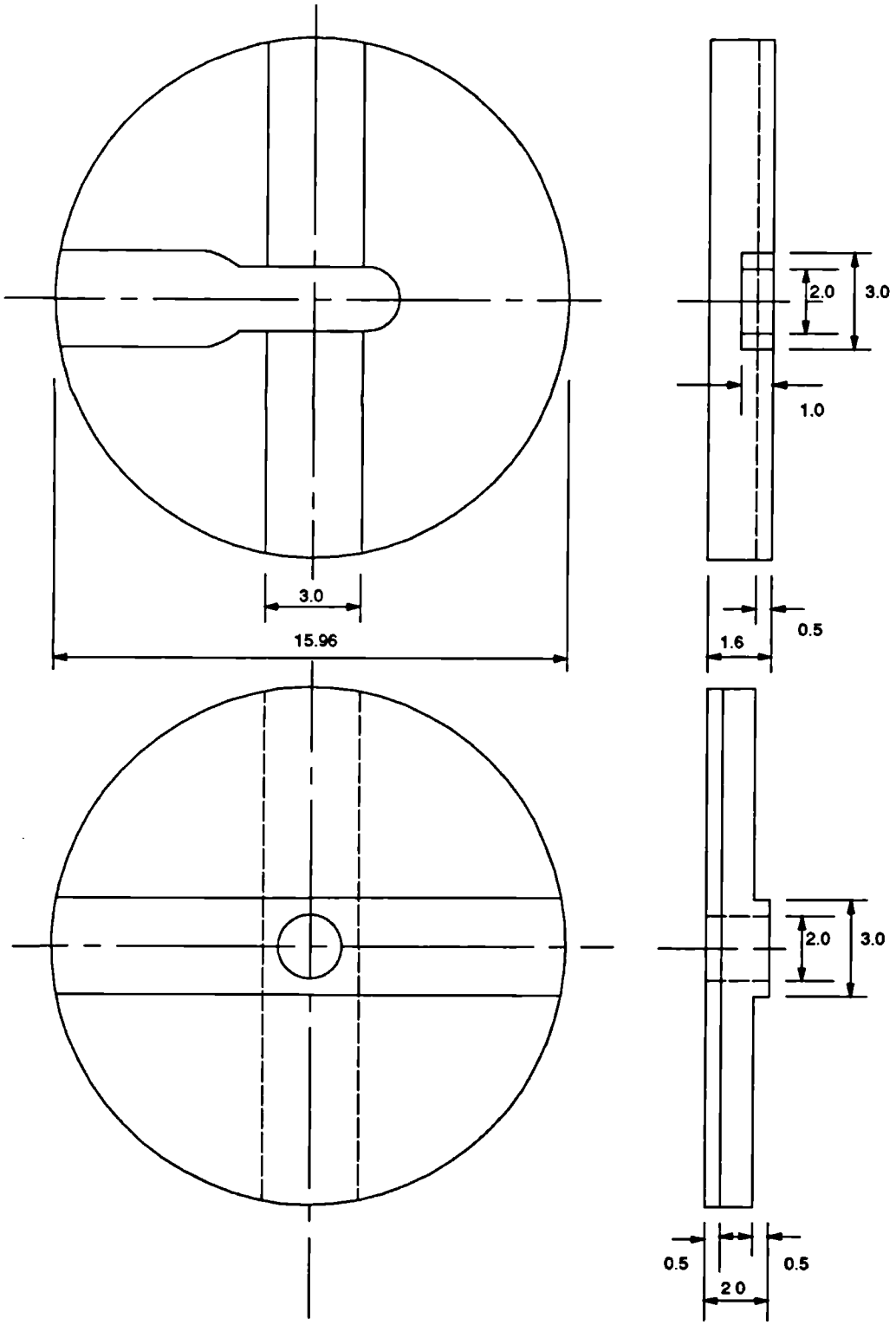

Figure 3.17. A diagram showing the dimensions of the discs used in the shear section of Design A, The top disc holds the FP110D155 magneto-resistor element and the bottom disc holds the Samarium Cobalt rod magnet.

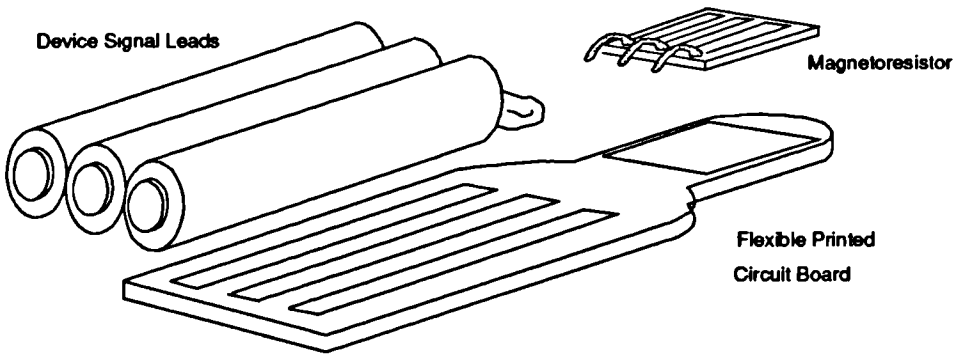

Figure 3.18. An exploded schematic of the signal lead and magneto-resistor element assembly, bonded to a thin flexible printed circuit board (35/50/35μm: Cu/Kapton/Cu).

3.2 Normal Section Design

The following presents the general design of the section of the transducer which converts normal stresses into electrical signals. It describes the principle of operation of this section and reports the process of selection of components for a prototype. Also presented are details of the assembly procedures and equipment for the prototype.

3.2.1 Principle of Operation

The approach adopted for the design of the section for sensing applied normal-stress was to use a combination of known technology and an unusual method of actuation. Following from the discussion in Chapter 3, it was decided to use a resistive strain-gauged diaphragm as the sensing mechanism.

The diaphragm is formed by machining a deep circular recess into the bottom surface of a metal disc. The thicker material at the disc circumference acts as the support for the thin central area or diaphragm. A strain gauge, is bonded to the face of the diaphragm at the bottom of the recess. Any forces applied normal to the opposite face of the diaphragm will cause it to distort and strain, consequently straining the gauge elements. This strain causes a change in resistance which can be measured and bears a direct relationship to the forces that are applied.

In using a strain-gauged diaphragm to measure applied normal forces; there is an inherent compromise between sensitivity (and ultimately resolution) and dynamic range. The amplitude of the output signal from this type of transducer is mainly a function of the type of gauge used, the excitation voltage, and the amount of bending (or deflection) of the diaphragm. The following subsections discuss these points.

3.2.2 Strain-gauge Properties

Resistive strain gauge theory was studied as far back as Lord Kelvin in the 1800's and Dr St.Lindeck in 1908. Since then the application of strain gauges to the measurement of stresses in many commonly used engineering materials has been well established. There are numerous texts that treat the subject fully **[Perry 1955; Potma 1967]** and it is not the intention to provide a rigourous discussion of the theory here. Instead, a brief summary and a report of the design considerations for an accurate and stable stress transducer is given.

Strain gauges can, in principle, only be used for the measurement of deformation or 'strain.' However it is possible to derive from these strains, information about the stresses occurring in the material caused by external forces or pressures exerted on it if the stress-strain relationship of the material is known.

When a strain gauge element (fine wire or semiconductor) is strained it changes its dimensions and resistivity. If the strain magnitude is restricted to be within the elastic limits of the material, the resistance of the element will change repeatably. The relation for this change in resistance is given as **[Peura 1978]**

$$R = \frac{\rho L}{A} \tag{3.18}$$

Where ρ is the resistivity [Ωm^{-1}], L [m] is the length of the element and A [m^2] is the cross-sectional area. When the element is strained the change in resistance can be found by differentiating (3.18) to give

$$\partial R = \frac{\rho \partial L}{A} - \frac{\rho L \partial A}{A^2} + \frac{L \partial \rho}{A} \tag{3.19}$$

By substituting Poisson's ratio, μ, which relates the change in diameter to the change in length by the relation **[Sears 1978]**

$$\frac{\partial D}{D} = -\mu\frac{\partial L}{L} \tag{3.20}$$

And by re-expressing (3.19) as the ratio of the original parameters we have :

$$\frac{\Delta R}{R} = (1+2\mu)\frac{\Delta L}{L} + \frac{\Delta \rho}{\rho} \tag{3.21}$$

Where the first term on the right hand side is the dimensional effect on the change in resistance, and the second term is the piezoresistive effect. In wire or foil gauges the dimensional effect is dominant while in semiconductor gauges the piezoresistive effect is dominant. A quantity often used to compare the sensitivity of strain-gauge materials is the gauge factor *G*,

$$G = \frac{\Delta R/R}{\Delta L/L} - (1+2\mu) + \frac{\Delta \rho/\rho}{\Delta L/L} \tag{3.22}$$

The choice of gauge type has a large bearing on the amount of change in its resistance for a given amount of strain (this is known as its gauge factor). Those types in common use are the metallic foil, semiconductor and deposited metal gauges. Foil gauges are the most common and are formed by rolling metal alloys into thin layers and bonding or moulding them onto various backing materials. A pattern, dependent on the application, is then etched into the foil. This backed foil is then bonded to the test structure with organic cements.

Semiconductor gauges (or piezoresistive gauges) are formed by depositing doped silicon in the appropriate patterns onto a suitable insulating substrate. The substrate is then bonded to the test structure in the same way as foil gauges.

Deposited metallic gauges are thin films of pure metals or alloys deposited directly onto pre-insulated structures. The various patterns are laid by using masks, or etching the films once deposited. Their chief disadvantage is the requirement for special facilities to effect the deposition (whereas the others can be installed in-house) and their slightly poorer performance than foils **[Measurements Group Ltd 1981]**.

The gauge factor of metallic gauges is comparable to foil types with a gauge factor of approximately *2.5*. Semiconductor materials have a gauge factor *50-70* times that of metal gauges, but their temperature coefficient of resistance is *35-350* times greater than metals **[Cobbold 1974]**. Also the deviation from linearity of metal gauges is significantly lower than semiconductor gauges. In order to reduce data processing overheads on data from semiconductor gauge systems the signal-path processing elements would need to be significantly more complex. It must also

be noted that the same semiconductor technology which created this type of gauge has also produced smaller, more accurate amplifiers with very high common mode (noise) rejection ratios, that compensate foil gauges for their low gauge factors.

As temperature stability was an important criterion then a combination of gauges was used. These could be arranged in a half or full Wheatstone bridge circuit that would provide some inherent cancellation of thermally induced apparent strain (assuming all the gauges have identical characteristics and sense identical temperatures).

It was also important to provide some environmental protection for gauges as air borne moisture and low-level contaminates could effect their long term stability. Moisture may attack the gauge cement and ultimately change the ability of the gauge to follow the structure's strain. Therefore it was necessary to thoroughly clean each gauge and coat it with a protective layer. The protective layer must also be flexible enough to allow the gauge to stretch unhindered as the diaphragm deflects. In this case a thin layer of polycrystalline wax or non-acetic acid based silicone rubber was applied. It should be noted here that some silicone rubbers give off acetic acid when they are curing. These types should be avoided as the acid is corrosive to the backing material of the strain gauge.

On discussion with twenty six strain gauge manufacturers/distributors and after inspection of their data sheets it became obvious that the majority of their product lines have very similar specifications. As none had significant advantage over another the choice of gauge was influenced mainly by availability, cost and supplier support (as initially the gauges were to be bonded to the diaphragms by the supplier). The following sample gauges were taken to compare sensitivity, temperature stability for full and half bridge configuration.

a) Technimeasure QFDPF-9-350; full bridge foil gauge.
b) Tokyo Sokki Kenkyujo Co LTD FT-2-350-4B; full bridge foil gauge.
c) Technimeasure FCA-3 ; half bridge foil gauge with external temperature compensation resistors.

The samples were mounted on diaphragms and subjected to a number of performance tests. The results of these are reported in Chapter 5.

3.2.3 Excitation Limits

The greater the excitation voltage applied to the straingauge, the greater the signal to noise ratio, for any given signal processing system, and hence the greater the dynamic range of the electrical signal. There is however, a functional limit to the amplitude of the excitation voltage. This will depend on the gauge configuration, size, thermal conductivity of the gauge backing material, and the thermal conductivity of the diaphragm material. Each gauge has a given resistance that dissipates electrical energy as heat. When the heat is generated faster than it can be dissipated then the device's performance will deteriorate and it will ultimately fail. Obviously to minimise support circuitry it would be preferable to use the same excitation voltage as for the shear stress transducer.

3.2.4 Diaphragm Considerations

Strain gauges sense strain or deflection in a diaphragm such that, the greater the deflection the greater will be the change in resistance of the gauge. Now, for any given applied force, the amount of deflection of the diaphragm is inversely related to its thickness. Also the greater the diameter of the diaphragm the greater will be the deflection. So the gauge output will be greater for large diameters and thin cross sections than that for small diameters and thick cross sections. Hence the stress resolution will also be greater - as the noise in any signal processing system is generally constant. But, the maximum force the diaphragm can safely experience before permanent deformation occurs, is inversely related to the diaphragm thickness. The stress at which this deformation begins is termed the *yield strength* of the material. Thus within the diameter and height constraints of the device, a diaphragm thickness was to be chosen so as to ensure the best compromise between stress resolution and stress range. Also the height of the diaphragm supporting walls was to be sufficient to allow maximum deflection of the diaphragm without impacting the gauge on the bottom of the shear-stress section.

The diaphragm described above can be thought of as a flat plate clamped at its circumference. When subjected to forces perpendicular to its face it will undergo flexure in all planes perpendicular to the face. In the following discussion of bending in the plate it is assumed that; the load is symmetrical; the thickness of the plate is small compared to its diameter; strain in the middle plane of the

diaphragm is negligible (I.e. the maximum deflection is less than approximately one quarter of the thickness); principal stresses perpendicular to the face are not significant; also that straight lines in the plate originally vertical become straight lines inclined to the vertical after strain.

Let the radius of the plate be 'r' and its thickness be 't'. If it is subjected to an evenly distributed load, of total magnitude P, over a small central area of radius, r_o, the plate can be treated as two separate regions. Where the radius is less than r_o and when it is between r_o and r. Figure 3.19 describes this arrangement.

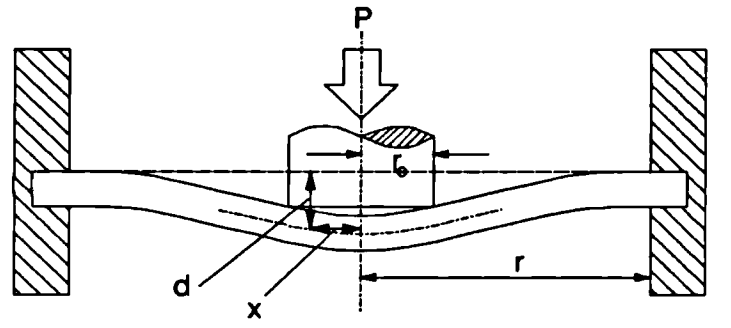

Figure 3.19. Schematic representation of a flat circular plate of radius, r, clamped at its circumference. The deflection distance, d, is due to a uniformly distributed force, of total load P, over a small central area of radius, r_o.

A simplified model of the stress in the plate is derived from the Bernoulli-Euler theory of bending in beams. It postulates that if r_o/r is small, then the maximum stress in the plate occurs at its centre and is given by **[Morley 1947]**:

$$S_R(\max) = S_T(\max) = \frac{-3(m^2-1)}{2\pi m t^2} \cdot \mathrm{P} \cdot (m+1)\left(\ln\frac{r}{r_o} + \frac{r_o^2}{4r^2}\right) \qquad (3.23)$$

where S_R and S_T are radial and circumferential stresses respectively, and $1/m$ is Poisson's Ratio for the plate material. Also the axial deflection of any radius, x, of the plate from its unloaded position is given by:

$$d = \frac{-3(m^2-1)}{4\pi m^2 t^3 \mathrm{E}} \cdot \mathrm{P} \cdot \left[r^2 + r_o^2\left(\ln\frac{x}{r} + \frac{1}{2}\right) + x^2\left(\ln\frac{x}{r} - \frac{1}{2} - \frac{r_o^2}{4r^2}\right)\right] \qquad (3.24)$$

where E is the modulus of Elasticity (Youngs modulus) for the plate material, and x is the radius from the centre.

By inspection of (3.23) and (3.24) it is clear that, for a given thickness of plate, as the radius of the loaded area (r_o) increases the internal stress per unit load decreases. Thus for greater stress sensitivity from a device the applied load should be concentrated through a small area.

Also it is clear that for a given total load, the deflection (and hence device output) and internal stresses will be greater for thin plates.

In general there is a compromise to be made in chosing the value of parameters in the diaphragm design. This being between achieving good sensitivity to stress and maximum working range - where internal stresses are limited to less than Yield Point stresses. From (3.23) $S\ max$ must not exceed the value of the Yield Point stress for the material. Of the factors of $S\ max$, the thickness (t) and the two radii (r, r_o) are variable, while the total load P and Poisson's ratio ($1/m$) are fixed by design.

The diaphragm material was silver steel (low carbon) in order to match the thermal coefficient of expansion of the strain gauge. That fixed Youngs modulus, Poisson's ratio and the Yield Point stress for the material as $2.069 \times 10^5\ Nmm^{-2}$, 0.29 and $770Nmm^{-2}$ respectively. The diaphragm radius (r) was bounded in the upper limit by; the radius of the shear section, minus the guide-pin hole diameter, minus a suitable hole clearance. The lower limit of radius was fixed by; the radius of the strain gauge ($4.75mm$), plus the width of the device's electrical lead ($1.27mm$). thus the radius had to fall within $6.02 \leq r \leq 6.45mm$. In terms of greatest stress sensitivity and internal stresses, the worst case radius was $r = 6.45mm$.

Of the remaining two parameters (t, r_o) it is obvious that there is a sensitivity advantage in minimising diaphragm thickness in priority to minimising loaded area. This can readily be seen from (3.23) and (3.24) where internal stresses are proportional to $1/t^2$ while deflection is proportional to $1/t^3$.

Reducing the loaded area also has a practical significance as is discussed in 3.2.5. It is difficult to maintain a uniform pressure over the entire diaphragm unless the forcing body exhibits load spreading and intimate surface conformity. But by

reducing the loaded-area radius, the variation in deflection across the area decreases, easing the conformity problem. Furthermore the physical requirements of the forcing body can be minimised by restricting the load to be applied uniformly distributed on the circumference of a circle of radius, r_o. Along the line of the circle the deflection must be constant. This can be achieved in an approximate fashion for instance by applying the load through a cylinder of radius r_o, which abuts the diaphragm. The maximum internal stress in the diaphragm is then described by:

$$S_R(\max) = S_T(\max) = \frac{-3(m+1)}{2\pi m t^2} \cdot \mathrm{P} \cdot \left(\ln\frac{r}{r_o} - \frac{1}{2} + \frac{r_o^2}{2r^2} \right) \qquad (3.25)$$

provided $\frac{r}{r_o} \geq 3.$

Deflection is a maximum at the centre of the circle and may be written as:

$$d(\max) \approx \frac{-3(m^2-1)}{4\pi m^2 t^3 \mathrm{E}} \cdot \mathrm{P} \cdot \left[r^2 - r_o^2 \left(1 + 2\log\frac{r}{r_o} \right) \right] \qquad (3.26)$$

Also comparison of (3.26) with (3.24) shows that loading the diaphragm on the circumference of a circle produces greater deflections than by loading over an area.

So by assuming a diaphragm radius of $r = 6.45mm$ and a maximum working load of $P = 100N$ then (3.25) and (3.26) produce values of t *min* and d *max* at the Yield Point stress, dependent on the value of r_o. These are given in Table 3.5.

r_o [mm]	2	1.5	1	0.5
t [mm]	0.24	0.28	0.33	0.41
d [mm]	0.15	0.11	0.07	0.03

Table 3.5 Calculated values of minimum thickness and maximum deflection at Yield Point stress (770N/mm ^{2}) for a diaphragm of radius 6.45mm loaded by 100N on the circumference of a circle of radius r $_o$.

By interpolation of Table 3.5 values of $r_o = 1mm$ and a thickness $t = 0.35mm$ were chosen for the diaphragm. These allows a maximum load of $P = 111N$ and a deflection $d = 0.096mm$ before permanent deformation occurs.

3.2.5 Indentor Mechanism

A major factor affecting the accuracy of the diaphragm-type stress transducer is that of ensuring the repeatability of the profile of force distribution over the diaphragm. In the two extremes a single point force applied near the supporting wall will deflect the diaphragm very little whereas the same point force applied in the centre of the diaphragm will produce maximum deflection. **Sanders et al [1990]** chose to place the normal-stress transducer on top of their three-axes device during clinical trials. In this situation the ability of the device to measure accurately the true stresses occurring at the body interface would depend on the possibility of tissue conforming to the surface of the diaphragm. In certain conditions, notably near or under bony prominences the major forces may be applied non-centrally. Even if a load spreading layer of material were interposed between the tissue and the device, there would be great demands on the properties and thickness of this material.

In order to ensure repeatability in the position and profile of any forces applied to the diaphragm used here, a fixed indentor is used. This is a flat plate with a cylindrical boss machined onto it. The plate is held central under the diaphragm, but free to move normal to it, by four guide pins inserted into the annular support wall of the diaphragm. This is most effective when the normal-stress transducer is attached to the bottom of the three-axis device. The indentor is also designed to provide overload protection. Its diameter is great enough that when the transducer is loaded by large normal stresses the indentor base plate impinges on the diaphragm support walls and therefore limits the maximum deflection of the diaphragm. Figure 3.20 shows a sectioned diagram of the pin-indentor arrangement and its operation.

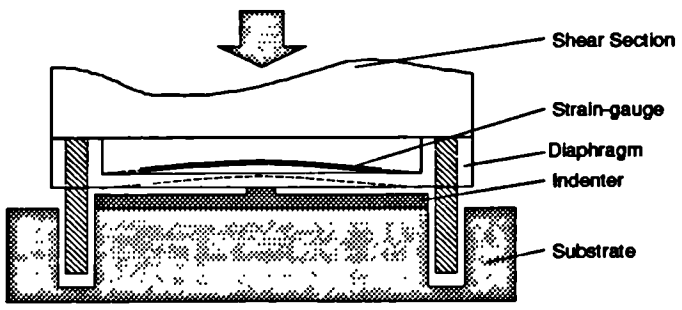

Figure 3.20. Sectioned view of the Normal-stress transducer showing the indentor mechanism.

3.3 Prototype Device Assembly

The combined prototype triaxial stress transducer is constructed from the two sub-assemblies; the biaxial shear-section and the normal-section. These sections are prepared and assembled separately before being bonded together.

In view of the size of the device as a whole compared with the forces it must sustain it is essential that component bonding be sound. To achieve a strong bond the careful preparation of the individual components and selection of the appropriate cement is vital. The sequence of assembly of each section is outlined below, along with any details of special preparations required at each stage.

During the assembly process achieving good alignment of the discs concentric to one another is essential. Any eccentricity in the shear section will appear as a displacement of the magnet and hence 'unbalance' of the MR output under no load. To facilitate alignment an assembly jig was made up that consisted of two plates and four rods. As the thickness of the silicone is also important shims were placed between the jig plates to regulate this. Figure 3.21 is a schematic of a device placed in the assembly jig while the cements dry.

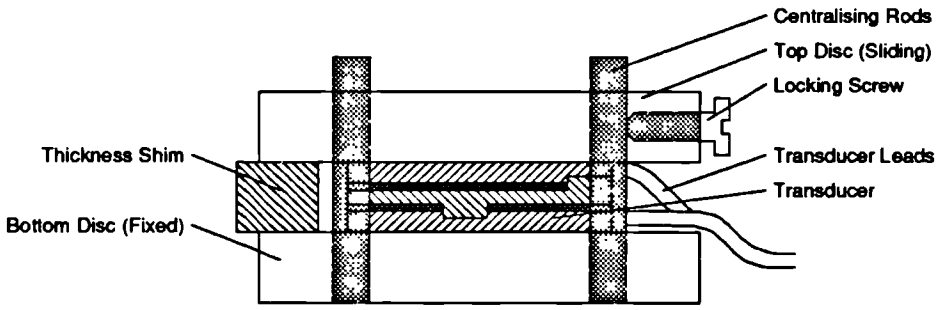

Figure 3.21. A diagram of the transducer captured in the assembly jig while the cement dries. Rods hold the device discs concentric and shims set the thickness.

3.3.1 Shear-section Assembly

The assembly procedure for the shear section began with the fabrication of the flexible PCB that was to hold each MR and device lead attachment. One was required for each axis. The flexible laminate was purchased externally, but the

photo etching and cutting out of the PCB were done in-house. The MR's were glued (cyanoacrylate) in place and their leads trimmed and soldered. After the section discs were inspected and deburred a lead and MR subassembly were cemented in each of the outer discs. The magnet was pressed into the centre disc and cemented in place (cyanoacrylate). All three discs were then cleaned prior to section assembly.

An outer disc was placed in the assembly jig and a layer of silicone applied. A thickness shim was placed on the outer side of the jig. The middle disc was inserted in the jig concentrically to the first and clamped down on the silicone to the height of the shim. Care was taken to ensure that the ridge and groove of the discs were engaged. When the silicone was cured the jig was unclamped and the same procedure followed for the remaining outer disc. A second thicker shim was used for that operation.

3.3.2 Normal-section Assembly

The assembly of the normal stress transducer section began with the manufacture of the diaphragm. After these were inspected and trimmed they were sent to the gauge supplier for mounting of the gauges.

Small rectangles of flexible PCB were cut and cleaned. On the diaphragm return, excess gauge cement was removed and the PCBs fitted. Gauge and device leads were soldered onto the PCB and the device lead insulation trimmed level with the annular wall. The indentor guide pins were fitted into their mounting holes and cemented in place.

3.3.3 Three Axis Device Assembly

The final assembly stage was where the normal-section was attached to the bottom face of the shear-section. In order to maintain some concentricity the assembly jig, of Figure 3.21, was used. The joint was to be capable of withstanding the maximum shear-stress applied to the device, so the adhesive used was an high-strength epoxy. Both faces of the join were lightly abraded and thoroughly degreased. The shear section was first inserted in the jig so that the bottom face was up. A thin

layer of epoxy was applied to the upper face of the normal-section's annular support wall. When the layer had gone tacky, the normal-section was inserted upside down in the jig. The two sections were pushed into contact by sliding the top plate of the jig down over the jig rods. Pressure was applied to force the jig plates together and the locking screw tightened. When the epoxy had hardened the devices were removed from the jig and the excess epoxy and silicone rubber removed. Each device was uniquely labelled to identify it with its own calibration data - as the component and assembly variables make each device different.

3.4 Mounting Considerations

A transducer must be placed at each measurement site of interest in a socket. This must be done in such a way as to maintain the integrity of the socket and provide a rigid fixing base for the transducer. To achieve this a device is recessed into the socket wall, sandwiching the indentor plate underneath it. The pin and hole combination allow the whole device to move in a direction normal to the socket but prevent translational or rotational motion. All forces are applied to the upper surface of the shear-stress subassembly. The normal components of these forces are transmitted through the shear-stress section driving the whole device onto the indentor plate. The coplanar force components react against the guide pins and move the discs of the shear-stress section.

In order for the shear sections to move unhindered there must be a clearance void surrounding the two sections. Care must be taken to keep the void width to a minimum. During clinical trials skin or stocking may be folded into it, impeding transducer movement. Figure 3.22 shows the mounting arrangement in the socket. In this schematic the transducer is shown with a disc of liner material bonded to the top shear section. The primary purpose of this is to attempt to match the frictional and stiffness properties of the transducer location to those of the surrounding material.

It is essential that the recess in the socket wall, into which the transducer locates, be a precision fit. Also, that the device top surface be coplanar to the inside face of the socket wall. To achieve this, a transducer shaped epoxy blank of the correct dimensions is lightly bonded to the liner fitted over the residual limb positive prior

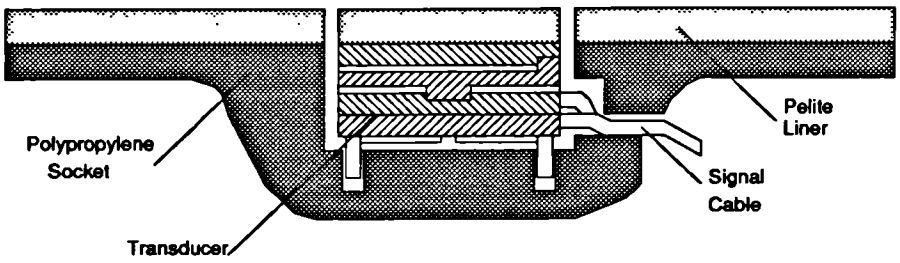

Figure 3.22 Simplified schematic representation of the mounting arrangement of the three-axis device in the socket wall.

to drape forming. During the forming process the softened polypropylene moulds itself around the blank. After the socket positive is withdrawn the blanks are removed and the recess trimmed for the correct fit.

The blanks themselves are made in a moulding process. The positive for the mould is machined from a single aluminium block. It has essentially the same shape as the assembled transducer, complete with leads and pins. The dimensions for it are shown in Figure 3.23. Its diameter must be that of the transducer, plus one millimetre for clearance when the shear section is displaced under applied stress. The stubs for lead exits are extended from their true exit depth to the top surface of the device (surface nearest the limb interface) so that the polypropylene does not form over the blank leads, preventing their removal. Its height includes the thickness of the indentor plate. Holes are drilled into the positive, and steel pins are fitted. These pins are oversized to provide a clearance fit for the transducer pins in the socket wall. Their length is also exaggerated to provide depth clearance.

The mould is made from low viscosity, low temperature coefficient silicone rubber, (Silcoset 105 - Ambersil UK Ltd). The silicone is poured into a small bowl - in this case the cap off a spray can. It is placed in a low-vacuum chamber for fifteen minutes to remove any air from liquid. The positive is mounted on a flat disc and placed inverted into the silicone. Figure 3.24 describes this arrangement. The bowl is then left in the vacuum chamber overnight while the silicone cures. The silicone is then removed from the bowl.

A low viscosity, low temperature coefficient two part epoxy, (Epotek 301 - Intertronics Ltd, UK), was used for the blanks. This was dimensionally stable at the temperatures

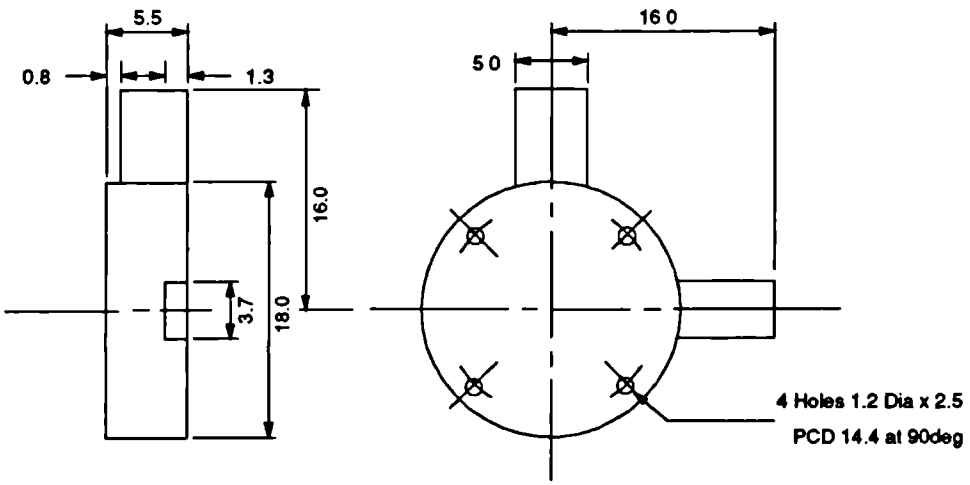

Figure 3.23 Dimensions of positive master used in making mould for epoxy blanks which form transducer recess in the socket wall.

experienced during drape forming. Epotek was mixed and poured into the mould. Only enough epoxy was poured to just fill the mould. A bent paper clip was used to encourage air bubbles out of the pin holes. The mould was placed in the vacuum chamber for thirty minutes to remove trapped air. A sheet of Mylar was placed on the mould and weighted. Epoxy does not bond to the Mylar and the weight ensures a smooth flat surface. Figure 3.24 describes this arrangement. To speed the cure of the epoxy the mould was placed in a laboratory oven at *80℃* for twelve hours. The blank is popped out of the mould and trimmed.

The intended measurement sites in the socket are marked on the liner, and blanks are lightly bonded in place at the correct orientation. After the drape forming process when the socket positive and liner are removed the blank stays in the socket wall. These are then levered out or broken. The remaining recess is then trimmed, and device-lead access holes cut through the socket wall. Discs, the diameter of the recess are cut from the liner at the marked sites. These have one millimetre trimmed off their radius for clearance. They are bonded to the top of each device. The liner is placed in the socket, and each device lead is split and passed through the holes in the socket wall. A view of a prepared recess and an instrumented socket is presented in Figure 3.25.

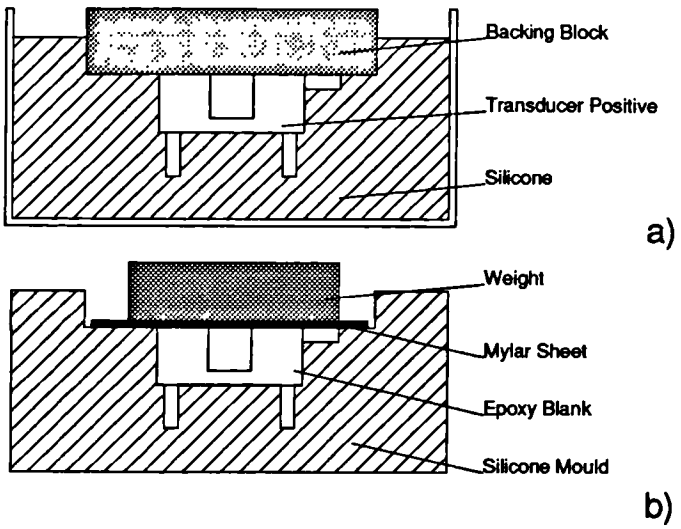

Figure 3.24 Schematic describing the making of the mould a) and the making of the epoxy blanks from the resulting mould b).

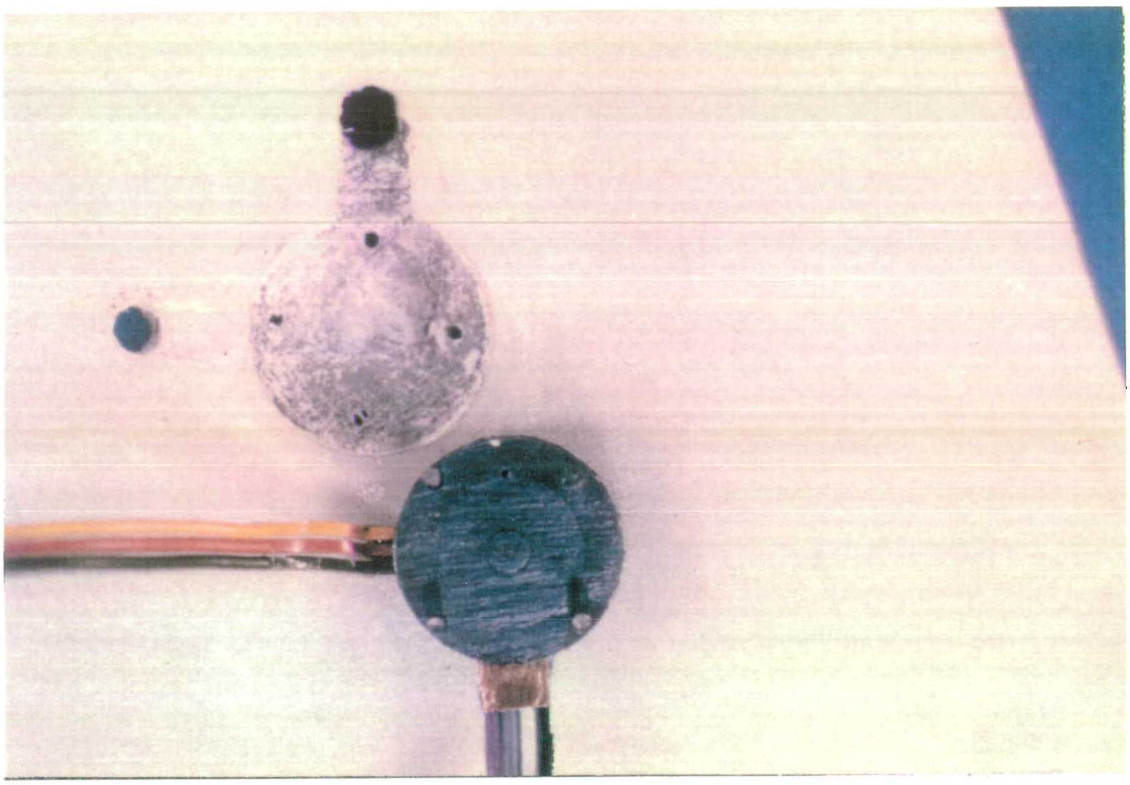

(a)

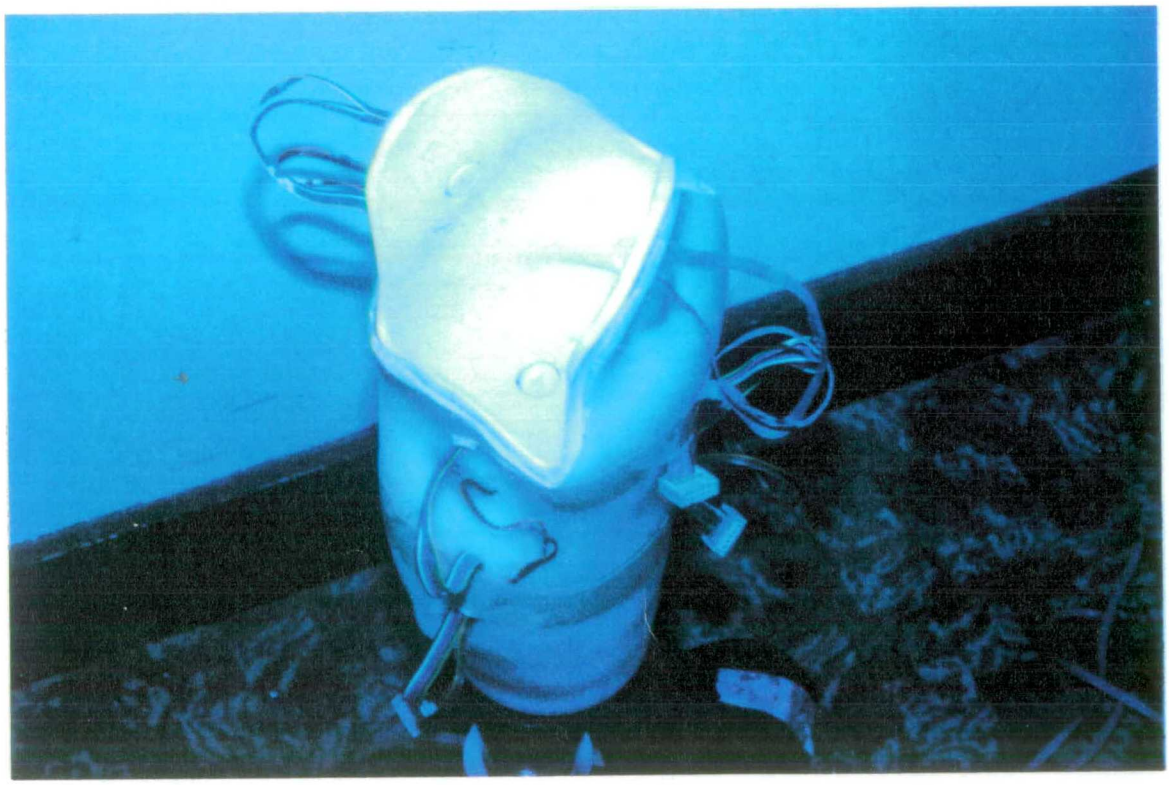

(b)

Figure 3.25 View of the recess in the socket wall after the removal of the epoxy blank a). Picture of an instrumented socket, showing the device lead exits through the socket wall b).

Chapter 4
Triaxial Stress Transducer
- Development to Requisite Form

It is the objective of this chapter to plot the progress of the design of the transducer and to record the best performance demonstrated with the final design - within the limits of the experiments performed. Notes are made of the critical areas of assembly and explanations are given of the testing phenomena observed. It is not the intention to discuss the manufacturability or likely production yield of this design. Variability in performance between devices was generally broad as these were hand assembled products. It is expected that the variation in experimental results presented here may well be reduced with a more automated manufacture process.

The prototype shear and normal stress transducer sections described in Chapter 3 were subjected to a number of tests. The effectiveness and adequacy of the critical components of each section were analysed and reported here. After modification and reselection of components, the sections were then reassembled and retested. On achieving a successful combination of components a triaxial device was assembled and tested. In the last part of the chapter, details of calibration tests are presented and the transducer performance compared to that of the requisite transducer specified in 2.6.

4.1 Shear-Stress Section Development

In this part of the chapter the development of the shear stress transduction mechanism is detailed. Overall there were many changes made to the section design at differing intervals. However for simplicity these changes are all collected into three design stages. The first prototype will be considered as **Design A**, the second as **Design B**, while the final form of the shear section is presented as **Design C**.

For each design stage a discussion is given of:

the considerations made for the selection of components
the performance test methods and equipment
the results reported from the tests

the limitations of, or necessary changes to be made to, the current design. At each stage the design was assessed for stress and temperature sensitivity as a whole section as well as at component level.

4.1.1 First Prototype Assessment - Design A

In order to obtain a 'feel' for the significance and interplay of each component's performance in the section, four identical sections (aluminium-silicone-aluminium) were constructed using the silicone, **Ambersil 1039N**, which was most highly recommended by the suppliers. Tests were run on these sections. In parallel, samples of each of the other silicones [3.1.2.4] were bonded between two transducer-sized blank aluminium discs and their stress-strain and creep properties assessed. The results of these investigations are reported in the following subsections, and a summary made in [4.1.1.4]

4.1.1.1 Test Regimes and Equipment

The test types, methods and equipments used in the initial appraisal of the prototype sections are reported here.

Each section was tested for sensitivity, linearity with applied load, and insensitivity to temperature changes. The properties of most importance were seen as ;

resolution of small forces
repeatability of any measurement
linearity of output with applied stress
sufficient dynamic range for clinical stresses
output independent of frequency and temperature

The device temperature tests were undertaken primarily to determine the stability of the device's output over the range of temperature changes normally expected in the clinical situation. Secondly it was necessary to ascertain if there may be any changes to the device's modulus of rigidity. Both of these would produce an apparent-strain error signal which would compromise the device accuracy and may invalidate its calibration curve.

Various testing equipments were used in carrying out these initial tests, some of which existed in the Department while others had to be constructed. The force tests were initially performed on an **Instron - 1195** Materials Testing Machine. This instrument attempts to deform a test sample by tension or compression between a moving crosshead and a rigid base. The degree of deformation is measured by an extensometer attached to the test sample, and the amount of force required to achieve the deformation is measured by a loadcell mounted on the crosshead or base. The rate of deformation, the maximum force applied and the maximum displacement can be separately controlled. With these functions it is possible to apply cyclic loads at specific rates and to given force limits. A strip chart in the instrument records the applied deformation and resultant forces developed in the test sample.

In order to apply shearing forces to the transducer a special calibration jig had to be designed. Figure 4.1 shows an exploded schematic of the construction of the jig. It consisted of two holding blocks (*A, B*) mounted between side walls. One block (*A*) was fixed to the Instron base loadcell and the other (*B*) to the crosshead. Block *B* was confined to move vertically and parallel to the other (*A*) by two linear bearings (*C*) fixed on to the side walls. Each of the blocks had a cylindrical hole machined out of its centre. Into each of these holes fitted one half of a cylinder (*D*). Each half cylinder had a recess cut into one end for holding the transducer. The transducer (*E*) was sandwiched between the cylinder halves which was then inserted into the holding blocks and fixed by screws. The cylinder could be rotated to allow stresses to be applied to the transducer from any angle in the shear plane. A photograph of the assembled jig is also given in Figure 4.1.

In the initial tests the output from the shear section was obtained by using a digital multimeter (Solartron 7045 - Schlumberger (UK) LTD) to measure the resistance of each 'arm' of the MR element. These readings each took about ten seconds to complete. Because of this the Instron was paused during its stroke and the displacement held while readings were taken. Thus linearity tests occurred as a multistage ramp. Unfortunately this method allowed stress-relaxation to add errors to each reading, but for a first approximation this scheme was acceptable.

To assess their temperature sensitivity the sections were placed in a small thermostatically controlled electric oven ($0.25m^3$). Hygroscopic gels in the oven assured a dry heat. The device leads and a temperature meter probe were introduced

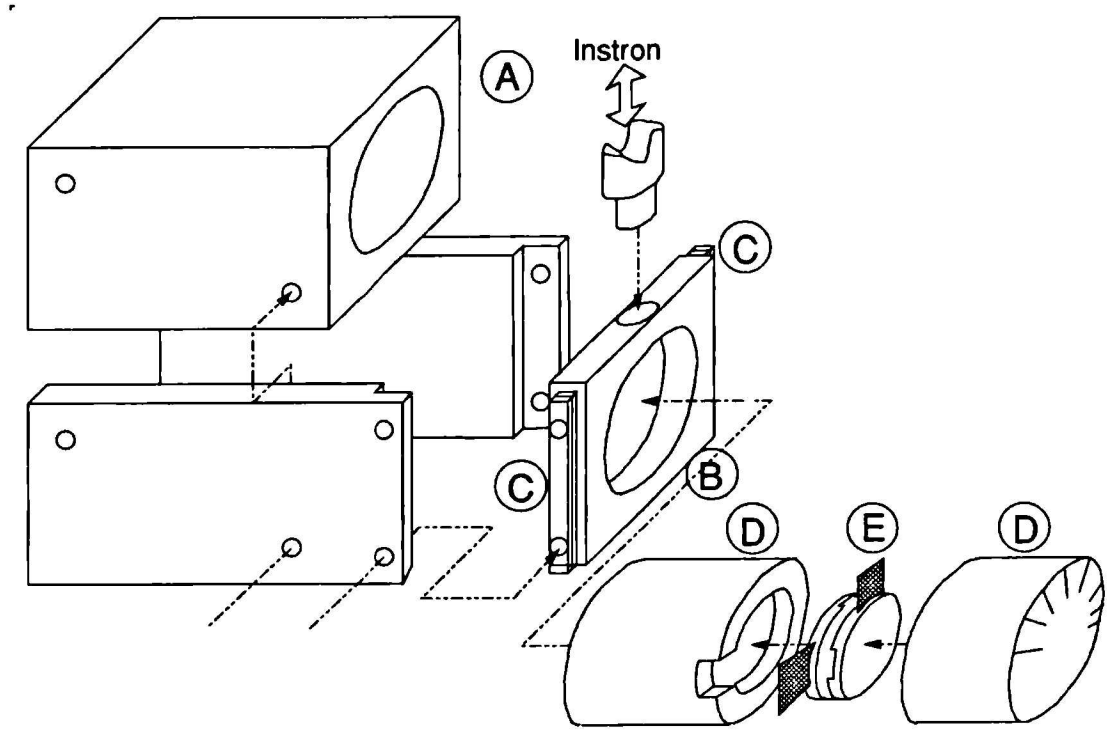

(a)

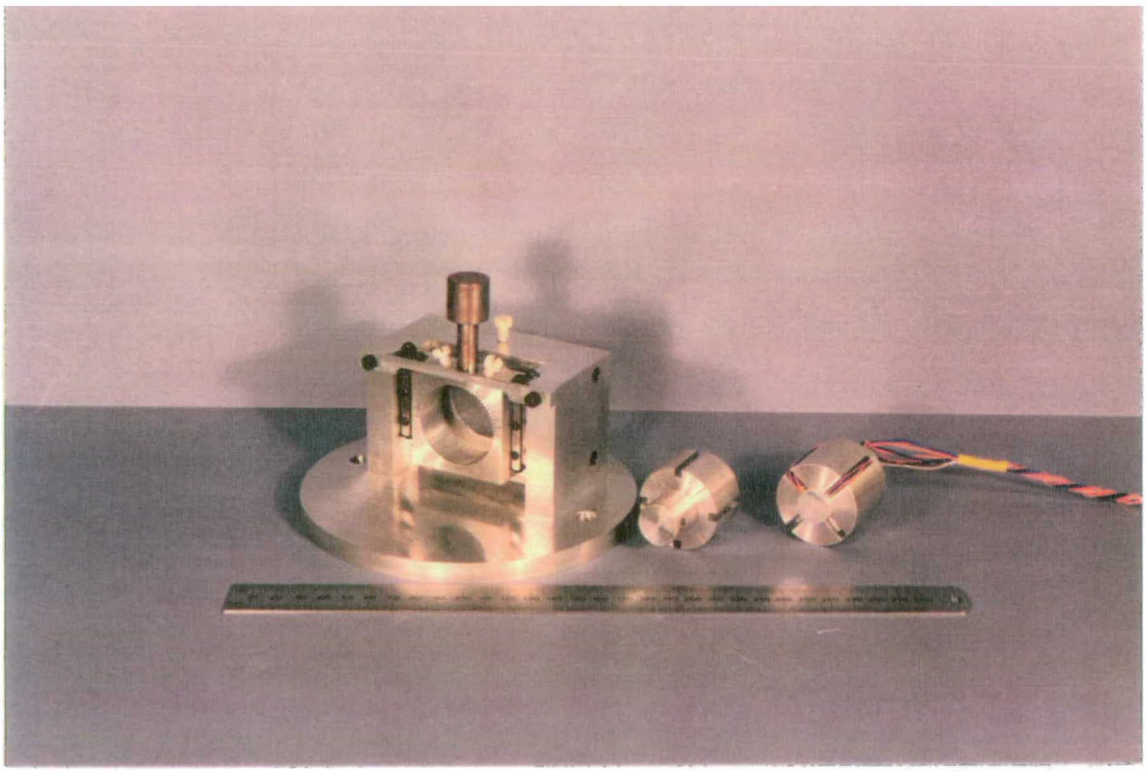

(b)

Figure 4.1 a) Exploded schematic of the construction of the calibration jig for applying shear forces to the transducer; b) photograph of the assembled jig.

into the oven via a baffled vent hole in the roof. The temperature meter (MEP123 - Medical Engineering and Physics, Dulwich Hospital, London) used for this measurement, had an accuracy of $\pm 0.1\,^{\circ}C$ over the range $-200\,^{\circ}C$ to $400\,^{\circ}C$.

During these tests the section's signal output was expressed in terms of the resistance ratio of the two arms of the magneto-resistor. This was calculated in the same manner as a resistive divider ratio. That is, given a device which had R_1 ohms in one arm and R_2 ohms in the other, then:

$$\Re = \frac{R_1}{(R_1 + R_2)} \tag{4.1}$$

the percentage change in the resistance ratio $\Re$ with force or temperature is then calculated as:

$$\Delta\Re_{\%} = \frac{(R_{max} - R_{min})}{R_{min}} \cdot 100 \tag{4.2}$$

This assumes a linear change in resistance ratio with applied stimulus. All the devices have an initial zero-stress ratio of approximately $\Re = 0.5$, so comparisons of sensitivity are possible.

From the work of **Pollard [1984]** it was considered that the maximum expected shear force on the plantar surface would be less than *50N* (over $2cm^2$). Over this force range the value of $\Delta\Re_{\%}$ was the full scale sensitivity (*FSS*) of the device, from which unit sensitivity was calculated [$\Delta\Re_{\%}/N$].

4.1.1.2 Static Stress Response

Two regimes of loading the devices were used. A multistage ramp increasing/decreasing displacements until a given load was reached (*0, 2...50N*), pausing at intervals for measurements. This test was designed to observe the linearity of the devices. Secondly, cycling between fixed loads pausing at force extremes for measurements (*0, 30, 0, 30N*), allowed changes in the stiffness of the rubber to be observed as a change in the slope of a stress strain plot. Similarly any viscoelastic changes due to heat build up from losses in the material or creep would translate the curve parallel to its initial curve.

The four assembled sections [4.1.1] and the silicone blanks (aluminium - silicone - aluminium) were subjected to force cycles at orientations of *0°,45°* and *90°* to the applied force vector. The silicone blanks were also orientated to preclude nonuniform bonding from elevating stress values. Measurements of the output ratio, $\Re$, and the deformation were taken at force intervals during loading and unloading. For the period of the measurement the applied stress was held constant.

4.1.1.2.1 Linearity and Range

Force versus resistance ratio curves typical of Design A are shown in Figure 4.2. They describe the change in resistance ratio for force applied in a multistage ramp to *50N* while the sections were at an orientation of *45°*. Also shown is the response to five force cycles - measurements were only taken at *0N* and *50N* - and the response to a *100%* overstress. From this it was seen that both axes exhibited a linear change in $\Re$ with applied stress; the force versus resistance ratio curve was repeatable; and the silicone was linearly elastic in its behaviour. Figure 4.2 also shows that the section design was typically able to withstand at least *100%* overstress. Table 4.1 lists the *FSS* of the sections under load at the three orientations.

Orientation	*FSS* $[\Delta\Re_{\infty}]$			
	1	*2*	*3*	*4*
0°	*5.04*	*5.3*	*4.8*	*4.7*
45°	*3.49*	*3.68*	*3.42*	*3.2*
90°	*0.06*	*0.69*	*0.3*	*0.5*

Table 4.1 Full scale sensitivity to load of four shear sections of Design A. Sections were orientated at 0°, 45° and 90°.

Figure 4.3 shows the FSS of two mutually perpendicular shear sections to tangential loads applied at different orientations. Sinewaves are superimposed on each plot for comparison. The phase offset seen between the two axes was due to transducer alignment errors in the calibration jig. The data indicates that the direction of load vectors can be derived with reasonable accuracy under this design.

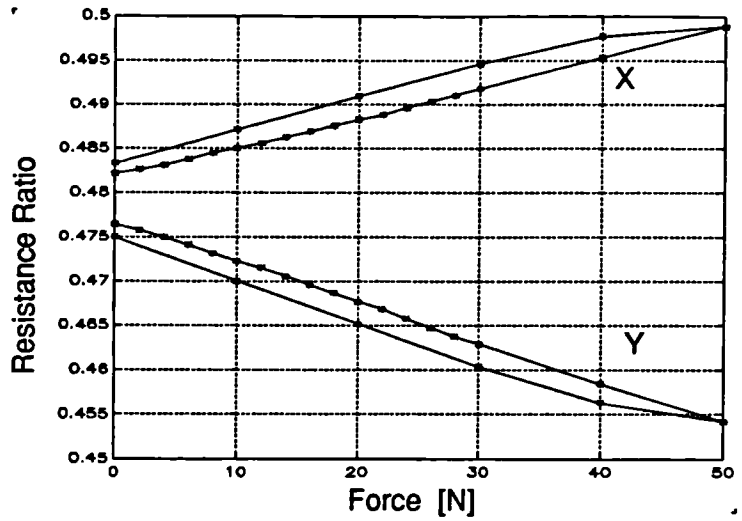

(a)

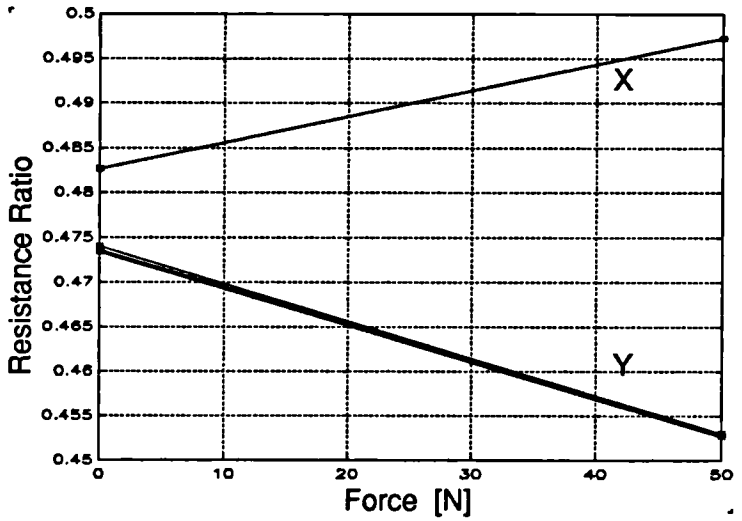

(b)

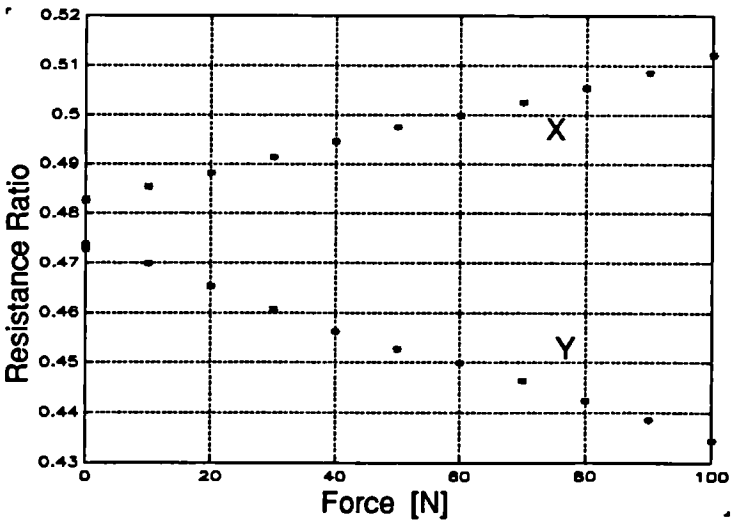

(c)

Figure 4.2 Force versus Resistance Ratio curves of th X & Y axes of a typical shear section of Design A. Linearity of response to 50N (a). Repeatability over 5 cycles to 50N (b). Response to a 100% overstress (c). All loads were applied at a 45° orientation.

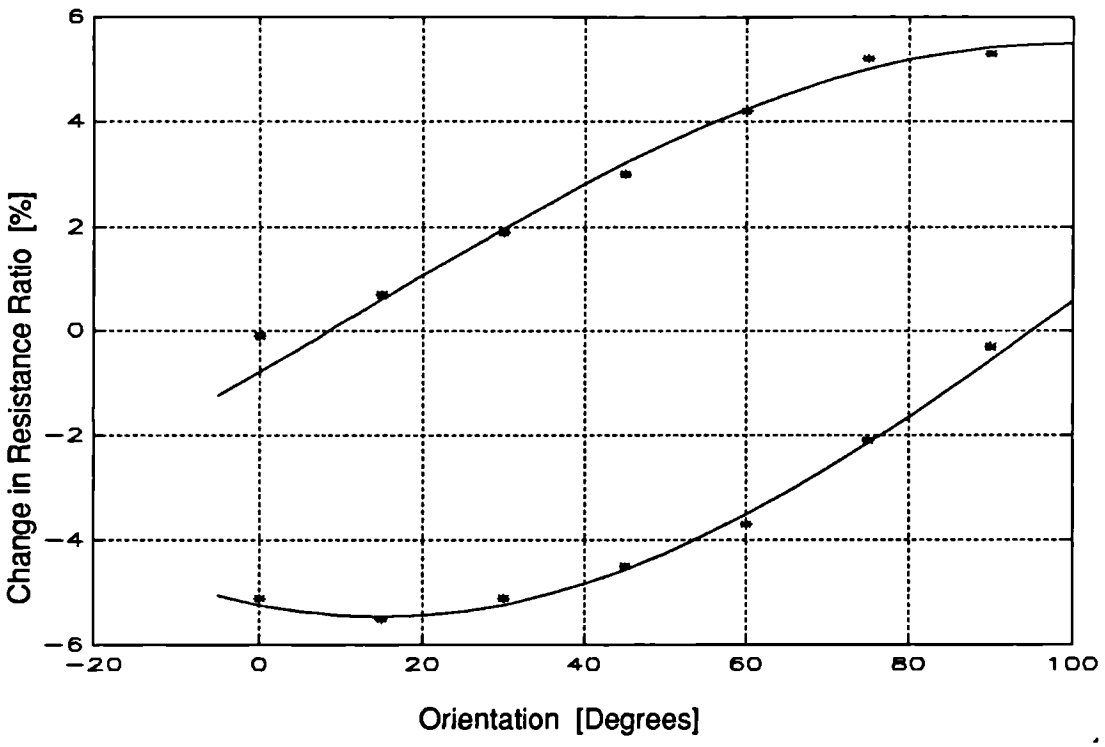

Figure 4.3 Typical Response of a shear section of Design A to force vectors applied at various orientations in the shear plane.

4.1.1.2.2 Creep and Hysteresis

It was noted from Figure 4.2 that there was significant hysteresis in the force versus resistance ratio curve. There were two major implications of this: heat build up under prolonged stress cycling may affect the viscoelastic property of the rubber; and an amount of uncertainty is introduced in assigning a resistance ratio to a given force. It was expected, however, that the former was less likely to be significant due to the small number of cycles occurring during clinical trials. This was supported in the laboratory as the transducer response was repeatable after several hundreds of cycles. Thus, the magnitude of the hysteresis was thought to be the more important problem.

It was also noted for the multistage cycle that the values of $\Re$ at zero load were not coincident. This was attributed to more periods of measurement and hence more stress relaxation occuring during loading than unloading. A period of unloading equal to the loading period was required to release completely the energy stored in the rubber.

The average magnitudes of hysteresis loops of the four sections are reported in Table 4.2. Each section was subjected to five cycles, to *50N*, at orientations of *0°*, *45°* and *90°*. The values measured were seen to be significantly large, for some sections, in relation to the FSS of the section.

Orientation	*Hysteresis [N]*			
	1	*2*	*3*	*4*
0°	*11.4(.89)*	*13.4(.55)*	*16.6(.89)*	*14(.71)*
45°	*14.2(1.1)*	*15.4(.89)*	*20.8(.84)*	*16.8(.84)*
90°	*12.1(.55)*	*13.8(.45)*	*15.6(1.14)*	*15(.71)*

Table 4.2 Average magnitude (standard deviation) of hysteresis in four shear sections of Design A. Each was subjected to five cycles to 50N applied at orientations of 0 °, 45 ° and 90 °.

To determine if the hysteresis seen was particular to the silicone used, a comparison of the mechanical properties of the three silicone samples - **Ambersil 1039N**(A), **Dow Corning RTV738**(DC) and **General Electric RTV157**(GE) - were made. Silicone test pieces (*0.8mm* thick) were sandwiched between two aluminium discs of the same diameter as the transducer. Each silicone was mixed in air and allowed to cure for their recommended times. Shear forces were applied to the blanks (aluminium - silicone - aluminium) using the transducer calibration jig coupled to the Instron. Each was subjected to a constant rate of strain (*0.5 mm/min*) until a force of *50N* was reached, at which point the strain was held. During the test the reaction force generated in the samples was recorded on the Instron chart recorder. Figure 4.4 shows the resultant force-time curves as traced from the chart.

From linear approximations of the initial parts of each curve, it was possible to derive average shear modulii for each silicone.

It is obvious that GE and DC silicones were less rigid than silicone A, and would therefore stretch further for any given applied force. In a transducer this would give rise to greater device sensitivity and a smaller range for a given thickness of the rubber layer. Both A and GE exhibit quite linear force response with applied strain, while DC was significantly non-linear. The latter part of the curves indicates that stress relaxation is occurring in the silicone. A and GE show similar relaxation

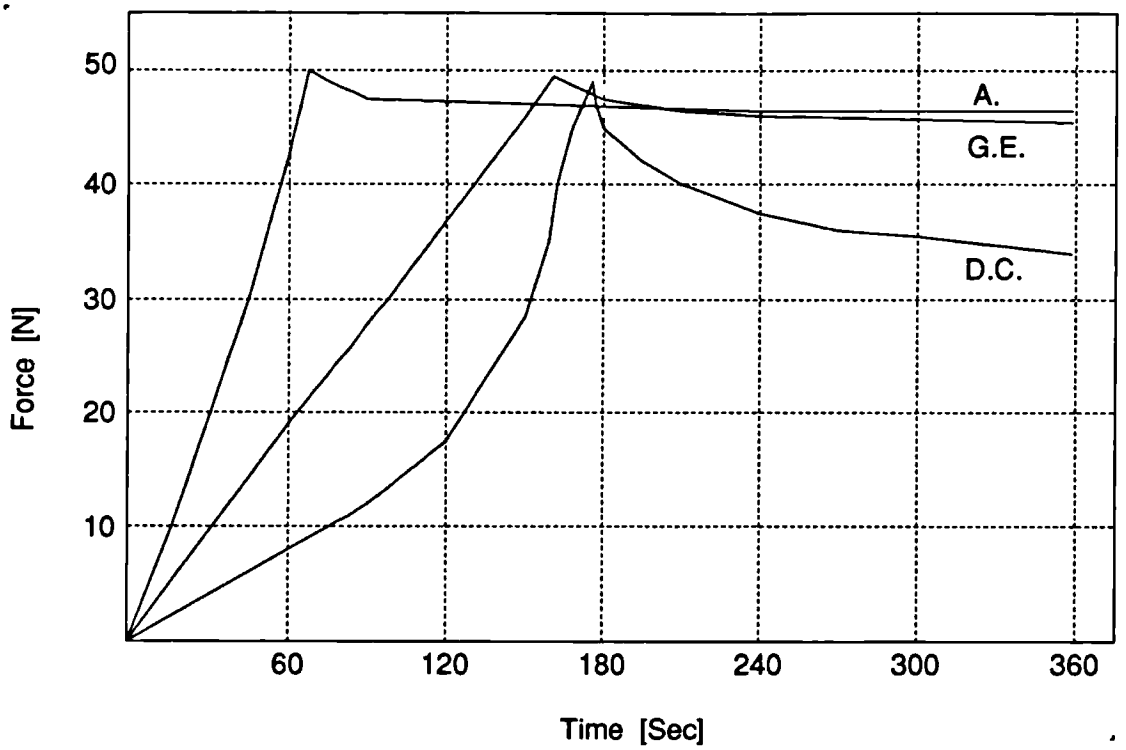

Figure 4.4 Reaction force occurring in three silicone rubber samples when subjected to constant strain rate (0.5 mm/min). After reaching 50N the strain was held constant.

but DC shows dramatically more. The use of DC in a measuring device would therefore result in a loss of accuracy for forces applied at low frequency. The greater the rate of relaxation the higher the low frequency limit of accuracy. The greater the amount of relaxation, the greater the magnitude of conversion inaccuracies.

It was felt that during clinical use where constant stresses are applied to the transducer, it would be more likely to experience creep than relaxation. Thus, in order to quantify creep reactions in each blank (aluminium - silicone - aluminium), they were subjected to a *30N* step load for *60sec*. The resultant displacements were measured with the Instron extensometer and logged on the chart recorder.

Table 4.3 presents the observed creep rate in the blanks. The values are expressed in terms of the percentage increase in displacement, over the instantaneous displacement (*1Sec*), with the logarithm of time (seconds).

In summary it was clear from Figure 4.4 that GE could replace A as the rubber in the shear section. With a layer of half the thickness the same displacement would arise for a given force but allowing a corresponding decrease in the magnet

Silicone	*Creep Rate [%strain/log(Sec)]*
General Electric - RTV157	*3.6 (.4)*
Ambersil -1039N	*4.6 (.2)*
Dow Corning - RTV138	*23 (3)*

Table 4.3 Average creep rate (standard deviation) in disc's of silicone (16 dia x 0.8 mm) when subjected to a 30N step shear stress.

element separation (for flush mounting magnets), so increasing the device sensitivity. Also, it was obvious that the GE silicone had similar stress relaxation resistance to that of A. So for improved performance the GE silicone was chosen to replace A for the next development stage.

4.1.1.3 Temperature Sensitivity

The temperature sensitivity of the shear section was assessed by measuring the resistance values of each axis when the unloaded section was heated from *20℃* to *50℃*. The four sections in turn and a temperature probe were suspended inside the oven [4.1.1.1]. The temperature was incremented in steps. At each temperature the sections were allowed to stabilize for thirty minutes before a measurement was taken. Figure 4.5 shows the resultant change in resistance ratio with temperature for each of the sections. There are three notable features in the data plots. Firstly, the temperature coefficients are constant (linear slope). Secondly, the coefficients are of opposite sign for sections with an initial resistance ratio greater than the balance value of *0.5*$\Re$. Thirdly, the coefficients corresponding to an initial $\Re$ value greater than *0.5*, are greater than those of initial $\Re$ value less than *0.5*.

The opposite signs of the coefficients were due to the magnetic field experienced by the MR being reduced with increasing temperature, so causing $\Re$ to return toward *0.5* - zero field value. A reduced magnetic field at the MR could have been caused by the magnet field strength decreasing or the magnet-element separation increasing. Thus, a possible theory for the differing magnitudes of the coefficients, above and below $\Re$=*0.5*, was that the symmetry of the MR resistances have a negative temperature coefficient which adds algebraically to the above phenomenon.

Now, over the range *20-40℃* the resistance ratio of a section may change by up to *1%* due to temperature effects alone. When compared to the FSS of a section (approximately *5%*) the above value becomes very significant. To explore the above theory and the origins of the device's temperature sensitivity, a number of experiments were carried out to determine the contribution of each component toward this error.

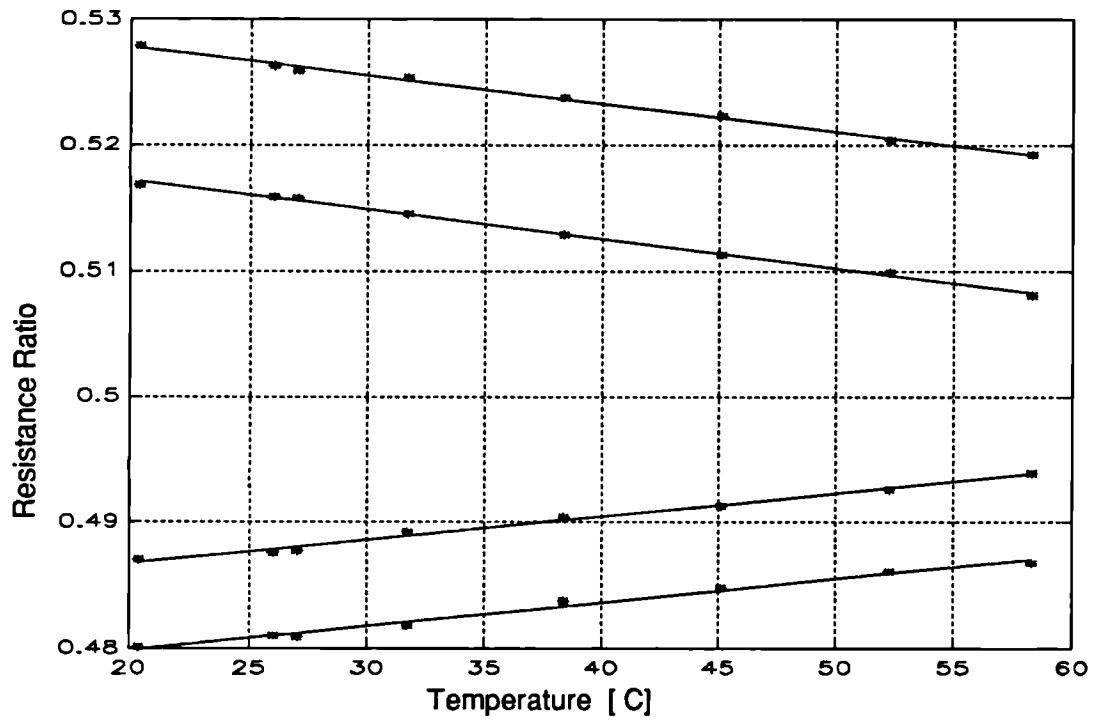

Figure 4.5 Change in the resistance ratio of four sections of Design A when subjected to temperatures from 20 - 58℃.

4.1.1.3.1 Magnetoresistor Contribution

Siemens, the manufacturer of the MR, advised that the distribution of In/Sb needles [Table 3.4] was not uniform for both arms, due to manufacturing tolerances. This may cause the centre point of the MR to change by *±1.5%* over the temperature range *20-40℃*. To verify this three elements were placed in the oven and the temperature raised from *20-50℃*, while the resistance ratio was measured. Figure 4.6 shows the change in resistance ratio for each element with temperature. The results were found to be of a smaller magnitude than the quoted value of the temperature coefficient [3.1.3.2] being only; *-0.0075, -0.0141, -0.0174* $\Delta\Re_{\alpha}/°C$. The tests were carried out under a *0.0T* field compared to the *0.3T* field, approximately,

found in the assembled section. Under the latter conditions the temperature coefficients and resistances would be larger, possibly resulting in a larger change in the centre point with temperature (refer to Figure 3.15). Additionally, the distribution of In/Sb needles is statistically random under production techniques so the elements tested here may only have moderate differences in needle distribution. All in all, the negative coefficient, supports the earlier theory of the unequal magnitude of the coefficients either side of $\Re=0.5$.

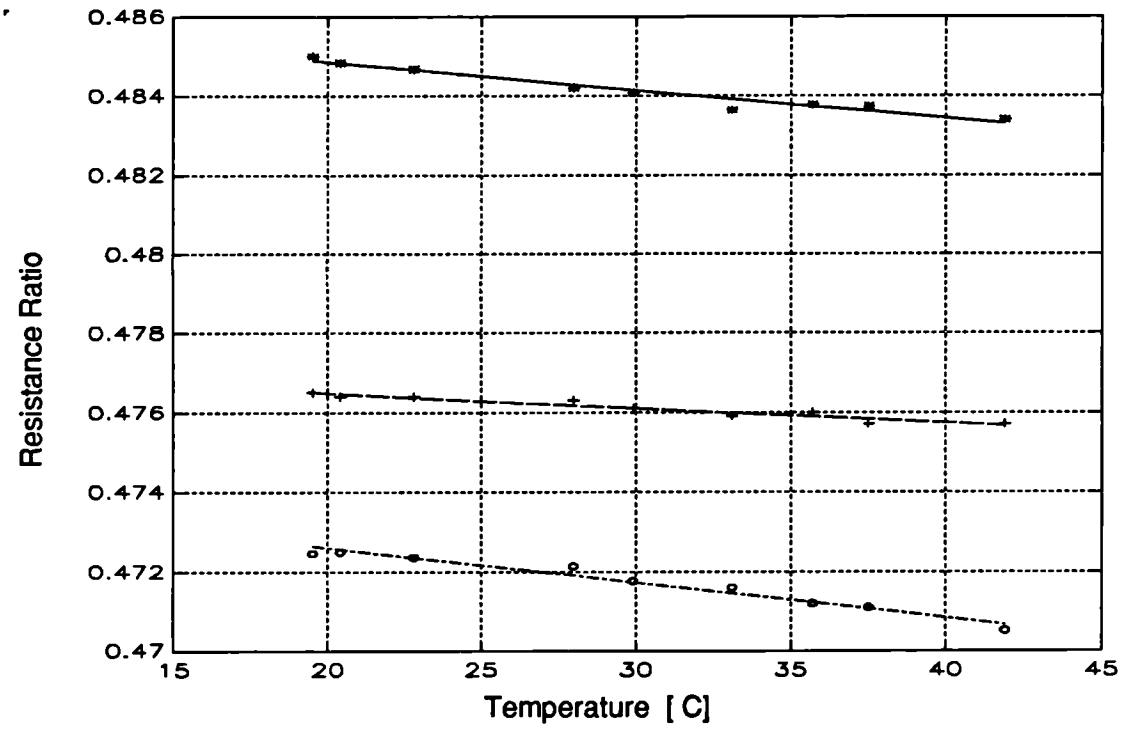

Figure 4.6 Experimental measurements of the change in resistance ratio of FP110D155 magneto-resistors with temperature.

4.1.1.3.2 Silicone Expansion

The change in resistance ratio due to temperature effects on the rubber layer was assessed by two related experiments. The axial expansion of the silicone layer was measured with increasing temperature. Secondly, the change in resistance ratio with magnet-element separation was determined.

Samples of the three silicones were mixed in air, as they would be when mixed for the transducer, and bonded between blank aluminium discs. The overall thickness

of each assembly was measured with a micrometer at *23 ℃* (room temperature) and then at *79 ℃*. The expansion of the aluminium was assumed negligible compared with the silicone. This assumption is thought valid due to the low linear coefficient of expansion for aluminium (*23 x 10^{-6} cm/cm/ ℃*), compared to that of the silicones (*10^{-4} cm/cm/ ℃*). The rubber was also assumed to expand linearly with temperature. The results of the experiment are presented in Table 4.4.

Silicone	*Aerated [cm/cm/ ℃]*	*Pure [cm/cm/ ℃]*
Ambersil (1039N) (A)	*3.4 x 10^{-4}*	*
Dow Corning (RTV738) (DC)	*4.5 x 10^{-4}*	*3.1 x 10^{-4}*
General Electric (RTV157) (GE)	*5.1 x 10^{-4}*	*2.7 x 10^{-4}*

* Value not specified by the manufacturer

Table 4.4 Linear thermal expansion of silicones A, DC and GE. Comparison of measured values for aerated silicones, with pure silicones.

The change in resistance of an MR element with magnet-element separation is dependent on three principle factors: the uniformity of In/Sb needle distribution in the active areas of the MR element; the magnitude, direction and homogeneity of the magnetic field; and the MR-magnet separation distance. To assess the combined effect of all these parameters, an MR element mounted on a PCB was fixed to the bed of a automated X/Y plotting table, while a magnet was held perpendicular to it at a separation of *0.1mm*. The resistance ratio of the arms cf the element was measured while the magnet was scanned across it in *0.15mm* steps. These measurements were repeated while incrementing the separation in *0.1mm* steps to reach a maximum separation of *1.5mm*. A summary of these measurements is presented in Figure 4.7. The nominal silicone thickness in a shear section is *0.5mm*. From Table 4.4 the likely expansion of silicone A, over the temperature range *20-40 ℃*, was *3.4μm* (*0.5mm* to *0.5034mm*). A change in the magnet-element separation of this magnitude may alter the MR output, in the worst case, by $0.019\Delta\Re_{\%}$ - [Figure 4.7.]

The expansion of the silicone layer resulting in an increase in magnet-element separation and subsequent decrease in the field at the MR is an additional mechanism causing $\Re \rightarrow 0.5$ with an increase in temperature.

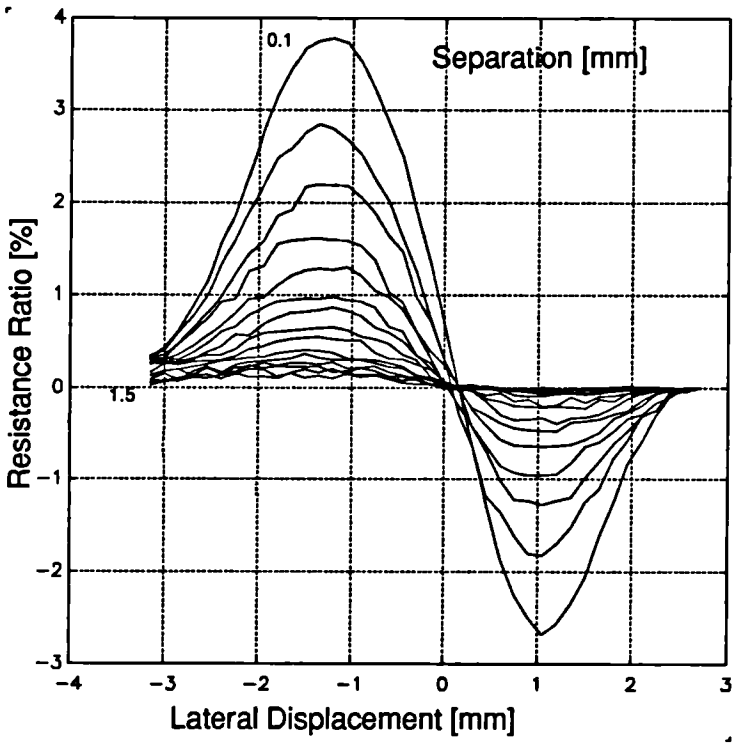

(a)

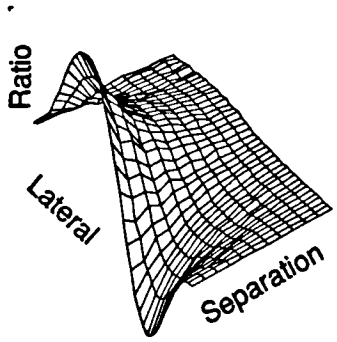

(b)

Figure 4.7 Resistance ratio variation as a function of magnet - magnetoresistor separation, for an FP110D155 differential magnetoresistor (Siemens (UK) LTD) and a 3x2mm diameter SmCo magnet (Magnet Developments LTD). Values were measured on a 0.15mm (lateral) x 0.1mm (vertical) grid. Data is shown in profile (a) and also as a 3D mesh (b).

4.1.1.3.3 Magnet Contribution

The last component assessment was the change in the magnet's field strength with temperature. The suppliers of the magnet (Magnet Developments LTD, UK.) advised that the temperature coefficient was approximately *0.1%/℃* for the range *0-100℃*. An attempt was made to verify this, but due to the lack of availability of a magnetometer with a probe size less than or equal to the magnet diameter, and which has a temperature stabilised output, the magnet temperature coefficient was estimated indirectly. An element was fixed to a solid base and a flat bottomed polystyrene dish supported immediately above it on spacers. The magnet was held against the bottom of the dish above the centre of the element. Water at *50℃* was introduced to the dish and allowed to cool, while the element resistance was measured at regular intervals. The change in the field strength of the magnet was measured by the change in resistance of the MR element. Figure 4.8 is a graph of the results. However, it was thought that the MR would experience some heating as well and therefore the change in its output would be due to both coefficients. Also the magnet-element separation was unavoidably greater than that used in the section. The change in the field strength detected by the MR at the separation used in this experiment would be less than those typically found in a transducer. Thus the derived temperature coefficient was thought to be an underestimate.

It was clear that the field strength of the magnet diminished with temperature (*-0.0088* $\Delta\Re_{\%}/°C$), further supporting the earlier theory where the sign of the temperature coefficients either side of $\Re=0.5$ are opposite.

4.1.1.4 Discussion

The following is a summary of the test results for Design A and their implications.

There are three observations that recommended this design. Firstly, from Figure 4.2 it is seen that the sections output response to applied stress is approximately linear. Thus the calibration and data processing of clinical measurements is simplified. Secondly, it also indicates that measurements are repeatable, with some minimal errors. Thirdly, Figure 4.2 shows that the design could withstand a *100%* overstress without its function being impaired.

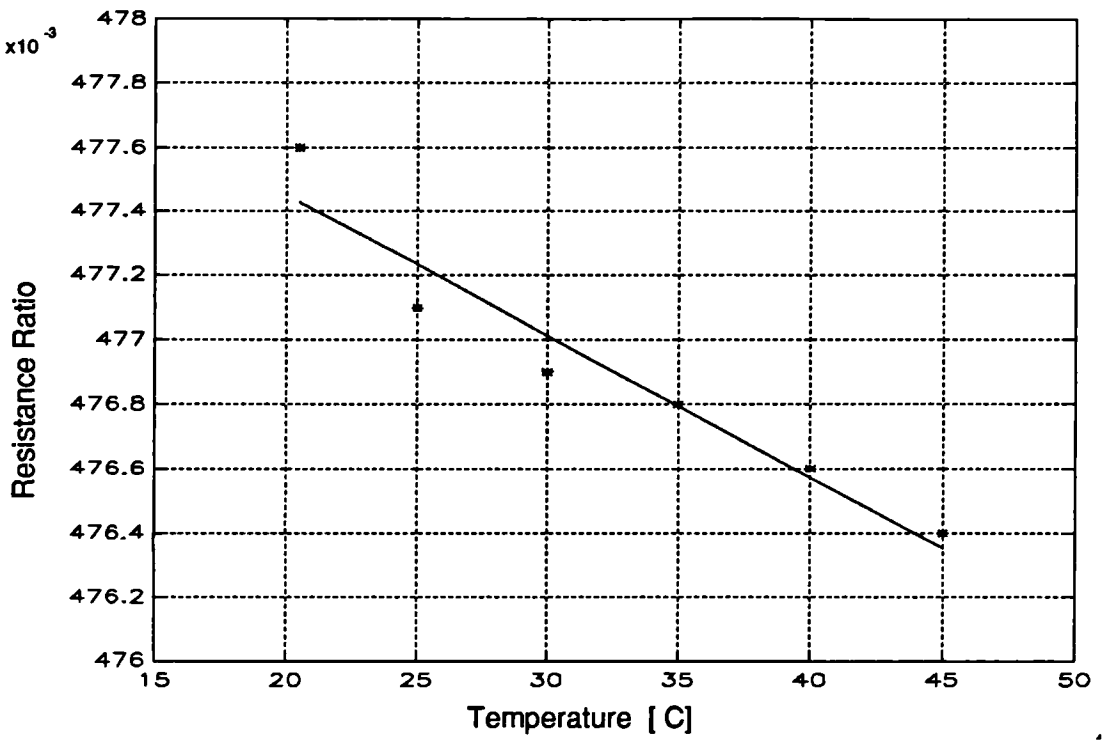

Figure 4.8 Experimental measurement of temperature induced changes in the field strength of a Samarium Cobalt magnet - evaluated by its effect on a magneto-resistive element.

Conversely the following observations describe negative aspects of the design. Firstly, the full-scale sensitivity (*FSS*) is typically only *5%* of the output value at zero stress. On its own this was not a deficiency - especially when compared with the magnitude of the output change from a strain-gauge device. However, when considered in conjunction with the temperature induced change in output, it was quite significant. Figure 4.5 shows that an extreme temperature change in the device, of *20℃*, may typically produce a change in $\Re$ of up to *1%*, equivalent to a *20%* error in full-scale measured stress. From the discussions in Chapter 2, even during strenuous exercise the likely increase in temperature in a prostheses will be an order of magnitude smaller than the test range. Thus, if the device temperature at the time of the clinical trial was known and the change during the trial was small, it would be possible to recover the true applied stress with a small uncertainty. However, to do this would require a measurement of temperatures during the trial and knowledge the devices stress response at each of these. Thus making the calibration and data processing procedures very complex. Alternatively the device temperature could be controlled electronically both at a compromise to the size and cost of the device and system.

So to minimise the potential temperature induced errors a redesign of the section or a reselection of components was necessary.

The theory of the mechanisms involved in producing the shear section's temperature sensitivity [4.1.1.3] was supported by the individual component tests. It was possible, from the tests, to estimate the relative contribution of each component to the overall temperature sensitivity [Table 4.5]. It is seen that the major apparent contributors are the magneto-resistor element and the magnet. As mentioned before, it was felt that the methods used produced indicative rather than definitive results.

Component	[$\Delta\Re_a$/°C]
Magneto Resistor	*- 0.013 ± 0.005*
Magnet	*- 0.01*
Silicone	*± 0.001*

Table 4.5 Summary of the relative contribution of each of the components in the shear section (Design A) to the overall section temperature sensitivity. All data is derived experimentally and expressed as a function of the percentage change in MR element resistance-ratio.

4.1.2 Component Reselection

From the measurements described in 4.1.1, the major problem with Design A was the magnitude of its temperature sensitivity compared with its stress sensitivity. With this in mind each component was re-examined for possible replacement to improve the overall design performance.

4.1.2.1 Magnetoresistor Replacement

As mentioned previously, the MR element being used was a differential device, so common-mode changes in temperature under a common magnetic induction would not affect the output. However, the attributes of the MR element responsible for its temperature sensitivity are the uneven distribution of In/Sb needles in each active area of the element and the doping grade. As these properties are intrinsic to the semiconductor and the manufacturing process, the only way of decreasing the

temperature induced apparent stress from these sources was to change the MR element to a type with a smaller overall temperature coefficient and a lower variation in its temperature coefficient with induction. Both of these, however, lead to an element with reduced field sensitivity to magnetic induction. So, replacement would need to be coupled with other methods for increasing the device sensitivity to applied stress.

A market survey revealed the most suitable alternative MR to be another Siemens MR (FP111L100). This MR element has a significantly smaller temperature coefficient (*-0.38%/℃*) compared with the FP110D155 (*-2.7%/℃*); while the relative resistance change, under the field strength in use in the prototype section (approximately *0.3T*), only decreases from *3* to *1.85*. Thus in using a FP111L100 the stress sensitivity of the device was increased relative to its temperature sensitivity.

4.1.2.2 Magnet Replacement

The device's stress sensitivity was further enhanced via two approaches. The first was to increase the magnetic field strength experienced by the MR. This could be achieved by employing a stronger magnet and/or moving the magnet closer to the MR. A field concentrator was already built into the substrate of both Siemens magneto-resistors. Also, the magnet diameter could be optimised to be approximately equal to the separation of the MR's active regions.

Previously when designing the prototype, the strongest magnet material readily available, to the author's knowledge, was Samarium Cobalt (**SmCo**), and the smallest parts obtainable were *2mm* diameter rods. A further search of magnetic material suppliers revealed a source of a relatively new material, Neodimium Boron Iron (**NdBFe**). It could be obtained in the form of a powder-sintered block which could only be ground to rectangular dimensions. The relative field saturation of the sintered NdBFe is *2-5* times that of Polymer bonded SmCo, while the quoted temperature coefficient of the NdBFe material was *-0.15 %/℃* compared to *-0.10 %/℃* for SmCo. Thus there was a relative advantage in using NdBFe magnets.

Stock samples of the new material with dimensions *3x2x2mm* were obtained. This longer length allowed the magnet face to be placed closer to the MR element by extending the height of the ridges of the central disc. The new MR element was

wider and longer than the previous one. In this case the relative increase in the dimensions of the element to those of the magnet enhances the device sensitivity to changes in magnet-element displacement. The original FP110D155 element was only *1.2mm* wide, whereas the FP111L100 element was *2.7mm* wide, compared to the magnet which was *2mm* across. When the magnet is large relative to the element, the field differential between either half of the element is small. Whereas for an element slightly larger than the magnet, there would be a greater difference in field distribution for either half. So for a given displacement of the magnet the latter will produce a greater change in the element resistance ratio. Figure 4.9 illustrates this. In the limit, if the magnet is much smaller than the element the resistance of either half will change very little while the other remains constant.

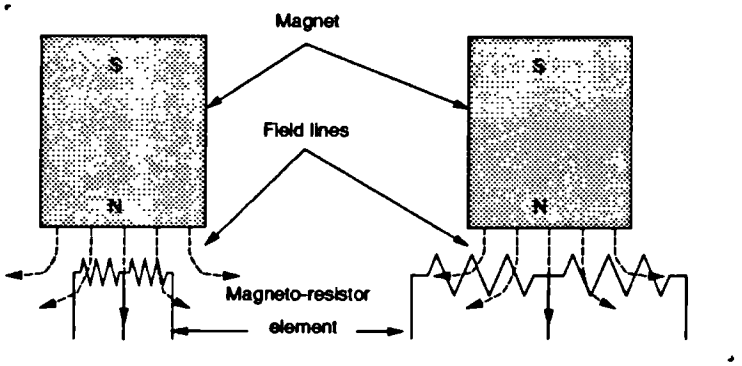

Figure 4.9 Relative exposure to magnetic field for two different widths of magneto-resistor element.

4.1.2.3 Silicone Replacement

The results of the constant strain tests [Figure 4.4 and Table 4.3] indicated that the General Electric RTV157 (GE) silicone exhibits a lower modulus of rigidity and has similar relaxation resistance than Ambersil 1039N (A). Thus by replacing A with GE the shear section thickness could be reduced and still result in the same range of displacements. In order to determine the appropriate thickness of the GE silicone, in a section with the new magnet and MR, two experiments were performed. Firstly, the maximum useful lateral displacement of the magnet across the MR was investigated. Secondly, the thickness of GE required to map the expected maximum clinical force ($\pm 50N$) onto that displacement range was determined. Figure 4.10 is a plot of the change in resistance ratio of a typical FP111L100 MR element when a *3x2x2mm* NdBFe magnet was moved over its surface at a vertical

separation of *0.1mm*. Figure 4.11 shows the resulting extension when four section-sized specimens of GE silicone, each of different thickness, was subjected to a *50N* stress. Bearing in mind that these are typical results, a useful displacement range of *±1mm* was chosen and a conservative layer thickness of *0.5mm* was set for the next design stage (Design B).

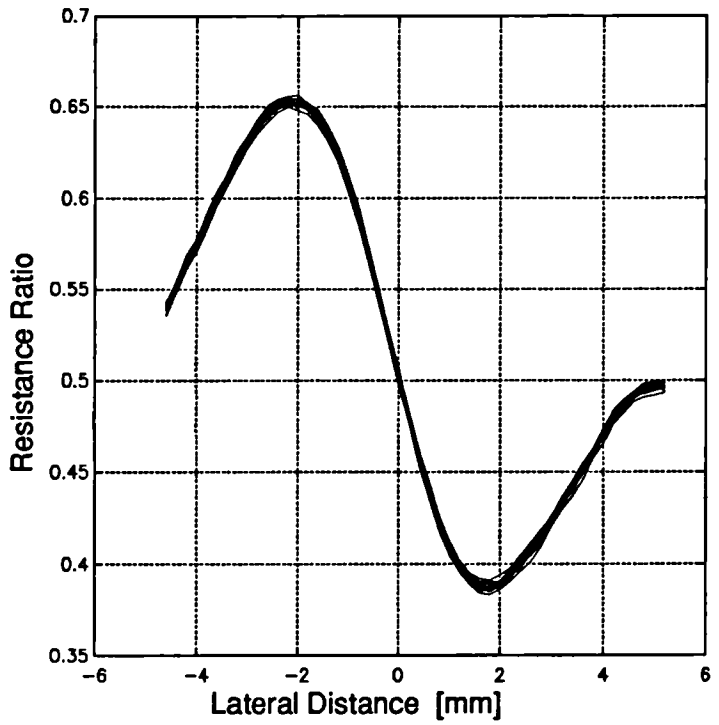

(a)

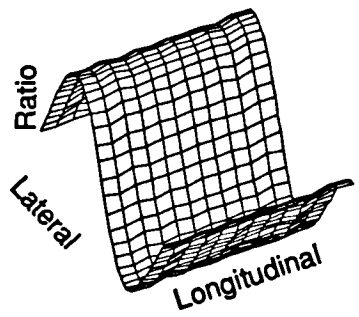

(b)

Figure 4.10 Field sensitivity of FP111L100 differential magneto-resistor (Siemens (UK) LTD) to 3x2x2mm NdBFe magnet (Magnet Developments LTD) stepped over its surface on a 0.2mm lateral x 0.1mm longitudinal grid at 0.1mm separation. Data is plotted in profile (a) and as a 3D mesh (b).

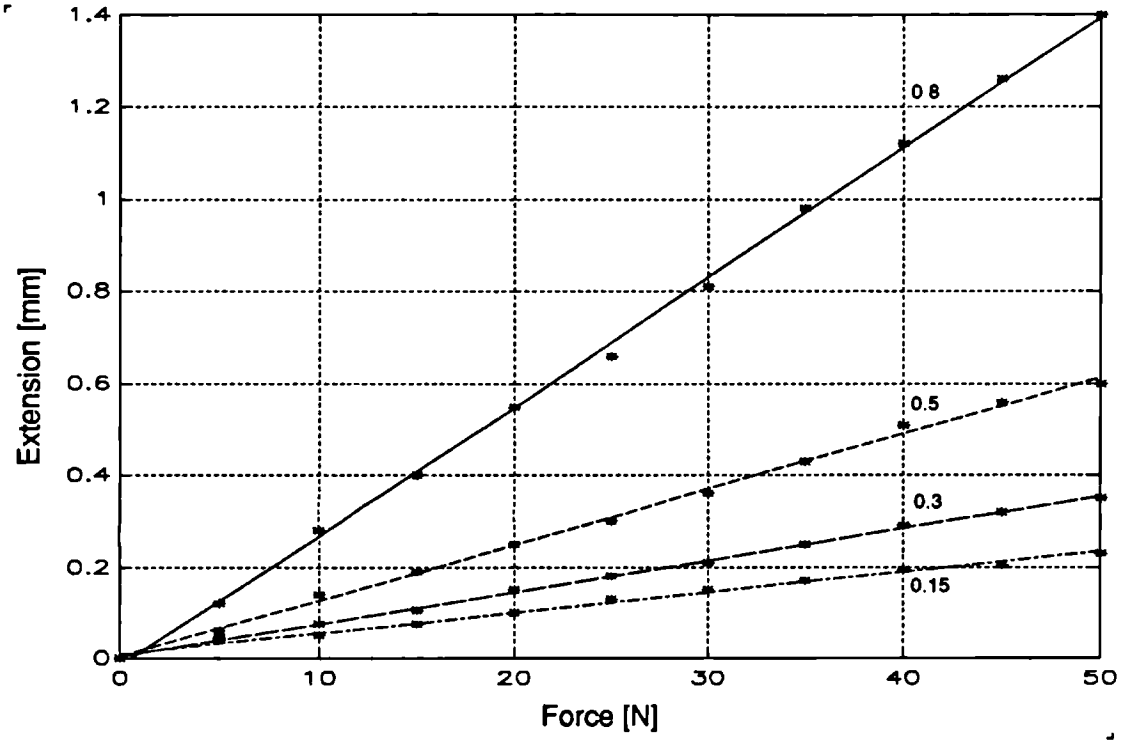

Figure 4.11 Force-displacement relationship for four disc's of RTV157 silicone (GE LTD) under 50N shear force. The dimensions of the disc's were 16mm dia x 0.15, 0.3 ,0.5, 0.8mm.

4.1.2.4 Dimensional Changes

During the assembly of the transducers several problems became apparent. Maintaining correct silicone thickness and hence disc separation was difficult, and ensuring an accurate alignment so that the ridge and channel mated was not always possible. By allowing the ridge to push home to the base of the channel, the alignment and silicone thickness problems were removed.

The ridge height on the middle disc was increased from *0.5mm* to *1.0mm*. This allowed the ridge to be pushed home into the channel, which was *0.5mm* deep, and maintain an accurate disc separation (silicone thickness) of *0.5mm*. This is illustrated in Figure 4.12.

Modifications were also made to the MR PCB shape and the PCB slot in the outer discs of the section to accommodate the reselected components [refer to 3.1.3.3, 3.1.3.4].

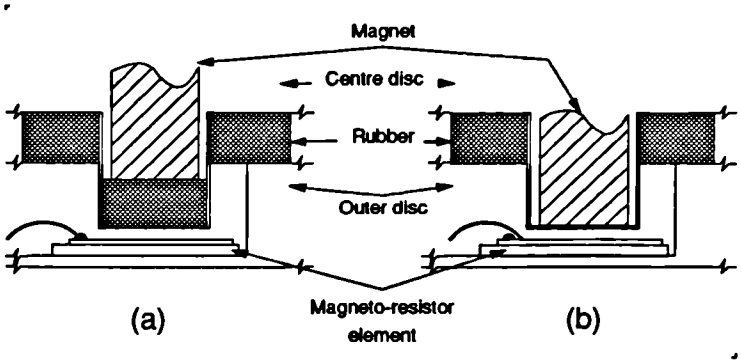

Figure 4.12 Schematic of the difference in geometry of the ridge and channel structure between Design A (a) and Design B (b).

4.1.3 Second Prototype Assessment - Design B

Design B is the second prototype shear section, derived from the first prototype (Design A), and modified according to the component changes discussed in [4.1.2]. The following part of this chapter, to [4.1.4], reports the performance assessment of Design B.

4.1.3.1 Test Equipment Modification

During the testing of Design B, in the Instron Materials Testing Machine, a locking bar in the calibration jig was accidently left in place during a force-strain test. The bar effectively stopped the sliding block of the jig from moving. The resulting plot on the Instron chart-recorder showed an unexpectedly significant hysteresis loop. To persue the origin of this a steel spring was placed directly under the sliding block and was compressed. A greater than expected hysteresis loop was again exhibited. Closer investigation showed that the cause of this exaggerated hysteresis to be an inherent lead or lag in the Instron chart drive controls. When an extensometer was in use the chart lagged the applied strain. Conversely when chart motion was made proportional to the cross-head displacement, the chart led the applied strain.

Thus for accurate calibration data the Instron force and strain signals needed to be monitored at a point prior to the machine's chart-recorder. This necessitated obtaining another recording system. Also from the experience gained in collecting the data described in 4.1.1, it became obvious that a more automated method of

data collection was required. Consequently, a signal conditioning unit was built to interface the shear section outputs to an analogue to digital (**A/D**) convertor. The A/D unit used was a DT2814 (Data Translation Inc), hosted in an IBM compatible personal computer (**PC**). It has an accuracy to *12 bits* over a *0-10V* input range. Software execution rates limited sample frequencies to *50Hz*. A circuit diagram of the signal conditioning unit is shown in Figure 4.13.

From a study of the Instron maintenance manuals, appropriate points were found in the extensometer and loadcell circuitry where the strain and force signals could be monitored. Coaxial leads conducted these signals to the signal conditioning unit where they were buffered and amplified. A similar scheme was followed to derive a signal from the **MEP123** temperature meter and buffer it. A driver circuit for the shear-stress section passed a constant current through both MR elements in series. Differential amplifiers were used to amplify the voltage developed between each elements' centre terminal and its lowest voltage terminal. The gain of the amplifiers was determined experimentally and then fixed. It was chosen so that the amplified output from any section under full load (*50N*) would map onto the full input range of the A/D convertor. Due to assembly variability each section has a different zero-stress output. The signal gain, therefore had to set low enough to take account of this offset and allow sufficient margin for most devices to map into the A/D input range. Conversely the gain must be large enough to provide adequate signal resolution. The other instrument signals were similarly buffered and digitised.

The A/D convertor was controlled by a short BASIC programme, specially written to capture the signals from all sources (shear section, loadcell, extensometer and temperature meter) in sequence, at a specified rate. The resultant data was stored on disk under a specified file name. This data was later analysed in an "off-line" mode using a commercial mathematical software programme (MATLAB - Mathworks Inc.)

During initial tests, in an attempt to get a feel for the dynamic response of the assembled device, the calibration jig [Figure 4.1] was uncoupled from the Instron crosshead and forces of approximately *50N* were applied by hand at various frequencies. The loadcell output and the transducer output were recorded on an X-Y plotter. For frequencies of approximately *0.1 - 1Hz* the hysteresis loop [Figure 4.2] did not change appreciably. However, for frequencies greater than about *1Hz*

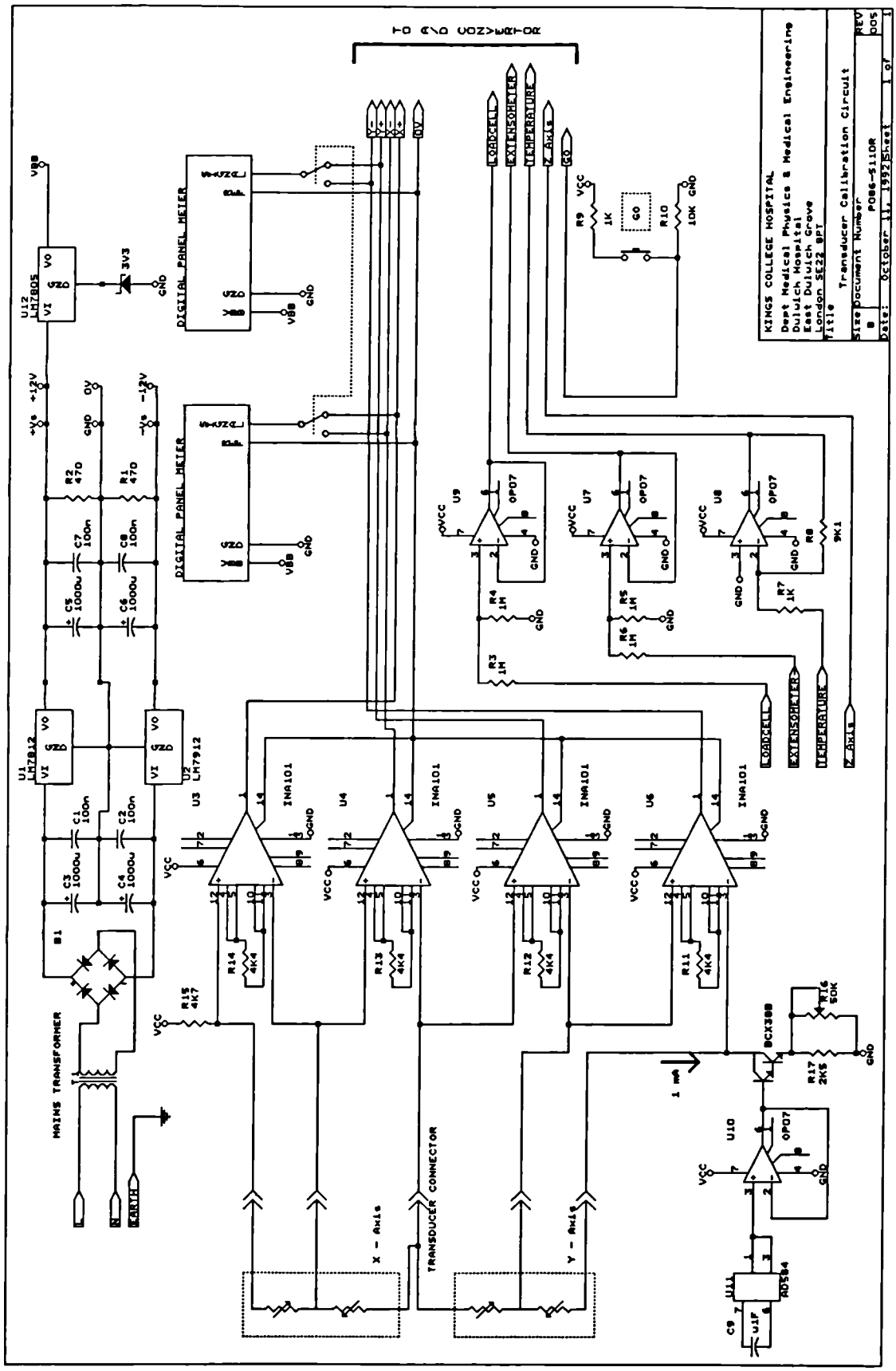

Figure 4.13 Circuit diagram of the signal conditioning unit used for interfacing to the transducer (Design B), loadcell, extensometer and temperature meter to the PC controlled A/D.

(i.e. clinical frequencies) the loop became much larger, with the transducer output decreasing much faster than the recorded force. The lag in recording the force indicated that there was inherent mechanical or electrical damping in the Instron above *1Hz*. Therefore in order to simulate forces at clinical frequencies alternative load testing equipment was required. (NB: The inherent damping in the Instron is due to its designed use as a static or low frequency stress testing platform).

4.1.3.2 Temperature Sensitivity

Component reselection [4.1.2.] was mainly concerned with reducing the overall temperature sensitivity, while increasing the stress sensitivity of the shear section. The following is a report of the assessment of the temperature sensitivity of Design B. Initially the temperature sensitivity of the individual components was assessed, followed by the temperature response of the device as a whole.

4.1.3.2.1 Magnetoresistor Contribution

Quoted temperature coefficients, as advised by the manufacturer (Siemens (UK) LTD), referred only to the change in resistance of any arm of the magneto-resistor element and so were of little use in determining offset (centre point) drift in the MR. The manufacturer was unable to provide data on the centre point drift for the FP111L100, although it was expected to be less than the FP110D155 (*±1.5%* over *20-40 ℃*). An experiment was performed to determine an approximate value for it's temperature coefficient and drift, to compare to those derived for the FP110D155. Four unmounted magneto-resistor elements were heated and cooled over the temperature range from *24-50 ℃*, while the resistance of the elements were recorded. The calculated resistance ratios of the elements are shown in Figure 4.14. A first order polynomial fit (least squares sense) to each of the curves resulted in slope coefficients of *-0.0064, -0.0068* and *-0.0086* $\Delta\Re_{\%}/°C$ respectively (top to bottom in Figure 4.14).

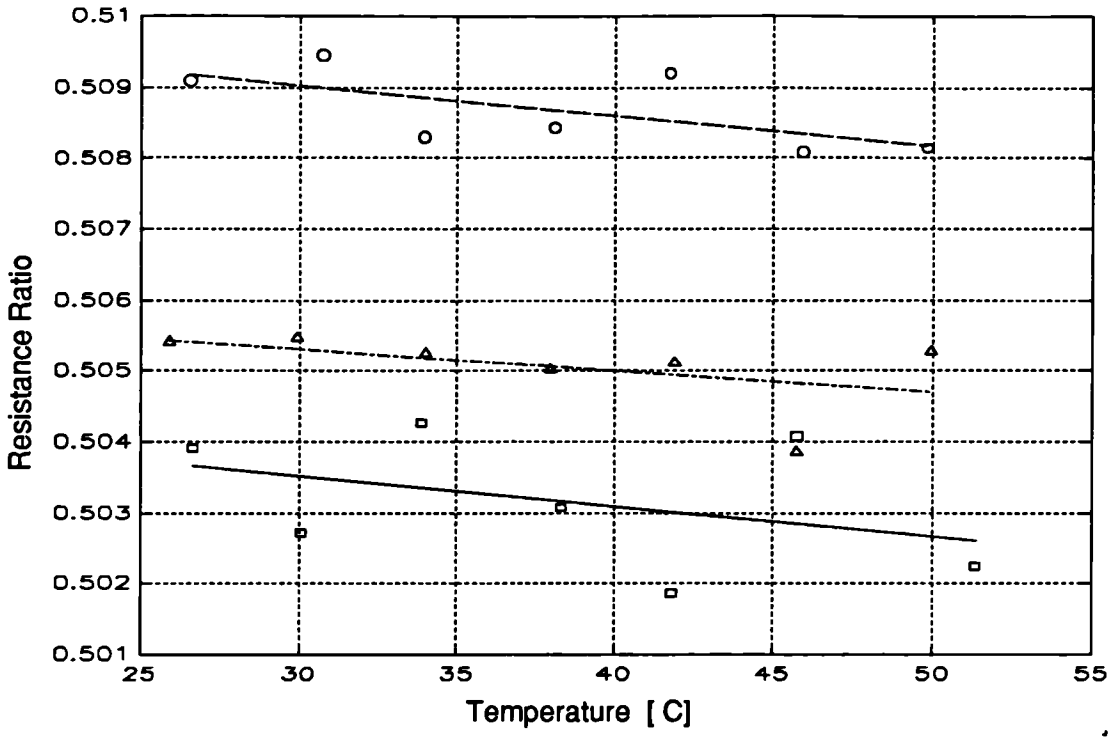

Figure 4.14 Variation in resistance ratio with temperature of three FP111L100 (Siemens (UK) LTD) differential magneto-resistors.

4.1.3.2.2 Silicone Expansion

The effect of expansion of the silicone layer on the MR resistance ratio was assessed next. The quoted coefficient of thermal expansion of the pure silicone, given in the manufacturers literature, was 27×10^{-5} *cm/cm/℃*. However during the construction process the silicone becomes aerated and it was anticipated that the thermal expansion would be greater than the quoted value. In order to assess any possible change in the resistance ratio due to the expansion of the silicone (and hence change in the magnet-element separation) the same two part test used in [4.1.1.3.2] was followed.

From Table 4.4 the measured thermal expansion coefficient for aerated GE silicone was 5.1×10^{-4} *cm/cm/℃*. Using this value and assuming a worst case temperature change of *20℃*, it was inferred that the silicone thickness, and hence magnet-element separation may increase by *5.1μm* (*0.5mm* to *0.5051mm*).

The second part of the test was conducted as before by fixing an MR element to the bed of an automated X/Y plotter table and positioning a magnet centrally over it. The MR resistance ratio was measured as the magnet was scanned across the element at various magnet-element vertical separations. The results are shown in Figure 4.15.

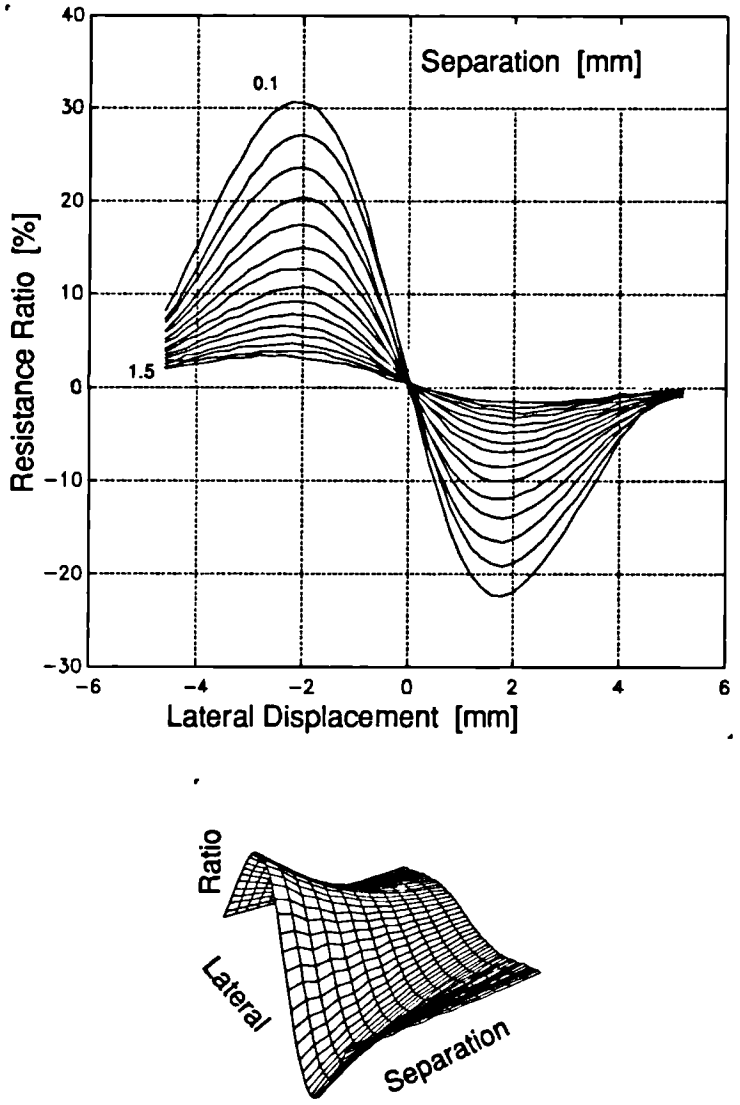

Figure 4.15 Resistance ratio variation as a function of magnet - magnetoresistor separation, for an FP111L100 differential magnetoresistor (Siemens (UK) LTD) and a 3x2x2mm NdBFe magnet (Magnet Developments LTD). Values were measured on a 0.2mm (lateral) x 0.1mm (vertical) grid. Data is shown in profile (a) and also as a 3D mesh (b).

From Figure 4.15 the rate of change of resistance ratio with separation was greater when the magnet was displaced by approximately *2mm.* In an assembled section the magnet-element separation is typically *0.1mm.* Thus in the worst case, a change in vertical separation of *5.1μm* (*0.1 to 0.105mm*) over *20℃* would cause a decrease in resistance ratio of approximately *0.2%.*

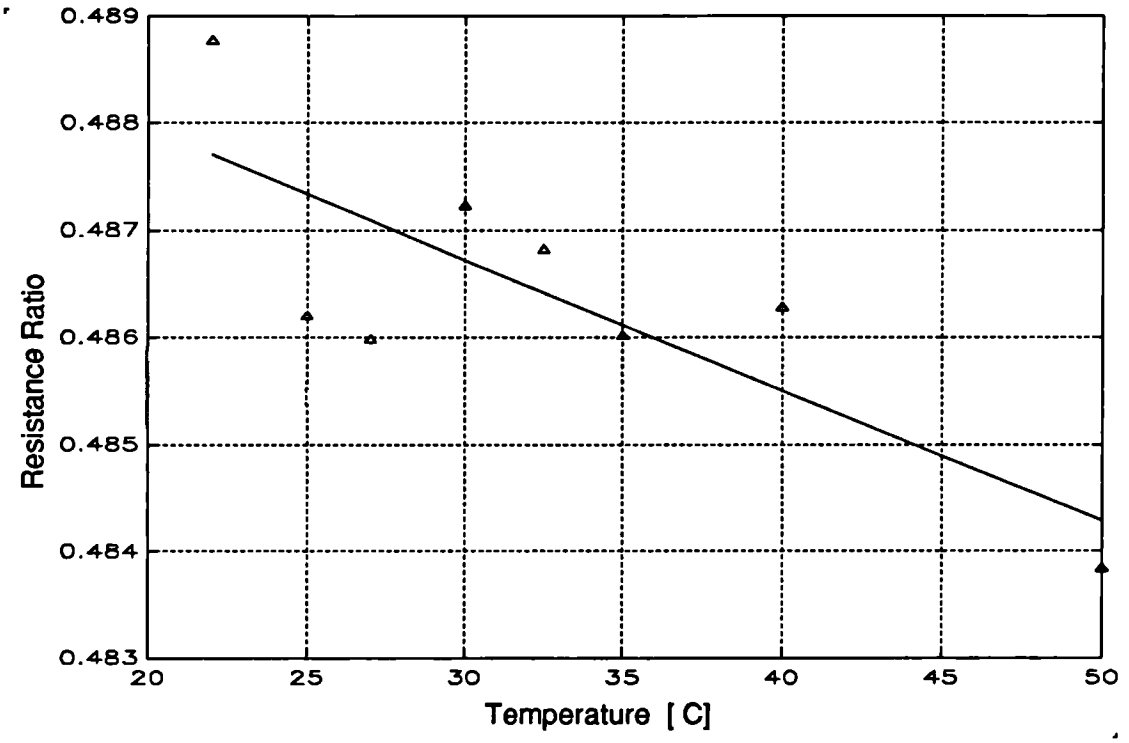

Figure 4.16 Experimental measurement of the temperature induced changes in the field strength of a NdBFe magnet, evaluated by the field effect on a magnetoresistor.

4.1.3.2.3 Magnet Contribution

In order to determine whether there was any significant change in the field strength of the magnet with temperature over the temperature range being considered. The magnet manufacturer quoted it's temperature coefficient as *-0.15%/℃.* In order to assess how this would effect the resistance ratio, a similar test was carried out as for the SmCo magnet [4.1.1.3.3]. Figure 4.16 displays the resultant data. Over a *20℃* temperature span there was a decrease of *-0.5%* typically. Again the test was not thought to be very accurate as the MR measuring the field experienced some heating and the MR-magnet separation was greater than in the shear section.

4.1.3.2.4 Component Summary

A summary of the response of the components in Design B to temperature stress is given in Table 4.6. These values are compared to those of Design A.

Component	Design A [$\Delta\Re_\omega/C$]	Design B [$\Delta\Re_\omega/C$]
Magneto-Resistor	-0.013 ± 0.005	- 0.008 ± 0.001
Magnet	- 0.01	- 0.024
Silicone	± 0.001	± 0.01

Table 4.6. Summary of the relative contributions of each component in the section, to the overall temperature coefficient of the shear stress section. Design B compared to Design A.

The salient features are; a reduction in MR element sensitivity; an apparent increase in magnet sensitivity; and an order of magnitude increase in the effect due to silicone expansion. Although the latter two compromise the shear stress section performance they must be viewed in the context of the sections stress response (presented later). Similarly the reduced field sensitivity of the MR must be offset against its lower temperature coefficient.

4.1.3.2.5 Device Temperature Sensitivity

To determine the temperature sensitivity of the biaxial shear stress section as a whole, a number of devices were assembled and their coefficients measured in both the loaded and unloaded state. Each section was mounted in the calibration jig at an orientation of *45°*. The jig was then positioned in the oven beneath the vent hole. A platform with an extended mounting post was attached to the sliding block of the jig through the vent hole. Masses were placed on the platform (external) to load the section whilst in the oven. A schematic of the equipment arrangement is shown in Figure 4.17.

Loads of *10, 20* and *30N* were placed on the platform at increments of temperature over the range *26-51°C*. After the loads were applied, a pause of five seconds was allowed before the temperature and output were recorded. Unloaded tests were

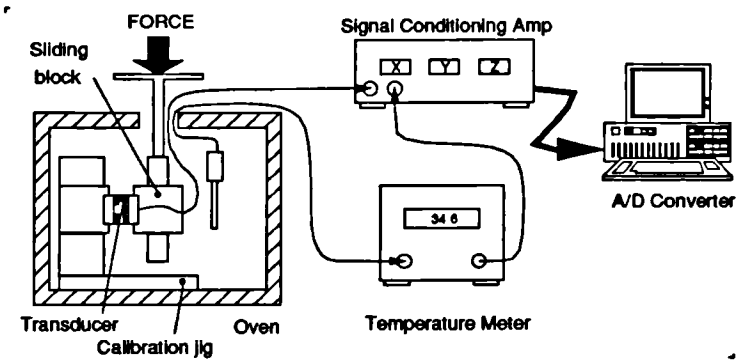

Figure 4.17 Schematic of the experimental setup used to assess the temperature sensitivity of shear stress sections of Design B. The section may be loaded by placing masses on the platform.

carried out with the sections fixed in turn in horizontal and vertical orientations on a shelf in the oven. The different orientations were intended to show up any drift in the zero-load output due to viscoelastic changes in the silicone. Figure 4.18 shows results representative of the batch of biaxial shear stress sections tested.

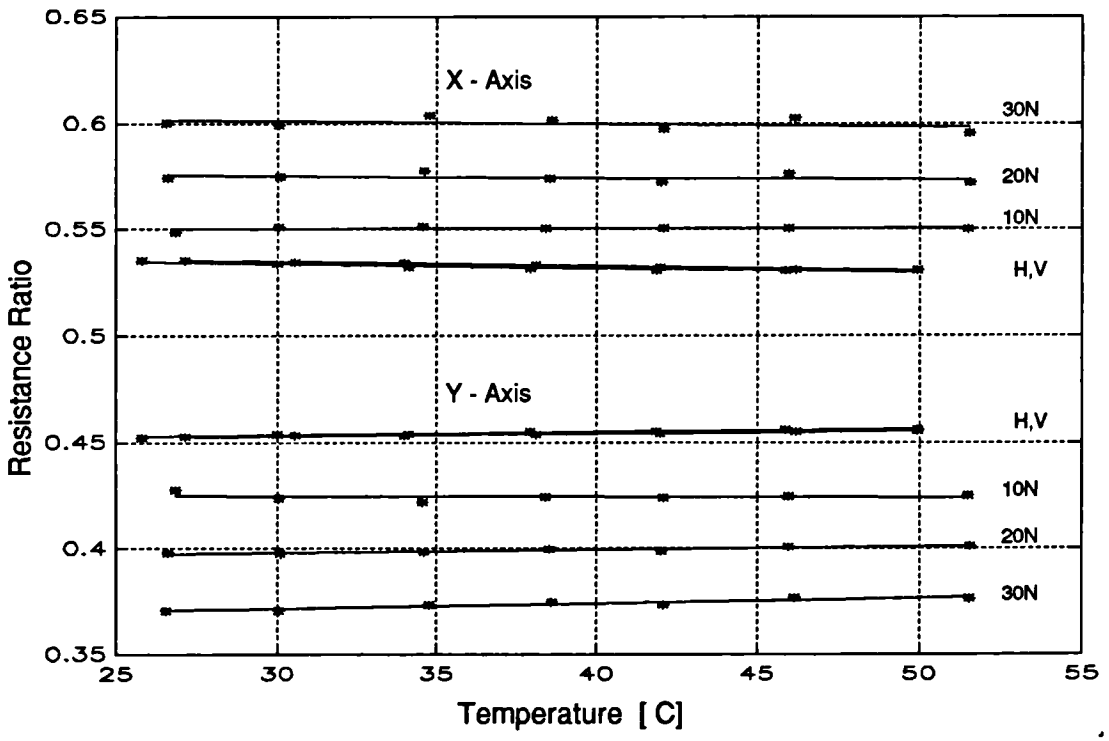

Figure 4.18 Typical variations of $\Re$ with temperature for shear stress sections of Design B. Over the temperature range the sections were loaded with 10, 20 and 30N masses, and placed horizontally and vertically when unloaded (H,V).

There are three observations of significance to be made from Figure 4.18. The first, that the gradients of each line are typically less than *0.4* $\Re_{\%}$ over *20* ℃. This demonstrates a temperature sensitivity significantly less than that of Design A - as was set out to be achieved. Secondly, the traces for the various loads remained reasonably parallel with temperature. The implication of this is that there was very little change in the viscoelastic properties of the silicone over the temperature range. The third observation was the relatively constant separation between the traces for each axis, implying a linear force-resistance ratio response for the section.

The results of these temperature tests imply that sections of Design B need only be calibrated at one temperature and possibly only under a few loads, both of which are desirable in the requisite transducer design.

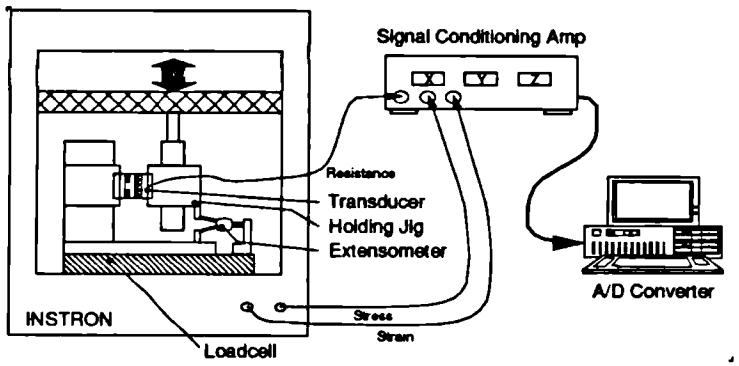

Figure 4.19 Schematic of test equipment setup used to assess the static stress characteristics of the shear stress sections of Design B.

4.1.3.3 Static Stress Response

The following, to [4.1.3.4], describes the methods used and results obtained in characterising the response of the Design B shear stress section to applied static forces.

Three biaxial sections were tested to determine their stress sensitivity and ability to resolve force vector direction. The test apparatus consisted of the Instron Materials Testing Machine, calibration jig, signal conditioning circuit and the PC with analogue to digital convertor. Figure 4.19 is a schematic of the experimental set up used.

4.1.3.3.1 Linearity and Range

The assembled sections were subjected to a cyclic force from *0N* to *50N*. Each was fixed in turn into the calibration jig at several orientations to the applied force. They were then subjected to *50N* force cycles at a constant rate of strain (*2mm/min*) while the force output from the load cell, and the changing resistance ratio of each axes was sampled at *20Hz*. The transducer was then rotated and fixed at a different orientation and the test repeated. Figure 4.20 shows a summary of the change in resistance ratio with applied force vector for a typical shear-stress section. As the direction of the applied force moves nearer to the orthogonal axis, the amount of displacement, and hence change in resistance ratio becomes smaller. It was clear that the curves were highly nonlinear at even moderate forces. Indicating that extreme stresses were being experienced in the silicone. This was also indicated by the presence of large hysteresis loops (*±5-±13N*). The implications were that the linear range was less than satisfactory, the uncertainty of measurements were large, and the calibration/signal processing requirements would be complex.

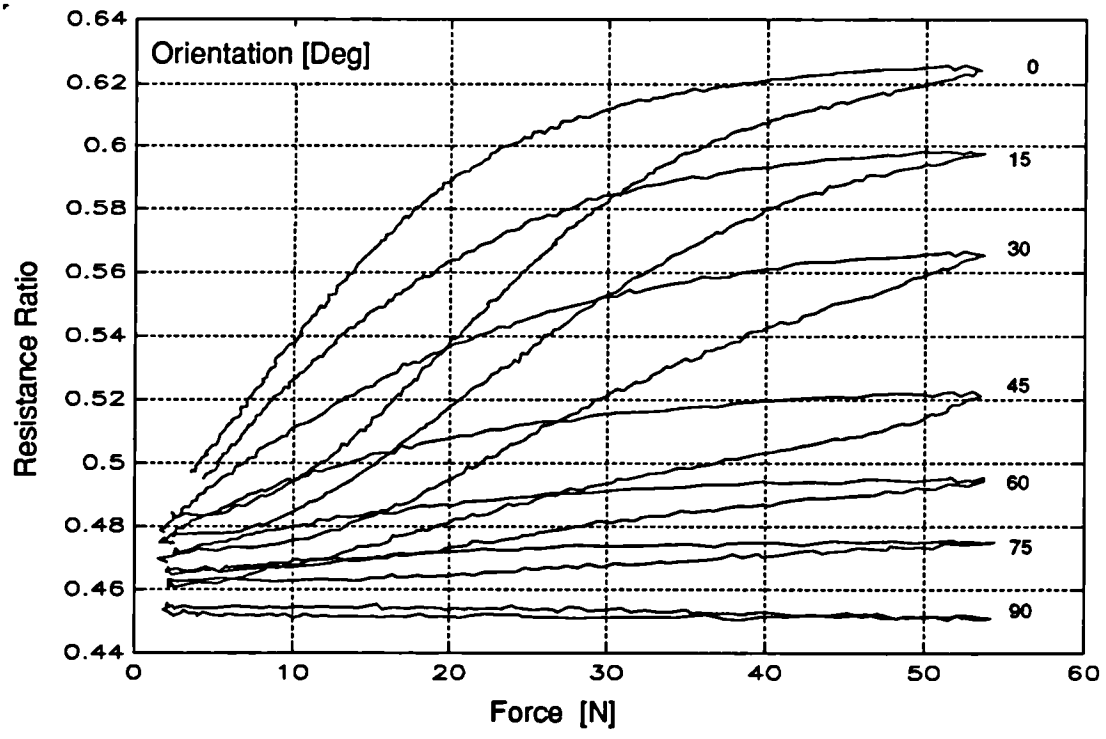

Figure 4.20 Typical force-resistance ratio response of a shear stress section of Design B. Loads cycles to 50N were applied at 15° intervals between 0 - 90°.

4.1.3.3.2 Force Resolution

The short horizontal region at the beginning of each trace in Figure 4.20 gave an idea of the amount of force required to begin displacement - overcome static friction. The value represents the minimum detectable force of the section. As the operation of the Instron was to effect a change in displacement and to record the force generated in the shear section, this is an indirect method of assessing the minimum detectable force. A more direct method was used.

During the creep measurement tests [4.1.3.3.4] the calibration jig was uncoupled from the Instron and a small platform attached to the sliding block. Masses were then placed on the platform until a change in output was observed. The minimum sensitivities of the sections of Design B were between *1-5N*. The probable cause of the resolution limit was frictional inertia - static friction. This is discussed later in [4.1.4.2]

4.1.3.3.3 Repeatability

To assess the repeatability of the section's response the devices were subjected to many load cycles between the set limits of *0-50N*. Initially, the Instron crosshead speed was set to *5mm/min* (i.e. a load cycling frequency of *0.083Hz*). After the first three cycles the trajectory of each force versus resistance ratio cycle was indistinguishable from the previous. Each cycle was repeatable to within *1%*.

4.1.3.3.4 Creep and Hysteresis

It was obvious from Figure 4.20 that the hysteresis present in the section was far in excess of desired levels. The load cycling test was repeated, first changing the crosshead speed to *10mm/min* (*0.17Hz*), then reducing the upper load limit to *25N*. Figure 4.21 shows these results plotted as resistance ratio against force for an orientation of *0°* (along the sensing axis).

Doubling the crosshead speed, and hence frequency, from *0.083Hz* to *0.17Hz* had no apparent effect on the size of the hysteresis loop. Halving the applied load

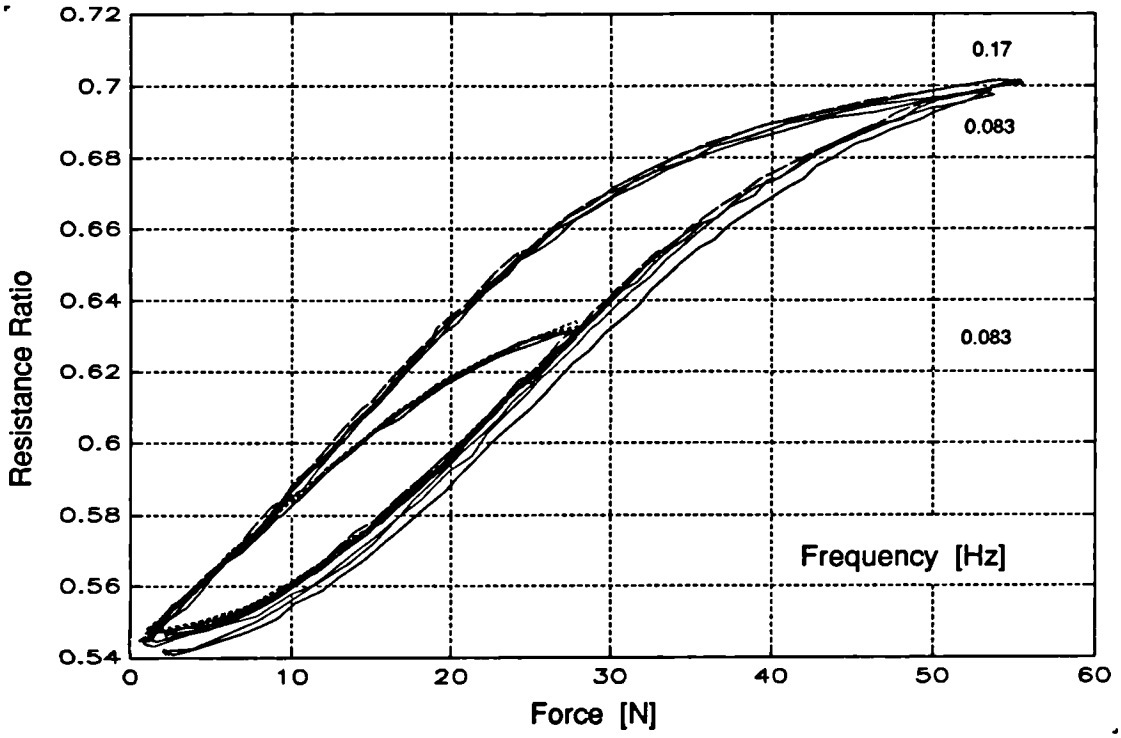

Figure 4.21 Typical Force - Resistance Ratio response with load cycle frequency of shear sections of Design B. Each was subjected to five load cycles of; 50N at 0.083Hz; 50N at 0.17Hz; and 25N at 0.083Hz.

from *50N* to *25N* also had little effect on the relative size of the hysteresis loop. The question arose as to whether the large hysteresis was due to the bulk properties of the silicone or to the manner in which it is assembled in the device. To answer this the stress-strain relationship of disc's of GE silicone were compared to that of the assembled shear-stress sections.

Three devices and three silicone blanks (aluminium - silicone - aluminium) were subjected to five *50N* stress cycles at *0°*, *45°*, and *90°* orientations. Their mid cycle hysteresis values were measured. Table 4.7 gives the mean and standard deviation of these values.

It was clear that the hysteresis loop for the pure silicone blank (aluminium - silicone - aluminium) was less than that of the assembled section at any orientation. This implied that there were additional hysteretic factors in the section design, which appeared to be random between axes and between sections.

Orientation	Assembled Section			Blank		
	1	2	3	1	2	3
0°	10.6(.55)	12.4(.55)	10.4(.55)	6.4(.55)	7(0)	6.2(.5)
45°	13.8(.84)	16.4(.55)	15.8(.45)	-	-	-
90°	11.6(.55)	10.6(.55)	11.8(.45)	-	-	-

Table 4.7 Mean (standard deviation) hysteresis values [N] of three sections, of Design B, and three blanks, of GE silicone. Each section was subjected to five cycles of 50N stress at 0.083Hz and orientations of 0°, 45° and 90°. Blanks were subjected to five cycles of 50N stress at 0.083Hz at one orientation.

On disassembly of the sections one of the contributing factors to the *excess* hysteresis was found to be due to thin films of silicone (less than *0.1mm* thick) between the ridge and the channel. Obviously they had been trapped during the assembly process. It is known that when rubbers are strained to high extensions (*300-400%*) exhibit hysteresis several orders of magnitude greater than those found at normal extensions (*20-200%*). This is due to physical changes in the material [**Ward 1971**]. Certainly the thin layers found would easily experience excessive extensions at even moderate stress levels.

It was also evident that the hysteresis present in the silicone itself was approximately *±3.5N* (*7% FSL*) which was greater than the desired accuracy of the requisite transducer.

It was observed from Figure 4.21 that for the first three cycles the hysteresis curve moved along a path above the original curve. When it reached the upper limit for the second time it appeared to continue on a cyclic path that was reasonably consistent. This behaviour is typical of 'creep' in the silicone. The hysteresis loop would continue to move up, but to a decreasing extent on each cycle - characteristic of the exponential decay in the rate of creep.

The creep in the design (Design B) was evaluated by applying a *30N* step load to sections mounted in the calibration jig. The resistance ratio in the section was sampled for *60Sec* at *5Hz*, and the creep rate calculated as before [4.1.1.2.2] by

plotting $\Delta\Re_{\omega}$, beyond the initial value, against the logarithm of time. The resultant curve was approximated by a first order polynomial and the slope taken as the rate value. Table 4.8 lists the values for the three sections.

	Section		
	1	*2*	*3*
Creep Rate [%/log(Sec)]	*5.6(.4)*	*5.0(.2)*	*4.9(.8)*

Table 4.8 Average creep rate (standard deviation) in sections of Design B when subjected to a 30N step load.

The values in Table 4.8 indicate that errors would grow to be significant (≈*15%*) over the course of a clinical trial - *1000 Sec.*

4.1.3.3.5 Alignment Errors in Testing

When straining the silicone blanks (aluminium - silicone - aluminium) regions of force versus displacement plots were observed where the displacement remained constant for a period after the cycle passed through a maximum or minimum [Figure 4.22]. That is, the test assembly (silicone blank in the calibration jig) had a large initial resistance to the change in displacement, symptomatic of the sliding mechanism of the jig seizing momentarily (frictional inertia). Both silicone blank test pieces and assembled sections were observed to exhibit this region during load cycles. Although the regions appeared to be larger for sections, and especially for orientations other than *0°* and *90°*. Therefore the cause could not be the ridge and channel mechanism. When a steel spring, of similar rigidity to a silicone blank, was compressed between the sliding block and the jig base, the region was not evident. This implies the cause lay in the way the forces were applied to produce shear. In previous shear stress tests the test specimen was fixed in the calibration jig so that it was in view of the Instron operator. This meant that there was a distance of approximately *15mm* between the line of applied stress and the centre of the specimen. Figure 4.23a illustrates the early method of positioning the blank/section in the calibration jig, where *d* is the moment-distance from the line of applied stress. Any moments about the plane of the sliding block could cause friction in the bearings, which may in turn cause some frictional inertia or *stiction* when

changing the direction of motion. After retesting the silicone blank it was evident that the size of the region was indeed related to the moment, *d*. The calibration jig was thus modified to reduce *d* to a minimum, as illustrated in Figure 4.23b. The silicone blank was subsequently found to exhibit *1.5-2N* less hysteresis than measured previously.

As a consequence of the misalignment in early tests, the force versus resistance ratio and creep curves of previous shear-stress transducer designs may have been exaggerated. However, it could reasonably be assumed that all sections suffered the same problem as none of the results were noted to be exceptional. Thus early results still serve to give a relative comparison between section designs.

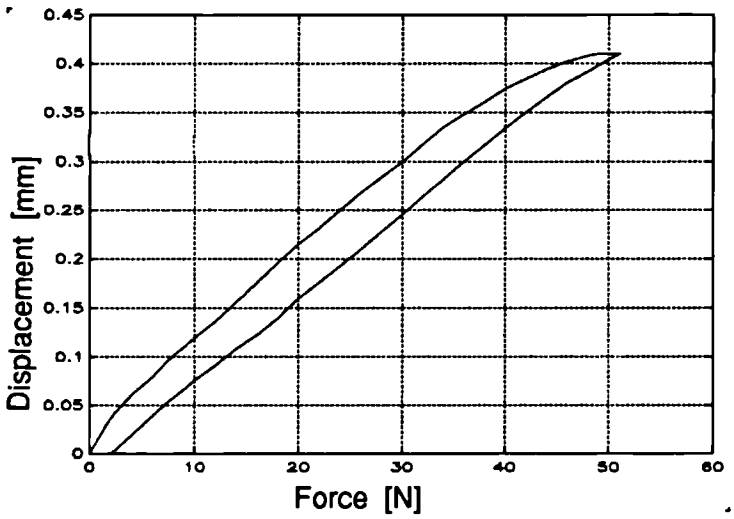

Figure 4.22 Force versus Displacement curve for a silicone blank (RTV157 - GE (UK) LTD). Note that at the extremes of the cycle there are short constant displacement regions. These are indicative of stiction/coulomb-friction.

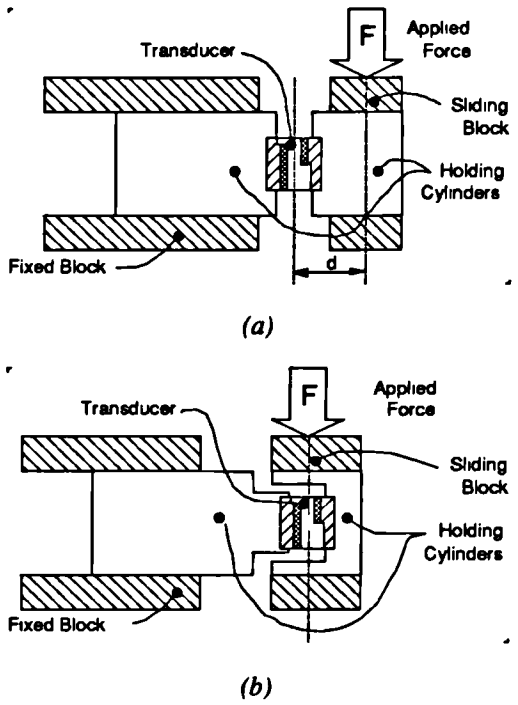

Figure 4.23 Schematic of the position of a test body (silicone blank or shear section) in the calibration jig, relative to the line of applied shear force. The moment arm is ***d*** *(a). The modified calibration jig, where the moment arm is eliminated (b).*

4.1.3.4 Discussion

In summary, comparing Design B with that of Design A: the stress sensitivity was *5-6* times greater and the temperature sensitivity was *2-3* times lower. The nett effect being that the temperature induced apparent stress was much less significant. It was also observed that both designs yielded repeatable and approximately linear force versus resistance ratio curves and were able to distinguish stress vectors.

Despite the above qualities there were major shortcomings of the Design B. Two of these were: the inherent hysteresis of the silicone; and the inclusion of trapped silicone layers between the ridge and groove during the assembly procedures. The prevention of these layers would have been difficult to achieve. Even pre-assembly of the discs before *injecting* the silicone would not guarantee success. For, to avoid air inclusions and ensure penetration, a low viscosity rubber would have been required which would have only exacerbated the migration of silicone into any gaps. Regardless of any solution being found to that problem it was evident that the silicone itself had unacceptable hysteresis.

It is worth noting here that although **Tappin et al[1980]** and **Pollard et al[1983]** had used silicone rubbers in their shear transducer they had only been able to perform static and simple dynamic calibrations on them. Under those conditions it may not have been possible for them to have appreciated the hysteresis present in the stress cycle of the silicone.

The highly non-linear shape of the section's force versus resistance ratio curve was most probably due to the extreme strain experienced in the thin layers of silicone trapped between the ridge and groove. This idea was supported by the linear shape of the stress-displacement curve for pure silicone blanks (aluminium - silicone - aluminium).

A further property of the silicone that made it unsuitable for use in the requisite transducer was the amount of creep demonstrated. Under low frequency stresses errors of up to *10% (FSL)* would occur after only *100 sec* loading, so compromising accuracy. The silicones tested, therefore, were not the preferred spring material because of inherent properties and the form they were applied in. It was necessary after these results to look closely at the alternative elastomers.

4.1.4 Further Component Reselection

4.1.4.1 Silicone Replacement by Natural Rubber

A natural-rubber (polyisoprene) was chosen to replace the silicone-rubber (polysiloxane) as the restoring mechanism in the shear-section in an attempt to improve performance. As discussed earlier [3.1.2.4] the potential problems with using natural-rubber in the application were: finding an adequate cold bonding technique; possible rigid boundary layer on the bonding surface; and deriving a formulation with acceptable physical properties. In seeking a better understanding of these potential problems and of the general suitability of various natural-rubber compounds, the advice of the **National Rubber and Plastics Research Association** was sought. It was their opinion that the UK authority on natural-rubber was the **Malaysian Rubber Producers Research Association** (MRPRA).

4.1.4.1.1 Natural Rubber Formulation

In achieving an acceptable formulation there were compromises to be made. The essential properties required were: low hysteresis; low creep and relaxation; moderate rigidity; and high resilience. In order to obtain good resolution in shear stress measurements the rigidity of the rubber must be such that *50N* stresses displace the magnet across the full face of the MR element. However, more rigid rubbers have lower creep and relaxation properties. Thus the gross trade off is between transducer thickness and minimising creep, stress relaxation, and hysteresis.

A similar layer thickness was used for the natural rubber layer (*0.5mm*) as was used for the silicone layer. From Figure 4.15 a *200%* strain would allow the magnet to displace over its full useful range. The shear-modulus in this case would need to be $0.25N/mm^2$. However, a low shear-modulus was less critical than minimising the creep and hysteresis. MRPRA were approached for advice on an optimum natural rubber formulation. Their proposed formulation is given in Table 4.9. Two sample sheets were donated by them, however, the tested hardness of this rubber implied that it would be twice as rigid as required (estimated at $0.48N/mm^2$).

Components	*Ratio by parts*
SMR CV	*100*
Zinc oxide	*5*
Stearic acid	*2*
Sulphur	*2.5*
CBS	*0.6*
Santoflex 13	*1*

Table 4.9 Formulation of Natural Rubber compound used as restoring force in shear-stress transducer.

4.1.4.1.2 Bonding Considerations

Beside being able to obtain a natural rubber compound with particular optimum physical properties the other major obstacle to be overcome was identifying an

adequate bonding technique. As discussed in [3.1.2.4] the preferred adhesion method of hot bonding rubber to metal was rejected because of the probable damage to the MR element and magnet, or the technical difficulty in, alternatively, trying to accurately place these components into the section after the bonding process.

However, MRPRA advised that effective cold-bonding techniques were known. **Lindley [1974]** conducted a study of the *then* commercially available adhesives and their recommended preparation methods. The three most effective adhesives were **Araldite AY105/HY953F** (Ciba-Geigy), **Chemlock 304** (Hughson Chemical Co) and **Eastman 910** (Emerson & Cummings). The first two are epoxies, both of which required pre-treatment of the rubber with concentrated acids - sulphuric or hydrochloric. The latter is a cyanoacrylate adhesive for which there are no required pre-treatments except degreasing the surfaces to be bonded with acetone. On approaching the company quoted by Lindley as suppliers of Eastman 910 (Emerson & Cummings) the author was told that it was not part of their product range. It was subsequently not possible to locate this product. Within Lindley's study, two other cyanoacrylate adhesives tested produced weak bonds which could be pulled apart by hand. For this reason it was decided to concentrate on the use of epoxies. MRPRA were also of the opinion that the surface boundary layer was a function of the length of exposure time to the pre-treatment process. For the stress levels expected in the transducer, adequate bonds could be obtained for shorter pre-treatment periods. Furthermore natural rubber compounds could be formulated with hysteresis levels better than silicone at strains of up to *300%*. Therefore any reduced effective thickness of the layer would still bring an improvement over Design B.

Epoxy adhesives

From a survey of fifty-six suppliers and manufacturers of epoxies only two expressed confidence in being able to bond natural rubber to aluminium. Samples of their recommended adhesives were obtained. They were **AY105/HY953F** (Ciba Geigy) and **556301** High strength and **554850** Quick set epoxies (RS Components Ltd). Unfortunately **Chemlock 304**, used by Lindley, was not available at the time due to importation delays. The rubber pre-treatments for these adhesives is acid based, which is aggressive to all the other materials used in the transducer. Thus, careful neutralisation of the acid is essential after pre-treatment of the rubber.

At this stage of the transducer development the centre disc material was replaced by an **Acetal** copolymer due to friction difficulties [4.1.4.2]. Three blanks (acetal-rubber-acetal) made using the **556301** epoxy were tested to characterize the rubber properties. Following this, ten complete shear-stress sections were built using acetal as the centre disc. These were then tested to characterize the section performance under force and temperature stresses. However, over half of them failed during a week of testing. All suffered structural failure of the acetal centre disc. On inspection the acetal appeared to have been chemically eroded. The cause of the erosion was found to be due to traces of acid that was used in the pre-treatment of the rubber. These traces had been absorbed into the rubber and consequently seeped out. There were many such failures with sections made using this bonding method - despite the extreme care taken to try to neutralize the acids without significantly affecting the treated condition of the rubber. It was felt that the assembly process had become very difficult and specialised with no simple method of quality assurance. Long term affects of any contaminates would also invalidate the device calibration curves, thus an alternative bonding method was sought.

Cyanoacrylate adhesives

MRPRA advised that **Loctite (UK) Ltd** had recently developed a cyanoacrylate adhesive that did not require pre-treatment of the rubber. Also, whereas previously cyanoacrylates were very ineffective in bonding to self-lubricating thermoplastics, a primer had also been formulated to overcome this limitation. Upon meeting with a Loctite chemist, samples of the adhesive **406** and primer **757** were obtained and demonstrated to form an effective shear stress bond between rubber and acetal. Further, another Loctite product **405** was demonstrated to form an effective bond between natural rubber and aluminium.

From tests using rubber blanks (aluminium - natural rubber - aluminium) and these adhesives the bond strengths were found to be acceptable for the expected clinical stress range. Also, the assembly process was considerably simplified. Complete shear-stress sections, subsequently constructed, showed superior hysteresis and creep properties and linear repeatable force-resistance ratio and force-displacement curves. So with these components - Natural Rubber, acetal discs and Loctite adhesives -

incorporated into Design B the shear-stress section design was finalised. A complete description of the section components and assembly along with a report of detailed performance characteristics is given in [4.3].

4.1.4.2 Low-Friction Polymer Central Disc

When a natural rubber layer was assembled in a shear-stress section, where all three sections were aluminium, it was observed that the force-displacement curves of the section showed flat regions at their minima and maxima, similar to those seen for the silicones [4.1.3.3.2]. As before, there was a large initial resistance to a change in the direction of the applied displacement. This phenomena was not observed when a natural rubber sheet was cemented between two blank aluminium discs and was stressed in the same manner, so implying that the cause was internal to the section assembly. The action was that of momentary seizing of the assembly, indicating some form of frictional inertia, possibly friction between the ridge and channel. After silicone oil was allowed to seep between the ridge and channel, there was a significant reduction in the size of the stationary displacement region. On disassembly and close inspection under a microscope it was observed that friction between the aluminium on aluminium sliding surfaces was the cause.

To overcome the friction problem outlined above, a survey was carried out for a substitute centre disc material that had "self-lubricating" properties and adequate bonding possibilities to rubber. Self-lubricating materials are difficult to bond to because of the very surface properties they are sought for. Many are found in the family of thermoplastics. They are easily machined but are not very strong materials. The molecules in their structure do not form many crosslinks to neighbouring molecules so they are not very resistant to chemical, particularly acid, attack. A survey of suitable thermoplastic materials resulted in the selection of an **Acetal** copolymer - mainly because of familiarity with its use in the authors Department. Rods of acetal were obtained and three test blanks (acetal-rubber-acetal) made. Sheets of rubber were bonded to these and the strength of these bonds tested in shear. The breaking stress levels were well above expected clinical stress levels (in excess of *5MPa*).

4.2 Normal-Stress Section Development

This part of the chapter [4.2] describes the design development of the normal-stress sensing section. It details the performances of three strain gauges under applied loads and concurrent temperature stresses and the appropriateness of the diaphragm dimensions.

The author acknowledges that much of the work on the design and performance assessment of the normal-stress transduction section was carried out with the help of a colleague Mr. D. Porter. For completeness it is reported here.

For each of the foil strain gauges referred to in [3.2.2], a specific disc shape (referred to as a diaphragm) was made. The diaphragm thickness was the same for each but a unique pattern of slots were cut from the support wall at a variety of angles to accommodate the different lead configurations of each strain gauge. Figure 4.24 describes the disc outlines and gauge patterns for each of the three gauges. The diaphragms were machined "in-house" and sent to the gauge manufacturer for mounting of the gauges. This was to ensure optimum gauge performance on the specified diaphragm.

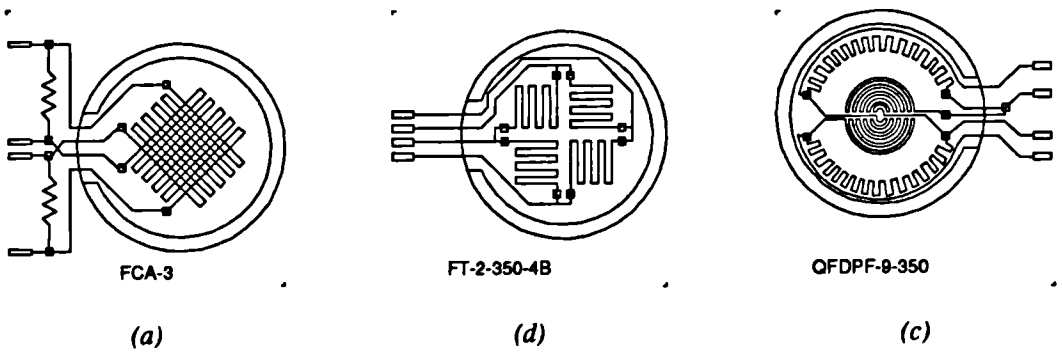

Figure 4.24 Schematic of the gauge pattern and diaphragm outline of the prototype normal-stress transducer sections (a) SG1, (b) SG2, (c) SG3.

The first gauge, which will be referred to as **SG1**, was a simple two element non-temperature compensated device. Two external resistors were connected to the gauge leads to complete a Wheatstone bridge configuration. The second and third gauges, **SG2** and **SG3**, were four strain element types, with their elements arranged as a bridge.

4.2.1 Test Equipment and Methods

Each of the sections was loaded and concurrently subjected to a range of temperatures. The experimental set-up shown in Figure 4.17 was used, with the exception that the sections were placed under the sliding block of the jig. In that way loads on the platform compressed the section between the sliding block and the stand. In order to provide the same load profile for each diaphragm a two millimetre diameter steel ball bearing was cemented to the centre of each diaphragm with epoxy. The sliding block then rested on top of the ball bearing. Each gauge was connected to a one volt bridge supply and amplifier - **SGA850** - donated by **Technimeasure Ltd**. The amplifier gain was fixed at an experimentally derived value for all sections to allow comparisons to be made. The output of the amplifier was input to an A/D convertor housed in a PC. Temperature measurements were made, as before, via the **MEP123** temperature meter, and interfaced to the A/D.

4.2.2 Temperature Sensitivity

The platform was loaded in sequence with *0, 0.5, 1, 2* and *3kg* masses as the temperature were increased from *20-50℃* in *3℃* steps. At each temperature step the section was allowed ten minutes to come to thermal equilibrium. The masses were then placed on the platform in turn for five seconds while measurements were made of the temperature and the gauge output. Figure 4.25 plots the typical gauge output as a function of temperature and applied load for SG1, SG2 and SG3 respectively.

The measured temperature coefficient of each gauge is given in Table 4.10. These are calculated using a linear approximation for the output change with temperature over the range *20-50℃*.

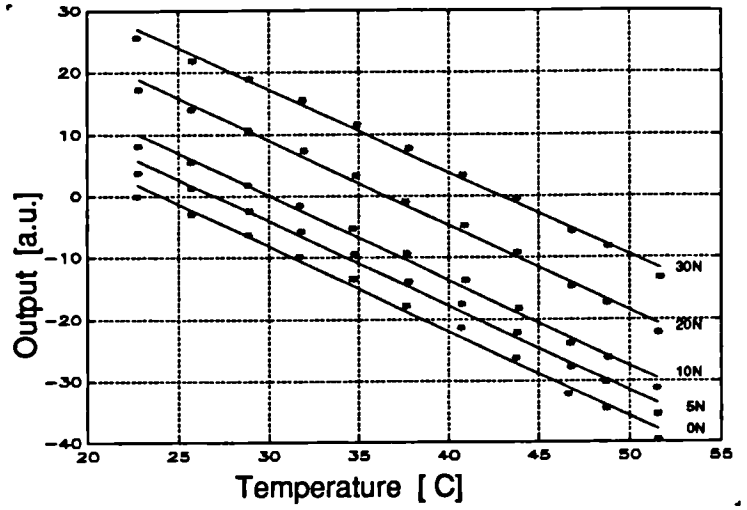

(a)

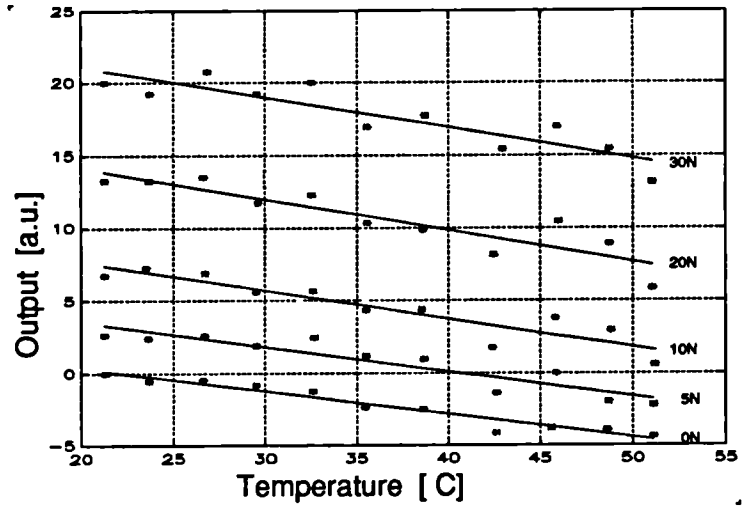

(b)

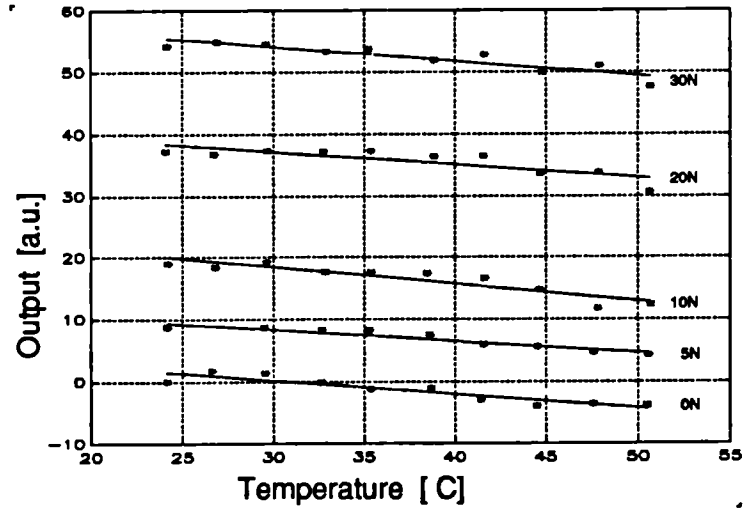

(c)

Figure 4.25 Relative section output as a function of temperature and load for the prototype normal-stress transducer ; (a) SG1, (b) SG2, (c) SG3. The excitation voltage was 1Vdc.

	SG1	SG2	SG3
Temperature Coefficient [a.u./℃]	-1.3702 (0.0168)	-0.1898 (0.0240)	-0.2230 (0.0345)

Table 4.10 Relative temperature coefficients of the prototype normal-stress sections. The mean (standard deviation) of three cycles over the range 20-50 ℃ is given.

SG2 and SG3 were comparable and clearly had significantly lower temperature coefficients than SG1.

4.2.3 Static Stress Response

Force sensitivity (gain) data taken from Figure 4.25 was rearranged in Figure 4.26 to show the section output linearity with force and temperature. Gain data is plotted for temperatures in the *20-40 ℃* range at *3 ℃* intervals. The slope of the curves gives the gain and their change in slope provides the gain drift (change in force sensitivity with temperature) values given in Table 4.11. From this data SG3 has greater force sensitivity than SG2 or SG1 at *20 ℃*, and exhibits less drift in force sensitivity with temperature than SG2 or SG1.

	SG1	SG2	SG3
Gain [a.u./N]	0.857 (0.017)	0.663 (0.034)	1.816 (0.042)
Drift [a.u./N/℃]	-1.6×10^{-5}	-1.5×10^{-3}	1.4×10^{-3}

Table 4.11. Mean (Standard deviation) of relative force sensitivity and drift values over the temperature range 20-40 ℃ for the prototype normal-stress sections.

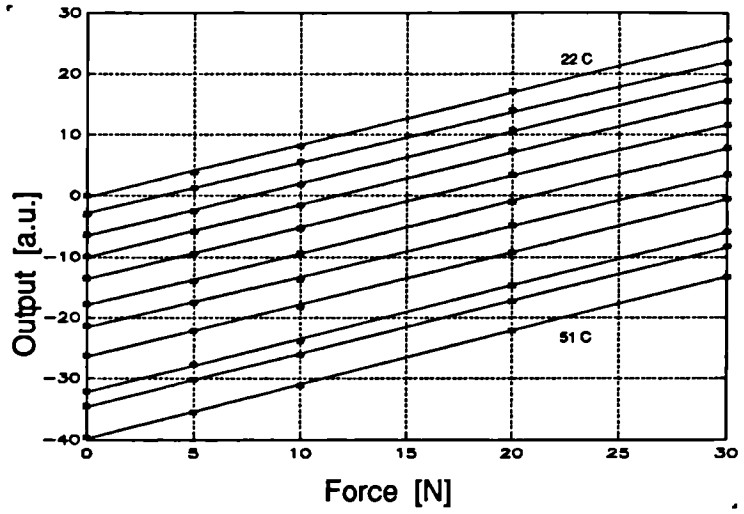

(a)

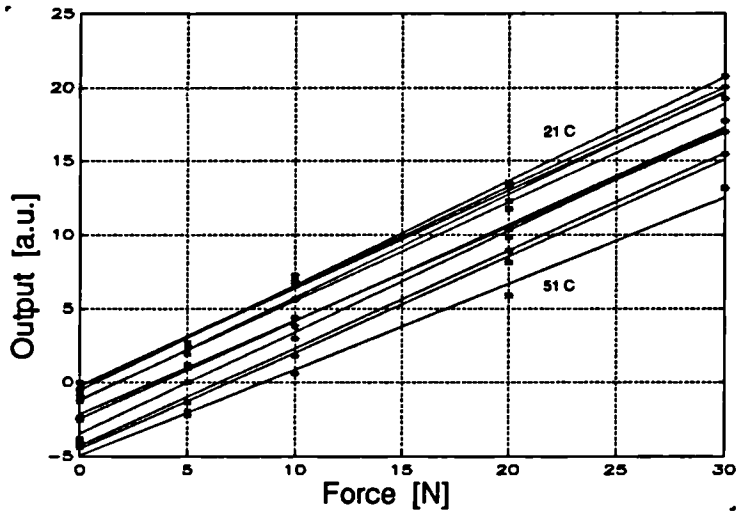

(b)

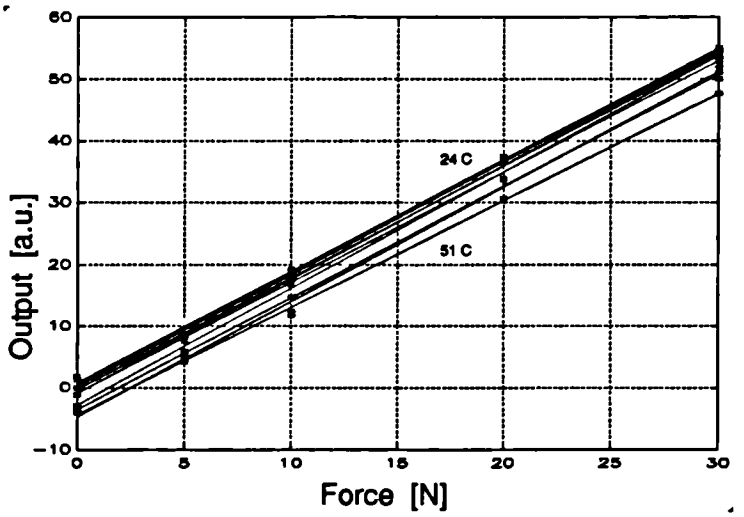

(c)

Figure 4.26 Relative force sensitivity as a function of temperature and load of the prototype normal-stress section ; (a) SG1, (b) SG2, (c) SG3. The excitation voltage was 1Vdc.

4.2.3.1 Non-axial Loading of Diaphragm

The calculations to determine the optimum diaphragm thickness [4.2.4] involved a compromise between diaphragm radius, and whether loads were uniformly distributed or centralised through a point. The theory of bending in beams predicts that the deformation (and therefore transducer output) will vary greatly with the size of the loaded area and its centre of application. To demonstrate this theory, load spreading layers and varying diameter spherical indentors were used to apply stresses to the SG3 section. Figure 4.27 plots the gauge outputs (one volt excitation) over five force cycles to *55N* at *0.1Hz*. Each plot has a small diagram indicating the load applications mechanism.

In clinical applications other researchers have mounted the normal stress section of their transducer next to the limb interface **[Sanders and Daly 1989]**. Clearly, form Figure 4.27, the dependence of the device response on the area and centre of force application is very strong. This indicates that measurement errors will occur when a strain gauge diaphragm is used directly at the interface surface, and these may be significant near bony prominences.

Now, the use of small layers of liner material interposed between the transducer and the skin interface may perform some load spreading function easing the conformability problem at the interface, as experienced by the limb. So, over the fleshy parts of the residual limb, interface loads may be quite uniformly applied across the face of the transducer, thus non-axial loading errors may be minimised. It also tends to maintain a consistent friction coefficient across the interface. The transducer described in this thesis was intended to be used at interface sites which may not be fleshy. Therefore, in order to minimise errors it was important to provide a mechanism for focusing the applied load in a consistent manner independent of its centre of application.

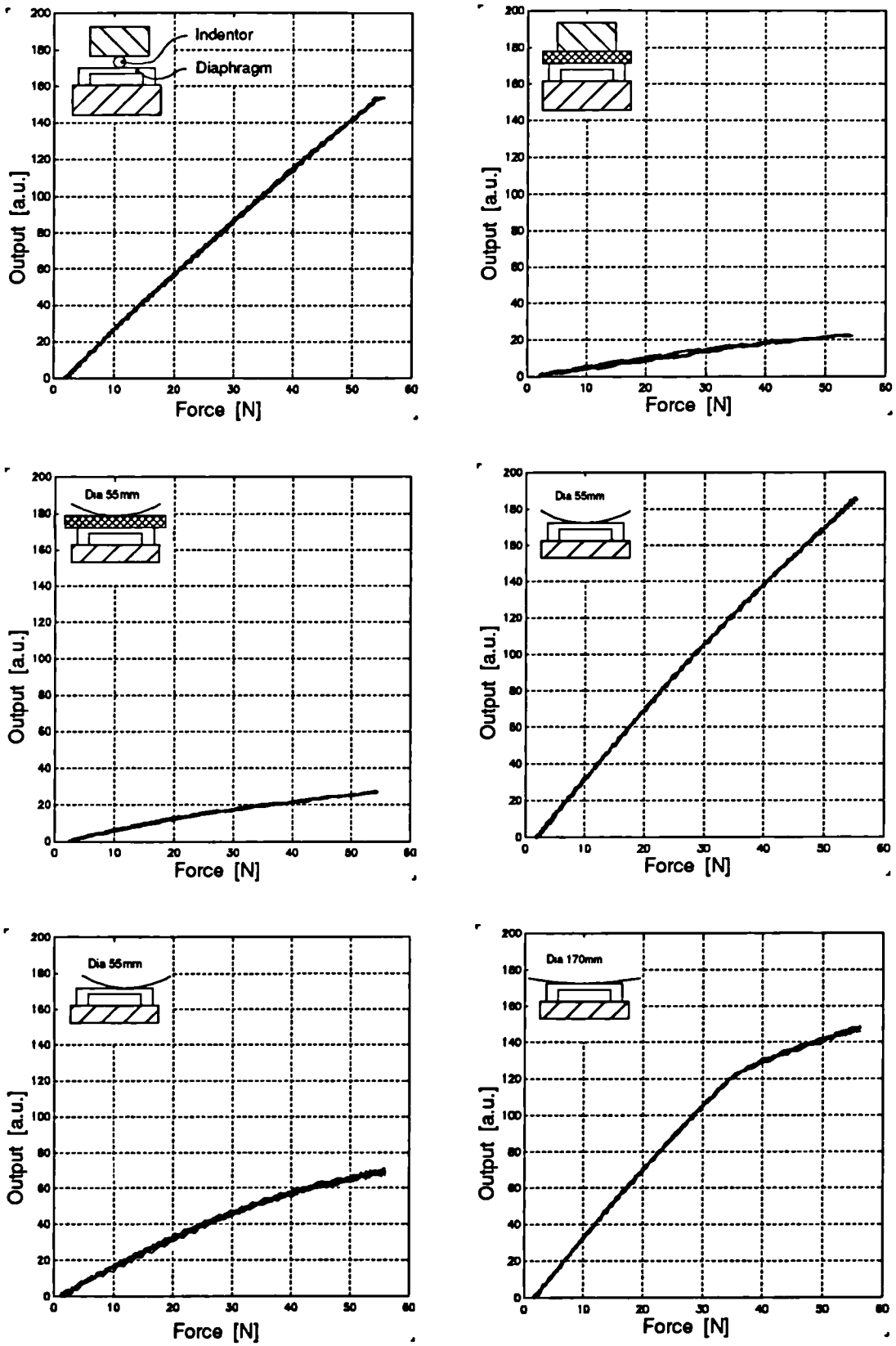

Figure 4.27 Relative output signals for SG3 strain-gauged diaphragm when 55N load applied to diaphragm via load spreading layers and various diameter indentors. Each was subjected to five cycles at 0.1 Hz. The excitation voltage was 1Vdc.

4.2.4 Discussion

It was clear that full bridge gauges SG3 and SG2 had superior temperature stability to the half-bridge SG1. Also, SG3 had greater force sensitivity and a more constant force-output curve with temperature.

The temperature and force sensitivities of SG3 were found to be adequate for the application considered here. Furthermore the driving and buffering circuits required for foil strain gauges are no more complex or costly than those for a comparable semiconductor gauge [3.2.2]. So on a cost and performance basis it was decided that SG3 (**QFDPF-9-350 Technimeasure LTD**) would be used in the normal-stress section of the triaxial-stress transducer.

4.3 Requisite Triaxial Transducer Design - Design C

In [4.1] and [4.2] details were reported of the various stages in the development of the shear and normal stress transduction sections. This part of the chapter [4.3-4.4] describes the construction and performance of a design that was accepted as the final iteration of the development process and formed the requisite triaxial transducer.

4.3.1 Device Construction

The following [4.3.1] gives details of the components used in the final three axis transducer design (Design C), along with assembly procedures and details.

Shear stress transduction section

The basic components of the shear stress transducer section consisted of three discs. These were cut from aluminium alloy bar stock (outer discs) and acetal rod (centre disc). Each was subsequently inspected and deburred. Their dimensions are given in Figure 4.28.

The PCB's, which hold the MR element and shear section leads, were fabricated from double-sided copper laminate (**EPS121RA - Fortin Inc or AKS121 - ISM**

Ltd). Squares of the laminate (*20 x 20mm*) were scrubbed to remove any oxide layer and grease, then washed with distiled water. They were coated with two layers of photo resist (**Positiv20+ - Electrovalue LTD**) and dried. A photo mask for creating the PCB pattern has the dimensions given in Figure 4.29. After exposure and developing they were etched and cut from the sheet. A low power microscope (*x8*) was necessary to achieve the precision required during cutting (*approximately 0.1mm*).

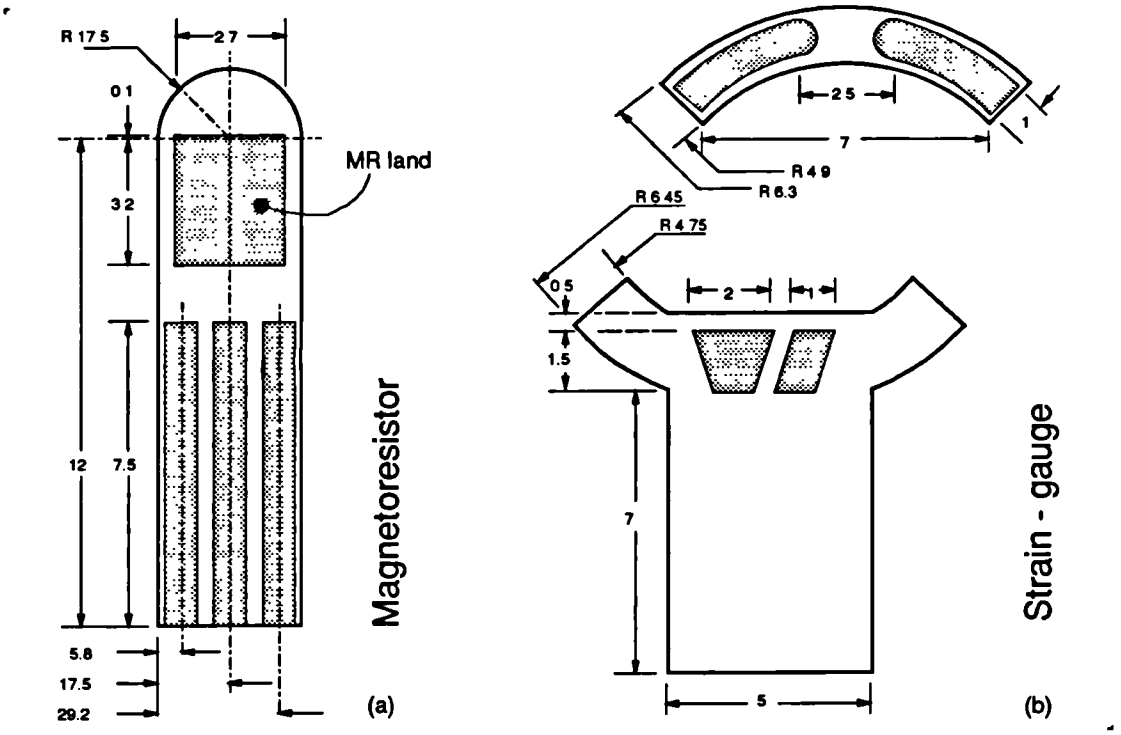

Figure 4.29 Dimensions (mm) of photomasks for the PCB's used in Design C. Magnetoresistor PCB from the shear stress section (a), and strain-gauge lead termination PCB from the normal stress section (b).

Each PCB was again degreased with low impurity Acetone and the MR element (**FP111L100 - Siemens (UK) LTD**) cemented onto the land on the PCB with cyanoacrylate adhesive (**405 - Loctite UK LTD**). Very accurate placement was essential to minimise output offset errors after assembly.

The MR element leads needed to have their insulating lacquer scraped off before being soldered to the tracks on the PCB. Because of the size of the element a miniature soldering iron was used and the procedure performed under the microscope. The temperature of the iron was carefully controlled and all actions were precise and quick to avoid melting the joint where the lead was attached to the element.

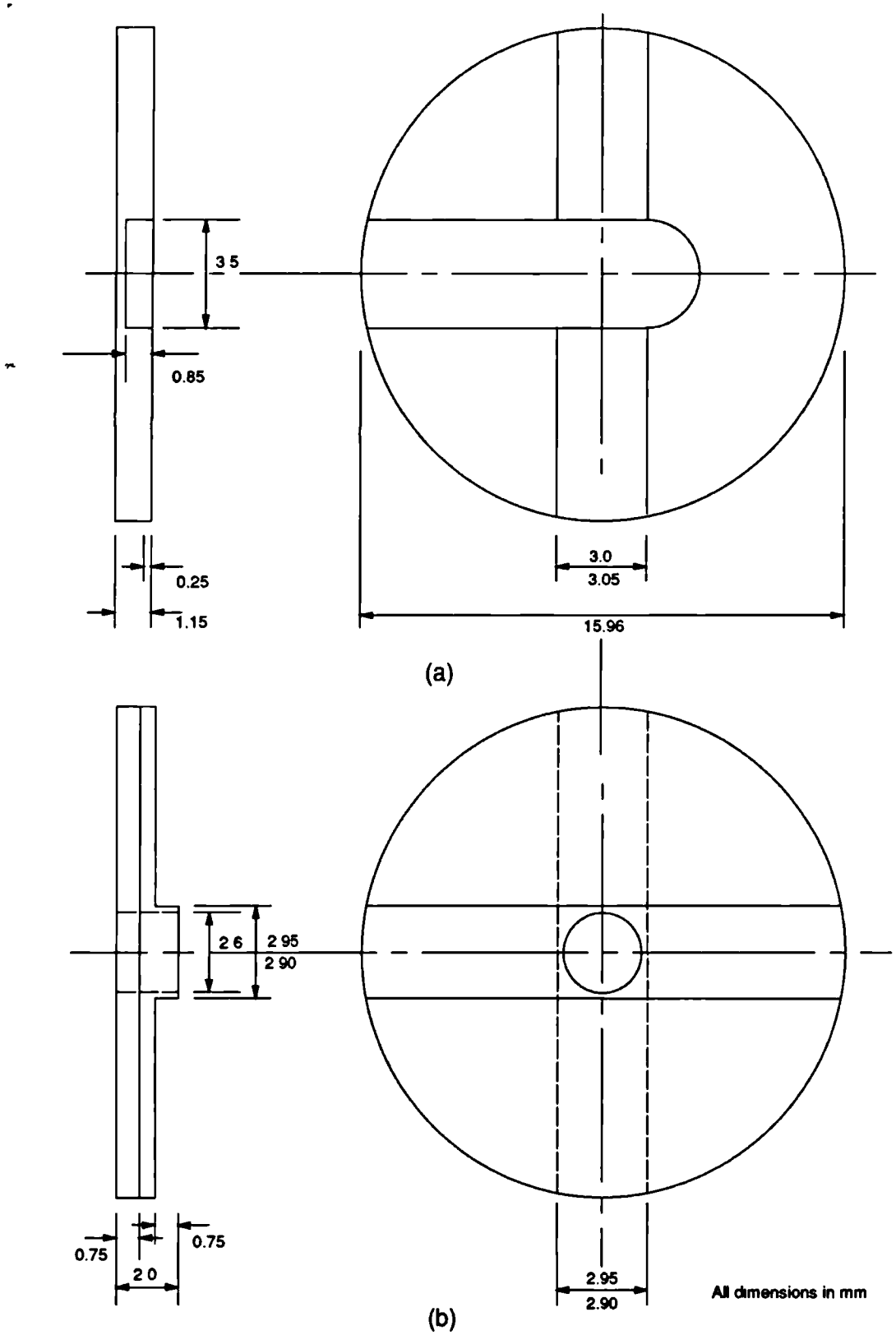

Figure 4.28 Dimensions (mm) of the disc's used in the shear section of Design C. Outer disc (aluminium alloy) with groove for housing the MR PCB (a) and the centre disc (acetal copolymer) with a central hole for containing the magnet (b).

A standard *1.27mm* pitch *10-way* ribbon cable (RS Components LTD) was used as the section lead. In the assembled device all the leads were formed, because entry to each of the two shear sections are mutually orthogonal. To facilitate this the cores of the leads specific to each section, were cut to predetermined lengths before being tinned. Also, to minimise the thickness of each section the top and bottom surfaces of the section lead insulation were cut flat. These would eventually fit into the slots milled into each outer disc and be flush with the surface of that disc. The pretrimmed leads were soldered to the PCB tracks so that their joints abutted the MR device lead joints. In order to provide maximum strain relief for the device leads, as much section lead insulation as possible was cemented inside each disc. The PCBs were fitted into their slots in the outer discs and cemented into place (**405 - Loctite (UK) LTD**). An interference fit between the PCB and slot was obtained for accurate alignment of the MR element with the magnet.

Four rectangles (*18 x 7mm*) of natural rubber sheet (*0.5mm thick*) [see 4.1.4.1 for formula] were abraded and cleaned with acetone. These were cemented to the two semicircular upper surfaces of each of the outer discs with a cyanoacrylate adhesive (**405 - Loctite (UK) LTD**). To minimise sliding friction the channel in each outer section was coated with a thin layer of PTFE (RS Components LTD) from an aerosol.

The bar magnet (**2x2x2 NdBFe - Magnet Developments LTD**) was inserted and cemented (**406 + 757 - Loctite (UK) LTD**) into the hole drilled in the centre of the acetal disc. Any excess length of the magnet was filed off so that the face of the magnet was flush with the surface of the acetal disc. This was necessary as any protuberances may impinge on the MR element during assembly or snag on the edge of the MR element slot when the disc slides under applied force.

Normal stress transduction section

The assembly procedure for the normal-stress section was carried out in parallel with the assembly of the shear-stress section. It began with the manufacture of the diaphragm from silver steel rod. The dimensions of the diaphragm and the indentor are given in Figure 4.30. It was important that the inside surface of the diaphragm was smooth, otherwise the strain-gauge may be damaged by being bonded to an uneven surface.

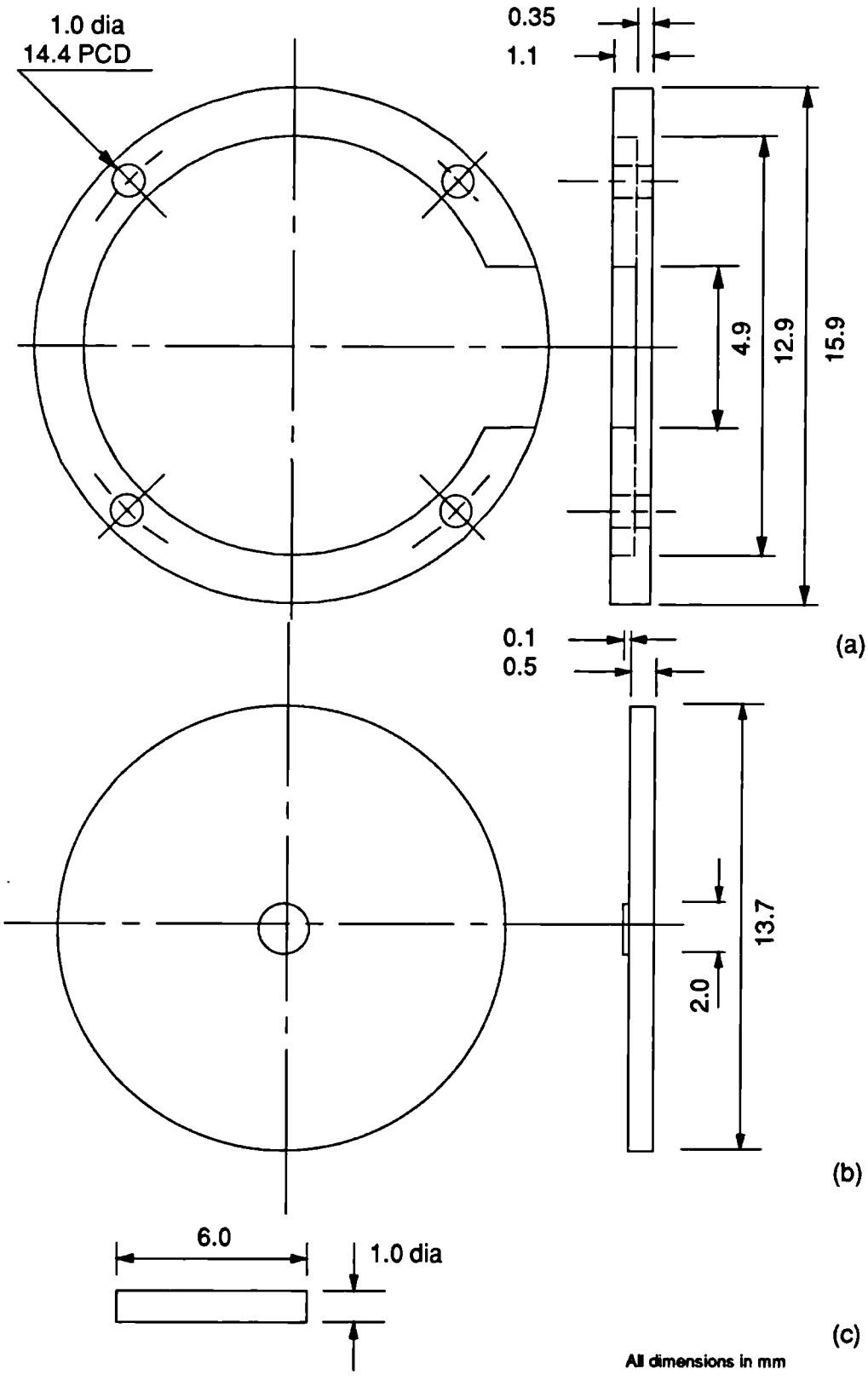

Figure 4.30 Dimensions (mm) of the diaphragm (a), indentor (b) and guide pins (c) used in the normal stress section of Design C. All are made from silver steel.

The strain gauge **(QFDPF-9-350 Technimeasure LTD)** was cemented **(P2 - Technimeasure LTD)** centrally on the diaphragm with tinned copper-wire leads soldered to the gauge terminals. Excess gauge cement was carefully removed and the diaphragm degreased.

Miniature PCB's were made in the same fashion as those for the shear section. Their use was to terminate the gauge leads and section leads as well as provide some strain relief. The dimensions for the PCB's are given in Figure 4.29. There was an upper and a lower (nearest the section lead entrance) PCB.

Both the gauge leads and the section leads required preparation before soldering. Under a microscope, a scalpel blade was used to scrape any oxide layer from the gauge leads. These were then cut to length and soldered to the copper pads on the PCB's. Each core of the section lead (remaining four cores of *10-way* ribbon above) was cut to a predefined length and its end stripped and tinned before soldering them to the PCB's. As before this operation was conducted using a miniature soldering iron and under a microscope. Again, to minimise the thickness of the section the upper and lower surface of the section lead's insulation was trimmed flat. Care was taken not to expose any of the conductors during the trimming operation.

Because of height restrictions under the diaphragm, any excess solder was trimmed away. A visual check was necessary to confirm that all conductive parts were below the level of the diaphragm support wall. This was done bearing in mind that the diaphragm will flex under load, so moving the gauge closer to the top of the shear section. The section leads are formed around the inner circumference of the diaphragm support wall and cemented in place with a small amount of contact adhesive, cyanoacrylate. It was important that the leads butt against the diaphragm support wall where they will cause minimum interference with the bending movement of the diaphragm under load. Also care was taken to ensure that no adhesive covers the top (or exposed) face of the gauge, as this would tear the gauge as the diaphragm flexes. A second trim made certain the section leads are flush with the support wall and the wall was free from adhesive.

When the normal section is assembled on to the bottom of shear section the joint was air tight. So, any air trapped in the diaphragm cavity would expand and contract with changes in ambient temperature. That would put pressure on the

diaphragm and cause it to flex, thus generating an error signal. To avoid this problem a small vent hole was drilled through the diaphragm close to the support wall. However, the gauge was then exposed to the environment and may be degraded by airborne contaminates. For protection a thin layer of silicone rubber (non-acetic acid based) was applied over the gauge.

The indentor guide pins were assembled next. Each hole drilled in the wall of the diaphragm and its associated pin was cleaned of debris and degreased with acetone. An interference fit was obtained between the guide pins and the holes in the diaphragm support wall. A small amount of high strength epoxy adhesive (RS Components LTD) was droppered down each hole and the pins inserted. It was sometimes necessary to force the pins with a small hammer so that they located with their upper end flush with the top of the support wall.

A photograph of the disc's at this stage of the construction is given in Figure 4.31.

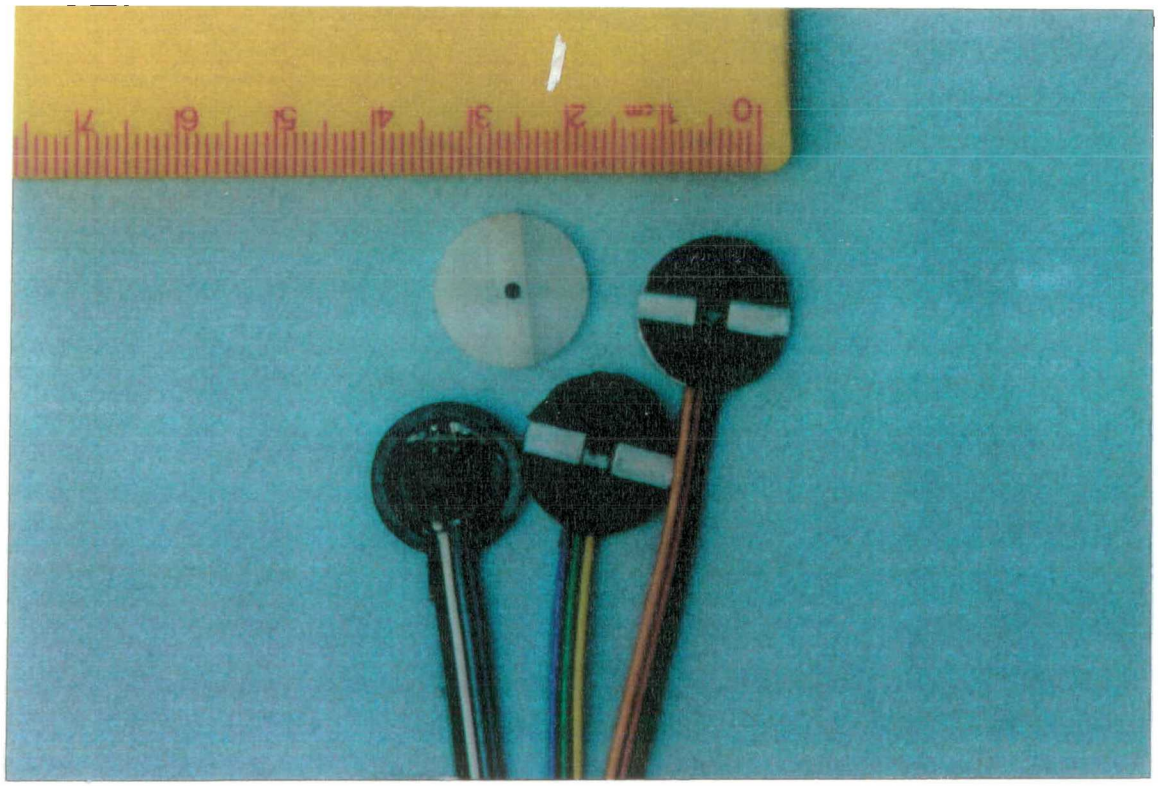

Figure 4.31 Photograph of the four transducer discs before final assembly.

The final stage of the assembly was to attach the normal section to the bottom face of the shear section. Concentricity was maintained by the assembly jig. The

Device assembly

A jig was constructed [Figure 3.21] for the assembly process to align the discs while the cement cured. All disc surfaces were cleaned with acetone. An outer disc (aluminium alloy) of the shear section was inserted into the base of the assembly jig and the adhesive (**405 - Loctite (UK) LTD**) applied to the top surface of its rubber layer. The centre disc (acetal copolymer) was primed (**757 - Loctite (UK) LTD**) and pressed on to the outer disc in the assembly jig. Care was taken to align the ridge and channel immediately as bonding only took seconds. The same procedures were followed for cementing the other outer shear section disc.

join must be capable of withstanding the maximum shear-stress applied to the device, so the adhesive used was an high-strength epoxy (**RS Components LTD**). Both surfaces to be joined were lightly abraded and thoroughly degreased with acetone. A layer of epoxy was applied around the circumference of the diaphragm. The two sections were mated and the assembly jig clamped. When the epoxy had hardened the devices were removed from the jig and excess cement removed from around the transducer.

Prior to calibration the resistances of each of the shear axes MR elements were measured. A small padding resistor (**1% metal oxide - RS Components LTD**) was added to the appropriate lead to ensure the zero-load resistance of both halves of the axis were equal, so that the output of the shear signal amplifiers would indicate zero volts at zero force. Thus a forward displacement would produce a positive voltage, and a reverse displacement a negative voltage. Each device was uniquely labelled to identify it with its calibration data [4.3.2.3], as component and assembly variables make each device different.

4.3.2 Dynamic Stress Response

In order that the measured stress signals accurately reflect the actual stresses occurring at the limb/socket interface it is essential that the transducer be able to closely track the changes in stress magnitude. It is important, therefore, that the magnitude response of the transducer is constant over the expected range of frequencies in the stress field. This part of the chapter [4.3.2] details the equipment, test methods and performance of the transducer design under applied load cycles. In contrast

to previous static or quasi-static stress response testing of Design A and B it was possible to carry out both dynamic and static assessments on the final design. Ten transducers were constructed and subjected to loads of varying magnitudes, frequencies and orientations. From these tests, conclusions have been made about the design's linearity, range, hysteresis, creep, stress vector resolution and frequency response.

4.3.2.1 Test Equipment

In order to apply dynamic loads to the devices under test over a range of frequencies, an industrial vibrator and power amplifier were purchased (**SS300, G100A - Gearing and Watson LTD**) [Figure 4.32]. The calibration jig for the shear transducer sections was clamped to a rigid platform designed to place the transducer level with the axis of the vibrator. A signal generator (**HP3314A - Hewlett Packard (UK) LTD**) provided the frequency source for the power amplifier. The vibrator and power amplifier were set in a constant-force mode so that cycles to given force magnitudes, at the signal frequency, could be applied to the jig. A universal joint was used to connect the vibrator to the calibration jig and address any misalignment between the two.

To apply dynamic forces to the normal stress section of the transducer a small aluminium alloy plate was drilled to accommodate the diaphragm guide pins. The indentor plate was positioned under the section as the section pins were inserted in the plate guide holes. The plate and normal section were then placed between the sliding block of the calibration jig and a vertical plate on the platform base. Forces applied to the sliding block were then transmitted to the section, driving it onto the indentor.

The forces applied to the calibration jig were measured at the point where the universal joint attached to the sliding block by interposing a bidirectional piezoelectric load cell (**9301A, 5007 - Kistler (UK) LTD**). The accuracy of the cell including nonlinearities, was better than *0.03%*.

Displacements of the sliding block, under the applied forces, were measured by an LVDT (**OD3, SM1 - Schlumberger (UK) LTD**). The core of the LVDT was attached to the sliding block and the body of the LVDT inserted into a hole in the vertical plate of the platform. The accuracy of the LVDT, including nonlinearities, was better than *0.5%*.

The transducer under test was powered and its signals buffered by a transducer interface unit (**MEP085B**) built specifically for the data collection unit [Chapter 6]. The excitation applied to each device was *1Vdc.*

Signals from the load cell, LVDT, and transducer were digitised (**DT2824PGH - Data Translation Inc**), to *12 bits*, and stored on a personal computer (**IBM-PCAT**) using the data capture software suite (**Global Lab - Data Translation Inc**). The accuracy of the A/D, including nonlinearities, was better than *0.2%.*

Figure 4.32 describes the setup schematically, and presents a photograph of the equipment.

4.3.2.2 Dynamic Measurement Considerations

When measuring dynamic stresses or dynamically testing devices it is essential to consider how the measuring or testing equipment may be affecting the desired measurand.

To be able to precisely measure dynamic stresses it is essential that the frequency response of the transducer is constant over the bandwidth of the measurand (*50Hz*). If this not the case then the transducer will not be able to accurately track changes in stress levels. Explicit measurements of the transducer frequency response can be made if the bandwidth of the transducer dynamic calibration facility is greater than that of the transducer. Otherwise, it can be implied that the transducer response is sufficiently constant, over the measurand bandwidth, by demonstrating that it's resonant frequency is very much greater than the measurand bandwidth. In either case it is also necessary to assess the actual nature of the dynamic response of the transducer in the measurand bandwidth. To do this, the calibration facility is used to evaluate the transducer response at an arbitrary frequency in the bandwidth. However, the bandwidth of the calibration facility with a transducer-like body in situ must be greater than this arbitrary frequency. Therefore the frequency response of the calibration facility was determined.

The calibration facility (jig) with transducer in situ [see Figure 4.32] form a single mode mechanical system under forced vibration. The rheological system model for this arrangement may be drawn, using Voigt elements, as in Figure 4.33.

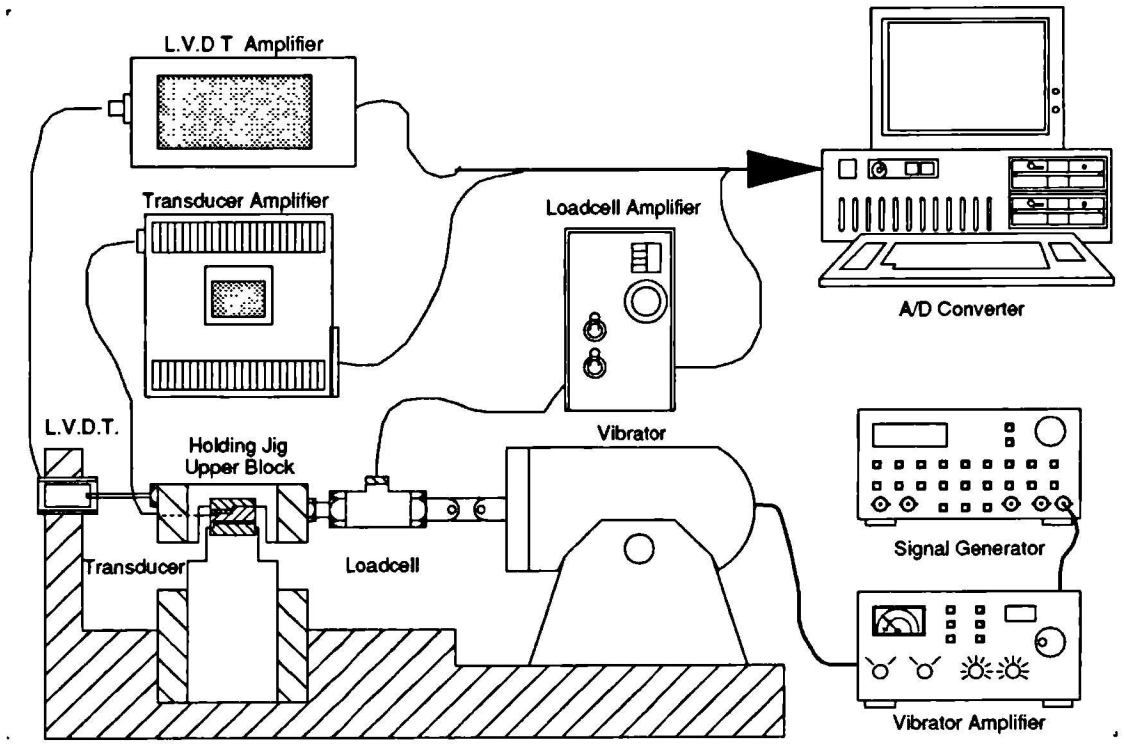

(a)

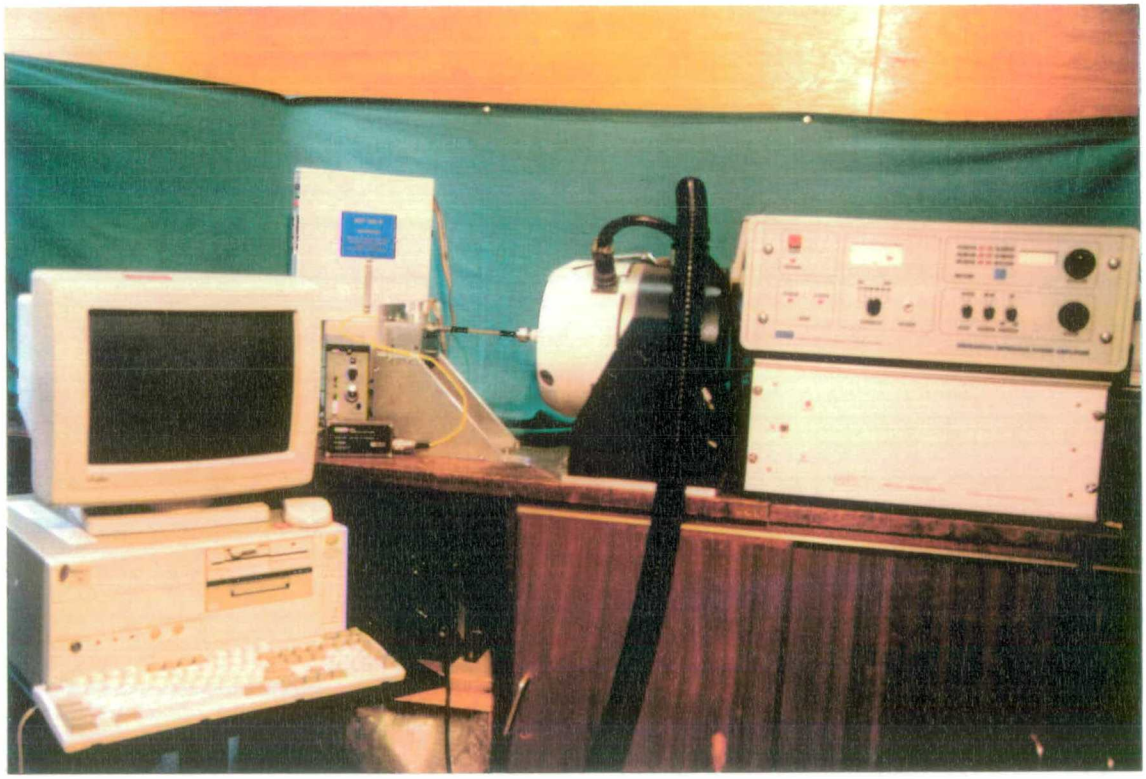

(b)

Figure 4.32 Schematic (a) and photograph (b) of the inter-connection of the components of the transducer dynamic calibration equipment.

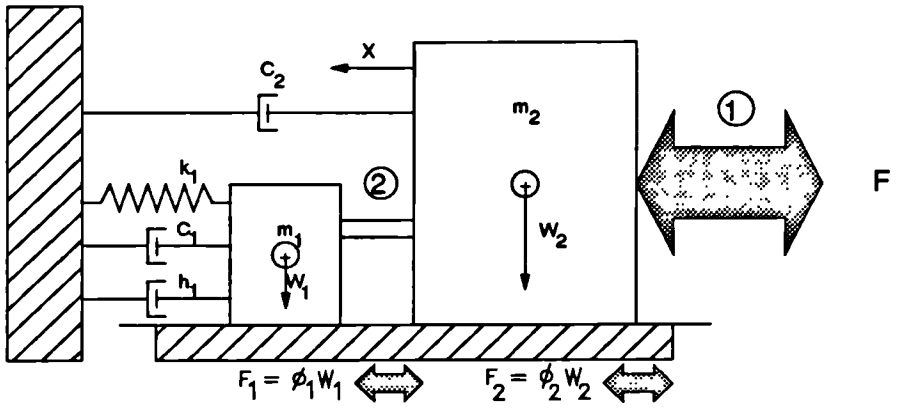

Figure 4.33 Rheological model of the shear transducer dynamic calibration jig with transducer in situ.

Where: M_1 and M_2 are the masses of the transducer and holding block respectively; c_1 and c_2 are the viscous damping coefficients of the transducer and the calibration jig respectively; h_1 is the hysteresis of the transducer and k_1 is its elastic stiffness; x is the displacement caused by the measured force F; F_1 and F_2 are the friction (coulomb or dry) forces in the transducer (shear section only) and the calibration jig bearings respectively; w_1 and w_2 are the weights of the transducer and holding block acting normal to their bearing surfaces; while ϕ_1, ϕ_2 are the coefficients of dry friction for the transducer ridge/channel (shear section only) and the jig bearings respectively. Two terms are used to describe the damping effects in the transducer. The hysteresis term, h_1, is used to discriminate between the energy losses which occur under cyclic loads that are independent of frequency, and those losses whose magnitude is frequency dependent are represented by c_1. In this case where the calibration jig bearings are lubricated with a low viscosity oil, the coulomb friction force in the bearings (F_2) can be assumed negligible. Also, the viscous damping coefficient for the jig (c_2), which is due to viscous friction in the lubricating oil and air friction during motion, will be small

The vibration of the system under steady state sinusoidal forces will be governed by the following force-balance equation **[Nagrath 1986]**:

$$(\phi_1 w_1 + h_1[x])sgn[\dot{x}] \quad + \quad (M_1 + M_2)\ddot{x} + (c_1 + c_2)\dot{x} + k_1 x \quad = \quad F \sin \omega t \qquad (4.3)$$

where, the function 'sgn' stands for 'algebraic sign of' (i.e. +ve or -ve) the given variable. The first term on the left hand side contains non-linear functions. The

first part of this term, $(\phi_1 w_1)$, representing coulomb friction in the transducer (shear section only), is constant but is manifest in two stages. From the transducer at rest there occurs an initial static (inertial) friction force which changes to a lower (dynamic) friction force once the body is in motion. This characteristic is generally small in the transducer due to the PTFE film applied to the ridge/groove construct and the self lubricating property of the Acetal centre disk. The second part of the term, $(h_1[x])$, represents hysteresis in the rubber layer (shear stress section) or the diaphragm (normal stress section) of the transducer and is a function of displacement. Hysteresis in rubbers is generally found to be a few percent of the applied stress magnitude **[Ward 1971]**, while in silver steel hysteresis is only a few tenths of a percent.

The calibration data for the transducer should relate its output signals to forces applied to it. In the calibration jig, described in Figure 4.32 and 4.33, the actual force being applied to the transducer, at **(2)**, is not being measured directly. Only the force at **(1)** is. Although, from (4.3), if $c_2 \ll c_1$ and $M_2 \ll M_1$ then the energy lost in moving the calibration jig would be small in comparison to the energy expended in moving the transducer. Thus, the frequency response measured will reflect closely that of the transducer.

Now, both c_1 and c_2 are small and may be comparable. The masses of the sliding block, holding cylinder (M_2) and transducer (M_1) are given in Table 4.12 (N.B. half the holding cylinder is attached to the transducer and is in motion during calibration). It is clear from Table 4.12 that in this case M_2 is about *50* times greater than M_1. This is due to its original intended use as a testing jig attached to the static test system (Instron Materials Tester). It is also clear that it is a non-trivial problem to reduce the mass of the gripping and supporting structure of the sliding block to be significantly less than the mass of the transducer. Therefore, the dynamic calibration jig cannot be used to explicitly measure the frequency response of the transducer. Unfortunately due to time and resource constraints it was impractical to tackle the considerable problem of designing a dynamic calibration jig to do this. However, another testing method was available which did imply that the frequency response of the transducer is constant over the measurand bandwidth, as required [4.2.3.5]. It, therefore remains, only to identify the bandwidth of the calibration jig, with a transducer-like body in situ. This is in order to select an arbitrary frequency in the measurand bandwidth at which to observe the typical dynamic response of the transducer.

Component	*Mass [gm]*
Sliding block and bearings	*108.3±0.1*
1/2 holding cylinder	*86.6±0.1*
Transducer (3 Axis) + 100mm cable	*4.2±0.4*
Shear Axis (single disc)	*0.7±0.1*
Normal Axis (single disc)	*2.5±0.1*

Table 4.12. Masses of the calibration jig components and transducer.

To determine the bandwidth of the calibration jig, with a transducer-like body in situ, the transducer in Figure 4.33 was replaced by a helical metal spring (negligible hysteresis and creep and of known stiffness - $k=30.5 \pm 0.5N/mm$) between the sliding block and the vertical plate on the jig. The model for that setup is given in Figure 4.34. The force balance equation describing the model under forced sinusoidal motion can be written as:

$$m\ddot{y} + c\dot{y} + ky = F(t) = F\sin\gamma t \qquad (4.4)$$

Where k is the stiffness of the steel spring, c is the viscous damping in the jig bearings, y is the displacement under applied force F, γ is the angular frequency of the forced oscillation and m is the mass of the sliding block. The mass of spring, viscous damping in the spring, and dry friction in the bearings are assumed negligible.

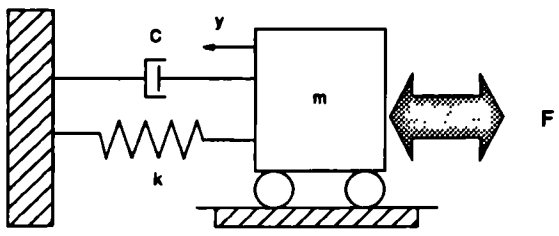

Figure 4.34 Rheological model of the experiment used to determine the frequency response of the transducer calibration jig.

Now, (4.4) can be rewritten as:

$$\ddot{y} + 2\lambda\dot{y} + \omega^2 y = \frac{F}{m}\sin\gamma t \tag{4.5}$$

where $2\lambda = \frac{c}{m}$, $\omega^2 = \frac{k}{m}$ and ω is known as the natural frequency of the system.

Obtaining the general solution to (4.5) involves solving its homogeneous and particular equations. There are three cases for solution of the homogeneous equation depending on the algebraic sign of $\lambda^2 - \omega^2$. For an underdamped system $\lambda^2 - \omega^2 < 0$, for an critically damped system $\lambda^2 - \omega^2 = 0$, for an overdamped system $\lambda^2 - \omega^2 > 0$. An impulse-like impact test on the calibration jig resulted in a decaying oscillatory motion, indicating that it is underdamped **[Kreyszig 1979]**. The general solution of (4.5), therefore, may be written as **[Zill 1989]**:

$$y = Ae^{-\lambda t}\sin(\sqrt{\omega^2 - \lambda^2}\,t + \phi) + \frac{F}{m}\cdot\frac{1}{\sqrt{(\omega^2 - \gamma^2)^2 + 4\lambda^2\gamma^2}}\cdot\sin(\gamma t + \theta) \tag{4.6}$$

where $\tan\theta = \frac{-2\lambda\gamma}{\omega^2 - \gamma^2}$ and A and ϕ are arbitrary constants

to satisfy any initial conditions.

The first term on the right hand side of (4.6) describes the transient response of the system and the second term the steady state response. After sufficient time under a steady harmonic excitation force the first term decays to zero, leaving:

$$y = \frac{F}{m}\cdot\frac{1}{\sqrt{(\omega^2 - \gamma^2)^2 + 4\lambda^2\gamma^2}}\cdot\sin(\gamma t + \theta) \tag{4.7}$$

or as is more commonly seen in engineering texts :

$$y = \frac{F}{k}\cdot\frac{1}{\sqrt{(1 - w^2)^2 + (2\zeta w)^2}}\cdot\sin(\gamma t + \theta) \tag{4.8}$$

where $\zeta = \frac{\lambda}{\omega}$, $w = \frac{\gamma}{\omega}$

The amplitude of the displacement (y) relative to the excitation force (F), for a given mass (m) and spring stiffness (k), is thus a function of both the damping (c) and the excitation frequency (γ). When damping is present ($c<>0$), the amplitude of (4.7) is bounded as $t \to \infty$, and reaches a maximum when :

$$\gamma = \sqrt{\omega^2 - 2\lambda^2} \tag{4.9}$$

or

$$w = \sqrt{1 - 2\zeta^2} \tag{4.10}$$

Clearly, for small damping $c \to 0$ $(2\lambda \to 0)$, the frequency of maximum oscillation approaches the natural frequency of the system. By substituting (4.9) into (4.7), the maximum value of the oscillation is given by :

$$y|_{max} = \frac{F}{m} \cdot \frac{1}{2\lambda\sqrt{\omega^2 - \lambda^2}} = \frac{F}{k} \cdot \frac{1}{2\left(\frac{\lambda}{\omega}\right)\sqrt{1 - \left(\frac{\lambda}{\omega}\right)^2}} \tag{4.11}$$

Written in terms of the resultant displacement relative to the maximum of the excitation function,

$$\left.\frac{y}{Y_0}\right|_{max} = \frac{1}{2\left(\frac{\lambda}{\omega}\right)\sqrt{1 - \left(\frac{\lambda}{\omega}\right)^2}} \tag{4.12}$$

or

$$= \frac{1}{2\zeta\sqrt{1 - \zeta^2}} \tag{4.13}$$

where $Y_0 = F/k$ is the static displacement under a static force (F). Clearly, for small damping $c \to 0$ $(2\lambda \to 0)$, the magnification approaches infinity.

The system described by Figure 4.34 was excited by sinusoidally varying forces to *20N* at various frequencies between *0.1Hz* and *200Hz*. After ten cycles at each frequency, when a steady state had been achieved, five cycles of section output, displacement and applied force were recorded. A plot of the resultant peak dynamic displacement to the static displacement with frequency is given in Figure 4.35. This type of plot is also called a magnification plot as it is a dimensionless ratio of dynamic to static displacements. The phase difference between the applied sinusoidal force and resultant displacement is also given. The curve exhibits the form of a lightly damped system, as the magnification ratio is large (y/Y_o=*22*), and the resonant frequency (*61-62Hz*) is close to that of the natural frequency of the system, $\omega = \sqrt{k/m}$ = *(61.8-62.8) Hz.*

Now, the measured stiffness of the shear section is typically *80±5N/mm*, and the stiffness of the normal section is typically *280±80N/mm*. Thus the resonant frequency of the calibration jig with a transducer in situ is approximately *100Hz* (shear stress section) or *190Hz* (normal stress section). This is sufficient to accurately observe the dynamic response of the transducer over the whole bandwidth of the measurand (*50Hz*). As will be shown later [4.2.3.5], the resonance of the transducer is significantly higher than the measurand bandwidth so its frequency response is constant over the whole bandwidth. Therefore, an arbitrary frequency of *1.0Hz* was selected at which to observe the dynamic performance of the transducer, and this was taken as a fair assessment of its performance over the whole bandwidth.

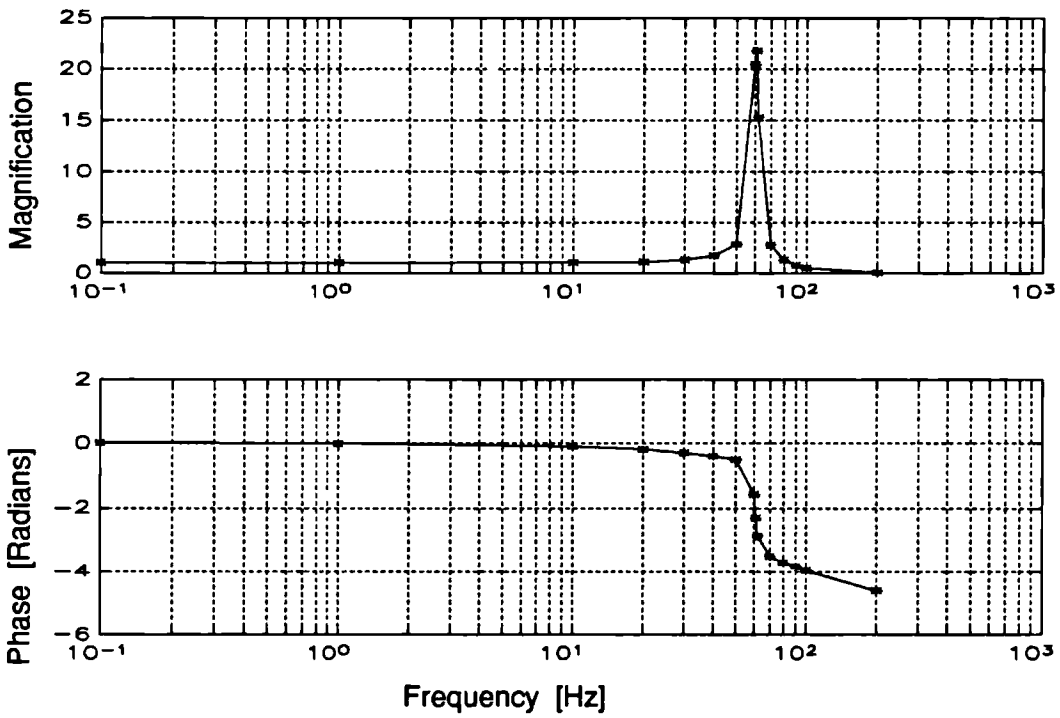

Figure 4.35 Magnification (a) and Phase lag (b) curves for a spring (k = 30.5 N/mm) in the calibration jig under forced steady state oscillation to 20N. The driven mass was 0.1991Kg.

4.3.2.3 Range, Hysteresis, Linearity and Accuracy

This part of the chapter describes the stress performance of the final transducer design. The form of the force versus output curve is discussed, noting any features, their causes and implications. The effect of nonlinearities, such as creep, hysteresis, saturation and friction, on linear range and accuracy are reported. As are the

methods used to convert recorded transducer output data back into the causative applied force. Again the shear and normal-stress sections of the transducer design are reported separately.

Shear-stress Section

The first part of the shear-stress section calibration was aimed at establishing the linear range and accuracy typical of the design. Ten transducers were assembled and the shear section of each was subjected to five load cycles of *±5, ±10, ±20, ±50N*, at *1Hz*. The load cycles was applied with the transducer at orientations of *0°* and *90°*. Figure 4.36 shows two examples of one shear axis output response to applied force. From records of the section displacement with applied force the measured stiffness of the shear section was typically *80±5 N/mm*. During testing four transducers was exposed to more than *100000* loading cycles, without degradation of their calibrated performance.

From Figure 4.36 it can be seen that the section output may be linear with applied force. However, hysteresis is present which tends to broaden at the extremes of the loading cycle. Also the calibration loop exhibits short horizontal regions at its extremes. This indicates momentary seizing of the ridge and channel construct when motion of the two ceases at the extremes (+ or *-50N*) of a load cycle. As the region is not uniform for all sections there is obviously some variation in the dimensions/fit of the ridge and channel within the batch of transducers. This could reasonably be due to trimming variations during assembly. The broadening of the calibration loop at the extremes of the load cycle is a combination of localised friction and energy losses occurring in the rubber.

The effect of friction on the force to output transfer function of the section is analogous to that of backlash in gears. There will be a loss in transfer magnitude and a phase lag between input and output wave forms. Both of which are dependent on the ratio of the applied force to the friction force, such that, if the ratio is large the loss in magnitude and the phase lag will be negligible [**Nagrath 1986**]. These effects are also true, in general, of hysteresis in rubber, where both magnitude distortion and a phase lag occur.

Saturation effects are also evident. These are caused by the magnet being displaced substantially off one half of the MR element. Therefore, although each device has

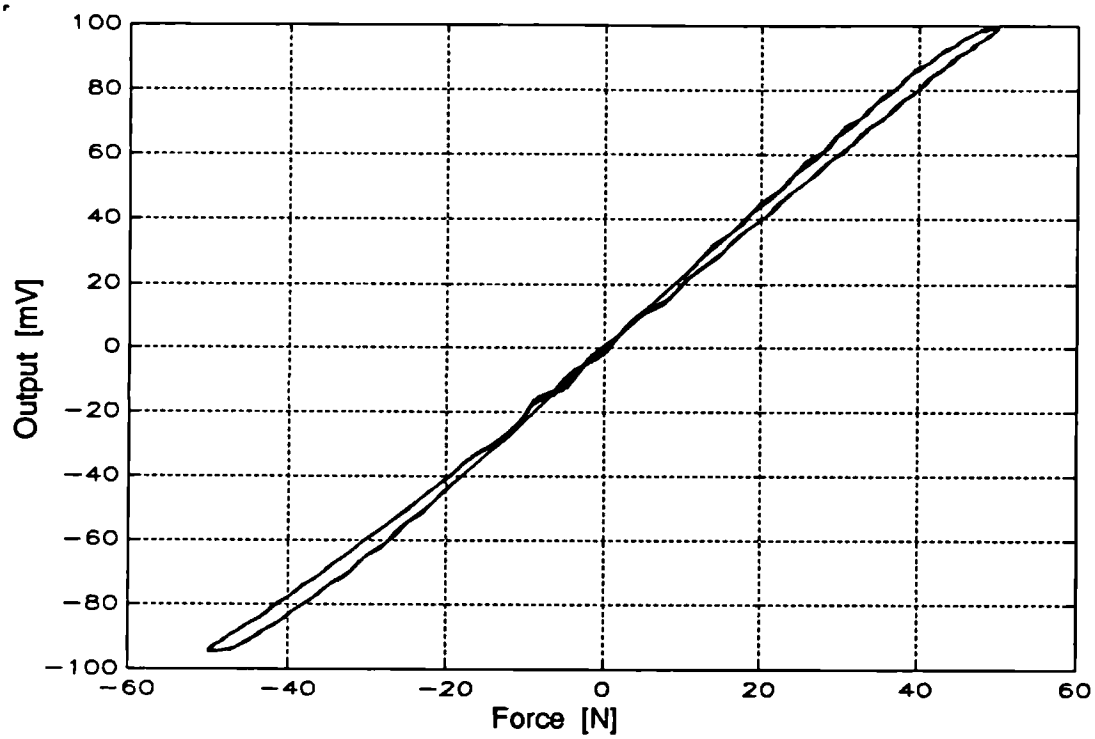

(a)

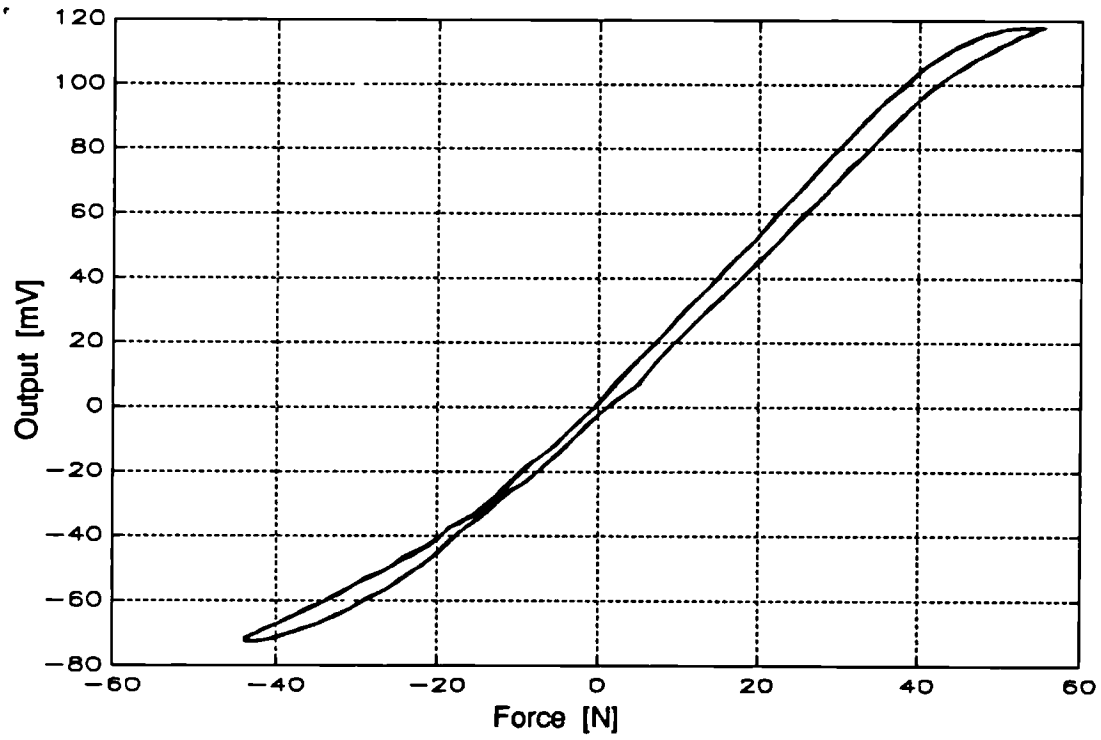

(b)

Figure 4.36 Example Force versus Output curves for shear sections of Design C. Five consecutive cycles to ±50 N at 0.1 Hz are described. The excitation voltage was 1V.

a working range of approximately *±50N*, the linear range is sometimes smaller. To define a linear range, a first order polynomial was fitted by matrix methods, under a least-squares criterion, through the central *±30N* of the calibration loop of each transducer. This was achieved through the use of the mathematics software package **Matlab** (Mathworks Inc). A second curve of higher order is fit to follow closely the centre of the calibration loop, and the difference between the two is then taken as a measure of the linearity error. The appropriate order of the second curve is found by minimising the residuals between it and the calibration loop, while keeping the order small. A fifth order polynomial was found to be sufficient. An example of a first and fifth order curve fitted to an hysteresis loop is given in Figure 4.37. The figure also depicts how the absolute linearity error varied over the load cycle for the best three sections tested. A linear range for a device may be derived directly from the linearity error plots. For example, the *5%* linearity range of *+33* to *-42N* is marked on Figure 4.37b.

The slope of the first order polynomial curve may be used as the conversion constant for the processing of clinical data. The error incurred in the use of the conversion constant was defined as the difference between any point on the calibration loop and the first order fit. This value thus includes both nonlinearity and hysteresis error sources. The user may choose to use the linearity information to define the uncertainty of any measurement he makes (E.g. *5%* linearity = *5%* accuracy). However the accuracy of the device may be better specified as follows.

It was observed that the width of the calibration loop decreased as the peak amplitude of the load cycle decreased - confirming that hysteresis is amplitude dependent. An example of this dependence is shown in Figure 4.38a-d. As conversion error is directly related to hysteresis, the accuracy of a conversion regime is dependent on the local amplitude of the applied force. To define an accuracy value for the first order polynomial conversion method, the maximum conversion error from the *±5, ±10, ±20, ±50N* load cycles was plotted against the cycle amplitude. Figure 4.38e is a plot of these maximum conversion errors for the best three sections tested. On this figure an arbitrary piecewise limit (line) is drawn. This bounds the maximum conversion errors by a percentage of the cycle amplitude and a fixed small force value. With these limits identified, any converted clinical data may then be described as accurate to a given percentage (*9%*) of its converted value or a fixed force (*0.5N*), whichever is the greatest.

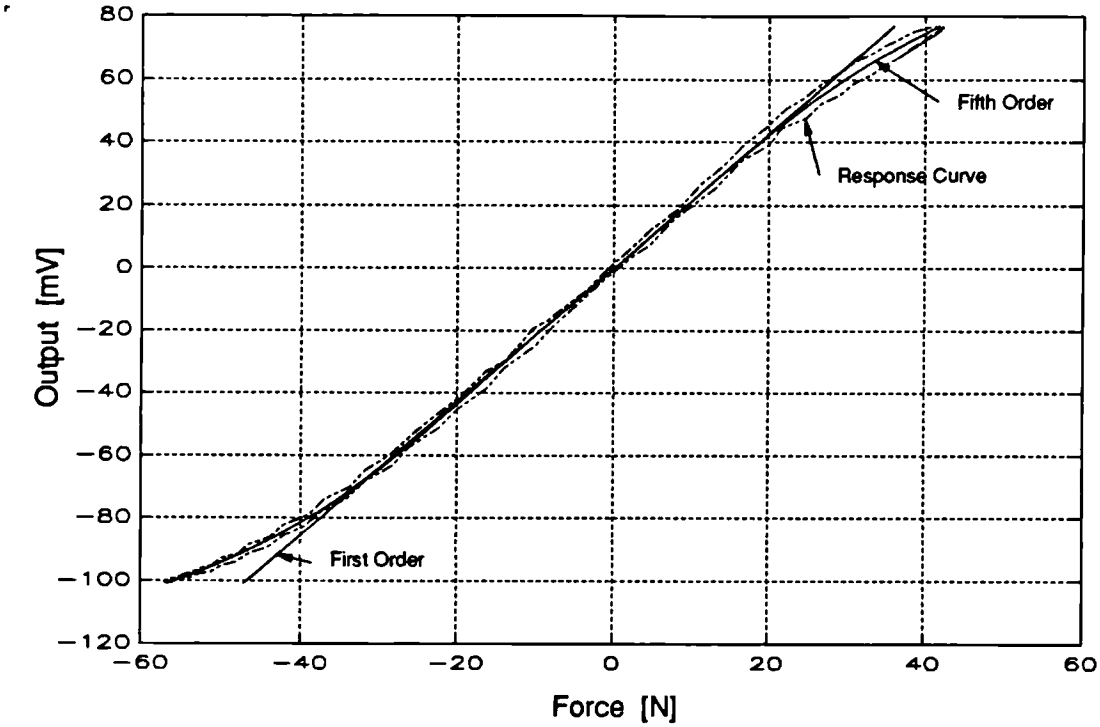

(a)

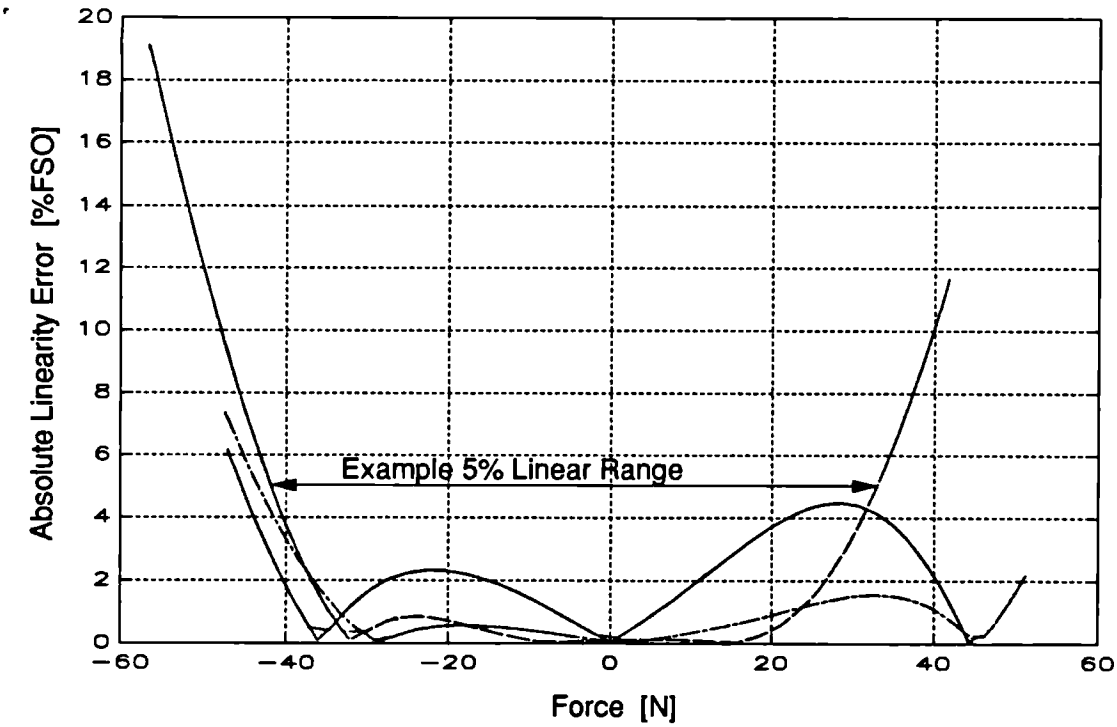

(b)

Figure 4.37 Example of a first order (linear) curve and a fifth order (central) curve fit to a force versus output calibration curve for a shear section of Design C (a). Absolute linearity error of the best three sections tested under a full scale (±50N) load cycle (b).

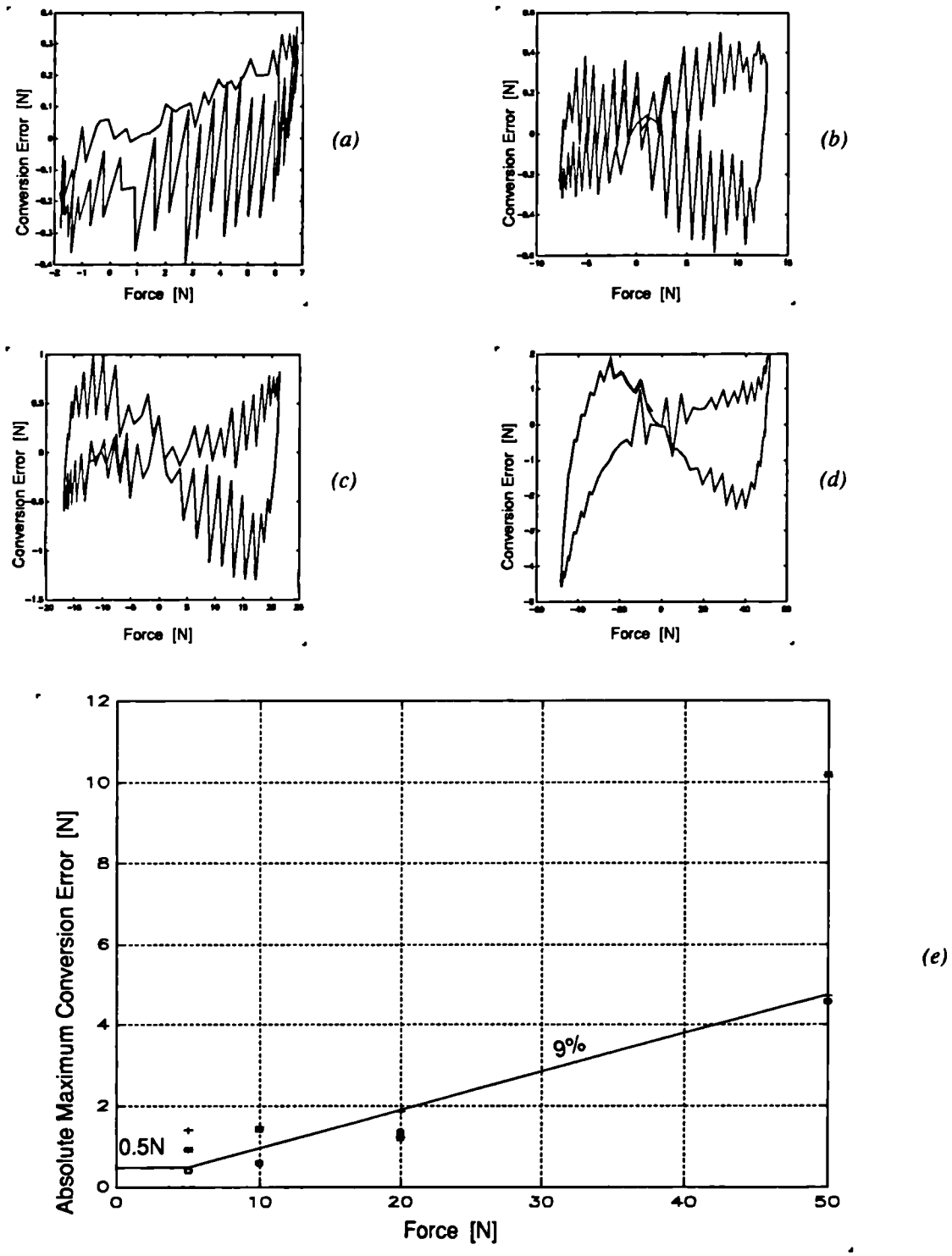

Figure 4.38 Examples of the errors arising from approximating the force versus output calibration curve by a first order polynomial. Conversion error over a single load cycle, for ±5, ±10, ±20, ±50N cycles (a)-(d). Absolute maximum conversion error as it varies with force cycle amplitude (e). Data from the best three sections of the Design C shear transducer are shown. Lines bound the markers of the device with the smallest 'percentage of applied force or a minimum force which ever is the greater'.

In some transducers, extreme friction in the sliding mechanism dominated the internal hysteresis of the rubber. In these cases the loop width tended to be constant with cycle amplitude, defining the accuracy as a fixed magnitude only.

Now, the coefficients of the fifth order polynomial, as used above, can be implemented as a 'conversion equation'. To find the polynomial coefficients a fifth order polynomial was fitted by matrix methods, under a least-squares criterion, through the calibration loop of each transducer. This was achieved through the use of the mathematics software package **Matlab** (Mathworks Inc). These coefficients would generally be unique to each device. Once determined they would be recorded in the documentation accompanying every device. The conversion error was then the difference between the polynomial fit and the calibration curve. Figure 4.39 plots the maximum conversion error of this method as a function of force cycle amplitude - for comparison with Figure 4.38e. Using a fifth order polynomial conversion equation , any converted clinical data may then be described as accurate to a given percentage (*6%*) of its converted value or a fixed force (*0.45N*), whichever is the greatest.

Normal-stress Section

The calibration of the normal stress section followed the same regime as for the shear stress section. Each of the ten sections was subjected to five loading cycles, of *10, 20, 50, 100* and *200N* loads at a cycle frequency of *1Hz*. Two example force versus output (calibration) curves are shown in Figure 4.40. From records of the section displacement with applied force the measured stiffness of the normal section was typically *280±80N/mm*. During testing four transducers was exposed to more than *100000* loading cycles, without degradation of their calibrated performance.

In the figure, one curve [Figure 4.40a] exhibits two distinct slopes and the other [Figure 4.40b] exhibits three. In the former case the initial slope corresponds to unhindered flexion of the diaphragm. While the shallow slope corresponds to the outer rim of the indentor plate impinging on the diaphragm support wall, inhibiting further flexure. In the latter case slopes at the beginning and end of the curve have the same causes as above. The middle portion of the curve show the diaphragm has greater stiffness or is hindered in its flexure. The cause of the hindrance was traced to the device leads which follow the inside rim of the diaphragm support

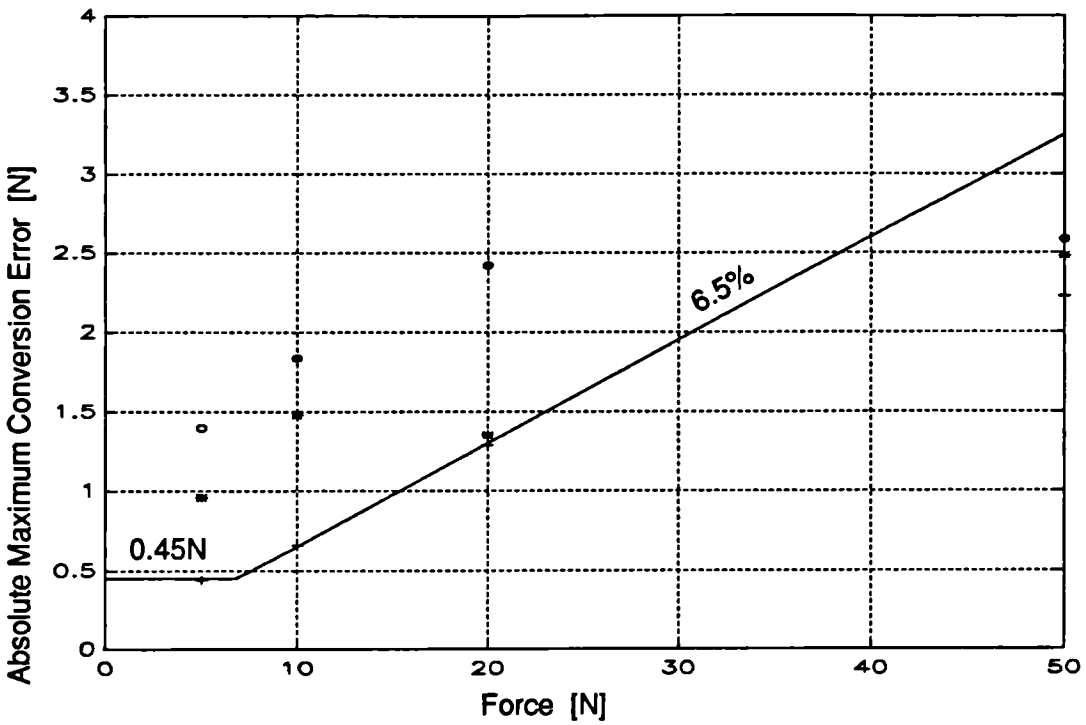

Figure 4.39 Examples of the errors arising from approximating the force versus output calibration curve by a fifth order polynomial. Absolute maximum error as it varies with force cycle amplitude. Data from the best three sections of the Design C shear transducer are shown. Lines bound the markers of the device with the smallest 'percentage of applied force or a minimum force which ever is the greater'.

wall. These were thick enough to be forced into contact with top of the shear section when the diaphragm is flexed. This in turn provides a reactionary support force on the diaphragm, decreasing its diameter and increasing its stiffness. This problem may be circumvented by using smaller diameter section leads.

The working range of the normal stress section may be defined as the magnitude of applied force at which the indentor plate impinges on the diaphragm support wall. At that point (the knee) the calibration curve changes slope. Initially the slope is relatively constant and a single data conversion constant can be defined. Now, the working range may be extended by defining a second (and third) conversion constant which is only applicable to the slope of the curve above the knee. However, the sensitivity of the device is diminished beyond the knee, and data conversion becomes more complex. The ranges of the normal stress sections under test varied considerably, with half of them having a range of less than *70N*. The sources of this variation were due to differences in diaphragm thickness and indentor boss height between the sections in the batch.

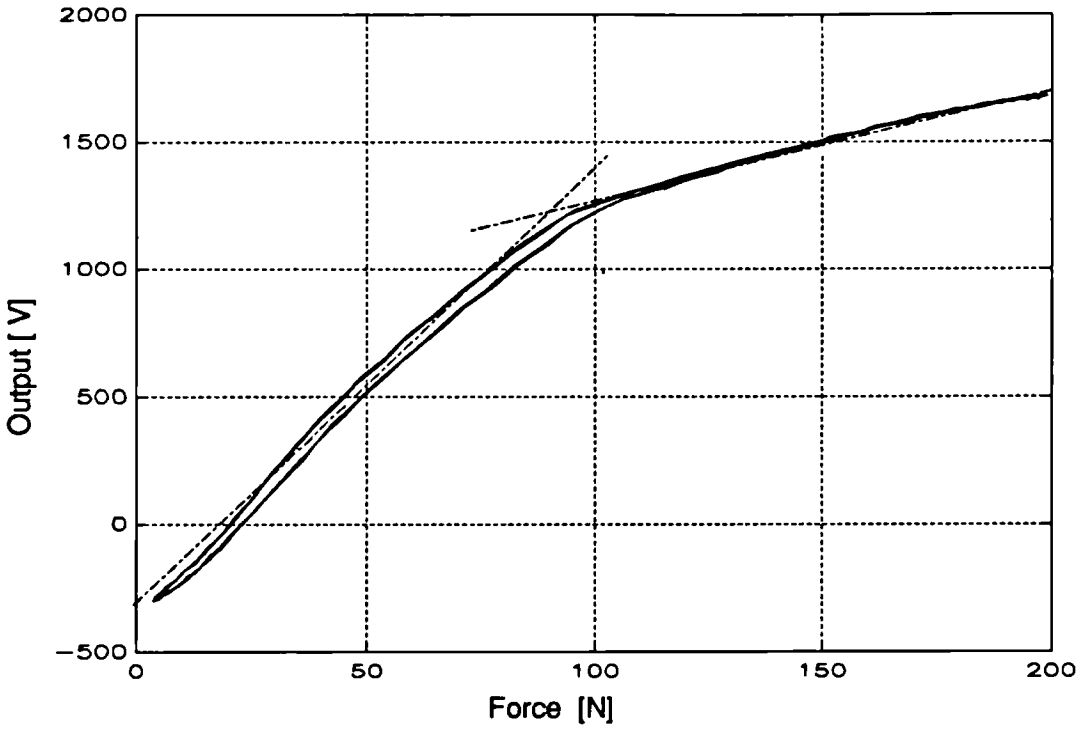

(a)

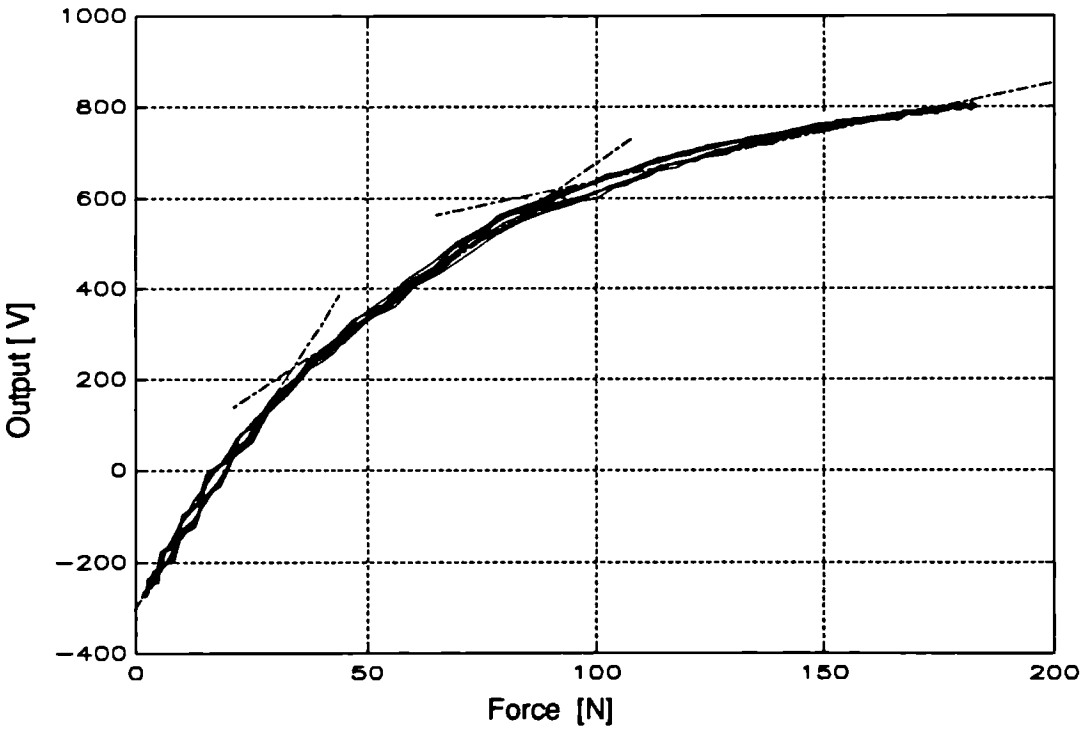

(b)

Figure 4.40 Example calibration curves for Normal transducer sections of Design C. Each was subjected to five cycles to 200N at 0.1Hz. The excitation voltage was 1Vdc.

There was hysteresis over the load cycle, but it was seen to be significantly less than that of the shear stress section. This was expected as hysteresis in silver steel is much smaller than that for rubber.

A conversion constant for transforming the recorded clinical data to its causative applied force, was defined. A first order polynomial was fitted by matrix methods, under a least-squares criterion, through the calibration loop of each transducer. This was achieved through the use of the mathematics software package **Matlab** (Mathworks Inc). The coefficient of this polynomial was used as the conversion constant.

Linearity error and linear range may be calculated by fitting a high order polynomial to the centre of the calibration loop and finding the difference between it and the first order polynomial fit. Figure 4.41 plots the linearity error over a full scale load cycle (*100N*) for the best three sections tested. A linear range for a device may be derived directly from the linearity error plots. For example, the *5%* linearity range of *67N* is marked on Figure 4.41a.

It was observed that the width of the calibration loop decreased as the peak amplitude of the load cycle decreased - confirming that hysteresis is amplitude dependent. As conversion error is directly related to hysteresis, the accuracy of a conversion regime is dependent on the local amplitude of the applied force. To define an accuracy value for the first order polynomial conversion method, the maximum conversion error from *±10, ±20, ±50, ±100N* load cycles was plotted against the cycle amplitude. Figure 4.41b is a plot of these maximum conversion errors for the best three sections tested. On this figure an arbitrary piecewise limit (line) is drawn. This bounds the maximum conversion errors by a percentage of the cycle amplitude and a fixed small force value. With these limits identified, any converted clinical data may then be described as accurate to a given percentage (*5%*) of its converted value or a fixed force (*1.9N*), whichever is the greatest.

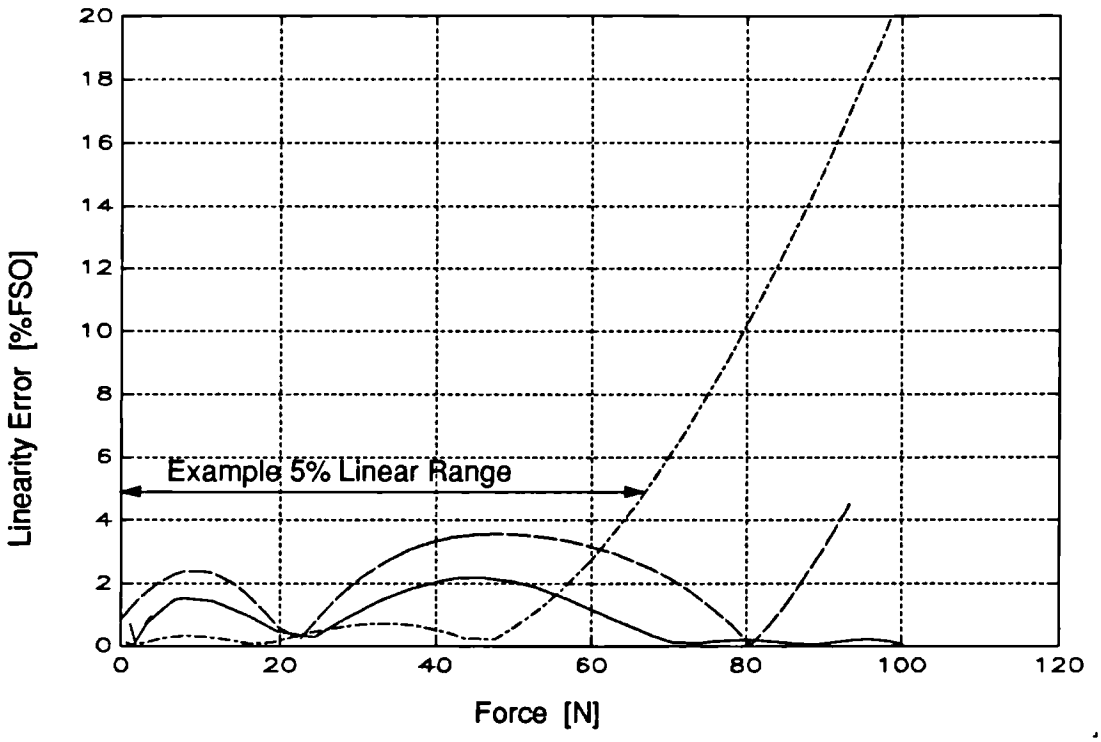

(a)

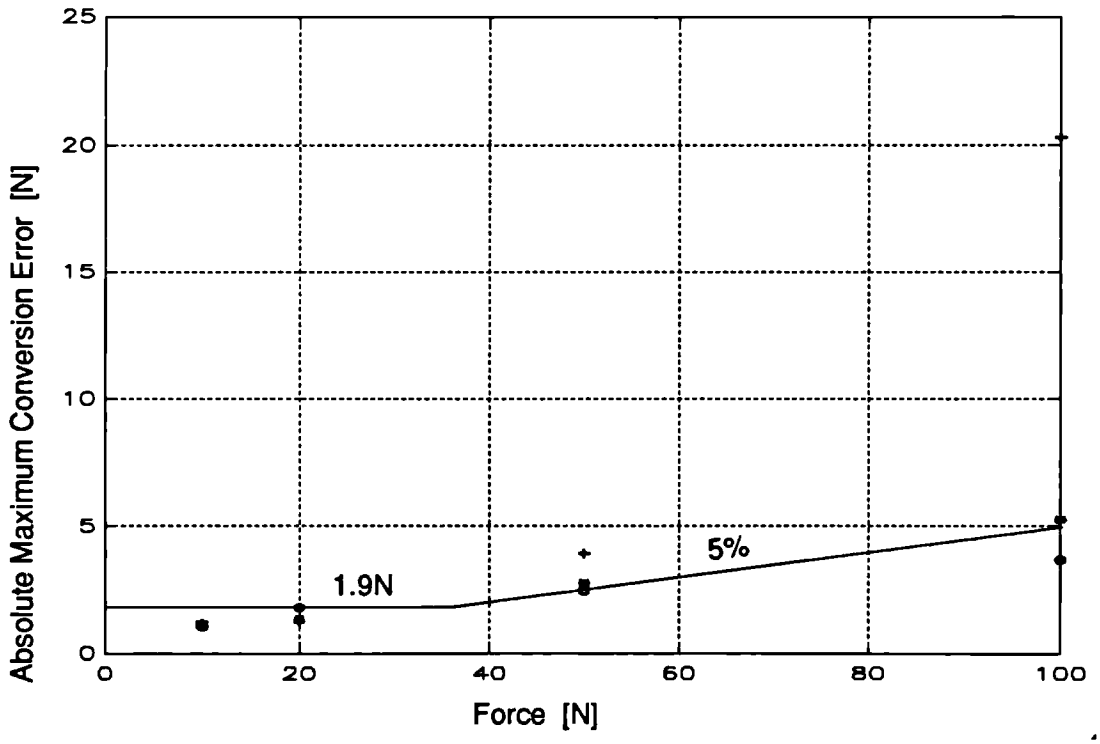

(b)

Figure 4.41 Absolute linearity errors over a full scale load cycle (100N) (a). Absolute maximum error as it varies with force cycle amplitude, arising from a first order approximation to the Force versus output curve (b). Data is from the best three normal stress sections of the Design C. Lines bound the markers of the device with the smallest 'percentage of applied force or a minimum force which ever is the greater'.

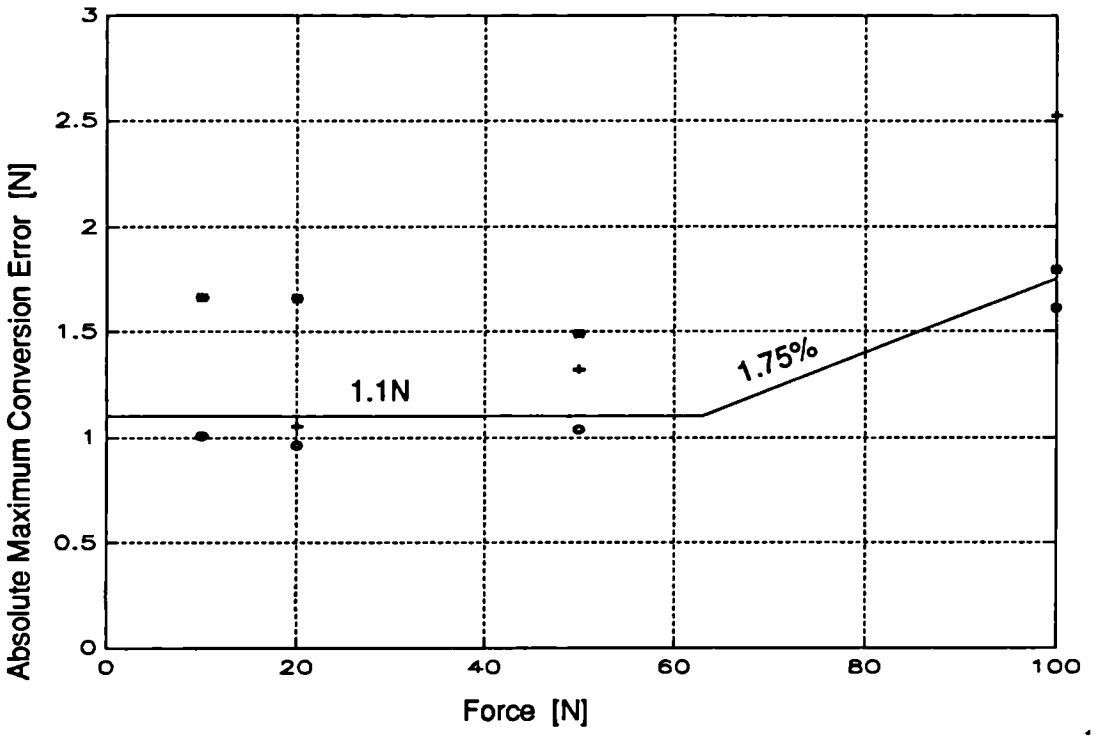

Figure 4.42 Absolute maximum error as it varies with force cycle amplitude. Errors are those arising from the use of a fifth order polynomial approximation to the force-output curve. Data is from the best three normal stress sections of Design C. Lines bound the markers of the device with the smallest 'percentage of applied force or a minimum force which ever is the greater'.

Now, the coefficients of the fifth order polynomial can be implemented as a 'conversion equation'. When a higher order polynomial approximation to the force versus output calibration curve is used, linearity errors are replaced by a smaller trend error. This generally reduces the conversion errors to that of the hysteresis induced uncertainty. Figure 4.42 plots the absolute conversion error for a fifth order approximation to the calibration curve. On this figure, as above, an arbitrary piecewise limit (line) is drawn. This bounds the maximum conversion errors by a percentage of the cycle amplitude (*1.75%*) and a fixed small force value (*1.1N*). The relatively high minimum force seen on the limit line is due to relatively coarse increments (approximately *1N* steps) in applied force, during load cycling, creating a jerky calibration curve. The applied force cycle was not smooth because very small changes in displacement were required and there was a coarseness in the movement of the bearings in the vibrator [Figure 4.32a].

4.3.2.4 Shear Stress Vectors and Crosstalk Errors

The assessment of linearity and hysteresis described in 4.3.2.3 was performed with each shear axis aligned to the direction of the applied force. As the two shear axes are arranged orthogonally the magnitude *and* direction of applied force can be resolved. The accuracy of this ability to distinguish the direction of applied loads relies on each axis being insensitive to the components of the load which are orthogonal to it. An induced change in the output of a given axis due to loads applied along either of the other axes is called *crosstalk*. An assessment of this action is described at the end of this section - [4.3.2.4].

To assess the accuracy of the direction resolution each device was subjected to $\pm 20N$ loading cycles, at $1Hz$, at 15° orientations from 0° through to 360°. The maximum and minimum output of each axis pair was recorded for the cycles at each orientation. The change in output with angle should ideally form a sine-cosine pair. Examples of the variation in output with orientation for the best three sections can be seen in Figure 4.43a. By calculating the inverse tangent of these pairs it was possible to determine the apparent or indicated angle of the applied force vector. When this was compared to the true angle the angular error was found. Figure 4.43b shows the angular errors for the above three sections as a function of the true vector angle. From this plot it can be seen that in the best case it was possible to resolve force vector angles to better than 6° with Design C.

There are two main causes of the error in the design. Firstly, as the vector angle approaches the orthogonal of an axis there will be an increasing frictional force occurring at the ridge and channel construct. This will hinder displacement and reduce the output magnitude for that axis. The resultant error in the apparent angle will be an over or under estimate of the true angle dependant on relative friction of the two axes. Secondly, as each MR element may not be truly uniaxial, any lateral play in the ridge and channel will disturb the output magnitude unpredictably.

Mechanical crosstalk between the transducer axes is where a given axis output changes when a force is applied in a direction orthogonal to it (ie. along one of the other two axes). This change in output falsely indicates that there is a component of the applied force acting along the direction of the given axis. This source of error in the transducer was assessed by observing the output variations of all three axes while a full scale loading cycle was applied parallel to each axis in turn.

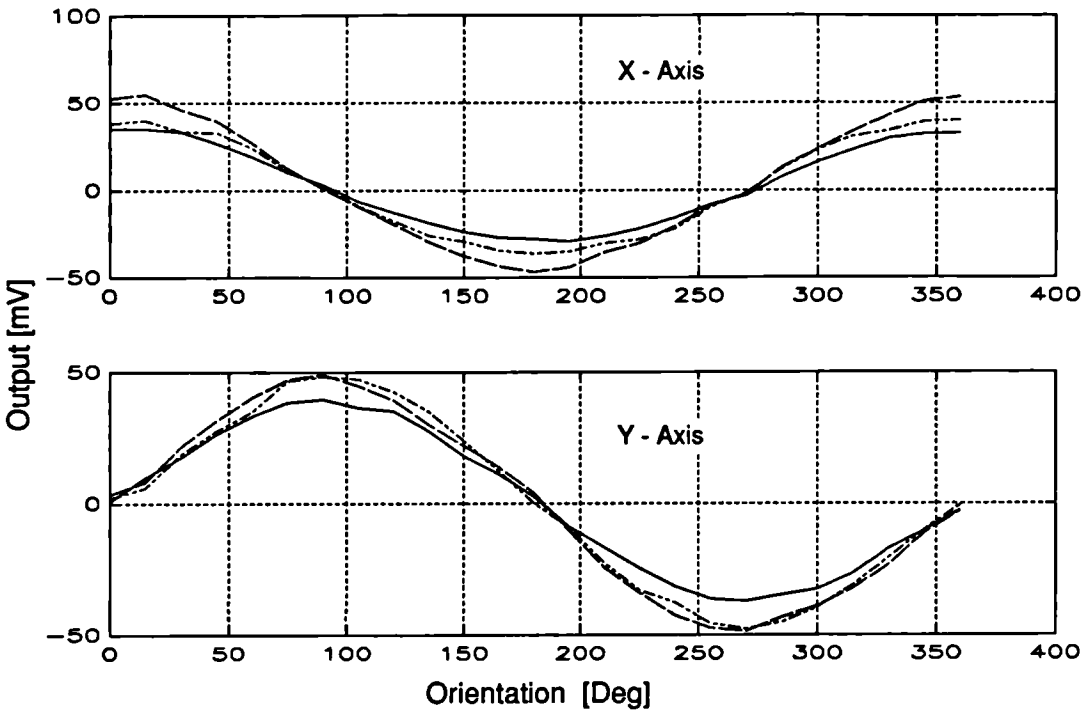

(a)

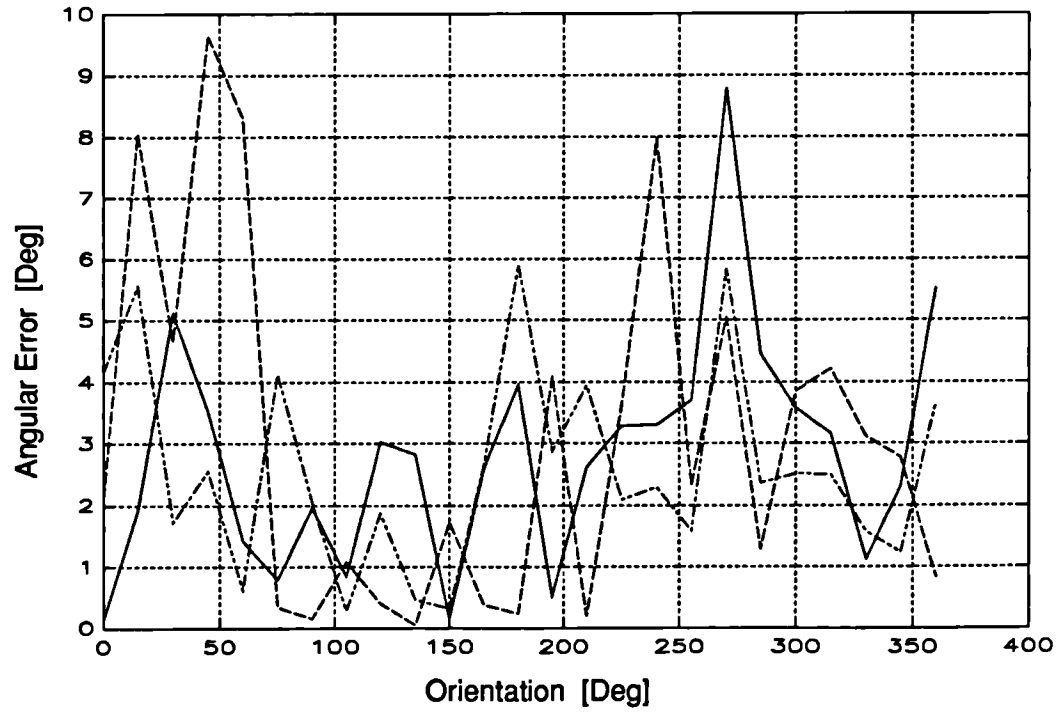

(b)

Figure 4.43 Output variation with orientation of the applied force vector (±20Npp loading cycle at 1Hz) (a). Error between measured orientation and applied force orientation (b). Data is from the best three shear stress sections of Design C.

The maximum variation in the output of each axis under orthogonal loading was taken as the maximum crosstalk error. The average crosstalk error on the shear axes due to full scale loading on the normal axis is *1.1% FSL (SD = 1.4)*. The mechanism of interference in the shear stress sections is the slight compression of the rubber layer, under normal loads, altering the magnet-magnetoresistor separation. This interference can be reduced by increasing the *area : thickness* ratio of the rubber layer or increase the magnet-magnetoresistor separation to a less sensitive region. Both of these schemes would decrease the stress sensitivity of the transducer. The interference in the normal stress section is due to the combination of force moments, from shear stresses, normal stresses and excess space in guide pin holes of the normal section. These create a small variation in normal force as the transducer rocks on the boss of the indentor plate. This interference can be reduced by lengthening the guide pins and improving their fit in their holes, which will provide greater opposing force moments and increased mechanical rigidity.

4.3.2.5 Creep and Frequency Response

The frequency response of both the shear and normal sections of the transducer will be bounded at both low frequencies due to creep phenomena and high frequencies due to inertial reactions. Creep in the normal stress section was indetectable, so there is no practical low frequency limit for normal stresses. Creep was observed in the shear stress section but was found to be completely reversible - so calibration data remains valid. The frequency response of the shear section will be predominated by the elastic response of the rubber - [3.1.2.3]. Thus at very low frequencies (< *0.01Hz*) the output is likely to exhibit a non-linear response to stress due to creep processes in the rubber. At intermediate frequencies (*0.1-1000Hz*) the output is approximately linear with stress. While, at very high frequencies (> *10000Hz*) the rubber becomes glassy and the output is negligible.

Four shear stress sections of the ten assembled transducers were subjected to *20N* step shear forces and their outputs sampled at *100Hz*. The data was plotted against the logarithm of time and a first order polynomial was fitted to the curve. The coefficient of the polynomial defines the creep rate in units of *%/log(sec)*. The value provides an indication of the error involved in using the conversion constant at very low frequencies. Table 4.13 contains the creep constants of the four sections tested.

Device	*Creep %/log(sec)*
1	*3.87*
2	*2.45*
3	*2.26*
4	*2.32*

Table 4.13. Measured creep rate of four shear sections of Design C. A 20N shear force was applied and left for 150 seconds.

Assuming that the stride time of amputees may generally vary from *1-5* seconds, the dynamic stresses, at the limb/socket interface, related to walking will generally be of this period or shorter. A clinical study may last for approximately *20* minutes, roughly two decades of time longer than a stride. Thus, from Table 4.13, longterm limb/socket stresses due to fitting, retention or stance forces will contribute less than *10%* errors by the end of a study. For accuracy it is therefore advisable to keep studies short. If an error in shear stress measurement of *10% FSL* is defined as the acceptable limit, the low frequency limit of the shear stress section is *0.1mHz*.

From [4.3.2.2] the resonance of the dynamic calibration facility, when a spring of similar stiffness to the transducer is being loaded, was identified as approximately *100 Hz*. Therefore the frequency response of the transducer could only be determined quantitatively, with this equipment, if its resonant frequency was below this. To explore this, four triaxial devices were each mounted in the calibration jig [Figure 4.32] and subjected to sinusoidally varying forces. Load cycles to *±20Npp* at frequencies ranging from *0.01Hz* to *200Hz* were applied to the shear stress sections and load cycles to *20Npk* at frequencies ranging from *0.01Hz* to *500Hz* were applied to the normal stress sections. After ten cycles at each frequency, when a steady state had been achieved, five cycles of section output, displacement and applied force were recorded. Plots of the resultant peak dynamic displacements to the static displacements with frequency (magnification plot) is given in Figure 4.44. The phase differences between the applied force and resultant displacement is also given. The curves exhibit the form of lightly damped systems. The magnification ratio is moderate for the shear stress section (y/Y_o=*5.3*), and the resonant frequency (*100-120Hz*), while the magnification ratio is low for the normal stress section (y/Y_o=*1.8*), and the resonant frequency (*100-200Hz*). Although, the test frequencies

for the normal stress section were coarsely separated around its resonance, so the magnification ratio may in reality be higher. In both cases the resonant frequency is close to that of the natural frequency of the calibration jig with spring of comparable stiffness in situ (*100Hz* shear : *190Hz* normal).

It was evident from the curves that the resonance of both the shear and normal stress sections was above that which the test facility could accurately measure. The curves suggest that the dynamics of both sections may reasonably be modelled by the Voigt model shown in Figure 4.33. Also the sections have slightly more viscous damping than is present in the jig bearings, but are nonetheless underdamped structures. Therefore their true frequency response has a similar form to that seen in Figure 4.44.

Now their resonant frequency can be determined by observing their impulse response. If an impulse force is applied to each section then from (4.6) the device will be excited into a decaying oscillation. The second term on the right hand side of (4.6) becomes negligible and the first, or transient term, dominates. The envelope of the decay is related to the damping in the section as described by $e^{(-\lambda t)}$. The frequency of the oscillation is the resonant frequency described by $\sin\sqrt{(\omega^2-\lambda^2)}+\phi$. From Figure 4.44 both sections are underdamped therefore their resonant frequency will be close to their natural frequency, which is:

$$\omega = \sqrt{\frac{k}{m}} = \sqrt{\frac{80(\pm 5)\,[Nmm^{-1}]}{0.7(\pm 0.1)\,[g]}} \approx 1700(\pm 170)Hz \quad (Shear) \quad (4.14)$$

$$= \sqrt{\frac{280(\pm 80)\,[Nmm^{-1}]}{4.2(\pm 0.4)\,[g]}} \approx 1300(\pm 250)Hz \quad (Normal)$$

To apply the impulse force a typical device was clamped to a large table top in such a way as to allow the section under test to vibrate freely. The shear stress section was struck a momentary (glancing) impact parallel to its axis by a metal bar. The normal stress section was excited by a metal ball bearing being dropped onto the transducer forcing it onto the indentor beneath it. In both cases output was recorded by a Digitising Storage Oscilloscope (DSO). The resultant transient outputs are presented in Figure 4.45.

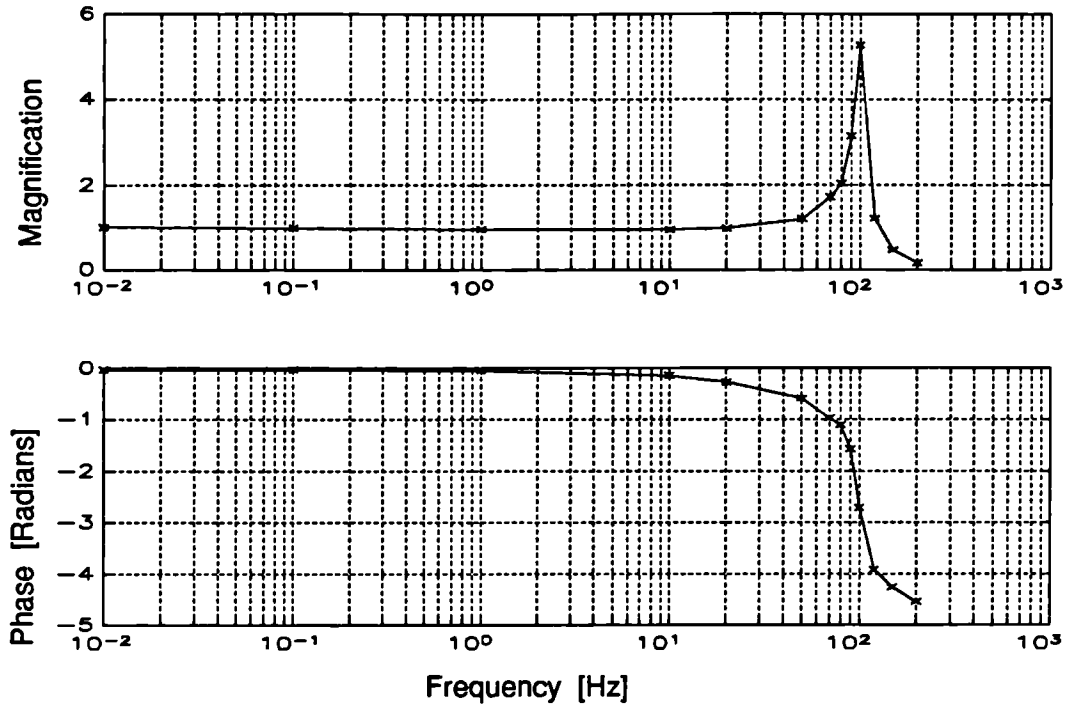

(a)

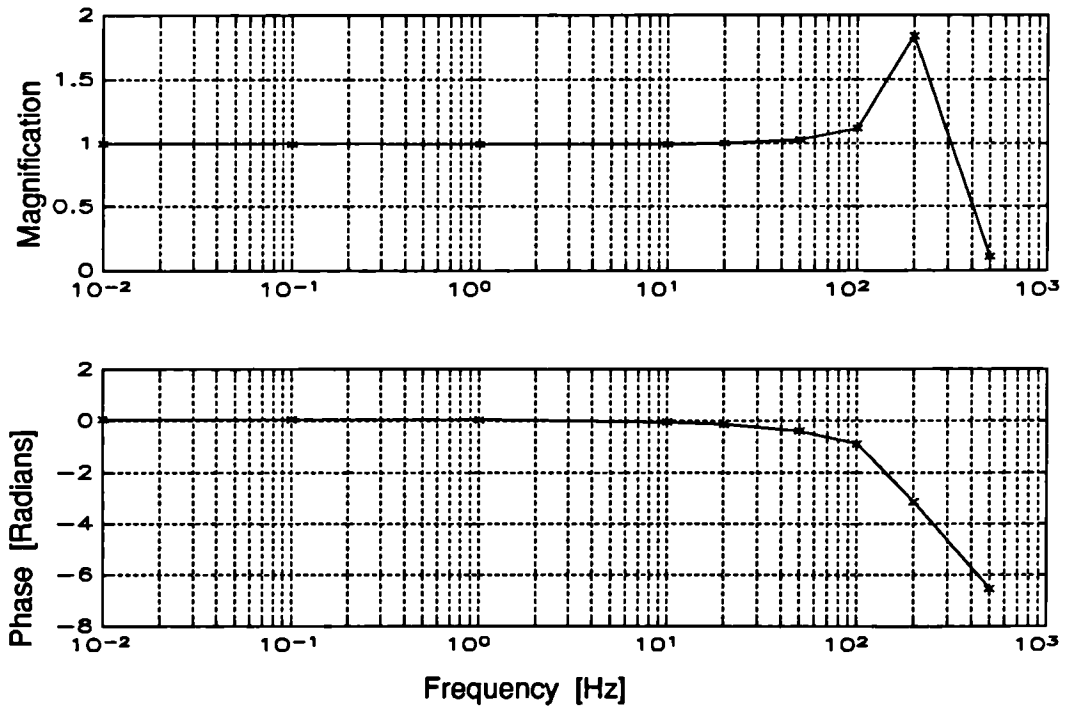

(b)

Figure 4.44 Example magnification and phase lag plots for the shear stress section (a), and normal stress section (b) of Design C, under steady state forced sinusoidal oscillation to 20N.

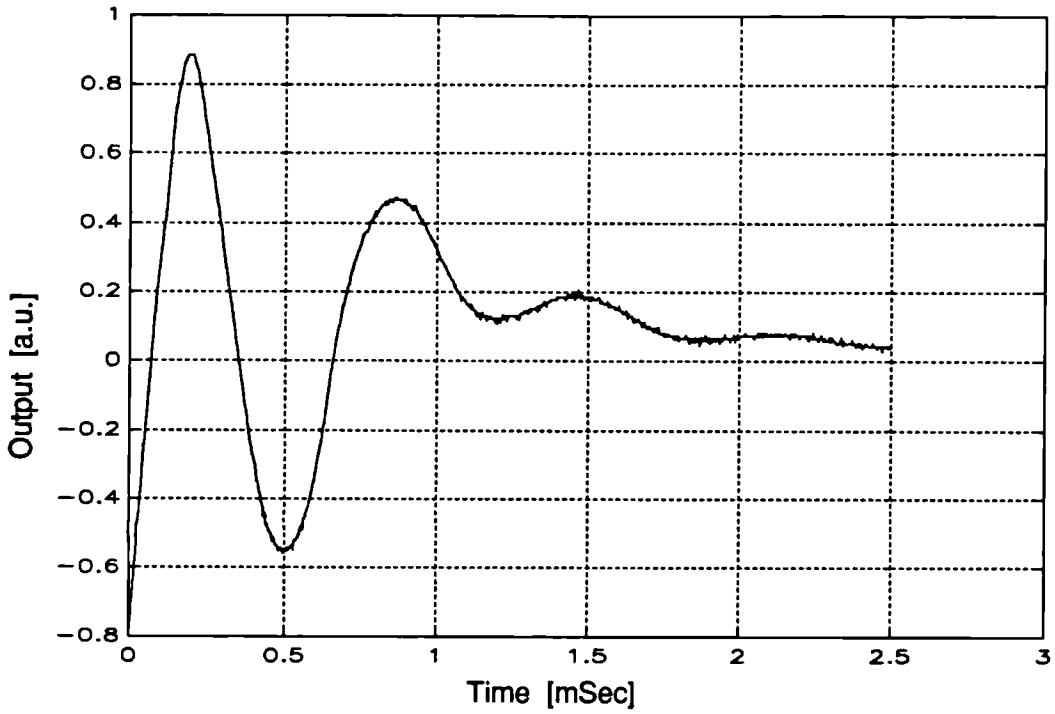

(a)

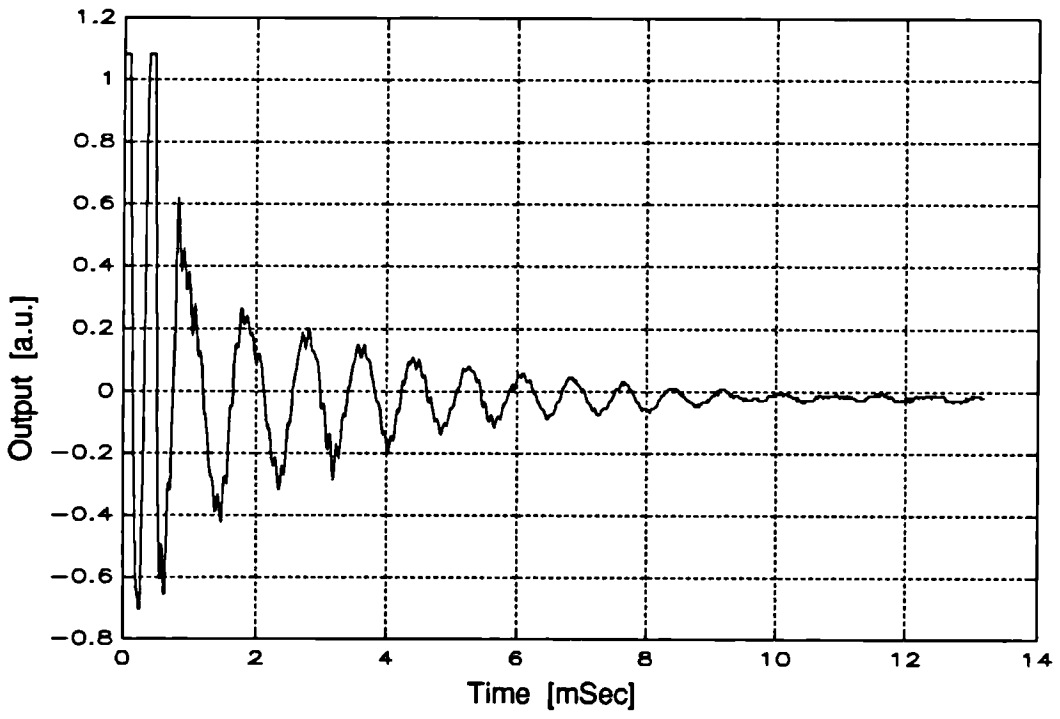

Figure 4.45 Impulse response of shear (a) and normal stress sections (b). Each section was excited by an impulse stress and allowed to 'ring'.

It is seen from the curves that the resonant frequency of the shear stress and normal stress sections are approximately *1500Hz* and *1200Hz*, respectively. Both these measured values are close to the predicted frequencies. Clearly the frequency response of both shear and normal stress sections of the device could reasonably be affirmed as constant up to and significantly beyond the measurand bandwidth of *0-50Hz*, as required.

4.3.3 Temperature Sensitivity

Having determined the designs' response to force magnitude, orientation to applied force and frequency, it was necessary to establish the extent to which the response was compromised by its temperature sensitivity. That is, where temperature induced changes in the output signal of the device may be falsely interpreted as stress signals.

4.3.3.1 Test Equipment and Methods

To assess the temperature sensitivity, three transducers chosen at random from the set of ten, were mounted, in turn, in the calibration jig and placed in the laboratory oven. The normal stress section tests were carried out with the device placed under the sliding block of the calibration jig - [4.3.2.1]. An external platform was attached to the sliding block of the jig via a connecting rod which projected out of a vent hole in the oven roof [Figure 4.17]. The temperature was raised from *27* to *50°C*. At approximately five degree intervals various loads were placed on the platform in succession and recordings of the temperature and section output were recorded. Signals from the section were buffered by the MEP086B unit [Chapter 6] and temperature measurements were made using the meter MEP123 platinum resistance thermometer. Signals were input to an A/D convertor (*DT2824-PGH - Data Translation Inc*) hosted in a personal computer (*IBM PC/AT*). Control of the A/D was via applications software Global lab (*Data Translation Inc*).

4.3.3.2 Sensitivity Data

From the recorded temperature and section output data, the change in output with temperature for the loaded sections was plotted. Figure 4.46 presents example plots of data from a shear stress and a normal stress section.

It was clear from Figure 4.46 that there were two temperature induced phenomena occurring. Firstly, there was a noticeable temperature coefficient of output (offset drift = slope) and secondly, there was an accompanying change in load sensitivity (gain drift = non parallel load lines). Therefore, the assessment of the potential temperature induced errors is quite complex so two assumptions are made to simplify the error estimates. Firstly, the change in offset and the change in gain are treated as independent parameters, and secondly as being linear. With reference to Figure 3.15 the above assumptions were seen to be valid for the MR, over the temperature range *20-40 ℃*.

Now, the output v force calibration curve for a normal stress axis is derived at room temperature and can be described by the equation :

$$y_c|_{T_{Room}} = m(x-A) \qquad [N] \tag{4.15}$$

Where y $[V]$ is the output, x $[N]$ is the applied force, m $[N/V]$ is the gain constant and A $[V]$ is the offset in output at zero-load. At any other temperature $T_{Room}+\Delta T$ the new output v force calibration curve can then be written as :

$$y|_{T_{Room}+\Delta T} = n(x-B) \qquad [N] \tag{4.16}$$

Where $n \neq m$ and $B \neq A$ due to the gain and offset drift.

Clearly, when converting recorded output data into apparent applied force, the difference between the performance curve and the calibration curve will lead to an over or underestimate of the force. The error can be derived as :

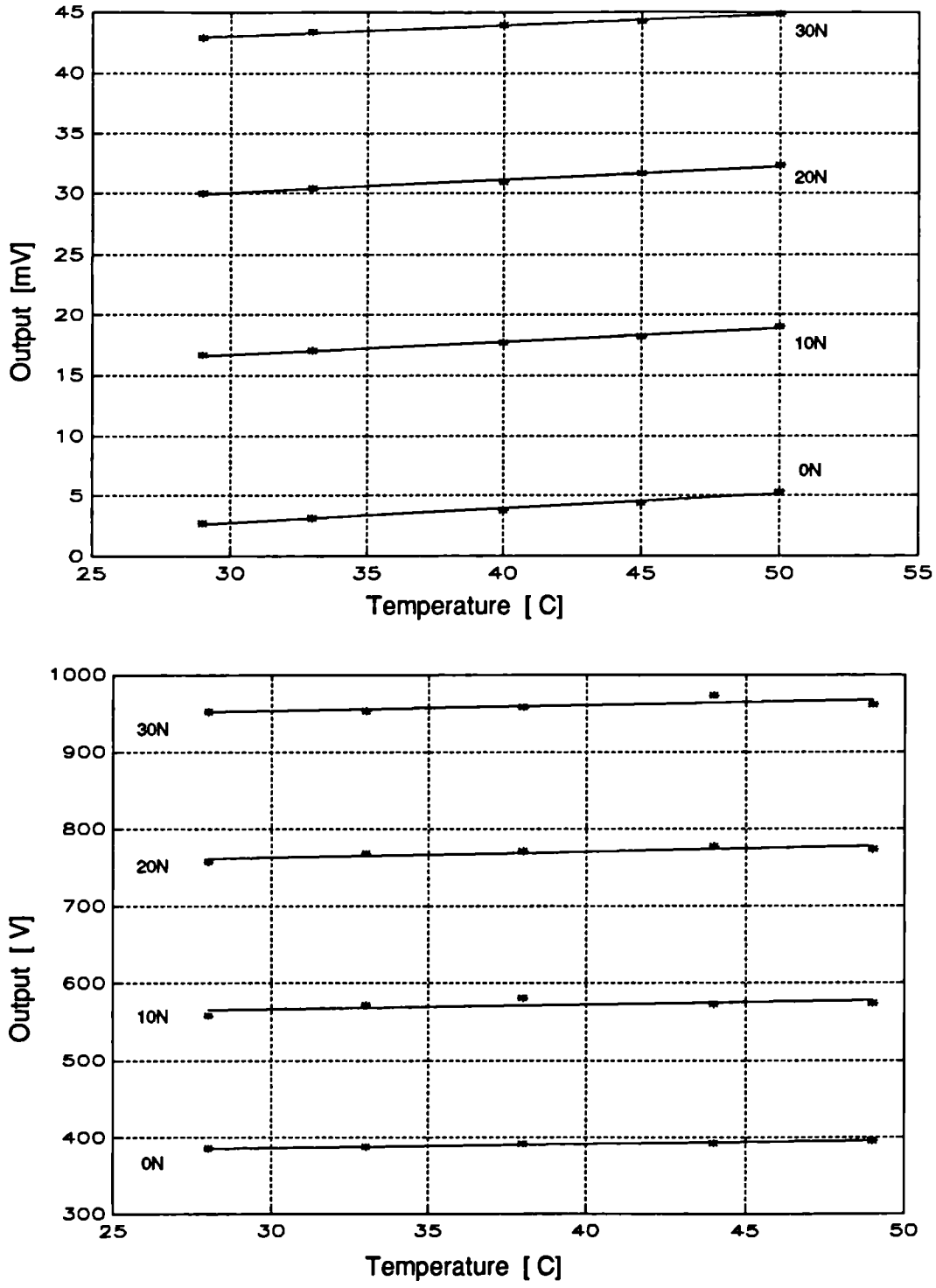

Figure 4.46 Example of the output variation with temperature of a shear stress (a) and normal stress (b) section of Design C, when loaded (0, 10, 20, 30N) and subjected to temperatures of 27-50 °C.

$$Error = \varepsilon = y - y_c = n(x-B) - m(x-A) \qquad (4.17)$$

Now, if the offset drift is s $[V/^{\circ}C]$ and the gain drift is g $[N/V/^{\circ}C]$

then $$B = A + s\Delta T$$

and $$n = m + g\Delta T \qquad (4.18)$$

So (4.17) can be written as :

$$\begin{aligned} \varepsilon &= (m + g\Delta T)(x - (A + s\Delta T)) - m(x - A) \\ &= (g(x - A) - ms)\Delta T - gs\Delta T^2 \end{aligned} \qquad (4.19)$$

Using (4.19), values were derived for the gain and offset at $20^{\circ}C$ and the maximum error over the range $20\text{-}40^{\circ}C$, for each of the sections tested. These are given in Table 4.14.

Section	Gain [N/mV]	Offset [mV]	Offset Drift [mV/°C]	Gain Drift [N/µV/°C]	Error [N]	Error [%FSS]
1	.5821	63.07	.1349	.53	1.58	3.16
2	.74	1.56	.1194	.51	1.78	3.56
3	.4131	34.72	-.0014	1.78	4.33	8.66
4	.6355	-21.02	.1417	1.89	1.91	3.82
5	.568	32.3	.0224	1.47	2.32	4.64
6	1.0037	-6.02	.2856	2.79	5.99	11.98

Table 4.14 Values of the Gain, Zero-stress Offset, Offset temperature drift, Gain temperature drift, and maximum data conversion error, for six sections of Design C.

Clearly the majority of devices of Design C may have temperature induced errors of less than 5% over their working temperature range. Thus implying that during any one clinical measurement session errors due to temperature related drifts in device performance may be considered minimal, if not negligible. The apparent outliers in the data set of Table 4.14 may possibly disappear if a more exact and consistent assembly procedure could be established. This is because: offset is

dependent on spatial alignment; gain is dependent on friction, stiffness, and magnet-MR separation; and both offset drift and gain drift are dependent on magnet-MR separation.

4.4 Summary

This chapter has described the progress of development of the three axis stress transducer from prototype to a requisite form. In this part a summary is given of the best performance demonstrated by a batch of ten transducers of the final design form. This will give an indication of the achievable performance of the design. Comparisons are made with the initial specification given in Chapter 2.

The assembled device measured *15.96mm* diameter by *4.9mm* thick with the indentor plate adding a further *1.1mm* total thickness. Each shear axis had a stiffness of *80±5N/mm* and the normal axis a stiffness of *280±80N/mm.*

The force versus output calibration curve for all axes exhibited hysteresis. That of the normal axis was small, less than *2%* indicated load, while for the shear axes was less than *6.5%* indicated load. It was demonstrated that the hysteresis was amplitude dependent.

Some nonlinearities occurred on all axes. A saturation effect was seen on the shear axis, due the displacement of the magnet approaching the outer edges of the magneto-resistor. Thus when a single conversion constant is used to transform recorded voltage to force, a linear range for the section must be defined. For example, the *5%* linearity range is typically only *±30N.* However, it has been demonstrated that it is possible to construct the shear stress section so that it has a total linearity error, over the full scale range (*50N*), of less than *6%FSO.* The nonlinearity in the normal axis was due to the device leads, bonded to the underside of the diaphragm, interfering with its flexure. It was demonstrated that it is possible to construct the normal stress section so that it has a total linearity error, over the full scale range (*100N*), of less than *2.5%FSO.*

Friction was a source of error in the shear stress section. Although most of the devices built exhibited some friction effects, it was demonstrated that sections could be made which were free of significant friction.

The above errors (hysteresis, nonlinearity and friction) for both shear and normal stress sections can be combined into a parameter which defines the accuracy to which the conversion method models the calibration curve. When the calibration curve was approximated by a first order polynomial, a single constant was used to convert recorded voltage data into apparent force data. The accuracy of this conversion method was expressed as percentage of indicated force or some minimal force whichever was the greater. It has been demonstrated that it is possible to construct the shear stress section so that it has a first order conversion polynomial with total accuracy , over the full scale range (*50N*), of *9%* indicated force or *0.5N* whichever is the greater. For the normal stress section the demonstrated best accuracy was *5%* indicated force or *1.9N* whichever is the greater. When the calibration curve is approximated by a higher order polynomial, nonlinearity errors are replaced with a trend error. Also the useful range of the device is extended as the polynomial fits into the previously nonlinear regions of the calibration curve. When a fifth order polynomial was fitted to the shear and normal stress calibration curves, the demonstrated best accuracy of data conversion was then found to be *6%* indicated force or *0.45N* and *1.75%* indicated force or *1.1N*, respectively.

The force sensitivity of the axes was taken from the first order polynomial fit and was approximately *0.6N/mV* and *0.05N/μV* for shear and normal stress axes respectively. The excitation voltage in each case was *1V d.c.* Both section designs are able to withstand *100%* overload. During testing four transducers was exposed to more than *100000* loading cycles, without degradation of their calibrated performance.

The frequency response of each section was deduced implicitly. Both were constant well beyond the expected clinical stress signal bandwidth of *50Hz.* Resonant frequencies were approximately *1500Hz* and *1200Hz* for the shear and normal stress sections respectively. From the shape of the magnification plots of Figure 4.44 it can be seen that the section response is constant up to approximately half of the resonant frequency. Creep was only significant in the shear axes. The measured rate was *2.7(0.77SD) %/log(Sec).* Over a typical *20* minute clinical measurement period, the constant pre-load forces will cause an apparent force increase of less than *10%FSL.* All instances of creep were seen to be reversible. If an error in shear stress measurement of *10%FSL* is defined as acceptable performance, the low frequency limit of the shear stress section is *0.1mHz*, while that of the normal stress section is negligibly small.

Temperature induced apparent stress errors were observed in both axes mechanisms. These were manifest as offset drift and sensitivity drift. They were assessed over the temperature range *20-40 ℃*. The values of offset and sensitivity at *20 ℃* were used as a baseline for calibration data. Errors due to both drifts combined were demonstrated to be less than *0.19* $\%FSL_{20}/℃$ and *0.1* $\%FSL_{20}/℃$ for the shear and normal stress sections respectively.

Table 4.15 presents some of the above data for comparison with Table 2.2 - the proposed performance specification.

Parameter	*Shear stress section*	*Normal stress section*
Measurement Range	*0 - 250 KPa*	*0 - 500 KPa*
Overload	*2500 KPa*	*1000 KPa*
Accuracy (first order conversion polynomial)	*± 9% indicated load or 2.5 KPa*	*± 5% indicated load or 9.5 KPa*
(fifth order conversion polynomial)	*± 6% indicated load or 2.25 KPa*	*± 1.75% indicated load or 5.5 KPa*
Temperature Range	*20 - 40 ℃*	
Frequency Range	*0.1 mHz - 750 Hz*	*0 - 600 Hz*
Lifetime (gait cycles)	*> 100000*	
Dimensions	*15.96 mm diameter x 4.9 mm*	
Mass	*4.6 ± 0.4 g*	

Figure 4.15 Performance data of the final design of the triaxial stress transducer.

Generally, it was felt that the specifications set out for the transducer had been met to a significant degree. And furthermore, to the extent of the author's knowledge has filled a gap in the general triaxial stress transducer market not occupied by any other device.

Chapter 5
Data Acquisition : Hardware

The previous chapter described the development path of the triaxial stress transducer from prototype to final form. In this chapter the design of the circuits and systems used to acquire and store transducer signals are detailed.

Figure 5.1 is a block diagram of the hardware units of the acquisition system. The transducers connect to a Transducer Interface Unit (TIU). Their signals are buffered and filtered and then passed to the Data Collection Unit (DCU) where they are digitised. Buffered digital data is transferred to a Personal Computer (PC) for archival and processing. Simultaneously, external event signals are also digitised and archived, for synchronising multi-system data sets.

Section 5.1 describes the circuitry and protocols for exciting the transducers and conditioning their outputs. Section 5.2 reports on the nature and interconnection of the equipment used to digitise and store the signals. Section 5.3 describes the interface circuitry for synchronisation to a video based kinematics measurement system. Section 5.4 describes the physical interconnection of each part of the system. Lastly, 5.5 discusses the safety considerations of the system.

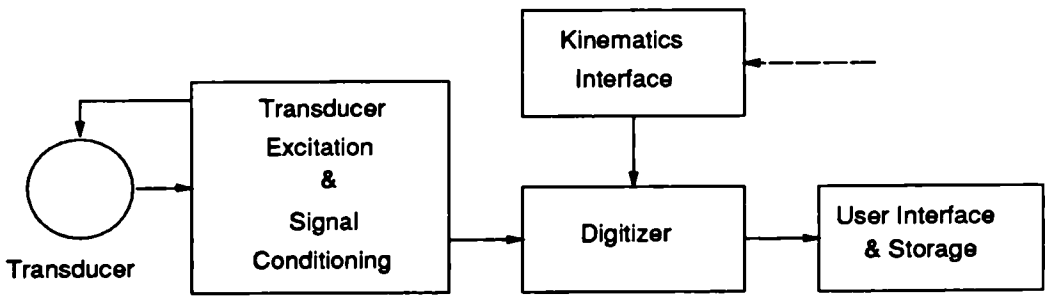

Figure 5.1 Block diagram of the hardware interconnection of the Data-Collection system

5.1 Transducer Interface Circuit

The following section describes the functional blocks and circuitry, in the TIU, used to interface to the transducers.

Each transducer was excited with a reference voltage which was then modulated by the applied stress to produce the electrical stress signals. Section 5.1.1 discusses the modes and implementation of circuits to do this. Section 5.1.2 describes the conditioning and buffering which is applied to the stress signals before they are input to the DCU. Also discussed is the expected noise in the clinical environment

5.1.1 Transducer Excitation

In order to devise the most effective method of exciting the transducer it is necessary to understand the electrical characteristics of the transduction elements. What follows is a discussion of the principle electrical properties of the magneto resistor (MR) (**FP111L100 - Siemens UK LTD**) and the foil strain gauge (SG) (**QFDPF-9-350 - Technimeasure LTD**).

5.1.1.1 Magneto-resistor Electrical Properties

The excitation circuitry will experience the MR as a two-port, three terminal device whose driving-point impedance is variable. Under the influence of a changing magnetic flux density, perpendicular to its face, the resistance component of the impedance will vary according to the approximate relationship.

$$R_\beta = R_o(1+K\mu^2\beta^2) \qquad (3.17)$$

Where R_β is the resistance when influenced by magnetic induction β, R_o is the resistance under zero induction, μ is the electron mobility of the material and K is a material dependant constant.

Heidenreich [1985] states that the MR's frequency response extends into the Gigahertz region, which implies that the reactive component of the impedance is small. Relative to the range of frequencies expected to be met in this application these reactive components are negligible. As discussed in Chapter 3 the MR appears as two magneto-resistors in series. The base resistance, R_o, (ie when not in the presence of a magnetic field) of each of these is $100\Omega \pm 20\%$. The difference in value of each resistor, compared with the other, is expressed in the centre symmetry parameter, M. Which is defined as the percentage difference of the single resistors (R_1, R_2) divided by the smaller of two resistances;

$$M = \frac{R_1 - R_2}{R_2} \cdot 100\% \qquad for R_1 > R_2 \qquad (5.1)$$

For this particular MR type the symmetry is typically *2%*. The relative resistance change, with the magnetic field used in this application, is approximately *1.5*. Thus in the assembled shear section with no shear-stress applied the driving-point impedance is approximately *300Ω ± 20%*. When the section is loaded the impedance may vary up to *50%*.

To improve noise rejection from the excitation supply, the MR of each axis was incorporated as one half of a Wheatstone bridge. The other arm of the bridge is formed from two fixed series resistors across the same supply. Figure 5.2 shows the arrangement. Output signal is taken between the centre point of each arm.

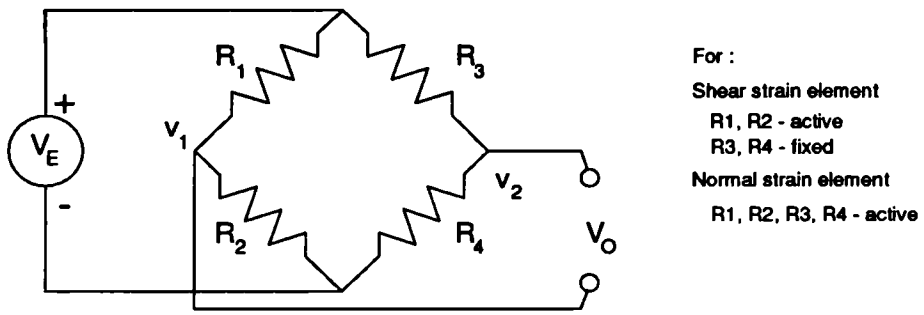

Figure 5.2 Schematic of a Wheatstone bridge circuit with two active arms.

Another advantage in this arrangement is that any imbalance in the MR can be zeroed out by padding resistors. Then, the direction of the stress induced displacements can be distinguished by the sign of the output voltage. With this arrangement the change in output voltage is related to the excitation voltage, the initial resistance and the change in resistance by;

$$\Delta V_o = \frac{\Delta R_o}{2 \cdot R_o} \cdot V_E \qquad (5.2)$$

Obviously the output magnitude may be increased by employing a large excitation voltage. However consideration must be given to the power dissipation in the device. From Chapter 4 it is seen that the MR element is adversely sensitive to temperature changes. Now, electrical power input to the element is converted to

heat, a proportion of which is conducted away by the surrounding material. If the thermal conductivity of this material is insufficient then the element will itself heat up, causing the output voltage to change erroneously. Therefore to determine the excitation voltage or current it is necessary to determine the thermal conductivity of the mounted MR. The quoted value for the MR lying on a metal surface is *15mW/K*. The actual value for the MR enclosed in the section will be lower. In this case it is surrounded by rubber and plastics which have lower thermal conductances than metal.

To experimentally determine it, the following simple test was undertaken. Firstly the assembled section was placed in an oven, heated to its maximum operating temperature, $T_{max} = 120°C$ and allowed to equilibrate for *30* minutes. The resistance of each MR was measured. Secondly the section was cooled to ambient temperature, $T_a = 23°C$, and allowed to equilibrate for *30* minutes. Each MR was then driven with a current that was increased until the resistance of the MR reached that of the first measurement. At that point the MR is operating at its maximum operating temperature, T_{max}, and the electrical power input is causing an increase in temperature of $T_{max} - T_a$. The thermal conductance is then given by:

$$G_{th} = \frac{P}{T_{max} - T_a} \quad [WK^{-1}] \tag{5.3}$$

In this case the electrical power input was measured as the product of the input current and voltage, *68mA* and *13.0V*. So rearranging (5.3) we have;

$$G_{th} = \frac{V \cdot I}{T_{max} - T_a} \tag{5.4}$$

$$= 9.1 \quad mWK^{-1}$$

Now from the relation for electrical power;

$$P = \frac{V^2}{R} \tag{5.5}$$

(5.4) can be rearranged to give:

$$V_{max} = \sqrt{(T_{max} - T_a) \cdot G_{th} \cdot R_{Tmax}} \tag{5.6}$$

Where V_{max} is the excitation voltage that will raise the MR to its maximum permissible temperature. This form can be used to determine the excitation voltage at which a given temperature rise will occur. By restricting T_{max} to be *1 ℃* above ambient and using the ambient value of resistance for $R_{Tmax} = 320\Omega$, The maximum excitation voltage allowed is $V_{max} = 1.7V$.

Before the excitation voltage could be finalised it was necessary to consider the excitation limits of the SG.

5.1.1.2 Strain-gauge Electrical Properties

It is common to excite full bridge strain-gauges by a constant voltage source. So, there was a possibility of using the same excitation circuit for both MR and SG. Before defining a circuit the electrical properties of the SG were investigated.

The excitation circuitry will experience the strain-gauge as a two port, four terminal device whose driving-point impedance is relatively constant. As the gauge is subjected to tensile stress the ratio of change in its impedance to its initial value is given according to the relationship :

$$\frac{\Delta R}{R} = (1+2\mu)\frac{\Delta L}{L} + \frac{\Delta \rho}{\rho} \qquad (4.21)$$

Where R is the initial resistance, L is the initial length, μ is Poissons ratio for the gauge material and ρ is its resistivity. The frequency response of the free gauge extends into the high Kilohertz. When the gauge is bonded, it is dependent on the stress-strain relationship of the substrate. For this application the reactive components of the gauge impedance are insignificant.

Under no-load conditions the driving-point resistance of the gauge used here is *350Ω ± 0.3%*. When the gauge is bonded and subjected to maximum tensile stress the resistance change is typically *2%* of this base value. The SG has a full bridge configuration with four active elements. So the change in output voltage is related to the excitation voltage, initial resistance and change in resistance as :

$$\Delta V_o = \frac{\Delta R_o}{R_o} \cdot V_E \qquad (5.7)$$

Again the magnitude of output signal is directly proportional to the excitation voltage. The limiting value of V_E is determined from the allowable power dissipation in the gauge. The QPFDPF-9-350 gauge is specifically designed for bonding to low-carbon steels. Manufacturing data supplied with each gauge summarises the power calculations and recommends a maximum excitation voltage of *1V*.

5.1.1.3 Excitation Circuit

From the previous discussion on allowable power dissipation it was decided that the same excitation circuit would be used for both the MR and SG. The voltage would be set at *1* Volt. Although small excitation voltages generally lead to poor signal to noise ratios, both the MR and SG are relatively low impedance devices. This tends to make them less sensitive to the relatively low power electromagnetic interference found in the typical clinical environment. However the stability of the excitation voltage is quite important. As will be discussed later the digitiser used has a *12* bit resolution and therefore is capable of resolving to *0.024%* of its input range. At the time of design the most cost effective high stability voltage reference available was the AD588 (**Analog Devices LTD**) with a regulation of *0.1%*. The following describes the various elements of the excitation circuitry.

The circuit diagram shown in Figure 5.3 describes the transducer excitation circuit. Components *C1-C4, R1, R2* provide a local power supply reservoir of *±12V*. *U1* is the precision voltage reference (AD588) with two internal buffer amplifiers *A3, A4*. The output of this reference is *±5.000V (±5mV)* so in order to create a *1V ±1mV* to apply to the transducers, *R3-R6* divide the output to *±0.5V (±50μV)*. These voltages are buffered by *A3* and *A4*. *Q1* and *Q2* act as output current buffers for *U1* as the load current with ten transducers connected (*150mA* maximum), exceeds the output current specification of the AD588. *R11* and *R12* provide *Q1* and *Q2* with output short-circuit protection. An analogue ground connection (*AGND*) to *U1* (*pin 9*) references the transducer excitation voltage to float at approximately ground potential. This affords the excitation voltage an extra degree of noise immunity from disturbances in the power supply.

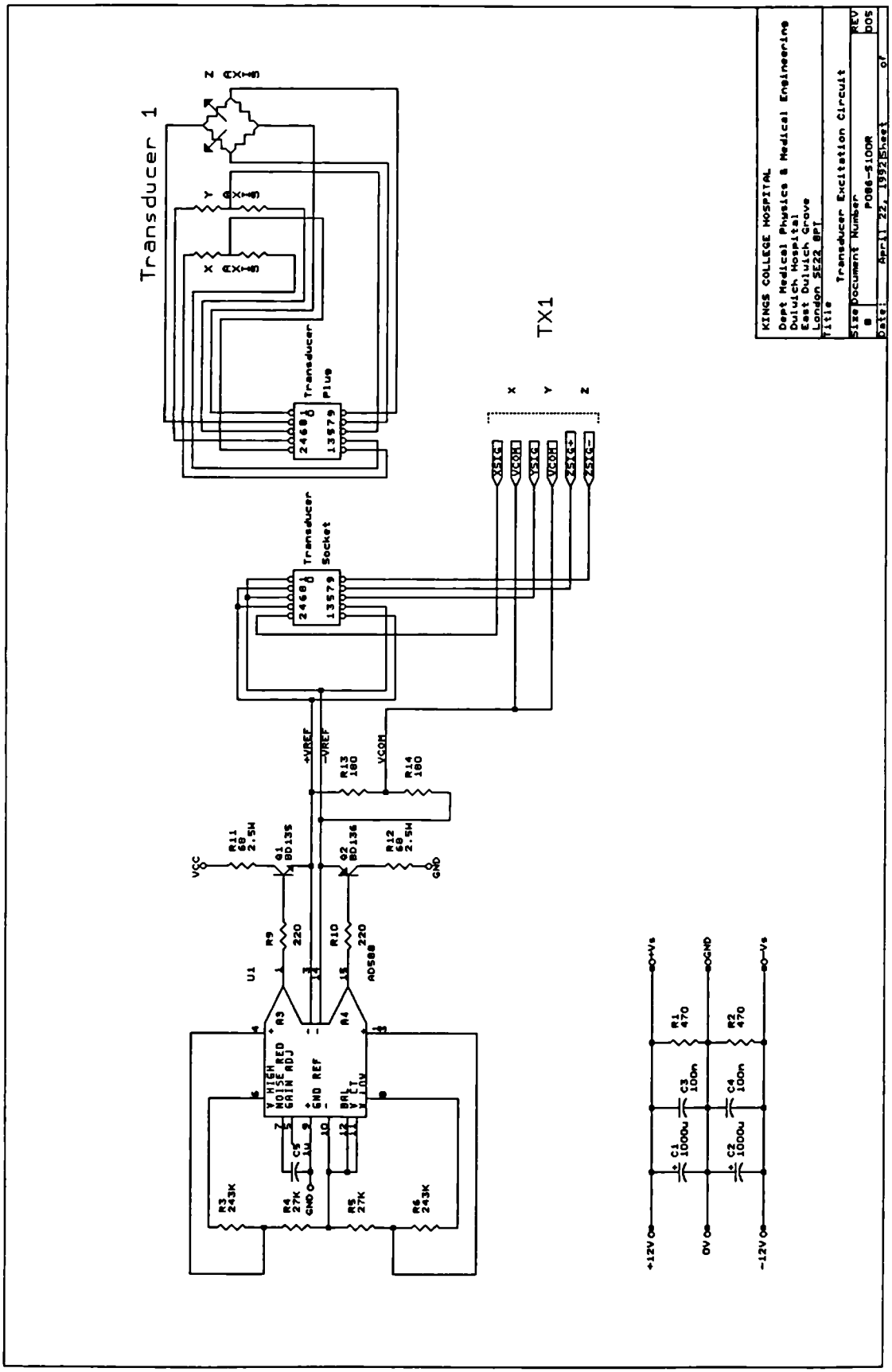

Figure 5.3 Diagram of the Transducer excitation circuit.

R13 and *R14* act as the second arm of the Wheatstone bridge for the MR's of the two shear sections. These resistors have approximately the same impedance as the MR so that the source impedance of both signal and reference are equal. This helps to minimise noise from bias currents of succeeding amplifier stages **[Seippel 1983]**. To further minimise interference from noise on power supply rails *U1* has decoupling capacitors *C6, C7* in close proximity. Also, every connection to the positive supply or *AGND* are star-point connections so that no component is directly connected to another's demand or return currents. **[Morrison 1977]**.

5.1.2 Signal Conditioning

The main function of this stage is to amplify and filter the signals from each axis of a transducer. The transducers themselves may be situated some one or two metres from the excitation circuit and signal buffers. Over this distance the lead wires become susceptible to electromagnetic interference. Thus, although the transducer elements of each axis have relatively low input impedance, any large noise signals, particularly from mains frequency sources may induce some voltages on the lead wires. Also the signals themselves are small and not much larger than the noise around them . With the use of appropriate amplifiers and filter circuits it was possible to separate the transducer signals from the environmental noise. The following subsections describe the reasoning and design steps for these circuits.

5.1.2.1 Amplification

It was the purpose of the amplifier circuits to magnify the transducer signals to be significantly above the background noise and to span the full range of the A/D input. By using differential signal amplifiers, careful track layout, impedance matching and earthing techniques most common-mode noise can be removed **[Brokaw 1988]**. Cable shielding and interleaved-ground-wire techniques would aid in reducing external interference signals. However, they can also add considerable size and weight to the transducer leads.

In the signal conditioning circuit, differential amplifiers are used. These have a sufficiently high input impedance and low bias currents, such that they don't significantly alter the current flowing in either the transducer elements, reference or excitation circuits. More importantly their high common mode rejection ratio

removes any significant noise commonly coupled onto the signal leads. Also the input circuits may be isolated from the output circuits allowing the use of floating excitation voltages, which has inherent noise minimisation advantages **[Morrison 1977]**.

The amplifier used in this application was required to have the following properties; differential input impedance of better than *500kΩ* (for minimal loading effects on the transducer signal); CMRR and PSRR greater than *72dB* (causes less than *1LSB* of noise on the A/D output - *12* bit); a bandwidth greater than *5KHz* (two orders of magnitude greater than the signal bandwidth); a noise figure of less than *2.4mV* [referred to the output] (*1LSB* of the A/D output); and an output voltage swing of *±5 Vpp* into the input impedance of the A/D converter.

The programmable gain instrumentation amplifier AD625 (Analog Devices LTD, USA) was chosen. It has excellent d.c. and low frequency gain stability, low nonlinearity, offset and gain errors and a high common-mode rejection ratio (CMRR). With most integrated circuits there is a price-performance trade off to be made where cost rises exponentially with a linearly higher specification. It was felt that the system performance requirements could be met with this device at moderate cost.

Figure 5.4 is a circuit diagram of the signal amplifiers used for each transducer in the system. The circuits for signals from the X and Y axes are identical while those for the Z axis differ only in the gain factor applied. It is sufficient here to describe only the function of one of these circuits (X axis) as the others follow the same regime.

A reference voltage (Figure 5.3) is fed to the inverting terminal of *U5*, and the transducer signal to the non-inverting terminal. The reference voltage ensures that at zero applied force the amplifier output is approximately *0V*. A positive applied force will thus result in a positive voltage, while a negative voltage implies a negative force vector.

Input protection for *U5* is provided by *R30, R31*. In choosing their value there were four considerations. They form a resistive divider with the amplifier input impedance and therefore will introduce a gain error. The amplifier input offset currents will flow through them creating an offset voltage. Any difference in their

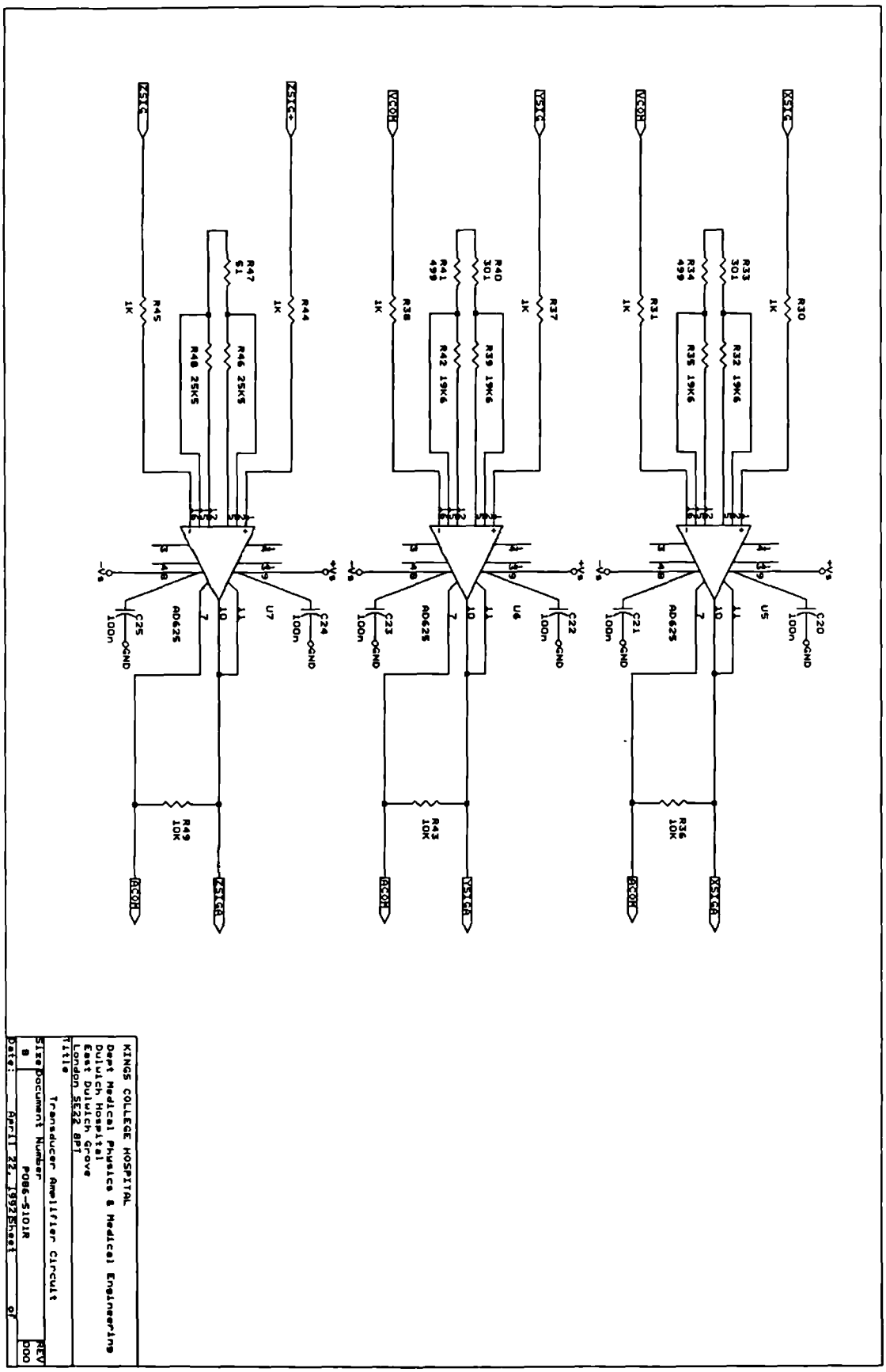

Figure 5.4 Diagram of the amplifier circuits for each Transducer signal.

value will increase the voltage offset and noise signal. They will be an additional noise source (Johnson Noise) with a magnitude proportional to the square root of their value. All these considerations recommend their value be minimised. However to limit overload current their value should be maximised. The values chosen were those recommended by the amplifier manufacturer, $1k\Omega$.

Gain error can be calculated from **[Analog Devices 1991]**:

$$Error = 1-\frac{Z_i}{Z_i+R_s} = \frac{R_s}{Z_i+R_s} \approx \frac{R_s}{Z_i} \quad \text{if} Z_i \gg R_s \qquad (5.8)$$

where $R_s = R_{v+}+R_{v-}+R_{Transducer}+R_{Reference}$

and $Z_i = Z_{Common-mode} || Z_{Differential}$

for the amplifier. Substituting in the values :

$$Error = \frac{(1+1+0.3+0.3)\times 10^3}{500\times 10^6} = 0.0005\%$$

This is obviously negligible. If the source impedances are unbalanced the common-mode (E_{CM}) and noise (E_N) voltages are unequally divided and a differential signal is developed. This error signal cannot be separated from the desired signal. In the worst case where one input has zero impedance and $E_{CM}+E_N = 10V$, say, then the error voltage developed at the amplifier input is:

$$Error = (E_{CM}+E_N)\left(\frac{R_T+R_{v+}}{Z_{CM}+R_T+R_{v+}}\right) \qquad (5.9)$$

$$= 10\cdot\left(\frac{1300}{10^9+1300}\right) \approx 13\mu V$$

For a full scale input signal ($\pm 100mV$ - shear, $2.5mV$ - normal) this becomes :

$$Error \approx 0.013 \quad \%FSO \quad \text{(Shear)}$$

$$\approx 0.52 \quad \%FSO \quad \text{(Normal)}$$

Thus as long as closely matching ($< 5\%$) input impedances are used these errors can be ignored.

The gain of the amplifier is set by *R32-R35*. These must be close tolerance components for accurate setting of the signal scale-factor. Also they must have

low temperature coefficients and high long term stability. In order to determine the gain required for each signal it is necessary to know the range and offset of the input signal and the range and offset the output must be mapped onto.

The transducer output signal will generally be a complex function of the stress applied to it. An exact determination of this relationship is impossible without precise knowledge of; MR resistance as a function of field strength; the field strength perpendicular to the MR at each point on the magnet face; the magnet and MR dimensions; the magnet - MR element separation; and the signal offset due to the non-central assembly of the magnet above the element. Of these the first five are dependent on manufacturing and assembly tolerances for which no individual part data are available. The latter property was measured and corrected by inserting a padding resistor in one lead of the MR. Without this the offset of any axis would be amplified, compromising the dynamic range and system resolution. **Kuny and Heidenreich [1985]** demonstrated that the magnetoresistor output is linear with magnet displacement over the range ±*3/4* width of the magnet.

The slope and extent of the linear region of each assembled device was determined experimentally. Full scale loads were applied to both the shear and normal sections of each transducer. The resultant output signals were measured and the gain factor, required to map this signal into the A/D input range, was calculated. Average values for a batch of transducer were used to derive an optimum gain value for the X and Y axes of *50* similar experiments with the Z axis indicated that a gain of *2000* was optimum. Those gain values mapped the linear range of each axis into the input range of the A/D.

An analysis of the inherent error sources in this circuit design is essential for confidence in its accuracy.

The differential amplifier is a two stage device consisting of a variable gain input stage and a fixed gain output stage. At high gains the input errors dominate while at low gains the output errors dominate. Now, offset voltages occur in both stages. The total offset may be referred to the input (**RTI**) or the output stage (**RTO**) and are calculated by:

$$E_{os}(RTI) = V_{Ios} + \frac{V_{Oos}}{Gain}$$

$$E_{os}(RTO) = V_{Ios} \times Gain + V_{Oos} \qquad (5.10)$$

Additionally the amplifier offset currents flowing through the input impedances increase the offset voltages such that :

$$E_{os}(RTI) = V_{Ios} + \frac{V_{Oos}}{G} + I_{os} \times R_s \qquad (5.11)$$

By substituting gain factor (*50*-shear, *2000-normal),* source impedance ($R_s = 1300\Omega$) and amplifier data, the worst case offset error is:

$$E_{os}(RTI) = 345\mu V = 0.3 \ \%FSO \quad \text{(Shear)}$$

$$= 250\mu V = 10 \ \%FSO \quad \text{(Normal)}$$

Clearly the worst case error for the normal stress signal is significant. However these offsets may be nulled at the amplifier during calibration procedures. In this case the shear signal offset error was ignored and the normal signal offset error nulled for each amplifier if required.

A more significant error source - since it cannot be nulled - is the temperature induced drift in offset voltage. The calculation of these errors is similar to (5.11). Over the range *20-40* ℃ the drift figures for the worst case were estimated to be :

$$\Delta E_{os}(RTI)\Big|_{T=20°C}^{40°C} = \Delta V_{Ios} + \frac{\Delta V_{Oos}}{G} + \Delta I_{os} \times R_s \qquad (5.12)$$

$$= 3.03\mu V°C^{-1} = 0.003 \ \%FSO°C^{-1} \quad \text{(Shear)}$$

$$= 2.08\mu V°C^{-1} = 0.08 \ \%FSO°C^{-1} \quad \text{(Normal)}$$

These values indicate that the offset drift error may effectively be ignored.
A final source of amplifier error is noise originating in each component. Major sources are shot, thermal (Johnson) and 1/f (flicker). All three occur in the amplifiers and are often combined into a voltage and current noise figure. Johnson noise, however, predominates over other noise sources in resistors. Each is specified in terms of a spectral density, and some are frequency and gain dependent. Thermal noise in the input resistances is given by the relation :

$$E_J = \sqrt{4KTR_s} \qquad [V\sqrt{Hz}^{-1} rms] \tag{5.13}$$

Where K is Boltzmann's constant, T is the absolute temperature (Kelvin). The amplifier current noise flows in the input impedance adding to the voltage noise. The quoted voltage noise for the amplifier acts as a voltage source in series with the stress signal. If it is assumed that these noise sources are random and uncorrelated then the total noise voltage can be estimated by :

$$E_N(RTI) = \sqrt{E_J^2 + E_N^2 + I_N^2 \times R_s^2} \times \sqrt{BW} \qquad [Vrms] \tag{5.14}$$

where BW is the bandwidth over which the amplifier operates **[Garrett 1981]**. Substituting values from the data sheet the worst case noise voltage is :

$$E_N(RTI) = 6.9\mu Vrms \approx 45.9\mu Vpp = 0.05 \quad \%FSO \quad \text{(Shear)}$$

$$= 1.4\mu Vrms \approx 9\mu Vpp = 0.36 \quad \%FSO \quad \text{(Normal)}$$

In summary, the amplifier circuit design described here maps the typical output of a shear and normal transducer (*100mV FSO, 2.5mV FSO*) onto a $\pm 5V$ input range of the A/D converter. Provided the offset nulls are trimmed if required, then offset drift errors are < *0.1 %FSO/℃* and noise is < *0.4%FSO.*

5.1.2.2 Interference and Filtering

This section discusses the expected form of the signal and noise. Then describes circuitry designed to maximise the signal to noise ratio and adjust the signal band-width for input to the A/D.

In general, Biomedical signals are wide spectra signals for which amplitude and phase information are important parameters. Any filters or amplifiers which are involved in conditioning the transducer signals before it is digitised, must faithfully reproduce the signal while attenuating noise. Achieving this aim is often beset with compromise as both signal and noise may be of similar magnitude and frequency. Before the filter and amplifier parameters can be set the likely form of signal and noise must be estimated.

In this application the expected signals would contain transients that approximate to step functions. From previous work the bandwidth is less than *50Hz* **Antonsson and Mann [1985].** And from the transducer design tests the magnitude will be *100mV* and *2.5mV* full scale from the X (Y) and Z axes respectively before amplification.

The likely form of the noise was determined by experiment. It was assumed that signals from the transducer or amplifier would be conveyed to the A/D over a trailing cable. The available gait laboratory space would require a ten metre cable. This cable in its unshielded form would act as a noise aerial. The circuit of Figure 5.5 was used to determine the magnitude and band-width of the noise signal. The cable was either terminated with *180Ω* into *0.5V* or driven with a constant voltage; to simulate both the transducer and buffered signal cable respectively. During the test all possible electrical noise sources were turned on, to simulate worst case conditions.

Both amplifiers used in this circuit were chosen for their inherent low noise and wide bandwidth. The magnitude and bandwidth of the measured a.c. Noise is given in Table 5.1

	Bandwidth [Hz]		
	300	*30K*	*1M*
Passive	*300 μV*	*2 mV*	*30 mV*
Driven	*200 μV*	*2 mV*	*20 mV*

Table 5.1 Noise signal magnitudes (pkpk) over the given bandwidths for a 10m length of unscreened wire with a passive (180Ω) *or active termination.*

The majority of the noise was removed by the differential amplifier. With a *300Hz* filter imposed on the remaining signal the noise magnitude will amount to less than one bit error in a *±5V* signal digitised to *12* bits.

Now, under the Nyquist criterion it is important to remove any signal components with a frequency greater than half the sample frequency of the A/D. Otherwise those components would be under sampled and appear in the digital signal as lower

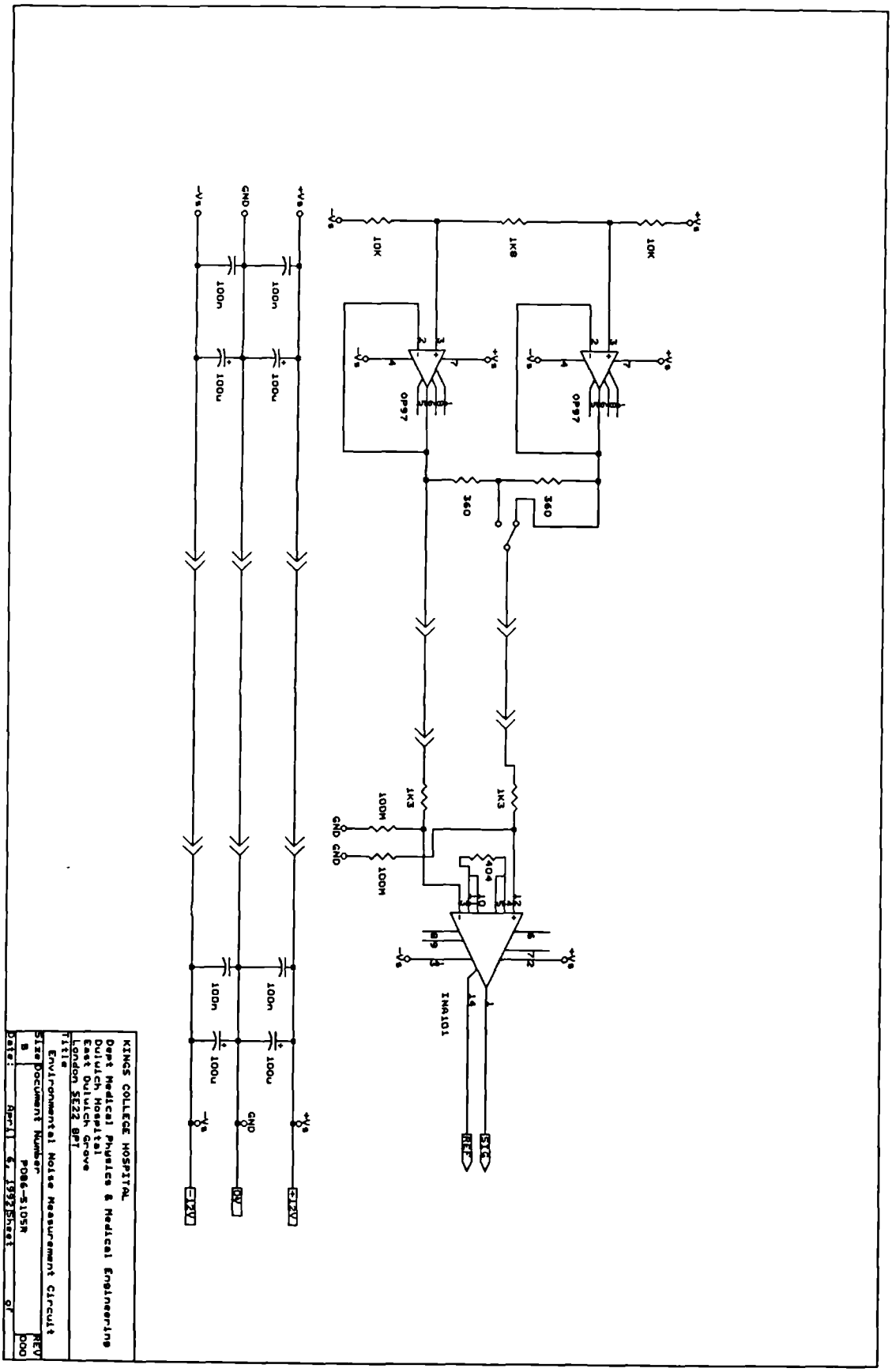

Figure 5.5 Schematic of the circuit used for determination of the likely environmental noise pickup from long signal leads.

frequencies. A process known as aliasing. The sampling rate of the A/D is *1000Hz*. To limit the signal bandwidth an analogue filter was applied to the amplified signal.

The four most commonly used filter types are Cauer (Elliptic), Chebyshev, Butterworth and Bessel (Thompson). Only a synopsis of each of their relevant characteristics is given here. For a more detailed description the reader is referred to more general texts, such as **Williams [1981]**.

The first two types are used primarily where very narrow frequency selectivity is important, at the expense of amplitude and phase integrity. Their gain factor is not constant over the pass band, exhibiting a periodic ripple. Also the signal delay through the filter is not constant over the passband but decreases with frequency. And in general they tend to have underdamped step responses. Both the passband ripple and the unequal delay may be minimised. However, that would involve a performance compromise or extra circuitry. In the present application narrow frequency selectivity is not critical. As Table 5.1 indicates, the likely noise is above *300Hz*, approximately a decade above the signals of interest. Because of these considerations attention was focussed on the latter two types of filter; Butterworth and Bessel.

Butterworth and Bessel filters have considerably less frequency selectivity than Cauer or Chebyshev types. But their time domain behaviour is more damped. The equations which specify Butterworth functions dictate that the filter gain is maximally constant over the passband. However, its phase response is non-linear resulting in a slightly underdamped step response. Bessel filters on the other hand have maximally linear phase response but non-constant gain in the passband. Thus their transient or step response may be optimised for critical damping at the expense of frequency selectivity and constant gain in the passband.

In summary, the signal bandwidth is expected to be less than *50Hz*; the likely environmental noise is only significant beyond *300Hz*; and Nyquist requires anti-alias bandwidth of less than *500Hz*; the signal may contain step-like transients; and in the worst case the signal to noise ratio is only *4:1*.

With the above considerations a fourth order Bessel filter with a cut frequency of *250Hz* was found to be optimum. This provides constant delay over the passband, with less than *1%* deviation in amplitude from d.c. to *50Hz*. Noise attenuation is greater than *60dB* above *2.5KHz* **[Zverev 1967]**.

The circuit shown in Figure 5.6 is a standard Biquad implementation of the fourth order Bessel filter. This form is most often used in low Q applications and is insensitive to passive component tolerance and ageing. The passband gain of the filter was set at unity and the corner frequency set at *250Hz*. Equations for derivation of the component values were determined by comparison of the generalised second order biquadratic equation and the transfer function of the circuit. Those equations were then solved from tabulated values of the Bessel polynomial roots **[Williams 1981]** and the arbitrary assignment of values for the capacitors. Metal film resistors (*0.1%* tolerance) and polystyrene capacitors (*1%* tolerance) were used for accuracy and long term stability. *U8* is a dual low noise operational amplifier, AD648 (Analog Devices LTD). The overall frequency response of the amplifier and filter combined is shown in Figure 5.7.

The actual noise signal at the output of the combined transducer-amplifier-filter-cable system was evaluated in the laboratory. A transducer, at rest, was connected to the amplifier unit (TIU) and the signal spectra and amplitude was observed at the input to the digitiser (DCU). The maximum magnitude of the noise signal was *10mV* (*0.24%FSO*) for the shear section and *10mV* (*0.25%FSO*) for the normal section. The bandwidth of the noise signal was *200Hz*. These figures indicated that with careful differential amplifier, grounding and filtering techniques environmental noise would not interfere significantly with stress signals.

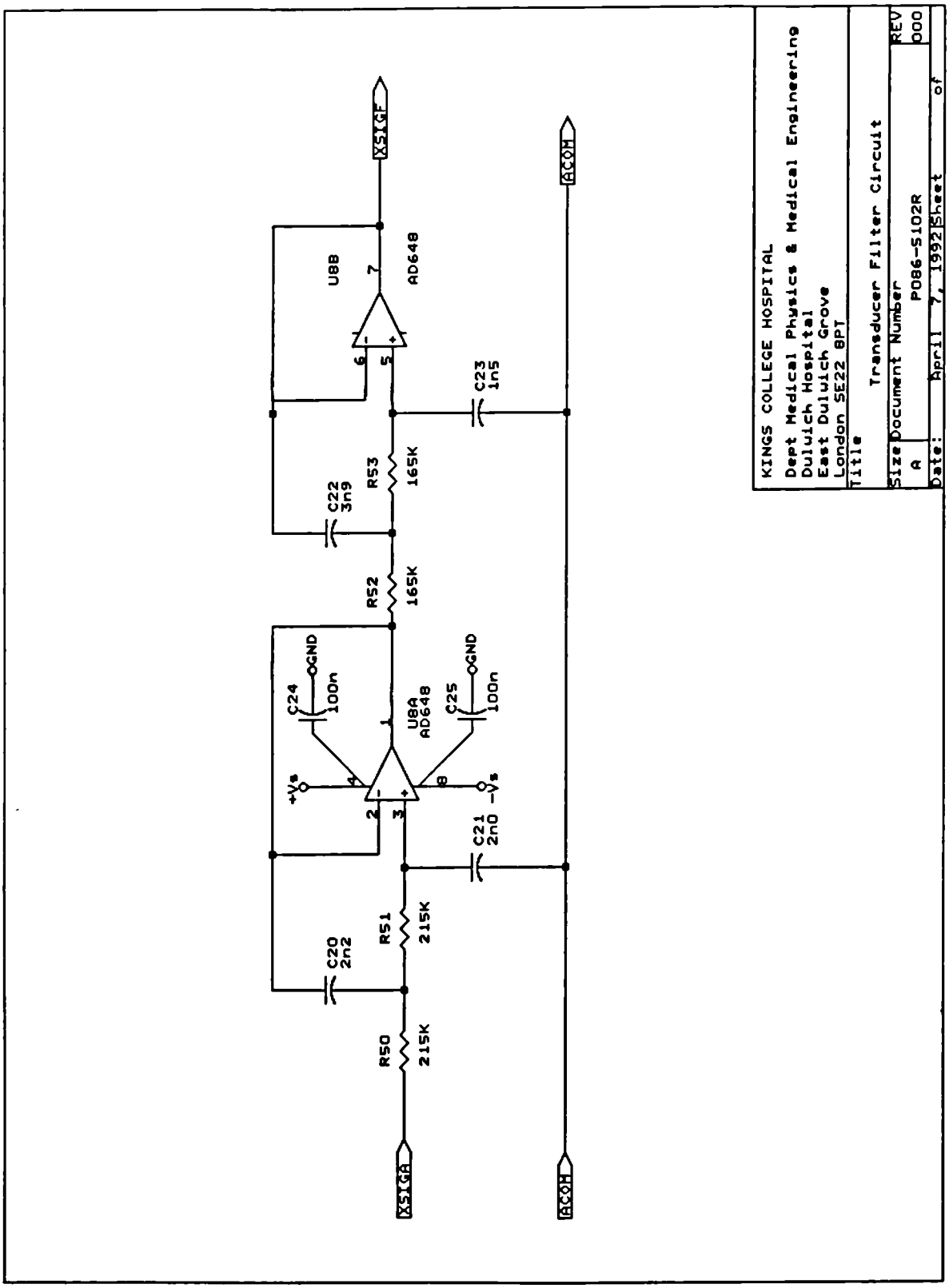

Figure 5.6 Diagram of the filter circuit - a standard Biquad implementation of a fourth order low-pass Bessel ($f_c = 250Hz$).

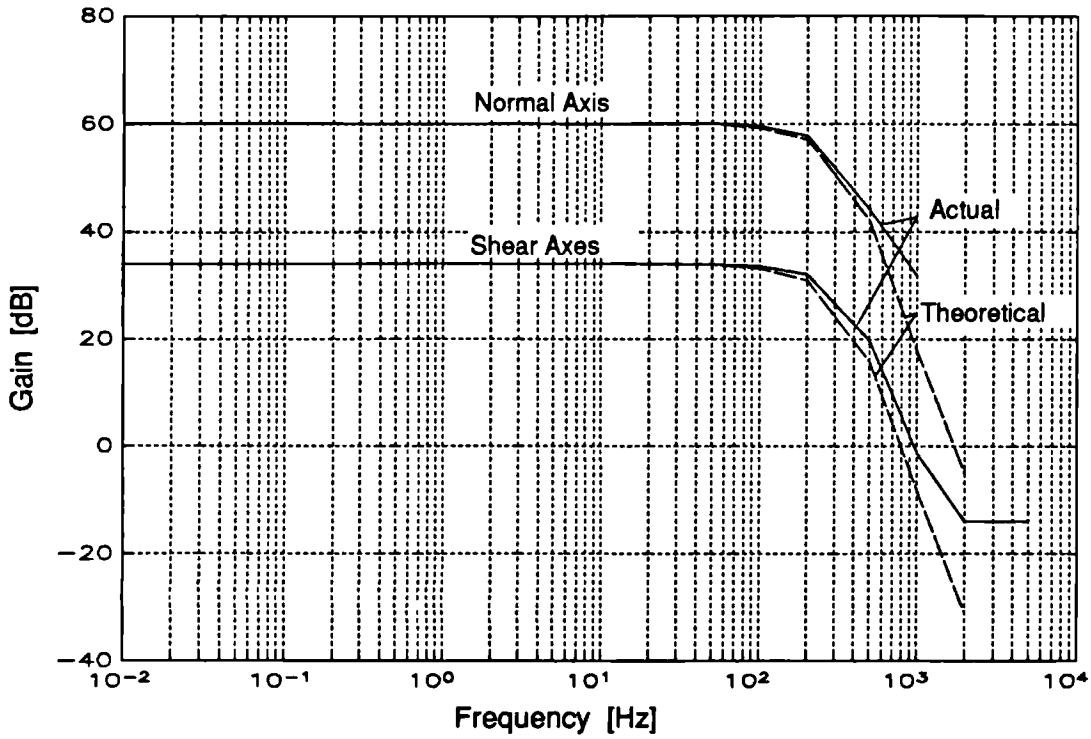

Figure 5.7 Frequency response of transducer amplifier and filter for both the shear stress signal path and the normal stress signal path.

5.2 Signal Conversion and Data Storage

This section discusses the hardware requirement and its implementation, for the analogue to digital conversion and subsequent archiving of transducer signals.

Section 5.2.1 outlines the specification for the A/D converter. This unit was purchased as a subsystem component from a commercial vendor. Section 5.2.2 details the specification and selection of a microcontroller unit used to manage the A/D and some high-speed data memory required to service the A/D output rate. Also, it describes the personal computer system which integrates the control of each unit and archives all the data for subsequent processing. Section 5.2.3 describes the necessary power supply requirements for the system.

5.2.1 Analogue to Digital Conversion

The A/D converter subsystem was specified in terms of the : number of signal channels; mode of signal input; input voltage range; number of bits; sample rate; input impedance; compatibility with existing systems; software support and ease of use.

Initially it was expected that at least five anatomical sites would be monitored simultaneously during clinical trials. Because of the expense and time involved in making an instrumented socket to fit each patient, it was more rational to insert as many transducers as practical. On inspection of the socket area in relation to the transducer size, an estimated ten devices could be fitted before the rigidity of the socket was compromised. Additionally, to transducer signals, two channels would be required for event signalling (e.g. foot switches). Thus the maximum number of active channels would be thirty two.

As the signal amplifiers may be some distance from the A/D, differential inputs were used to maximise noise rejection. Although the event signal was only two-valued and therefore suitable for single ended inputs, most A/D's are unable to accommodate both differential and single ended inputs on the same unit. So this channel was differential also.

The A/D input range must equal the output range of the signal amplifiers which was $\pm 5V$. While its input impedance must be significantly greater than the preceding stage (filter) to avoid loading effects, causing signal degradation. In this case it must be a minimum $10k\Omega$. The number of bits or the size of the digital result required was defined by the resolution limit desired of the input signal. In the case of the normal-stress transducer $100N \pm 0.5N$ is mapped into $0\text{-}5V$ of signal. Therefore at least 200 discrete levels must be discriminated. So an 8 bit or greater A/D converter is required.

The sample rate required was dependent on the bandwidth of the transducer signal. It was assumed that the maximum likely frequency in the signal would be $50Hz$. Under the Nyquist criterion the minimum sample rate would need to be $100Hz$. However this would only provide two sample points per cycle. To allow a more accurate reconstruction of the waveform; ten or more points per cycle would be desirable. Thus a sample rate of $500Hz$ per channel was required.

The design of an A/D unit is a complex exercise which has been surmounted by many designers already. So initially a commercial unit which fitted the specification was sought. Ideally the unit should reside in a standard computing platform where the data could be archived and processed. In this case the PC was the desired platform However a survey of the market failed to find a PC unit with thirty-two differential channels. The only available format was a VME based unit (Plessey Microsystems LTD). The relevant specifications for the unit are given in Table 5.2.

Model	*PME 98-06*
Sample Rate	*1 KHz per channel*
Input Ranges [V]	*±5, ±10, 0-5, 0-10*
Number of Channels	*64 SE, 32 Diff*
Gain	*1, 10, 100 Software programmable*
	1-1000 Presettable (resistor)
Number of Bits	*12*
Output Format	*Binary, Offset binary, 2's complement*

Table 5.2 Specifications of the A/D convertor used.

As the unit was a slave of the VME bus, it required a host controller and software to enable it to function. This could not be provided by the PC directly. A central processing unit (CPU) was sought from the same company for compatibility.

It is noted here that the A/D described above would have very readily fulfilled all of the project requirements. Unfortunately the unit used was an early version and was subsequently found to contain many operational faults. Four of the five modes of operation did not function at all. The fifth mode was only made to work in a very unconventional manner. Unfortunately it was a very processor intensive method, resulting in significantly reduced throughput rates. To the authors surprise the product support from the supplier was woefully inadequate. Despite admitting that there were many design faults with the PM 98-06 they were not prepared to upgrade it or offer any advice short of purchasing the latest version. As a result significant effort was expended in achieving an acceptable sample rate of 500*Hz* per channel using this faulty equipment.

5.2.2 Conversion Control and Data Storage

As the A/D unit was a slave on the VME bus, a CPU was required to perform the necessary control functions. It would have to initialise the channel sampling sequence and gains; initiate conversions at a specified rate; buffer the A/D output data; and communicate with the user.

Initially a PC was considered for this purpose. However there were a number of difficulties to be overcome. Firstly, providing an interface from the PC bus to the VME bus was a complex problem. There were no commercially available units appropriate for this task, and the design effort required would be considerable. Secondly at the desired sample rate, data transfer from the A/D would demand the uninterrupted attention of the CPU. A difficult requirement to achieve with a standard PC. Thirdly at maximum sample rate the data memory would be filled at *32 Kbytes/sec.* As both programme and data occupy the same memory, data size must be traded against programme complexity. At the time PC memory was restricted to less than *640 Kbytes.* Now, although storing data directly to disk would have provided more data space, disk access is too slow for the data rates needed. However, a purchased VME bus based CPU was shown to provide enough memory for both large programme and data space. Further, an application specific operating system allowed the core processor sufficient uninterrupted time to maintain data transfer rates. Also, being VME based the interface to the A/D was trivial. Moreover a serial port provided a link to the user via a standard terminal. The CPU chosen was PME 68-12 (Plessey Microsystems LTD). It contained a Motorola MC68000 processor, 1 Mbyte DRAM, 16 Kbyte fast SRAM, 19200 Baud serial port, and EPROM based resource table for input/output control.

However, with this CPU there were no archiving facilities provided. Nor were there any data processing software readily available. In comparison there was a wealth of software and standard disc storage on the PC. So to make use of this, the PC was used as the terminal to the PME 68-12. This was a relatively common mode for the PC to operate in. Thus the system comprised of two physical boxes. One an IBM compatible PC with a minimum of configuration of: 80286 processor; *512 Kbytes* of RAM; *1.2 Mbyte* FDD or *10 Mbyte* HDD; serial port (capable of 19200 Baud); CGA monitor. The other, a VME bus rack containing; PME 68-12 CPU; PME 98-06 A/D; Power supply; transducer signal termination unit; VME backplane (*3* slot) and bus termination. All of the latter was designated MEP086A

as this was the in-house project reference code. It will however be referred to as the Data Collection Unit (DCU) throughout this thesis. The last unit in the DCU was a PCB which terminated the signal cable from the transducer interface circuits-discussed in 5.1. The transducer signal termination unit contained differential input single pole RC filters ($f_c = 250Hz$) for each signal channel, a ground reference point, and it re-routed the channels to the appropriate A/D connector pin. The filter provided some noise suppression from interference picked up along the cable. An RS232 serial cable was used to link the PC to the PME 68-12 of the DCU.

With this arrangement the user enters the trial parameters, patient comments, and data file names to the PC via menu based software. This information is preprocessed on the PC. Commands and control parameters are sent to the DCU over the serial link. There they are translated into A/D control instructions and the relevant data structures are set up. When data has been collected and resides in the memory of the PME 68-12, it is transferred back to the PC over the same serial link. Then they are archived to disc file for subsequent processing.

To improve data transfer time the serial ports of both PC and DCU were set to *19200 Baud.* Extensive software was written to effect: the user interface menus; preprocess trial parameters; handle the communication links; drive the A/D unit; provide data butter structures; transfer data; and create data files on disc. The details of this are presented in Chapter 6.

5.2.3 Power Supplies

The PC for the User interface and data storage contains its own supply, deriving power from the mains. Both the DCU and TIU are powered from the same supply. Mains voltage is passed through an isolating transformer and fed to a switched-mode regulator housed in the DCU. This is a standard commercial design SPG312 (Schroff UK LTD), capable of *5V @ 11A, ±12V @ 2.25A.* The three voltages and *0V* are fed directly to the VME backplane. The PME 68-12 and PME 98-06 take their power from this backplane on the standard designated VME connector pins.

There were two options for supplying power to the TIU, by battery or cable from DCU. The estimated maximum power consumption of the unit was *±12V @ 0.7A*. It was possible to supply this by either method. However, in order to reduce the weight carried by the patient a cable supply was preferred. So a small multicore power lead was run from the DCU alongside the transducer signal cable.

5.3 Registration of Foot Contact Events

In order to correlate the measured stresses with the various temporal phases of the gait cycle, heel strike and toe off events for each foot were recorded. These were detected by contact switches attached to the plantar surface of each footwear. Signals from the switches are conveyed to the TIU by ribbon cable. There they are modified and passed on to the DCU.

The foot-switches used were types FSW12 for the Toe, and FSW7 for the Heel (Medical Research LTD, UK). Two were used for each foot, one under the toe area and the other under the heel. The circuit of Figure 5.8 detected each switch closure and produced two binary signals, one trinary signal and a visual indication of the switch states.

On each switch closure the relevant LED (*D1-D4*) lights to indicate contact with the ground has been made. Heel and toe switch closures are OR'd together through diodes *D5-D6* (*D7-D8*), so the signal at the collector of *Q3*(*Q4*) will be binary in nature. In normal gait the signal states will have the interpretation given in Table 5.3.

Output state	*Foot action*
Low	*Swing phase*
Low → High	*Heel strike*
High	*Stance phase*
High → Low	*Toe off*

Table 5.3 State table of binary footswitch signal for normal gait.

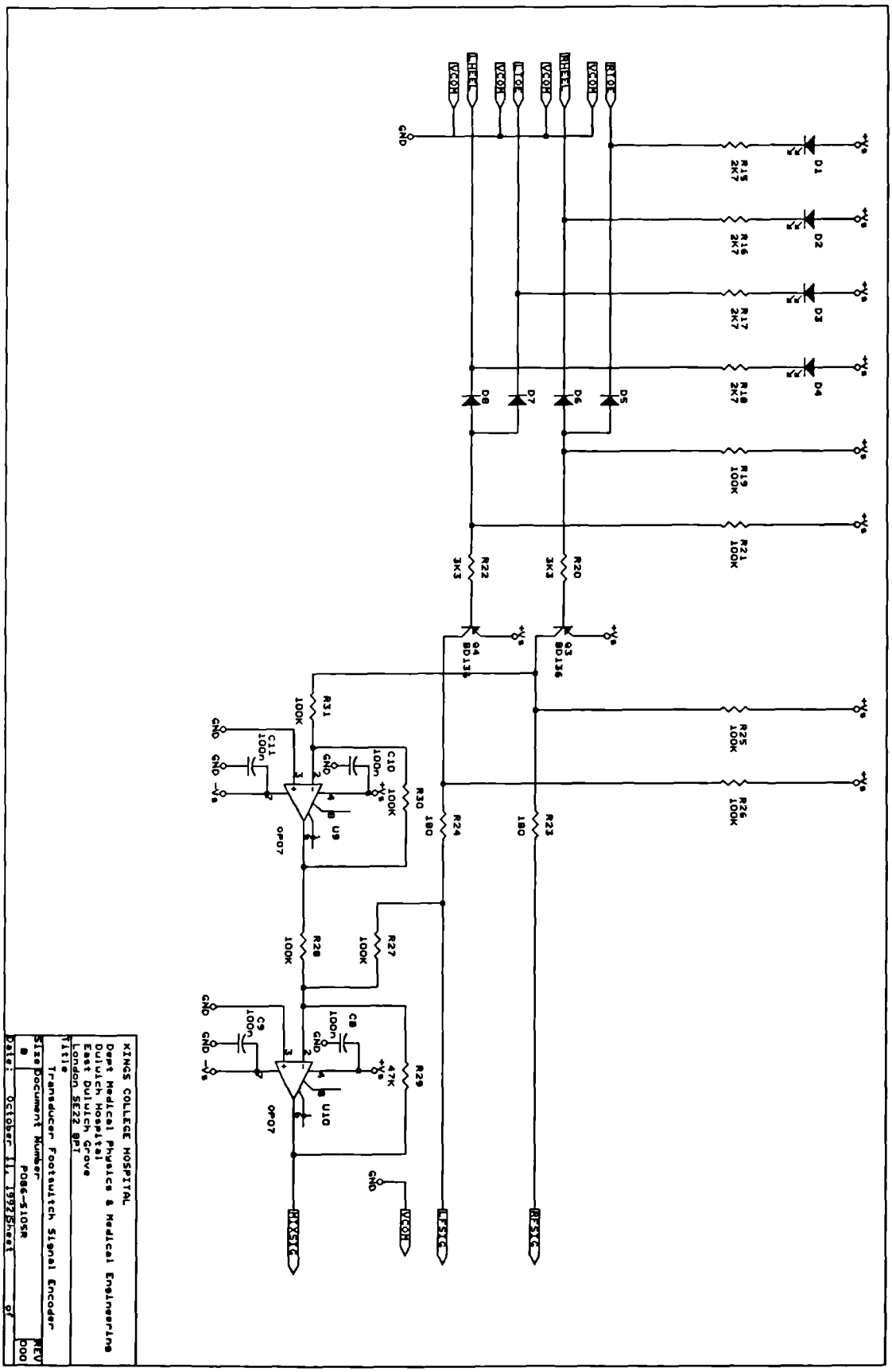

Figure 5.8 Footswitch conditioning circuit. Provides LED indication of switch states; Left and Right foot contact signals (binary); combined left and right contact signals (trinary).

The binary signals from each foot are combined to form a trinary signal. *U3* inverts the right foot signal. This is then summed with the left foot signal at *U2*. Table 5.4 describes the output states of *U2* for combinations of left and right foot action with normal a gait pattern.

Output State	*Foot action*
Zero	*Double support phase (or None)*
Zero → Positive	*Left Toe-off*
Positive	*Right support phase*
Positive → Zero	*Left Heel-strike*
Zero → Negative	*Right Toe-off*
Negative	*Left support phase*
Negative → Zero	*Right Heel-strike*

Table 5.4 State table of trinary footswitch signal for normal gait.

This trinary signal is passed to the DCU where it is digitised with the stress signals.

5.4 Interface to Kinematic Measurements

From analysis of the stress-time recordings much can be learned about the magnitude, direction and timing of stresses occurring during gait. Further information can be gained by relating these stresses to joint angles, body position and limb motion - especially during abnormal gait.

The University Department at which this research was undertaken has the use of a **VICON** Kinematics Measurement system (Oxford Metrics LTD). This is a video based technique which records the spatial trajectories of reflective markers on a subject, during a gait cycle. It is also capable of simultaneously recording force plate, EMG and other event data.

By providing a signal, which contains identifiable events, to both the stress measurement and kinematics measurement systems, then both data sets will contain sufficient timing markers for correlation. There will, of course, be some correlation uncertainty, as both systems are sampling data asynchronously to each other. The

worst case lag in detecting an event will be one sample period of the fastest sampling system. Similarly the worst case error in synchronisity will be the same period.

Two signals were passed between the two systems. Either of these could be used for synchronising both data sets. The first and simplest was the footswitch signal sent from the DCU to VICON. This is recorded by both systems simultaneously. The second was a signal from VICON which reflects its Run/Halt status. In the DCU this signal is digitised with the stress signals and serves two purposes. It identifies which gait cycles were recorded on VICON and is used as an optional trigger for initiating data conversion in the DCU. If the software selects the Run/Halt signal as the trigger, the DCU continuously digitises the signal looking for a low to high transition. When detected, stress data conversion begins.

The previous section described circuitry to capture and output footswitch events. A combined left and right foot signal was digitised by the DCU in synchronism with the stress signals. Two separate signals, from left and right feet, are passed via the DCU to the VICON system. Figure 5.9 describes an interface circuit built for this. Both signals were transferred to the VICON event channels through opto-isolators then converted to TTL levels.

A similar circuit to that above was used to transfer the VICON Run/Halt signal to the DCU.

5.5 System Integration

The whole stress measurement system consists of three separate enclosures with connecting cables.

Up to ten triaxial stress transducers plug into the transducer interface unit. Each has a cable length of *1-2m.* Sufficient to span from the socket to the TIU without impeding the free movement of the subject. The TIU itself is carried by the subject in a backpack. The specially made pack is sewn from a polyester cover and includes padded straps. Openings are provided on the sides for transducer and signal cable access. Shoulder and waist straps were provided. A fully populated (ten transducer) unit and pack have dimensions of approximately *250 x 300 x 50mm*

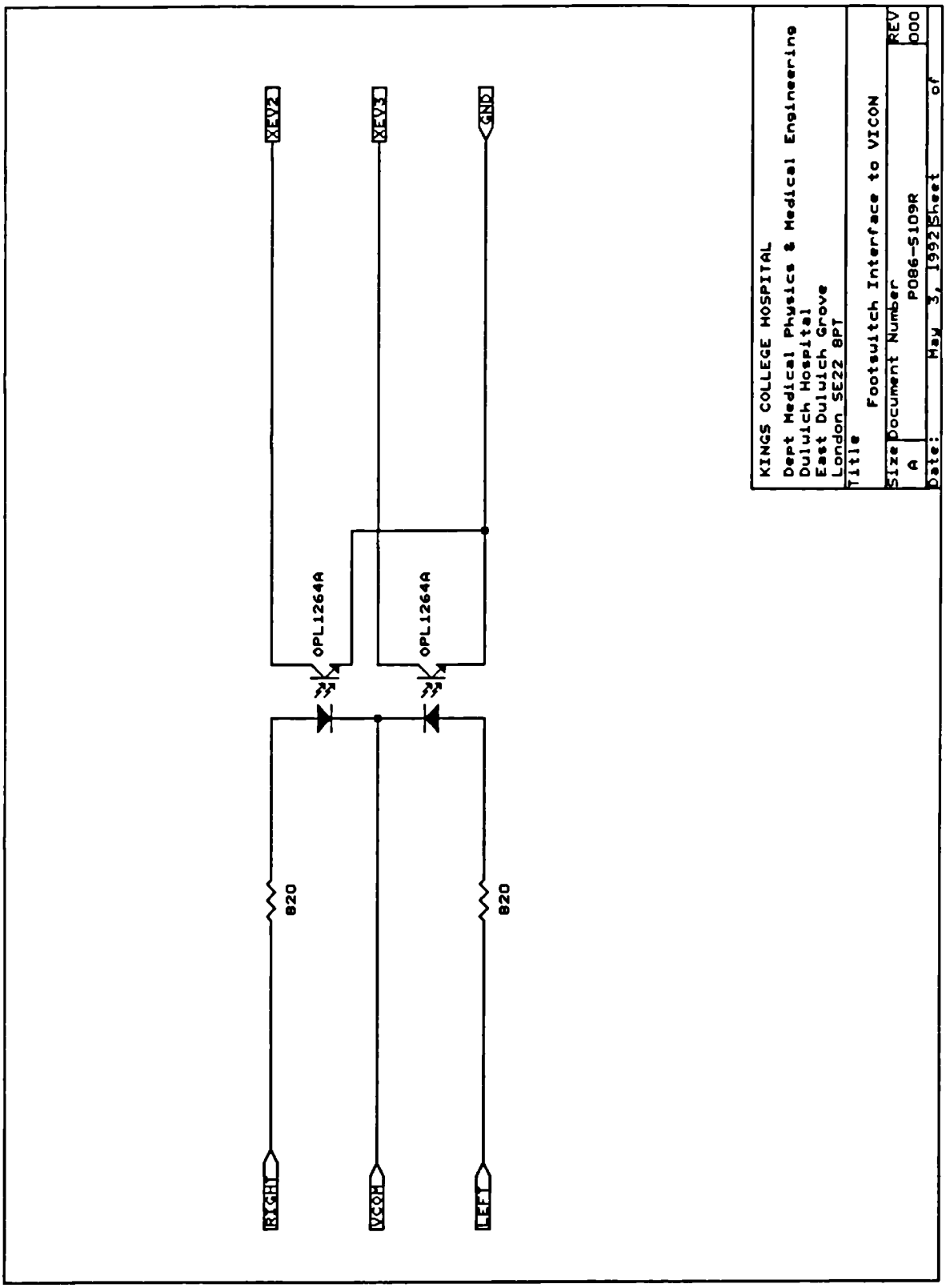

Figure 5.9 Interface circuit used to transfer Footswitch signals from the Data Collection Unit to the VICON Kinematics system.

and weighs *1.3Kg*. Although it was thought that its size may be a difficulty for smaller elderly subjects. If this was the case then a smaller unit with fewer transducers could be built, or the researcher could follow closely behind the subject holding the pack. In all cases care must be taken not to distract the subject from their usual gait pattern.

Signals from the TIU are conveyed to the DCU by a ten meter length of ribbon cable. The cable length was chosen to equal the length of the kinematics laboratory. This would allow between ten and thirty steps. The limit to the cable length (walkway length) is a function of; the drive capability of the transducer buffers; noise susceptibility; and memory size at a given sample rate and stride time. With the cable used here the output drive and noise pickup on the cable was found to be satisfactory [5.1.2.2] and the number of steps adequate for planned studies. The drag force of the cable on the subject was measured as $< 8N$ on linoleum flooring. This was thought not to have a significant effect on the gait of an active amputee.

The DCU enclosure is positioned near to the PC. It is a mains powered stand alone unit. The signal cable from the TIU connects to the rear of the unit. After passing through the cable termination PCB the signals are separated and output to the A/D. Four, *26* way jumpers link the termination PCB to the A/D via their front panels. A serial communications cable spans one or two meters from the PME 68-12 front panel to the serial port on the rear of the PC. Two five meter signal cables run between the DCU and VICON. Footswitch signals, left and right, are sent to the VICON, while the VICON Run/Halt status is sent to the DCU. The first two signals can be used as additional information to the Kinematic data sets, or provide common synchronising events to correlate stress and kinematic data. The latter signal is digitised with the stress signals and may provide; a record of which gait cycles were captured on VICON; a correlating signal; or a trigger signal to initiate sampling on the DCU.

The PC consists of the monitor, processor box and keyboard. When the system is used in conjunction with the VICON system, the PC is usually positioned near to the VICON controls. The User can then operate each independently if required.

Figure 5.10 shows the three enclosures with cables and pack.

Figure 5.10 Photograph of the units and cables which comprise the stress measurement system. From right to left; transducer and footswitch; Transducer Interface Unit; transducer signal cable; Data Collection Unit; serial link; PC for control and archiving.

5.6 Safety

During the design and construction of the equipments described in this thesis care was taken to ensure that all the electrical safety recommendations of BS5724 were followed.

To reduce the potential shock hazard, voltages in the TIU were restricted to be below *24V* d.c. Voltages in the transducers were supplied from a *1V* quasi-floating source. It is not a true floating source as it is restricted to be within the *±12V* supply of the unit. Additionally the TIU power supply is derived directly from the DCU which is fed via an isolating transformer. All voltages and currents in the patient circuit are isolated from mains and earth potentials. The DCU conforms to Class 1B of BS5724 and the TIU to Class 2. The chassis and accessible panels of the DCU are bonded to mains earth.

In order to maintain isolation the serial link from the DCU to the PC was opto-isolated. An RS232 to RS422 to RS232 conversion was made using two Model 262 (Teledata INC, USA) opto-isolating modems. Isolation from the VICON potentials was also necessary. Again opto-isolation was used in the signal paths between the VICON and the PC.

5.7 Discussion

The data acquisition system is made from a number of interconnecting hardware units. The transducers connect to a Transducer Interface Unit (**TIU**) which supplies an excitation voltage and buffers and filters their signals. These are then passed to the Data Collection Unit (**DCU**) where they are digitised. Buffered digital data is transferred to a Personal Computer (**PC**) for archival and processing. Simultaneously, external event signals are also digitised and archived, for synchronising multi-system data sets.

The transduction elements of the triaxial stress sensor are: a magnetoresistor and moving magnet system in the shear stress section; and a strain gauged diaphragm and pre-shaped indentor in the normal stress section. The principle electrical properties of the magneto resistor (**MR**) (**FP111L100 - Siemens UK LTD**) are that it is a low impedance (*300*Ω) three terminal device whose impedance varies (±*25%*) with the magnitude of magnetic flux density perpendicular to its active face. It is configured as one half of a Wheatstone bridge and excited by *1V* d.c. The strain gauge is a four terminal metallic foil gauge configured as a full Wheatstone bridge. Its impedance is low (*350*Ω) and varies only fractionally under stress (±*2%*). Excitation is from the same source as for the magnetoresistor, and is set at *1V*d.c. The low impedance of both elements minimises their susceptibility to electromagnetic interference, and the low excitation voltage minimises thermally induced errors due to resistance heating. A high stability voltage reference maintains the excitation voltage regulation to better than *0.1%*.

Amplifier and filter circuits separated the transducer signals from any environmental noise coupled on to the transducer leads. Differential amplifiers were used to take advantage of their high common mode rejection (CMRR) to remove any significant noise commonly coupled onto the signal leads. The high input impedance minimised input bias current drain from the transducer signal currents. Also, the input circuits

were isolated from the output circuits allowing the use of floating excitation voltages, which had inherent noise minimisation advantages. System gains were set at *50* and *2000* for the shear and normal sections respectively. Input protection resistances on the amplifier contributed negligibly to gain errors and CMRR degradation. Input offset errors were *0.3%FSO* and *10%FSO* (worst case) for the shear and normal sections respectively, although these may be nulled at the assembly stage. Temperature induced offset drift was not significant. Inherent noise from electrical components was also not significant.

The expected stress signals could contain transients that approximate to step functions, thus the type of the filter employed was Bessel. From a consideration of the expected bandwidth of the stress signals and the environmental noise, determined by experiment, the bandwidth of the filter was set at *250Hz*, and a *4th* order implementation used.

The stress signal digitiser in the DCU was purchased as a subsystem unit to capitalise on cost, time and design effort savings. However, because of the number of differential channels to be digitised (*32*), the digitisation rate (*500Hz*) and the required memory size (*≈1Mbyte*), a PC format unit was not available. A commercial unit was found, with a suitable performance specification, on VME format. A subsystem controller was also purchased for directing the digitiser, buffering its data output and transferring the data to the PC at a manageable rate. The digitiser input range was set to *±5V* to just exceed the maximum output range of the signal amplifiers. A resolution of *8bits* was sufficient for this application, although, a *12bit* unit was obtained for the same cost. The controller processor (*MC68000*) was run at a clock speed of *10MHz* to enable it to store digitised data at *32Kbytes/Sec*. Software to effect control was run from SRAM for speed of execution. Data transfer rate, from the DCU to the PC, was set at *19200Baud* to minimise transfer time. The PC used was an IBM-AT-compatible (*80286*) running at *8MHz*. Its data archive was a *10Mbyte* HDD or *1Mbyte* FDD. User control of the whole acquisition system was via software being executed on the PC.

In order to correlate the measured stresses with the various temporal phases of the gait cycle, heel strike and toe off events for each foot were recorded. These were detected by contact switches attached to the plantar surface of each footwear. Signals from the switches are conveyed to the TIU by ribbon cable. There they were modified and passed on to the DCU. There they were digitised with the

stress signals and also passed on to an external kinematics measurement system. A second signal, which contains identifiable events from the kinematics measurement system, was input to the DCU and also digitised with the stress data. Thus both DCU and kinematics data sets contained sufficient timing markers for correlation.

The DCU power was derived from an transformer isolated mains supply and the TIU was in turn powered from it by a low voltage supply (*12V*) to ensure patient safety from electrical shock. Data transfer to the PC was effected over an opto-isolated RS232 link to isolate the patient from currents derived from the PC. The signals to and from the DCU and the kinematics system were also opto-isolated to effect patient safety.

Chapter 6
Data Acquisition : Software

The previous chapter described the development and function of the required data acquisition hardware for this system. In this chapter details of the software developed to control the hardware and to manage the acquired data are presented.

Section 6.1 describes the minimum hardware required to run the software and the development environment under which it was created. Section 6.2 provides an overview of the system control strategy. It outlines the software structure, hardware interaction and the user interface. Sections 6.3 to 6.6 are detailed descriptions of the operation of the many programme modules which make up the system software. Flowcharts of these modules are presented in each section.

Listings of the code written for each of the modules discussed are not presented here as they total some six thousand lines. They are however recorded in a Departmental report (**P086-SOFTMAN**) which is available on request from Kings College (Dulwich) Hospital[1].

It should be noted here that two sections of the programme code were written to control the Data Collection Unit (DCU) in an unorthodox manner. These code sections were written in Motorola *68000* Assembler and acted to control the A/D and the serial port on the CPU board. Although these sections comprise less than *5%* of the total software they absorbed almost *70%* of the code writing time.

It was necessary to write the serial port control code to achieve the higher data throughput rates. The DCU code was 'hand-crafted' to work around the multiple errors in the technical manual supplied with the A/D and CPU boards. An extensive amount of effort was expended in writing code to coerce the A/D board into digitising any signal. As supplied, the board did not operate in any mode recommended by the supplier. More surprisingly, the supplier would not officially support the product despite acknowledging its faults. However a confidential copy of the circuit diagrams was obtained. By studying the interconnection of the control

1 Department Medical Engineering and Physics, Kings College (Dulwich) Hospital, East Dulwich Grove, London SE22 8PT, UK.

logic a method was devised for initiating and terminating conversions under software control. Eventually, successful, although less than optimum, operation of the DCU was achieved with the software reported here.

Despite these unique sections of code the programmes are quite portable to other Motorola *68000* based computers. Modular programming techniques were followed throughout with a clear distinction between machine specific and machine independent code modules. Therefore portability is assured by replacing only the machine dependent code modules.

6.1 System Hardware and Programming Environment

This section describes the minimum hardware required on which to run the data acquisition and processing software. It also describes the programming languages and environments used to develop the software.

In order to acquire new data there are two hardware units required. These are an **IBM-PCAT** (PC) or compatible and an **MEP086A** data collection unit (DCU). The PC must have; an *80286* CPU running **MS-DOS** v *3.0* or later; *512* Kilobytes of **RAM**; **CGA** colour monitor (minimum); **RS232** serial port capable of *19200* Baud on COM1; and standard *102* key keyboard.

The MEP086A unit is described in detail in Chapter 5. In outline it consists of a **PME68-12** processor board (**CPU**) and **PME98-06** analogue-to-digital convertor (**A/D**) board on a VME (RevC) bus (**Radstone Technology PLC**). The PME68-12 board must have a Motorola *68000* CPU and a **PLUM** monitor (v *3.3*) - as supplied by Radstone - and *1* Megabyte of RAM. Additionally, an **MEP086B** transducer interface unit (**TIU**) may be used to buffer the transducer signals into the A/D.

All the data processing was carried out using an interactive mathematics programming environment and language called **MATLAB386 (Mathworks INC)**. This software was run on an IBM compatible **COMPAQ DESKPRO** *386/20*. Because of the unique characteristics of each transducer under calibration, the interactive environment was efficient at exploring these characteristics and producing semi-automatic signal processing functions. To run MATLAB386 the COMPAQ must have a mathematics coprocessor - *80387*. Various processing routines were written in MATLAB386 language to: perform data file conversions; display and plot performance curves;

calculate linearity, hysteresis, frequency, creep and temperature parameters; and to perform curve fitting operations. These routines are recorded in the departmental report mentioned above.

The development of the data acquisition software was carried out on the PC. Programmes to run on the PC were written in the 'C' language under the **MICROSOFT QUICK C** v *2.05* compiler. Also some *80286* assembly routines were written under **MICROSOFT QUICK ASSEMBLER** v *2.05*. Programmes running on the DCU were written in 'C' and *68000* Assembler under the **MANX AZTEC C68K** Cross-compiler/Assembler. Machine independent code was debugged between two IBM-PC compatibles while the machine-specific code was downloaded to the DCU and debugged under the PLUM monitor control.

6.2 Software Overview

This section presents an overview of the system control strategy. It outlines the structure of the software, the hardware interaction and the user interface. Figure 6.1 is a diagram of the interconnection of system units.

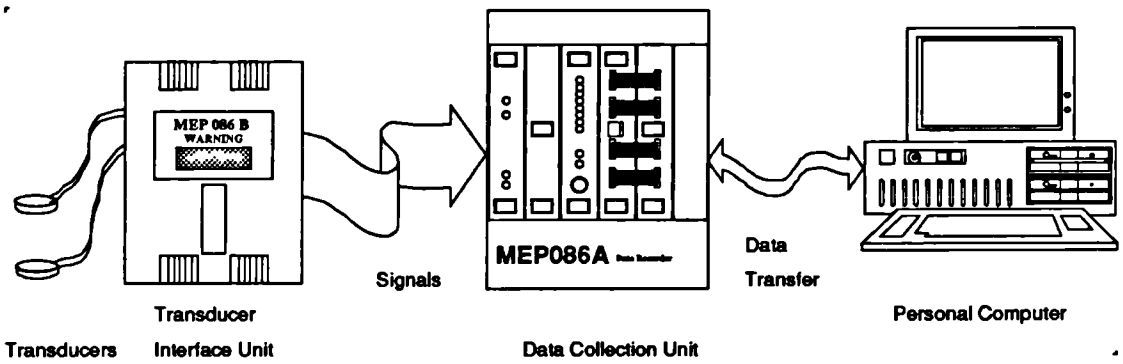

Figure 6.1 Schematic of the interconnection of the system units.

The PC is the host controller of the whole system. Software running on it provides the user interface and controls the functions of the DCU. Signals from the PC are sent via the serial port to the DCU to initiate data collection; transfer data and perform file maintenance. The DCU in turn captures signals from the TIU carried by the subject. These signals are digitised and stored temporarily in the DCU before transfer to the PC for archiving. The number of transducer signals and the rate of conversion are dictated by the user via the PC.

The reasons for using two independent units in the data acquisition system were covered in detail in Chapter 5. These were essentially the lack of a commercially available PC-based digitiser with sufficient: number of differential channels; conversion rate; and memory capacity. Although these conditions were met by VME based units, there was no available software for high-level user control. Thus there was a need to develop a considerable amount of programming skills for both low-level machine-dependent and high-level machine-independent software.

There are two main programme suites for the system, one running on the PC and one running on the DCU. These run asynchronously to one another and communicate by passing command codes and data over the serial link.

The purpose behind the design of the software for controlling these units, was to provide an easy to follow step-by-step interface for the user who might be unfamiliar with the details of PC operations. It should require the minimum knowledge of IBM PC-DOS command line syntax, and provide an infallible route to quickly obtain data once the various inter-unit cables have been installed. Also it must be general enough to provide the user with a tool for collecting transducer calibration data as well as clinical data.

For these reasons a menu-based approach was adopted. From the first screen the user sees he is offered a menu of all the valid operations for that Level in the programme. As the options from the menu are chosen further levels are entered and new menus of valid operations are offered. And so on throughout the data collection and archiving process. Each menu option is self explanatory and are easily selected by use of the cursor keys on the keyboard. Reminders and warning messages are flashed up for certain critical operations prompting the user to confirm the course of action before executing it. Thus the user is relieved of having to remember sequences of command options and is buffered from accidental loss of data.

On the PC the programme is divided into three levels On the DCU the programme has only two levels, these correspond with levels two and three of the PC programme. Figure 6.2 shows diagrammatically the system control strategy and the links of interaction between the programmes running on each machine. Initially the user executes the PC programme.

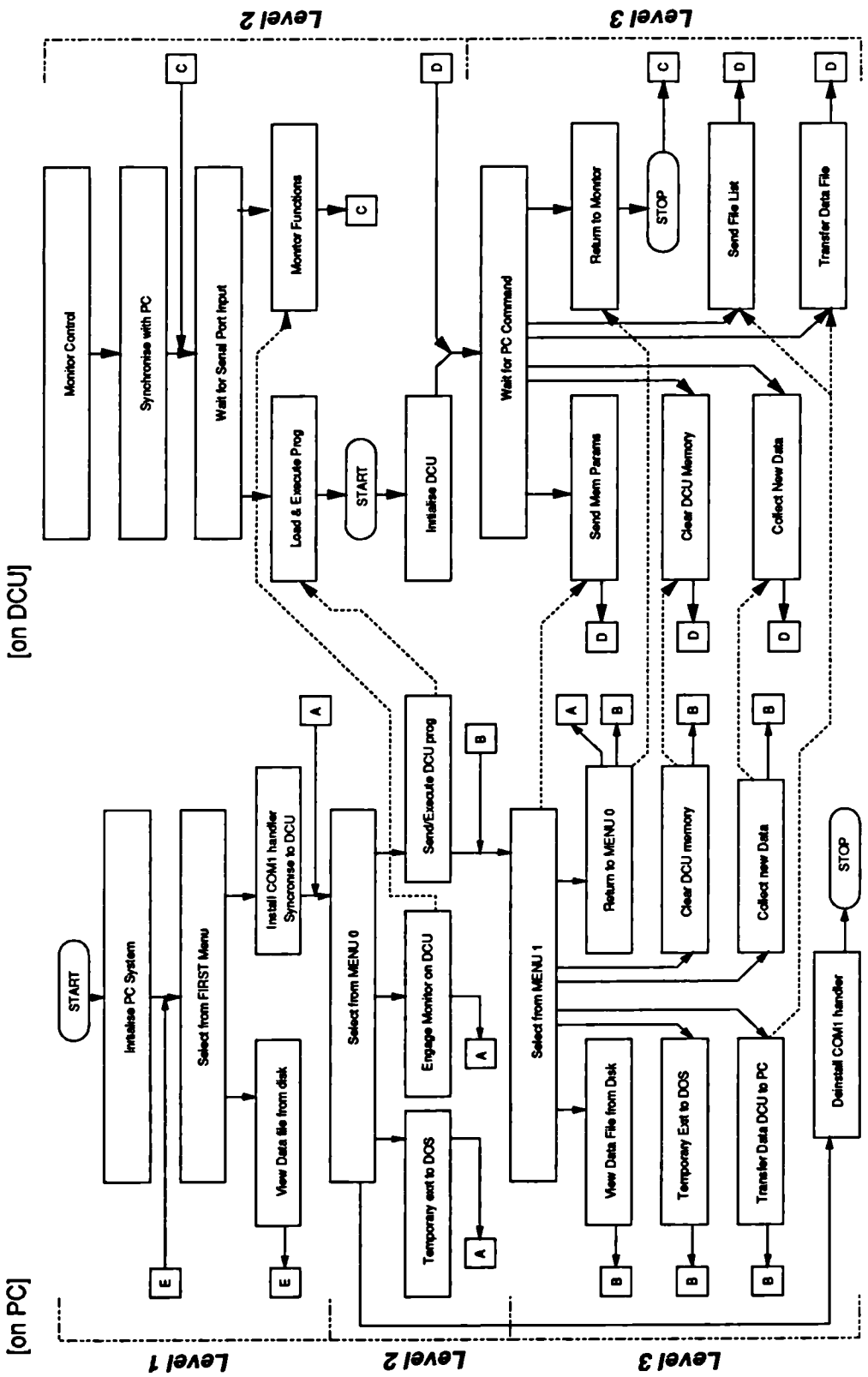

Figure 6.2 System diagram of control flow and interaction of the software running separately on the PC and the DCU. To ease confusion some flow lines have been replaced by annotated boxes on the diagram. All boxes with the same character are connected together and the arrows denote the direction of flow.

At this level (**Level1**) the user can view existing data files, or begin a new data collection session. At further levels the DCU is required to be connected to the PC.

At **Level2** the user has options of initialising the DCU prior to data collection, communicating directly with DCU's monitor programme (used only for emergency data recovery) or executing any PC-DOS function (again used mainly in conjunction with emergency data recovery). To re-iterate what was discussed in Chapter 5, the DCU has a monitor programme (PLUM) stored in EPROM that is executed when it is powered up. This is a low-level control programme that cannot perform the complex functions required for data collection. After initialisation the DCU waits for commands input via the serial port. In order for the DCU to function the PC programme must download the DCU's operating programme and run it.

At **Level3** the user has the options of Collecting new data, Transferring the data to the PC, Viewing a data file, Clearing the DCU memory, or executing a PC-DOS function. These options send specific command codes to the DCU programme which are received, checked and executed. Before collecting new data the user must specify the number of transducer signals to digitise, the digitisation rate, and any comments to be stored with the datafile. When the user is finished they can return to **Level2** and exit the session.

6.3 Level1 - File Viewing

Level1 of the software is entered on execution of the PC programme where upon the PC is initialised. The PC screen is set to its default mode and all screen handling is done in text mode rather than graphics mode. During all menu driven sections of this programme the screen cursor is turned off. The Control-C (^C) facility is enabled to allow the user to abort the programme at any time. The COM1 port is initialised to; *9600* Baud, No parity, *8* bits, *1* stop bit. The 'First' menu is then displayed on the screen. This offers options to *QUIT, VIEW A DATA FILE, RUN MEP086.* A photograph of the PC screen showing the **Level1** menu is given in Figure 6.3. Figure 6.4 shows diagrams of the programme sequences for this Level. If the *QUIT* option is selected the programme is terminated after returning the screen and serial port to their original configurations. If the *RUN MEP086* option is selected then control passes to **Level2.**

(a)

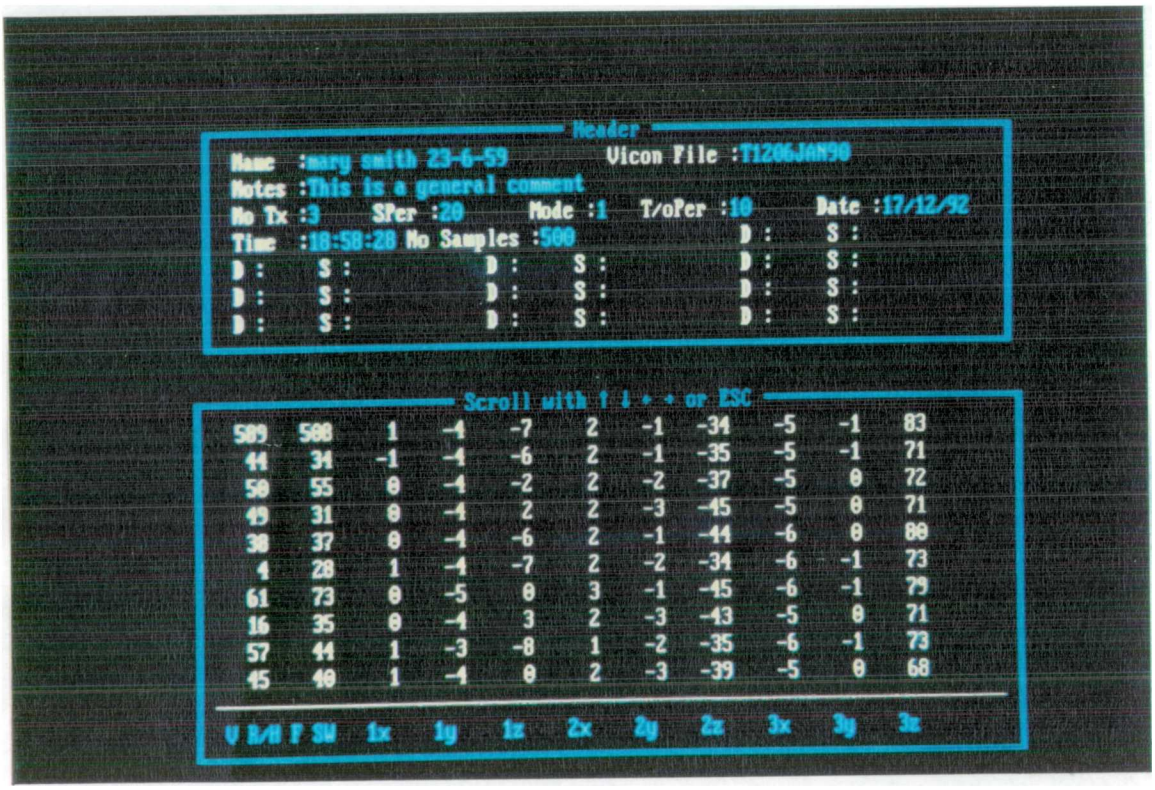

(b)

Figure 6.3 User screens for **Level1** *menu a) and a displayed data file b).*

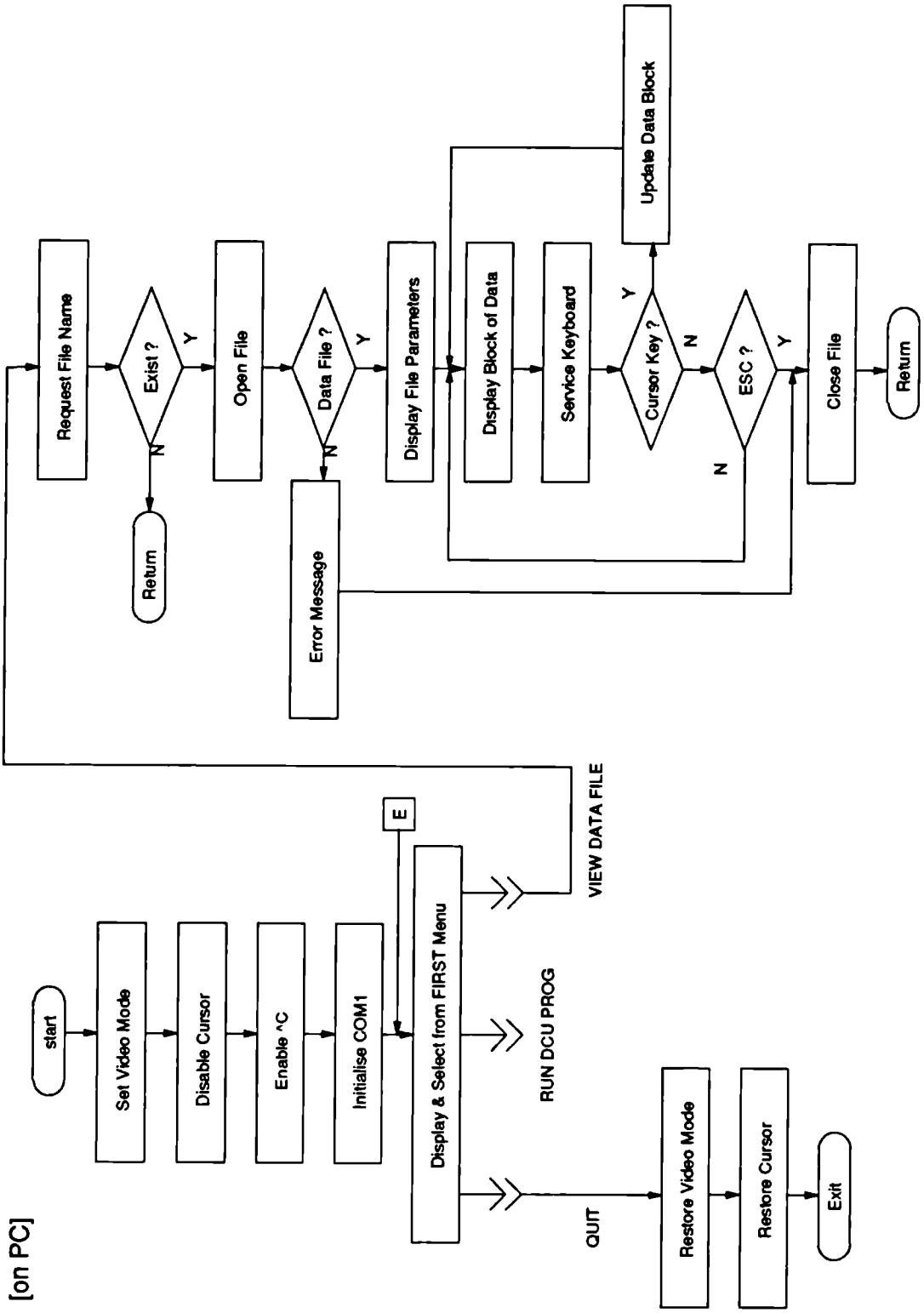

Figure 6.4 Flow chart of the programme sequence for the **Level1** *menu, VIEW A DATA FILE, QUIT, and RUN MEP086 options.*

6.3.1 View Data Files

Selecting *VIEW A DATA FILE* will display a previously saved data-file that is stored on the PC. It must be a Transducer data file and it must be in the current directory. Figure 6.3 is a photograph of the user screen with a displayed data file. Figure 6.4 is the flow chart for this operation. The expected file structure is defined in Appendix A. A message will prompt the user for a file name. Wildcards can be used to obtain a list of all files in the current directory. The list will be displayed and the appropriate file may be selected.

The file's existence is checked. Then it is opened and read to confirm that it is a transducer data file. If either of these checks fail, the file is closed, an error message written to the screen and the function is terminated. If both checks pass then the data file is opened in binary read-only mode. This mode allows both binary data and ASCII text to be read but protects against accidental overwriting of the data. A header in the file contains all the notes and experimental parameters (number of transducers, sample rate etc.) in ASCII text. These are read from the file and displayed in a panel at the top of the screen. Data is then displayed in a lower panel in columns according to the transducer and axis it refers to. The cursor keys and the Page Up, Page Down keys can be used to scroll through the data. If the ESC key is pressed the file is closed, the screen cleared and the function returns to the **Level1** menu.

6.4 Level2 - Data Collection Unit Initialisation

At this point the user is requested to check all hardware connections are in place and to switch on the DCU.

On switch-on the DCU is under control of the EPROM based monitor (PLUM) on its CPU card. At this stage, the PC programme communicates with the monitor. To synchronise the PC with the DCU the user is instructed to reset the DCU via its front panel RESET switch. The programme waits up to ten seconds to recognize the reset prompt sent from the DCU before continuing. The sequence of operations for the synchronisation of the two machines is given in Figure 6.5.

Characters arriving at the COM 1 port cause an interrupt of the PC which calls an assembly routine to store the data in a buffer. This routine is installed before communicating with the DCU. By default the DCU serial port baudrate is *9600*. When the two units are synchronised this is changed to *19200* for faster data transfer rates. The **Level2** menu (Menu O) offers the options of *QUIT, LOAD AND RUN DCU* programmes, interact with the *MONITOR,* or *TEMPORARY EXIT TO DOS.* At this point the PLUM monitor still controls the DCU. Selection of *MONITOR* will invoke a terminal emulator programme that will allow the user to interact with PLUM in emergencies. *QUIT* will cause the COM1 service routine to be de-installed and the entire programme to terminate. *LOAD AND RUN DCU* will initiate sending and executing the suite of programmes that will control the DCU. Figures 6.6 shows the user screen for the **Level2** menu.

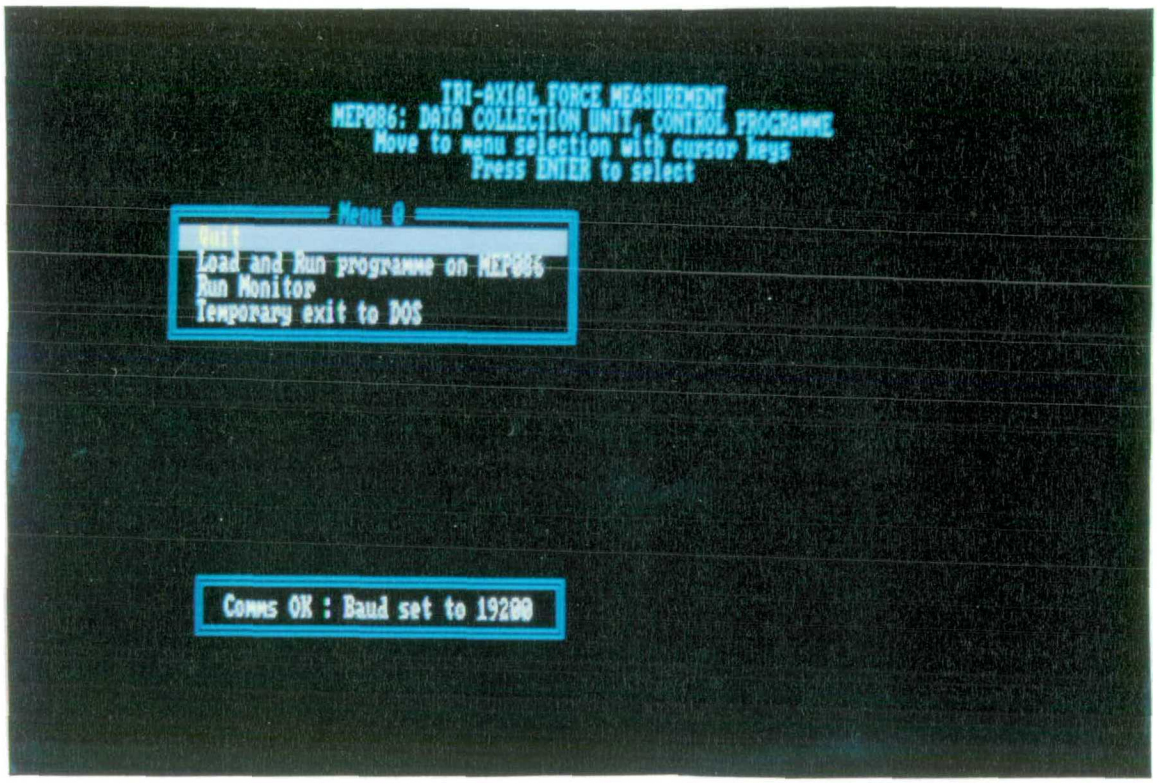

(a)

Figure 6.6a User screen for the ***Level2*** *menu.*

(b)

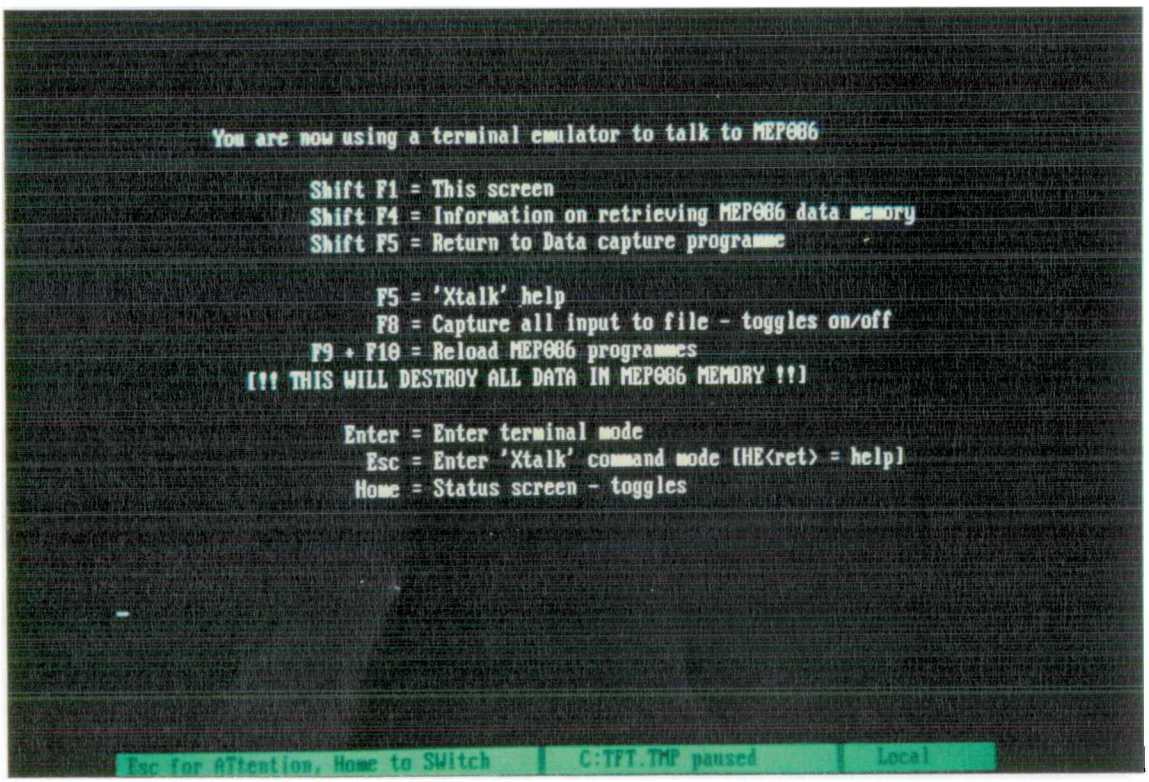

(c)

Figure 6.6b,c User screens for b) TEMPORARY EXIT TO DOS and c) MONITOR.

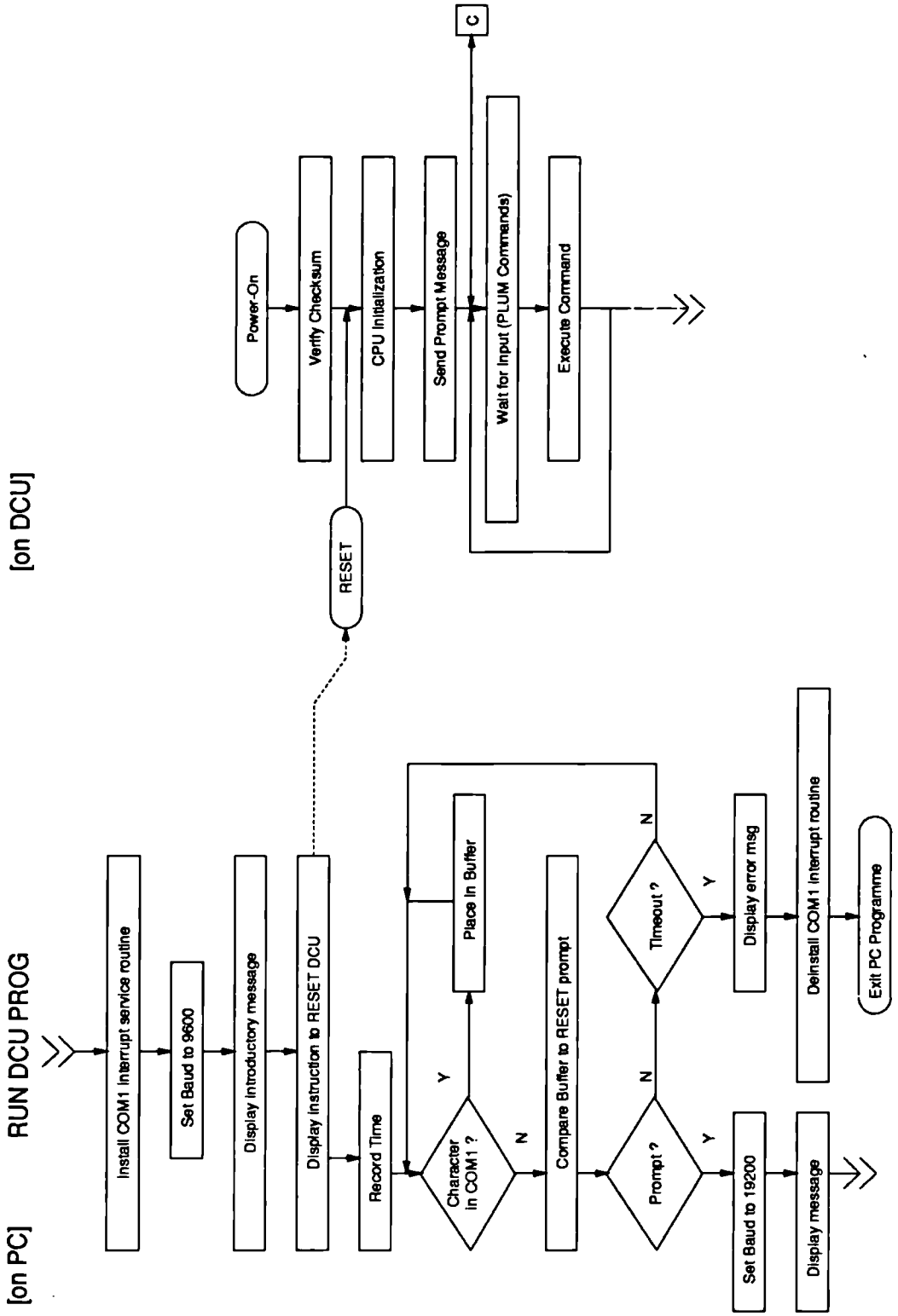

Figure 6.5 Flow chart of the programme sequence required to synchronise the DCU to the PC.

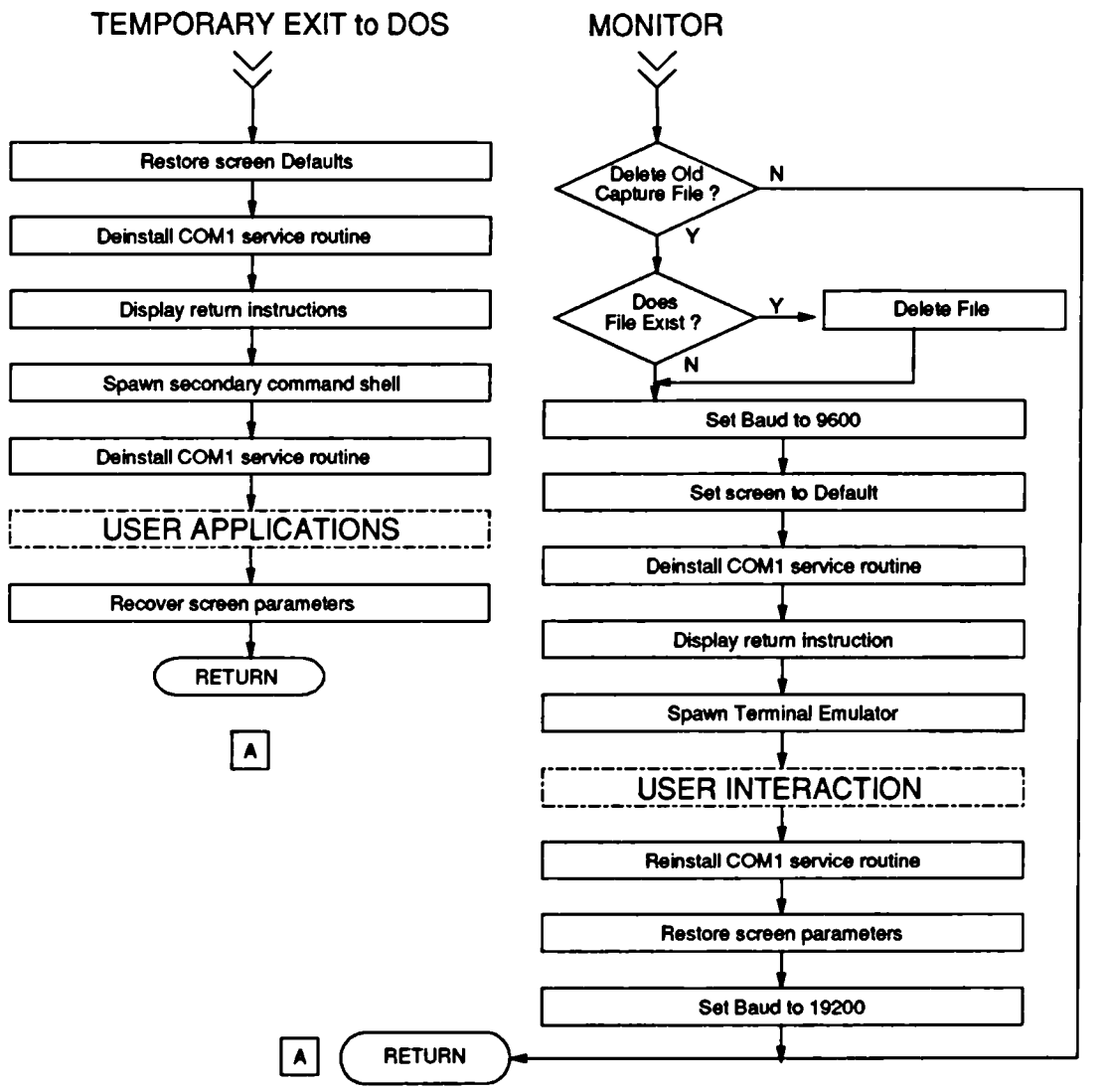

Figure 6.7 Flow chart of the programme sequence to execute a) a TEMPORARY EXIT TO DOS and b) the MONITOR option.

6.4.1 Dos Functions

In a *TEMPOARY EXIT TO DOS* a secondary command shell is generated to allow the user to execute other PC-DOS applications while the control programme stays resident in memory. A diagram of the programme sequence for this operation is given in Figure 6.7. By the user typing "**EXIT**" the shell is removed and the execution of the programme will continue from its last executed instruction. Inside the shell the user may execute any programme that may fit into the remaining memory. The COM1 service routines are removed before the shell is built to

avoid its corruption or causing a fatal error. On exit from the shell the service routine is re-installed and the screen handling parameters returned to those last in use by the control programme.

6.4.2 Monitor Functions

To interact with PLUM a terminal emulation programme is invoked under a secondary command shell. The use of this emulator may be necessary to recover data files from the DCU memory in the event of a fatal error. Figure 6.7 shows the programme sequence for this operation. A number of files were written to complement the terminal emulator, specifically for interacting with DCU. As described above the programme status is saved and the COM1 service routine de-installed before the shell is invoked. On return from the emulator, the programme status is restored and the COM1 service routine re-installed before execution of the programme is resumed.

6.4.3 Programme Transfer and Execution

Before the DCU can be used to collect data the necessary control programme must be sent to it from the PC and executed. The DCU does not have any non-volatile storage to save this programme so it must be down-loaded for every session. Figure 6.8 describes the sequence of events to effect this operation.

At this point the PC programme is communicating with the DCU's PLUM monitor. It sends monitor-specific commands to the DCU which are echoed back. These echoes are used to check that no errors have occurred.

The programme which runs on the DCU has been compiled and encoded into Motorola "S" record format and stored on the PC's disc. To send this and have it installed in the DCU, the PLUM command "LOAD" is sent. After the command is echoed the encoded programme is sent. To execute it the PLUM "EXECUTE" command is sent. On the DCU the control programme is loaded into *3* Kbytes of fast SRAM for maximum speed of execution. Appendix A contains a description of the DCU memory map. The first action the DCU programme takes is to initialise its working environment (stack pointers and memory map etc.). It then

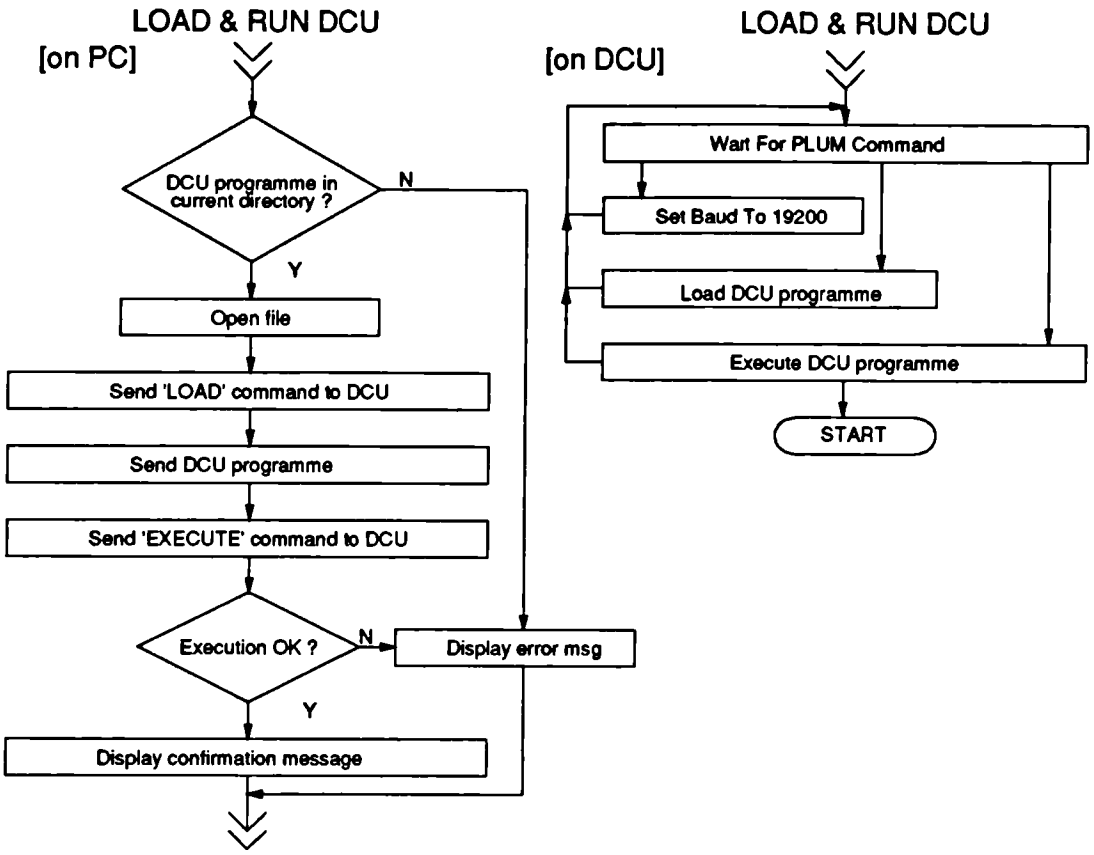

Figure 6.8 Flow chart of the programme sequence to transfer programme code to the DCU and execute it.

initialises the A/D, the data file tables and memory pointers. When these have been successfully carried out it sends a startup message to the PC. Any error in this operation returns the user back to the **Level1** menu.

6.5 Level3 - Data Collection

When the DCU programme has initialised its hardware it sends a message to the PC to indicate that it is successfully in control of the DCU. On receipt of this message, the PC programme is synchronised with the DCU programme. Commands are issued to the DCU from the PC in much the same way as with the PLUM monitor. These commands are echoed back to the PC to acknowledge their receipt.

The DCU waits for a command input from the PC, checks the validity of the code and tests for errors. When an error occurs an error number is set which defines the module in the programme where the error occurred. The handling of these error conditions is described in 6.6.

Before displaying the **Level3** menu (Menu 1) information about the memory available in the DCU is requested. The memory parameters sent are:

number of Kbytes total memory
number of Kbytes used
number of files stored
number of Kbytes free

Figure 6.9 is a flowchart of the units interaction for these operations.

Menu 1 offers the options of *RETURN TO PREVIOUS MENU, VIEW a DATA FILE* from PC, *COLLECT NEW DATA* on DCU, *TRANSFER DATA FILE* from DCU, *CLEAR MEMORY* on DCU or *TEMPORARY EXIT TO DOS.* Figure 6.10 shows the format of this menu on the PC screen before the memory on the DCU is cleared.

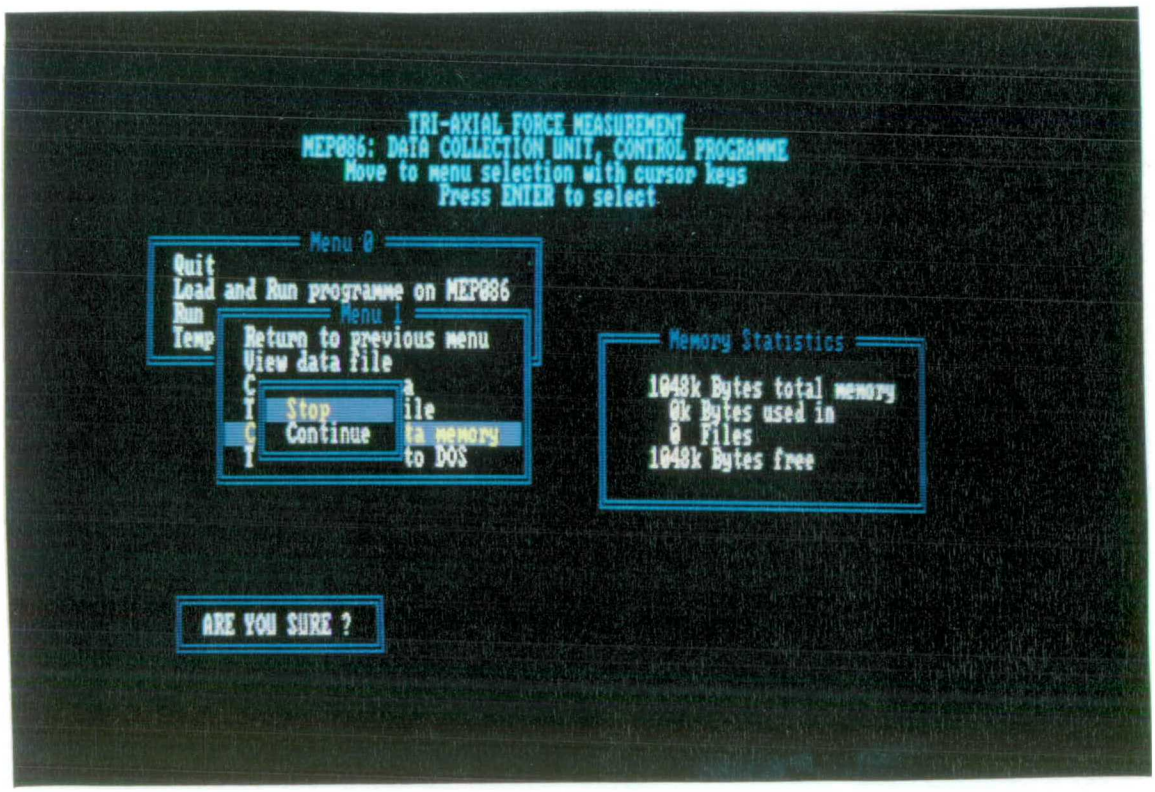

Figure 6.10 User screen for ***Level3*** *menu. A confirmation of memory clearance is requested.*

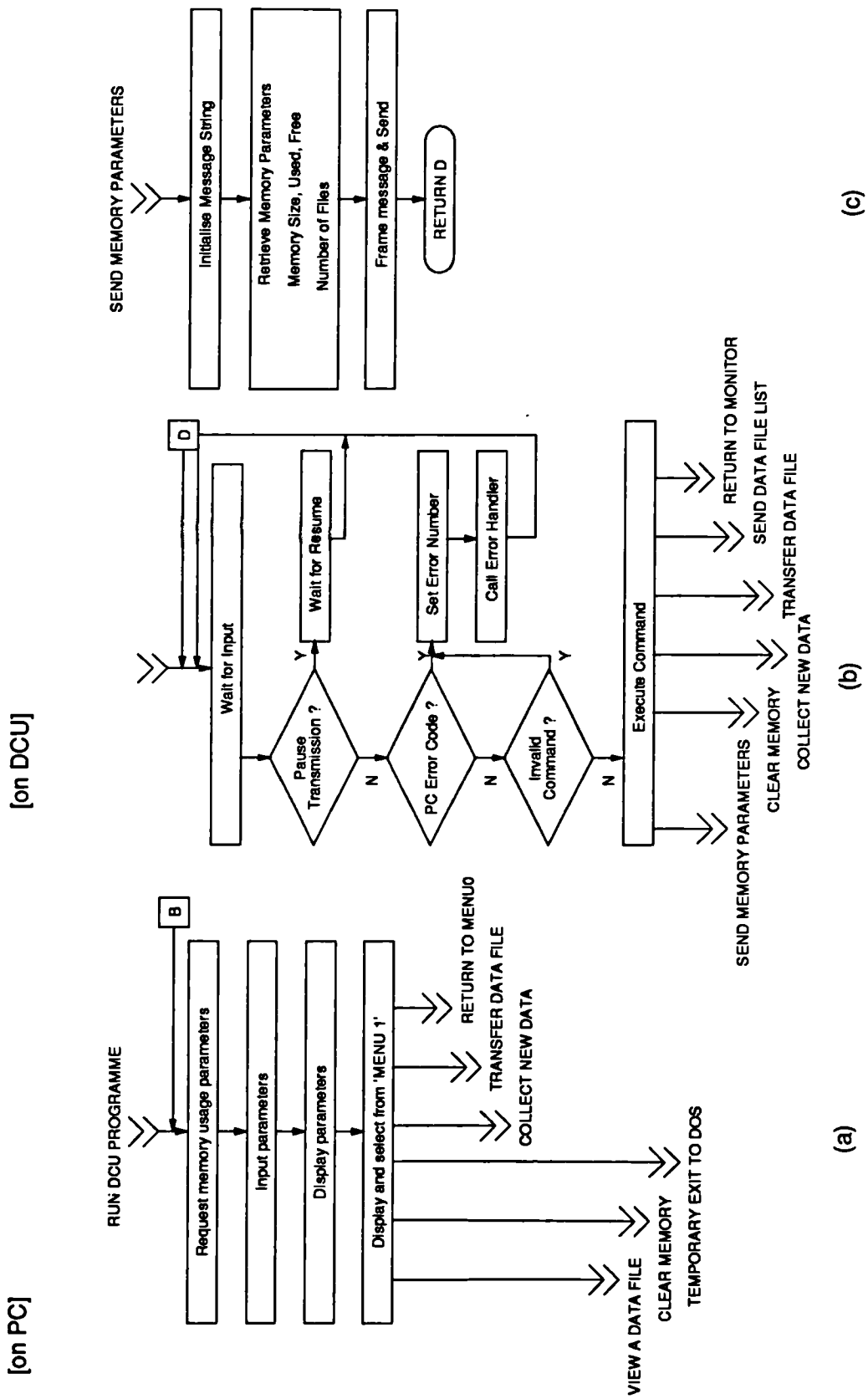

Figure 6.9 Flow chart of the programme sequence to request and execute commands on the DCU.

6.5.1 Support Functions

These functions are small relatively simple routines which act in support of the main functions of **Level3**. They are the *RETURN TO PREVIOUS MENU, CLEAR MEMORY* on DCU and *TEMPORARY EXIT TO DOS* options from the menu.

When data collection is finished the user returns to **Level2** where control of the DCU is handed back to the PLUM monitor programme. At this point data still exists uncorrupted in the DCU memory and emergency access to this data can be made through a terminal emulator package, if required. Further, if the option *LOAD AND RUN MEP086 PROG* is subsequently selected from Menu 0 this data will be overwritten by new data. Thus, before sending the *RETURN TO PREVIOUS MENU* command from the PC to the DCU the user is prompted to confirm the action. Figure 6.11 describes the sequence of this operation.

Once all data files on the DCU have been transferred to the PC, the user may clear the DCU memory ready for new data collection. Selection of the *CLEAR MEMORY* option from the **Level3** menu, begins a global delete of all data files on the DCU. Before sending this command the user is prompted to confirm the action. On the DCU a table is kept that holds pointers to where each of the data files are stored in its memory. On receipt of the *CLEAR MEMORY* command, the memory itself is not cleared directly, but the table entries and memory pointers are reset to default values. Subsequent data collections will re-allocate the pointers and overwrite the current data. Figure 6.11 shows the sequence of events for this operation.

The selection of the *TEMPORARY EXIT TO DOS* option is executed in the same way as described in 6.4.1. Its main uses in the module are; to check that duplicate filenames are not given when files are transferred to the PC; and to make disc space available for data files - which may be up to *1000* Kbytes in size.

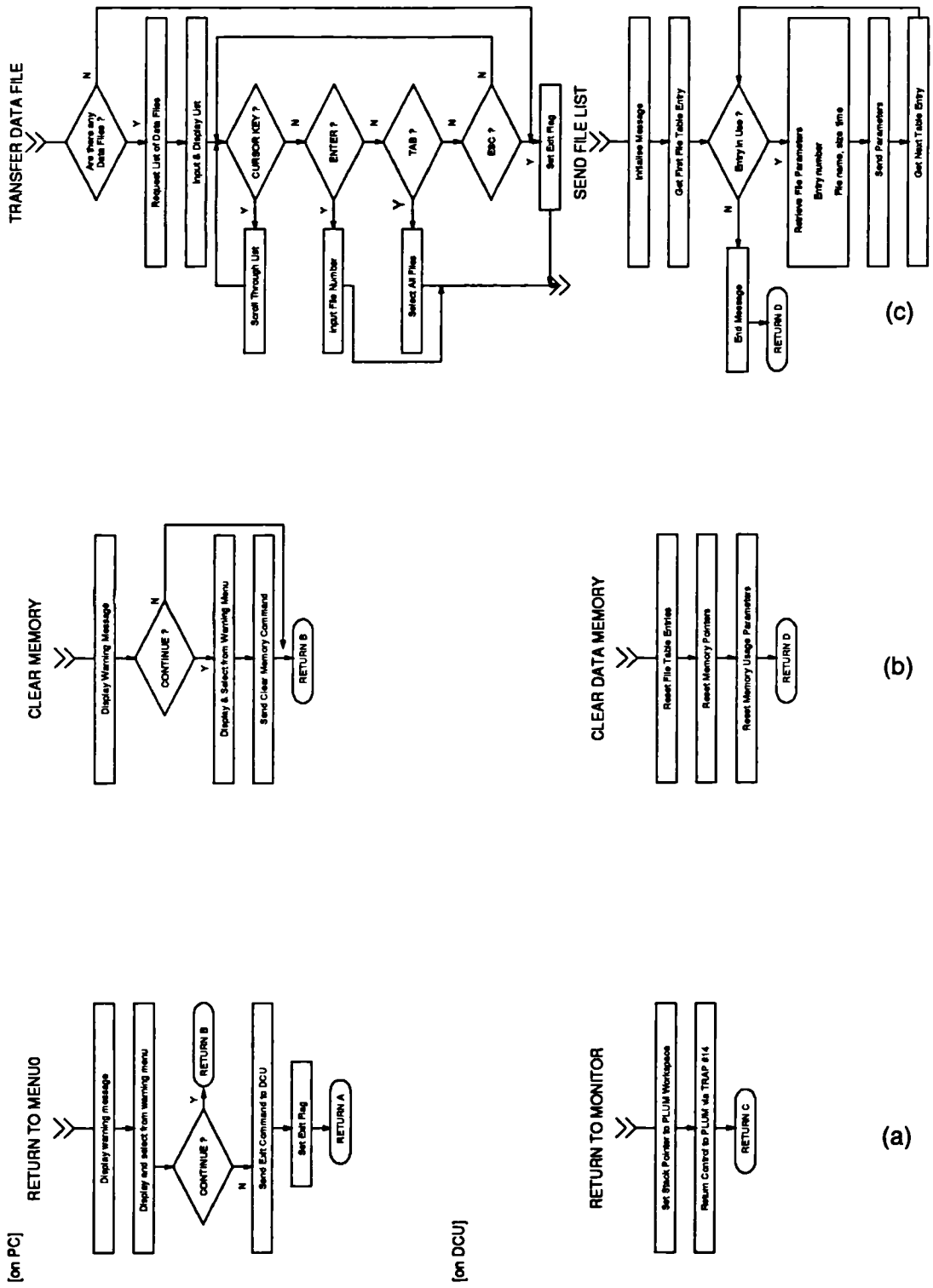

Figure 6.11 Flow chart of the programme sequence to, return to **Level2** *(Menu 0) a), CLEAR MEMORY on DCU b), and TRANSFER A DATA FILE to PC c).*

6.5.2 Transfer Data Files

Data captured on the DCU must be transferred to the PC for archiving and processing. Many data files from individual clinical trials may be temporarily stored on the DCU. Before requesting the transfer of any of these data files from the DCU, it must be indentified from the others currently in memory. On selection of the *TRANSFER DATA FILE* option from the **Level3** menu, the *number of files stored* parameter [see 6.5] is evaluated. If there are no files stored then the option is terminated. If there are files present then a list of these files is requested from the DCU.

The list sent by the DCU contains the file number, name, creation time and size of each file in its memory. To form the list the DCU scans through its file table in sequence. Each file's sequence number (file number) and size are copied from the table then the file name and creation time are retrieved from the file header in memory. This continues until an unused table entry is met. These parameters are then encoded and sent to the PC. Figure 6.11 describes the sequence of events for this operation.

The file list is displayed on the PC screen and the user may scroll through the list using the cursor keys. Figure 6.12 shows the screen format of this list. By pressing ESC the *TRANSFER DATA FILE* option is aborted. Pressing TAB selects all files, in numerical sequence. Pressing ENTER allows the user to type the file number of the file he wishes to transfer. The sequence of events for the transfer operation of the selected file(s) is described in Figure 6.13.

Before transfer takes place the disc space in the current directory of the PC is compared to the current file size. If there is not enough free space then the process is terminated. (N.B. the Menu1 option *TEMPORARY EXIT TO DOS* can then be used to make disc space available). The user is then prompted for a filename under which the transferred file will be archived to disc. If this filename is already in use then the user is offered the choice of overwriting named file or aborting the transfer process.

The named disc file is opened and an identifier written into it. This identifier is recognized under the *VIEW DATA FILE* option and infers that the present file is indeed a DCU data file.

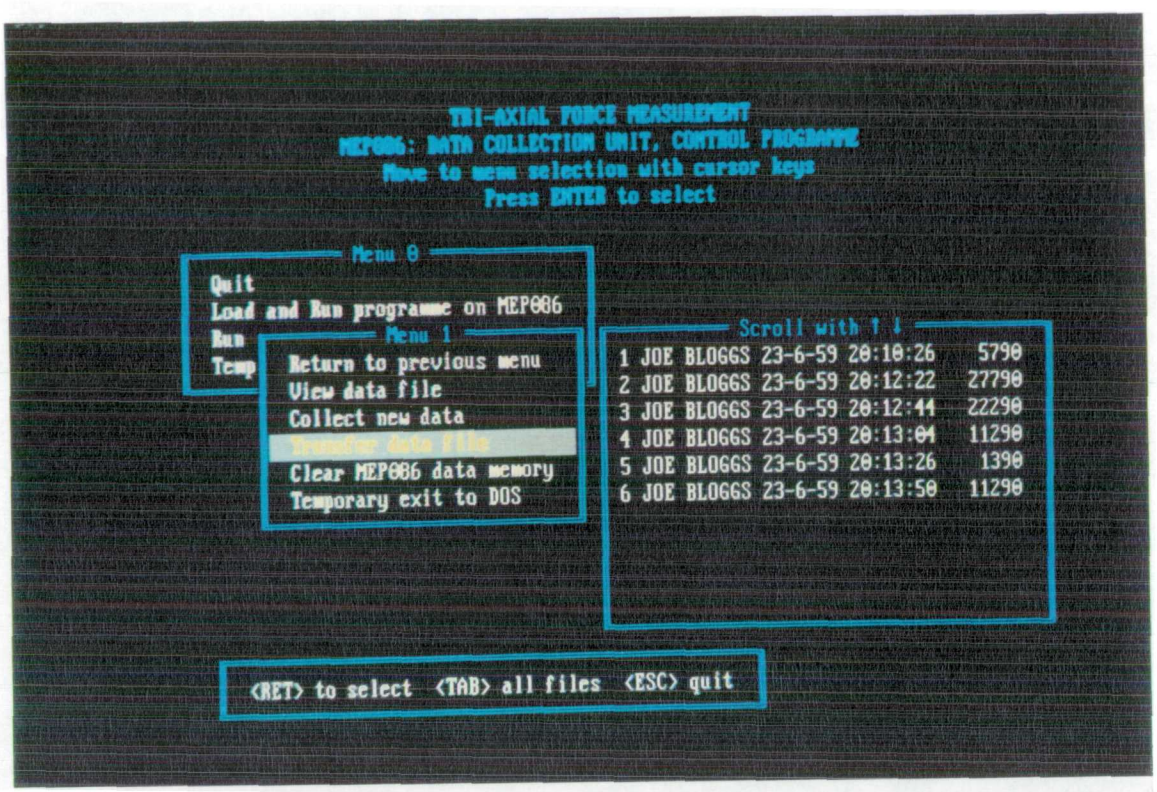

Figure 6.12 User screen listing files stored on the DCU, ready for transfer to the PC.

A transfer command is then sent to the DCU along with the file number of the first of the selected files. The header of this numbered DCU file is transferred first and written to disc, followed by the file's data section. On the DCU the header of a transferred file is stored as an ASCII string and the file's data is stored as binary characters. Now, control of the communication link between the PC and DCU, over which the files are sent, is effected by the sending of certain binary characters. Thus, to avoid characters in the file's data section looking like control characters all data is coded before it is sent and decoded on arrival at the PC.

On the PC, disc access is much slower than memory access. Also, each write to the disc must be precursored by a head positioning manoeuvre. Therefore when writing small amounts of data, relatively large time overheads are incurred. Thus, the incoming decoded data from the DCU is saved to a large temporary buffer (*32Kbytes*). When this buffer is full it is written to the disc file, and new incoming data is allowed to fill the buffer again. When the end of transmission is met the buffer is emptied to the disc file and the disc file closed. During any file transfer the PC may request a pause in the transmission while it writes the file to disc. The DCU then waits for a 'resume' command.

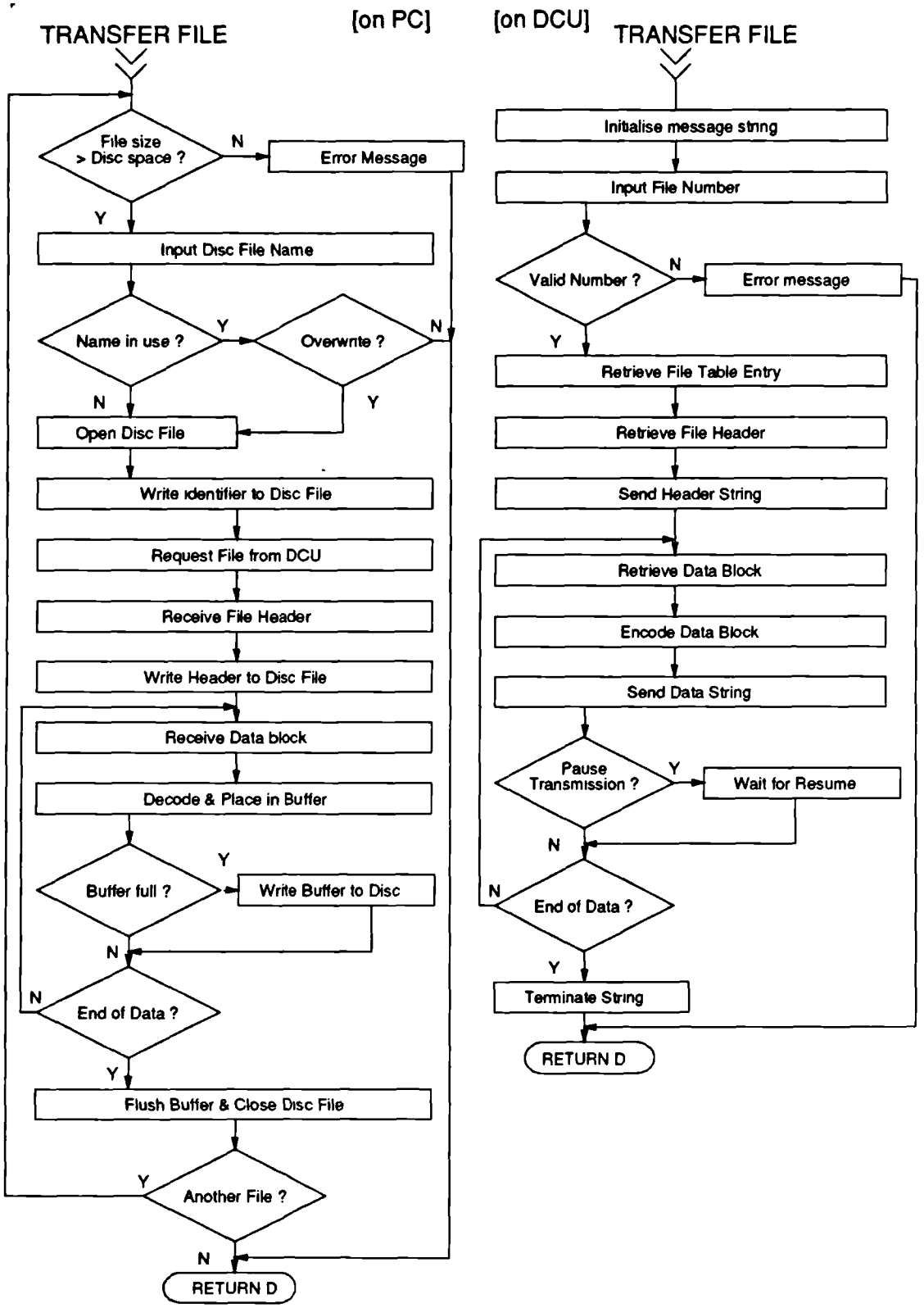

Figure 6.13 Flow chart of the programme sequence to TRANSFER A DATA FILE from the DCU to the PC.

If a single file was selected from the list then the *TRANSFER DATA FILE* option is terminated. If all files were selected then the file number and size of the next file in the sequence is evaluated. The disc space necessary to archive it is assessed, and if space permits, a transfer command and the file number is sent to the DCU. That file is then sent and archived. And so on until all files are transferred.

6.5.3 Collect New Data

There are two phases to initiating collection of new data. The first is the input of values for the experiment parameters. The second is the transfer of these parameters and the provision of a trigger to begin sampling. At first a software module is called which controls the input of parameter values.

A panel showing the parameters and their default values is displayed on the screen. The user may cycle through the parameter fields by use of the up and down cursor keys. Figure 6.14 shows the screen format of this panel while Figure 6.15 describes the sequence of operations in this routine. To edit a field the user positions the cursor in the field and presses the space bar. The programme then saves the region of the screen that is about to be edited. This region is replaced once editing is ended and the amended text is written into the field. The fields are classed according to the type of parameter to be input and the way in which the parameter is implemented. **Notes** and **name** fields are input without checking. The **digit** fields are checked against limits that are predefined. If the input exceeds these limits the nearest limit is used instead of the input. The *Sample Period* and *Timeout Period* are implementation dependent and are restricted to values selected from a menu. When all editing is finished the user presses INS to collect new data using the new parameter values. The user can abort the data collection process by pressing ESC (N.B. all edited fields are saved).

The second phase is a routine which controls the collection of new data using the current parameters. Figure 6.16 describes the sequence of operations in this routine.

To initiate the collection of new data the PC sends a command code. On receipt of the command the DCU checks that there is sufficient free space in its memory for at least one sample plus the file header. If there is not, an error is flagged, the process aborted, and control returns to the **Level3** menu. Otherwise the new

parameter values are sent to the DCU. These parameters constitute part of the header for that file. The DCU then finds the next unused file table entry but does not allocate it until successful completion of the experiment. Memory pointers to the files header and data space are calculated. The parameters are written into memory and the PC is informed that the A/D is being initialised.

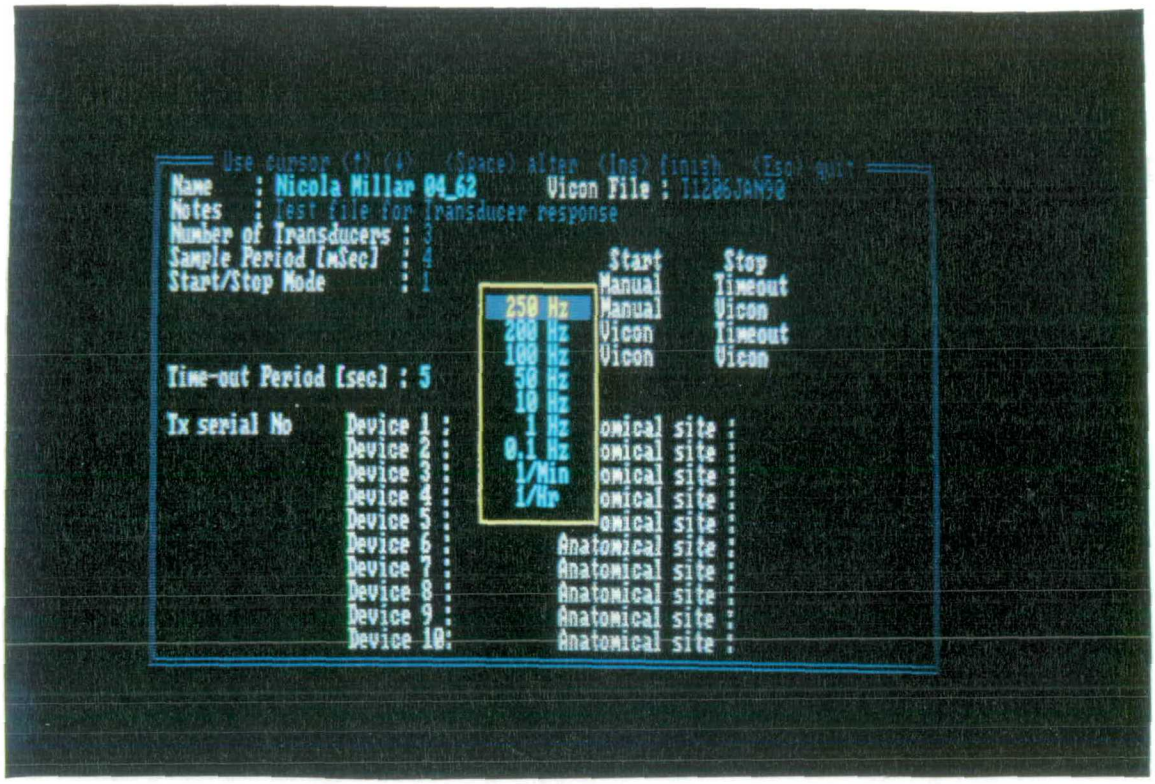

Figure 6.14 User screen for inputting new parameter set. Defaults shown in low-light colours. New parameter values set in high-light.

From the parameter set the number of A/D channels to be used is calculated. The A/D is then initialised to operate in the **transient** mode with end-of-conversion determined by polling of its status register. **Transient** mode is where each active channel is converted in sequence at the maximum possible rate. Then this process is repeated at the next sample interval. Conversions are initiated by software using the real-time-clock (**RTC**) on the CPU board to provide interrupt at the required sample interval. On each RTC interrupt a service routine sets a flag to indicate that a period has passed. The CPU reads this flag, clears it and starts another conversion. The interrupt service routine and A/D control routines were written in assembly language for speed.

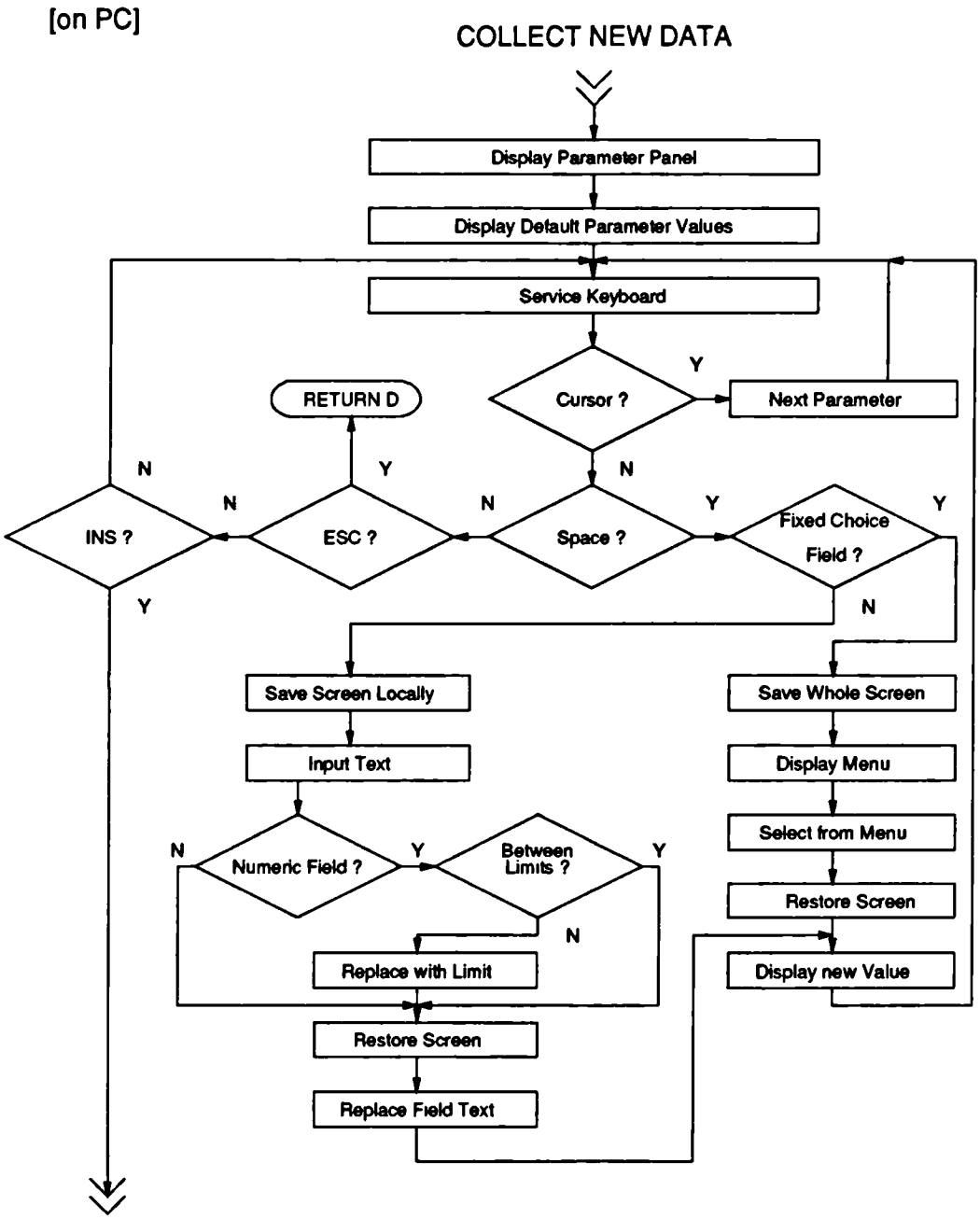

Figure 6.15 Programme sequence for inputting new parameter set.

After initialising the A/D the time-out period is set and the **start/stop** (trigger) mode determined. The DCU then waits for a trigger. The start trigger can be issued by an external system (VICON kinematics measurement system) or by the PC, on a key press. The trigger mode is specified as one of the experiment parameters.

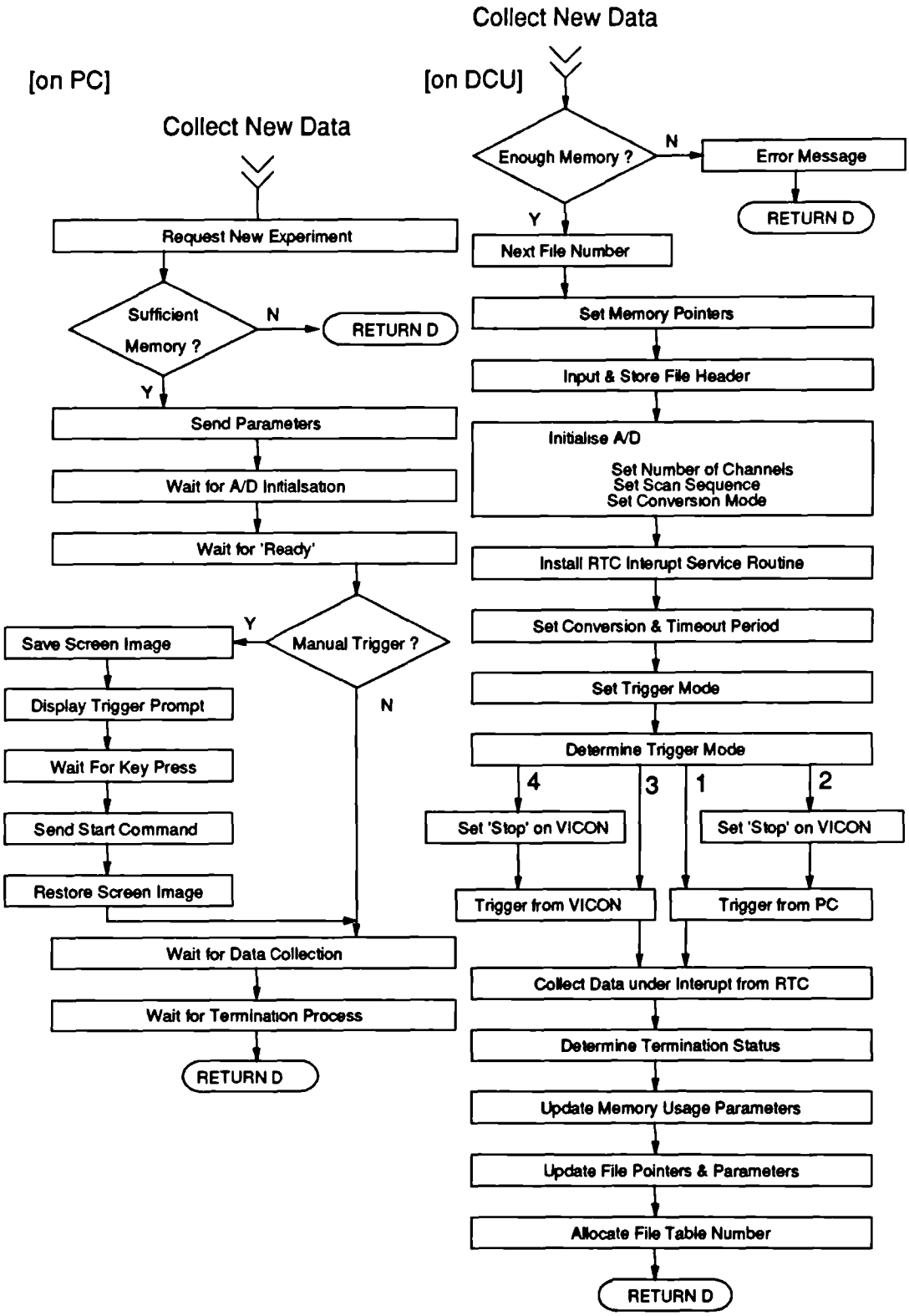

Figure 6.16 Programme sequence for controlling the data conversion process.

The VICON kinematics measurement system records the body position, limb motion and joint angles of the patient being studied [see 5.4]. In order that the kinematic data set can be correlated with the interface stress data set, the footswitch signals from the patient are recorded by both systems. Additionally, the collection of data on both systems may be started by a signal from the VICON - called the RUN/HALT signal. If the trigger mode requires a manual start the user is prompted to press the PC's enter key for the start trigger. A VICON start calls an assembly routine to monitor the VICON RUN/HALT signal, input to channel *1* of the A/D, and returns a flag when the channel value rises above *400* Hex (half the signal range).

On receiving a start trigger, the DCU sends a confirmation to the PC, whereupon the user is informed that data collection is in progress. An assembly routine is called to control the A/D and RTC for the experiment duration. On successful completion it returns a termination status which indicates the reason for the end of sampling. The DCU then informs the PC what the cause of termination was - either VICON stop; timeout; or out of memory. On correct termination the file table entry is allocated and the file table parameters updated. Each file table entry contains 5 parameters:

file number
header pointer
data pointer
end pointer
file size

The memory usage parameters and the experiment duration are also updated.

6.5.4 View Data Files

When this option is selected the user is offered the same route to viewing previously archived data file as described in 6.3.1 .

6.6 Error Trapping

The detection of unexpected or erroneous input and subsequent orderly recovery without data loss, is a major requirement in any software package. In this instance where two machines are attempting to maintain synchronisity while gathering and transferring unique data it is paramount. Not only might an error cause a loss of data that may have taken days of organisation to collect, but there would be great inconvenience to the patient under study.

Therefore, in any routine in both PC and DCU programmes when input is expected, the incoming data is checked against both its expected form (where this is possible) and also against the system error code. If the input is not what is expected then on the DCU the global error parameter 'errno' is set to a given value, dependent on which part of the programme the error was detected in. The ERROR function is then called and passed the given error number.

Figure 6.17 shows the sequence of operations carried out when unexpected input is received by the PC and the DCU respectively. The DCU programme is only running a single tier deep thus on an error it returns to await another command sent from the PC. On the PC the programme may be several tiers deep and an error may require a return up more than one tier. The ERROR function handles the recovery from the error condition to a controlled state. It returns a status code to the calling routine which in turn aborts returning the status code to its calling routine. This status code determines the action taken by the parent routine depending on the seriousness of the error. Figure 6.17 also describes the arbitration of the code significance by the PC programme. The difference in error number passing on the DCU to that on the PC is so that if the stack checking routine on the DCU detects an error the stack can be reset and the error recovered from in a predictable way.

The principle operations of ERROR on the PC and DCU can be seen in the flow chart of Figure 6.18. In the PC programme the error number passed to the ERROR function is checked if the number is < 99 then the error occurred on the PC. If so, the input buffer is flushed. Only certain error conditions on the PC need to notify the DCU of their occurrence. A flag is set if this is necessary and the PC sends a system error code to the DCU. The PC then displays a message for the user, sets a status code and sends a continue code to the DCU before returning to

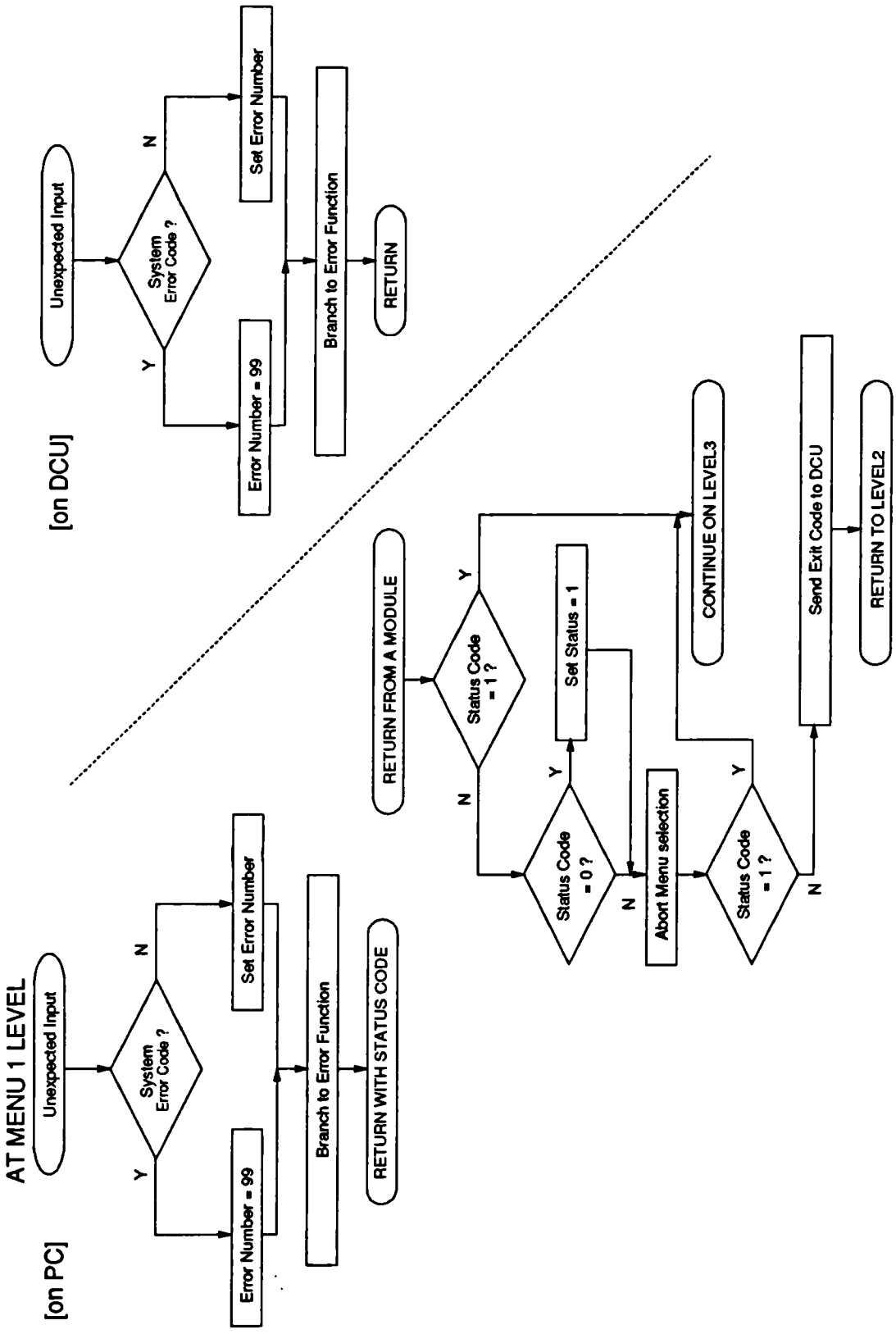

Figure 6.17 Programme sequence when unexpected input is received on either unit.

its calling function. If the number is *99* then the error occurred in the DCU. The PC waits for an error number to be sent to it. If this number is *200* then a stack overflow occurred on the DCU so the status code returned by ERROR is *-1*. If the number sent is < *200* the appropriate message is displayed, the status code set and the continue code sent back to the DCU.

On the DCU the error number passed to the ERROR function is checked. If it is *99* the error occurred on the PC and the DCU waits for the continue code before returning to its calling routine. If the error number is < *99* the error occurred on the DCU during an input. The input buffer is flushed, the system error code is sent to the PC followed by the error number *100*. It then waits for the continue code before returning to the calling routine.

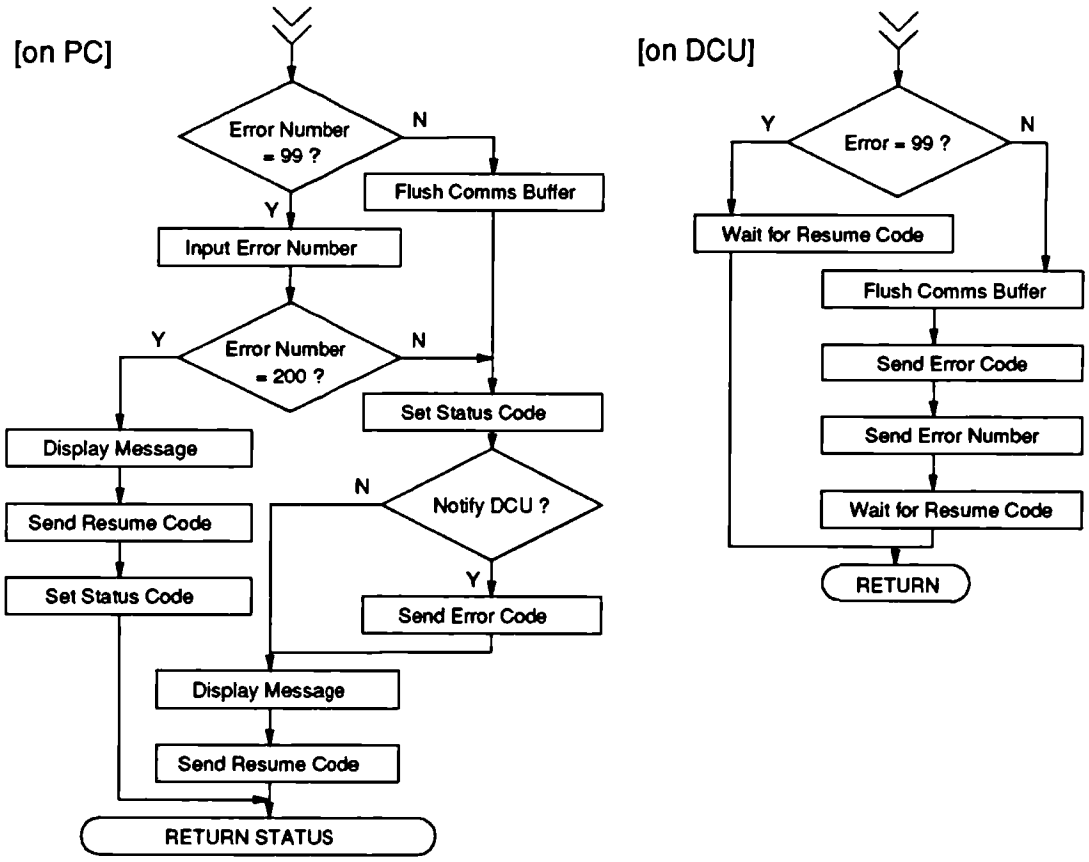

Figure 6.18 Principle operation of the error handling routine.

6.7 Discussion

The software described in this chapter was developed to control the data acquisition hardware and to manage the acquired data. The operation of the many programme modules which make up the system software are detailed. Listings of the code written for each of the modules discussed are recorded elsewhere [6.1]. Each of the modules was coded and tested individually. The entire system software was also tested and executed without errors. It has been used successfully to acquire transducer calibration data and subject trial data.

Chapter 7
Clinical Evaluation

7.1 Introduction

Subsequent to calibration and performance assessment of the transducers, it was felt necessary to verify their appropriateness and to identify possible application problems, via two short clinical evaluations. In particular this would provide patient/subject feedback and design information on the efficacy of the mounting methodologies used.

This chapter describes the two evaluations which were carried out at Kings College Hospital (Dulwich)[1].

The first was a short rudimentary investigation to set the ground work for a long term study being carried out by other researchers at the Hospital. A method of instrumenting a below knee supracondylar patella-tendon bearing (**PTB**) socket with several transducers was developed and measurements were made of the interface stress patterns over several gait cycles. The mounting technique was appraised and the stress patterns were correlated to gait events using footswitches. These findings were compared to those of other researchers in the field. Two different foot/ankle assemblies were attached to the prosthesis and measurements taken. A comparison of the gait cycle interface stress patterns related to each foot/ankle assembly was also made.

The second evaluation was not related to the measurement of interface stresses in lower limb prostheses but demonstrated the effective use of the devices to measure shear stresses at other body/support interfaces. In this case a device was mounted in a shoe insole. This was part of the preliminary work to assess the suitability of the transducer to quantify interface stress patterns under diabetic feet, during gait. In the evaluation study the plantar stresses of normals were recorded to

1 Kings College Hospital (Dulwich), East Dulwich Grove, London SE22 8PT, UK

establish baseline data for the Diabetic study. The investigation was instigated by a colleague (**Hosein and Lord[1991]**), with the author involved as a technical adviser.

For both evaluations attention was focussed on: transducer robustness; identifying problems in the mounting regime; and observing typical stress magnitudes, timings and spectra. No conclusions were sought as to the clinical significance of the observed patterns as the data sets were too few.

7.2 Evaluation Study 1 - Limb/Socket Stresses in Amputees

This study was performed to assess: the robustness of the transducer; to identify possible problems with their mounting and system inter-connections; and observe the magnitude and bandwidth of clinical stresses. One patient was studied. The patient was a 62 year old male, weighing 70kg, and had had a left below knee amputation sixteen months earlier. He was an active retired person who walks *2-8km/day* and wears his prosthesis for *8-12hrs/day*. The limb he was supplied with was a supracondylar PTB socket with a Multiflex foot/ankle assembly (**Chas.A.Blatchford & Sons LTD**).

The proposed sites for measurement of shear and normal stresses at the limb/socket interface were based on considerations of the general pressure-sensitive and pressure-tolerant areas of the limb **[Rae and Cockrell 1971]**. The areas chosen are those known to be pressure-tolerant and will carry the greatest stresses. With the aid of the patients prosthetist five sites were chosen for the transducers. These were:

the medial and lateral femoral condyles
the popliteal
and the medial and lateral paratibials.

These sites are similar to those used by **Rae and Cockrell [1971]**, **Pearson et al [1973]** and **Burgess and Moore [1977]**.

The procedure outlined below was followed for fabricating a test socket and mounting the transducers. A fresh casting was taken of the patients residual limb and a plaster positive made. At this stage of the prosthetic fitting process the wrap cast was normally destroyed to recover the positive. This was a potential problem for

a study proposing to look at the effect of rectification variables on the interface stress patterns. However, with care in some cases it is possible to recover the wrap cast and make copies of the positive.

The standard rectifications were effected by the prosthetist as per the patient's records on file. A pelite liner was prepared and fitted to the rectified positive. Five transducer blanks were fixed to the Pelite with double-sided tape at the chosen measurement sites. The orientation of the blanks were set to give: a positive X axis indication for a proximal to distal stress vector along the longitudinal axis of the socket shank; a positive Y axis indication for stress vectors tangential to the socket circumference in an anti-clockwise sense (as viewed from above); and Z axis indications for radially applied stress (i.e. orthogonal to the plane of the interface). These orientations were aligned by eye and therefore the X and Y axes carried an angular uncertainty. It was estimated at the time that this uncertainty was likely to be less than *11°*. The placement of the blanks in order to achieve good location with anatomical sites, was effected by the prosthetist visually comparing the positive and the residual limb. Again this was an inexact process with estimated errors of *±2-3mm.*

After the drape forming process, the blanks were removed and the recesses trimmed. This later procedure was difficult to perform, especially for locations deep inside the socket, where visual inspection is limited and manual dexterity is required. Circular sections were cut from the Pelite liner at each transducer site. These were trimmed to a smaller diameter so that when mounted on the transducer there was a small clearance between the disc and the surrounding liner (*approximately 1mm*). This aided in isolating the stresses applied to the site. Access holes for the transducer leads were cut through the socket wall and each transducer was mounted. A brief inspection was made to ensure that there was sufficient freedom of movement for the normal section guide pins and the shear section disc displacement. The liner was then inserted and the pelite disc sections bonded to the top of each device.

The patients standard foot/ankle assembly (Multiflex) was fitted to the shank of the prosthesis. A thin cotton stocking was worn over the residual limb which was the patients normal practise. After the patient had donned the socket, final alignment and length adjustments were made by the prosthetist. Two footswitch pads were placed under each foot, one at the dorsal edge of the heel and the other just

forward of the ball of the foot. These switches were OR'd together [see 5.3] so that a *high* to *low* signal transition occurs when the heelstrikes and a *low* to *high* signal transition occurs at toe-off. The transducer and footswitch leads were secured in place by cloth tape (Micropor - 3M Inc), ensuring that there was sufficient slack for full limb movement during gait.

A fifteen metre length of carpeted corridor was commandeered as a walkway and the patient was allowed to walk a few lengths to accustom himself with this particular prosthesis. When he felt comfortable he was asked to walk the fifteen metres at his normal walking pace. Interface stress and footswitch data were collected at *50Hz* over the twenty second period it took to complete one length of the walkway. The signal cable was 'played' out behind the patient to minimise drag and the possibility of entanglements. The walk was repeated five times and five sets of data were collected.

Without removing the patient's limb from the socket the Multifex foot/ankle assembly was exchanged for the Quantum (**Vessa LTD**) foot/ankle assembly. The necessary length and alignment adjustments were made by the prosthetist. Again the patient was allowed some time to become familiar with the prosthesis before the above series of walks were repeated.

As no clinical relevance was being assigned to this data Figure 7.1 and Figure 7.2 show example data sets from sites which show a marked change in stress pattern with a change ankle/foot assembly. The data corresponds to the popliteal and lateral paratibial sites respectively. The first part of each figure shows the stress vector components and footswitch information recorded with the Multiflex foot/ankle assembly fitted. While the second part shows data recorded when the Quantum foot/ankle assembly was fitted.

The third data set of the series of five walks recorded is used as the example data of the figures. The first three steps of each walk were disregarded as this was the acceleration phase of the walk. Only steps four to nine of the walk are shown in the figures.

Without seeking to explain in detail or place too much clinical relevance on this data, a few general observations can be made. Both sites were regarded as areas intended for weight bearing. The normal stress at the popliteal site exhibited a

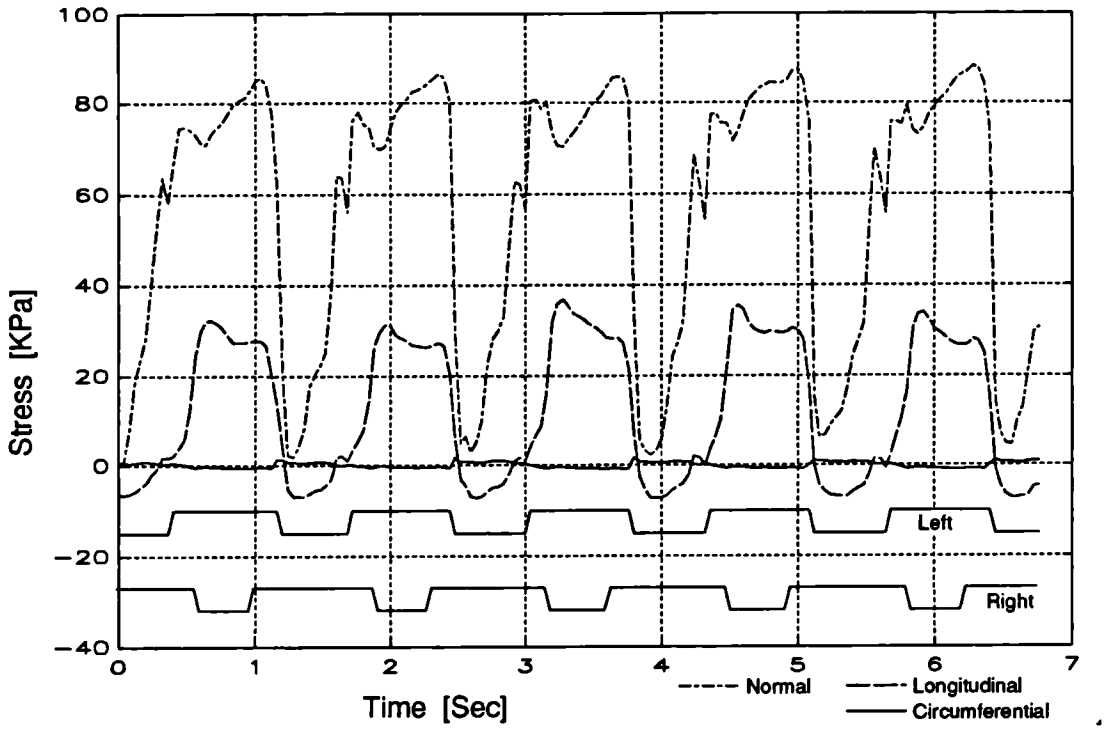

(a)

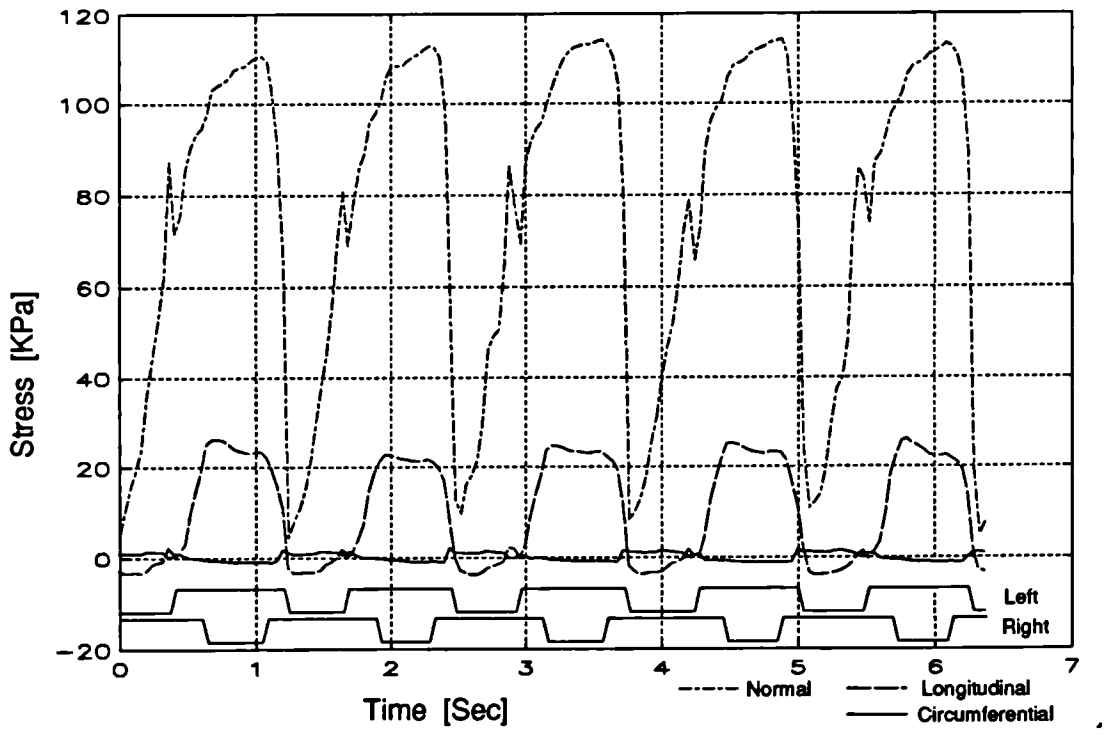

(b)

Figure 7.1 Interface stresses between residual limb and socket at the popliteal site. The patient was fitted with a below knee supracondylar PTB socket and Multiflex (a) and Quantum (b) foot/ankle assemblies.

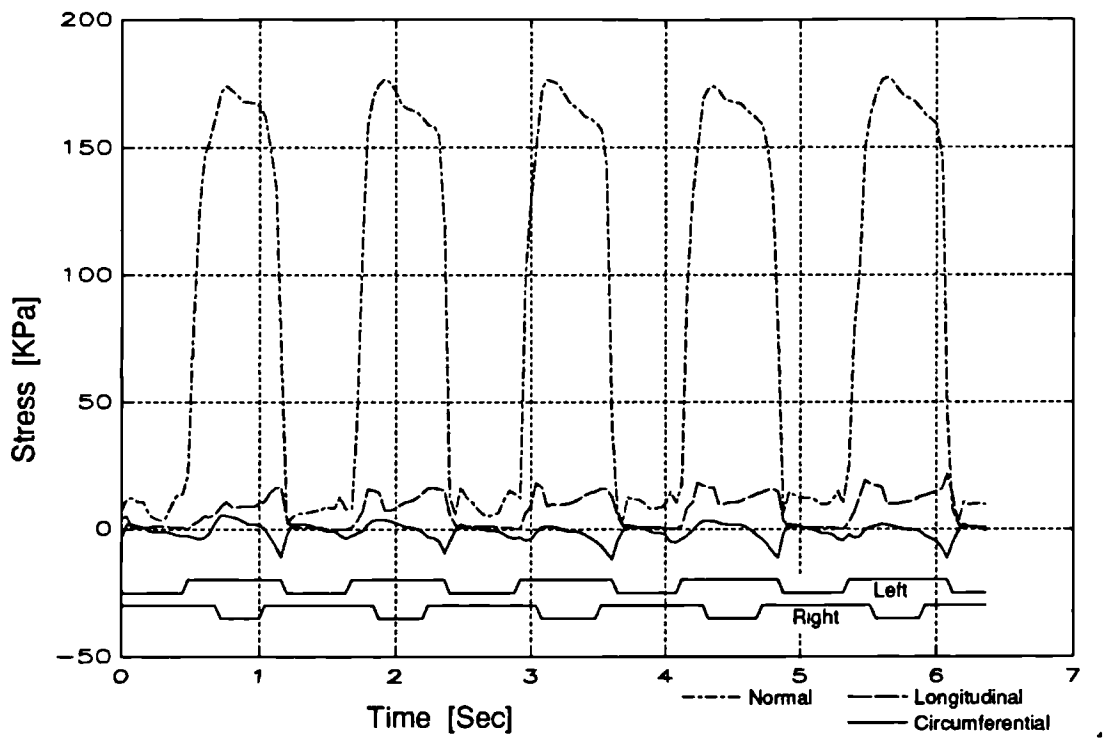

(a)

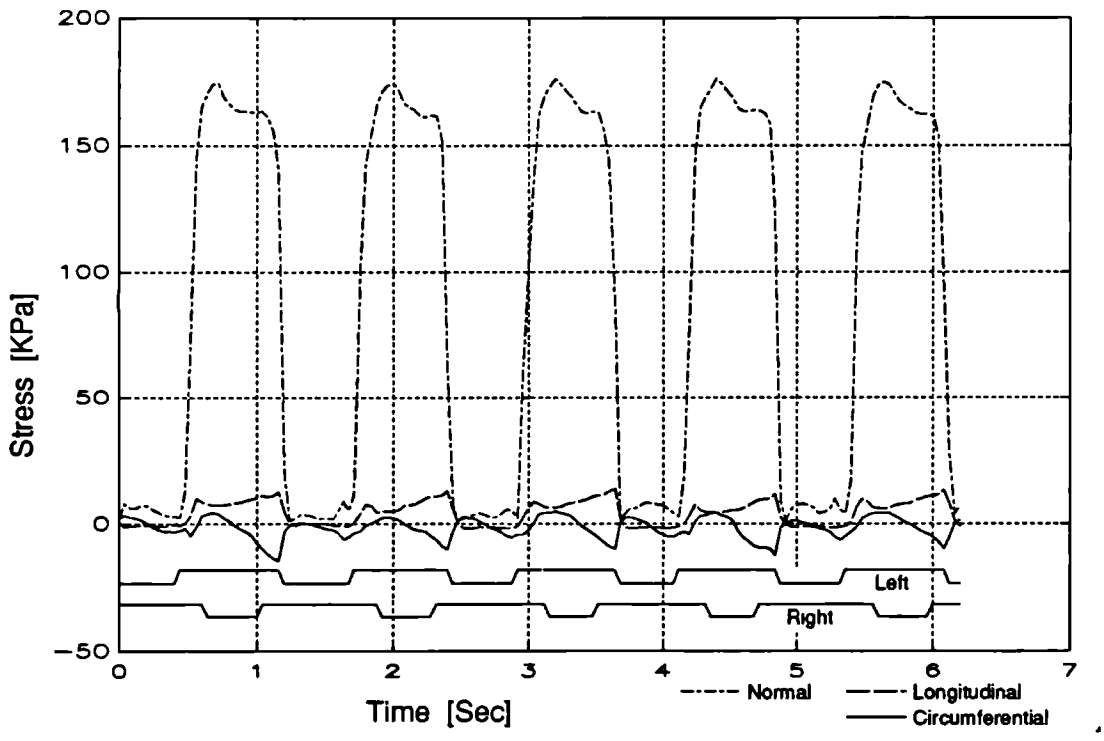

(b)

Figure 7.2 Interface stresses between residual limb and socket at the lateral paratibial site. The patient was fitted with a below knee supracondylar PTB socket and Multiflex (a) and Quantum (b) foot/ankle assemblies.

distinct double peak characteristic, as observed by **Sanders and Daly [1989]** and **Sanders et al [1990, 1992]**. The first peak occurring shortly after heelstrike on the prosthetic side (left). The second maximum was just prior to toe-off. Both resemble typical ground reaction forces at the plantar surface of the foot, as observed by other workers. The first peak is caused by the reaction forces during rapid deceleration of the body as the foot strikes the floor. This is followed by a trough during transfer of weight to the forefoot and the second peak is caused by an increasing reaction generated by the upward acceleration of the body during push-off. It was noted however, that normal stresses began to increase while the prosthetic limb was only part way through the swing phase. The cause of this was not clear. Though, the coincident increase in the longitudinal stress implies that the limb is being accelerated into the socket where the muscle bulk may bulge against the socket wall. Or, perhaps this is due to moments about the distal end of the limb forcing rotation of the prosthesis onto the posterior aspect of the limb.

It was also observed that a significant level of longitudinal shear stress occurred as the limb pistoned into the socket during the stance phase and out again during swing phase. To a lesser extent, a double peak of longitudinal shear stress was evident during stance. The first peak was due to reaction forces during deceleration, followed by falling off as the body rolls onto the forefoot. The second peak, which is coincident with the maximum normal stress, is probably due to the patient pushing down onto prosthesis to gain some spring from the artificial foot before toe-off. It may also be due to muscle flexion as the patient gains a stable purchase on the prosthesis before lifting it into the swing phase. **Appoldt et al [1970]** recorded only single peak shear stress waveforms from AK amputee sockets during gait. The maximum stress was seen to occur near toe-off. Circumferential shear was seen to be much smaller than longitudinal shear, as observed by **Sanders and Daly [1989]** and **Sanders et al [1990, 1992]**. **Appoldt et al [1970]**, however, observed that the shear stresses on both axes may be comparable, in the AK amputee socket. The circumferential forces could possibly be reflecting the torsion imposed on the limb due to the lack of rotational freedom in the prosthetic ankle mechanism. **Appoldt et al [1970]** comment that toe-in rotations are commonly observed in force plate and instrumented pylon studies of prosthetic gait.

There are slight variations in the stress waveforms between steps, although, the peak stresses remain similar. These variations presumably reflect the patients attempts to achieve stable gait by changes in step to step loading of the prosthesis.

Both normal stress and longitudinal shear stress exhibit a small reverse transient at heelstrike, the cause of which is not certain. It may however, be due to a sudden limb movement (slip) into the socket, as described by **Appoldt et al [1968b]** and as observed in the stress patterns recorded by **Sanders et al [1992]**. During the swing phase the limb may have moved proximally in the socket. Small distal and radial stresses at the initial moments of heel-strike may have been supported by interface friction. Then with the rapid rise in stress magnitude during deceleration the friction forces were overcome and the limb slipped distally into the socket, momentarily releasing the stresses in the process. As the limb meets with stronger opposing forces in the socket the stresses increase again.

Comparison of the limb/socket interface stresses at the popliteal site, revealed an increased maximum normal stress and a decreased peak in longitudinal shear, using the Quantum foot, as opposed to the Multiflex. Changes in circumferential shear were relatively indetectable. The double peak in the normal stress pattern was diminished significantly. Suggesting that the heel strike deceleration was cushioned by the foot, and perhaps spread over a greater part of the stance phase. A double peak was still present in the longitudinal stress pattern although it was less pronounced. Generally, the amount of longitudinal shear during stance was lower, though the transient at heelstrike was still present.

At the lateral paratibial site normal stresses were predominant over the shear stresses. During stance phase there was a peak in normal stress shortly after heelstrike, which reduced to a plateau in midstance before falling off quickly at toe-off. There appeared to be little difference in the normal stress patterns corresponding to the two prosthetic terminal devices. Longitudinal shear stress was approximately half that observed at the popliteal site. A double peak pattern during stance phase was apparent for both foot assemblies. However the peaks were reduced with the Quantum foot. There was a significant amount of circumferential shear, its pattern indicated there were counter clockwise stresses (as viewed from above) at heelstrike and clockwise stresses leading toward toe-off. Again these are possibly reactions due to limited ankle rotation after the heel had been planted.

The stress patterns observed at the medial paratibial site showed similar trends to those seen at the lateral site. While stresses at the medial and lateral femoral condyles were smaller in magnitude than those at the paratibials.

The frequency content of the signals was obtained by taking the Fourier transform of each data set. Plots of these show that there was no significant frequency components above *15Hz*. A plot of the frequency components of the data sets of Figure 7.1 and Figure 7.2 are given in Figure 7.3.

Subjectively the mounting design was considered satisfactory from the patients point of view. Clinically there were no marks on the skin to indicate significant localised pressure deviations. Nor were there any indentations to indicate that soft tissues had moved into the annulus between the transducer and the housing.

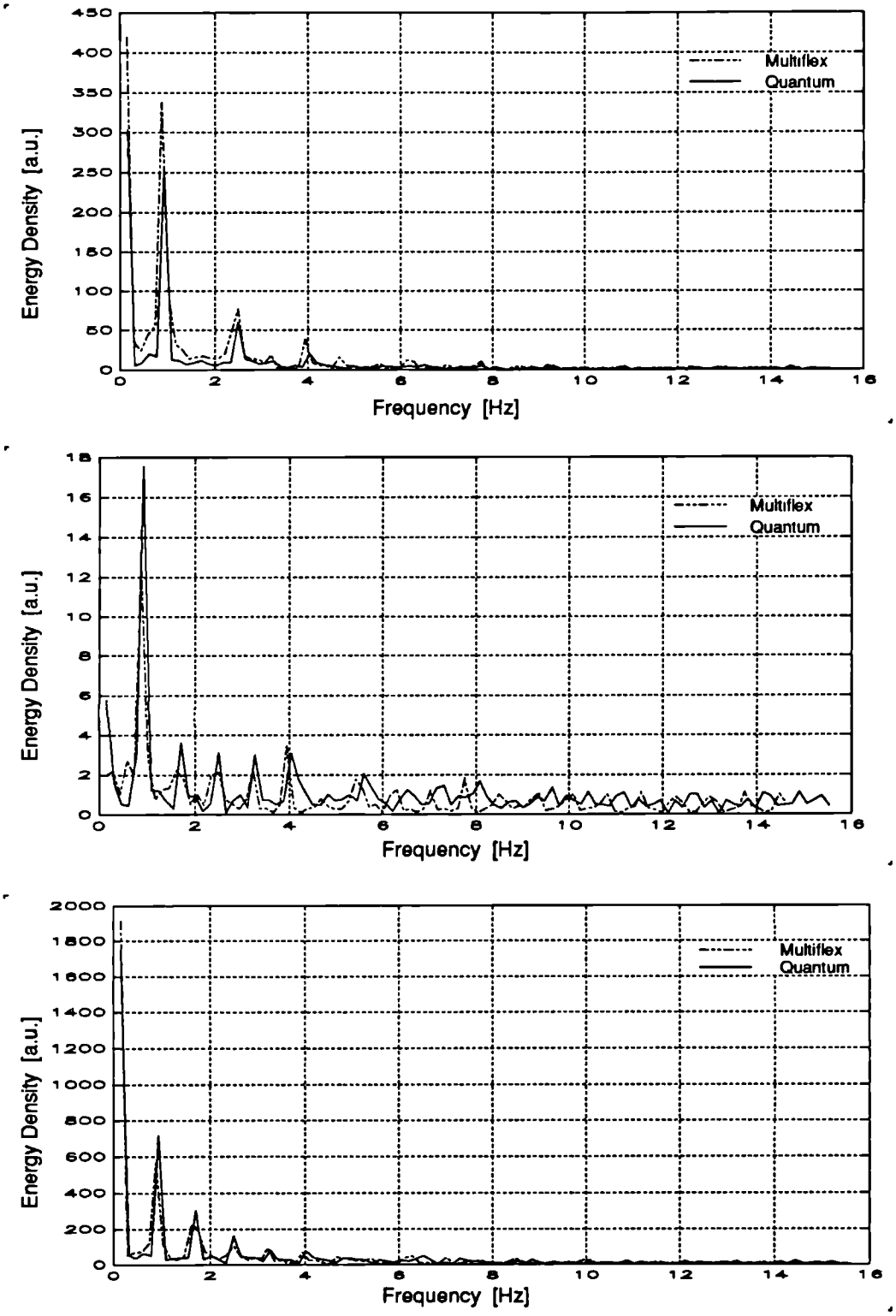

Figure 7.3a Frequency components of the limb/socket interface stresses when the socket is fitted with a Multiflex or Quantum foot/ankle assembly. Measurements were taken at the mid popliteal site. The longitudinal (Proximodistal), circumferential (anti-clockwise) and normal (radial) stress curves are shown, top to bottom respectively.

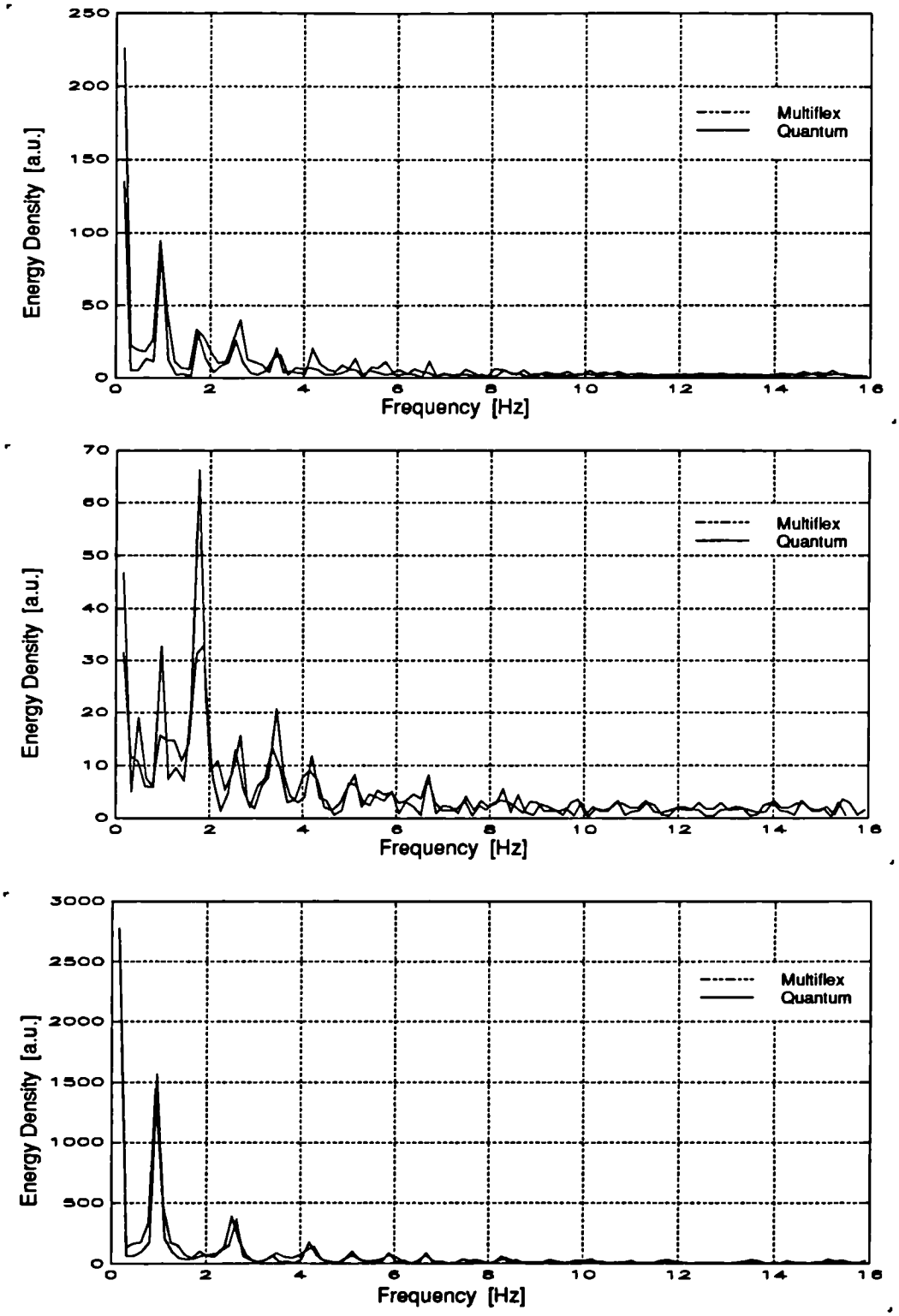

Figure 7.3b Frequency components of the limb/socket interface stresses when the socket is fitted with a Multiflex or Quantum foot/ankle assembly. Measurements were taken at the lateral paratibial site. The longitudinal (Proximodistal), circumferential (anti-clockwise) and normal (radial) stress curves are shown, top to bottom respectively.

7.3 Evaluation Study 2 - Plantar Stresses in Normals

In parallel with the intended application of these transducers to study stresses in lower limb prostheses, investigations were begun into measuring plantar stresses at the foot-shoe interface. Generally, the mechanical stresses which occur during asymptomatic gait in normals, are not such as to cause serious tissue damage. However, in cases of impractical footwear or foot pathology, these stresses may cause serious lesions. The result of which is either reduced tolerance to further stresses in plantar tissues or an altered plantar load distribution. Clinical studies have established a clear relationship between areas of high normal stress and ulcer formation, particularly in the region of the plantar metatarsal heads. In order to better understand the relative contribution of shear and normal stresses toward tissue damage, the transducers developed here were used to quantify plantar loads during normal gait.

The majority of the work carried out in this pilot study was performed by colleagues of the author and is more fully reported in **Lord et al [1992]**.

The method used to mount the transducer in the shoe was as follows. A transducer was set into an inlay/insole which was suitable for inserting in a standard orthopaedic (extra-depth) shoe. As an inlay is normally provided with these type of shoes the foot would still experience a normal freedom of movement when the instrumented inlay replaced the insole. The inlay was made from a combination of materials. An open cell foam sheet (**Cleron : Footman & Co LTD**) was chosen to absorb the extra depth in the shoe - six millimetres - and covered the majority of the plantar surface. A band of more rigid material was inserted across the insole in a strip under the metatarsal heads. In that region the top surface of the insole was required to remain flush with the top surface of the transducer during applied normal stresses. A high-density low compressibility material was used for the band (**Plastazote : BXL Plastics LTD**).

The posterior extent of the band was at the metatarsal 'break' where the shoe sole flexes during heel-lift. The transducer was fitted in a mounting which was clamped into the Plastazote band. Figure 7.4 is a simplified schematic of this arrangement.

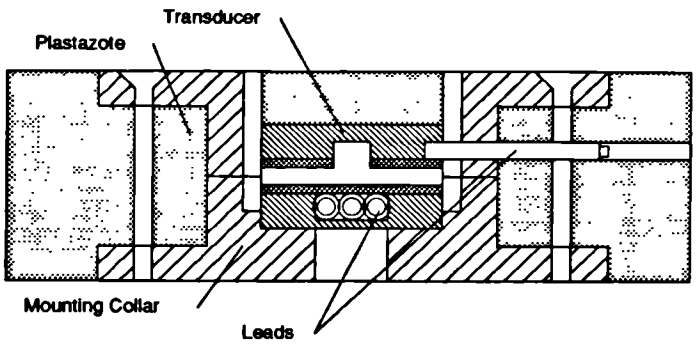

Figure 7.4 Schematic of the transducer mounting in the shoe inlay. A aluminium alloy two part annulus clamps the transducer to the Plastazote band of the inlay.

The mount was a two part annular housing of aluminium alloy. The bottom of the annulus held the transducer while the top collar clamped it to the inlay. Slots were cut in both top and bottom parts to accommodate device lead exits. The transducer had the normal section removed, leaving a two axis shear device. This was glued into the base plate of the mounting with a contact adhesive.

The regions of high normal stress were located with the aid of a pressure measuring insole (**F-Scan Gait Analysis System : Tekscan Inc**). This was a thin flexible insole of *960* load cells each of approximately five square millimetres. An insole was trimmed to the shoe size and stress measurements taken during normal gait. Analysis of the records enabled the location of the peak pressure under the first metatarsal head to be found. The corresponding site on the transducer inlay was marked, and a mounting hole was cut.

A hole was drilled through the inlay at the site and an oversized rebate cut around the hole, top and bottom. These were to accommodate the transducer mounting collar. Slots are cut through the Plastazote for the device lead holes. The housing base and transducer were then inserted in the hole. The top collar of the housing was screwed down onto the base, clamping the Plastazote.

Four asymptomatic subjects of similar shoe size, three male and one female, were selected for the evaluation. All could fit a size *7½* (UK) stock orthopaedic shoe (**LSB Orthopaedic LTD**). It was found that the location of their peak normal stress under the first metatarsal head was coincident to within *±5mm*. Therefore a single common location for the shear transducer, and thus inlay, was used for them all.

Five shear recordings were made with each subject wearing the shoe without socks. The subjects feet were allowed to air-dry and equilibrate to room temperature before donning the shoes. A footswitch (**FSW7: MIE Medical Research LTD**) was attached to the posterior of the heel of the instrumented shoe - right foot. Each subject was asked to walk along an eleven metre wooden walkway - right foot first. The signals were digitised at *50Hz* per channel after they had been amplified and filtered (*25Hz* corner frequency). A sample of the recordings are presented in Figure 7.5. These are the third set of the five for two of the subjects.

It was immediately obvious that shear patterns vary significantly between subjects. Possibly due to differing frictional coefficients or tissue elasticity. Anterior stress (positive values in Figure 7.5) occurred shortly after heel strike, but varied greatly in magnitude between subjects. A large posterior stress was seen to occur after heel lift, probably just prior to toe-off. These features relate to the deceleration and acceleration of the body, respectively. Stress patterns in the mediolateral direction appeared to follow the same trend as the anteroposterior pattern. Although, the magnitudes were generally smaller. There were exceptions with some subjects where lateral shear was greater than posterior shear at the end of the stance phase [see Figure 7.5b]. Stresses along this axis are generated to help the subject balance and provide a centralising thrust at toe off.

The frequency content of the signals was obtained by taking the Fourier transform of each data set. Plots of these showed that there were no significant frequency components above *15 Hz*. Plots of the frequency components for the data sets of Figure 7.5 are given in Figure 7.6.

Again, the mounting design was considered satisfactory from the subjects point of view. Clinically there were no marks on the skin to indicate significant localised pressure deviations. Nor were there any indentations to indicate that soft tissues had moved into the annulus between the transducer and the housing.

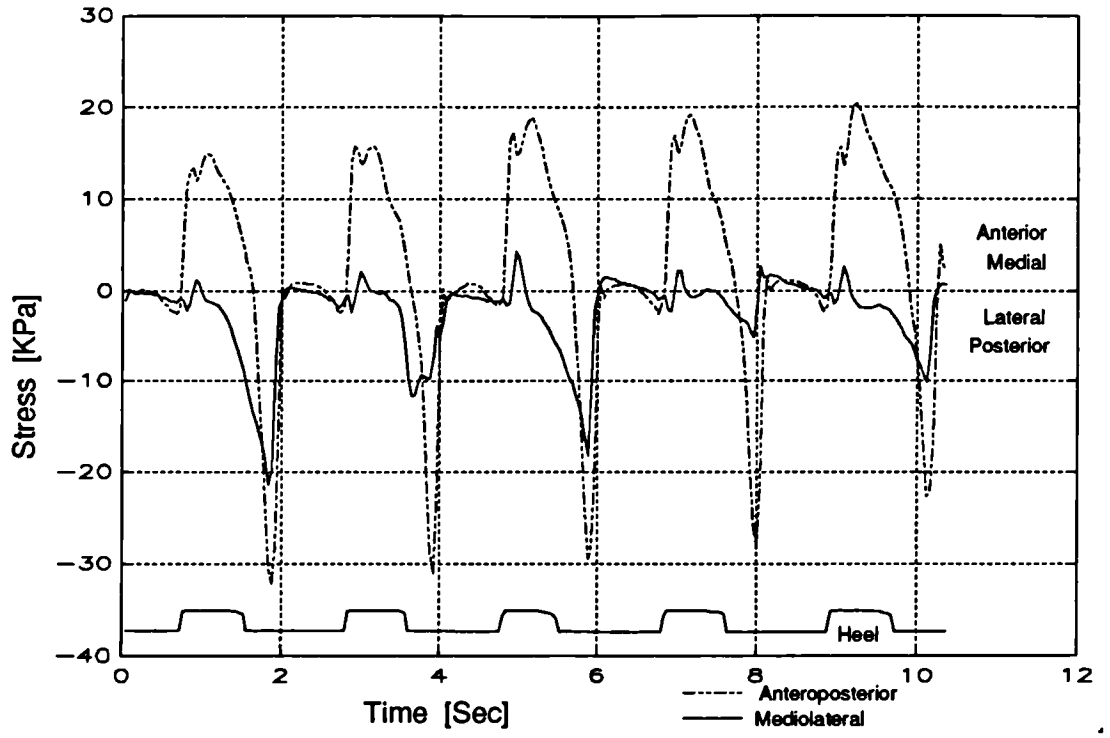

(a)

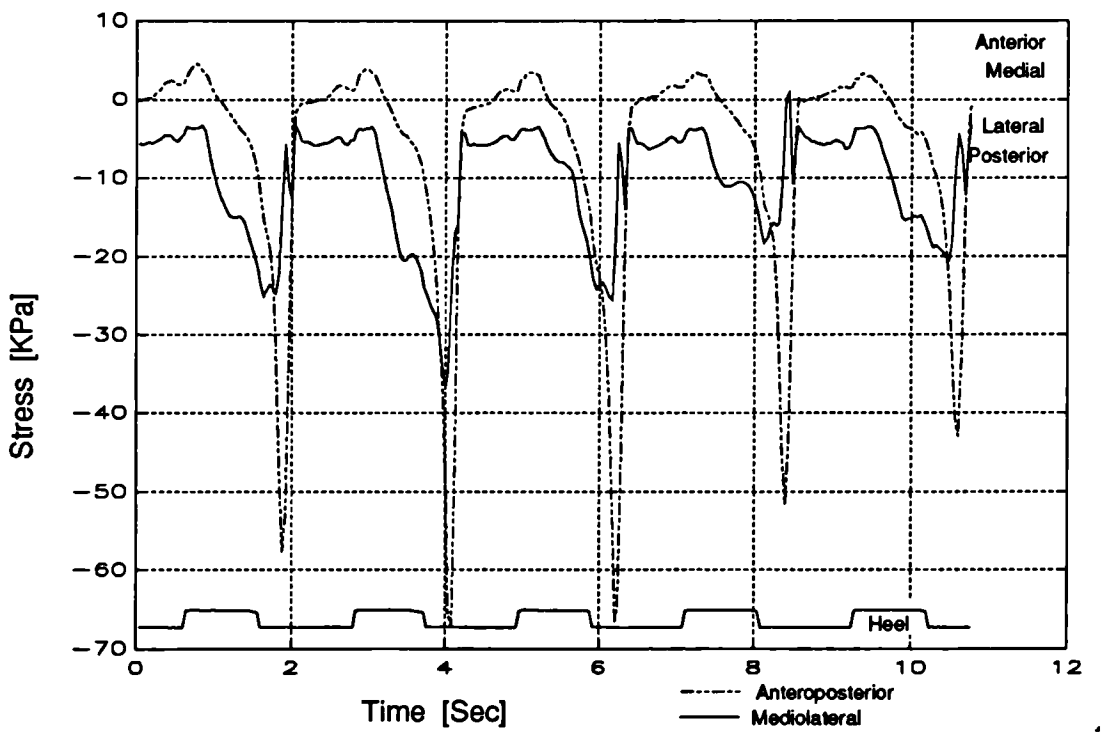

(b)

Figure 7.5 Anteroposterior and mediolateral shear stresses under the first metatarsal head of two asymptomatic subjects wearing orthopaedic shoes without socks. The transducer is recessed into an inlay made from Cleron and Plastazote. Right heel switch data is overlaid for reference.

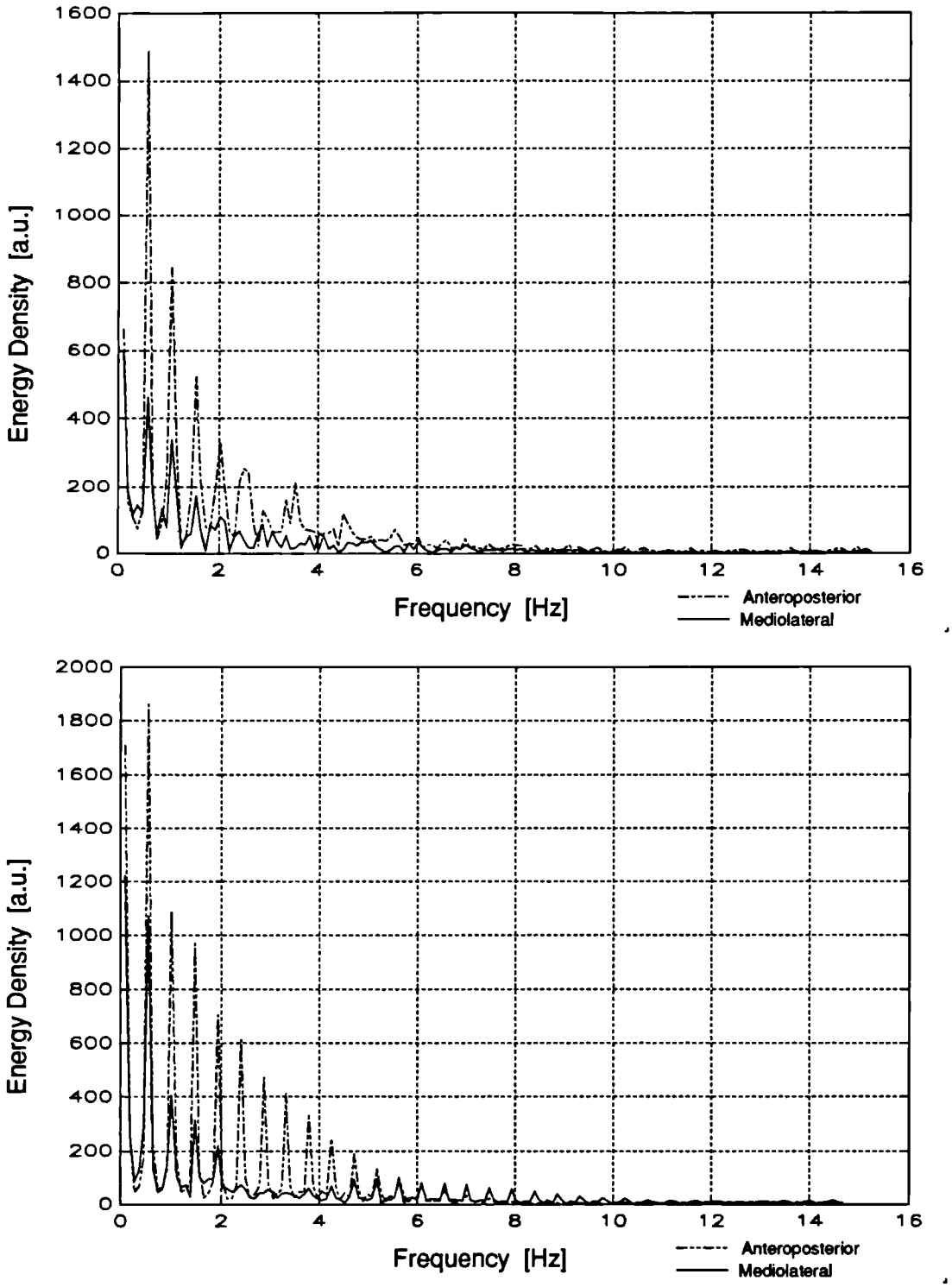

Figure 7.6 Frequency components of the foot-shoe interface stresses (Figure 7.5) at the first metatarsal head of two asymptomatic subjects. Both feet were in standard orthopaedic shoes without socks.

7.4 Performance and Mounting Notes

During the clinical evaluations above, a number of performance factors and mounting considerations were highlighted. These are discussed here in relation to the design specification for the transducer and system, and mounting requirements.

The relative magnitudes of the stresses measured in both studies were found to fall well within the full-scale-output limit set as part of the design specification. Normal stresses did not exceed *200kPa*, while shear stresses never exceeded *75kPa* on either axis. These findings are very similar to those of **Sanders et al [1992]** where peak magnitudes were up to *205kPa* for normal stresses and *54kPa* for shear stresses. Indicating, perhaps, there was a case for increasing the sensitivity of all the axes, especially for studies of plantar interface stresses. These evaluation studies, however, were not exhaustive and therefore the findings can only be taken as indicators.

The frequency content of the recorded signals indicated that there was not significant activity in the spectrum beyond *15Hz*. This was taken as confirmation that the choice for system bandwidth of *250Hz* was probably excessive.

The patient felt comfortable with the position and weight of the system units and the associated cabling. The security of the transducer leads, signal cable and their connectors between the distributed components of the data acquisition hardware was found to be acceptable.

From a mounting perspective, it was found that the requirement to have the Pelite liner installed in a socket before the subject 'dons' the prosthesis, was very limiting. The pre-insertion of the liner in the socket was necessary to avoid accidental dislocation the pelite discs from the top surface of the devices when the limb is inserted. Unfortunately this is a major drawback. The subject in this evaluation was able to achieve this only with difficulty.

Generally amputees normally fit the liner to their limb before inserting it into their sockets. Many of them will find it impossible to insert their limb if the liner is already in place. This limits the range of patients one can study.

A further problem found with the mounting method was the difficulty in accurately trimming and preparing the transducer recess in the socket. Access is limited for

tools and for visual inspection. Especially when preparing precision guide holes for the normal section pins. An error in this respect may render that site unusable for that socket.

Thus an alternative method of putting the transducers in place was determined which would overcome this limitation. It would allow each transducer to be fitted from the outside of the socket and still maintain the device face coplanar to the interface. An investigation in to its practical difficulties are only now being investigated, although technically it is quite feasible.

The simplest method of transducer insertion from the outside would be to drill a hole through the socket wall, from the outside, once it had been fabricated. This method, however, embodies a source of potential misalignment errors. The residual limb is a three dimensional curved surface. Although the inside of the socket shell is encouraged to conform to the shape of the positive model of the limb, by vacuum forming, the outside surface may not necessarily remain parallel to the inside. It is important to ensure that the top of the transducer is coplanar to the residual limb/socket interface. Mounting the drill perpendicular to the outside surface of the socket, and cutting a transducer mount hole, will not necessarily achieve coplanarity.

The alternative method, similarly to that described in 3.4, employs an epoxy blank mounted on the limb positive. This forms a recess in the socket wall during the vacuum forming process. The blank is transducer sized but is ring shaped with a central hole moulded through it, and no guide pins. After the limb positive is removed from the socket a small hand drill is used to cut a hole from inside the socket to the outside, using the central hole of the blank as a guide. Figure 7.7a is a schematic of this procedure. The newly cut hole is then perpendicular to the plane of the interface. Then, using this new hole in the socket wall as a guide, a radial cutting tool or boring drill can be used to cut a transducer mounting hole from either the outside or inside of the socket [Figure 7.7b]. An external mounting assembly incorporating the normal stress section indentor and holes for its guide pins can contain the transducer in such a manner that it can be inserted through the socket wall. The mounting hole may be threaded or external screws may be used to provide a securing mechanism for the transducer assembly [Figure 7.7c].

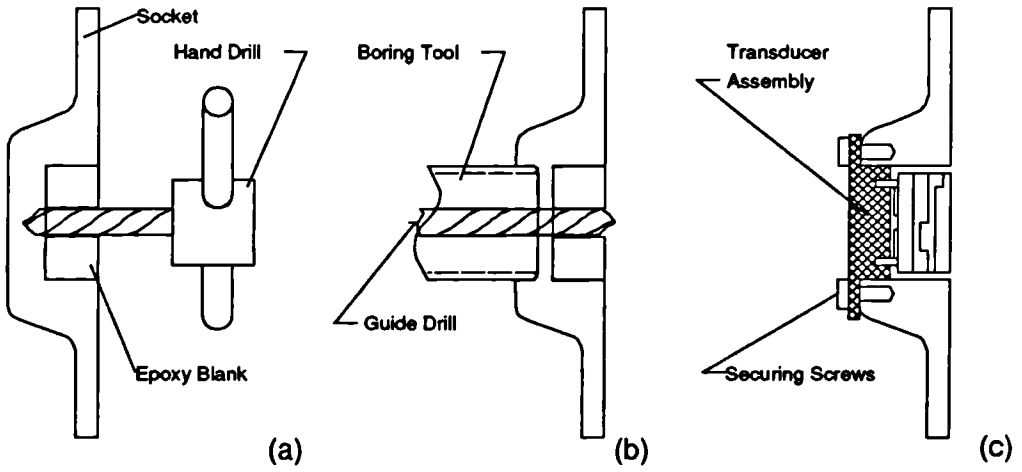

Figure 7.7 Schematic of a method of mounting a transducer from the outside of the socket and maintaining coplanarity with the limb interface. An epoxy blank with central hole, creates a recess in the socket wall. A small drill cuts a guide from the inside (a). A boring tool with a centre rod cuts a perpendicular mounting hole, using the drill hole as a guide (b). The transducer assembly is secured by external screws (c).

In general the results reported in 7.2-7.3 are too few to allow any statistically significant conclusions to be drawn. However, they do constitute some interesting and previously unobserved stress patterns, encouraging further detailed study. The performance specification of the transducer was observed to be broad enough to encompass the magnitude and frequency range of measured normal and shear stress waveforms at the limb/socket interface.

Chapter 8
Discussion and Future Work

This chapter discusses the work presented in this thesis. It is split into five sections. Section 8.1 contains a brief reiteration of the case for the requirement of the system developed here. Section 8.2 describes the overall conclusions from the transducer development, its performance and the mounting technique used. A discussion of the performance of the data collection system is presented in section 8.3. The findings from the clinical evaluation are summarised in section 8.4, and section 8.5 details suggested further work in continuation of this research.

8.1 Overview of the Imperatives

The estimated rate of new amputees, in the UK, is about *10000* each year **[Dormandy and Thomas 1988]** and about half of these are referred for artificial limb fitting. The majority are over *60 years* (*75%*) **[DHSS 1986]** and the life expectancy for the majority (*50-75%*) of them is only *5 years* **[Dormandy and Thomas 1988]** . It is therefore essential that optimum mobility and independence be achieved as soon as possible after amputation. The current prosthetic design and provision is a craft based practise carried out by skilled prosthetists. In *1986* the average time from amputation to delivery of a definitive conventional below knee prosthesis was *69* working days *(4.5 months)* **[McColl 1986]**. At the same time approximately *33%* of amputees complained of poorly fitting or uncomfortable prostheses. In *1984* it took an average of *3.2* visits to the prosthetist to rectify the amputee's prosthesis problems.

A standard prosthesis is issued to each new amputee, regardless of their age or ability. The socket of the prosthesis forms the interface between the amputee and the artificial limb. It is this component which is modified to uniquely accommodate the individual amputee's limb shape. Its function is threefold: to provide safe and comfortable transmission of ambulatory and stance forces from the residual limb to the prosthesis; to afford stability of the prosthesis on the limb; and it must enable the amputee to exert sufficient control over the prosthesis. The forces which act on the limb are static and dynamic in nature and encompass both normal and shearing stresses. It is known that some areas of the limb are relatively tolerant

of normal stresses while others are particularly stress sensitive. The socket geometry must be designed to direct load through stress tolerant areas and to relieve the stress intolerant areas.

Current socket design principles are referenced to the normal stress tolerant areas of the limb, but are ignorant of the shear stress sensitivity of the limb tissues. There is presently a lack of knowledge about the duration, magnitude, distribution and tissues' tolerance of shear stresses imposed on the limb during normal activities. This is primarily due to a lack of instrumentation with which to measure both normal and shear stresses at the residual limb/prosthetic socket interface. The transducer and data collection system described in this thesis overcomes this technical deficiency and facilitates the advancement of knowledge in this area.

Concurrently, attempts are being made to transform the current manual craft of socket design into a supervised automatic process. The proposed process relies on accurate knowledge-based mathematical models of the mechanical behaviour of the amputee's limb and the socket. Intensive calculations (finite element analysis) with the models try to predict a socket shape and stiffness which is optimum for each limb. Initial studies indicate that this process is feasible, provided that accurate models can be formulated. Again, there is a lack of knowledge about the shear stress response of limb tissues in sockets. Without which it is extremely difficult to refine the models needed. The interface stress measurement system described in this thesis can be employed to address this problem.

In addition, there are a number of other body/support interfaces which require the same knowledge but which lack the instrumentation with which to obtain it (i.e foot/shoe, bedsores, wheelchair seating). The system documented here may, also, be applied to the measurement of stresses at these interfaces.

Soft tissue responds to applied stress in either of two general modes; tissue breakdown or tissue adaptation. Breakdown is a degenerative and destructive process where the tissues become intolerant of stresses, while adaption is a disruptive and modifying process where tissues become more stress tolerant. Whether a particular individual's limb tissue will undergo breakdown or adaption under a given stress regime depends on a number of factors, most of which are not quantitatively defined as yet.

The mechanical stress induced breakdown of tissue is a complex process dependent on the resilience of the organs, vessels, cells and intra-cellular structures. It may also be precipitated/modified by concurrent medical and nutritional conditions. Tissue damage appears to be proportional to a normal *stress-magnitude x duration* function, and inversely proportional to the *length-of-recovery-period* between normal stresses. There is no relational hypothesis for shear stresses as yet, due to the paucity of data. Although, shear stresses are thought to be equally as destructive as normal stresses. Also, there is evidence that the combination of the two stress modes is particularly injurious.

The effect of moderate stresses applied at regular intervals can alter the normal structure of soft tissue, as is evidenced by the formation of callus'. The new adapted structure maintains or improves the tissues ability to sustain applied stress. It has also been demonstrated in animal studies, that wound healing rates and the strength of the resultant tissue are improved by moderate passive motion of the wound or physical activity during healing. Thus with a sufficient understanding of tissue healing and growth mechanisms it may be possible to design mechanical stimulation or surgical regimes to modify the stress tolerance of limb tissues. So with a combination of socket design and soft tissue modification, more tolerant limbs and comfortable prostheses may be engineered.

In order to begin to define safe limits for stress magnitude, duration and length of relief periods, it is necessary to study the damaging effects of simultaneous normal and shear stresses on the soft tissues of the limb. To the author's knowledge a study of this nature has not been attempted on the lower limb and no device has been proposed for the stress measurements. The transducer and data acquisition system described in this thesis can be utilised for such a study and to provide direct measurement of the stresses in individual prosthetic socket designs for comparison with any proposed limits.

8.2 Transducer Development

The transducer developed here is original in that it is the first device in the world which is demonstrably suitable for accurate measurements of simultaneous normal and shear stresses at any site on the residual limb/prosthetic socket interface of BK PTB prostheses. Additionally, it is also uniquely able to be applied to stress

measurements at other body/support interfaces where they have not previously been possible. The specifications for this device were determined from a consideration of previous researchers interface stress measurements coupled with informed estimates of some unquantified parameters. The final form of the device was demonstrated to meet these requirements to a significant degree. The transducer is capable of detecting forces applied normal to its active surface and is able to resolve shear forces applied in the plane of its active surface into two orthogonal components. The device is constructed as three individual axes, bonded together.

The shear stress sensitive axes are uppermost in the device, closest to the residual limb/prosthetic socket interface. They are fabricated from three rigid discs and two interposed layers of rubber bonded together in a cylinder. Ridge and groove constructs are employed to restrict movement of the outer discs along defined axes with respect to the centre disc. Their motion is orthogonal with respect to each other. Shear forces applied to the outer discs are opposed by internal stresses in the rubber layers and the discs displace with respect to the centre disc. The linear stress strain relation of the rubber layer in pure shear results in a linear shear force versus displacement function. The displacement, and hence applied force, is detected by a magnetoresistor-magnet pair. By fixing a small rod magnet to the centre disc and the magnetoresistor to each outer disc, relative motion of the magnet with respect to the magnetoresistor can be measured.

The normal stress sensitive axis is furthest from the residual limb/prosthetic socket interface, being bonded to the underside of the shear stress sensitive section. It consists of a rigid disc with a wide cylinder cut from its centre, leaving a bottle cap (diaphragm) type construct. The top of the cap is strain-gauged on its under surface. Indentations of the diaphragm are detected by resistance changes in the strain-gauge. Forces applied normal to the active face (uppermost surface) of the shear stress section are transmitted to the bottom of the section, and drives the diaphragm of the normal stress section on to a separate indentor plate. This plate has a boss machined on its centre which impinges on the centre of the diaphragm. The natural spring in the diaphragm construct opposes the applied normal force and it deflects a distance proportional to the force. The unique implementation of the indentor mechanism obviates the potential errors, faced by all previous researchers designs, caused when non uniform normal stresses are applied to the active face of the transducer.

Several design iterations were necessary before the requisite transducer performance was achieved. The greatest difficulties were encountered in the selection of the materials for each of the mechanical components of the device.

The most problematic material was the rubber spring layer of shear stress section. This was required to be: linearly elastic over large deformations *(≈100-200%)* in shear modes; incompressible under normal stress; dimensionally stable with temperature; resilient without hysteresis, creep or stress relaxation; and must be easy to bond to plastics and metals. These requirements were eventually, satisfactorily met by a special formulation of a natural rubber compound. Natural rubber is an inert, robust material which retains its properties with age. It is also easy to handle in sheet form. Transducer construction is thus greatly simplified by the use of preformed solid components.

In order to minimise friction in the ridge and groove constructs the centre disc was fabricated from a low friction material (Acetal). However, Acetal is also an extremely inert material and proved difficult to bond to. Additionally, traditional processes for bonding rubber, using epoxies, involved a chemically aggressive pre-treatment which is corrosive to Acetal. Failures in transducer integrity due to corrosion problems were experienced with early designs. But, these were overcome by employing cyanoacrylate adhesives and an etching primer, originally designed for PTFE. Transducer construction was thus simplified by the use of non-aggressive easy to apply brush-on adhesives.

Another difficulty was that the relative temperature sensitivity of the device with respect to its stress sensitivity was initially very large. An analysis of the relative contribution of each component to the overall temperature sensitivity resulted in the reselection of some components to others with lower temperature coefficients. This was coupled with other component reselections designed to improve the overall stress sensitivity. The resultant combination of components yielded a device with an acceptable temperature induced error figure. Over the range of temperatures assumed to be found in the clinical trial (*20-40 ℃*), temperature induced errors were less than *0.19%FSO/˚C* and *0.1%FSO/˚C*, for the shear and normal stress sections respectively. As the temperature of the interface was not expected to vary much (within the range *32-37˚C*) throughout the trial, the temperature sensitivity of the device was not significant. It is interesting to note that no other researcher in this field has presented any temperature sensitivity data for their devices.

The last major problem was the variability in the offset, linearity and range of devices in an assembled batch. The origins of which lay firmly in the assembly process tolerances and fabrication tolerances of some components. Especially as the transducer assembly was carried out by hand. The alignment of the shear stress sensor pair was critical in establishing a balanced offset and symmetrical range in either direction. Machining tolerances were similarly critical in realising low friction slides with minimal backlash and consistent diaphragm deflection distances. However, in order to prove the design it was only necessary to demonstrate that at least one assembled device consistently meets the proposed performance criteria.

During device calibration, practical difficulties were encountered in mechanically exciting the transducer over its full bandwidth. So, the bandwidth of each section was determined by impulse force methods, and calibration was carried out a frequency well within its passband. Calibration (force versus output voltage) curves were obtained from plots of device output variation during forced sinusoidal mechanical oscillation.

It was demonstrated that it is possible to construct a transducer, of the design described in this thesis, which has a linear response of better than *6%FSO* for each shear stress axis and better than *2.5%FSO* for the normal stress axis. However, hysteresis, nonlinearity and friction errors were present on all axes. When a first order (linear) conversion polynomial was employed to approximate the calibration curve, the accuracy of the conversion was: *9%* of indicated force or *0.5N* (whichever was the greater) for the shear stress axis; and *5%* indicated force or *1.9N* for the normal stress axis. When a fifth order conversion polynomial was employed the demonstrated accuracy of the conversion was: *6%* indicated force or *0.45N* for the shear stress axis; and *1.75%* or *1.1N* for the normal stress axis. The frequency response of the shear stress axis was *0.1mHz-1500Hz* and for the normal stress axis was *DC-1200Hz*. Both the stress and frequency performance were comparable or better than all other devices used in this field.

The assembled device measured *15.96mm* diameter by *4.9mm* thick. These dimensions precluded its use by insertion between the limb and socket. It has been demonstrated that by creating a recess in the socket wall the transducer could be positioned so that it was flush with socket's inside surface. Furthermore, to maintain uniform frictional and mechanical stiffness fields across the interface a small disc of socket

liner material was bonded to the top (active) surface of the transducer. Those procedures ensured that measurement errors due to device protuberance and interface discontinuities, experienced by other researchers, were minimised.

The formation of accurately dimensioned recesses at specific sites in the socket wall was accomplished by the innovative use of cast epoxy transducer dummies attached to the limb model positive prior to vacuum forming the socket. That approach fulfilled three important functions: registering the correct device orientation; ensuring the device was flush with the socket's inside surface; and guaranteed the active surface of the transducer was parallel with the inside surface of the socket. The latter function has not been addressed by other workers.

8.3 Data Acquisition System Development

A complete measurement system for quantifying stresses at the interface has been designed and built. Exacting requirements exist for the transducer excitation and signal amplifying circuits to ensure the accuracy and resolution of low amplitude transducer output signals. To minimise space, weight and costs, a common excitation circuit was implemented for both normal stress (strain-gauge) and shear stress (magnetoresistor) transduction elements. The stability of the circuit was of the order of *0.1%*. To minimise ohmic heating of the transduction elements and therefore temperature induced errors, the excitation voltage was low *(1V)*. Consequently, output signals were small and required precision amplification. The accuracy of the amplifier circuitry used was dominated by random thermal noise in circuit components, and was calculated to be better than *0.4%FSO* at worst case.

The stress signal bandwidth was expected to be less than *50Hz*. It was also expected to contain step-like transients. Preservation of these transients and maintainence of a constant signal gain over the bandwidth, required the use of Bessel type filters for the noise rejection circuits. Environmental noise signals in the clinical area were found to have their greatest magnitude in the spectrum above *300Hz*. Thus, the stress signal filters were set for a cut-off frequency of *250Hz*. The resultant measured electrical noise magnitude, and therefore signal uncertainty, in the complete stress signal amplifier-filter-cable system was found to be *0.24%FSO* for the shear stress signal path and *0.25%FSO* for the normal stress signal path.

Synchronisation signals were also generated, to give reference points in signal traces and to provide synchronisation events to external third party systems. Foot contact events were utilised for these signals. They were detected by attaching heel and toe switches to the plantar surface of both prosthetic and natural feet of the amputee subject. Captured stress signals could thus be related to heel strike and toe off events in the gait cycle. Interface circuits were built to allow synchronisation signals to be exchanged with a third party gait kinematics analysis system (VICON). Those allowed stress signal patterns to be related to kinematic events in the gait cycle, a process which has only been partially implemented by two other researchers.

Stress and synchronisation signals were captured and digitised by the data acquisition system specifically built for this research. A commercial 12-bit Analogue to Digital (A/D) conversion subsystem and Central Processing Unit (CPU) were purchased for the control, digitisation and buffering of the clinical signals. The system was able to digitise and store *32* channels of data (*10* transducers and *2* footswitch signals) at a rate of *500Hz*, for about *30* seconds per run. PC-bus based subsystems were not commercially available with these specifications, therefore, a separate VME-bus system was assembled. This was interfaced to a PC through which it could be controlled and onto which its data could be archived. However, significant difficulties were encountered in getting the commercial subsystem to perform in any of the modes it was claimed to be able to. This was due to incompetence, design errors and poor technical support by the vendor. Despite this major disadvantage, custom software and minor hardware alterations were able to effect a working system. Considerable software, written in C, was designed and coded to create a menu based user interface with which to control all data acquisition and archival. Third party software was utilised to display and process the archived data off-line.

All equipment was designed to comply with British and International Medical Safety standards.

8.4 Clinical Findings

A limited clinical evaluation was carried out in order to: determine the suitability of the transducer design specifications; assess the performance of the transducer; evaluate the efficacy of the mounting methodology; and identify potential problems from the patients perspective. From the evaluation it was concluded that the system

was effective, could readily be used as a research tool at more than one body/support interface and that meaningful results can be obtained. It was, however, identified that changes were needed in the transducer mounting method, in order to reduce socket preparation time and to enable a greater number of PTB socket users to be studied. The details of the changes are discussed in [8.5].

Despite the fact that the results were too few to admit that significant conclusions to be drawn, they do constitute the first observations of their kind, ever. Additionally, they provide some interesting indicators which confirm earlier related findings and they show that the effect of some prosthetic variables is not uniform nor isotonic at all sites across the interface. The trial confirmed that during gait, shear stresses at the residual limb/prosthetic interface are much smaller in magnitude than normal stresses at the same site - less than one third. The ratio of shear to normal stress varies with site and with changes in prosthetic variables - like type of foot/ankle assembly. Longitudinal (proximodistal) shear stresses are greater than circumferential (mediolateral) shear stresses. Normal stresses were found to have peak values in the range *50-170kPa*, shear stresses had a peak value range of *10-40kPa* (longitudinal) and *2-20kPa* (circumferential)

Some sites exhibit biphasic normal and shear stresses during the stance phase of gait, while others are monophasic. These appeared to be influenced by prosthetic variables. The maxima of the stress waveforms at different sites did not appear to be coincident. They indicated that a stress wave travels over the limb in a proximomedial direction. The waveforms were also non-symmetric over the stance phase suggesting that the resultant shear vectors had different directions at heelstrike and toe-off.

The stress patterns seemed to indicate that immediately following heelstrike significant slip occurred at some sites, while it was barely distinguishable at others. Some sites loaded during stance phase were also partially loaded during swing phase, although, this did not appear to be the norm. It was likely that at those sites, relearned muscle activity sequences were engaged in aiding socket suspension during the swing phase. It also appeared that it was at these sites that slip was greatest.

The variation in stress waveforms between steps in a given trial appeared to be minimal. There was also little change in the base stress levels over a trial, indicating

low transducer drift and minimal changes in socket fit over the duration of the trial. The bandwidth of the significant frequency components of both normal and shear stresses was found to be less than *15Hz.*

Subjective assessment by the patient considered the position and weight of the system components to be acceptable and the layout of leads and cables was not restrictive. It was felt, however, that the requirement to don the prosthesis when the liner was already in situ in the socket was restrictive and difficult to perform.

A short clinical trial was implemented where the transducer was employed to measure the shear stresses at the foot/shoe interface. This demonstrated the versatility of the device and system. Again, this data was the first example of its kind to be acquired. The results clearly demonstrated significant variation in stress patterns between individuals but little difference between successive steps of any one individual in a given trial. The principle direction of shear stress at various phases of the gait cycle differ from individual to individual. The bandwidth of significant spectral components was approximately *15Hz.*

8.5 Outline for Future Developments

The work described in this thesis has provided a solution to a long standing problem, however, as with most research it is just the beginning of future work and it is only one solution which itself may benefit from further refinements. This section outlines suggestions for improvements in the transducer and data acquisition equipment, and presents proposals for the application of this measurement system.

The major limitation of the system as a clinical research tool was in its requirement for the liner to be installed in the socket before the patient dons his prosthesis. This was necessary in order to avoid dislocating the cylinders of liner material bonded to the top of the transducers recessed into the socket wall. As this requirement was contrary to normal practice and was difficult to effect, it limited the number of patients who could take part in studies. It was also found that accurately trimming and preparing the transducer recess was a very difficult task requiring great dexterity where visual inspection was limited. An alternative mounting method has been proposed (details are given in [7.4]) whereby the transducer is inserted through the socket wall from the outside. A recess is still to be formed

in the socket, during its fabrication, but its function is to act as a guide for cutting a transducer insertion hole. Additionally, it ensures that: the active face of the transducer is aligned parallel with the interface; the transducer is inserted until flush with the inside socket wall; and facilitates accurate placement of the transducer with respect to an anatomical site. Trimming of the transducer mounting holes is thus made redundant and precision external mounts can be utilised.

Currently, the alignment of the transducer axes with some reference axis on the limb, or socket, is performed by eye. The accuracy of this could be improved by designing a mechanical scribing jig, which attached to the limb model mandrill, for cutting alignment marks.

Greater precision in the manufacture of the disc, diaphragm and indentor components will promote an improvement in device performance consistency across a batch. Equally effective in this area would be the implementation of a more precise or automated assembly process.

The digitiser and data buffer subsystems of the data acquisition system were developed around the VME-bus architecture, while the data archival and processing used a PC-bus architecture. The rationale for this was the lack of suitable commercial PC-bus digitisers with the required specification. A working acquisition system has been demonstrated here which fulfilled all the project requirements. However, the mode of its internal operation was unconventional due to technical errors on the commercial VME-bus subsystems purchased. Also, the necessity for a precision high speed data link between the VME units and the PC, the extra set of system units, and separate software to run on each, added complexity to the system. During the course of this research, technology in digitising and data buffering for PC-bus subsystems has advanced considerably. It is now possible to replace the VME-bus units with smaller faster subsystems which can be installed directly into a PC. Additionally, a significant amount of third party software is available to control these subsystems and process the acquired data. Thus, a reduction in complexity, trial time, cost and maintenance could be achieved by developing the current acquisition system to employ this new technology.

A further avenue of system development which could be explored is in utilising data telemetry concepts to conduct stress signal data from the patient to the acquisition system. The benefit of this is to endow the patient with a greater freedom of

movement, where the trailing cable currently used is thus removed. The compromise for this benefit is the additional cost and the need to make the patient-carried circuitry battery powered.

If the data trend observed here is supported by further clinical measurements then further changes could be made to the transducer and acquisition hardware to improve their performance or manageability. These are discussed below.

It was observed that the range of peak stresses measured at the limb/socket interface did not exceed *200KPa (40N)* in the normal direction, and *75KPa (15N)* in the tangential (shear) directions. This indicated that the transducer may be over specified in terms of measurement range. By reducing the range the resolution and accuracy of the device may be increased, however, as device accuracy is dominated by its hysteresis the overall improvement may be small. The device diameter may be reduced to allow greater resolution in stress field mapping. If this is undertaken, the reduced surface area of rubber will incur a decrease in the linear range of the device. However, this may be counteracted by a reducing the measurement range or by implementing a high order voltage to stress conversion polynomial. By increasing the gain on the data acquisition amplifiers to reduce the measurement range, resolution would be improved and the signal to noise ratio of the system enhanced.

A further improvement in the signal to noise ratio could be gained by reducing the bandwidth of the signal filters. It was observed that the stress signal bandwidth was approximately *15Hz*, while the filter bandwidth had been set at *250Hz*. This latter bandwidth was determined by the use of a Bessel filter type to achieve precise transient response over the expected stress signal bandwidth of *50Hz*. The observed bandwidth implies that the transient response may be relaxed, thus the filter bandwidth may be significantly reduced and the filter type revised to one with a faster frequency roll-off in the stop band.

The next phase of this research is undoubtedly the instigation of laboratory and clinical studies with the equipment designed here. These would concentrate in four main areas.

Firstly, there is a need to establish baseline data about the stress fields inside prostheses and the patients ability to endure them. This would involve obtaining

an appreciation of: the pattern, duration and magnitude of stresses found during both static and dynamic states of prosthetic use; and the stress tolerance of various limb sites, tissue types, disease states and individuals. This would involve instrumenting a large number of sockets of known rectification for a substantial range of patients/conditions. Also, a study of the response of tissue types to applied stress magnitude and duration would be required to define the conditions under which tissue adapts or breaks down. This may be supplemented by a parallel study into forms of surgical or chemical intervention which may alter the ability of the tissue to adapt to or tolerate stresses.

Secondly a study needs to be undertaken to map the influence on the stress field, of changes in prosthetic variables such as liner materials, alignment, socket flexibility and prosthetic foot/ankle assemblies. This may need to be conducted, initially, with limb models under laboratory conditions, in order to perform controlled tests. It would be necessary to correlate these findings with the first study, proposed above, to assess how tolerable the variations in the stress field are for the patient.

Thirdly, in parallel, models of the limb/socket interaction can be formulated using mathematical methods. Their ultimate use being to predict the shape and properties of an optimum socket/prosthesis for any individual, given a minimal set of measurements of their limb properties. These models would need to be verified or iteratively modified by experimental measurements on mechanical models or real limbs.

Lastly, there are many other body/support interfaces for which there has been a lack of appropriate instrumentation for triaxial stress measurements. The system described in this thesis can be applied to some of these areas, in particular to the foot/shoe and buttock/seat interfaces.

There are presently two studies being undertaken at the Department of Medical Engineering and Physics, Kings College Hospital (Dulwich), London, which are attempting to address the third and fourth issues above using the transducers and data acquisition system components developed in this research. Some of the suggested modifications/developments given here have been, or are being, implemented on these projects.

With the information to be gained from the application of this research, described in this thesis, in the current and future studies, improvements in the function, comfort and fit of lower limb prostheses will be realised. Thus, a more optimum independence and quality of life for the lower limb amputee will be promoted.

Appendix
Data File Format & Memory Map

This Appendix describes the format of all data files captured using the MEP086A Data Collection Unit (DCU). It also describes the memory map of the DCU.

A.1 Data-File Format

Data captured on the DCU is uploaded to a Personal Computer (PC) via a serial link, for archiving and processing. The software required to run on the PC and DCU to effect the data exchange are TFT.EXE and MEP086.EXE, respectively. These programmes were written by the author. A copy of the code is registered with Kings College Hospital (Dulwich)[1] under the title **P086-SOFTMAN**. Data files stored on the PC contain an ASCII *header* followed by three byte-wide two's complement BINARY *data*. The header contains the experimental parameters used to collect the data, as well as notes on the patient and transducer sites.

Information fields within the header are delimited by ','. The data field is packed and does not contain delimiters.

The file format is given in Table A1.

1 Department of Medical Engineering & Physics, Kings College Hospital (Dulwich), East Dulwich Road, London SE22 8PT, UK

	Field	Size [bytes]	Data Type	Description
	Identifier	7	Ascii	MEP086 data file identification tag
	BEG	1	Binary	BEGinning of header field
	Name	21	Ascii	Patient identifier
	VICON-name	21	Ascii	Associated VICON file
	Comment	61	Ascii	General comment field
	N°Transducers	3	Ascii	Number of transducers
	Sample Period	5	Ascii	Period between data points [mSec]
	Trigger mode	2	Ascii	Start/Stop triggers
	Time out	6	Ascii	Period of data collection before timeout [Sec]
x 10	Serial number	3	Ascii	Serial number of transducer - for calibration
	Site	11	Ascii	Anatomical site of transducer placement
	Date	9	Ascii	Creation date of file
	Time	9	Ascii	Creation time of file
	N°samples	8	Ascii	Number of data points for each transducer
	END	1	Binary	END of Header field
x N°	VICON status	3	Binary	State of VICON data collection [ON/OFF]
samples	Footswitch data	3	Binary	Three state footswitch data
	T1x	3	Binary	Transducer 1 : X Axis
	T1y	3	Binary	Y Axis
	T1z	3	Binary	Z Axis
	T2x	3	Binary	Transducer 2 : X Axis
	T2y	3	Binary	Y Axis
	T2z	3	Binary	Z Axis
	.....	...	....	.....
	T10x	3	Binary	Transducer 10 : X Axis
	T10y	3	Binary	Y Axis
	T10z	3	Binary	Z Axis
	END	1	Binary	END of data field

Table A.1 File format of the MEP086 DCU data files archived on the PC.

A.2 DCU Memory Map

The DCU has a Motorola 68000 CPU, thus its address space is not segmented like the IBM PC. It is capable of directly addressing $FFFFFF_{16}$ bytes of memory. In this unit $FFFFF_{16}$ bytes of RAM, 4000_{16} bytes of fast SRAM and 80000_{16} bytes of EPROM are installed. The input/output devices (such as A/D and serial port) devices are also mapped into the address space. The location or address of each of these areas is given below in Table A2.

Address Range	*Memory Type*	*Usage*
000000 - 400000	*SRAM*	*Programme Instruction Space*
400000 - 1FFFFF	*NONE*	--
200000 - 2FFFFF	*RAM*	*Programme Data Space*
300000 - DFFFFF	*NONE*	--
E00000 - E7FFFF	*EPROM*	*PLUM Monitor*
E80000 - F0FFFF	*NONE*	--
F10000 - F1003F	*I/O*	*Serial Port*
F10040 - F11800	*I/O*	*UNUSED*
F11801 - F1182F	*I/O*	*Real Time Clock*
F11830 - FFEFFF	*I/O*	*UNUSED*
FFF000 - FFF1FF	*I/O*	*Analogue to Digital Convertor*
FFF200 - FFFFFF	*I/O*	*UNUSED*

Table A.2 Memory map of the MEP086 DCU address space.

Publications

The research described in this thesis has led to the presentation and publication of the following papers.

Williams.R.B, Porter.D, Roberts.V.C, (1989), Assessment of stresses at the stump/socket interface, *Abstracts 6th World Congress ISPO*, Kobe Japan, November, 142

Porter.D, Williams.R.B, Regan.J.F, Roberts.V.C, (1990), A triaxial force transducer for investigating stresses at the limb socket interface, *Proc. Ann. Conf. ISPO(UK)*, April, Edinburgh

Williams.R.B, Porter.D, Roberts.V.C, Regan.J.F, (1992), Triaxial force transducer for investigating stresses at the stump/socket interface, *Med. & Biol. Eng. & Comput.*, **30**, 89-96

Lord.M, Hosein.R, Williams.R.B, (1992), Method for in-shoe shear stress measurement, *J. Biomed. Eng.*, **14**, 181-186

References

Adamson.M, (1978), *Skin temperature monitoring*, PhD thesis, University of Strathclyde, Glasgow, Scotland.

Akashi.K, Katsuki.T, Hayashi.K, Funaki.K, (1986), Stress analysis of a below knee prosthetic socket, *5th World Congress ISPO*, Copenhagen, June 25-July4, 354

Alexander.I.J, Chao.E.Y.S, Johnson.K.A, (1990), The assessment of dynamic foot-to-ground contact forces and plantar pressure distribution: A review of the evolution of current techniques and clinical applications, *Foot & Ankle*, **11 (3)**, 152-167

Analog Devices, (1991), *Error calculations for instrumentation amplifiers*, Application Note, Analog Devices, Norwood M.A.

Angel.J.C, (1979), Amputation below the knee, in *Operative Surgery: Orthopaedics Part I*, Rob.C, Smith.R. (Eds), Butterworths, London, 311-315

Antonsson.E.K, Mann.R.W, (1985), The frequency content of gait, *J. Biomechanics*, **18(1)**, 39-47

Appoldt.F.A, Bennett.L,(1967), A preliminary report on dynamic socket pressures, *Bull. Prosthet. Res.*, **10 (8)**, 20-55

Appoldt.F.A, Bennett.L, Contini.R, (1968a), Stump-socket pressure in lower extremity prostheses, *J. Biomechanics*, **1**, 247-257

Appoldt.F.A, Bennett.L, Contini.R, (1968b), The results of slip measurements in above-knee suction sockets, *Bull. Prosthet. Res.*, **Fall**, 106-112

Appoldt.F.A, Bennett.L, Contini.R, (1969), Socket pressure as a function of pressure transducer protrusion, *Bull. Prosthet. Res.*, **10 (11)**, 236-249

Appoldt.F.A, Bennett.L, Contini.R, (1970), Tangential pressure measurements in above-knee sockets, *Bull. Prosthet. Res.*, **10 (13)**, 70-86

Bader.D.L, (1990), The recovery characteristics of soft tissues following repeated loading, *J. Rehabil. Res. & Dev.*, **27(2)**, 141-150

Bader.D.L, Barnhill.R.L, Ryan.T.J, (1986), Effect of externally applied skin surface forces on tissue vasculature, *Arch. Phy. Med. Rehab.*, **67(11)**, 807-811

Barbenel.J.C, Evans.J.H, Finlay.J.B, (1973), Stress-strain time relations for soft connective tissues, in *Perspectives in Bio-medical Engineering*, Kenedi.R.M, (Ed), MacMillan Press, London, 165-172

Barbenel.J.C, Payne.P.A, (1981), In-vivo mechanical testing of dermal properties, *Bioeng. Skin*, **3**, 8-38

Barbenel.J.C, Sockalingham.S, (1990), Device for measuring soft tissue interface pressures, *J. Biomed. Eng.*, **12**, 519-522

Baumann.J.U, Sutherland.D.H, Hanggi.A, (1979), Intramuscular pressure during walking: An experimental study using the wick catheter technique, *Clinical Orthop. & Related Res.*, **145**, 292-299

Bennett.L, (1971), Transferring load to flesh Part II: Analysis of compressive stress, *Bulletin Prosthet. Research,*, **Fall**, 45-63

Bennett.L, (1972a), Transferring load to flesh Part III: Analysis of shear stress, *Bulletin Prosthet. Research*, **Spring**, 38-51

Bennett.L, (1972b), Transferring load to flesh Part IV: Flesh reaction to contact curvature, *Bulletin Prosthet. Research*, **Fall**, 60-67

Bennett.L, (1973), Transferring load to flesh Part V: Experimental work, *Bulletin Prosthet. Research*, **Spring**, 88-103

Bennett.L, (1974), Transferring load to flesh Part VII: Gel liner effects, *Bulletin Prosthet. Research*, **Spring**, 23-53

Bennett.L, Kavner.D, Bok.K.L, Trainer.F.A, (1979), Shear vs Pressure as causative factors in skin blood flow occlusion, *Arch. Phys. Med. Rehabil.*, **60**, 309-314

Bergel.D.H, (1961), The static elastic properties of the arterial wall, *J. Physiol.*, **156**, 445-457

Billmeyer.F.W, (1971), *Textbook of Polymer Science*, 2nd Ed, Wiley, New York

Brand.P.W., (1975), *Repetitive stress on insensitive feet*, U.S. Public Health Service Hospital, Carville, Louisiana

Brokaw.A.P, (1988), *An IC Amplifier Users Guide to Decoupling, Grounding and making things go right for a change*, Application Note, Analog Devices, Norwood M.A.

Brown.I.A, (1973), A scanning electron microscope study of the effects of uniaxial tension on human skin, *Brit. J. Dermatol.*, **89**, 383-393

Burgess.E.M, (1968), The below-knee amputation, *Bull. Pros. Res.*, **10**, 9

Burgess.E.M, (1985), Below-knee amputation, in *Surgical Techniques Illustrated: A Comparative Atlas*, Malt.R.A, (Ed), Saunders, Philadelphia, 563-568

Burgess.E.M, Matson.F.A, (1981), Determination of amputation levels in peripheral vascular disease, *J. Bone Joint Surg.*, **63-A**, 1493-1497

Burgess.E.M, Moore.A.J, (1977), A study of interface pressures in the below knee prosthesis (Physiological suspension: an interim report), *Bull. Prosthet. Res.*, **10 (28)**, 58-70

Burgess.E.M, Romano.R.L, Zettle.J,H, Shrock.R.D, (1971), Amputations of the leg for vascular insufficiency, *J. Bone Joint Surg.*, **53A**, 874-890

Butler.C.M, (1986), The vascular amputee, *MS Thesis*, University of London

Butler.D.A, et al, (1984), Effects of structure and strain measurement technique on the material properties of young human tendons and fascia, *J. Biomech.*, **17**, 579-596

Callen.S, (1981), Hexcelite temporary prosthesis for lower-limb amputees, *Physiotherapy*, **67**, 138-139

Cappozzo.A, Figura.F, Gazzani.F, Leo.T, Marchetti.M, (1982), Angular displacements in the upper body of AK amputees during level walking, *Prosthet. Orthot. Int.*, **6(3)**, 131-138

Cardi.M, Ferguson-Pell.M, Minkel.J, Bhansali.L, (1991), *Development and evaluation of an advanced pressure mapping system for prescription of seating and positioning systems*, Report of Centre for Rehabilitation Technology, Helen Hayes Hospital, New York

Carton.R.W, Bainouskas.J, Clark.J.W, (1962), Elastic properties of single elastin fibres, *J. Appl. Physiol.*, **17**, 547-551

Childress.D.S, Steege.J.W, (1987), Computer-aided analysis of below-knee socket pressure, *J. Rehabil. Res. & Dev.*, **25**, 22-24

Cobbold.R.S.C, (1974), *Transducers for Biomedical Measurements*, Wiley, New York

Cockrell.J.L, (1971), Point measurement of normal pressures, in *The effect of pressure on soft tissues*, A workshop report sponsored by the Committee on Prosthetic Research and Development, National Academy of Sciences, Washington D.C.

Coddington.T, (1988), Why are legs amputated in Britain?, in *Limb Salvage and Amputation for Vascular disease*, (Greenhalgh.R.M, Jamieson.C.W, Nicolaides.A.N, Eds) Saunders, London, 331-337

Comaish.S, Bottoms.E, (1971), The skin and friction: Deviations from Amonton's laws and the effects of hydration and lubrication, *Brit. J. Dermatol.*, **84**, 37-43

Cook.T, Alexander.H, Cohen.M, (1977), Experimental method for determining the 2-dimensional mechanical properties of living human skin, *Med. Biol. Eng. Comput.*, **15**, 381-390

Cox.H.T, (1944), The cleavage lines of the skin, *Br. J. Surg.*, **29**, 234-240

Cua.A.B, Wilhelm.K.P, Maibach.H.I, (1990), Frictional properties of human skin: relation to age, sex and anatomical region, stratum corneum hydration and transepidermal water loss, *Brit. J. Dermato.*, **123**, 473-479

Culham.E.G, Peat.M, Newell.E, (1986), Below knee amputation : a comparison of the effect of the SACH foot and SINGLE AXIS foot on electromyographic patterns during locomotion, *Prosthet. Orthot. Int.*, **10(1)**, 15-22

Daly.C.H, (1969), The role of elastin in the mechanical behaviour of human skin, *Proc. 8th Int. Conf. Med. Biol. Engg.*, Chicago, 17-18

Daly.C.H, (1982), Biomechanical properties of dermis, *J. Investig. Dermat.*, **79**, Supplement, 17s-20s

Daniel.R.K, Priest.D.L, Wheatley.D.C, (1981), Etiologic factors in pressure sores: An experimental model, *Arch. Phys. Med. Rehabil.*, **62(10)**, 492-498

Davies.R.M, Lawrence.R.B, Routledge.P.E, Knox.W, (1985), The RAPIDFORM process for automated thermoplastic socket production, *Prosthet. Orthot. Int.*, **9**, 27-30

Dean.D, Saunders.C.G, (1985), A software package for design and manufacture of prosthetic sockets for trans-tibial amputees. *IEEE Trans. Biomed. Eng.*, **BME-32(4)**, 257-262

Dewar.M, Reynolds.D, (1986), Development of the UCL Computer Aided Socket Design system, *Annual Report*, UCL Bioengineering Centre, University of London.

Dewar.M.E. Judge.G, (1980), Temporal asymmetry as a gait quality indicator, *Med. & Biol. Eng. & Comp.*, **18**, 689-693

DHSS, (1986), *Amputation Statistics for England, Wales and N. Ireland 1976-1986*, Statistics and Research Division, DHSS

Dick.J.C, (1951), Tension and resistance to stretching of human skin and other membranes, *J. Physiol.*, **112**, 102-113

Doillon.D.J, Dunn.M.G, Silvert.J.H, (1988), Relationships between mechanical properties and collagen structure of closed and open wounds, *J. Biomech. Eng.*, **110**, 352-356

Dormandy.J.A, Thomas.P.R.S, (1988), What is the natural history of a critically ischaemic patient with and without a leg?, in *Limb Salvage and Amputation for Vascular Disease*, (Greenhalgh.R.M, Jamieson.C.W, Nicolaides.A.N, Eds), Saunders, London, 11-26

Dupuytren.G, (1834), *Traité Théorique et Pratique des Blessures par Armes de Guerre*, Maison, Paris, **1**, 66

Ebskov.B, (1988), Trends in lower extremity amputation (Denmark 1979-1983), in *Amputation Surgery and Lower Limb Prosthetics*, Murdoch.G (Ed), Blackwell Scientific, Oxford, 3-8

Engsberg.J.R, Clynch.G.S, Lee.A.G, Allan.J.S, Harder.J.A, (1992), A CAD CAM method for custom below-knee sockets, *Prosthet. Orthot. Int.*, **16**, 183-188

Fairs.S.L.E, Ham.R.O, Conway.B.A, Roberts.V.C, (1987), Limb perfusion in the lower limb amputee - a comparative study using a laser-doppler flowmeter and a transcutaneous oxygen electrode, *Prosthet. Orthot. Int.*, **11**, 80-84

Faulkner.V, Walsh.N, Gall.N, (1986), Ultrasound as an aid to prosthetic socket design, *J. Rehab. Res. & Dev.*, **24**, 7

Fawcett.D.W, (1986), *A textbook of histology*, 11th Ed, Saunders, Philidelphia, 543-578

Ferguson-Pell.M.W, (1980), Design criteria for the measurement of pressure at body/support interfaces, *Eng. in Medicine*,**9(4)**, 209-214

Ferguson-Pell.M.W, Bell.F, Evans.J.H, (1976), Interface pressure sensors: existing devices their suitability and limitations, in *Bedsore Biomechanics*, Kenedi.R.M, Cowden.J.M, Scales.J.T (Eds), MacMillan Press, London

Ferguson-Pell.M.W, Cardi.M, (1992), Pressure Mapping Systems, *Team Rehab. Report*, **3(7)**, 28-32

Ferguson-Pell.M.W, Reddy.N.P, Stewart.S.F.C, Palmieri.V, Cochran.G.V.B, (1985), Measurement of physical parameters at the patient-support interface, in *Biomechanical Measurement in Orthopaedic Practice*, Whittle.M, Harris.D (Eds), Oxford, 133-144

Fernie.G.R, Griggs.G, Bartlett.S, Lunau.K, (1985), Shape sensing for computer aided below-knee prosthetic socket design, *Prosthetics & Orthotics*, **9**

Fernie.G.R, Halsall.A.P, Ruder.K, (1984), Shape sensing as an educational aid for student prosthetists, *Prosthet. Orthot. Int.*, **8**, 87-90

Ficarra.B.I, (1943), Amputations and prostheses through the centuries, *Medical Record*, **156**, 154-156

Finlay.B, (1969), Scanning electron microscopy of the human dermis under uni-axial strain, *Biomed. Eng.*, **4**, 322-327

Fisher.S.V. Gullickson.G.Jr, (1978), Energy cost of ambulation in health and disability: a literature review, *Arch. Phys. Med. Rehab.*, **59(3)**, 124-133

Flint.M.A, (1976), Langer's lines: A commentary, *Surg. Annu.*, **8**, 24-46

Franke.E.K, (1950), Mechanical Impedance of the surface of the human body, *J. Applied Physiol.*, **3**, 582-590

Frigo.C, Tesio.L, (1986), Speed-dependent variations of the lower limb joint angles during walking, *Am. J. Phys. Med.*, **65(2)**, 51-62

Fung.Y.C, (Ed), (1972), *Biomechanics: Its Foundations and Objectives*, Prentice-Hall, Englewood Cliffs, New Jersey

Fung.Y.C, (Ed), (1981), *Biomechanics: Mechanical Properties of Living Tissues*, Springer-Vertag, New York

Fung.Y.C, (1987), Mechanics of soft tissues, in *Handbook of Bio-engineering*, Skalak.R, Chien.S, (Eds), McGraw-Hill, New York

Garfin.S.R, et al, (1981), Role of fascia in the maintenance of muscle tension and pressure, *J. Appl. Physiol.*, **51**, 317-320

Garrett.P.H, (1981), *Analogue I/O Design*, Reston Pub C°, Reston V.A.

Gibson.T, (1965), Biomechanics in plastic surgery, in *Proc. Symp. Biomechanics and Related Bio-engineering Topics*, Kenedi.R.M, (Ed), Pergamon Press, London, 129-134

Gibson.T, Kenedi.R.M, (1970), The structural components of the dermis and their mechanical characteristics, in *Dermis*, Montagna.W, Bentley.J.P, Dobson.R.L, (Eds), Appleton-Century-Crofts, New York, 19-38

Gibson.T, Kenedi.R.M, Craik.J.E, (1965), The mobile micro-architecture of dermal collagen: bio-engineering study, *Brit. J. Surg.*, **52**, 764-770

Gibson.T, Stark.H, Evans.J.H, (1969), Directional variation in extensibility of human skin in-vivo, *J. Biomech.*, **2**, 201-204

Gilbert.J.A, Maxwell.G.M, McElhaney.J.H, Clippinger.F.W, (1984), A system to measure the forces and moments at the knee and hip during level walking , *J. Orthop. Res.*, **2(3)**, 281-288

Gray.H, (1989), *Gray's anatomy,* 37th Ed, Williams.P.C, Warwick.R, Dyson.M, Bannister.L.H (Ed's), Churchill-Livingstone, Edinburgh

Greenshaw.R.P, Vistnes.L.M, (1989), A decade of pressure sore research: 1977-1987, *J. Rehab. Res. & Devel.*,**26**, 63-74

Guyton.A.C, (1963), A concept of negative interstitial pressure based on pressures in implanted perforated capsules, *Circulation Research*, **12**, 399-414

Guyton.A.C, (1981), *Textbook of Medical Physiology*, 6th Ed, Saunders, London

Ham.R, Cotton.L, (1991), *Limb Amputation : From aetiology to rehabilitation*, Therapy in Practice Series:23, Chapman & Hall, London

Ham.R.O, Luff.R, Roberts.V.C, (1989), A five year review of referrals for prosthetic treatment in England, Wales and Northern Ireland 1981-1985, *Health Trends*, **21**, 3-6

Ham.R.O, Regan.J.M, Roberts.V.C, (1987), Evaluation of introducing the team approach to the care of the amputee: the Dulwich study, *Frosthet. Orthot. Int.*, **11**, 25-30

Hargens.A.R, et al, (1977), Interstitial fluid pressure in muscle and compartment syndromes in man, *Microvascular Research*, **14**, 1-10

Heidenreich.W, Kuny.W, (1985), Magnetic-field-sensitive semiconductor position sensors, *Elecktronik Industrie*, **6**, 7-10

Hennig.E.M, Cavanagh.P.R, Albert.H.T, Macmillan.N.H, (1982), A piezo-electric method of measuring the vertical contact stress beneath the human foot, *J. Biomed. Eng.*, **4**, 213-222

Henriksen.O, Marsch.G, Persson.B, (1978), The Tulip prosthesis, *Acta Orthop. Scand.*, **47**, 107

Holstein.P, Hansen.H.J.B, (1988), How do we determine the level of major amputation?, in *Limb Salvage and Amputation for Vascular Disease*, (Greenhalgh.R.V, Jamieson.C.W, Nicolaides.A.N, Eds), Saunders, London, 85-92

Hosein.R, Lord.M, (1991), Shear force measurement on the plantar surface of the foot., *Proc. 31st Ann. BES Scientific Meeting*, Univ. Birmingham U.K., 18-19 Sept.

Houston.V.L, Burgess.E.M, Childress.D.M, Lehneis.H.R, Mason.C.P, Garbarini.M.A, LeBlanc.K.P, Boone.D.A, Chan.R.B, Harlan.J.H, Brncick.M.D, (1992), Automated fabrication of mobility aids (AFMA): Below-knee CASD/CAM testing and evaluation program results, *J. Rehabil. Res. & Dev.*, **29(4)**, 78-124

Hunter.J.A.A, McVittie.E, Comaish.J.S, (1974), Light and electron microscope studies of physical injury to the skin: II Friction, *Br. J. Dermatology*, **90**, 491-499

Husain.T, (1953), An experimental study of some pressure effects on tissues, with reference to the bed-sore problem, *J. Path. Bact.*, **66**, 347-358

Hussein.H.MG, Thompson.D.E, Perritt. R.Q, (1978), Impedance of human soft tissue under various static pre-loads, *31st ACEMB*, Atlanta Georgia, 21-25 Oct, 260

Hutton.I.M, Rothnie.N.G, (1977), The early mobilisation in the elderly amputee, *Br. J. Surg.*, **64**, 267-270

Isherwood.P.A, (1980), The controlled pressure distribution system for prosthetic casting, *PhD Thesis*, University of London

Jones.D, Paul.J.P, (1978), Analysis of variability in pylon transducer signals, *Prosthet. Orthot. Int.*, **2**, 161-166

Katz.K, et al, (1979), End-bearing characteristics of Patella-Tendon-Bearing prostheses - A preliminary report, *Bull. Prosthet. Res.*, **10 (32)**, 55-68

Keier.A.N, Rozhokov.A.V, Shatilov.O.Y, (1988), The management of short stumps, in *Amputation Surgery and Lower Limb Prosthetics*, Murdoch.G (Ed), Blackwell Scientific, Oxford, 327-334

Kendrick.R.R, (1956), Below-knee amputation for arteriosclerotic gangrene, *Brit J.Surg.*, **44**, 13

Kenedi.R.M, Gibson.T, Daly.C.H, (1965a), Bio-engineering studies of the human skin; II, in *Proc. Symp. Biomechanics and Related Bio-engineering Topics*, Kenedi.R.M. (Ed), Pergaman Press, Oxford, 147-158

Kenedi.R.M, Gibson.T, Daly.C.H, (1965b), The determination, significance and application of the biomechanical characteristics of human skin, *Digest 6th Int. Conf. Medical Electronics and Biological Engineering*, Tokyo

Kenedi.R.M, Gibson.T, Evans.J.H, Barbenel.J.C, (1975), Tissue Mechanics, *Phys. Med. Biol.*, **20(5)**,699-717

Kirkby.R.L, Stewart-Gray.J.F, Creaser.G.A, (1985), Usefulness of foot sequence analysis in lower limb amputees, *Phys. Ther.*, **65(1)**, 31-34

Klasson.B, (1985), Computer aided design, computer aided manufacture and other computer aids in prosthetics and orthotics, *Prosthet. Orthot. Int.*, **9**, 3-11

Knight.P, Urquhart.J, (1989), Outcomes of Artificial Lower Limb Fitting in Scotland, *I.S.D. Publications,* Scottish Health Service

Kohler.P, Lindh.L, Netz.P, (1989), Comparison of CAD-DAM and hand made sockets for PTB prostheses, *Prosthet. Orthot. Int.*, **13**, 19-24

Kosiak.M, Kubicek.W.G, Olson.M, Danz.J.N, Kottke.F.J, (1958), Evaluation of pressure as a factor in the production of ischial ulcers, *Arch. Phys. Med. & Rehab.*, **Oct**, 623-629

Kreyszig.E, (1979), *Advanced Engineering Mathematics*, 4th Ed, Wiley, New York

Krouskop.T.A, Brown.J, Goode.B, Winningham.D, (1987b), Interface pressures in above-knee sockets, *Arch. Phys. Med. Rehabil.*, **68**, 713-714

Krouskop.T.A, Malinauskas.M, Williams.J, Barry.P.A, Muilenburg.A.L, Winningham.D.J, (1989), A computerised method for the design of above-knee prosthetic sockets, *J. Prosthet. Orthot.*, **1(3)**, 131-138

Krouskop.T.A, Muilenburg.A.L, Doughtery.D.R, Winningham.D.J, (1987a), Computer-aided design of prosthetic socket for above-knee amputee, *J. Rehabil. Res. & Dev.*, **24**, 31-38

Kuhn.W, Kunzle.O, Preissmann.A, (1954), Relaxation time spectrum, Elasticity and Viscosity of Rubber I, *Rubber Chemistry and Technology*, **27**, 36-73

Kuny.W, Heidenreich.W, (1985), *Magnetic-field-sensitive semiconductor position sensors*, Elecktronik Industrie, **5**, 5-6

Langer.K, (1861), Zur Anatomie und Physiologie der Haut: I Uber die Spaltbarkeit der Cutis, *Sitzungber Akad. Wiss. Wein.*, **44**, 19-46

Lanir.Y, (1987), Skin mechanics, in *Handbook of Bio-engineering*, Skalak.R, Chien. S, (Eds), McGraw-Hill, New York

Lanir.Y, Fung.Y.C, (1974), Two-dimensional mechanical properties of rabbit skin: II - Experimental results, *J. Biomech.*, **7**, 171-182

Lanshammer.H, (1982), Variation of mechanical energy levels for normals and prosthetic gait, *Prosthet. Orthot. Int.*, **6(2)**, 97-102

Laughman.R.K, Asken.L.J, Bleimeyer.R.R, Chao.E.Y, (1984), Objective clinical evaluation of function: Gait analysis., *Phys. Ther.*, **64(12)**, 1839-1845

Lawrence.R.B, Knox.W, Crawford.H.V, (1985), Prosthetic shape replication using a computer controlled carving technique, *Prosthet. Orthot. Int.*, **9**, 23-26

Leavitt.L.A, Zuniga.E.N, Calvert.J.C, Canzoneri.J, Perterson.C.R, (1972), Gait analysis and tissue-socket interface pressures in above-knee amputees, *Southern Med. J.*, **65(10)**, 1197-1207

Lee.G.C, Kopping.J.G, (1972), Lung elasticity, in *Biomechanics: Its Foundations and Objectives*, Fung.Y.C (Ed), Prentice-Hall, Englewood Cliffs, New Jersey, 317-336

Lee.M.M.C, Ng.C.K, (1965), Post-mortem studies of skinfold caliper measurement and actual thickness of skin and subcutaneous tissue, *Human Biology*, **37**, 91-103

Levit.F, (1981), Skin problems in amputees, in *Atlas of Limb Prosthetics: Surgical and Prosthetic Principles (American Academy of Orthopaedic Surgeons)*, C.V.Mosby Co, St. Louis, 443-447

Levy.S.W, (1956), The skin problems of lower-extremity amputee, *Artific. Limbs*, **3(1)**, 20-35

Levy.S.W, (1962), Skin problems of the leg amputee, *Arch. Dermatology*, **85**, 65-81

Lindley.P.B, (1974), Cold bonding vulcanised rubber to metal, *Natural Rubber Technology*, **5(3)**, 52-57

Lindley.P.B., (1978), *Engineering Design with Natural Rubber*, 4th Ed, NR Tech Bulletin Malaysian Rubber Producers Research Association, Brickendonbury, Herts, 26-28

Lindner.J, (1972), Skin ageing: A review, in Connective tissue and Ageing, *Int. Cong. Series No 264*, Excerpta Medica Amsterdam

Little.J.M, (1985), Below knee amputation, in *Surgical Techniques Illustrated: A Comparitive Atlas*, Malt.R.A, (Ed), Saunders, Philadelphia, 553-556

Liu.G.H.W, Mak.A.F.T, Lee.S.Y, (1992), Indentation properties of the soft tissues around below-knee stumps, *Proc. VII World Cong. ISPO*, June-July, Chicago, 150

Lord.M, (1981), Foot pressure measurement: A review of methodology, *J. Biomed. Engng.*, **3**, 91-99

Lord.M, Davies.R.M, (1988), Shape management: Systems concepts and the impact of information technology, in *Amputation Surgery and Lower-Limb Prosthetics*, Murdoch.G. (Ed), Blackwell Scientific, Oxford, 345-349

Lord.M, Hosein.R, Williams.R.B, (1992), Method for in-shoe shear stress measurement, *J. Biomed. Eng.*, **14**, 181-186

Love.A.E.H, (1943), *The Mathematical Theory of Elasticity*, 2nd Ed, Cambridge University Press, London

Lyquist.E, (1970), Recent variants of the PTB prosthesis (PTS, KBM, and air cushion sockets), in *Prosthetic and Orthotic Practice*, Murdoch.G. (Ed), Edward Arnold, London, 79-88

Malone.J.M, Moore.W.S, Goldstone.J, Malone.S.J, (1979), Therapeutic and economic impact of a modern amputation program, *Am. Surg.*, **189(6)**, 798-802

Markenscoff.X, Yannas.I.V, (1979), On the stress-strain relation for skin, *J. Biomech.*, **12**, 127-129

McColl.I, (1986), *Review of Artificial Limb and Appliance Centre Services*, DHSS, London

McCollum.C.N, (1985), Posterior flap below-knee amputation, in *Vascular Surgical Techniques: An Atlas*, Greenhalgh.R.M (Ed), Saunders, London, 340-346

McCollum.P.T, Spence.V.A, Walker.W.F, Murdoch.G, (1985), A rationale for skew flaps in below-knee amputation surgery, *Prosthet. Orthot. Int.*, **9**, 95-99

McCord.C.P, (1963), Cork legs and iron hands: the early history of artificial limbs, *Indust.Med.Surg*, **32**, 102-112

Measurements Group Ltd., (1981), Modern Strain Gauge Transducers - Their design and construction, *Epsilonics*, **1(1)**, 5-7

Meier.R.H, Meeks.E.D, Herman.R.M, (1973), Stump-socket fit of below-knee prostheses: comparison of three methods of measurement, *Arch. Phys. Med. Rehab.*, **54 (12)**, 553-558

Mensch.B, Ellis.P.M, (1987), Pre-operative and post-operative care and the responsibility of the physical therapist, in *Physical Therapy Management of Lower Extremity Amputations*, Heinmann Physiotherapy, London, 45-200

Merbit.C.T, et al, (1985), Wheelchair pushups : Measuring pressure relief frequency, *Arch. Phys. Med. Rehabil.*, **66(7)**, 433-438

Middleton.J.D, (1973), The influence of temperature and humidity on stratum corneum and its relation to skin chapping, *J. Soc. Cosmet. Chem.*, **24**, 239-243

Minns.R.J, Soden.P.D, Jackson.D.S, (1973), The role of the fibrous components and ground substance in the mechanical properties of biological tissues: A preliminary investigation, *J. Biomech.*, **6**, 153-165

Mizrahi.M, et al, (1985), Biomechanical evaluation of an adjustable patella-tendon-bearing prosthesis, *Scand. J. Rehabil. Med.*, **12** supplement, 117-123

Monster.A.W, (1972), Sensory augmentation in weight-bearing training, in *The effect of pressure on soft tissues*, A workshop report sponsored by Committee on Prosthetics Research and Development, National Academy of Sciences, Washington, D.C.

Moore.T.J, (1970), A survey of the mechanical characteristics of skin and tissue in response to vibratory stimulation, *IEEE Trans. Man-Mach. Sys.*, **MM5-11 (1)**, 79-84

Morley.A, (1947), *Strength of Materials,* 9th Ed, Longmans Green and C°, London

Morrison.R, (1977), *Grounding and Shielding Techniques in Instrumentation,* 2nd Ed, Wiley, New York.

Mridha.M, Odman.S, (1985), Characterization of subcutaneous oedema by mechanical impedance measurements, *J. Invest. Dermatol.*, **85**, 575-578

Mubarek.S.J, et al ,(1976), The wick catheter technique for measurement of intramuscular pressure, *J. Bone Joint Surg.*, **58-A**, 1016-1020

Murdoch.G, (1968), The 'Dundee' socket for the below-knee amputee, *Prosthetics Int.*, **3(4-5)**, 15-21

Murphy.E.F, (1971), Transferring load to flesh Part I: Concepts, *Bulletin Prosthet. Research*, **Fall**, 38-44

Naeff.M, Van Pijkeren.T, (1980), Dynamic pressure measurements at the interface between residual limb and socket - the relationship between pressure distribution comfort and brim shape, *Bull. Prosthet. Res.*, **10-33 (Vol 17 No 1)**, 35-50

Nagrath.I.J, Gopal.M, (1986), *Control Systems Engineering*, 2nd Ed, Wiley, Singapore

Nakajima.H, Surauki.M, Inatomi.Y, (1982), Application of CAD/CAM technology for socket design of artificial legs, *Proc. Conf. on CAD/CAM technology in Mech. Eng*, MIT, 134

Narang.I.C, Jape.V.C, (1982), Retrospective study of 14400 civilian disabled (new) treated over 25 years at an Artificial Limb Centre, *Prosthet. Orthot. Int.*, **6**, 10-16

Naylor.P.F.D, (1955a), The skin surface and friction, *Brit. J. Cermatol.*, **67**, 239-248

Naylor.P.F.D, (1955b), Experimental friction blisters, *Brit. J. Dermatol.*, **67**, 327-342

Nevill.A, (1991), A foot pressure measurement system utilising PVdF and copolymer piezo-electric transducers, *PhD Thesis*, University of Kent at Canterbury

Pagliarulo.M.A, Waters.R.L, Hislop.H.J, (1979), Energy cost of walking of below-knee amputees having no vascular disease, *Phys. Ther.* , **59(5)**, 538-542

Papir.Y.S, Hsu.K.H, Wildnauer.R.H, (1975), The mechanical properties of stratum corneum: I, The effect of water and ambient temperature on the tensile properties of newborn rat stratum corneum, *Biochim. Biophys. Acta*, **399**, 170-180

Patterson.R.P, Fisher.S.V, (1979), The accuracy of electrical transducers for the measurement of pressure applied to the skin, *IEEE Trans. Biomed. Eng.*, **BME-26(8)**, 450-456

Pearson.J.R, Grevsten.S, Almby.B, Marsh.L, (1974), Pressure variation in the below-knee patella tendon bearing suction socket prosthesis, *J. Biomechanics*, **7**, 487-496

Pearson.J.R, Holmgren.G, March.L, Oberg.K, (1973), Pressures in critical regions of the below-knee patella-tendon-bearing prosthesis, *Bull. Prosth. Res.*, **10 (19)**, 52-76

Perry.C.C, Lissner.H.R, (1955), *The Strain Gauge Primer,* McGraw-Hill, New York

Persson.B.M, Liedberg.E, (1983), A clinical standard of stump measurement and classification in lower limb amputees, *Prosthet. Orthot. Int.*, **7**, 17-24

Peura.R.A, Webster.J.G, (1978), *Medical Instrumentation - Application and Design,* Webster.J.G(Ed), Houghton Mifflin Co, Boston

Pierard.G.E, Lapiere.C.M, (1987), Micro-anatomy of the dermis in relation to relaxed skin tension lines and Langer's lines, *Amer. J. Dermatopathology*, **9**, 219-224

Pohjolainen.T, Alaranta.H, (1988), Lower limb amputation in Southern Finland 1984-1985, *Prosthet. Orthot. Int,* **12**, 9-18

Pollard.J.P, (1984), *The mechanics of diabetic forefoot ulceration*, MS Thesis, Cambridge, UK

Pollard.J.P, Le Quesne.L.P, Tappin.J.W, (1983), Forces under the foot, *J. Biomed. Eng.*, **5**, 37-40

Porter.D, Roberts.V.C, (1989a), A review of gait assessment in the lower limb amputee. Part 1: Temporal and kinematic analysis, *Clinical Rehab.*, **3**, 65-74

Porter.D, Roberts.V.C, (1989b), A review of gait assessment in the lower limb amputee. Part 2: Kinetic and metabolic analysis, *Clinical Rehab.*, **3**, 157-168

Potma.T, (1967), *Strain gauges - Theory and Application,* Phillips paperbacks, Illife Books, London

Potts.R.O, Brewer.M.M, (1983), The low-strain viscoelastic properties of skin, *Bioeng. Skin*, **4**, 105-114

Pritham.C.H, (1988), Prosthetic fitting: General Concepts, in *Amputation Surgery and Lower Limb Prostheses*, Murdoch.G. (Ed), Blackwell Scientific, Oxford, 29-33

Pye.G, Bowker.P, (1976), Skin temperature as an indicator of stress in soft tissue, *Eng. Med.*, **5**, 58-60

Quesada.P.M, Skinner.H.B, (1992), Finite element analysis of the effects of prothesis model alterations on stump/socket interface stresses, *Proc. VII World Cong. ISPO*, June-July, Chicago, 275

Radcliffe.C.W, Foort.J, (1961), *The Patellar-Tendon-Bearing below-knee prosthesis*, Biomechanics Laboratory, University of California, Berkely

Rae.J.W, Cockrell.J.L, (1971), Interface pressure and stress distribution in prosthetic fitting, *Bull. Prosthet. Res.*, **10 (15)**, 64-111

Rang.M, Thompson.G.H, (1981), History of amputation and prostheses, in *Amputation Surgery and Rehabilitation - The Toronto Experience*, J.P.Kostuik Ed, Churchill Livingstone, New York, 1-12

Rausch.R.W, Khalili.A.A, (1985), Air splint pre-prosthetic rehabilitation of lower extremity amputated limbs, *Phys. Ther.*, **65**, 912-914

Redhead.R.G, (1979), Total surface bearing self suspending above-knee sockets, *Prosthet. Orthot. Int.*, **3**, 126-136

Redhead.R.G, (1983), The early rehabilitation of lower limb amputees using a pneumatic walking aid, *Prosthet. Orthot.Int.*, **1**, 84-88

Reichel.S.M, (1958), Shearing force as a factor in decubitus ulcers in paraplegics, *J. Amer. Med. Ass.*, **166**, 762-763

Renstrom.P, (1981), A follow-up study of 200 below-knee amputations amputated between 1973-1977, in The Below-Knee Amputee, *MD Thesis*, University of Gothenburg, Sweden, 7-25

Renstrom.P, (1986), Circulation, muscle and volume changes in below-knee amputee stumps, *Proc. V ISPO World Cong.*, Copenhagen June 29-July 4, 234

Reynolds.D, (1988), Shape design and interface load analysis for below knee prosthetic sockets, *PhD Thesis*, University of London

Reynolds.D.P, Lord.M, (1992), Interface load analysis for computer-aided design of below-knee prosthetic sockets, *Med. Biol. Eng. Comput.*, **30**, 419-426

Ridge.M.D, Wright.V, (1966), The directional effect of skin - A bio-engineering study of skin with particular reference to Langer's lines, *J. Invest. Dermatol.*, **46**, 341-346

Rivlin.R.S, Saunders.D.W, (1949), Cylindrical Shear Mountings, *Trans. I.R.J*, **24**, 296-306

Roaf.R, (1976), Causation and prevention of bedsores, in *Bedsore Biomechanics*, Kenedi.R.M, Cowden.J.M, Scales.J.T (Eds), University Park Press, Baltimore

Robb.H.J, Jacobson.L.F, Hordon.P, (1985), Midcalf amputation in the ischaemic extremity: the lateral and medial flap, *Arch. Surg.*, **91**, 506-511

Robinson.J.L, Smidt.G.L, Arora.J.S, (1977), Accelerographic, temporal and distance gait factors in below-knee amputees, *Phys. Ther.*, **57(8)**, 898-904

Robinson.K.P, (1982), Skew flap myoplastic below-knee amputation: a preliminary report, *Br. J. Surg.*, **69**, 554-557

Robinson.K.P, (1988), Skew-flap below-knee amputation, in *Limb Salvage and Amputation for Vascular Disease*, (Greenhalgh.R.M, Jamieson.C.W, Nicolaides.A.N, Eds), Saunders, Philidelphia, 373-382

Robinson.K.P, (1989), Skew-flap below-knee amputation, in *Surgical Techniques : an atlas*, Greenhalgh.R.M (Ed), Saunders, London, 348-353

Rockborn.P, Jernerberger.A, (1986), Measurement of stump volume changes by impedance, *Proc. V ISPO World Cong.*, Copenhagen June 29-July 4, 232

Rogers.W.E, Crawford.R.H, Faulkner.V.F, Beaman.J.J, (1992), Fabrication of an integrated prosthetic socket using solid freeform fabrication, *Proc. VII World Cong. ISPO*, June-July, Chicago, 23

Rovick.J.S, (1992), An additive fabrication technique for the computer-aided manufacturing of sockets, *Proc. VII World Cong. ISPO*, June-July, Chicago, 24

Rovick.J.S, Chan.R.B, Van Vorhis.R.L, Childress.D.S, (1992), Computerised manufacturing in prosthetics: various possibilities using industrial equipment, *Proc. VII World Cong. ISPO*, June-July, Chicago, 22

Ruder.K, Fernie.G.R, Kostuik.J.P, (1977), Techniques of lower limb prosthetic manufacture using Lightcast II, *Prosthet. Orthot. Int.*, **1**, 84-88

Rush.D.S, Huston.C.C, Bivins.B.A, Hyde.G.L, (1981), Operative and late mortality rates of above-knee to below-knee amputations, *Am. Surg.*, **47(1)**, 36-39

Rutkow.I.M, Marlboro.P.H, (1986), Orthopaedic operations in the United States 1979 through 1983, *J. Bone and Joint Surg.*, **68-A**, 716-719

Saleh.M, Murdock.G, (1985), In defence of gait analysis; Observation and measurement in gait assessment, *J. Bone Joint Surg. (Br)*, **67(2)**, 237-241

Sandberg.L.B, Soskel.N.T, Leslie.J.G, (1981), Elastin structure, biosynthesis and relation to disease states, *N. Engl. J. Med.*, **304**, 566-577

Sanders.G.T, (1985), History, in *Lower Limb Amputations: a Guide to Rehabilitation*, F.A.Davis Co., Philadelphia, 13-33

Sanders.J.E, Daly.C.H, (1989), Normal and shear interface stresses in lower-limb prosthetics, *IEEE Conf. Engg. in Med. & Biol.*, Seattle WA, November, 1443-1444

Sanders.J.E, Boone.C.P, Daly.C.H, (1990), The residual limb/prosthetic socket interface: Normal stress and shear stress, *Proc. 13th Ann. Conf. RESNA*, Washington .D.C., RESNA Press, 234-235

Sanders.J.E, Daly.C.H, Burgess.E.M, (1992), Interface shear stress during ambulation with a below-knee prosthetic limb, *J. Rehab. Res. & Dev.*, **29(4)**, 1-8

Saunders.C.G, Fernie.G.R, (1984), Automated prosthetic fitting, in Special Sessions, *2nd Int. Conf. on Rehab. Eng.*, Ottawa Canada, June 17-22, RESNA, Bethesda MD, 239-242

Saunders.C.G, Foort.J, Bannon.M, Lean.D, Panych.L, (1985), Computer aided design of prosthetic sockets for below-knee amputees. *Prosthet. Orthot. Int.*, **9**, 17-22

Sears.F.W, Zemansky.M.W, Young.H.D, (1978), *University Physics*, 5th Ed, Addison-Wesley, Sydney

Seippel.R, (1983), *Operational Amplifiers*, Reston Publications Co, Reston Virginia.

Seliktar.R, Mizrahi.J, (1986), Some gait characteristics of below knee amputees and their reflection on the ground reaction, *Eng. Med.*, **15(1)**, 27-34

Shock.R.B, Brunski.J.B, Cochran.G.V.B, (1982), In-vivo experiments on pressure sore biomechanics: Stresses and strains in indented tissues, *1982 Advances in Bioengineering*, Thibault.L (Ed), 88-91

Shuster.S, Black.M.M, McVitie.E, (1975), The influence of age and sex on skin thickness and skin collagen density, *Brit. J. Dermatol.*, **93**, 639-643

Sienko-Thomas.S, Supan.T.J, (1990), A comparison of current biomechanical terms, *J. Prosthet. Orthot.*, **2(2)**, 107-114

Silver-Thorn.M.B, Childress.D.S, (1992a), Sensitivity of below-knee residual limb/prosthetic socket interface pressures to variations in socket design, *Proc. VII World Cong. ISPO.*, June-July, Chicago, 148

Silver-Thorn.M.B, Childress.D.S, (1992b), Use of generic geometric finite element model of the below-knee and prosthetic socket to predict interface pressures, *Proc. VII World Congress ISPO*, June-July, Chicago, 272

Silver-Thorn.M.B, Steege.J.W, Childress.D.S, (1992), measurements of below-knee residual limb/prosthetic socket interface pressures, *Proc. VII World Cong. ISPO*, June-July, Chicago, 280

Skalak.R, Chien.S, (Eds), (1987), *Handbook of Bioengineering*, McGraw-Hill, New York

Smith.D.M, Crew.A, Hankin.A, Silhouette shape sensor, *Annual Report,* UCL Bioengineering Centre, Uni of London, 1986

Sonck.W.A, Cockrell.J.L, Koepke.G.H, (1970), Effect of liner materials on interface pressures in below-knee prostheses, *Arch. Phys. Med. Rehabil.*, **51(11)**, 666-669

Southwell R.V, (1953), *An Introduction to the Theory of Elasticity*, 2nd Ed, Oxford University Press, London, 101-133

Spence.V.A, McCollum.P.T, (1985), Evaluation of the ischaemic limb by transcutaneous oxymetry, in *Diagnostic Techniques and Assessment Procedures in Vascular Surgery*, Greenhalgh.R (Ed), Grune & Stratton, London, 331-341

Steege.J.W, Schnur.D.S, Childress.D.S, (1987a), Finite element analysis as a method of pressure prediction at the below-knee socket interface, *Proc. 10th Ann. Conf. RESNA*, San Jose, California, 814-816

Steege.J.W, Schnur.D.S, Childress.D.S, (1987b), Prediction of pressure at the below-knee socket interface by finite element analysis, *ASME Symposium on Biomechanics of Normal and Prosthetic Gait*, Boston, **BED 4**, 39-43

Steege.J.W, Silver-Thorn.M.B, Childress.D.S, (1992), Design of prosthetic sockets using finite element analysis, *Proc. VII World Cong. ISPO.*, June-July, Chicago, 273

Steinberg.F.U, Sunwoo.I, Roettger.R.F, (1985), Prosthetic rehabilitation of geriatric amputee patients: a follow-up study, *Arch. Phys. Med. Rehabil.*, **66**, 742-745

Stevens.J.C, Jones.N.B, (1972), A review of apparatus for investigating the mechanical properties of soft animal tissue in-vitro, *Eng. Med.*, **6**, 112-119

Stoughton.R.B, (1957), Mechanisms of blister formation, *A.M.A. Arch. Dermatology*, **76**, 584-590

Symington.D.C, Lowe.P.J, Olney.S.J, (1979), The pedynograph: a clinical tool for force measurements and gait analysis in lower extremity amputees, *Arch. Phys. Med. Rehabil.*, **60(2)**, 56-61

Tappin.J.W, Pollard.J, Beckett.E.A, (1980), Method of measuring 'shearing' forces on the sole of the foot, *Clin. Phys. Physiol. Meas.*, **1(1)**, 83-85

Termansen.N.B, (1977), Below-knee amputation for ischaemic gangrene. Prospective randomised comparison of a transverse and saggital operative technique, *Acta Orthop. Scand.*, **48**, 311-316

Tibarewala.D.N, Ganguli.S, (1982), Pattern recognition in tachographic gait records of normal and lower extremity handicapped human subjects, *J. Biomed. Eng.*, **4(3)**, 233-240

Topper.A.K, Fernie.G.R, (1990), An evaluation of computer aided design of below-knee prosthetic sockets, *Prosthet. Orthot. Int.*, **14**, 136-142

Torres-Moreno.R, Foort.J, Morrison.J.B, Saunders.C.G, (1989), A reference shape library for computer-aided socket design in above-knee prostheses. *Prosthet. Orthot. Int.*, **13**, 130-139

Torres-Moreno.R, Saunders.C.G, Foort.J, Morrison.J.B, (1991), Computer-aided design and manufacture of an above-knee amputee socket. *J. Biomed. Eng.*, **13**, 3-9

Torres-Moreno.R, Morrison.J.B, Cooper.D, Saunders.C.G, (1992), A computer-aided socket design procedure for above-knee prostheses. *J. Rehabil. Res. & Des.*, **29(3)**, 35-44

Tortora.G.J., Angnostakos.N.P, (1990), *Principles of Anatomy and Physiology,* 6th Ed, Harper Collins, New York

Treloar L.R.G., (1958), *The Physics of Rubber Elasticity,* 2nd Ed, Oxford Univ Press, London, 85-98

Tsuchiya.K, Morimoto.S, (1986), Measurement of stump shape using Moiré topographyand picture processing technology, *Proc. 5th World Cong. ISPO*, Copenhagen, June-July, 310

Vachranukunki.T, Seliktar.R, Besser.M, Demopoulos.J.T, (1986), Optimization of residual limb-socket load bearing of below knee prostheses, *5th World Cong. ISPO*, Copenhagen, June 29-July 4, 355

Vailas.A.C, et al, (1981), Physical activity and its influence on the repair process of medial collateral ligaments, *Connective Tissue Research*, **9**, 25-31

Van Pijkeren.T, Naeff.M, Kwee.H.H, (1980), A new method for the measurement of normal pressure between amputation residual limb and socket, *Bull. Prosthet. Res.*, **17(1)**, 31-34

Van Royen.B.J, et al, (1988), A comparison of the effects of immobilisation and continuous passive motion on surgical wound healing in mature rabbits, *Plas. Reconst. Surg.*, **78**, 360-366

Viidik.A, (1987), Properties of tendons and ligaments, in *Handbook of Bioengineering*, Skalak.R, Chien.S (Eds), McGraw-Hill, New York

Vitali.M, Robinson.K.P, Andrews.B.G, Harris.E.E, Redhead.R.G, (1986), *Amputations and prostheses*, Bailliere Tindall, London

Vogel.H.G, (1982), Mechanical properties of rat skin as compared by in-vivo and in-vitro measurement, *Bioeng. Skin*, **3**, 198-209

Vogel.H.G, Denkel.K, (1982), Methodological studies on biomechanics of rat skin comparing in-vivo and in-vitro results, *Bioeng. Skin*, **4**, 71-79

Vossoughi.J, Vaishnav.R.N, (1979), A comment, *J. Biomech.*, **12**, 481

Waddell.J.P, (1981), Below-knee amputation, in *Amputation Surgery and Rehabilitation: The Toronto experience*, Kostwick.J.P, (Ed), Churchill-Livingstone, New York, 63-80

Wall.M, (1988), Lower limb amputation stump descriptions, in *Amputation Surgery and Lower Limb Prosthetics,* Murdoch.G (Ed), Blackwell Scientific, Oxford, 403-417

Ward.I.M, (1971), *Mechanical Properties of Solid Polymers*, Wiley-Interscience, London, 77-109

Waters.R.L, Pery.J, Antonelli.D, Hislop.H, (1976), Energy cost of walking of amputees: the influence of level amputation, *J. Bone Joint Surg.* , **58(1)**, 42-46

Weiss.M, (1969), Physiological amputation, immediate prosthetic and early ambulation, *Prosthetics Int.*, **3(8)**, 38-44

Whitkowski.J.E, Parish.L.C, (1982), Histopathology of the decubitus ulcer, *J. Am. Acad. Dermatol.*, **6(6)**, 1014-1021

Wildnauer.R.H, Bothwell.J.W, Douglass.A.B, (1971), Stratum Corneum biochemical properties: I, Influence of relative humidity on normal and extracted human stratum corneum, *J.Invest. Dermatol.*,**56**, 72-78

Wilkinson.J.C, Dewar.M.E, (1990), The UCL system for computer-aided socket design: Clinical results, *ISPO workshop report on CAD/CAM in Prosthetics and Orthotics*, Davies.R.M, Donovan.R.G, Spiers.R.W (Eds), ISPO, 25-27

Williams.A.B, (1981), *Electronic Filter Design Handbook*, McGraw-Hill, New York.

Williams.R.B, Porter.D, Roberts.V.C, (1989), Assessment of stresses at the stump/socket interface, *Abstracts 6th World Congress ISPO*, Kobe Japan, November, 142

Williams.R.B, Porter.D, Roberts.V.C, Regan.J.F, (1992), Triaxial force transducer for investigating stresses at the stump/socket interface, *Med. & Biol. Eng. & Comput.*, **30**, 89-96

Wu.Y, Binack.M.D, Krick.H.J, Pitman.T.D, Stratigos.J.S, (1981), Scotchcast PVC interim prosthesis for below-knee amputees, *Bull. Prosthet. Res.*, Fall, **10(36)**, 40-45

Zill.D.G, (1989), *A first course in differential equations with applications*, PWS-Kent, Boston

Zverev.A.I, (1967), *Handbook of Filter Synthesis*, Wiley, New York.

LONT
UNI